Fault Characterisation in the Pre-Zechstein Succession of the Anglo-Dutch and East Pennine Basins

Victoria Elizabeth Elliott

St. Peter's College

Thesis submitted to the University of Oxford for the degree of

Doctor of Philosophy (DPhil)

Michaelmas Term 2019



Supervised by Professor Joe A. Cartwright and Professor Mike C. Daly

Declaration

I declare that the work presented in this thesis is wholly my own, except where otherwise stated. The views and interpretations expressed herein are mine, and do not reflect those of any other person of group except where this is cited to be the case

Acknowledgements

Firstly, I would like to thank my primary supervisor, Joe Cartwright for giving me the opportunity to undertake this exciting challenge, and providing me with the best guidance and encouragement throughout the project. I have learnt so much from Joe over the years and I am very grateful for his shared knowledge. I would also like to thank my secondary supervisor, Mike Daly. Thank you for the great supervision and the many thoughtful discussions and excursions that greatly contextualised this research.

I am very grateful to BP and the studentship that I received from them, enabling me to undertake such an exciting project. Specific thanks to Laura Banfield, Deirdre Hay, Keith Mills and David Ashby for their help in developing the project and insightful feedback. Thank you to Scott Carmichael for help with the data navigation for compiling the workstation product. I would also like to thank PGS for providing me such an extensive and exciting dataset of 3D seismic. Thank you to the UKOGL for providing me with the 2D seismic dataset.

A big thanks to all members of the 3D Lab group (past and present), for making the lab a positive a friendly environment. A special thanks to Gemma, Martino and Chris for all the technical support throughout the years, for whom which I would not have been able to complete the finished document.

Finally, I would like to thank my family for their continued support and understanding throughout the years. A big thank you to the Kings, for giving me a roof and roasts in the final months. A special thank you to James' Taxi service. Thank you for enduring this with me, sorry for all the long days and late nights. Most of all, the biggest thanks goes to my Mum for her unrelenting support and understanding throughout the duration of the project.

Extended Abstract

There has been a recent revolution in the recognition of and production from low permeability ‘tight’ gas reservoirs. The distribution of faults within a unit of rock, as well as the origin and timing of these faults is of key importance in the evaluation of prospective ‘unconventional’ formations. This project explores the origin, characteristics and distribution of the faults within the Pre-Zechstein succession of the onshore and offshore Carboniferous basins of the eastern United Kingdom.

The datasets utilised in the project include new 3D seismic data from the offshore southern North Sea, vintage 2D seismic data from the onshore Stainmore Trough and western Cleveland Basin, coalmine plan maps from the East Midlands region of the Pennine Basin and surface geological observations of the stratigraphically equivalent succession in North East England. The methods used to characterise the faults include (1) the detailed analysis of 3D seismic attributes, sampled at various Carboniferous intervals offshore; (2) fault throw mapping performed on areas in which good reflection correlations could be mapped, and (3) the sampling of fault frequency and spacings using the 1D scanline method, so that it can be applied to different data types. Through these methods, the fault geometries, spatial distribution, kinematics and possible formation and reactivation mechanisms have been addressed.

A distinct difference in fault pattern is observed at Rotliegend and Intra-Carboniferous levels in the offshore Anglo-Dutch basin. Observation of these horizon-variance surfaces reveals a selective reactivation of faults has occurred within the Pre-Zechstein succession. Concealed fault trends have been highlighted on intra-Carboniferous isoproportional variance slices at selected intervals below the Base Permian Unconformity. Some of the longest faults that were thought to be

one continuous thoroughgoing structure have been found to be highly segmented after detailed observation of seismic attributes and lateral throw variations. The detailed analysis of geometries and kinematics of faults across case study areas have resulted in the characterisation of over 25 distinct fault types.

The relative timing of fault initiation and reactivation across the Anglo-Dutch Basin has been further characterised by throw distribution analysis. Five main t-z profile types have been recognised. Faults have been found to exhibit either a single distinct end-member type or a combination of types. The observation of the gradient of throw-distribution profiles has aided in the relative dating of fault movement histories that are otherwise obscured by the overlying mobile Zechstein overburden. Faults that previously appear to be single phase (Type-V) are found to have a phase of slip previously and later reactivated (Type-IV).

Three distinct structural style types have been recognised based on their lateral and vertical extends, how much of the Pre-Zechstein succession they offset and the nature of their basal tip terminations. These three structural style types are; throughgoing, superficial and layer bound. The throughgoing faults offset the entire Pre-Zechstein succession, the superficial Faults offset the upper Carboniferous (and/or Rotliegend) with a normal basal tip out, and the layer bound detach from the underlying stratigraphy offsetting the Upper Devonian – Lower Carboniferous stratigraphic layer only. Each structural style type is found to exhibit a distinctive t-z profile type (or distinct combination of types) and most importantly reactivation styles. The throughgoing faults are the only fault type that exhibit a compressional movement (Type III profile) sense as well as extensional and strike-slip, and have been reactivated most frequently through time. The superficial faults have fewer reactivation episodes through time with their movements being exclusively normal

(Type IV and Type V). The layer bound faults also have exclusively normal throws and their magnitude of reactivation is negligible (<20ms). Strike-slip movements on throughgoing faults were constrained by measuring the lateral offsets of faults or channels that they intersect, using horizon-variance maps.

The recognition of a family of layer bound faults detaching in the Upper Devonian - Lower Carboniferous interval is novel, as these faults have previously been attributed to regional extension, despite their clear decoupling from underlying stratigraphy and their apparent timing not conforming to the regional direction of extension during the Middle-Late Carboniferous.

Fault intensity (frequency) and spacing is highly variable across the sampled case study areas. The unified sampling method of 1D scanline grid surveys has allowed for the comparison of three different data types over a range of different areas.

The most obvious conclusion was that the lower the fault offset detection threshold was for each individual dataset (higher resolution), the greater the fault intensity and spacing values were. A surprising result was that despite the nature and age of the 2D seismic data, the fault spacing and abundance values were similar to that of some of the offshore areas, indicating that the 2D data may be as capable as 3D data to image faults in the interval of interest. This is thought to be due to the Carboniferous succession being of a relatively high resolution, and the main issues controlling fault detection being due to seismic noise, poor data and 2D seismic line spacing. 2D data having a relatively high resolution in the

The high frequency of faults intersected in the Visean onshore in the Stainmore Trough and Cleveland Basin and offshore on the Elbow Spit High,

suggests that the lower fault density intersected in the Visean interval in case study areas located in the deeper areas of the basin is purely a resolution artefact.

It was found that areas that with throughgoing parallel spaced faults, such as the Silverpit Basin and Stainmore-Trough – Cleveland Basin, exhibited a far less pervasive orthogonal trend (with offsets greater than the seismic resolution), with most smaller faults sharing the same orientation. This is thought to be controlled by 1) the structural inheritance of Caledonian basement structures and 2) stress perturbations caused by these throughgoing structures.

Areas of multiple larger scale faults (higher throws/vertical and lateral extents) generally have fewer seismic scale faults between them. This is interpreted to be due to the decreased necessity for more new meso-scale faults to be formed through time to accommodate stress field rotations, due to the presence of and strain concentrated on the larger faults. Alternatively, faults that do form do not propagate further, enough to be seismic scale faults. The presence of one or two smaller faults around these larger faults is observed and the frequency of these faults decreases with distance from the larger fault. The presence of faults clustered around these larger faults below the seismic resolution that accommodate the displacement is likely but not quantified. The frequency and spacing of faults observed in the large scale footwall blocks i.e. the Alston Block and Elbow Spit High is observed to be significantly less than in the hangingwalls (Stainmore Trough and Step Graben respectively).

Five structural domains have been recognised across the Anglo-Dutch and East Pennine Basin, each displaying distinctly different fault orientations, structural styles and patterns and nature of reactivations. The domains are mostly bounded by major fault zones such as the Dowsing Hewett Fault zone (Between Domain 5

and 2), The Murdoch Fault Zone (2 and 1/4/3), the Elbow Fault (Step Graben – Central Graben complex) that separates Domains 1 and 3. Structural inheritance of basement heterogeneities is a likely control in the patterns of fault formation and reactivation in these domains.

The detailed fault patterns across the East Pennine and Anglo-Dutch Basins therefore exhibit a complex formation and reactivation history that cannot be explained only by rotations of the regional stress field and the alternation of periods of tectonic extension and compression alone. There is a clear relationship between three profoundly different structural style types. A primary faulting mechanism resulting from regional tectonic stresses (throughgoing), and two secondary faulting processes that are in response to the tectonic fault formation and the accompanying deformation (superficial and detachment).

The key controlling factors on the timing, frequency, sense and magnitude of reactivations occurring on Pre-Zechstein faults are fault size and therefore coupling with basement stresses, proximity/relationship to throughgoing faults and the mechanical stratigraphy of the Pre-Zechstein succession. This explains why the throughgoing faults are active more frequently through time in nearly all senses. The secondary meso-scale (superficial and detachment) faults are therefore suspected to have formed in response to (superficial) or as a consequence of (detachment) movement on the larger structures and therefore are a consequence of regional tectonic strain. The superficial faults are reactivated on fewer occasions due to the stress shielding effect by the larger extensional throughgoing faults.

List of Abbreviations

ADB – Anglo-Dutch Basin

BPU – Base Permian Unconformity

BCU- Base Cretaceous Unconformity

CBH – Cleaver Bank High

EPB – East Pennine Basin

EPC – East Pennine Coalfield

ESP – Elbow Spit Platform

ESH – Elbow Spit High

FW - Footwall

HW - Hangingwall

MNSH – Mid North Sea High

MB – Murdoch Block

MS/ms – milliseconds

NWECB – Northwest European Carboniferous Basin

PZF – Pre-Zechstein Fault

PZS – Pre-Zechstein Succession

SB – Silverpit Basin

SNS - Southern North Sea

ST-CB – Stainmore Trough – Cleaver Bank High

Tmax – Point of maximum recorded throw on a fault

Tmin – Point of minimum recorded throw on a fault

TWT- Two-Way Time

Table of Contents

1 Introduction 2

1.1 Thesis Purpose 2

1.2 Thesis Background 3

1.3 Aims of Thesis 10

1.4 Approach 11

1.5 Data & Methods 13

1.5.1 Data 13

1.5.2 Methods 19

1.6 Structure of Thesis 27

1.7 Publications from this Thesis 28

2 Regional Structure of the Northwest European Carboniferous Basin ... 30

2.1 Introduction 30

2.2 Crustal Framework 30

2.3 Tectonostratigraphic Evolution 36

2.3.1 Early Ordovician – Middle Devonian 36

2.3.2 Late Devonian – Late Carboniferous 37

2.3.3 Late Carboniferous – Late Permian 47

2.3.4 Triassic 55

2.3.5 Early Jurassic – Early Cretaceous 57

2.3.6 Late Cretaceous – Cenozoic 58

2.4 Mid North Sea High 62

2.4.1 Elbow Spit Platform and High 62

2.5 Offshore Central Anglo-Dutch Basin 69

2.5.1 Silverpit Basin and Adjacent Areas 70

2.5.2 Cleaver Bank High 73

2.6 East Pennine Basin 78

2.6.1 Stainmore Trough and Cleveland Basin 80
2.6.2 South East Pennine Basin 85

3 The Geometry and Kinematics of Structures within the Pre-Zechstein Succession 91

3.1 Introduction 91
3.1.1 Chapter Rationale 91
3.1.2 Chapter Aims and Research Questions 91
3.2 Elbow Spit Platform (ESP) 93
3.2.1 Background 93
3.2.2 General structural and stratigraphic context 95
3.2.3 Structural Sets 101
3.3 Silverpit Basin and Murdoch Block (SB-MB) 115
3.3.1 Background 115
3.3.2 General structural and stratigraphic context 115
3.3.3 Murdoch Block Structural Sets 120
3.3.4 Silverpit Basin Structural Sets 132
3.4 Southern Cleaver Bank High (S/CBH) 143
3.4.1 Background 143
3.4.2 General structural and stratigraphic context 143
3.4.3 Structural Sets 146
3.5 Stainmore Trough – Cleveland Basin (ST-CB) 158
3.5.1 Background 158
3.5.2 General structural and stratigraphic context 159
3.5.3 Structural Sets 160
3.5.4 Coupling of the Pre- and Post-Zechstein 168
3.6 Dating Periods of Fault Activity 168

3.6.1 Early Carboniferous Extensional Slip – Not Reactivated after the Early Permian 168
3.6.2 Early Carboniferous Contractional Deformation (3) 171
3.6.3 Late Carboniferous-Early Permian Extensional Slip – Not Reactivated post BPU (4) 172
3.6.4 Late Carboniferous Reverse Slip/Contractional Deformation – Not Reactivated post BPU (5) 173
3.6.5 Late Carboniferous Strike-Slip – Not Reactivated post BPU (6) 174
3.6.6 Early-mid Carboniferous extensional slip – reactivation after the deposition of the Rotliegend 174
3.6.7 Mid-Late Carboniferous extensional slip – extensional reactivation after the deposition of the Rotliegend (7) 175
3.6.8 Late Carboniferous Extensional Slip – Reactivated post BPU 175
3.6.9 Extensional Post-BPU Structures (10) 176
3.6.10 Contractional Post-BPU Structures (11) 177
3.6.11 Strike Slip Post-BPU structures (12) 179
3.6.12 Timing further investigated 180
3.7 Classification of Fault Families 180
3.7.1 Scale 180
3.7.2 Structural Style 181
3.7.3 Net Slip 183
3.8 Conclusions 184
4 The Kinematics, structural styles and mechanisms of Pre-Zechstein Faults 186
4.1 Introduction 186
4.1.1 Project Rationale 187
4.1.2 Aims and Research Questions 188
4.2 Data and Methods 189

4.2.1 Throw-Depth Analysis....189
4.2.2 Throw-Distance Analysis....194
4.2.3 Throw Distribution Analysis Limitations....195
4.2.4 Seismic Attributes....196
4.3 Throw-Depth Analysis....199
4.3.1 T-z Profile End-Members....199
4.3.2 Fault examples with mostly Type I Profiles....202
4.3.3 Fault examples with mostly Type II Profiles....206
4.3.4 Fault examples with mostly Type III Profiles....213
4.3.5 Fault examples with mostly Type IV Profiles....217
4.3.6 Fault examples with mostly Type V Profiles....226
4.4 Intersecting Relationships....231
4.4.1 T-x Plots....231
4.4.2 Cross cutting fault relationships....239
4.4.3 Relationships between faults and channels....245
4.5 Discussion of Fault Tip Configurations....248
4.5.1 Basal Tip Geometries....248
4.5.2 Upper Tip Geometries....253
4.6 Discussion of Fault Slip and Reactivation Timings....261
4.6.1 Fault Activity....261
4.6.2 Timing Summary for each T-Z Profile....271
4.6.3 Patterns of Reactivation....272
4.7 Discussion of Fault Forming Mechanisms....273
4.7.1 Layer Bound/Detached Faults....273
4.7.2 Throughgoing and Superficial Faults....277
4.8 Conclusions....279
5 Fault Intensity and Spacing in the Pre-Zechstein Succession....283

5.1 Introduction 283
5.1.1 Project Rationale 283
5.1.2 Aims and Research Questions 286
5.1.3 Fault Intensity 286
5.1.4 Fault Spacing 287
5.2 Chapter Specific Datasets 290
5.2.1 3D Seismic Volumes 290
5.2.2 2D Seismic Lines 291
5.2.3 Coal Mine Fault Map 291
5.3 Methods 294
5.3.1 3D Seismic Dataset Methods 294
5.3.2 2D Seismic Line Methods 303
5.3.3 East Pennine Coalfield 304
5.3.4 Method Limitations 306
5.4 Fault Intensity 307
5.4.1 Elbow Spit Platform 307
5.4.2 Murdoch Block 310
5.4.3 Silverpit Basin 310
5.4.4 Southern Cleaver Bank High 311
5.4.5 Stainmore Trough – Cleveland Basin 311
5.4.6 East Pennine Coalfield 312
5.5 Fault Spacing Results 315
5.5.1 Elbow Spit Platform 315
5.5.2 Murdoch Block 320
5.5.3 Silverpit Basin 324
5.5.4 Southern Cleaver Bank High 328
5.5.5 Stainmore Trough – Cleveland Basin 332
5.5.6 South East Pennine Basin 335

5.6 Synthesis of Key Results 340
5.7 Discussion of Fault Abundance 344
5.7.1 Limitations 344
5.7.2 Impact of data resolution on Fault Intensity results 345
5.7.3 How does the fault intensity vary by stratigraphic interval and why? 347
5.7.4 Can the sub-seismic fault abundance in seismic data areas be estimated using the EPC results? 351
5.8 Discussion of Fault Spacing Characteristics 352
5.8.1 Limitations 352
5.8.2 What causes the paucity of a pervasive orthogonal trend in the Silverpit Basin 352
5.8.3 Which case study area would be most suitable for unconventional hydrocarbon production based on fault abundance and spacing? 353
5.9 Further Work 356
5.10 Conclusions 357
6 Summary and Discussion 361
6.1 Introduction 361
6.2 Phases of major fault activity in the Anglo-Dutch Basin study area 361
6.2.1 Late Devonian – Early Carboniferous (Famennian-Brigantian) Rifting, (~374-329Ma) 363
6.2.2 Early Carboniferous (Brigantian) Inversion (~328-326Ma) 364
6.2.3 Mid Carboniferous (Late Namurian - Early Westphalian) thermal subsidence (~321-310Ma) 368
6.2.4 Late Carboniferous – Early Permian (Stephanian-Sakmarian) Inversion (~306-290Ma) 370
6.2.5 Late Carboniferous – Early Permian Fracturing and Strike-slip (290-285Ma).... 372
6.2.6 Early Permian (Saalian) rifting, (~285-279Ma) 374
6.2.7 Early Triassic (~255-247Ma) 376

6.2.8 Late Triassic- Early Jurassic Rifting (~236-224Ma) 378
6.2.9 Late Jurassic – Early Cretaceous Rifting and Strike-slip (~151-139Ma) 380
6.2.10 Late Cretaceous – Cenozoic, Inversions (~89-20Ma) 383
6.3 Selective Reactivation of Pre-Zechstein Faults 386
6.3.1 Superficial Faults 388
6.3.2 Detachment Faults 389
6.3.3 Throughgoing Faults 389
6.4 Regional Tectonic Relationships between Structural Styles 390
6.4.1 Throughgoing (crustal/tectonic) and detachment (gravity driven) 390
6.4.2 Throughgoing (meso-scale) and superficial 390
6.4.3 Basement Folds and Superficial Faults 392
6.4.4 Fractal relationships between fault styles 392
6.5 Open and closed faults in the Pre-Zechstein Succession 395
6.6 Summary 400
7 Conclusions 403
7.1 Introduction 403
7.2 Overall Conclusions 403
7.2.1 The onshore East Pennine Basin and offshore central Anglo-Dutch Basin together comprise five structural domains that exhibit distinctly different primary fault patterns and styles of reactivation. 403
7.2.2 Process of faulting and fracturing: Meso-scale faults are formed as a consequence of, or in response to, the regional tectonic stress, but not directly from these stresses. 404
7.2.3 The key controlling factors for the timing and styles of fault reactivation are coupling with the basement, the relationship with crustal scale and through-going faults and the mechanical stratigraphy of the Pre-Zechstein succession. 405
7.2.4 Two other profoundly different fault processes are identified that result in the detailed structural complexity of the Anglo Dutch Basin 406

7.3 Chapter Conclusions 406

7.3.1 Detailed 3D seismic interpretation and the use of seismic attributes has 1) enabled the recognition of previously undetected fault trends in the offshore Anglo-Dutch Basin and 2) highlighted the fact that large structures are highly laterally segmented. 407

7.3.2 The use of 3D seismic attributes has enabled the recognition of the selective reactivation styles of faults within the Pre-Zechstein of the ADB.....407

7.3.3 Only a limited comparison can be made between the resulting offshore fault network (3D seismic) to the patterns onshore (2D seismic) 408

7.3.4 The presence of the mobile Zechstein halite unit offshore has profound decoupling and erasing effects on the record of structural evolution of fault systems in the Anglo-Dutch Basin.....408

7.3.5 Throw distribution mapping can be performed on intra-Carboniferous horizons in areas with good reflections and enables a better estimation of fault timings, intersecting relationships and fault tip configurations.....409

7.3.6 Three structural style types have been recognised that have different relationships with the underlying stratigraphy.....409

7.3.7 Detachment faults in the Lower Carboniferous – Upper Devonian on the southern Mid North Sea High. 410

7.3.8 Comparing fault spacing and frequency at seismic and map scale may enable the prediction of sub-seismic fault populations in offshore areas 410

7.3.9 Onshore 2D seismic data appears to be sufficient in resolution to capture the presence of faults, however, their definition of throw is poor. The 2D data however lacks the spatial extent to fully characterise the fault population that exists due to the 2D grid. 411

REFERENCES 412

APPENDIX 428

Figure 1.1 Structural map of the Southern North Sea, Mid North Sea High and Eastern England (Grant et al. 2020) 5

Figure 1.2 Published interpretations of Lower Carboniferous highs and basinal locations and geometries in the UK offshore and Eastern onshore areas. After Besly (2018). 7

Figure 1.3 Comparison of 2D and 3D seismic data. 8

Figure 1.4 Top Carboniferous structure maps illustrating the aliasing in fault interpretation of 2D data compared to 3D data, after Oudmayer & De Jager (1993). 9

Figure 1.5 Schematic of intersecting normal fault blocks illustrating the complexity in the estimating the movement of fault blocks and presence of a particular horizon in the subsurface (Dickinson 1954) 11

Figure 1.6 The locations of the seismic data Case study areas across the Anglo-Dutch Basin, relative to the major tectonic features (Fault positions from PESGB 2008 & Doornenbal and Stevenson 2010) 12

Figure 1.7 a) Area covered by the megamerge 3D seismic dataset (PGS) b) seismic transects of combined 2D seismic lines from various surveys, onshore UK (UKOGL) 14

Figure 1.8 Interval velocities, dominant frequencies, dominant wavelengths, vertical resolution thresholds and effective throw detection limits for the key stratigraphic intervals in the case study areas 17

Figure 1.9 Illustration of how the effective throw detection in the Carboniferous was ascertained to be half of the dominant wavelength. 18

Figure 1.10 The variance slices through the seismic volume at a fixed interval and is therefore does not sample a particular horizon. 20

Figure 1.11 Regionally correlated Top Rotliegend horizon with the variance attribute extracted onto it 22

Figure 1.12 Average interval velocities used in the conversion from time to depth. 25

Figure 1.13 Method of correlating horizons around a fault when a free lateral tip is present 26

Figure 2.1 Palaeotetctonic setting of Northwest Europe during the Early Carboniferous. The position of the NWECB is highlighted by the white dashed line. Modified after Kombrink (2008)... 31

Figure 2.2 Crustal structure and basement terranes beneath the Anglo-Ducth Basin, Pennine Basin and MNSH. 33

Figure 2.3 Major upper crustal terranes a structures underlying eastern England and the Southern North Sea. After Gutertch et al. 2010. 35

Figure 2.4 Paleogeographic maps showing the Late Paleozoic tectonic evolution. Reconstructions by Scotese, C. After Pharaoh et al. 2010. 38

Figure 2.5 The tectonic terranes that formed the palaeocontinent Laurussia. After Pharaoh (2010).....39

Figure 2.6 Bouguer (onshore) and free air (offshore) gravity map. Locations of the case study areas are shown by the black polygons. After Gutertch et al. (2010). 40

Figure 2.7 Simplified model by Coward (1993) illustrating the continental explusion of the North Sea Baltic Block resulting in dextral transpression in the SNS. Modified after Schroot & De Haan (2003). 42

Figure 2.8 Schematic cross section by Fraser & Gawthorpe (1990) illustrating the configuration of the Variscan thrust belt in the south of England and the Variscan Foreland failed rift system in the north of England, separated by the Midlands Microcraton. 44

Figure 2.9 Carboniferous sub-basin/half graben development in the Late Devonian - Early Carboniferous. Cross section through the Widmerpool Gulf and Hathern Shelf. After Fraser & Gawthorpe (1990) 45

Figure 2.10 Palaeofacies maps of northern England (Early Brigantian to Late Westphalian). After Fraser et al. 1990 46

Figure 2.11 Simplified models of the Variscan inversion observed across the Variscan Foreland. After Corfield et al 1996 48

Figure 2.12 Tectonic model by Coward (1993) illustrating the reinsertion of the North Sea Baltic Block and the resulting sinistral transpression in the SNS during the Variscan Orogeny 50

Figure 2.13 Base Permian subcrop map with main structural features within the PZS. After Kombrink et al. (2010).....51

Figure 2.14 Major tectonic phases throughout the Permian and their subsequent unconformities. After Pharaoh et al. (2010).....53

Figure 2.15 Regional upper Rotliegend facies distribution in the SPB (after McKie 2011). 54

Figure 2.16 Late Triassic tectono-stratigraphic map with main structures and depositional environments. After Pharaoh et al. (2010), modified after McKie (2011) 56

Figure 2.17 Late Jurassic (Kimmeridgian, 152 Ma) Tectonic Elements of eastern England and the Southern North Sea. VB = Vlieland Basin. CNB = Central Netherlands Basin. Modified after Pharaoh et al. (2010). 59

Figure 2.18 Late Cretaceous – Cenozoic tectonic phases and inversion events. After Pharaoh et al. (2010). 60

Figure 2.19 Synthesis and summary of the main tectonic phases through time and resulting structures 63

Figure 2.20 Structural overview of the Devonian and Carboniferous Basins across the Mid North Sea High and Northern England. From Monaghan et al. (2017) 65

Figure 2.21 Carboniferous chrono and lithostratigraphy for the Pennine Basin, Anglo-Dutch Basins and Mid North Sea High. After Kombrink et al. (2010). 66

Figure 2.22 Structural framework for the northern Dutch Offshore by Ter Borgh et al., (2018). 67

Figure 2.23 Structural framework of the Anglo-Dutch Basin during the early Carboniferous. After Besly (1998). 72

Figure 2.24 Seismic section imaging an E-W trending fault in the Silverpit Basin.. 74

Figure 2.25 Seismic section imaging a reverse NW-SE fault in the Silverpit Basin.. 75

Figure 2.26 Fault pattern in the Pre-Zechstein interval of the Silverpit Basin by Oudmayer & De Jager (1993) 75

Figure 2.27 a) Intra-Westphalian fault map of the Cleaver Bank High by Schroot & De Haan (2003) indicating fault types. 77

Figure 2.28 Seismic section through E-W orientated 'Type B' faults that exhibit normal throw at intra-Carboniferous level. After Schroot & De Haan (2003) 78

Figure 2.29 Summary of the Variscan inversion structures across the UK and Ireland. After Corfield et al. (1996) 79

Figure 2.30 Summarized stratigraphy of the Variscan plate cycle in the East Midlands. Megasequences and sequence development is indicated. After Fraser & Gawthorpe (1990). 81

Figure 2.31 Principle Carboniferous structural features for the British Isles, onshore and offshore. After Waters et al. (2007). 83

Figure 2.32 The Stainmore Trough and Cleveland Basin after Cossey et al. (2004) and Collier (1991). 84

Figure 2.33 Structure of the East Midlands region of the East Pennine Basin. After Fraser and Gawthorpe, 1990 and Bailey et al. 2005). 87

Figure 3.1 The locations of the case study areas overlain on a Base Permian sub-crop map. Major (Doornenblad & Stevenson, 2010). 92

Figure 3.2 Intra-Carboniferous isoproportional slice, -50ms below the Top Rotliegend horizon on the ESP. 94

Figure 3.3 a) 3D seismic section highlighting the data quality in the ESP area. 96

Figure 3.4 Mapped horizons in the Pre-Zechstein succession of the ESP. 97

Figure 3.5 Structural elements of the northern Dutch sector from Ter Borgh et al. (2018) & Smit et al. (2016)....97

Figure 3.6 SW-NE Geoseismic section across the ESP 98

Figure 3.7 Interpreted seismic section across the ESP....99

Figure 3.8 Seismic stratigraphy units in the Pre-Zechstein on the Elbow Spit Platform. ..100

Figure 3.9 a) Intra-Carboniferous isoproportional slice -50ms below Top Rotliegend horizon/BPU b) Summary map of each fault set visible in the Brigantian and their movement sense. 102

Figure 3.10 The WNW- fault set....104

Figure 3.11 Slope geometry of the Elbow Spit High and Elbow Spit Platform. 105

Figure 3.12 Seismic section across the ESP indicating the different Pre-Zechstein seismic stratigraphy units....106

Figure 3.13 Histogram of fault dips for faults on the ESP. Different fault types are indicated by the colour key. 107

Figure 3.14 Histogram of Tmax values for faults on the ESP. Different fault types are indicated by the colour key....107

Figure 3.15 The A-E_NE- fault set. 109

Figure 3.16 Seismic section oriented W-E normal to the A-E_N-S faults....111

Figure 3.17 The A-E_ENE- fault set. 113

Figure 3.18 Map of the Murdoch Block indicating Base Permian Subcrop chronostratigraphy and the position of known Carboniferous Hydrocarbon fields..... 116

Figure 3.19 Murdoch Block a) Data quality map b) Isochore map of Zechstein thickness. Blue areas indicate thick salt structures and white/yellow where the Zechstein is thinner. 117

Figure 3.20 Silverpit Basin a) Base Permian Subcrop Map b) Data quality map of the Silverpit Basin case study area 118

Figure 3.21 N-S Geoseismic section transecting the Murdoch Block. 119

Figure 3.22 Seismic stratigraphy units in the Pre-Zechstein on the Anglo-Dutch Basin.. 121

Figure 3.23 a) Top Rotliegend horizon map with variance extracted and overlaid, in the Murdoch Block..... 122

Figure 3.24 Composite fault map of all faults in the Pre-Zechstein of the Murdoch Block. Different fault sets are indicated by the colour key. 123

Figure 3.25 ENE-WSW seismic cross section through the PZS of the Murdoch Block, sub-normal to the NNW- faults. Location of section in Figure 3.24 124

Figure 3.26 North-South seismic cross section through the the PZS of the Murdoch Block. 126

Figure 3.27 Histogram of Pre-Zechstein Tmax values on sampled faults in the Murdoch Block, Silverpit Basin and Cleaver Bank High. 127

Figure 3.28 The 44-D_ENE and WNW- faults. Seismic cross section illustrates the variability between ENE- fault vertical profiles..... 130

Figure 3.29 N-S seismic cross sections at three points along the push down structure inbetween WNW-_1 and E-W_4. Observed thickening of upper Carboniferous before post-Rotliegend uplift, indicating the structure formed before the deposition of the Rotliegend.. 131

Figure 3.30 Variance slices across the Silverpit Basin case study area a) intra-Westphalian variance slice -100ms below the BPU. 133

Figure 3.31 Composite structural map showing all faults and folds within the Pre-Zechstein succession in the Silverpit Basin case study area. 134

Figure 3.32 Seismic cross section normal to the NW- trending structures in the Silverpit Basin. Location of section on figure 3.30..... 136

Figure 3.33 Histogram of Pre-Zechstein fault dips sampled from faults in the Murdoch Block and the Silverpit Basin. 137

Figure 3.34 3D map of the Top Rotliegend horizon in the Silverpit Basin Case Study area. 139

Figure 3.35 Seismic cross section normal to a NW-_T fault.....140

Figure 3.36 WNW-ESE interpreted seismic transect through the NE- strike slip faults. Location of seismic cross section on Figure 3.30.....142

Figure 3.37 a) Structural elements and subcrop map of the Cleaver Bank High.....144

Figure 3.38 Variance maps at different intervals on the Cleaver Bank High 145

Figure 3.39 NW-SE oriented seismic cross section across the Cleaver Bank High. 147

Figure 3.40 SW-NE oriented seismic cross section across the Cleaver Bank High. 148

Figure 3.41 Composite structural map for all faults imaged in the PZS in the Cleaver Bank High study area. Different fault sets are colour coded. 150

Figure 3.42 Reverse fault from type NW-_TR.. 153

Figure 3.43 Histogram of Pre-Zechstein fault dips recorded on faults in the Cleaver Bank High. 156

Figure 3.44 3D map of the Top Rotliegend horizon illustrating the overprinting of various fault trends creating the complex intersection geometries observed. 157

Figure 3.45 Major structural elements of the Cleveland Basin, Stainmore Trough and surrounding areas. Key transect locations are indicated.....158

Figure 3.46 Schematic of fault types observed on seismic data from the Stainmore Trough and Cleveland Basin. These fault types are categorised based on their throw profile. 161

Figure 3.47 N-S composite seismic cross section that transects the western Cleveland Basin. Location of transect on Figure 3.45.....162

Figure 3.48 N-S seismic section transecting the Alston Block and Stainmore Trough.....164

Figure 3.49 N-S interpreted seismic sections transecting the northern Stainmore Trough. Types-1a, 1b and 1d are recognised. 165

Figure 3.50 Comparison of the Zechstein succession onshore and offshore and the resulting structural coupling or decoupling. 169

Figure 3.51 Schematic of observed fault throw profiles in 2D observed in the Pre-Zechstein succession across the Anglo Dutch and East Pennine Basin study areas. 170

Figure 3.52 Fault classification diagram for all the fault sets identified across the study areas. 182

Figure 3.53 Structural style categories of faults within the Pre-Zechstein succession based on their vertical extent and basal tip geometries and relationships with underlying stratigraphy .. 183

Figure 4.1 The location of each fault sampled for throw distribution analysis presented in this chapter. 190

Figure 4.2 Summary of the sampling, measurement and plotting methods used in the throw distribution analysis. 192

Figure 4.3 Combined plotted throws for NNW-_1 MP1-4 aligned with the sonic log for nearby well 44-19, demonstrating that changes in throw in ms are unrelated to the velocity, which stays almost constant with depth in this interval 193

Figure 4.4 Schematic showing the corrections that were made to throw measurements for stratal folding adjacent to the fault plane From Mansfield & Cartwright (1996)..... 197

Figure 4.5 Method of correlating a horizon across a fault cut off.. 198

Figure 4.6 i) t-z profile end-member types observed on the faults sampled across the ADB ii) Schematic idealised cross sections expected for each profile. 200

Figure 4.7 t-z plots from four selected measurement points along strike on Fault ENE-_1, located on the Murdoch Block. 203

Figure 4.8 t-z plots for measurements performed at four positions along fault WNW-_4. 205

Figure 4.9 t-z plots displaying measurements performed at four positions along fault WNW-_1 on the Elbow Spit Platform. 209

Figure 4.10 t-z plots for measurements performed at six positions along strike of fault WNW-_2 on the Elbow Spit Platform. 211

Figure 4.11 a) idealised C-type fault displacement-length profile b) idealised M-type fault displacement-length profile c) idealised strain distribution on a C-type fault d) idealised strain distribution on a M-type fault. From Muraoka & Kamata 1983. 212

Figure 4.12 t-z plots for measurements performed at four positions along strike of fault E-W_1 on the Murdoch Block. The plots exhibit mostly type-III plots..... 214

Figure 4.13 t-z plots for measurements performed at four positions along strike of fault E-W_2 on the Murdoch Block. The plots exhibit type-I and type-III plots.....215

Figure 4.14 t-z plots for measurements performed at three positions along strike of fault NE-_2 on the Elbow Spit Platform. The plots exhibit type-I and type-III plots. 219

Figure 4.15 t-z plots for measurements performed at intersections with 7 parallel faults from set NW-_P in the Silverpit Basin. 222

Figure 4.16 Sampling transect of faults across the NW-_P faults in the Silverpit Basin ...223

Figure 4.17 Syn-sedimentary fault t-z profile, example from Baudon & Cartwright 2008. 225

Figure 4.18 t-z plots for three measurements performed at positions along strike of fault NE-_1 located on the Elbow Spit Platform. 227

Figure 4.19 t-z plots at four measurement points along strike of fault NWW-_1 located on the Murdoch Block. The plots exhibit mostly type-V profiles. 230

Figure 4.20 Throw distribution on fault NNW-_1 as recorded by three key horizons.....232

Figure 4.21 Map of four representative faults from each of the major fault sets in the Murdoch Block in which t-x analysis has been performed. 234

Figure 4.22 t-x plots showing the throw distribution on three major faults b) fault ENE-_1 c) ENE-_1 and d) WNW-_1.....235

Figure 4.23 t-x plots for faults NNW-_1 and WNW-_1 overlain from the point of X-type intersection.....240

Figure 4.24 t-x plots overlain at point of intersection between faults a) ENE- and E-W b) NNW- and ENE- and c) NNW- and E-W. 242

Figure 4.25 t-x distribution for the intra-MCM horizon on each of the four representative faults plotted onto the composite structural map 243

Figure 4.26 combined t-x for segments ENE_A and E-W_B on horizon intra-MCM illustrating the reactivation of these segments independently. 244

Figure 4.27 Top Rotliegend horizon map with variance overlain.....247

Figure 4.28 Analogous detachment faults from other areas.....249

Figure 4.29 Possible extrapolation of the t-z plots for fault E-W_1 below the last coherent horizon measurement in the instance of mechanical restriction and no restriction 252

Figure 4.30 Extrapolation of t-z plots into three characteristic throw-depth distributions at two intersection points along the strike of fault WNW-_4 255

Figure 4.31 Compilation of maximum displacement and length datasets for different published fault datasets. 258

Figure 4.32 Models illustrating how the decoupling effects by a mobile evaporite layer vary due to different controlling factors (Withjack & Calloway 2000). 260

Figure 4.33 Reconstruction of the main stages of evolution for the A-E_1 fault set and BPU erosional surfaces U1 and U2. 263

Figure 4.34 t-z plot for fault NE-_2. This profile can be interpreted as a Type-IV or Type-V profile 268

Figure 4.35 3D schematic of cutoff stretch accommodation faults that form perpendicular to a major normal fault (Stewart 2001). 269

Figure 4.36 Schematic illustrating the simple systems illustrating the generally accepted concepts of a) gravity gliding and b) spreading (after Ramberg (1980) and c) Model of gravity deformation on multiple blocks in which the individual blocks are gliding but the large scale system is spreading after Schultz-Ela (2001). 275

Figure 4.37 Schematic NE-SW cross section transecting the ESP illustrating the proposed gravity gliding-spreading hybrid mechanism that is forming the A-E_WNW- faults. 278

Figure 5.1 Illustration showing the possibility of faults that have offsets below seismic resolution. 285

Figure 5.2 Schematic representation of a fractal/self similar fault pattern (after Yielding et al., 1992) 285

Figure 5.3 Map of the study area indicating the case study locations and their scanline survey geometry. 288

Figure 5.4 Two end-member fault population geometries with different spacing characteristics 289

Figure 5.5 Scanline transect grid across the East Pennine Coalfield map (Bailey et al 2005).. 293

Figure 5.6 Scanline survey across the Elbow Spit Platform. Example transects in later figures are indicated by bolder coloured lines. 295

Figure 5.7 Scanline survey across the Murdoch Block. Positions of example transects in later figures are indicated by bolder coloured lines. 296

Figure 5.8 Scanline survey across the Silverpit Basin. Positions of example transects in later figures are indicated by bolder coloured lines. 298

Figure 5.9 Scanline survey across the Cleaver Bank High. Example transects in later figures are indicated by bolder coloured lines. 299

Figure 5.10 Examples of throw logs formed from 1D sampling scanlines from six other fault datasets 300

Figure 5.11 Criteria for what was recorded as a fault with an example on both very good and average seismic imaging. 302

Figure 5.12 Example scanline that samples fault throw at intersection, orientation, apparent dip and slip sense 302

Figure 5.13 Location of the Stainmore Trough-Cleveland Basin area with 2D scanline survey superimposed. 305

Figure 5.14 The plotted fault intensity (FI) values are calculated from the mean of all scanline FI values. 308

Figure 5.15 Spacing population plots for joint datasets a) and b) Cumulative frequency population curves for spacing c) – h) frequency distributions of joint spacing for six joint datasets (after Gillespie et al., 1993). 309

Figure 5.16 Frequency distributions for the distances between seismically resolvable faults in the Pre-Zechstein succession. 314

Figure 5.17 Fault Intensity and Average Spacing for each scanline set. Each scanline set is representative of a dominant orthogonal fault trend, these trends are indicated in the legend. 316

Figure 5.18 Representative scanline transects from each orientation set, sampling; fault spacing, orientation, throw sense, throw value and dip direction in the Lower Carboniferous of the Elbow Spit Platform. 318

Figure 5.19 Same set fault spacings in the Elbow Spit Platform study area.. 319

Figure 5.20 Representative scanline transects from each orientation set in the Murdoch Block. 322

Figure 5.21 Same set fault spacings in the Murdoch Block study area. 323

Figure 5.22 Same set fault spacings in the Silverpit Basin study area. 326

Figure 5.23 Representative scanline transects from each orientation set in the Silverpit Basin. 327

Figure 5.24 Same set fault spacings in the Cleaver Bank High study area. 329

Figure 5.25 Representative scanline transects from each orientation set in the Southern Cleaver Bank High. 331

Figure 5.26 Spacings between faults on each scanline transect set the Cleveland Basin. 333

Figure 5.27 Representative scanline transects from each orientation set in the Cleveland Basin. 334

Figure 5.28 Frequency distributions for fault spacings for various fault types in the East Pennine Coalfield 338

Figure 5.29 Four example scalines from the East Pennine Coalfield. 339

Figure 5.30 Scanline examples from the Alston Block and Stainmore Trough illustrating that there are significantly less faults observed in the footwall highs than in the hangingwalls 343

Figure 5.31 The FI and ETDL for each of the case study areas. 346

Figure 5.32 Comparison of two scanlines that sampled two different stratigraphic intervals in the Cleaver Bank high, compared with a scanline of the Westphalian interval in the Stainmore Trough-Cleveland Basin. 349

Figure 5.33 Representative scanlines from all case study areas. All scanlines can be found in Chapter 5 supplementary material. 355

Figure 6.1 The five structural domains across the Pennine and Anglo-Dutch Basins. orientation 362

Figure 6.2 Structural map indicating the faults present during the Late-Devonian to Early Carboniferous time period in the Pre-Zechstein succession in the central ADB. 365

Figure 6.3 Structural map indicating the faults and folds present and active in the Pre-Zechstein succession during the Brigantian, in the central ADB. 367

Figure 6.4 Structural map indicating the faults and folds present and active in the Pre-Zechstein succession during the late Namurian-early Westphalian in the central ADB. 369

Figure 6.5 Structural map indicating the faults and folds present and active during the Late Carboniferous (Westphalian D-Stephanian) time period in the Pre-Zechstein succession in the central ADB. 371

Figure 6.6 Structural map indicating the faults and folds present and active during the Late Carboniferous – Early Permian (Sakmarian) time period in the Pre-Zechstein succession in the central ADB. 373

Figure 6.7 Structural map indicating the faults and folds present and active during the Early Permian (Artinskian) time period in the Pre-Zechstein succession in the central ADB. 375

Figure 6.8 Structural map indicating the faults and folds present and active during the Early Triassic time period in the Pre-Zechstein succession in the central ADB. 377

Figure 6.9 Structural map indicating the faults and folds present and active during the Late Triassic-Early Jurassic time period in the Pre-Zechstein succession in the central ADB. 379

Figure 6.10 Structural map indicating the faults and folds present and active during the Late Jurassic to Early Cretaceous time period in the Pre-Zechstein succession in the central ADB. ... 382

Figure 6.11 Structural map indicating the faults and folds present and active during the Late Cretaceous to Late Cenozoic (Neogene) time period in the Pre-Zechstein succession in the central ADB. 385

Figure 6.12 Fault activity through time for example throughgoing, superficial and detached faults. 387

Figure 6.13 Schematic showing the structural relationships between the various structural style types 391

Figure 6.14 Detached fold in the Visean on the Northumberland Coast.. 394

Figure 6.15 Cliff exposure of an E-W striking, southward dipping normal fault downthrowing Namurian stratigraphy against Visean, at Howick on the Northumberland coast. 399

Chapter 1

INTRODUCTION

1 Introduction

1.1 Thesis Purpose

There has been a recent revolution in the recognition of and production from low permeability hydrocarbon reservoirs. The secondary permeability that is necessary for the extraction of hydrocarbons in low permeability formations is either present due to the existence of a natural fault and fracture network or created by the process of hydraulically fracturing the formation. An understanding of the natural fault and fracture distribution within a prospective formation (fault abundance, geometry and connectivity of the fault population) along with their kinematics is therefore of key importance. This is particularly important for example in the assessment of a formation for hydraulic fracturing, enhanced oil recovery and CO^2 sequestration operations, as faults can either act as a conduit or barrier to fluid flow, depending on the fault zone composition and displacement profiles (Holubnyak et al. 2018, Abdullah et al. 2020).

This thesis explores the origin, characteristics and distribution of faults within the Pre-Zechstein succession of a large area of the onshore and offshore Carboniferous basins of the eastern United Kingdom and identifies the processes that control fault development within the Carboniferous stratigraphic interval in particular. In doing so it attempts to aid the problem of a predicting fault characteristics such as orientation and density in different structural domains and to account for the different structural styles that may be present.

1.2 Thesis Background

The geology of the Carboniferous succession of northern England and the southern North Sea and the component hydrocarbon system have been extensively researched (Leeder, 1988, Fraser and Gawthorpe, 1990, Leeder and Hardman, 1990, Besly, 2019). Renewed interest has been sparked by the possibility of potentially significant shale gas reserves onshore in the UK Carboniferous Basins and tight gas reservoirs offshore in the Southern North Sea basins (Andrews, 2013, Langford et al., 2014a). The hope being to emulate the significant tight gas basins of the USA such as the Permian Basin and Barnett Shale, (Jarvie et al., 2005, Bowker, 2007).

A re-examination of the fault network within Carboniferous shales and low permeability Carboniferous sandstones is needed in order to evaluate the hydrocarbon potential of the low permeability formations. Knowledge of the nature, distribution and origins of the various types of faults present in these formations may be able to aid the process of highlighting areas of secondary permeability and predicting stress regimes, thereby improving the chances of an economic gas discovery.

Considerable shale gas reserves are suspected to be present within the Visean and Namurian aged Carboniferous mudstone successions in the Bowland and Cleveland Basins of northern England (Andrews 2013, Slowakiewicz et al., 2015, Hughes et al., 2016) and the Midland Valley Basin in southern Scotland (Monaghan, 2014). Various studies have aimed to quantify the organic carbon content of these formations but there has been little study into the distribution and nature of either the fault or fracture networks.

The relatively underexplored Mid North Sea High (MNSH) area has received a renewed interest sparked by the discovery of the 20 billion m^3 Lower Carboniferous Breagh field in 2008, located on its southern margin (McPhee et al., 2008). The hydrocarbon potential of the Mid North Sea High area was previously considered to be low due to the potential absence of Rotliegend reservoir rocks and the absence of a mature Upper Carboniferous source rock due to erosion at the Base Permian Unconformity (Geluk 2007, Ter Borgh et al. 2018). The Breagh field discovery has changed these opinions and renewed exploration in these areas.

The current exploration and production challenges and uncertainties regarding the Carboniferous of the southern North Sea were summarised by Besly (2019). A key uncertainty reported by Besly (2019) was the geometry of the sub-basins and their bounding structures. It has been found that sub-basin bounding structures vary from a single main fault to a complex set of flexural structures and ramps. Detailing which style is present in each instance is key to understanding sediment routing and fluid migration pathways. The lack of agreement that remains regarding sub-basin architecture and the location of the bounding faults is illustrated in Figure 1.2 with the map by Corfield et al. (1996) as the most widely cited.

A key difficulty in the characterisation of the Pre-Zechstein is due to imaging problems created by the thick Zechstein salt overburden which has undergone extensive mobilization (Stewart and Coward, 1995). This complicates seismic ray paths and distorts the base Permian subcrop imaging, particularly directly beneath the Base Permian Unconformity (BPU) (Cooper et al., 2005)

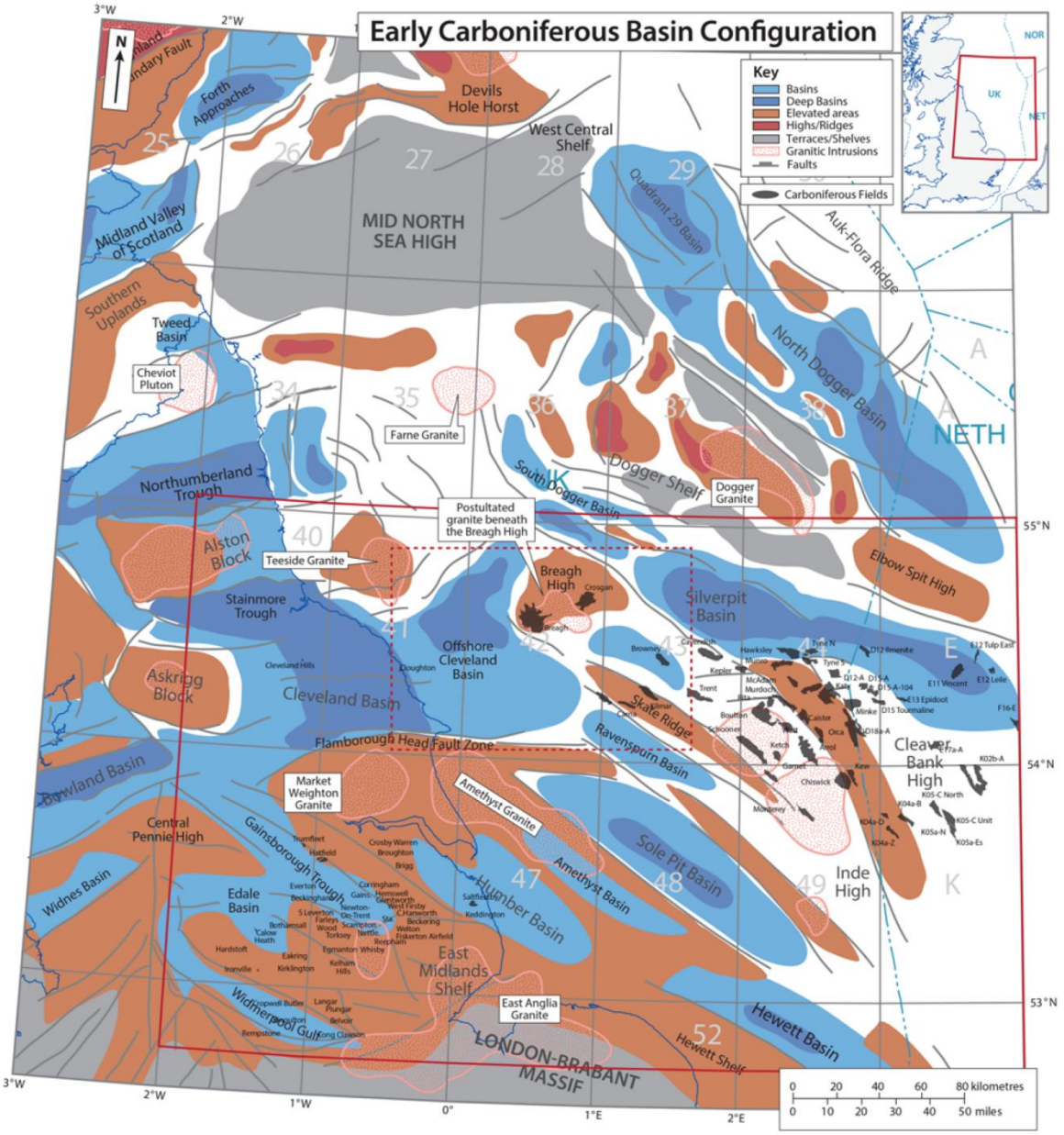


Figure 1.1 Structural map of the Southern North Sea, Mid North Sea High and Eastern England (Grant et al. 2020). The map shows the Early Carboniferous basin configuration along with the locations of major basin bounding faults, granites including the Breagh granite and Carboniferous Breagh oil field. The map was originally compiled from a number of sources including Arsenikos et al. (2018), Corfield et al. (1996), Smit et al. (2018), Rollin (1982), Donato et al. (1983), Leeder and Hardman (1990) and George and Berry (1997)

However, three dimensional seismic data can image the complex and abundant network of minor faulting that was only suggested from 2D seismic interpretation of the Carboniferous (Oudmayer & de Jager 1993, see Figure 1.4). Studies analysing the sub-seismic resolution faulting of the Yorkshire coal fields, onshore UK (Bailey et al. 2002) concluded that sub-seismic faulting likely results in complete connectivity of reservoir sandstone bodies in the Coal Measures succession. The detailed fault movement histories are of key importance as undrilled fault blocks may not contain the reservoir formation due to both truncation at the BPU (Figure 1.5). The careful correlation of horizons across faults and knowing their kinematics is therefore key to this assessment.

The characterisation of the fault population within the Pre-Zechstein succession is of paramount importance in the assessment of the presence, connectivity of and fluid flow through reservoirs. Detailing the structural configuration of pre-Zechstein succession (PZS) across the Anglo-Dutch and Pennine basins has been made more feasible by newly acquired and reprocessed 3D seismic data. Through the examination of improved quality 3D seismic data, the PZS has been found to exhibit great structural complexity, with a variety of structural styles co-existing within the same stratigraphic interval, despite being apparently subjected to the same regional tectonic stresses.

The complex intra-basinal fault patterns which are the result of over 300Ma of structural overprinting make it difficult to predict sub-seismic fault and fracture networks (Figure 1.5). Observations in this thesis challenge the views that the meso-scale structures visible within the PZS are formed and reactivated purely due to tectonic processes.

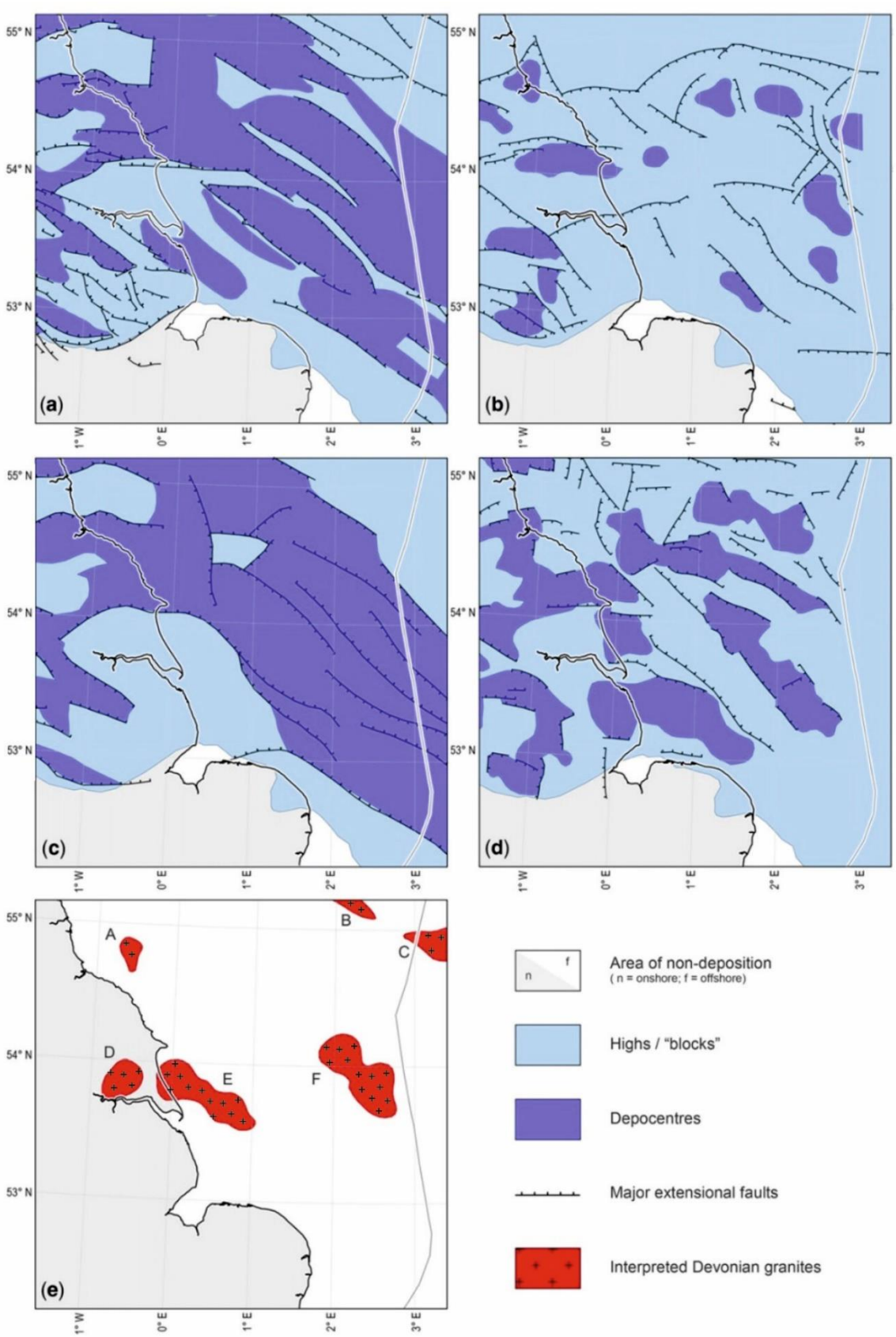


Figure 1.2 Published interpretations of Lower Carboniferous highs and basinal locations and geometries in the UK offshore and Eastern onshore areas: (a) Fraser & Gawthorpe (2003), Corfield et al. (1996), Kombrink 2008, (b) Collinson et al. (1993) (c) Cameron & Ziegler (1997), (d) Maynard & Dunay (1999), (e) positions of inferred granites in underlying basement highs (Donato et al 1983; Donato & Megson 1990: Donato 1993; EBN 2015). After Besly (2018).

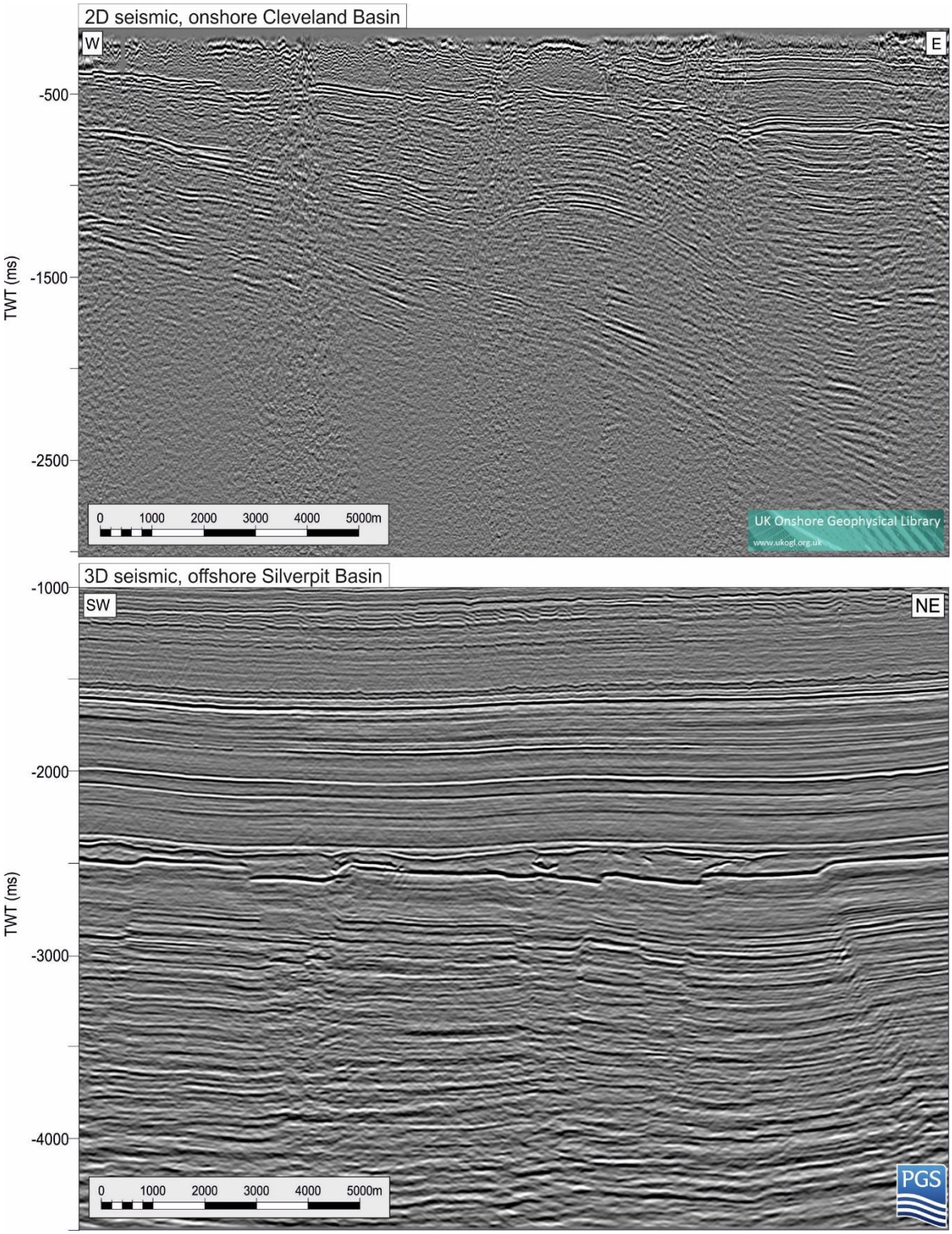


Figure 1.3 Comparison of 2D and 3D seismic data a) a relatively good quality 2D seismic line from the western area of the Cleveland Basin imaging the mid-lower Carboniferous succession. Faults and other structures are difficult to characterise and a sense of throw values are unclear. Reflections can be mapped but are discontinuous in areas. Unclear what is and is not an artefact. b) a relatively good 3D seismic line from the eastern Silverpit Basin. Faults can be clearly identified in the Carboniferous and younger. Reflections are continuous enough to be mapped locally with confidence and throw can be measured.

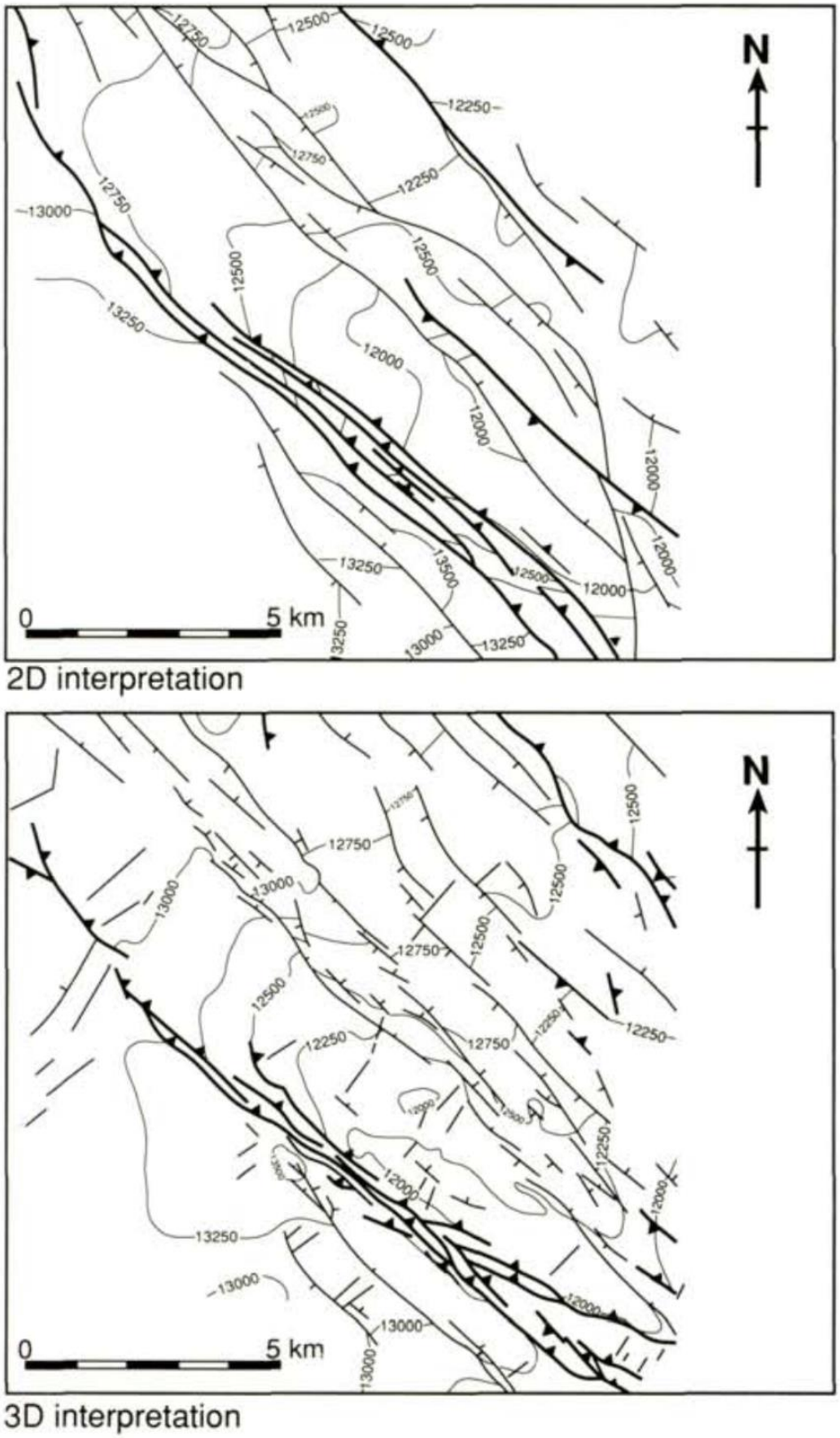


Figure 1.4 Top Carboniferous structure maps illustrating the aliasing in fault interpretation of 2D data compared to 3D data, after Oudmayer & De Jager (1993).

This thesis develops this thinking by unravelling the detailed fault histories and fault and fracture distributions, and mechanisms for formation and reactivation, and in doing so, explains some of the contradictions evident in the literature regarding structural configurations (see Chapter 2), offering a way forward to identifying prospective areas.

1.3 Aims of Thesis

The objective of this thesis is to examine the complex structural styles, movement histories and distributions of faults within the Pre-Zechstein succession across the Anglo-Dutch and Pennine Basins. The availability of 2D and 3D seismic data has allowed the mapping and definition of a series of structural domains, outlining their distinctive patterns and identifying the mechanics and process or processes that caused them.

The thesis aims to answer the following questions:

1. What are the detailed fault, fracture and geometries observed within the Pre-Zechstein at meso-scale?
2. What are the kinematic histories of the identified fault sets and their structural relationships?
3. What is the density and spacing of faults within the Pre-Zechstein fault population and what factors control any variation in these parameters?
4. What are the mechanisms for fault formation and subsequent reactivations within the Pre-Zechstein Succession and what factors lead to the observed complexity of the structural relationships?

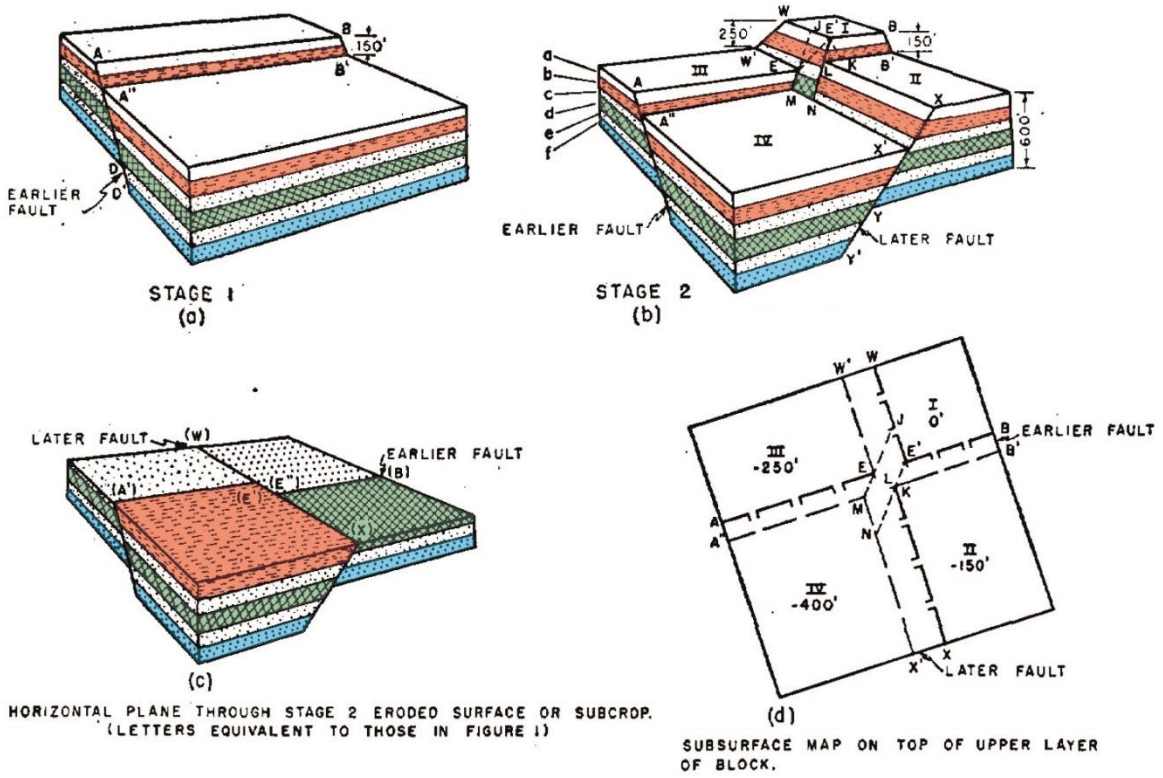


Figure 1.5 Schematic of intersecting normal fault blocks illustrating the complexity in the estimating the movement of fault blocks and presence of a particular horizon in the subsurface (Dickinson 1954)

1.4 Approach

Due to the lack of good quality basin wide imaging of the Carboniferous section, this project used a variety of case study areas across the Anglo-Dutch and Pennine basins to address the questions of section 1.2. The case study areas were chosen on the basis of good Pre-Zechstein imagining within the Carboniferous interval (Figure 1.6). Four areas of 3D seismic data and one area of 2D seismic data were used (Figure 1.4) together with an area drawn from pre-existing mapping. This approach allowed the extrapolation of detailed findings to a regional scale and enabled comparisons between areas.

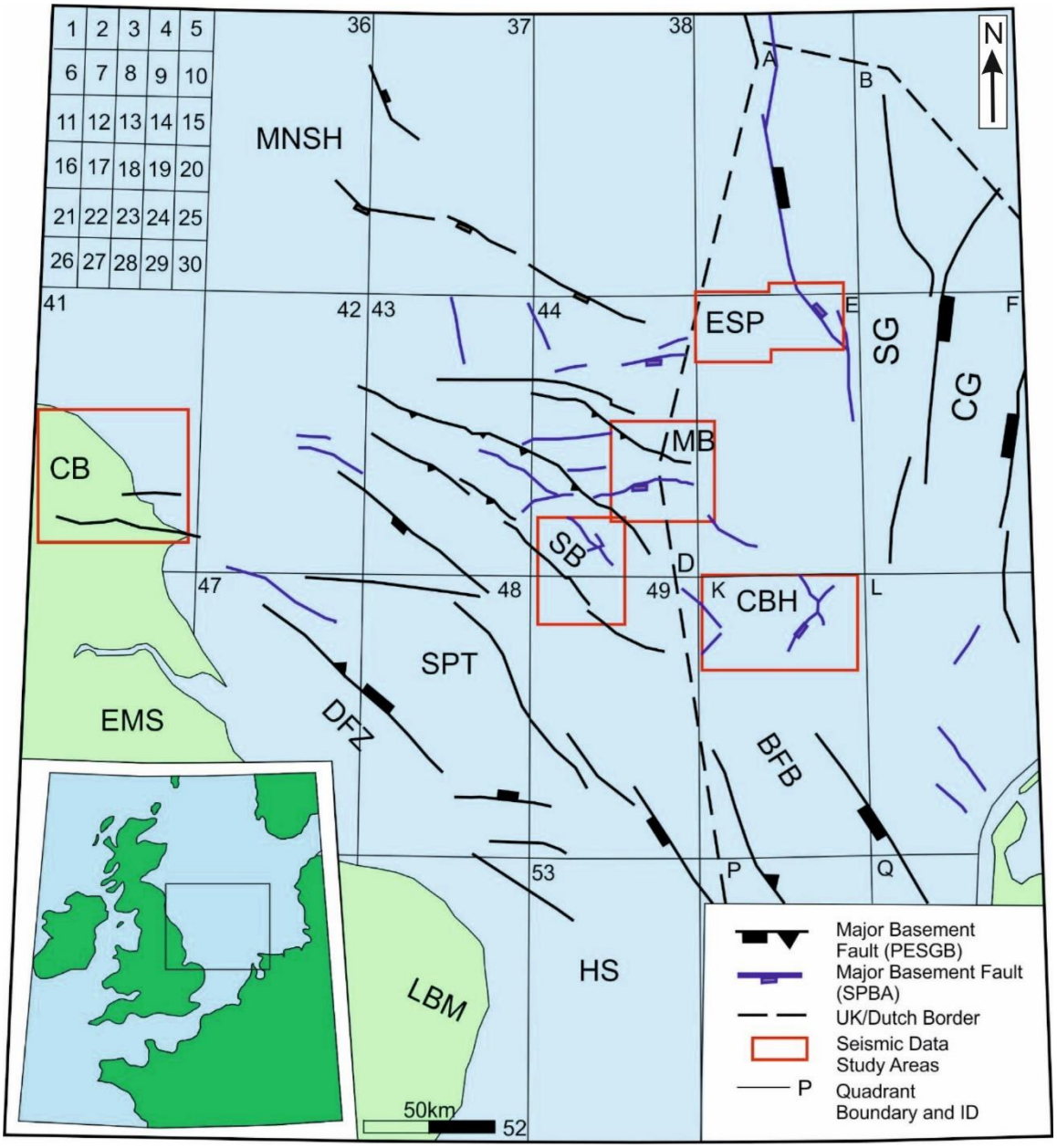


Figure 1.6 The locations of the seismic data Case study areas across the Anglo-Dutch Basin, relative to the major tectonic features (Fault positions from PESGB 2008 & Doornenbal and Stevenson 2010)

1.5 Data & Methods

1.5.1 Data

1.5.1.1 3D Seismic

The primary dataset for the analysis of the Pre-Zechstein is the PGS Southern North Sea Megamerge. This megamerge is an amalgamated and reprocessed mosaic of individual 3D surveys acquired since 1998, and covers 65,632km^2 of the UK and Netherlands sectors of the southern North Sea (Figure 1.7a). Data for the individual seismic surveys were acquired by air gun and streamer and with the most recent phase of reprocessing undertaken in 2015. The dataset is a post stack, time migrated 3D volume. Inlines have a bearing of 130 (NW) and crosslines 045 (NE), with a spacing of 25m by 25m. A depth migrated seismic volume for certain areas in the UK sector of the Southern North Sea was used for certain analysis such as detailed strike parallel throw mapping, in which it is useful to know depths in metres rather than two way time (TWT). Due to the lateral discontinuity of this data type into the Dutch sector, and the presence of areas in which the time to depth conversion has compromised imaging of complicated structure, the time migrated volume was used for the most of the structural and stratigraphic interpretation, and depth converted where necessary.

The 3D seismic has a phase shift 180 degrees and a positive polarity indicated by the hard reflection reflecting the Top Cretaceous Chalk. The volumes in the Southern North Sea have variable dominant frequencies at the Carboniferous interval due to the merging of individual surveys. The dominant frequencies range from approximately 20 hertz to 60 hertz.

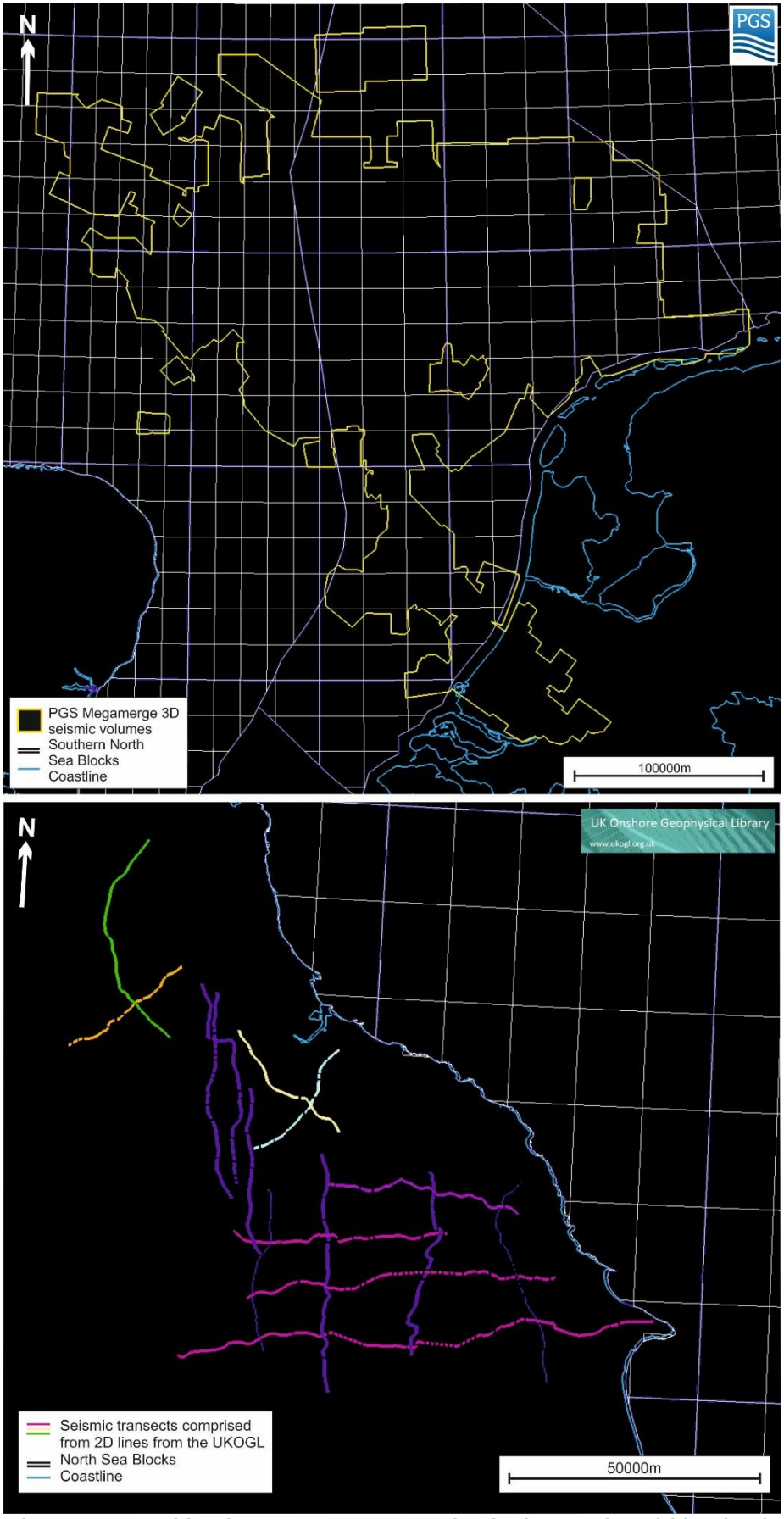


Figure 1.7 a) Area covered by the megamerge 3D seismic dataset (PGS) b) seismic transects of combined 2D seismic lines from various surveys, onshore UK (UKOGL)

Assuming an estimated average velocity of 4000m/s for an interval 100ms below the BPU (Westphalian-Namurian), the vertical resolution ranges from 66-200m. Resolution decreases at Namurian intervals (around 500ms below BPU) where the velocity is closer to 4500m/s to 75-300m.

The seismic image quality across the PGS megamerge is variable due to a variety of factors: Firstly, the combination of multiple surveys with different acquisition dates and processing parameters accounts for lateral image quality variability for the entire imaged section. Secondly, the presence of a variably thick Zechstein salt overburden accounts for image quality variations within the underlying PZS. Areas of thick salt accumulations, such as salt walls that have accumulated thicknesses of over 3000m from multiple phases of remobilisation, cause ray path distortion and transmission losses of the acoustic wave (Hollywood, 1993), distorting the pre-Zechstein subcrop in these areas. Thirdly, due to the decrease in resolution with depth, areas in which the Carboniferous succession is at a shallower are generally better imaged than the deeper areas of the basin. Lastly, many true Carboniferous reflectors close to the BPU are obscured by multiples parallel to the lower Permian reflections. Due to these reasons, it is no coincidence that each of the case study areas have relatively low thicknesses of Zechstein salt in the overburden, are relatively shallower depths and are located in areas less affected by halokinesis.

1.5.1.2 2D Seismic

A selection of public domain 2D seismic lines from the UK Onshore Geophysical Library were received for academic study in a post-stack time migrated SEG-Y format. Formation top information for certain areas of the Dutch sector were

The lines are located in North East Yorkshire across an irregular area of approximately 4,800km^2 (Figure 1.7b). The 2D seismic has a variety of acquisition and processing parameters due to the selected lines being from a variety of different surveys acquired from ~1960 onwards. The 2D seismic lines were shot by vibroseis and dynamite by a variety of contractors. Due to the nature of onshore seismic acquisition (Vibroseis vehicles following UK B Roads), the line spacing is irregular and the individual profiles are often highly curvilinear.

Dominant frequencies for the PZS across the onshore study area range from 25-50 Hz (Figure 1.8). Assuming an interval velocity of 4354m/s and 5080m/s (constrained Cloughton-1) for the Namurian and Dinantian (Visean) successions respectively, the dominant wavelength at these Carboniferous intervals are ~90m and ~200m. Since the effective throw detection limit was ascertained to half a wavelength in the Carboniferous (λ/2) (Figure 1.9), the resolution for each interval ranges from ~40-45m and ~100m. This difference in acquisition and processing parameters results in the quality of the seismic lines not only being variable within the same line or survey, but highly variable when different lines are joined to create composite transects.

1.5.1.3 Wells

The Megamerge survey is stratigraphically constrained by hundreds of exploration wells with accompanying wireline log and stratigraphic formation top information tied to the data. Data sources for these wells include BP, the British Geological Survey, UKOGL, IHS, and the Geological Survey of the Netherlands. These data enabled a direct stratigraphic calibration to be achieved in most interpreted areas.

There remains to be uncertainty regarding the deeper stratigraphy however, as most of these wells only have shallow penetrations, terminating in the Upper Carboniferous stratigraphy or younger. The deep stratigraphy in the basin is therefore still largely unconstrained; with correlations from wells penetrating deeper stratigraphy from the MNSH margin to the north challenging to make accurately due to facies changes.

Sonic logs were used to calculate interval velocities for the pre-Zechstein succession for use in conversions from two way travel time to depth. The well information for the Dutch sector was restricted to stratigraphic well tops. Key well reports for areas in the thesis are contained in Appendix A.

Area	IV Well Log	Strat/Seismic Interval	Interval Velocity (m/s)	Dominant Frequency (htz)	Dominant Wavelength (m)	Vertical resolution threshold (m)	Effective throw detection limit (m)
ESP	E2-2	Brigantian - Asbian	4119	40	103	26	51
ESP	E2-3	Asbian - Arundian	4400	20	220	55	110
ESP	A17-1	L. Carboniferous	5080	50	102	25	51
MB	44/19-3	Rotliegend	4689	30	156	39	78
MB	44/19-3	Westphalian B - U. Namurian	4354	30	145	36	73
MB	44/24-4	Westphalian B - U. Namurian	4763	30	159	40	79
SPB	44/27-1	Rotliegend	4916	25	197	49	98
SPB	44/27	Westphalian D - Westphalian B	4733	30	158	39	79
SPB	44/27	Westphalian B - Upper Namurian	4064	40	102	25	51
CBH	K03-3	Rotliegend	4549	50	91	23	45
CBH	K03-3	Maurits Fm	5080	60	85	21	42
CBH	K03-3	Klaverbank Fm	5542	50	111	28	55
Cleveland E	Cloughton	Namurian-Dinantian	4354	50	87	22	44
Cleveland E	Cloughton	Dinantian	5080	25	203	51	102
Cleveland W	Cloughton	Namurian	4354	55	79	20	40
Stainmore	Cloughton	Namurian-Dinantian	4354	50	87	22	44
MWH	Great Hatfield	Westphalian B-A	4064	50	81	20	41
Gainsborough	EPC map	Westphalian	-	-	-	-	1

Figure 1.8 Interval velocities, dominant frequencies, dominant wavelengths, vertical resolution thresholds and effective throw detection limits for the key stratigraphic intervals in the case study areas

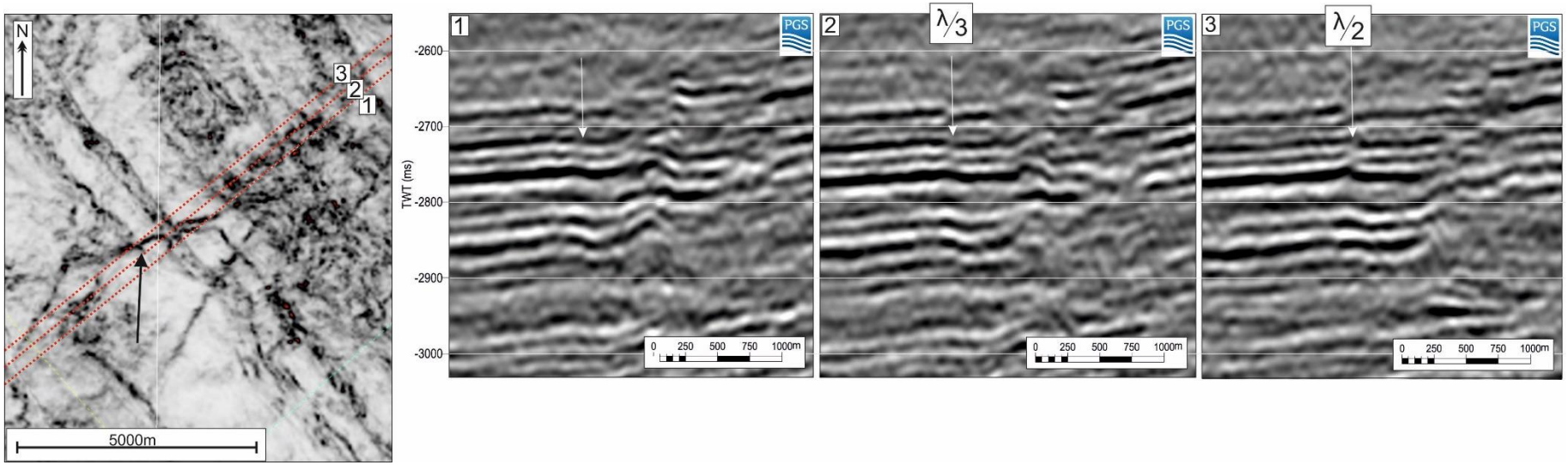


Figure 1.9 Illustration of how the effective throw detection in the Carboniferous was ascertained to be half of the dominant wavelength.

1.5.2 Methods

1.5.2.1 Structural interpretation of seismic data

The 3D seismic dataset was interpreted on a Microsoft Windows workstation running Petrel 2016. The regional structural trends were identified in map view using the computation of the variance attribute. The variance attribute (inverse of the coherency attribute) visually displays the calculated dissimilarity between trace amplitudes (Brown, 2011). The variance cube was computed from the original 3D seismic volume in which time slices (Z slices) could be observed throughout the 3D volume at chosen intervals (Figure 1.10). The variance attribute was of most use in this study as it quickly and effectively reveals the planform structural patterns within the PZS that cannot be easily visualised by horizon mapping of highly discontinuous stratal reflections. In areas where there is a significant dip of the stratigraphic units, isoproportional slices were computed 100 milliseconds below the BPU so that a chrono-stratigraphically consistent structural framework can be viewed (Figure 1.10). Slicing the volume in this way accounts for stratigraphic dip in comparison to horizontal slicing. This was of key importance due to the folding of the Pre-Zechstein succession, as evident in Figure 1.9.

The most laterally continuous, coherent horizons in the PZS were mapped extensively across the Anglo-Dutch Basin to reveal regional structural trends. An important regionally extensive horizon is the Top Rotliegend/TRot (Figure 1.11). The Top Rotliegend is a high amplitude, negative reflection produced by a soft reflection interface created by the Zechstein halite and dolomite interval juxtaposed above a higher acoustic impedance sandstone interval (Silverpit Formation).

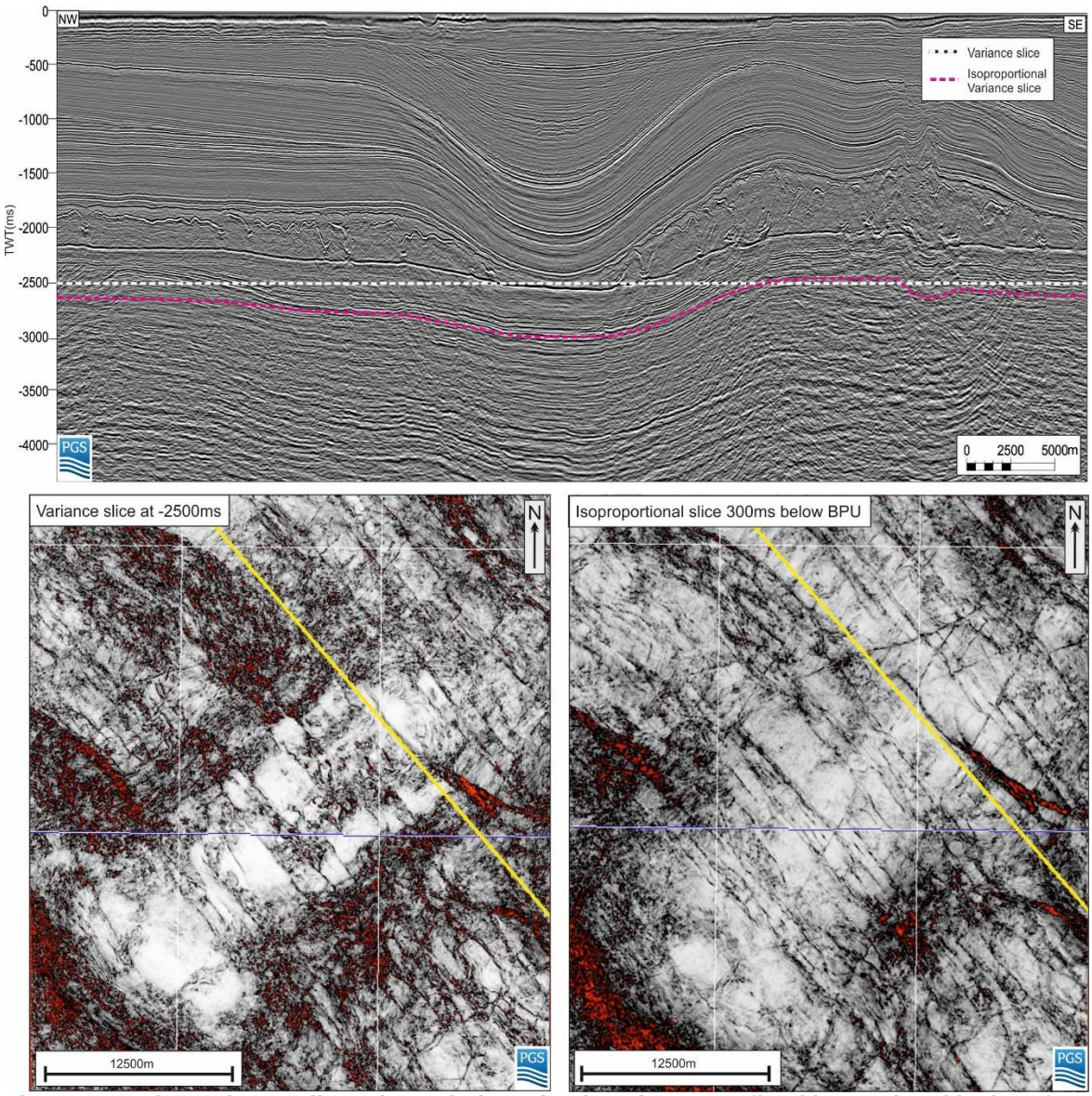


Figure 1.10 The variance slices through the seismic volume at a fixed interval and is therefore does not sample a particular horizon. The variance slice above slices through Carboniferous, Westphalian and Zechstein units which is not stratigraphically representative. Isoproportional slices however can be tied to a horizon and offset at fixed intervals from this horizon. Therefore when an intra-Carboniferous horizon cannot be mapped, this is of key utilization.

The extensive mapping of this horizon over a 250km by 250km area was carried out using the 3D autotracking and manual tracking features depending on reflection continuity. This horizon maps reveals an extensive and highly variable fault network across the basin.

In areas of good quality intra-Carboniferous reflections, these horizons were mapped in local areas across the basin to delineate the pre-Permian structuration, and to particularly highlight faults unaffected by post-Carboniferous reactivation. Detailed intra-Carboniferous horizon mapping is only possible on a local scale due to the discontinuity of reflections over large areas. Horizons with laterally continuous high amplitudes were chosen for picking, these were later given age constraints by tracing to the nearest deep well. The importance of mapping these horizons is justified by the revelation of structure that is not visible on the extensive Top Rotliegend horizon map. Tracing intra-Carboniferous reflections across discontinuities with high certainty is challenging due to the high density of fault intersections, which in turn cause distortion of the seismic image with fault planes causing wave diffractions (Brown 2011).

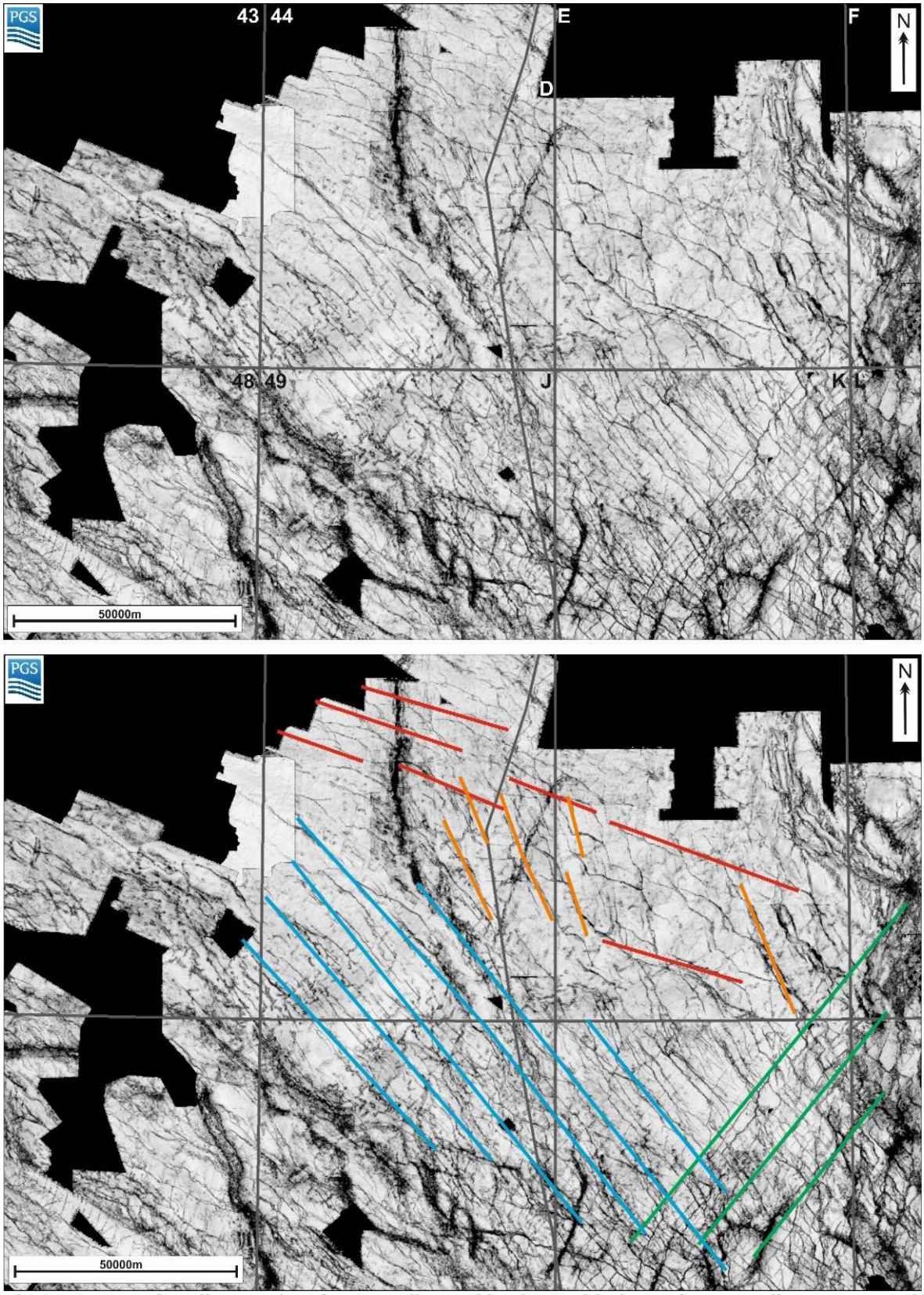


Figure 1.11 Regionally correlated Top Rotliegend horizon with the variance attribute extracted onto it. Four main fault trends are expressed by this map; a WMW-ESE (red), a NNW-SSE (orange). a NW-SE trend (blue) and a NE-SW trend (green). Areas of high variance (thick black lines/areas) correspond to the seismic distortion underneath areas of thick evaporite accumulations i.e. salt walls.

1.5.2.2 Reflection mapping across faults

Fault tips are rarely isolated and thus the standard correlation method of tracing horizons around fault tips (Figure 1.13) cannot be used in many cases. Seismic imaging becomes poorer at intersections, adding to the ambiguity. For these reasons, in some areas, seismic packages of similar reflection character were mapped rather than individual reflectors. Horizons that could be traced with confidence across fault intersections were computed into surfaces in order to reveal the 3D fault block geometries. Amplitude extractions for the variance attribute were applied to regionally and locally mapped horizon surfaces which enhanced the positioning of fault interpretations and intersections between faults, effectively creating a 3D variance slice where possible.

Pre-Zechstein faults within the study were identified and roughly picked in the interpretation window using the fault-mapping tool. The area in which the fault was picked is characterised by a seismically dim zone that cross cuts the reflections at an oblique angle, which then offsets the reflections (Nelson 2006). Due to the low resolution and image quality throughout much of the Carboniferous succession, key faults were mapped in 2D seismic section orthogonal to the strike of the fault between 250m (where detail was required) and 1250m (for larger scale faults). Fault planes were delineated by horizon mapping rather than detailed picking of the fault surface itself due to limitations of fault positioning related to data quality. Mapped faults were given a unique identification code based on their location in within UK or Dutch Southern North Sea quadrants and blocks, orientation and order of identification. An example of this is Fault Q44_B24_E-W_5, which is found in Block 24 of Quadrant 44 and was the 5th E-W trending fault to be mapped.

1.5.2.3 Measurement of Throw

The measurement of throw from the offset of seismic reflections is a method used widely throughout the thesis using mostly time migrated 3D seismic data. Reflections that have been mapped across the fault are measured at their horizon cut offs, with the distance between the two reflections being recorded in milliseconds (ms) two way travel time (TWT) or metres on pre-depth converted data (UK sector).

The error in this throw measurement has two components; 1) Error from the sampling interval (where the measurement is taken on the wavelet. This usually ranges from 1-2ms (Mansfield and Cartwright 1996) and 2) Error created by the inaccuracy of reflection correlations i.e. which reflection horizon is measured at the stratal termination (Mansfield and Cartwright 1996). This portion of the error increases with depth due to decreasing resolution and the effects of noise being more pronounced with depth. This component of error is estimated to range from 4-8ms with the value being higher in the range with depth and data quality. The highest error value for a particular area is used as standard for all measurements in that area. An error margin of 6-10ms is therefore used across the datasets depending on quality.

1.5.2.4 Time to Depth Conversion

Throw values in TWT were converted from milliseconds to metres in areas that P wave velocity is variable throughout the faulted succession. This conversion was performed by using the average velocity for the interval of interest, from the closest well (Figure 1.8) and imputing it into the formula of (V/D*2)/1000 where V is the average velocity in metres per second and D is the throw is milliseconds. This is an important consideration as throw variations in ms can sometimes be an

artefact of velocity variations. In areas of constant P wave velocity (as shown by the sonic log in Chapter 4) this conversion was not required.

Area	Faults	Seismic Interval	Average Interval Velocity (m/s)	Throw Measurement Error (ms)	Throw Measurement Error (m)	Sonic Well Logs
ESP	Throughoing	Rotliegend - Courceyan	4533	8	18	E2-2, E2-3 and A17-1
	Superficial	Rotliegend - Asbian	4260	6	13	E2-2 and E2-3
MB	Throughoing	Rotliegend - L. Carb.	4708	10	23	44/19-3, 44/24-4 and A17-1
	Superficial	Rotliegend - Namurian	4522	8	18	44/19-3, 44/24-4
SB	Throughoing	Rotliegend - Visean	4698	8	18	44/27 and A-17
	Superficial	Rotliegend - Namurian	4825	6	14	44/27
CBH	Throughoing	Rotleiegnd - L. Carb.	4903	8	20	K03-3 and A-17
	Superficial	Rotliegend - Westphalian	4815	6	15	K0-3
CB-ST	Throughoing	Visean - Tournaisian	5080	8	18	Cloughton-1
	Superficial	Namurian	4354	6	13	Cloughton-1

Figure 1.12 Average interval velocities used in the conversion from time to depth. The measurement error for each area, composed of (1) the sampling interval error (2ms) and (2) the correlation inaccuracy error (4-8ms). The values for (2) in ms are determined for each area based on the dominant frequency and data quality for that interval and added to the sampling interval error (1).

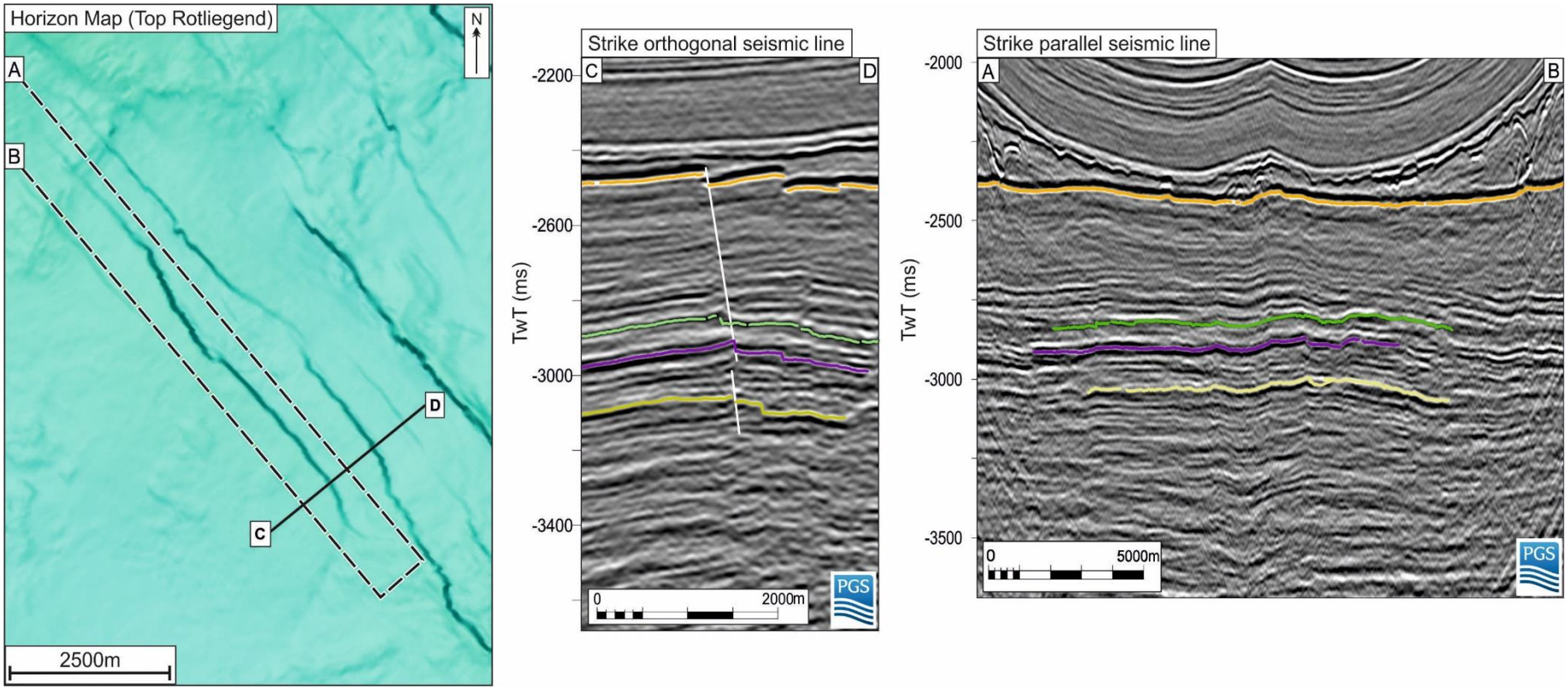


Figure 1.13 Method of correlating horizons around a fault when a free lateral tip is present

1.6 Structure of Thesis

The thesis comprises seven chapters. ***Chapter 1*** presents the purpose and structure of the DPhil project. It introduces the problem and outlines the existing literature regarding the challenges associated with creating structural models for the pre-Zechstein. The main aims and research questions are also introduced along with the datasets used and approach taken to address the questions. The principle methods of interpretation and analysis of seismic data are introduced.

Chapter 2 provides an overview of the regional crustal structure and evolution of the wider study area (The Northwest European Carboniferous Basin) through the relevant plate motions from the early Palaeozoic to present day. The current ideas regarding the basin scale and sub-basin scale structural patterns, styles and formation mechanisms of faults within of the Pennine Basin, Anglo-Dutch Basin and the Mid North Sea High are presented.

Chapters 3, 4, 5 contain the results of the research project. The results are presented thematically rather than geographically in order to present the key conclusions and themes as a synthesis of all the different case study areas in each chapter. ***Chapter 3*** presents a general structural characterisation of the case study areas across the Anglo-Dutch and Pennine Basins based on the seismic interpretation of 3D and 2D data. ***Chapter 4*** presents the results from throw distribution analysis from key representative faults from the 3D seismic case study areas. ***Chapter 5*** presents the analysis of the density and spacing of faults across the Pennine and Anglo-Dutch basins.

Chapter 6 synthesises and discusses the results of chapters 3-5, their meaning and uncertainties, and addresses the wider questions posed by the results of the thesis.

Chapter 7 presents the basic outcome of the thesis as four regional conclusions and nine more detailed conclusions from the quantitative fault analysis presented in the results chapters.

1.7 Publications from this Thesis

The following list outlines the articles that are currently in preparation, derived from the research contained within this thesis.

- Detachment Faults in the Upper Devonian – Lower Carboniferous of the Elbow Spit High - *In prep*
- Fault-channel interactions: a case study from the Rotliegend of the Murdoch Block – *In prep*
- Faulting processes and their inter-relationships in the Anglo-Dutch and Pennine Basins - a case study - *In prep*
- Fault characterisation in the Pre-Zechstein succession of the Anglo-Dutch Basin – *In plan*
- The intensity and spacing of faults in the Pre-Zechstein succession of the Anglo-Dutch and Pennine Basins – *In plan*

Chapter 2

REGIONAL STRUCTURE OF THE NORTHWEST EUROPEAN CARBONIFEROUS BASIN

2 Regional Structure of the Northwest European Carboniferous Basin

2.1 Introduction

The Northwest European Carboniferous Basin (NWECB) is a non-genetic, east – west orientated region of Late Devonian to Late Carboniferous subsidence and sedimentation, presently located in Northwest Europe (Kombrink, 2008). The NWECB (Figure 2.1) is part of a large shelf complex comprised of smaller basins, which then contain sub-basins and highs (Fraser and Gawthorpe, 1990, Corfield et al., 1996, Besly, 1998). The NWECB underlies the Southern Permian Basin (SPB), an intracontinental basin which began to thermally subside in the early Permian (Guterch et al., 2010).

This chapter provides a regional tectonic and structural context for the meso-scale structure examined by the smaller case study areas. This chapter also reviews the current ideas of the smaller sub-basinal scale structure. The key themes that are reviewed include fault orientations and geometries, structural styles, timing of formation and reactivation of structures, structural inheritance and fault forming and reactivation mechanisms.

2.2 Crustal Framework

The deep crust underlying the Anglo-Dutch Basin (ADB), Mid North Sea High (MNSH) and Pennine Basin is composed of the East Avalonia Terrane Assemblage (EATA). The EATA is a Gondwana-derived continental terrane (Winchester et al., 2002, Winchester et al., 2006) that ranges in crustal thickness from 24-38km. The EATA forms a junction with Laurentia to the north west and Baltica to the north east

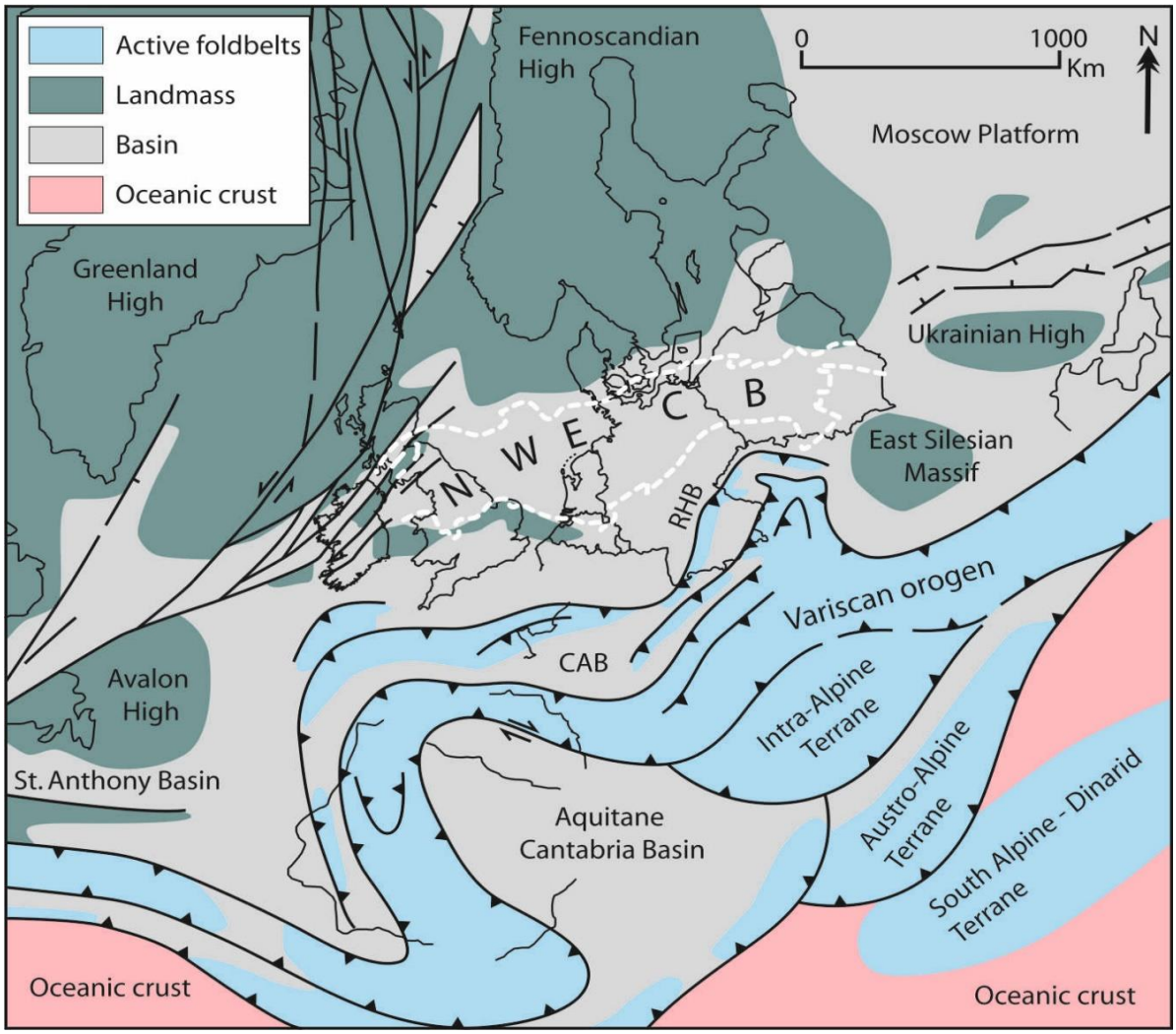


Figure 2.1 Palaeotetctonic setting of Northwest Europe during the Early Carboniferous. The position of the NWECB is highlighted by the white dashed line. Modified after Kombrink (2008)

(Figure 2.2) which consolidated during the Caledonian and Variscan orogenies. The southwest portion of this terrane is uplifted as a flexural response to the load created by the Variscan mountain range, this foreland bulge is called the London-Brabant Massif (Rijkers et al., 2009). The EATA is bound to the south by the Rheic suture, which marks the closure of the Rheno-Hercynian back arc-ocean basin, which opened during the Early Devonian between the EATA and the Armorican Terrane Assemblage and closed during the Carboniferous (Ziegler and Dezes, 2006). Deep seismic reflection and refraction studies revealed the Moho depth below the UK sector to range from 27 to 36km (Chadwick and Pharaoh, 1998, Lyngsie et al., 2006). The Moho is

deepest under Central and South-East England and shallowest beneath the Central North Sea Basin.

The pre-Permian sedimentary succession in the North Sea attains a thickness of up to 10km (Guterch et al., 2010). Older sediments have little stratigraphic age control, however some deeper well penetrations near the MNSH margin, Danish Central Graben and Rinkobing Fin High (Ziegler, 1990, Cartwright, 1990) reveal a strongly folded and sheared upper crustal layer with igneous intrusions. This highly deformed layer has poor seismic reflectibity and lies at depths of 18-21km (6-7s TWT). The Midlands Microcraton was a stable, defomation resistant identer (Soper, 1987) during the early Palaeozoic sedimentation and Acadian tectonism. The Acadian tectonism was most intense surrounding the microcraton, forming the slate belts of North Wales and Northern England and concealed Caledonides beneath eastern England and the Southern North Sea (Pharaoh, 1995). The concealed Caledonides of eastern England contain a number of discrete thrusts that have a NW-SE structural fabric. The most visible thrusts are seen under Eastern England basmement. A number of igneous intrusive bodies are also present (Guterch et al., 2010).

In the Southern North Sea, NW-SE deep mid-crustal reflections that dip to the north east are thought to represent either Mesozoic extensional shear zones (Reston and Blundell, 1987) or Caledonian basement thrusts. The Dowsing Line, a major lower crustal feature in which the geophysical characteristics vary on either side (Figure 2.3), bounds the concealed Caledonides with the Southern North Sea Terrane. The Thor suture between Baltica and Avalonia also follows this NW-SE trend, with a southwest dipping reflective unit (Figure 2.2).

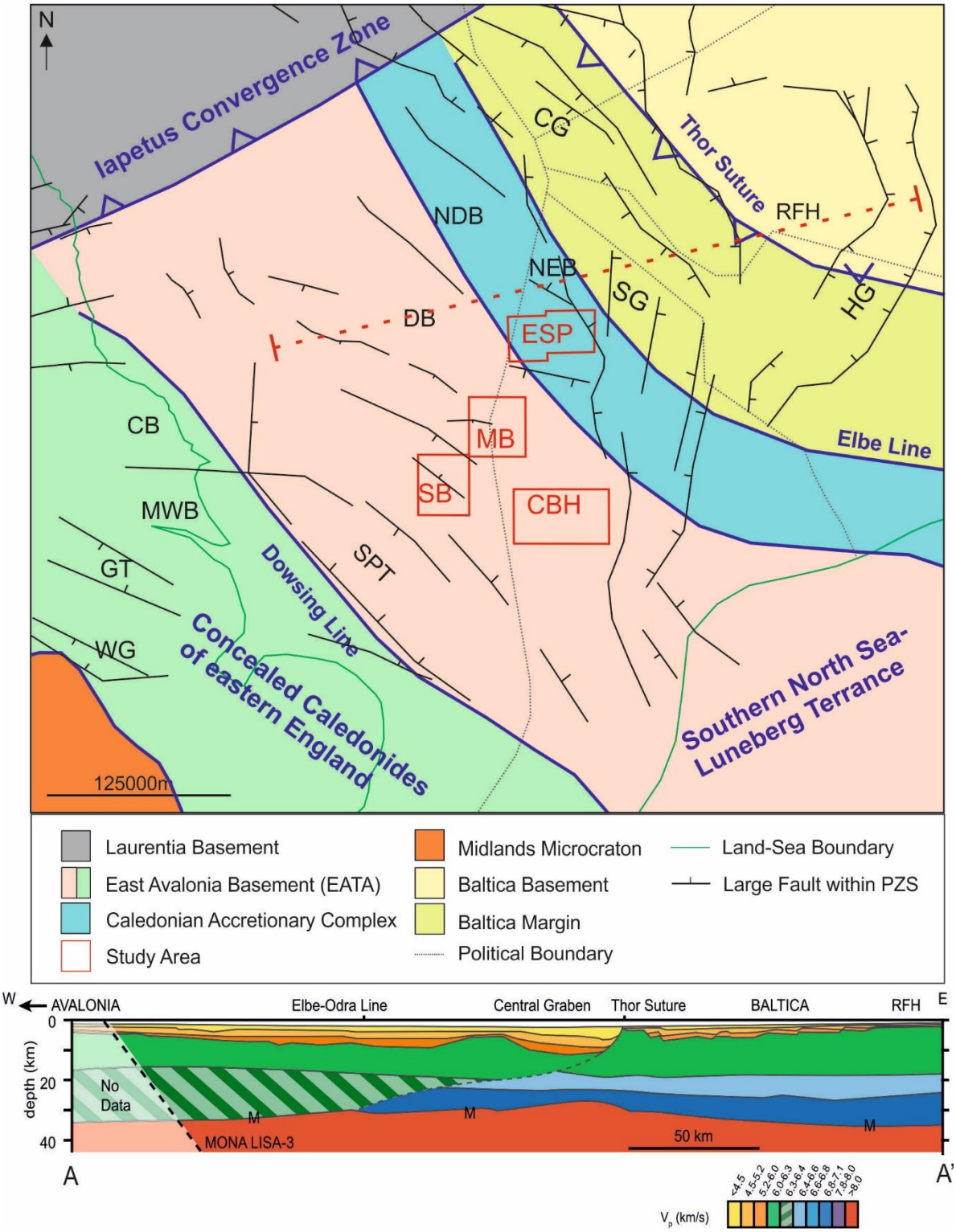


Figure 2.2 Crustal structure and basement terranes beneath the Anglo-Ducth Basin, Pennine Basin and MNSH. Blue lines represent plate boundaries and tectonic lineaments. Major faults offseting Pre-Zechstein Structure are overlain. Modified after Leslie et al. 2015; Smit et al. 2016; Ter Borgh et al. 2018

The Variscan Front Thrust (Figure 2.5) defines the northern limit of Variscan thick-skinned deformation and metamorphism and is the limit of the Variscan fold and thrust belt. The northern tip of the Variscan Front Thrust is the boundary between the Rhenohercynian Zone and Variscan 'Foreland' (Corfield et al., 1996). The Variscan Foreland is the area north of the Variscan fold and thrust belt and the research within this thesis is concerned with the deformation within this area.

The tectonic sutures and large scale features across the NWECB area are reflected by anomalies on gravity data maps. The Trans European Suture Zone (TESZ) between Baltica and Avalonia (Figure 2.2) has a NW-SE lineation trend on gravity anomlaie maps (Figure 2.6) which is thought to also represent the Caledonian deformation front. This lineament is likely a result of the difference in lower crustal density between each terrance on either side of the suture (Smit et al., 2016).

There is a strong contrast between the magnetic response of the crust of the East European Craton (Baltica) and the less magnetic Palaeozoic accreted terranes of Cental Europe (Avalonia and Armorica). The magnetic basement of Baltica dips to the southwest through the entire crust to 30-35km, beneath an overriding non-magnetic Avalonian wedge of crust. This results in the Caledonian suture between Avalonia and Baltica being easily identified on magnetic maps (Krawczyk et al., 2008).

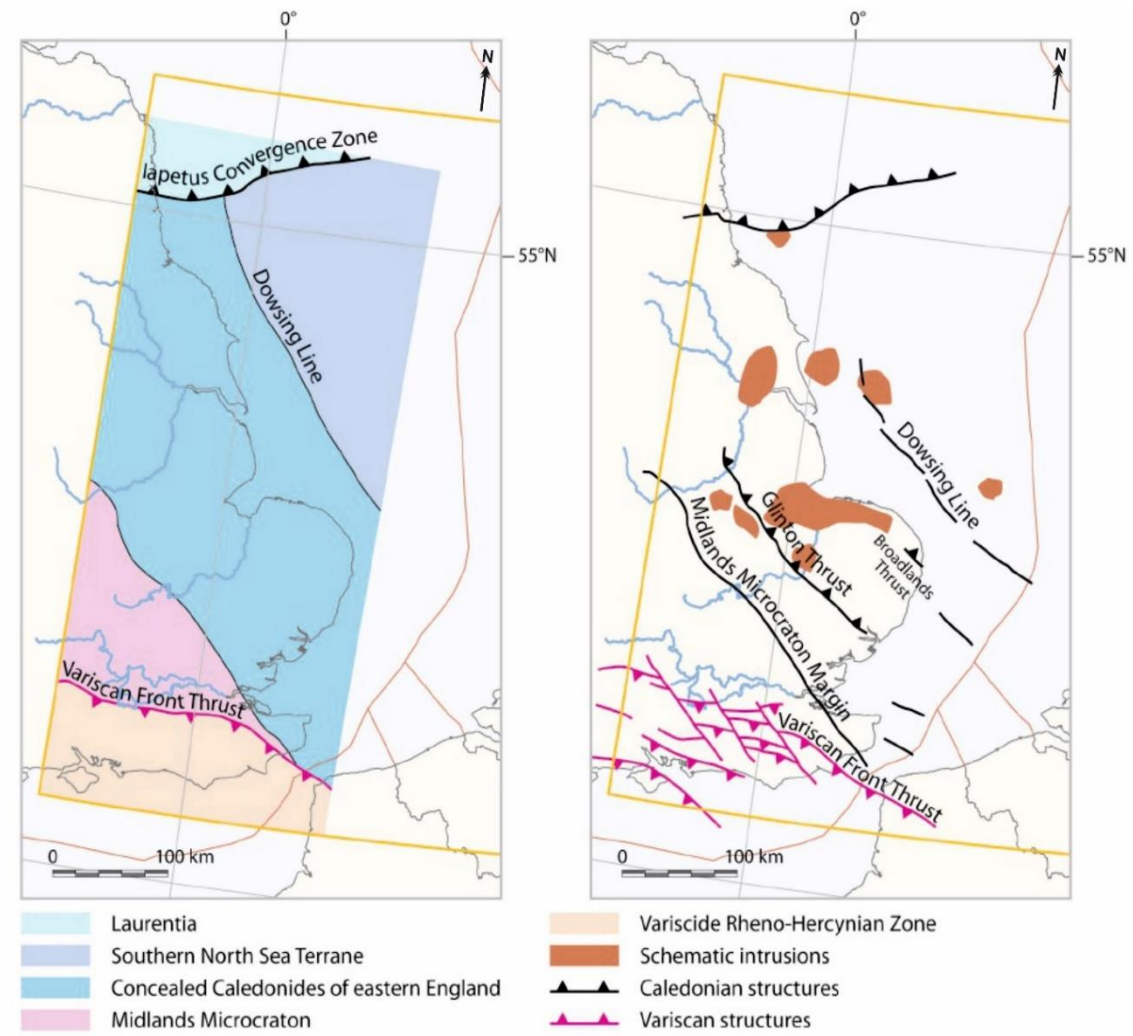


Figure 2.3 Major upper crustal terranes a structures underlying eastern England and the Southern North Sea. Lineaments/ faults like the Dowsing Line and Glinton Thrust have been repeatedly reactivated and have influenced proceeding structures. After Gutertch et al. 2010.

2.3 Tectonostratigraphic Evolution

An understanding of the key stages within the plate tectonic cycle undergone by the NWECB area is necessary context to assess formation and evolution of structures observed at smaller scales. This section will briefly outline the tectono-stratigraphic evolution of the northwest area of the NWECB from the Early Palaeozoic to Cenozoic times. A detailed account of the tectonic evolution across the entire NWECB area is documented by Guterch et al. (2010) and Pharaoh et al. (2010).

2.3.1 Early Ordovician – Middle Devonian

In the Early Ordovician, Avalonia rifted away from Gondwana (Trench and Torsvik, 1992), driven northwards towards Baltica by the opening of the Rheic Ocean (Nance and Linnemann, 2008, Nance et al., 2010, Cocks and Fortey, 1982). This was during the Caledonian plate tectonic cycle and resulted in the formation of the palaeocontinent Laurussia.

2.3.1.1 Shelvian Tectonic Phase (Late Ordovician)

The Shelvian tectonic phase (~435Ma) involved the collision of eastern Avalonia with Baltica during the closure of the Tornquist Sea on the southern margin of the Iapetus ocean (Toghill, 1992). The closure of the Tornquist Sea resulted from a dextral oblique mechanism and produced the NW-SE trending Thor Suture (Berthelsen, 1998, Pharaoh, 1999, Smit et al., 2016) between Avalonia and Baltica (Figure 2.5). Major crustal lineaments such as the Tornquist Line acted as a later locus for Carboniferous-Mesozoic strike-slip displacement and Alpine compressional induced basin inversion (Pharaoh et al., 2006).

2.3.1.2 Scandian Tectonic Phase (Late Silurian ~431-428Ma)

The closure of the Iapetus Ocean took place in the Late Silurian during the Scandian Orogenic Phase) (Kirkland et al., 2006). The northwest directed subduction of Baltica beneath Laurentia led to the final closure of the Iapetus and the amalgamation of Laurussia (Ziegler, 1989).

In the early Devonian, the Caledonian Ardennes fold belt that marked the Rheic Suture (Figure 2.5) was disrupted by rifting, controlling the subsidence of the Rheno-Hercynian basin. This Rheno-Hercynian basin developed in a back-arc position relative to the northerly dipping subduction zone (Ziegler, 1989, Nance and Linnemann, 2008). Collapse of the Arctic-North Atlantic Caledonides occurred parallel to the Variscan Orogeny under a sinistral transtensional setting. This collapse is evidenced by the intramontane Old Red Sandstone basins in the North Sea and widespread granitic plutonism in Northern England (Ziegler, 1989).

2.3.1.3 Acadian Tectonic Phase (Middle Devonian)

An initial compressional phase affected the Rheno-Hercynian back-arc basin in the Middle Devonian. The two Caledonian structural grains that emerge from this plate tectonic model are NE-SW and N-S to NW-SE. The Southern North Sea lies in the Tornquist structural domain (Corfield et al., 1996) with the dominant NW-SE structural grain inherited from the Lower Palaeozoic thrust and fold belt.

2.3.2 Late Devonian – Late Carboniferous

The Late Devonian to Late Carboniferous is a time period associated with the Assembly of Pangea and the beginning of the Variscan plate cycle. A Late Devonian episode of extension and volcanism (Ziegler, 1989, Ziegler, 1990) was followed by a build up of compressional stresses. During this time, Gondwana was beginning to converge with Laurussia in a clockwise-rotational mode and closure of the Rheno-Hercynian oceanic basin resumed (Franke, 2000, McKerrow et al., 2000).

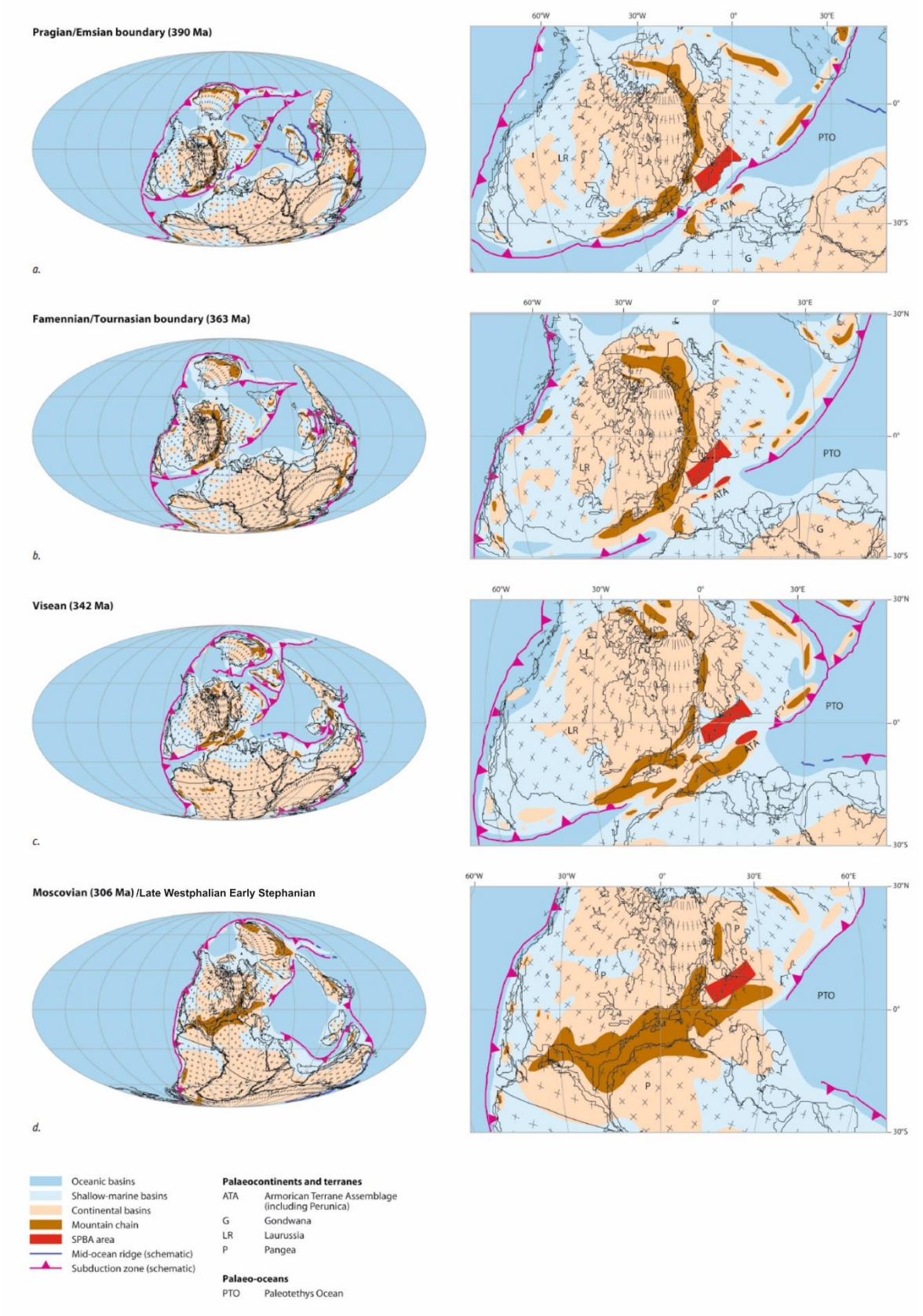


Figure 2.4 Paleogeographic maps showing the Late Paleozoic tectonic evolution. Reconstructions by Scotese, C. After Pharaoh et al. 2010.

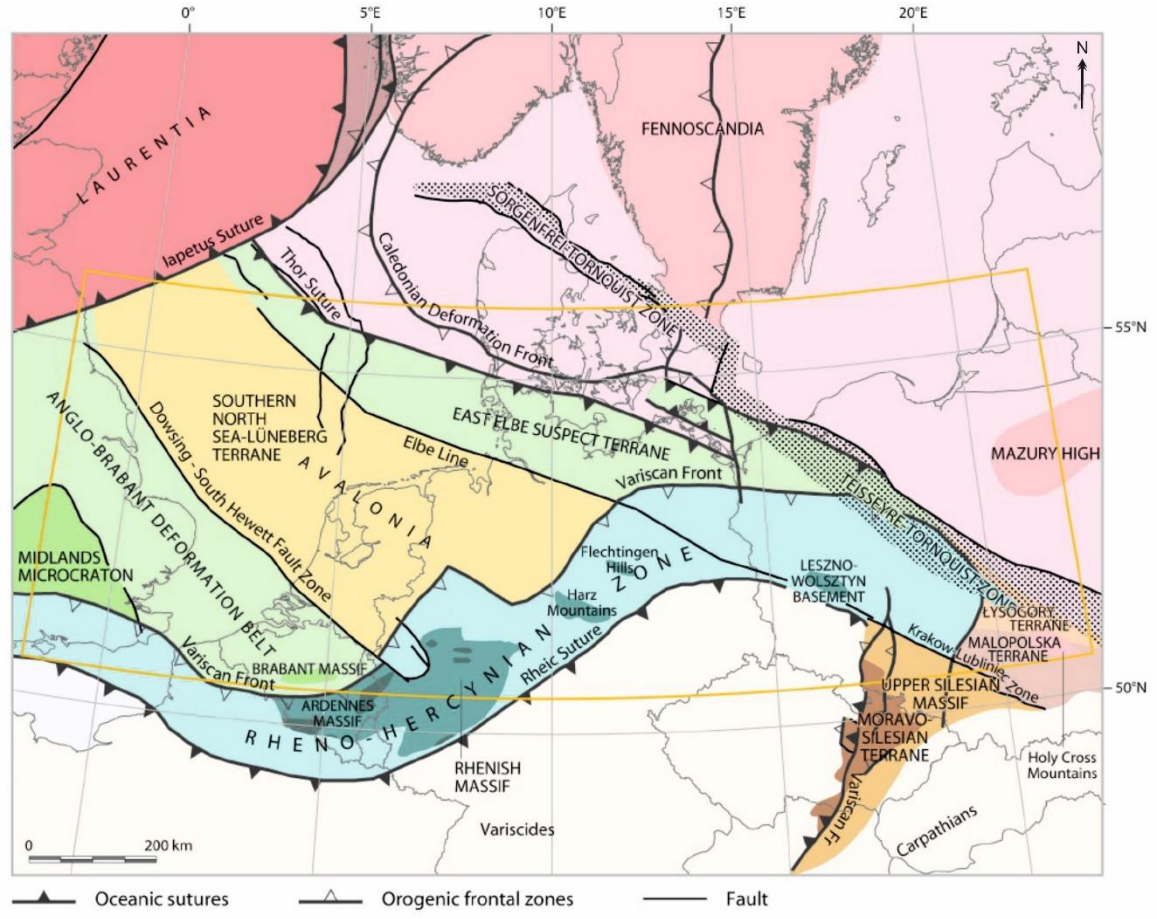


Figure 2.5 The tectonic terranes that formed the palaeocontinent Laurussia. After Pharaoh (2010).

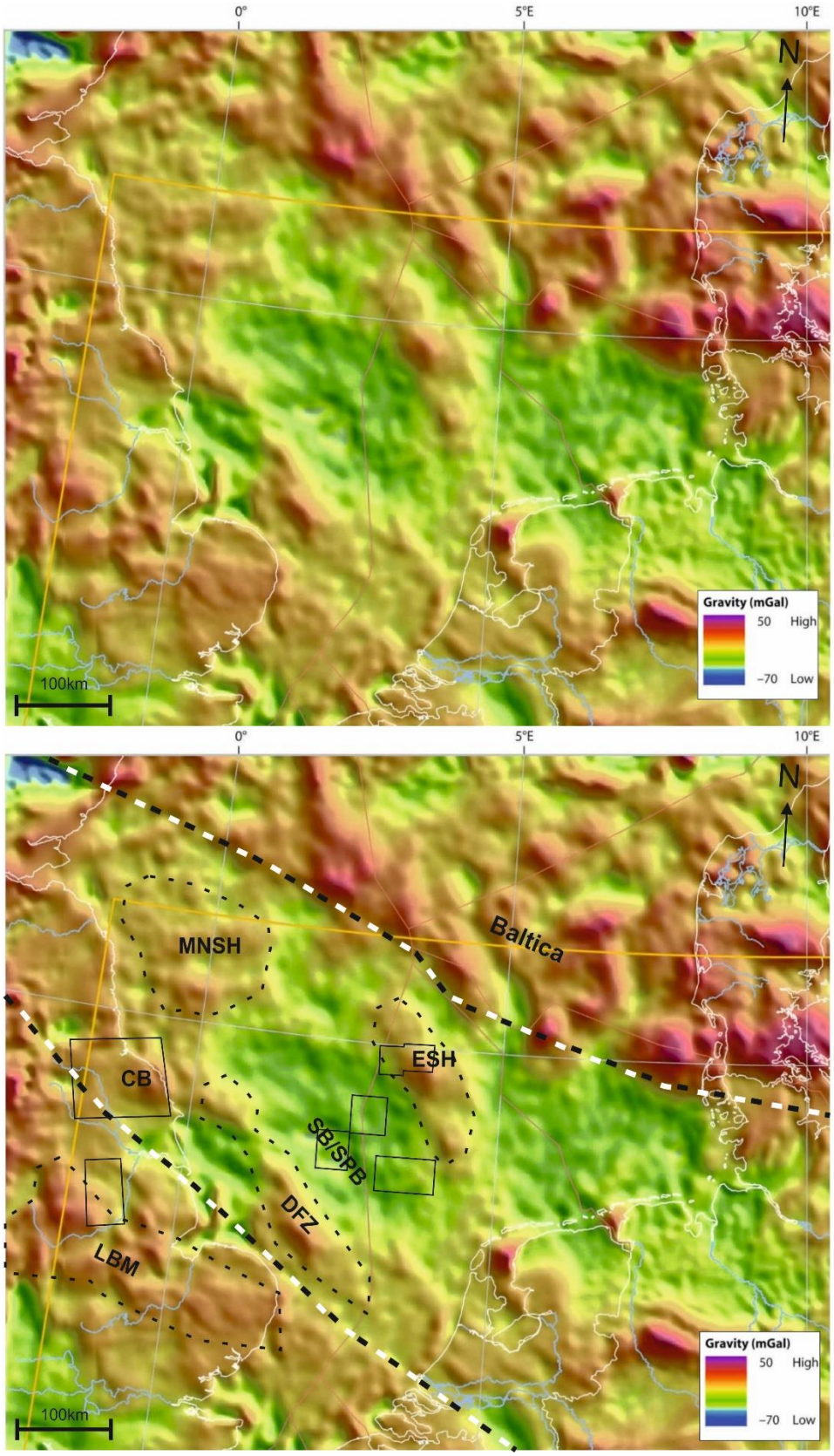


Figure 2.6 Bouguer (onshore) and free air (offshore) gravity map. Locations of the case study areas are shown by the black polygons. Areas of highest Bouguer gravity offshore to the north east of the map corresponds to the Baltica basement, with a sharply defined contact. Higher gravity anomalies are also present underneath the Elbow Spit High (ESH), Cleveland Basin (CB), Mid North Sea High (MNSH), Dowsing Fault Zone (DFZ) and London Brabant Massif (LBM). The Southern North Sea has a low gravity signal overall i.e. the Silverpit Basin and Sole Pit Trough. After Gutertch et al. (2010).

2.3.2.1 Bretonian Tectonic Phase (Late Devonian-Early Carboniferous)

A main phase of rifting began in the Late-Devonian with N-S extension reactivating the inherited NW-SE fault trend in the Southern North Sea obliquely (Fraser and Gawthorpe, 1990). Leeder and Hardman (1990) identified that most of the known onshore horst blocks at this rifting event had a late Caledonian granite pluton at their core. Recent discoveries have also suggested that a series of granite core highs is also the model in the MNSH terrane (Ter Borgh et al., 2018).

The extension at this time was caused by the formation of a back-arc basin ahead of the Variscan front, due to the northward subduction of the African portion of Gondwana under the European portion of Laurussia, closing the Rheic Ocean (Nance and Linnemann, 2008). Coward (1990) also argued for an escape tectonic model occurring at this time, in which a triangular shaped block called the North Sea Baltic Block was expelled from the colliding plates of Gondwana and Laurasia in a north east lateral expulsion and rotation (Figure 2.7). The implications of his model assigned a dextral transtensional regime in the SNS. Maynard et al. (1991) argued that the Late Carboniferous deformation is more likely due a combined back-arc extension and escape tectonic model.

During the Middle-Late Devonian, the Pennine, Anglo-Dutch and MNSH basins were infilled by continental clastic Old Red Sandstone facies. Marine intercalations of Mid Devonian age are found in the UK onshore, the MNSH, the Central Graben and Southern North Sea (Pharaoh et al., 2010). A Late Devonian (Fammenian) regression occurred forming coastal sandbars of the Buchan/Condroz Group (Kearsey et al., 2015).

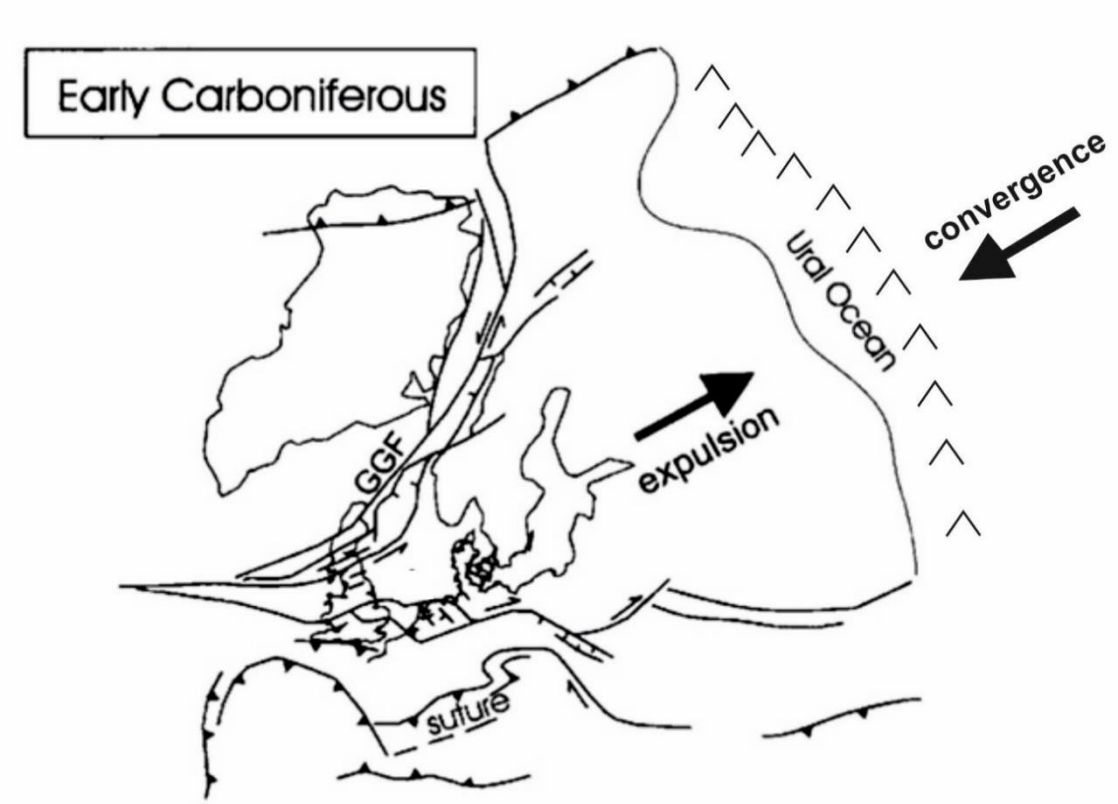


Figure 2.7 Simplified model by Coward (1993) illustrating the continental explusion of the North Sea Baltic Block resulting in dextral transpression in the SNS. Modified after Schroot & De Haan (2003).

In the Early Carboniferous (Tournaisian-Visean), regional extension across the Variscan Foreland was accommodated on mostly east-west to NW-SE orientated asymmetrical half-grabens. Throws up to 5000m are presently recorded on basement reflections (Ter Borgh et al., 2018). In the Visean, carbonate platforms accumulated on the granite cored highs with the accompanying deposition of more distal sediments into the half-grabens. Up to 4000m of these sediments were deposited in northern England half grabens which were big enough to be considered sub-basins i.e. the Bowland Basin in NW England (Fraser and Gawthorpe, 1990). These anoxic sub-basins were widespread during Visean - Early Namurian times and involved the accumulation of the black shales which are the prolific source rocks for the UK and Netherlands; the Bowland, Edale Shale and Geverik Formations respectively (Pharaoh et al., 2010).

Collision related compressional stresses exerted on the foreland at the Visean-Namurian boundary caused disruption of the Visean carbonate platforms (Zeigler 1990) and the development of a regional mid-Visean angular unconformity, described by Fraser and Gawthorpe (2003a) as a sequence boundary.

2.3.2.2 Sudetian Tectonic Phase (Early Namurian)

In the mid-late Namurian, the Variscan flexural foreland basin was infilled by post-rift deltaic and coal bearing clastics totalling several kilometres derived from the orogenic mountains. This was said to be a period of roughly 20 Ma relative tectonic quiescence that continued until the Westphalian C (Schroot and De Haan, 2003). Uniform thermal subsidence occurred throughout this time along an intracratonic basin with a NW-SW trend. According to the model by McKenzie (1978), this period is classed as a thermal sag phase and was related to a gradual cooling and strengthening of the lithosphere (Schroot and De Haan, 2003). Namurian transgressive marine shales infilled the topographic lows such as the Visean half grabens. Paralic conditions prevailed throughout the Westphalian with short lived marine incursions (Ziegler, 1978).

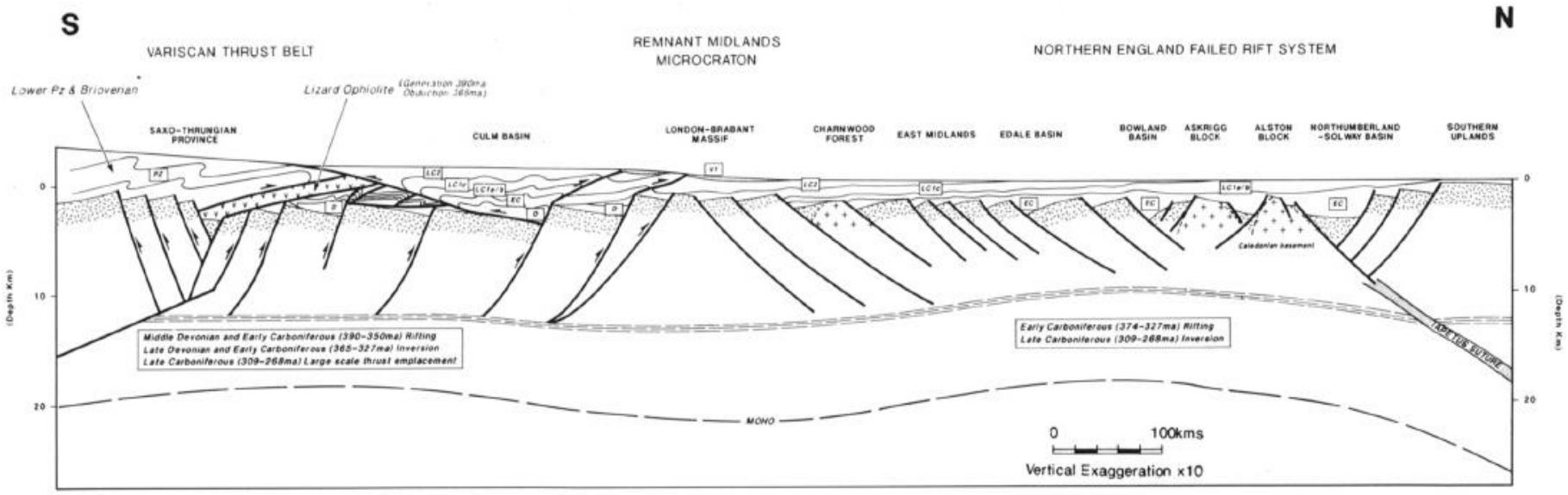


Figure 2.8 Schematic cross section by Fraser & Gawthorpe (1990) illustrating the configuration of the Variscan thrust belt in the south of England and the Variscan Foreland failed rift system in the north of England, separated by the Midlands Microcraton.

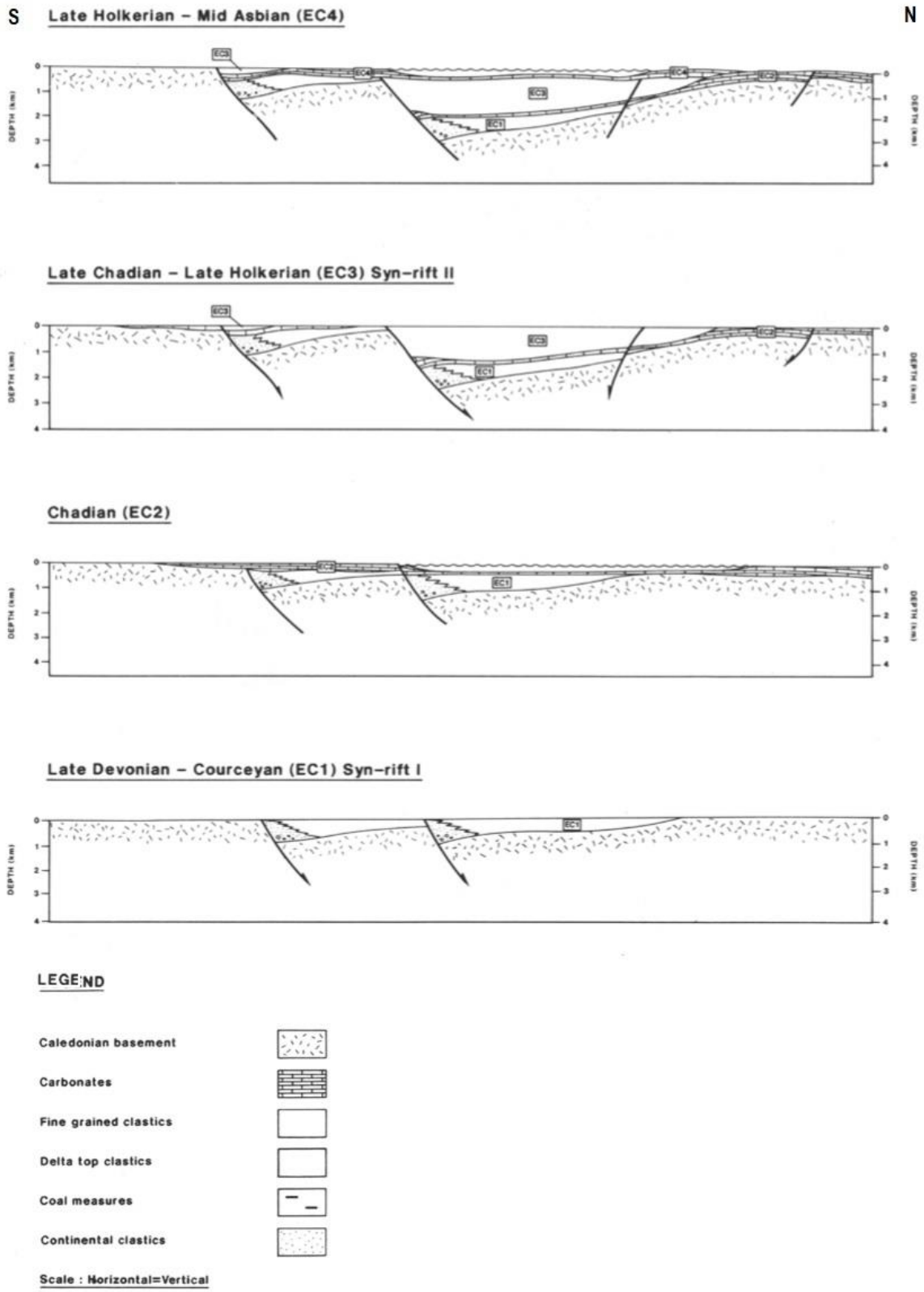


Figure 2.9 Carboniferous sub-basin/half graben development in the Late Devonian - Early Carboniferous. Cross section through the Widmerpool Gulf and Hathern Shelf. After Fraser & Gawthorpe (1990)

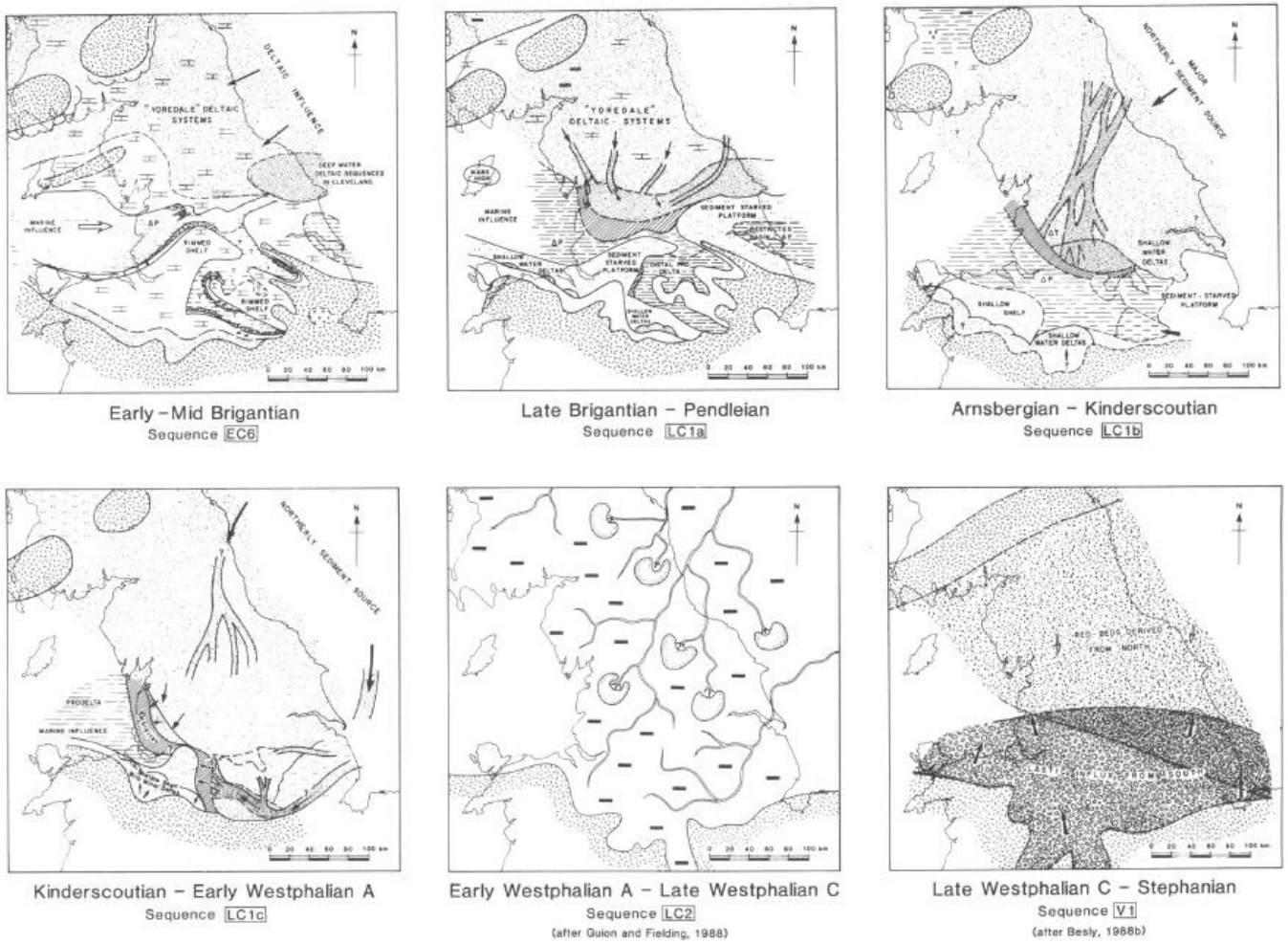


Figure 2.10 Palaeofacies maps of northern England (Early Brigantian to Late Westphalian). The fundamental control on Carboniferous sedimentation in northern England (and supposedly the Southern North Sea) was the presence of a major clastic source area to the north, with a predominantly north to south sediment transport direction. The Namurian and Westphalian sedimentary facies in the Anglo-Dutch Basin are indicative of the progressive of this large-scale delta system. After Fraser et al. 1990

2.3.3 Late Carboniferous – Late Permian

The Late Carboniferous to Late Permian is a time period associated with uplift and inversion followed by post orogenic collapse.

2.3.3.1 Variscan Tectonic Phase (Late Westphalian-Early Rotliegend)

In the Late Carboniferous (Westphalian D – Stephanian), the inversion of the Variscan foreland led to folding and reverse faulting across much of onshore UK and the southern North Sea (Fraser et al. 1990, Corfield et al.1996). The inversion of the NW-SE trending Carboniferous basins is the SNS was much less pronounced than the NE-SE oriented basins in onshore northern England (and the Irish Sea). The was due to their orientation in regards to the dominantly NW-SE to NNW-SSE direction of maximum shortening (Corfield et al. 1996, Figure 2.11). The inversion that took place on the NW-SE faults was suspected to have a significant component of oblique slip, though few lateral movement indicators have been identified (Schroot and De Haan, 2003).

Corfield et al. (1996) also concluded that the trends of the inversion anticlines were determined by local basement grain rather than by orientation of the compressive stress. Stewart and Coward (1995) also agreed that the Late Carboniferous inversion that occurred within the Anglo-Dutch Basin, and NE-SW shears that formed in Acadian times were reactivated as strike-slip faults in Variscan times.

The Stephanian history of the NWECB is poorly understood due to the uplift and erosion occurring simultaneously with Variscan compressional stresses. The model by Coward (1993) (Figure 2.12) illustrated that the North-Sea Baltic Block was being reinserted at this time due to the Ural plate collision to the north east. This caused sinistral transpression in the SNS along E-W shear zones.

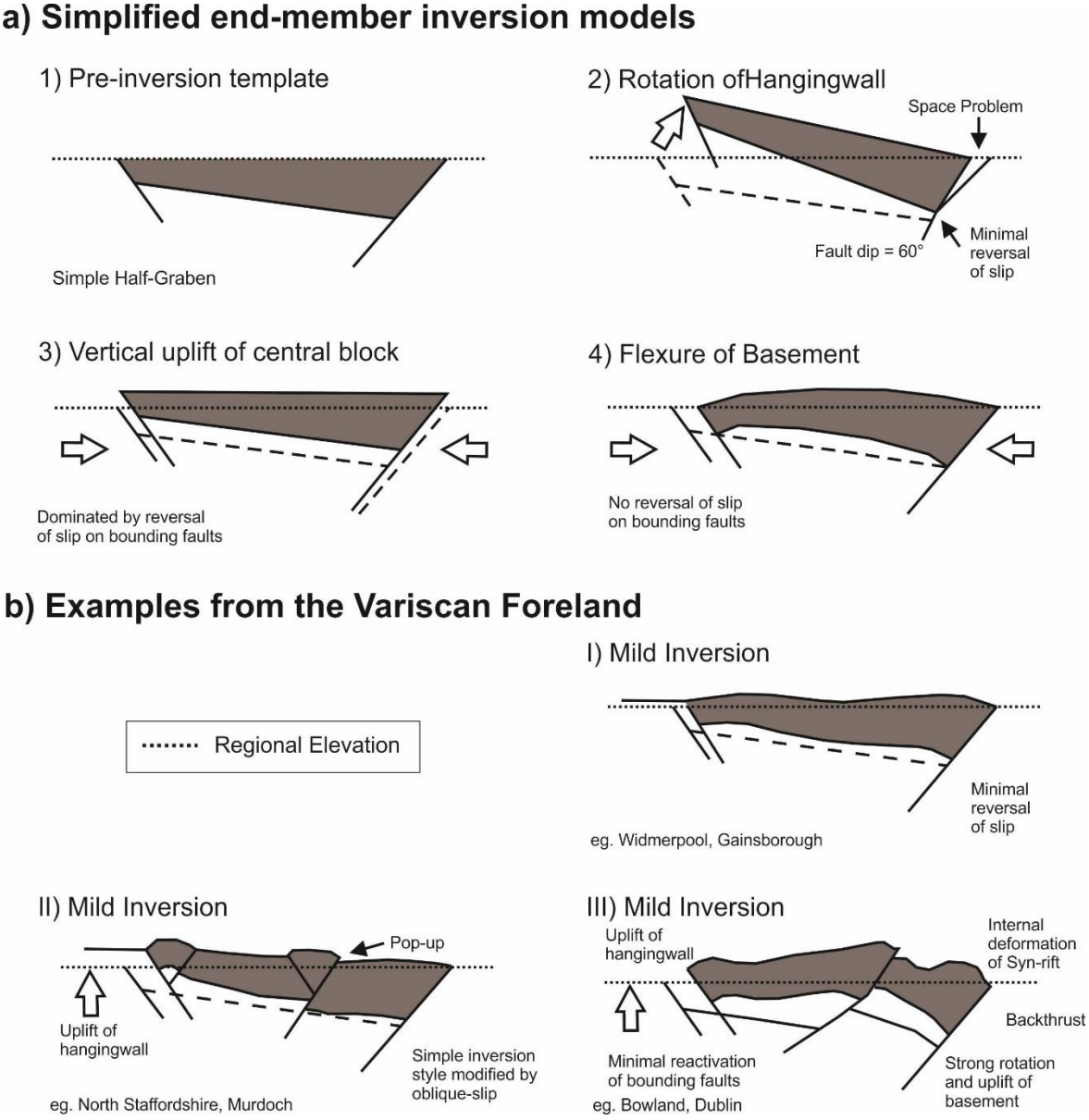


Figure 2.11 Simplified models of the Variscan inversion observed across the Variscan Foreland. After Corfield et al 1996

Transpressive tectonics in the SNS are indicated by locally deep truncation of Namurian and Westphalian Strata (Pharaoh et al. 2010). Stephanian sediments overlie the Westphalian unconformably in the West Netherlands Basin and the Cleaver Bank High (Figure 2.13).

The final suturing of Laurussia and Gondwana and the formation of Pangea occurred at the end of the Carboniferous – early Permian (Alleghenian). A dextral mega shear system connected ongoing crustal shortening between the Urals and Appalachians (Coward 1990). This system transected the Variscan Orogen, controlling the orogenic collapse (Arthaud and Matte, 1977, Ziegler, 1989).

The Northward compression in the Late Carboniferous reactivated NW-SE orientated dextral strike-slip faults and NNE-SSW striking sinistral faults (Lamarche et al., 2002). The strike-slip tectonics caused fracturing of the deep crust and significant disruption of the sedimentary cover (Arthaud & Matte 1977). During this time, punctuated intense volcanic and intrusive activity was occurring in the NWECB (Wilson et al., 2004). The Whin Sill of northern England, a thoelitic dolerite intrusion (Goulty, 2005), evidences this period of magmatic activity.

Compressional tectonic forces, regional strike-slip faulting and magmatism caused uplift and widespread erosion across the Anglo-Dutch Basin during this time. This formed a regional unconformity between Late Carboniferous and Early Permian strata known as the Variscan Unconformity or Base Permian Unconformity (BPU). The BPU is a term for the unconformity that represents several unconformities of Late Carboniferous to mid Rotliegend age across the NWECB (Glennie, 1998).

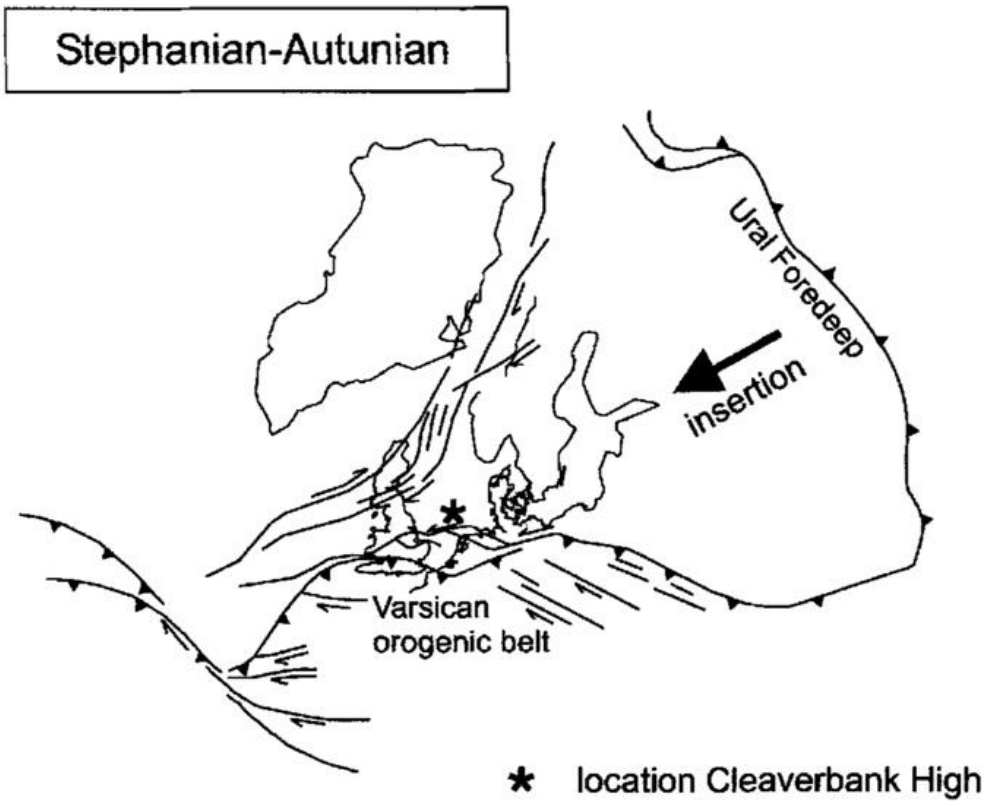


Figure 2.12 Tectonic model by Coward (1993) illustrating the reinsertion of the North Sea Baltic Block and the resulting sinistral transpression in the SNS during the Variscan Orogeny

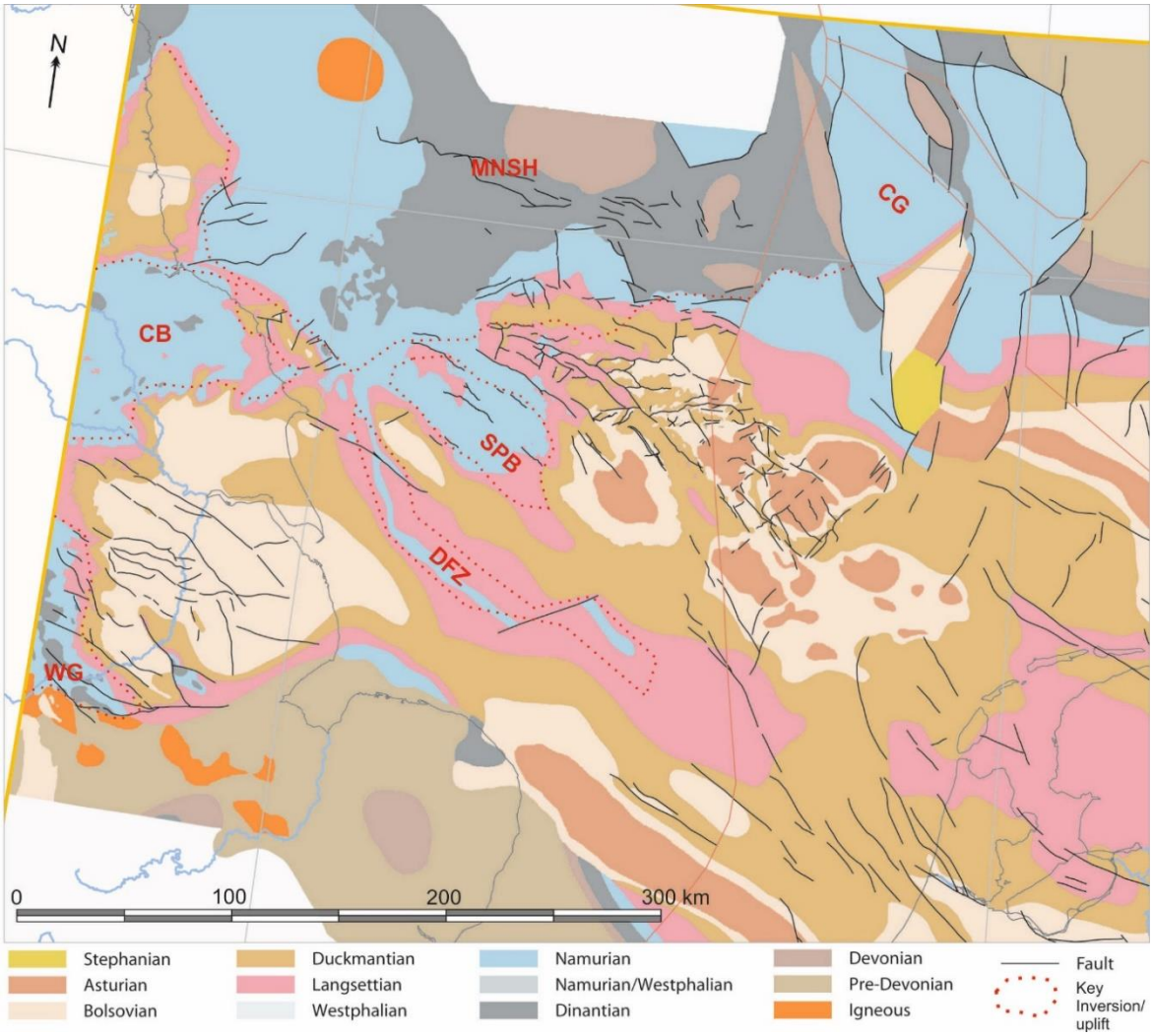


Figure 2.13 Base Permian subcrop map with main structural features within the PZS. After Kombrink et al. (2010)

2.3.3.2 Saalian Tectonic Phase (Early-mid. Rotliegend)

The detachment of subducted lithospheric slabs during the strike-slip induced collapse of the Variscan Orogen, caused upwelling of the asthenosphere and resulting thermal thinning and subsequent regional uplift, with possible partial delamination of the lithospheric mantle (Pharaoh 2010). Crustal thinning in the order of ~30km continued through the mid-Permian resulting from the subsequent regional erosional unroofing. The Saalian Unconformity (Glennie, 1997) represents the early Rotliegend stratigraphic hiatus (20-30Ma) and is the most widely recognised BPU throughout the Netherlands (Figure 2.14).

Thermal subsidence of the lithosphere began when asthenospheric temperatures returned to ambient levels in the early Permian (Ziegler and Dezes, 2006). At the end of the early Permian, the subsidence of the NWECB in response to thermal contraction of the lithosphere continued, however the volcanism associated with widespead strike-slip faulting ceased.

The Southern Permian Basin (SPB); the collective name for the Permian sedimentary basin overlying the NWECB, had formed by Rotliegend times and was isolated from the world's oceans. The SPB had drifted north to reach a position in the northern hemisphere in the Permian, at a desert belt latitude of 10° and 30° (Glennie, 1998). The Pennine High, Mid North Sea High, Ringkobing-Fin High and London Brabant Massif were persistent highs at this time, evidenced by the onlapping of Rotliegend sediments (Cartwright, 1990).

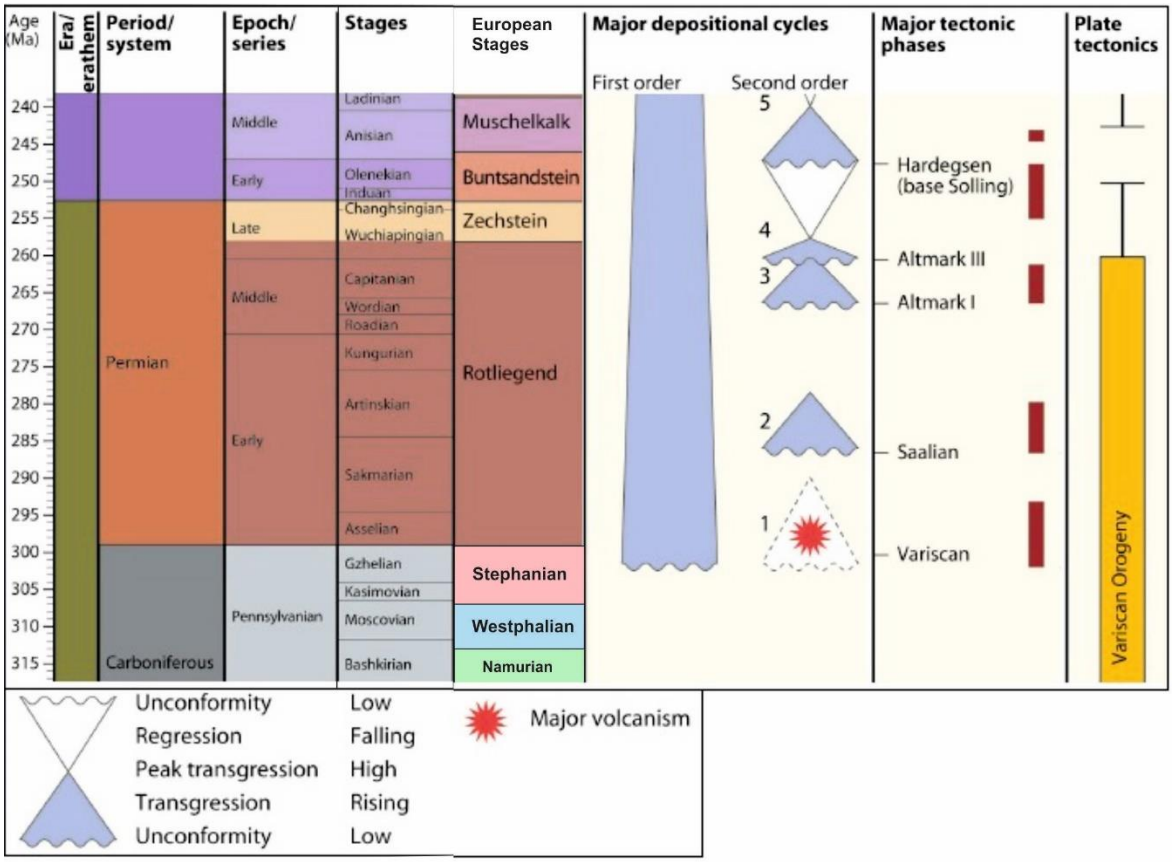


Figure 2.14 Major tectonic phases throughout the Permian and their subsequent unconformities. After Pharaoh et al. (2010)

In the Late Rotliegend, sediments were deposited in an inter-montane basin, structurally bound by the East Midlands shelf to the south, and the Mid North Sea High to the north (Howell & Mountney 1997). These Upper Rotliegend sediments can be lithostratigraphically divided as the Silverpit Claystone Formation and the Leman Sandstone Formation. They were deposited in a desert environment, which unconformably eroded Upper Carboniferous stratigraphy. Ephemeral fluvial systems drained off the London Brabant massif and flowed north towards the Silverpit Lake (Figure 2.15, McKie 2011). The Leman Formation is predominantly fluvial and aeolian sandstones, while the Silverpit Formation consists of playa lake mudstones and siltstones with discrete halite horizons (Glennie 1986).

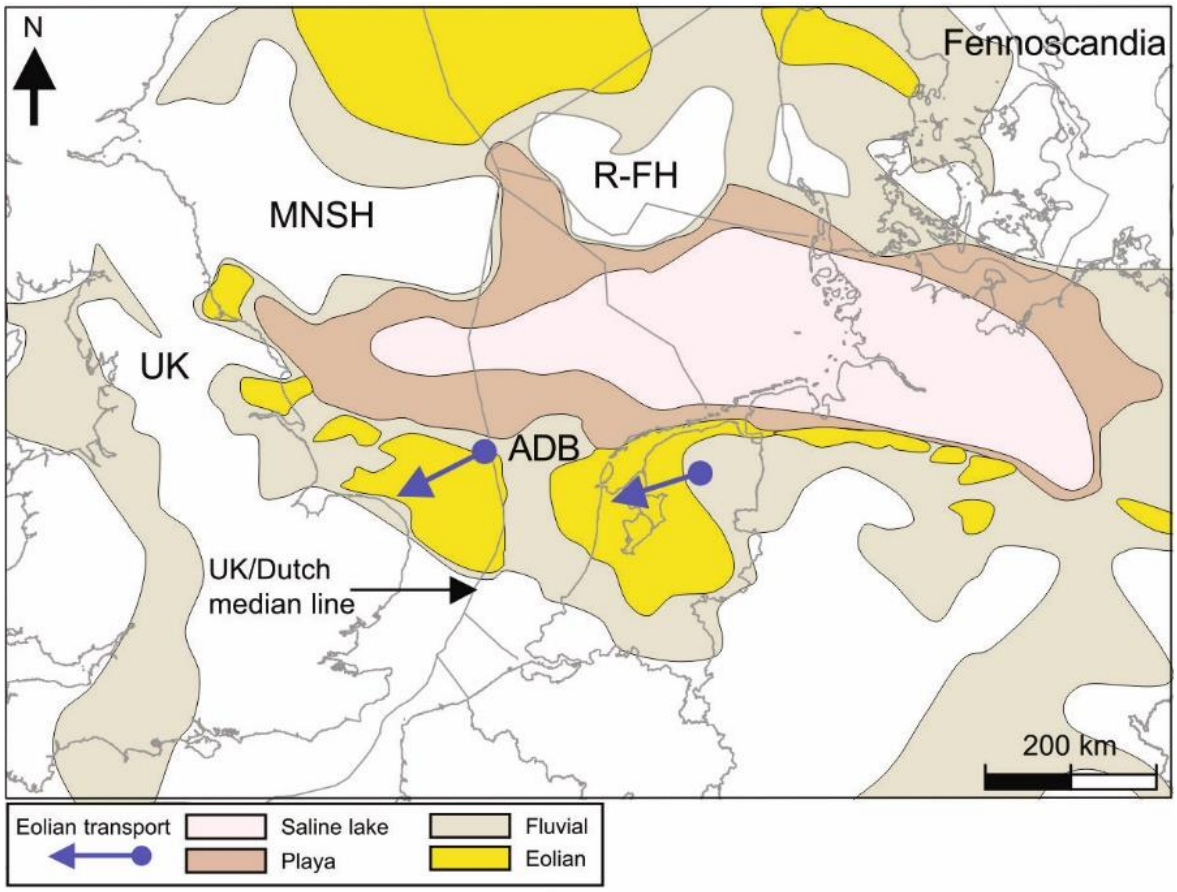


Figure 2.15 Regional upper Rotliegend facies distribution in the SPB (after McKie 2011). Playa and saline lake facies define the Silverpit Formation. Aeolian/eolian and fluvial facies define the broad distribution of the Leman Sandstone Formation.

The deposition of the Rotliegend was accompanied by minor faulting, evidenced by growth packages in the hanging wall of the Dowsing Fault (Quirk, 1997). The Cleaver Bank High and Elbow Spit High were present at this time but poorly defined (Van Hoorn 1987).

In the Late Permian, thermal relaxation of the lithosphere continued as did the northwards subduction of the Paleotethys Ocean beneath the southern margin of Europe. The SPB had been flooded by Arctic seas at this time (Zeigler, 1988) and restricted marine conditions resulted in the accumulation of the Zechstein evaporites and carbonates, controlled by thermal subsidence (Ter Borgh, 2018). The Zechstein sediments onlap the Mid North Sea High and Ringkobing-Fin High (Cartwright, 1990), indicating that they were still topographic highs at this time.

2.3.4 Triassic

The Triassic development of the NWECB is mostly concerned with the rifting of Pangea. Continued northward subduction of the Paleotethys ocean beneath Eurasia was accompanied by the northward drift of the Cimmerian superterrane that rifted off Gondwana's northern margin during the Permian (Pharaoh et al., 2010).

2.3.4.1 Hardegsen Tectonic Phase (Early Triassic)

A North Sea rift system (Figure 2.16) transected the Northern and Southern Permian basins (Ziegler, 1992) in the Early Triassic, forming the Central Graben system. Extension was orientated E-W to NE-SW forming a system of N-S faults.

2.3.4.2 Early Cimmerian Tectonic Phase (Middle Triassic)

Sediments were deposited in a shallow marine environment in the SPB during a global sea-level highstand in the Middle Triassic (Aigner and Bachmann, 1992). The development of salt walls at the central graben bounding faults suggests that rifting was occurring at this time (Remmelts, 1996).

The Danish Central Graben was undergoing active faulting in the Late Triassic (Cartwright, 1989). Salt diapirism began due to the rapidly developing sedimentary load. Syn-depositional displacement occurred on the Dowsing and South-Hewett faults from the Late Triassic to Mid-Jurassic (Coward and Stewart, 1995). Strike-slip faults and negative flower structures were formed by a dextral transtensional regime. The Cleaver Bank High formed an intermediate platform at this time (Pharaoh et al., 2010).

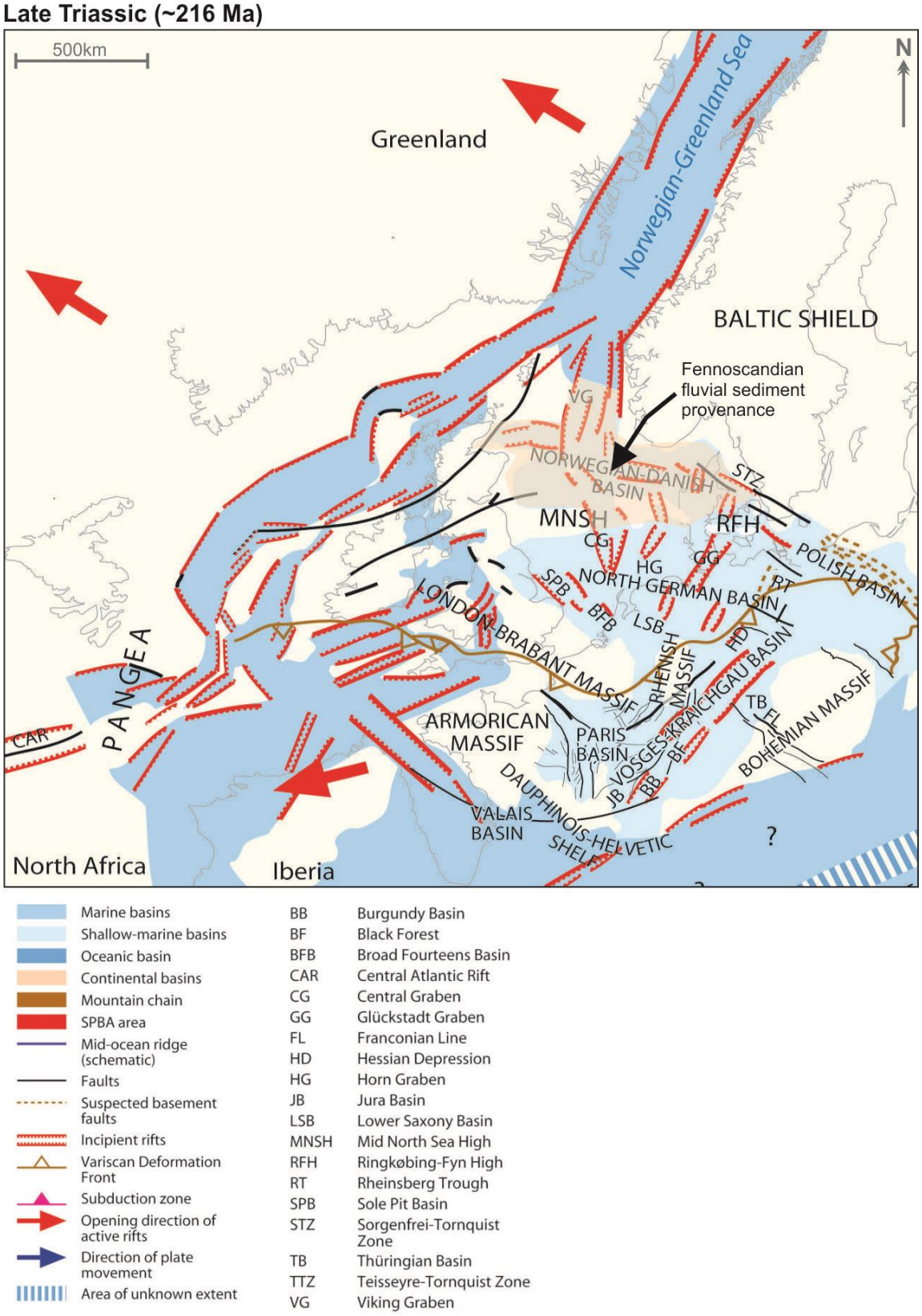


Figure 2.16 Late Triassic tectono-stratigraphic map with main structures and depositional environments. After Pharaoh et al. (2010), modified after McKie (2011)

2.3.5 Early Jurassic – Early Cretaceous

2.3.5.1 Early Jurassic Rifting

The North Sea rift system remained active in the Early Jurassic, with rifting in the Dutch Central Graben and Viking Graben (Pharaoh 2011). Apart from rifting in these areas, and the exception of the Broad Fourteens Basin, the Early Jurassic was a time of relative tectonic quiescence in the Anglo-Dutch Basin. Subsidence of the Sole Pit Trough was controlled by movements on the Dowsing-South Hewett and Flamborough Head Fault zones at this time (Van Hoorn 1987). The Cleaver Bank High was a platform during this time and is postulated to have accumulated a sedimentary succession hundreds of metres thick (Schroot & De Haan 2003).

2.3.5.2 Middle Jurassic (Middle Cimmerian)

Doming and uplift in the Central North Sea began in the Mid Jurassic (Aalenian) known as the Mid-Cimmerian event. This doming was postulated to be in response to the impingement of a transient mantle plume on the lithosphere (Underhill and Partington, 1993). The Mid-Cimmerian event resulted in uplift of the Dutch offshore and subsequent erosion of the Cleaver Bank High, locally down to the Carboniferous. The most severe erosion took place in the north of the Cleaver Bank High, adjacent to the Dutch Central Graben. An estimated 2000m of Lower Jurassic and Triassic sediments were eroded on the Cleaver Bank High from the Mid-Cimmerian event (Glennie, 1986). This left Permian and Triassic strata unconformably overlain by post-rift Lower Cretaceous. The Step Graben was also uplifted and eroded down to the Triassic and Lower Jurassic. Meanwhile, subsidence continued in the central graben accumulating a thick and complete Jurassic succession (Heybroek 1975, Ziegler 1990, Underhill & Partington 1993)

2.3.5.3 Late Jurassic - Early Cretaceous rifting (Late Cimmerian Tectonic Phase)

In the Late Jurassic (Figure 2.17), a strike-slip faulting regime was initiated and later intensified in the Early Cretaceous at the southern end of the North Sea rift system. This involved the transtensional subsidence of N-S oriented basins and transpressional uplift of intervening highs. Regional erosion occurred at this time across western and central Europe due to a eustatic lowstand and lithospheric deflection/doming (Ziegler, 1990).

Fault controlled subsidence of the Sole Pit Trough and Cleveland Basin continued, still controlled by the Dowsing Fault Zone evidenced by syn-depositional packages of Lower Cretaceous (Cameron et al., 1992). Sea floor spreading in the North Atlantic began in Aptian - Ablian (Pharaoh et al., 2010).

2.3.6 Late Cretaceous – Cenozoic

The transition into the Late Cretaceous involved the cessation of the strike-slip system and the deactivation of the North Sea rift, with rifting moving to the Atlatic between Norway and Greenland. The Late Cretaceous-Cenozoic tectonic evolution was driven by the convergence of Africa-Arabia and Eurasia, related to the crustal separation between Africa and South America in the equatorial South Atlantic (Dewey et al., 1989). Repeated fluctuations in the magnitude and orientation of the regional intraplate stress field caused subtle reactivations of the majority of pre-Cenozoic structural elements (Kley and Voigt, 2008). These fluctuations were controlled by the Alpine (~90-35Ma) and Pyrenean (34-31Ma) orogens. The earliest Eocene crustal separation between Greenland and Europe due to increasing ridge push forces exerted by the Arctic-North Atlantic sea-floor spreading axes (Ziegler et

al., 1998). This Alpine plate tectonic phase was punctuated by four phases of inversion from the Late Cretaceous to Cenozoic (Figure 2.18).

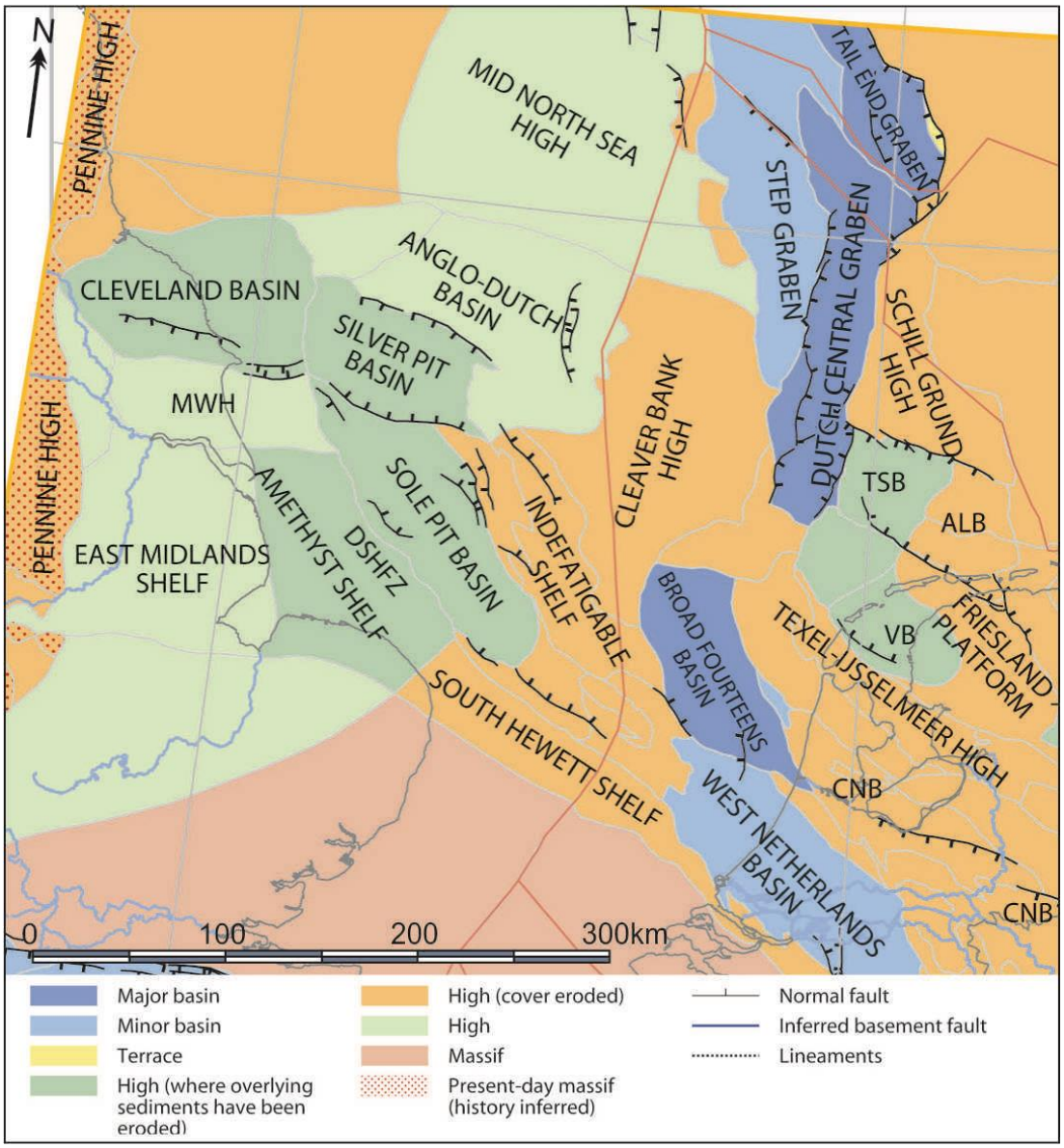


Figure 2.17 Late Jurassic (Kimmeridgian, 152 Ma) Tectonic Elements of eastern England and the Southern North Sea. VB = Vlieland Basin. CNB = Central Netherlands Basin. Modified after Pharaoh et al. (2010).

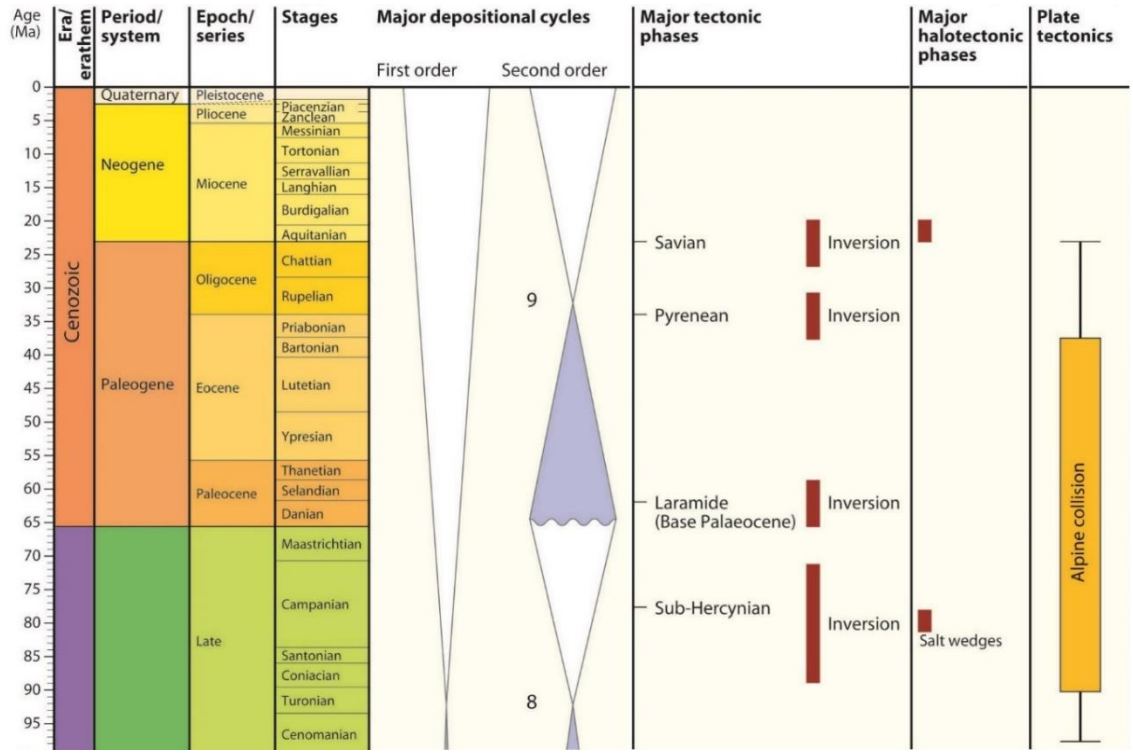


Figure 2.18 Late Cretaceous – Cenozoic tectonic phases and inversion events. Four main inversion events are recorded during the Alpine plate cycle and two phases of halokinesis. After Pharaoh et al. (2010).

2.3.6.1 Sub-Hercynian Inversion (Coniacian-Maastrichtian)

Contractional reactivation of pre-existing structures began in the late Turonian (Pharaoh et al 2010). In the Coniacian, tensional and transtensional Mesozoic basins experienced pulsating phases of inversion. NW-SE striking fault zones were the locus for deformation in the SPB. The geometry of the inversion structures produced, and the transpressively reactivated NW-SE faults, indicates a N-S to NE-SW compression (Scheck-Wenderoth et al., 2008).

The NW-SE trending Sole Pit Basin underwent a strong inversion during the Sub-Hercynian event (Badley et al., 1989). The Danish Central Graben (Cartwright, 1989) was also inverted during the Cenomanian. The Cleaver Bank High area was affected by the compression, generating localised pop-up structures at Rotliegend levels, following NW-SE, NE-SW and WNW-ESE trends. Reverse reactivation of prominent WNW-ESE faults formed prominent ridges and an anastomosing and

complex fault pattern, possibly due to periodic changes in the orientation of compressional stress during the Alpine orogeny.

2.3.6.2 Laramide Inversion (Palaeocene)

The western area of the SPB was incorporated into subsiding North Sea thermal sag basins, evidenced by the high thicknesses of the North Sea Group deposits. The Laramide pulse of intraplate compression began in Early Cenozoic times with a period dominated by crustal deformation and a change to a clastically dominated sedimentation regime. The N-S to NE-SW direction of regional contraction continued (Nalpas et al., 1995).

2.3.6.3 Pyrenean Inversion

A riedel fault pattern at the base Cenozoic level suggests dextral shearing during the Pyrenean, controlled by the reactivation of deeper faults (Oudmayer & De Jager, 1993). In the Silverpit Basin, the reactivation of basement faults under the dextral transpressive regime triggered widespread diapirism of the Zechstein salt, producing NW-SE trending salt pillows and walls (Pharaoh et al., 2010). In the Mid North Sea High area, the southern bounding fault for the North Dogger Shelf shows evidence for a Mid-Cenozoic reverse reactivation (Cameron et al., 1992).

2.3.6.4 Savian Inversion (End Oligocene-Early Miocene)

The Savian compressional pulse resulted in further uplift and inversion across the NWECB. The Cleveland Basin was particularly affected, with maximum uplift estimates of 2500m (Bulat and Stoker, 1986). The east-west trending Vale of Pickering-Flamborough Head Fault Zone may have developed at this time by sinistral transcurrent Mesozoic movement on a deep basement lineament, followed by dextral compression (Pharaoh et al., 2010).

2.3.6.5 Present Day

The present day stress field measurements reveal an overall NNW-SSE maximum horizontal compressive stress across the NWECB. This is attributed to the ridge push mechanism ongoing at the North Atlantic rift and the collisional coupling of the foreland lithosphere with the Alpine-Carpathian Orogen (Golke and Coblentz, 1996). For the Anglo-Dutch Basin, present day stress trajectories are predominantly northwesterly. There is a strong decoupling caused by the Zechstein salt which is evidenced by the differences in SHmax for sub-salt and supra-salt (Lempp & Lerche 2006). The table in

Figure 2.19 presents a summary of this tectonic evolution in this section.

2.4 Mid North Sea High

The Mid North Sea High is a terrane that lies between the Northern and Southern Permian Basins (Figure 2.20). Contrary to the name, it is not a single high mass but a series of basins and intervening granite cored highs and terraces (Donato et al., 1983). The basins are filled with Devonian-Carboniferous sediments (Figure 2.21) up to 6km in thickness (Leslie et al., 2015).

2.4.1 Elbow Spit Platform and High

The Elbow Spit Platform is the southernmost platform high within the MNSH terrane area. It is located in the northern Dutch sector, of the Southern North Sea. It overlies a major basement terrane boundary between the two large palaeocontinents Avalonia and Baltica (Figure 2.2). At this boundary, a separate crustal unit consisting of a collapsed Caledonian accretionary complex is postulated to exist (Smit et al., 2016).

Event Name	Period	Epoch	Stage	North Sea Stage	Plate Tectonic Cycle	Tectonic Event	Regional Stress orientation	Unconformities	Halotectonics	SNS Faulting regime	Resulting structuration	References
Caledonian	Devonian-Carboniferous	Late-Early			Variscan Orogeny	Extension from back arc basin formation	N-S/NNW-SSE			Oblique extension on NW-SE faults	NE-SW and N-S to NW-SE (NW inhertied from Lower Pal fold and thrust belt)	Leeder & Hardman 1990, Corfield et al 1996
Variscan	Carboniferous	Pennsylvanian	Gzhelian - Asselian	Stephanian	Variscan Orogeny	Regional Compression/Dextral mega shear	N-S/NNW-SSE	Variscan/Base Permian	-	Dextral and Sinistral Strike Slip	NW-SE dextral strike-slip, NE-SW/NNE-SSW sinistral strike-slip faults, intrusive and extrusive magmatism	Arthuad & Matte, 1977; Zeigler, 1989; Lamarche, 2002;
Saalian	Permian	Early	Sakmarian - Artinskian	Rotliegend	Variscan Orogeny	Thermal Uplift	-	Saalian/Base Permian	-	Extensional faulting	Cessation of Variscan Magmatism, Saalian Erosion and Unconformity	Stille, 1924; Glennie, 1998
Altmark (I,III)	Permian	Middle	Wordian - Wuchiapingian	Rotliegend	Variscan Orogeny	Thermal Subsidence	-	Base Permian	-		Active faulting on the Dowsing-Hewett Fault Zone	Ziegler 1990, Bachmann & Hoffman, 1997; Van Wees et al. 2000
Hardegsen	Triassic	Early	Olenkian - Anisian	Buntsandstein	-	Regional Extension	E-W/ NE-SW	Base Solling	Rafting		Central Graben System and N-S trending faults	Zeigler 1990; Ter Borgh et al. 2018,
Early Cimmerian	Triassic	Late	Carnian - Norian	Keuper	Pangea Breakup	Regional extension (rifting) and subsidence	NW-SE	Base Arnstadt, Base Norian, Base Rhaetian	Salt Diapirism	Rifting (normal faulting) Dextral Transtension	Syn-depositional displacement on DSHFZ, active faulting on Dutch Central Graben and Broad Fourteens Basin, negative flower structures in upper Triassic, Cleaver Bank High was a Platform, NE-SW trending faults	Ziegler 1988, 1990a; Van Hoorn 1987;
Middle Cimmerian	Jurassic	Middle	Aalenian - Bathonian	Dogger	Pangea Breakup	North Atlantic Sea Floor Spreading, Doming and uplift	-	Base Dogger	Y		Subsidence of Sole Pit Trough controlled by the DZFZ movements, erosion of Cleaver Bank High down to the Carboniferous. Erosion of the Step Graben down to the Triassic.	Underhill & Partington 1993; Surlyk & Ineson 2003,
Late Cimmerian	Jurassic-Cretaceous	Late-Early	Kimmeridgian - Ryazanian	Malm	Pangea Breakup	Regional Extension	E-W	Base Buckberg	Y	Transtensional subsidence, strike-slip	Transtensional subsidence of north-west oriented basins and transpressional uplift of interveining highs, continued fault controlled subsidence of Sole Pit Trough and Cleaver Bank High	Cameron et al. 1992,
Sub-Hercynian	Cretaceous	Late	Coniacian	Maastrichian	Alpine Collision	Inversion/Regional Compression	N-S/NE-SW	-	Salt wedges	Transpressive reactivation	Transpressive reactivation of NW-SE faults, Inversion of Sole Pit, Broad Fourteens and Dutch Central Graben,	Scheck-Wenderoth et al. 2008; Kley and Voigt, 2008
Laramide	Paleogene	Paleocene-Eocene	Danian - Thanetian	-	Alpine Collision	Inversion/Regional Compression	N-S/NE-SW	Base Palaeocene	N	Transpressive reactivation	Inversion of the Danish Central Graben, localised pop-up structures at Rotliegend levels on the Cleaver Bank High that trend	Nalpas et al. 1995, Cartwright 1989
Pyrenean	Paleogene	Eocene - Oligocene	Priabonian - Rupelian	-	Alpine Collision	Inversion/Regional Compression		-	Salt diapirism NW trending salt walls and pillows	Dextral Transpressional reactivation/reverse reactivation	Riedel fault pattern at Base Cenozoic, reactivation of basement faults in the Silverpit Basin, reverse reactivation of North Dogger Shelf bounding fault	Oudmayer & De Jager 1993, Pharaoh et al. 2010, Cameron et al 1992
Savian	Paleogene - Neogene	Oligocene - Miocene	Chattian - Aquitanian	-	Alpine Collision	Inversion/Regional Compression		-	Y		Uplift in the West Netherlands and Cleveland Basins	De Jager 2007
Present	-	-	-	-	Alpine Collision	Ridge push in north atlatic	NW-SE	-	-		Borehole breakouts and hydraulic fractures and sub salt levels	Golke et al. 1996

Figure 2.19 Synthesis and summary of the main tectonic phases through time and resulting structures

This is characterised by a zone of lower P wave velocity in the lower crust above the Moho (Figure 2.2). The ESH is a granite cored high calibrated by Well 17-A which is postulated to be a batholith, supported by the area having a higher Bouguer gravity anomaly (Figure 2.6).

2.4.1.1 Fault Systems

The structure of the Elbow Spit Platform area was relatively unknown until recently when Ter Borgh et al. (2018) used 2D and 3D seismic data (DEF survey 2011-12) to develop a structural framework for the northern Dutch Offshore for Palaeozoic to recent. They identified three different fault trends in the northern Dutch sector. A WNW-ESE trending set of normal faults with throws from 10s-100s of metres, identifiable on 3D seismic data on the southern and northern margins of the ESP. These faults have a moistly Carboniferous offset with smaller Rotliegend offsets. Ter Borgh et al. (2018) attribute the formation of these faults to regional extension in the Late Devonian-Early Carboniferous, despite the faults having a layer bound geometry, no syn-rift packages in the Lower Carboniferous stratigraphy and appear detached from underlying stratigraphy. This interpretation is also surprising considering the orientation of extension during this time is considered to be N-S to NNW-SSE (Fraser et al .1990, Leeder & Hardman 1990), and they do not appear to be basement faults. Could it be therefore that these faults were formed by a different mechanism than regional extension?

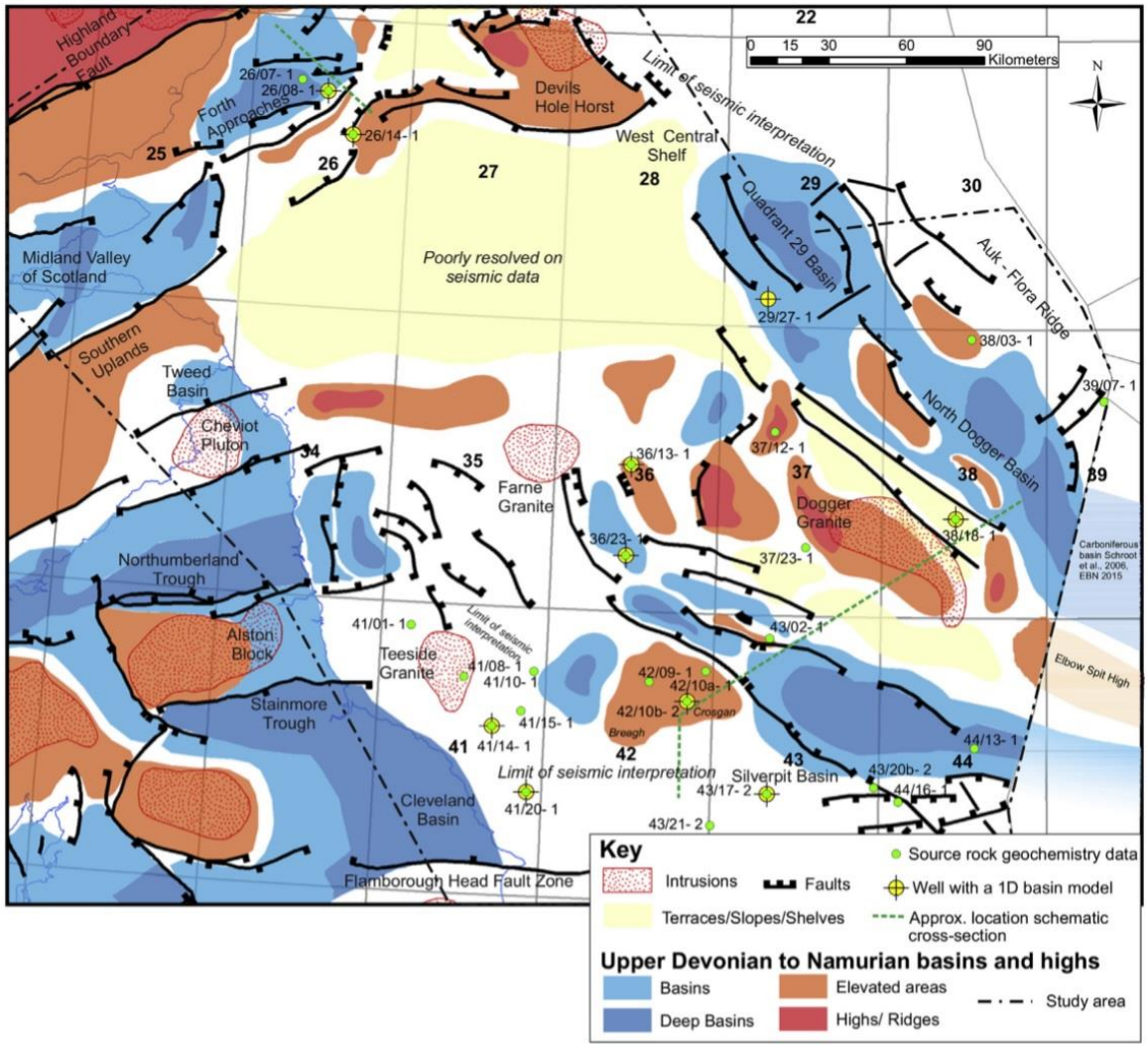


Figure 2.20 Structural overview of the Devonian and Carboniferous Basins across the Mid North Sea High and Northern England. From Monaghan et al. (2017)

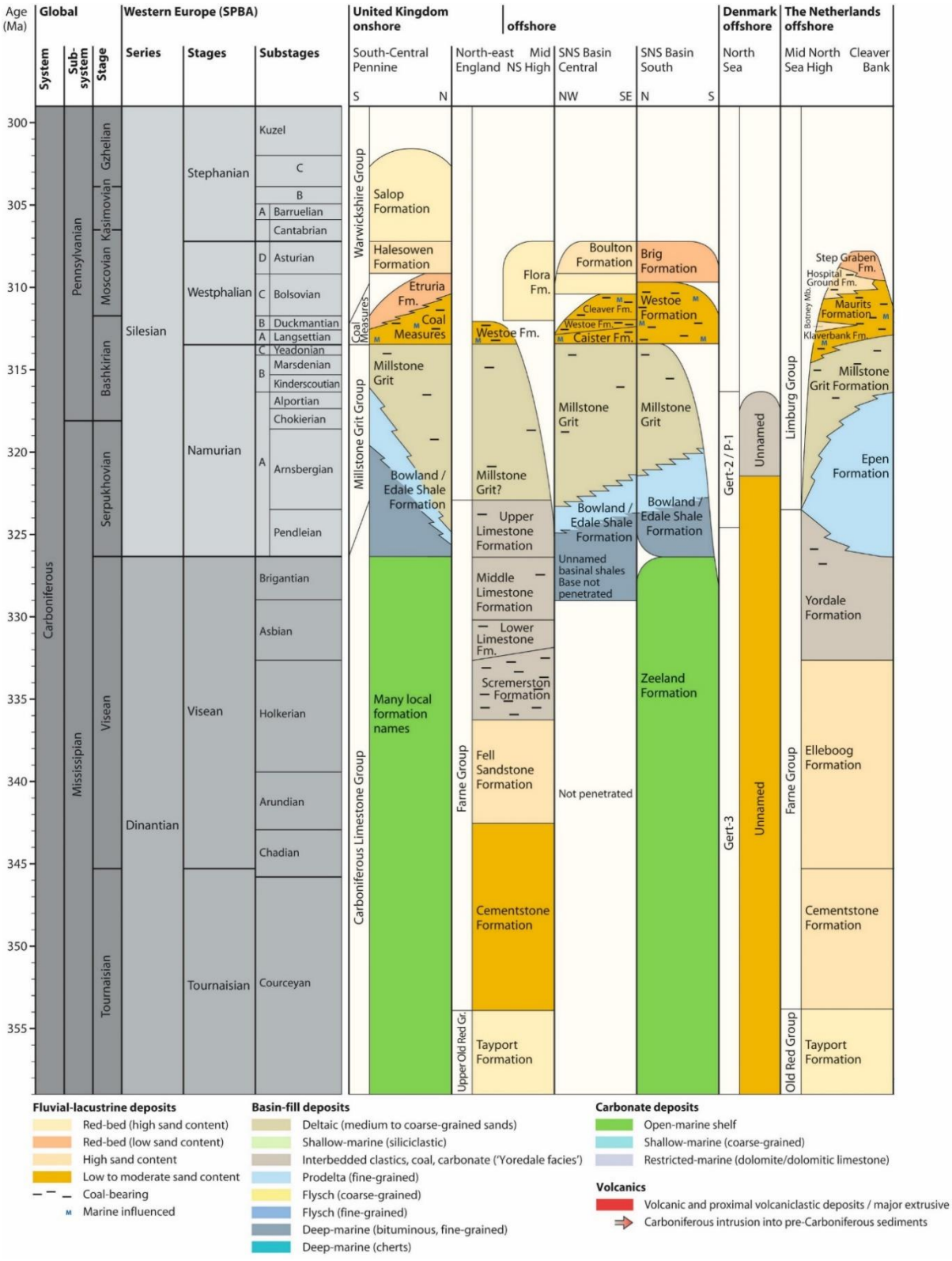


Figure 2.21 Carboniferous chrono and lithostratigraphy for the Pennine Basin, Anglo-Dutch Basins and Mid North Sea High. After Kombrink et al. (2010).

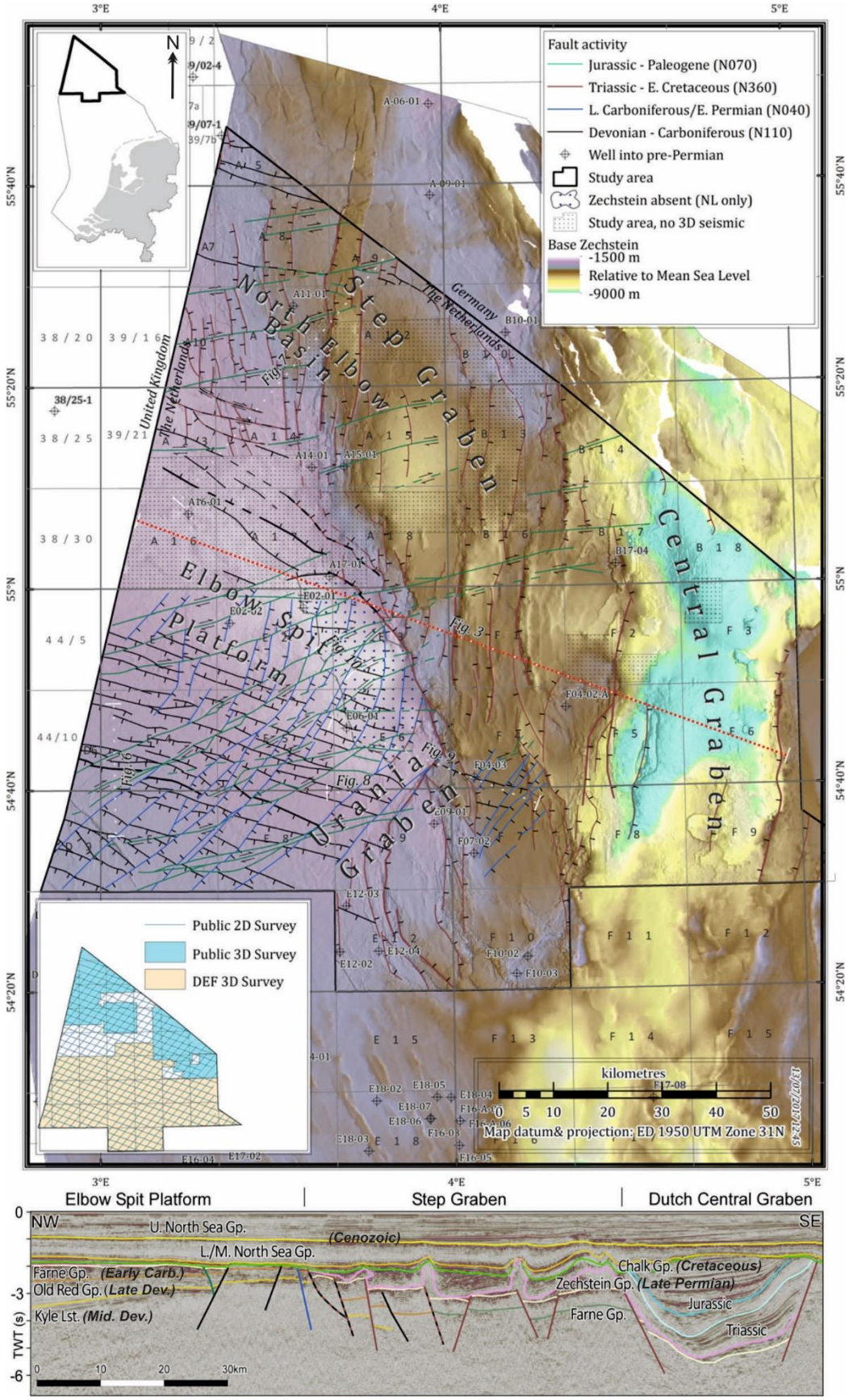


Figure 2.22 Structural framework for the northern Dutch Offshore by Ter Borgh et al., (2018). Faults are shown at Base Permian level or for older faults the shallowest offset reflection. Posiiton of cross section is indicated by the red dashed line.

A NE-SW trend of normal faults were also identified by Ter Borgh et al. (2018). The authors report that these faults have throws ranging from 10s to 1000s metres and offset intra-Carboniferous reflections with no significant offset of the Upper Rotliegend. They conclude that their movement was post Visean and pre-deposition of the Rotliegend. Their formation mechanism is attributed to regional extension from the Late Carboniferous – Early Permian.

A set of ENE-WSW strike-slip faults are also identified by Ter Borgh et al. (2018) They interpret visible dextral offsets of other fault trends of up to 1km. Mapped over 90km on the ESH. Offset units from Devonian-Palaeogene. Transpressive push-ups and transtensional pull-apart structures are observed in cross section that utilise the older fault trends to control the deformation. The authors argue that the Zechstein salt had a controlling effect on the structural styles, with overlying units showing only mild deformation where the salt is present and stronger deformation where it is absent. Ter Borgh et al. (2018) attribute these faults to an initial movement in the Early Cretaceous with a reactivation in the Late Cretaceous-Palaeogene. The mechanism they give is due to strain partitioning between the between the Danish Central Graben to the north and Dutch central graben due to alternations between extension orientation. The heterogenous underlying basement may contribute to this.

There is a paucity of NW-SE faults in the Elbow Spit Platform compared to most of the Dutch offshore (Ter Borgh et al. 2018). They are not observed north of block E12 which coincides to Caledonian accretionary complex basement (Smit et al., 2016). Ter Borgh et al. (2018) suggest that the contrast in structural patterns is from this difference in basement.

The current published literature (Ter Borgh et al. 2018) attributes the formation of all the faults on the ESP to regional extension, even when it is contradictory to the direction of regional extension evidenced by coeval structures. This suggests another mechanism for formation and is explored in the research Chapters of this thesis.

2.5 Offshore Central Anglo-Dutch Basin

The Anglo-Dutch basin (previously called the Southern North Sea Basin) is a Carboniferous depocentre comprised of sub-basins and half grabens. It is bounded to the west by the genetically related Pennine Basin and to the north by the Mid North Sea High terrane (Corfield et al., 1996). This contrasts with the interpretation by Coward (1990) who asserted that the area to the north east of the Dowsing Fault Zone was a morphologically smooth and almost horizontal depositional area during the Early Carboniferous' (Figure 1.2).

The sub-basins follow the dominant NW-SE structural grain that curves to join the mostly E-W onshore sub-basin trend. The orientation of the major Mesozoic basins across the Southern North Sea mirrors this and clearly demonstrates the structural inheritance of this trend (Leeder, 1982). These basins are controlled by major NW-SE orientated faults such as the Dowsing-South Hewett fault system, which are reactivated Caledonian basement lineaments (Pharaoh, 1999). The dominant NW-SE fault pattern, which has been attributed to an inherited structural grain from as early as the Late Silurian closure of the Tornquist Sea (see section 2.3.1.2), was first indisputably active in a dextral transpressional sense during the Stephanian/Autunian (Oudmayer & de Jager, 1993).

2.5.1 Silverpit Basin and Adjacent Areas

The Silverpit Basin is NW-SE trending Carboniferous sub-basin located in the UK southern North Sea within Quadrants 43, 44, and 49. It is bounded to the northeast and southwest by the shelf areas of the Murdoch block and Skate Ridge respectively (Figure 2.23). Fraser et al.(1990), Fraser & Gawthorpe (1990), Corfield et al. (1996) argue that the NW-SE orientated Silverpit Basin only underwent a mild regional inversion (less than 2% shortening) due to its orientation relative to the N-S to NNW-SSE compressive stress from the south in the Late Carboniferous.

The Pre-Zechstein fault patterns in the Silverpit Basin and Murdoch Block have been studied previously using 2D and 3D seismic data. Corfield et al. (1996) Hollywood & Whorlow (1993) use only 2D data while Oudmayer & de Jager (1993) and Quirk & Aitken (1997) use 2D and 3D data. They have collectively identified four fault sets across the Silverpit Basin and adjacent areas, with controversy existing regarding their formation mechanisms and timing of movement.

2.5.1.1 E-W Faults

A suite of E-W orientated normal faults are documented by Hollywood & Whorlow (1993) & Quirk & Aiken (1997). They are described as being very straight in map view with lengths up to 10s of kilometres. Intra-Carboniferous throws up to 500m are observed and stratal reflections in the hangingwall are folded into rollover anticlines (Figure 2.24). They exhibit limited reverse throw at Rotliegend levels that is expresses mild doming at Rotliegend levels (Oudmayer and de Jager, 1997). Uniform thicknesses of Rotliegend and Carboniferous sediments across the fault exhibit a lack of syn-depositional faulting at these times. Their timing of formation is assigned by Hollywood and Whorlow (1993) to be Late Carboniferous, pre-dating the formation of the NW-SE faults and deposition of the Rotliegend. Quirk and

Aitken (1997) attribute their formation to Early Permian rifting associated with thermal doming in the Saalian event (300-290Ma). Their reactivation is assigned to the Late Cretaceous by Hollywood and Whorlow (1993).

2.5.1.2 NW-SE Reverse Faults

A set of NW-SE reverse faults and associated folds were identified by Leeder & Hardman (1990). They are described by the authors and Hollywood & Whorlow (1993) to have consistent throws at Carboniferous and Rotliegend levels (Figure 2.25). The authors report that they have younger stratigraphy in the footwall indicating that they were initially active prior to the BPU erosion and reactivated once again after the deposition of the Rotliegend.

There is controversy in the literature regarding the slip histories of the NW-SE faults. Quirk and Aiken (1997) argue that they were compressionally reactivated Caledonian faults due to the observed normal offset of the Pre-Permian. They further claim that the monoclines are extensional rollovers and not formed by buckling generated by NE Variscan compression (Hollywood & Whorlow 1993).

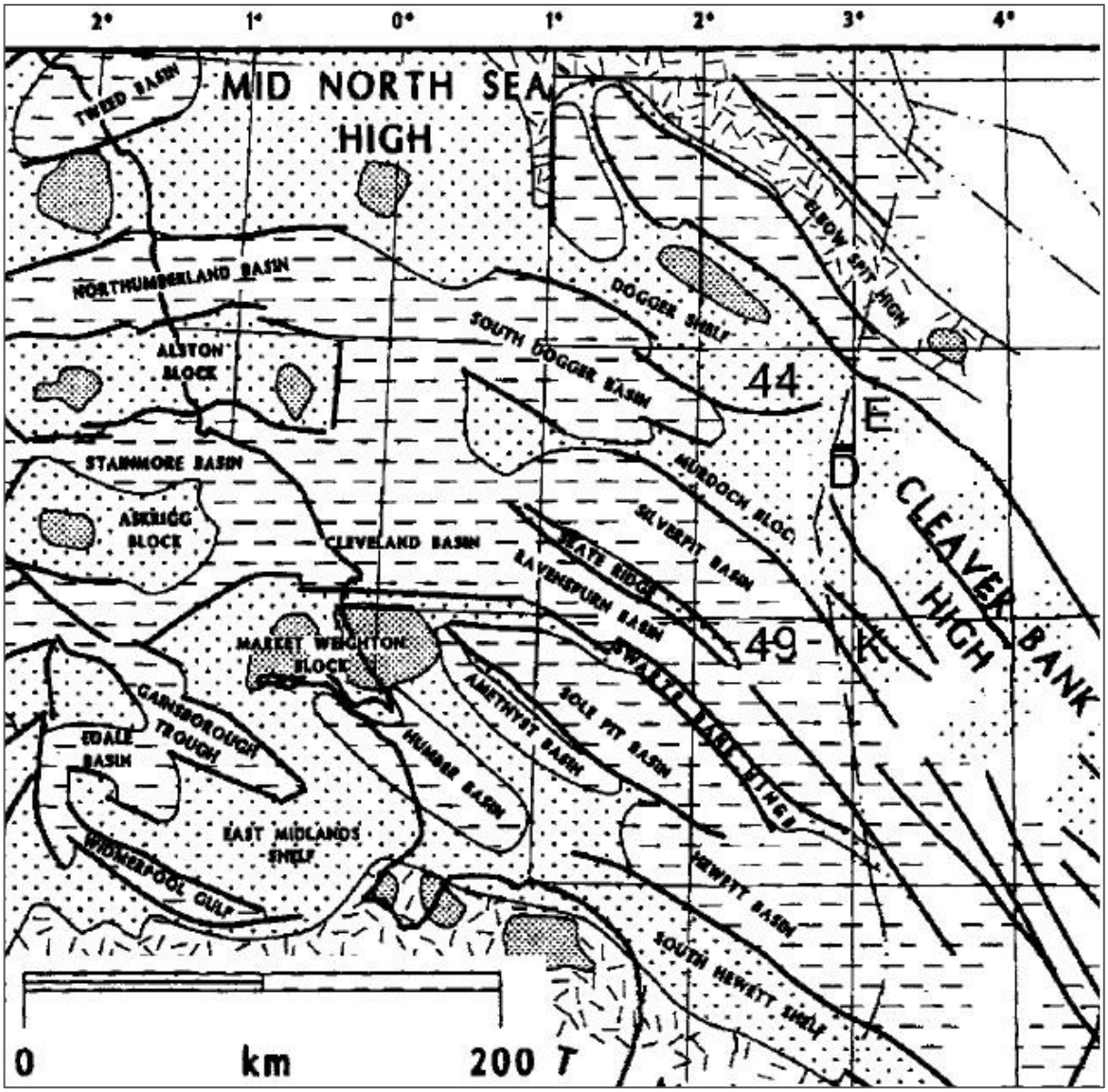


Figure 2.23 Structural framework of the Anglo-Dutch Basin during the early Carboniferous. Structural highs separating basins were found to be located over granite masses. After Besly (1998).

2.5.1.3 Other sets

Oudmayer & de Jager (1997) report high length to throw ratios observed on NW-SE faults and attribute these to the repeated reactivations. It is unclear however if they are referring to the reverse NW-SE faults or an additional set of NW-SE trending normal faults (Figure 2.26). A NE-SW cross fault trend is briefly mentioned by Oudmayer & de Jager (1997) with having minimal vertical offset, but no movement sense or timing is described. The confusion and controversy regarding the classification of faults in the Silverpit Basin suggests that the fault geometries and kinematics are more complicated than the currently defined fault sets.

2.5.2 Cleaver Bank High

The Cleaver Bank High is a Carboniferous platform area that is bound to the SW by the Silverpit Basin and to the NE by the Central Graben rift complex (Besly 1998). It experienced uplift in the Jurassic during the Late Cimmerian tectonic phase (Van Hoorn 1987). This coincided with the major rifting episode responsible for the formation of the Dutch Central Graben.

Fault sets identified within the Pre-Zechstein succession of the Cleaver Bank High have been studied previously using 2D and 3D seismic data (Quirk, 1997, Schroot and De Haan, 2003 Oudmayer & de Jager 1993).

2.5.2.1 Type A, B and C Faults

Instead of grouping faults by orientation, Schroot & de Haan (2003) classified the fault types based on their observed throw, grouping them into sets A, B and C (Figure 2.27a). Type A faults show normal offset at Base Permian and intra-Carboniferous levels, but these offsets do not have to be equal. This fault set includes the NW-SE high length/throw ratio faults discussed by Oudmayer & de

Jager (1993). These authors claim that Type A faults with equal offsets at Permian and intra-Carboniferous levels are Lower Jurassic in age.

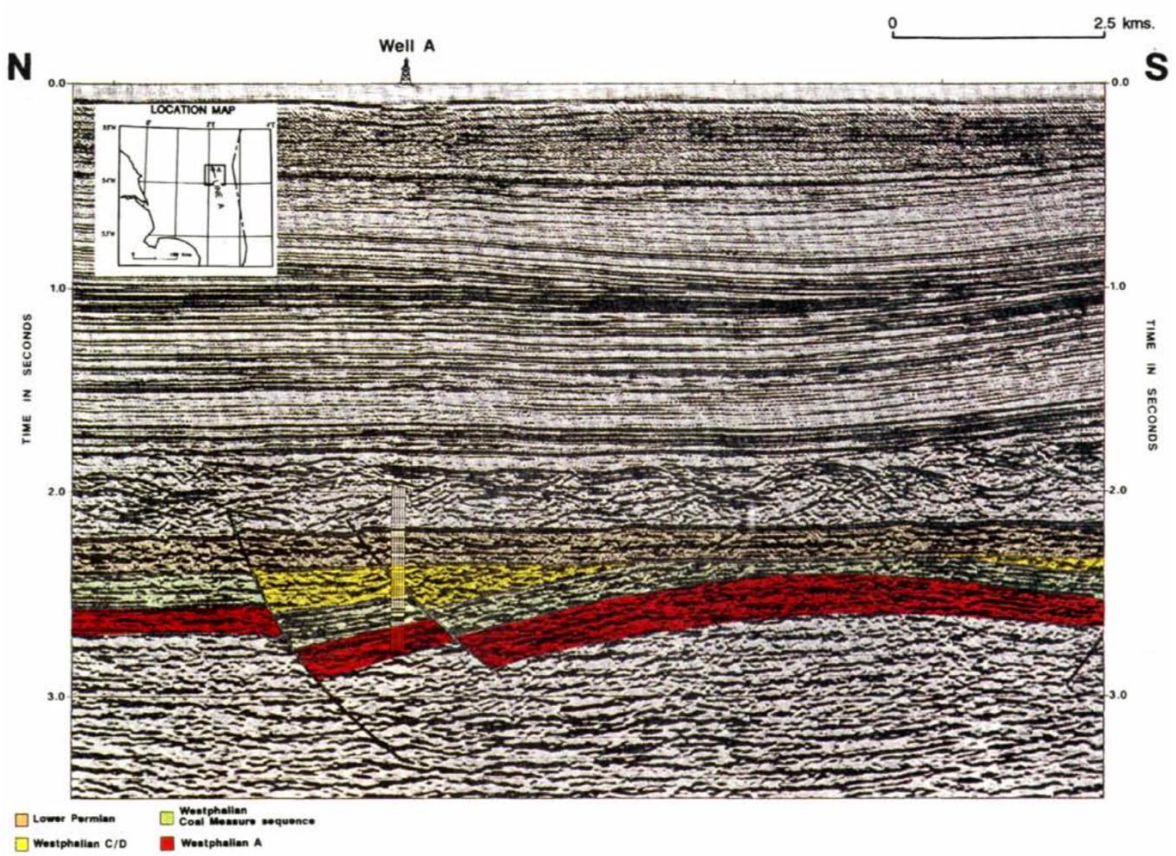


Figure 2.24 Seismic section imaging an E-W trending fault in the Silverpit Basin. Interpreted by Hollywood & Whorlow (1993) to have undergone normal offset in the Late Carboniferous with a slight reactivation after the deposition of the Rotliegend.

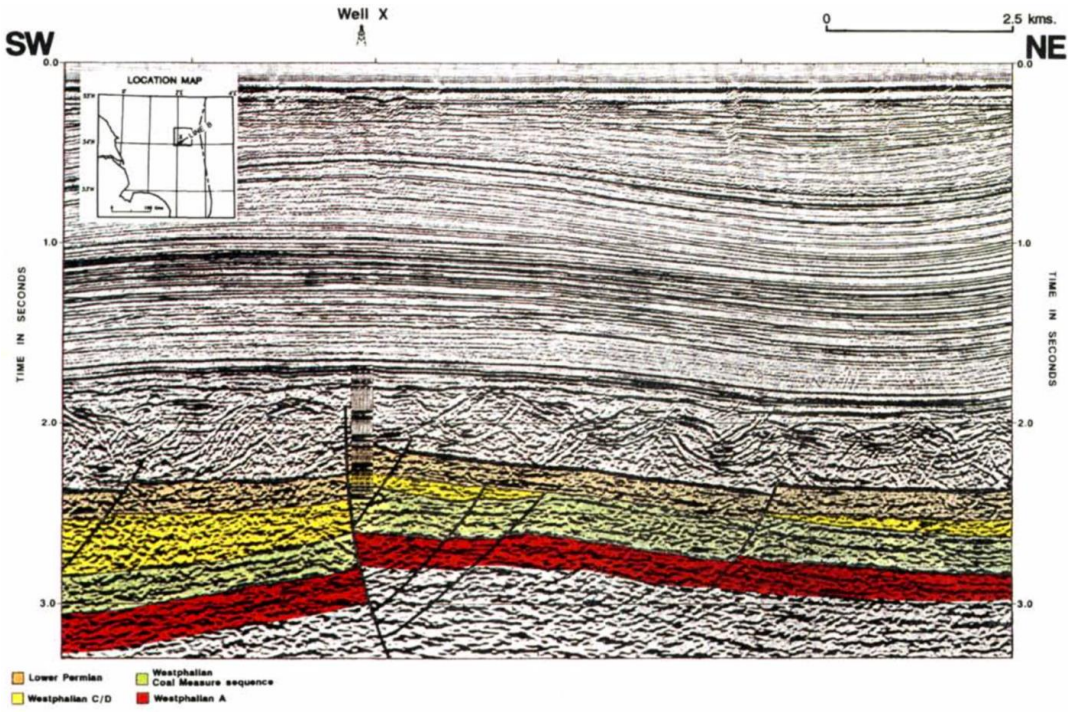


Figure 2.25 Seismic section imaging a reverse NW-SE fault in the Silverpit Basin. Interpretation of younger stratigraphy in the footwall by Hollywood & Whorlow (1993) suggesting that the fault originated before the Base Permian and was then reactivated after the deposition of the Rotliegend.

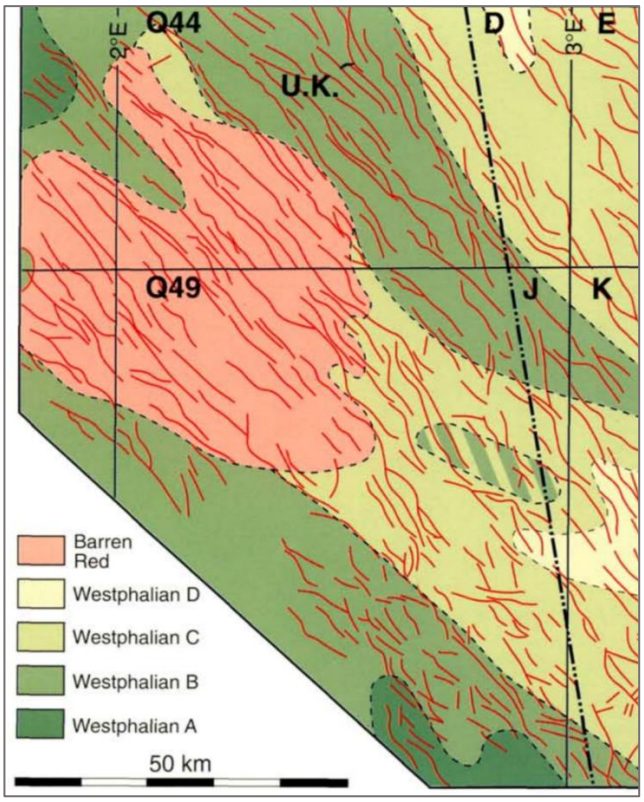


Figure 2.26 Fault pattern in the Pre-Zechstein interval of the Silverpit Basin by Oudmayer & De Jager (1993)

Type B faults exhibit a reversed throw at the Base Permian and trend E-W or NW-SE (Figure 2.28). Throw at Intra-Carboniferous levels are either reverse and smaller than BPU and Rotliegend throws, or are net normal. Their formation is attributed to be normal offset in the Late Carboniferous with a reverse reactivation in the Sub-Hercynian tectonic event in the Late Cretaceous (see section 2.3.6.1). Type C faults are reported to have normal throw at intra-Carboniferous level but no offset (or very slight offset) at the Base Permian. These faults have orientations of NE-SW, NW-SE and E-W in the CBH area (Schroot & de Haan 2003).

2.5.2.2 Folds

Folds oriented NW-SE with long wavelengths are also reported in the Carboniferous (Schroot & de Haan 2003), with intra-Carboniferous reflections truncated at the BPU across the area. This truncation concludes the folds were formed after the Westphalian D but before the deposition of the Rotliegend (Autunian).

2.5.2.3 E-W Shear Zones

Schroot & de Haan (2003) also postulate the existence of major E-W shear zones across the north of the CBH (Figure 2.27b). They are reported to be difficult to detect on 2D and 3D seismic data as net lateral throws are small due to repeated reactivations in opposite senses. They typically show strike-slip features such as flower structures and pull apart basins. The authors argue that the origin of these shear zones were extensional faults in the Devonian-Tournaisian, in which normal east-west trending faults were formed. Late Carboniferous compression then reactivated these faults as left lateral strike-slip zones, associated with the westward insertion of the North Sea-Baltic Plate (Coward 1990). Parts of the system were then locally reactivated in a normal sense during Late Carboniferous extension.

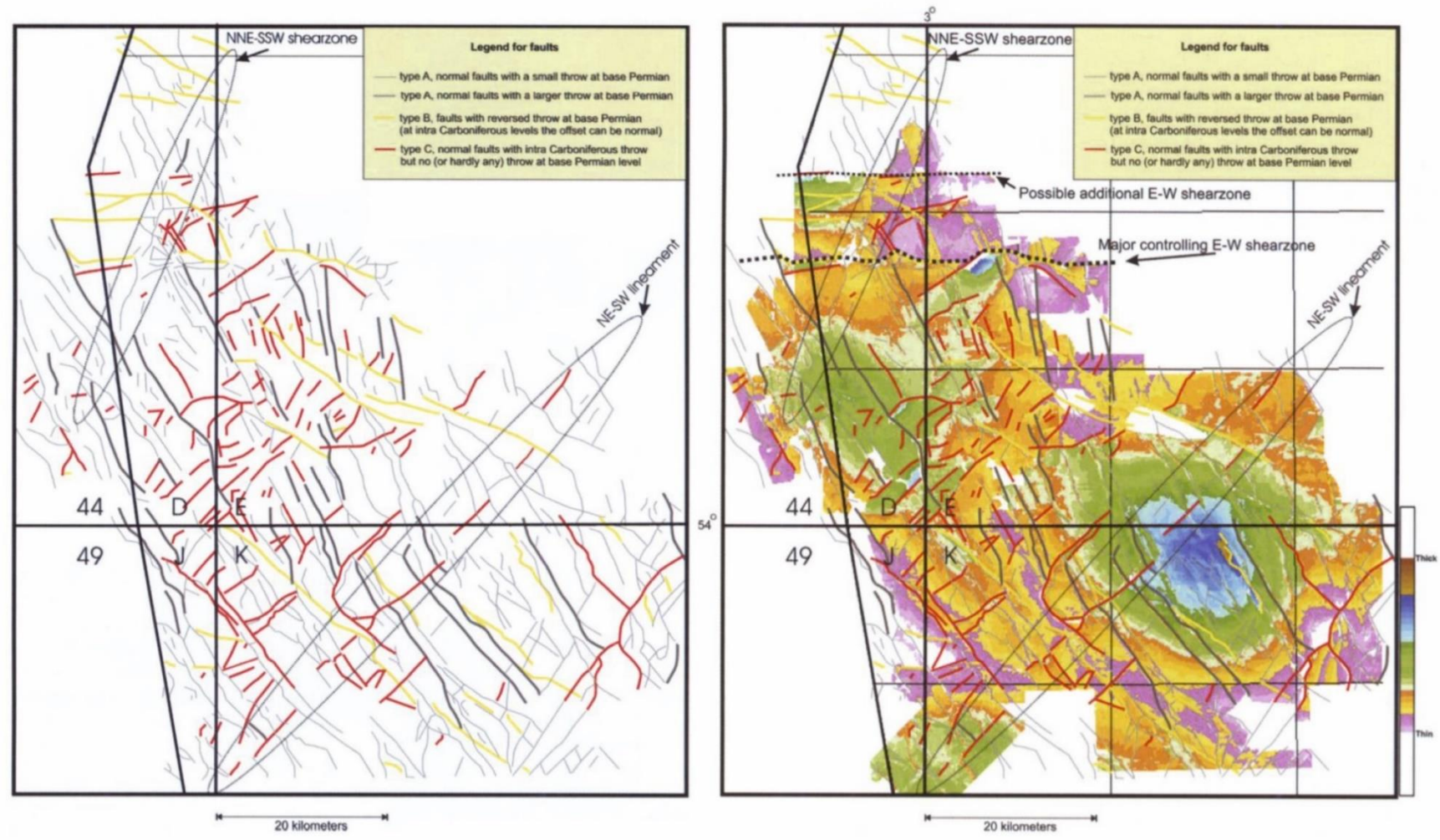


Figure 2.27 a) Intra-Westphalian fault map of the Cleaver Bank High by Schroot & De Haan (2003) indicating fault types. The authors indicate the presence of regional NE-SW and NNE-SSW lineaments b) Westphalian thickness map and positions of E-W shear zones. After Schroot & De Haan (2003)

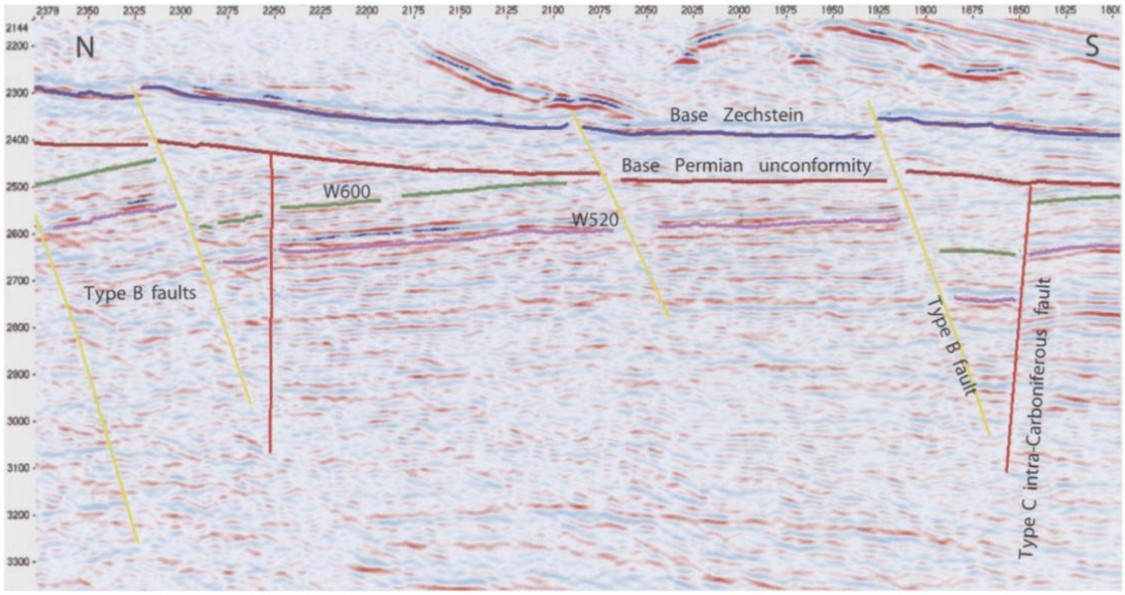


Figure 2.28 Seismic section through E-W orientated 'Type B' faults that exhibit normal throw at intra-Carboniferous level. Some 'Type C' faults are also intersected and show no reactivation after the BPU. After Schroot & De Haan (2003)

Finally, the Late Carboniferous faults were reverse reactivated in the Sub-Hercynian event (see section 2.3.6.1).Oudmayer and de Jager (1993) and Schroot and De Haan (2003) recognised that the NW-SE trending Type A faults have high length/throw ratios and attribute this to repeated reactivations. Since the stress regime would have only rarely been perpendicular to the trend, oblique slip along these faults is assumed. There is no strong evidence for lateral movements along these faults, there may be another reason for the high length-throw ratios observed on these faults.

2.6 East Pennine Basin

The East Pennine Basin is a terrane of genetically linked Carboniferous sub-basins on the East side of the Pennines, onshore England. The sub-basins are rhomb shaped half grabens that are orientated following the ‘Tornquist Trend’

(Fraser & Gawthorpe 2003). In the north east area of the Pennine Basin, they follow an E-W to ENE-WSW orientation i.e. Northumberland Trough, which they then progressively rotate to a WNW-ESE towards the south i.e. the Widmerpool Gulf. The basins are separated by intervening granite cored highs (Fraser & Gawthorpe 1990, Corfield et al 1996).

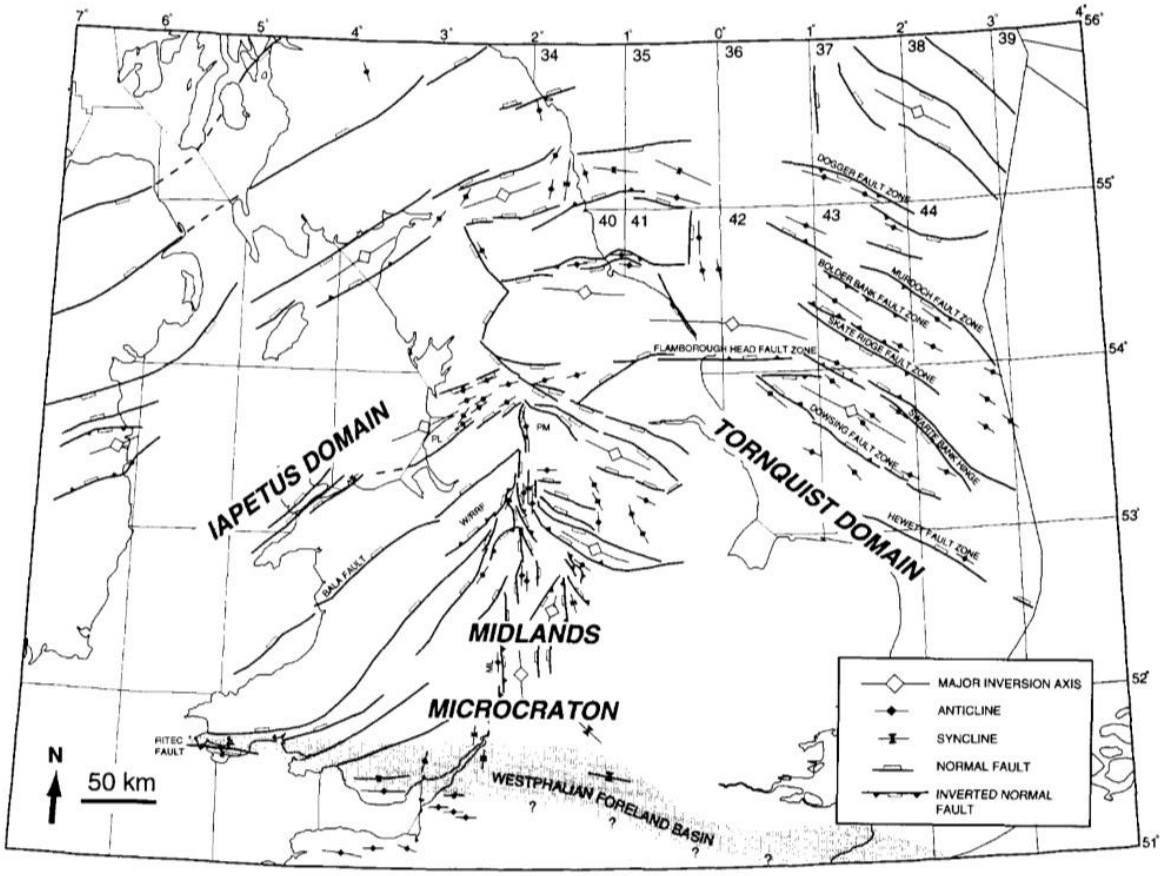


Figure 2.29 Summary of the Variscan inversion structures across the UK and Ireland. After Corfield et al. (1996)

The East Pennine basin lies within the Variscan foreland (Figure 2.29, Corfield et al., 1996), and contains an extensive Carboniferous sediment infill that was divided into three unconformity-bounded megasequences by Fraser & Gawthorpe (1990) based on the interpretation of reflection packages on 2D seismic data. The *syn-rift* megasequence was deposited in the late Devonian-Dinantian (Tournaisian-Visean) and was driven by rift controlled subsidence with deposition of fluvio-deltaic sediments into the half grabens and the development of Carbonate platforms on the highs. The post-rift megasequence was deltaic sediments deposited regionally in with overall equal thicknesses (Leeder & Hardman 1990) from the late Brigantian to late Westphalian due to thermal sag. The inversion megasequence was deposited from late Westphalian C to early Permian and consists of red clastics identified by the basal onlap into inversion anticlines in the hangingwall of major faults. The further subdivision of seismic stratigraphy units that represent depositional units is summarized in Figure 2.30.

2.6.1 Stainmore Trough and Cleveland Basin

The Stainmore Trough and Cleveland Basin are E-W trending sub-basins in Northeast England (Figure 2.31). The Cleveland Basin was identified as the onshore extension of the Sole Pit Trough (Van Hoorn). It is separated from the East Midlands Shelf by the Market Weighton High (Cossey et al., 2004). It is bound to the west by the Askrigg Block and has a merged northern margin with the Stainmore Trough. The basin can be simplified structurally in the form of two half grabens, offset by a major intra-basinal transfer system (Fraser & Gawthorpe, 2003a).

The Cleveland Basin received a predominantly clastic infill during Visean times due to the proximity of this basin to the prograding Fennoscandian delta system (Fraser and Gawthorpe, 2003b). Wedge shaped geometries are seen on 2D

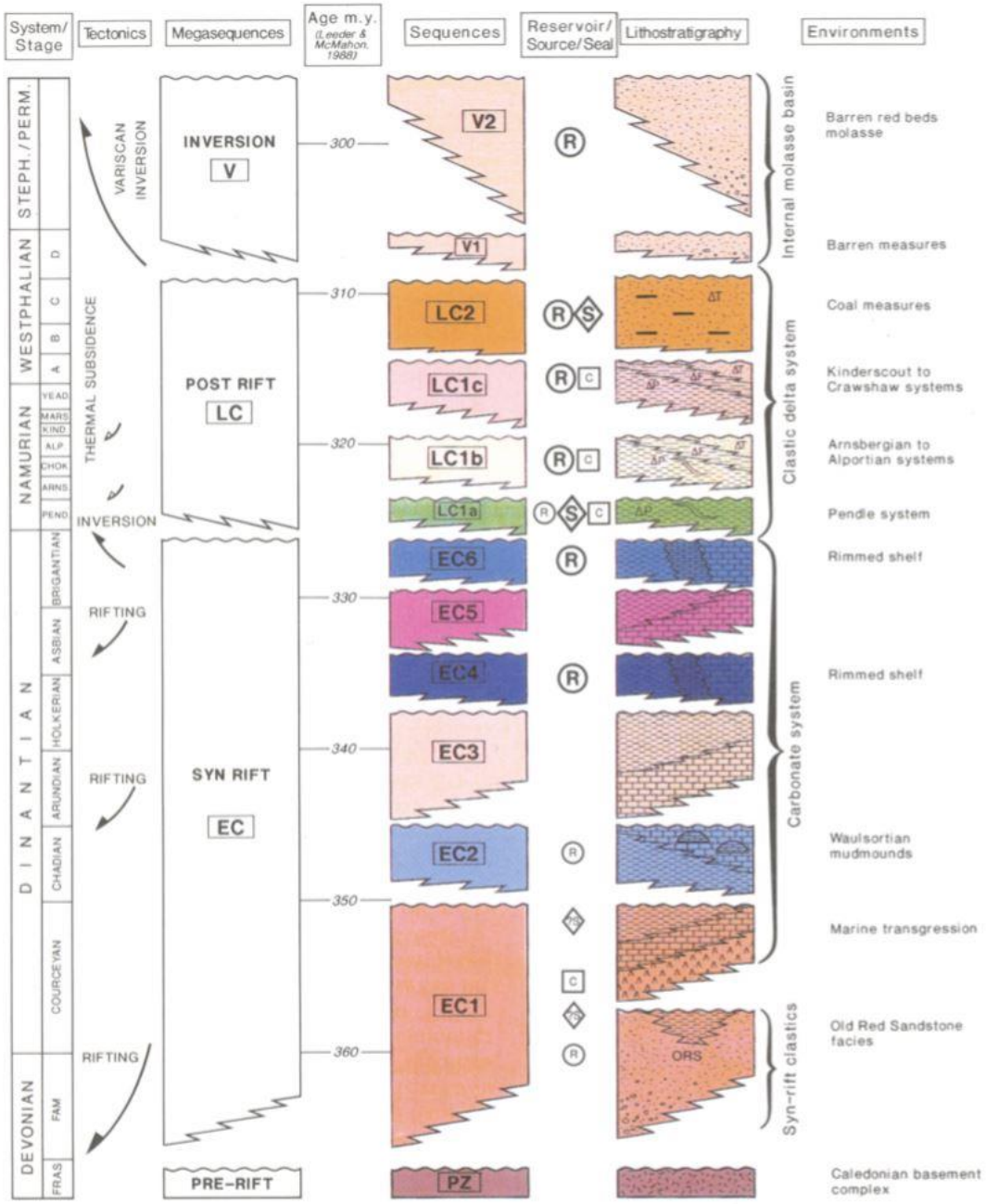


Figure 2.30 Summarized stratigraphy of the Variscan plate cycle in the East Midlands. Megasequences and sequence development is indicated. After Fraser & Gawthorpe (1990).

seismic and an angular unconformity has been observed in the deeper parts of the basin (Fraser and Gawthorpe, 2003b). Uplift during the Late Carboniferous eroded the majority of the Namurian and Westphalian sediments from the central part of the basin. The Barton Fault bounds the Cleveland Basin at its southern margin and has a 2500m thick footwall succession of Yoredale, Millstone Grit and Coal Measures facies detailing the expected full delta sequence. The thickness of the post-rift succession here is postulated to represent the lower limit for the thickness of the succession across the basin.

The Stainmore Trough lies to the north of the Cleveland Basin and is a major E-W trending half graben (Figure 2.31 and Figure 2.32). It is separated from the Cleveland Basin to the south west by the Askrigg Block, an uplifted granite cored block (Kent 1966, Figure 2.31). It merges with the Cleveland Basin to the south east to form a composite basin that extends offshore. The northern basin bounding faults are the Lundale-Butterknowle normal faults. They dip to the south and with a combined length of over 50km. North of these faults is the Alston Block, another uplifted granite cored high with Carboniferous platform Carbonate accumulations.

2.6.1.1 Fault Systems

There is a high level of uncertainty regarding the pre-Permian intra-basinal structure and stratigraphy within the Cleveland Basin. The Carboniferous succession is not exposed at the surface in the basinal areas and is only exposed on the highs such as the adjacent Alston and Askrigg Blocks (Figure 2.31). Due to the present depth of this interval, it is poorly imaged by 2D seismic data and the highly irregular 2D grid of seismic complicates the mapping of intra-basinal structures.

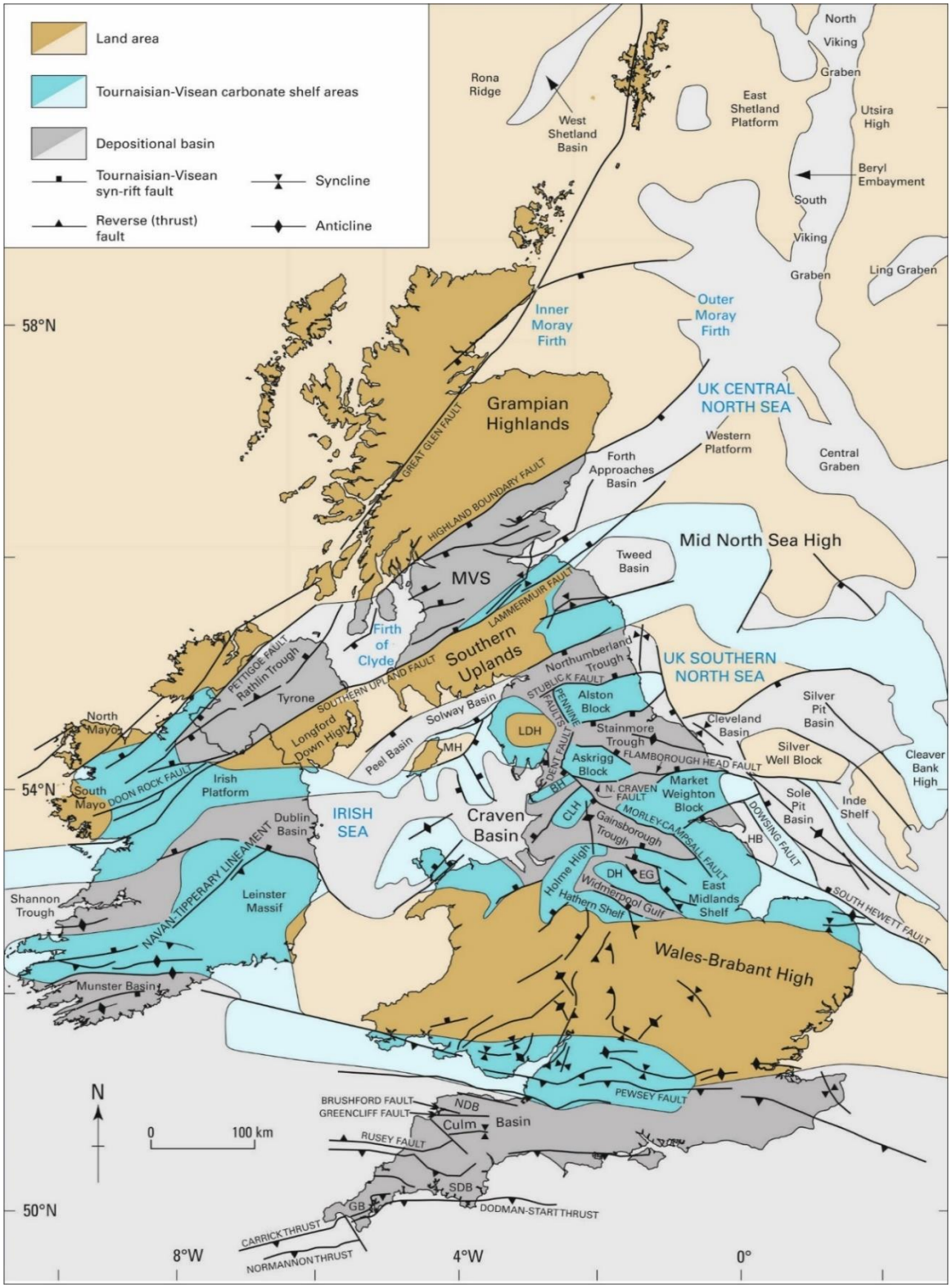


Figure 2.31 Principle Carboniferous structural features for the British Isles, onshore and offshore. After Waters et al. (2007).

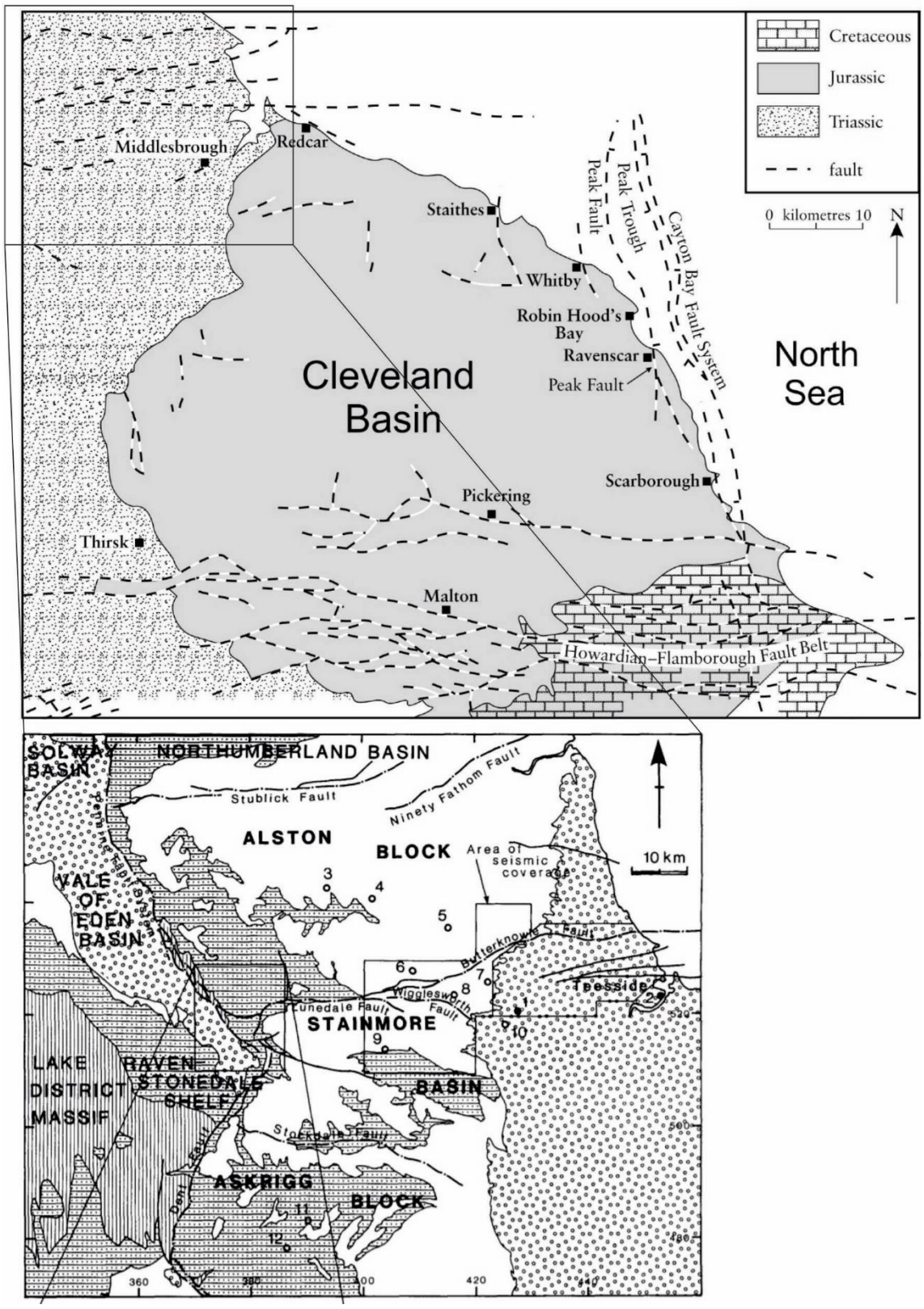


Figure 2.32 The Stainmore Trough and Cleveland Basin after Cossey et al. (2004) and Collier (1991).

For these reasons, intra-basinal Carboniferous structure maps remain largely blank except for a series of E-W trending faults to the south such as the Vale of Pickering and Flamborough Head fault zones (Figure 2.32).

To summarise, the approximate sub-basinal geometry of the Stainmore Trough and Cleveland Basin have been constrained by 2D seismic data, but due to the sparse grid of the 2D seismic data, the intra-basinal structure remains relatively uncertain.

2.6.2 South East Pennine Basin

The South East Pennine Basin encompasses the southern NW-SE orientated Carboniferous sub-basins and highs (Figure 2.31). The structure largely follows the Tornquist trend, with the Eakring fault being an extensional reactivation of the Caledonian Glinton thrust (Figure 2.3), demonstrating Caledonian structural inheritance (Fraser et al. 1990).

2.6.2.1 Sub-Basinal Faults

The dominant fault trends observed in the EPB includes major NW-SE and WNW-ESE asymmetric half grabens with kilometre scale displacements (Bailey et al., 2005). These faults are interpreted to have formed due to the ~N-S extension during Dinantian rifting, with this extension being accommodated on the pre-existing WNW-ESE and NW-SE Caledonian trends (Leeder 1990). Reactivations of these faults include a minor reactivation during the deposition of the post-rift megasequence evidenced only on large faults i.e. the Askern Spital Fault (see Figure 2.33) on which syn-rift displacement is observed (Rippon, 1997, Fraser and Gawthorpe, 1990). More commonly, these faults exhibit a mild inversion at the end-Carboniferous after the deposition of the Post-Rift. This event caused gentle folding and the creation of inversion anticlines within the hangingwall. This subsequent

erosion of the post and sometimes even syn-rift sediments (Bailey et al., 2005) can be viewed on 2D seismic data. Some strike-slip movements are also observed on these faults (Rippon, 1997). Sub-ordinate amounts of extensional reactivation are observed on some of these faults with offsets of the BPU and younger horizons. The origin and timing of this reactivation however is reported to be unknown (Bailey et al., 2005).

2.6.2.2 EPC Faults

On a smaller scale, an orthogonal network of NE-SE, NW-SE and WNW-ESE faults cross cut the East Pennine Coalfield (Bailey et al., 2005). These faults are predominantly extensional and exhibit drag folding or Variscan inversion anticlines in the hangingwalls (Goossens, 1973).

The faults are said to be formed between Late Westphalian to Early Permian after lithification (Walsh and Watterson, 1988b, Walsh and Watterson, 1989) but prior to Variscan uplift and erosion. Generally 10% of the total displacement occurred after the deposition of the overlying Permian (Bailey et al., 2005).

The network of NW-SE, NE-SW and WNW-ESE faults across the EPC have normal offsets and throws up to 200m (Watterson et al., 1996). Each orientation set dips in both directions at roughly equal amounts. Bailey et al report that many major NW-SE striking EPC faults coincide with the larger Dinantian half grabens.

No clear cross cutting relationships are observed between the NE-SW and NW-SE faults and they are considered to be contemporaneous. The WNW- faults zones show dextral offsets of the NW- and NE- faults meaning they have a movement that post dates these faults. This strike slip movement is attributed to late Carboniferous deformation related to the dextral shear occurring east of the Pennine high.

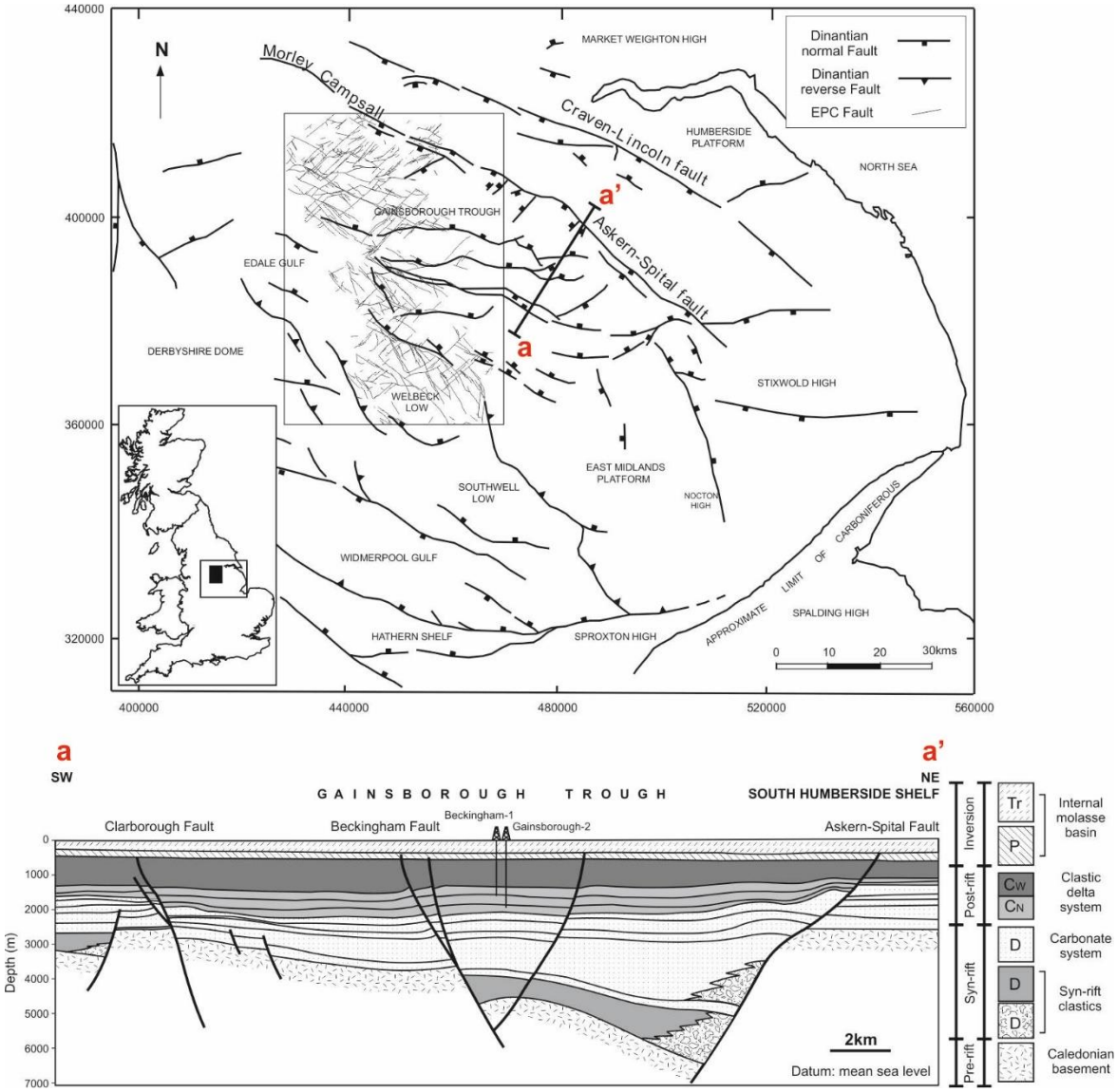


Figure 2.33 Structure of the East Midlands region of the East Pennine Basin. Two scales of faults are observed. Below is a cross section through the Gainsborough Trough, position of section is indicated (after Fraser and Gawthorpe, 1990 and Bailey et al. 2005).

Compaction and gravity-slide syndepositonal faults are also observed in the EPC. They are arcuate in map view with throws of less than 50m and are less pervasive than tectonic faults within the Westphalian succession (Bailey et al., 2005). These faults were formed due to slumping of the Namurian-Westphalian delta system (Fraser et al. 1990).

Structural styles in the East Pennine Coalfields are formed by varied origins and reactivation histories. This produces distinct differences in fault plane geometries and linkages. Mechanical stratigraphy also plays a part when there is a gross lithological change as well as compaction prior to faulting. Two scales of tectonic faults networks are identified in the EPB that formed at different times. The sub-basinal scale faults have kilometre offsets and were formed during the Visean due to north south extension, while the EPC faults were supposedly formed at the end Carboniferous related to Variscan compression.

2.6.2.3 Summary

- Faults are broadly classified across large areas in the ADB based on largely on orientation alone. This causes confusion across the literature as the detailed structural styles and kinematics vary due to fault size and related attributes.
- The structure of the ESP has only been characterized recently through new 3D data and formation mechanisms have been explored in little detail
- Current literature assumes the majority of meso-scale fault formation and reactivation across the MNSH and ADB is due to rotations of the regional stress field and reactivation of existing structures.

- Fault formation mechanisms are infrequently discussed by authors and when they are they are attributed to regional extension even if the resulting structures are not what would be expected from the paleostress regime.
- Most of the faults observed and discussed across the Anglo-Dutch and Pennine Basins and are thick skinned, planar normal tectonic faults. The gravity glide/syndepositional faults in the Gainsborough Trough are the exception.

Chapter 3

THE GEOMETRY AND KINEMATICS OF STRUCTURES WITHIN THE PRE-ZECHSTEIN SUCCESSION

3 The Geometry and Kinematics of Structures within the Pre-Zechstein Succession

3.1 Introduction

3.1.1 Chapter Rationale

The structure of the Pre-Zechstein of the Anglo-Dutch and East Pennine Basins is well documented by the interpretation of 2D and 3D seismic data (Chapter 2). Previous classifications and characterizations of faults in the Anglo-Dutch basin have been based broadly on fault orientation of larger scale trends (see Chapter 2, section 2.5). This method may result in the generalizing and aliasing of the discrete fault types that are present.

New 3D seismic data with better imaging of the PZS allows for a more detailed recognition of fault patterns at various scales defined by throw magnitude, that was not previously possible on 2D data.

3.1.2 Chapter Aims and Research Questions

The overall purpose of this chapter is to examine the geometries and kinematics of structures within the PZS. A number of detailed case studies (Figure 3.1) are presented to give a regional perspective of this large basinal area and to highlight their commonalities and differences to develop a tectonic model for their formation.

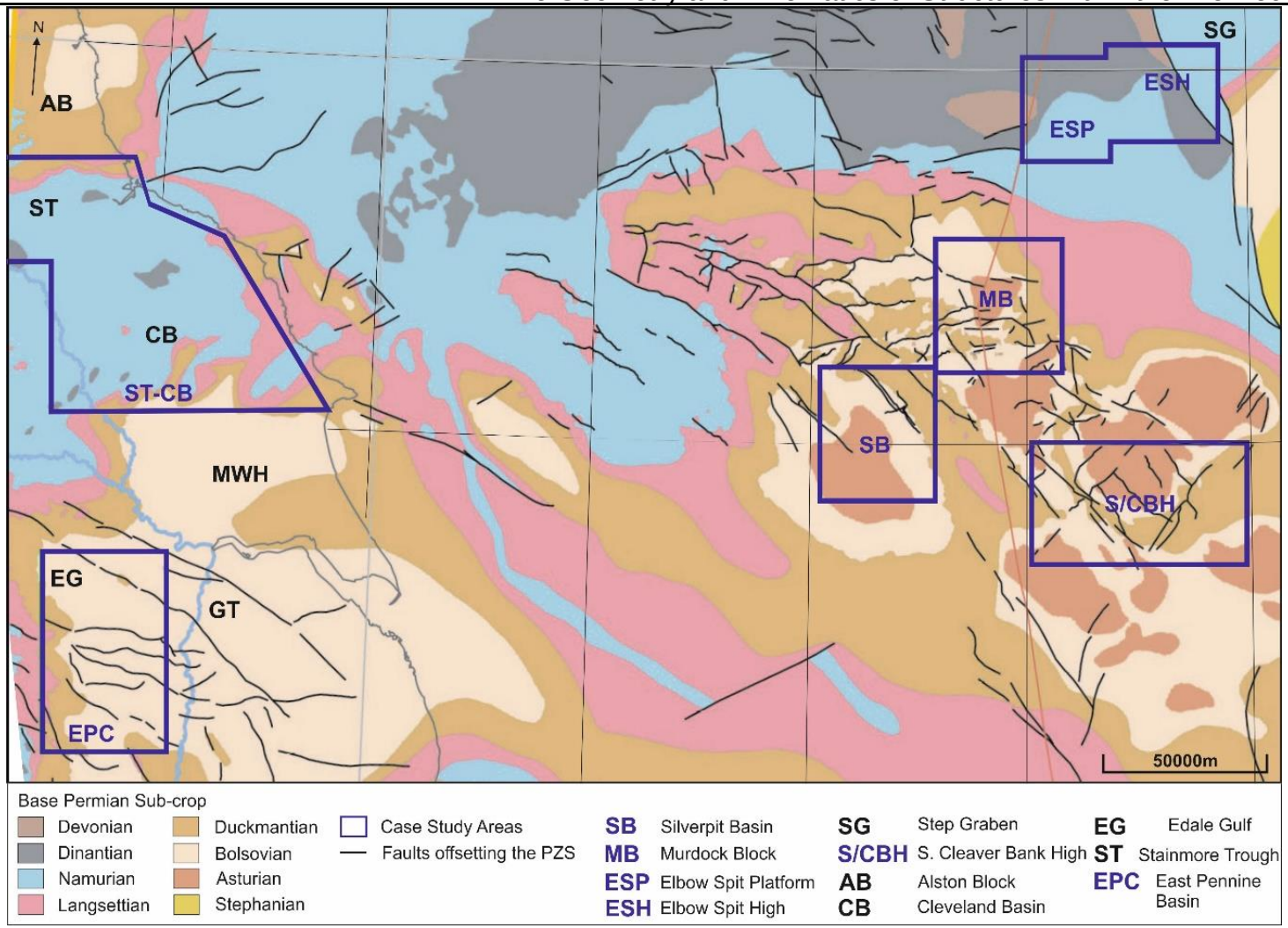


Figure 3.1 The locations of the case study areas overlain on a Base Permian sub-crop map. Major Pre-Zechstein faults are indicated along with the boundaries of the southern north sea Quadrants and UK/Dutch sector (Doornenblad & Stevenson, 2010).

This chapter begins with descriptive accounts of the main structural elements and sets out foundation on which later chapters build to address more specific questions. The questions that this chapter aims to answer are:

1. What fault types and inter-relationships are exhibited by fault arrays in the Pre-Zechstein succession of the Anglo-Dutch Basin?
2. What are the timings of formation and reactivation of the observed structures across the case study areas?
3. Are these fault sets opened or closed and how might this transmissibility affect production?

3.2 Elbow Spit Platform (ESP)

3.2.1 Background

The ESP is located in the northern Dutch sector of the Southern North Sea (Figure 3.2). The ~2,000km^2 3D seismic volume used to study the ESP is a portion of the PGS megamerge (see section 1.5.1.1). The volume spans blocks E/1-4 and has three key Pre-Zechstein well penetrations (Figure 3.2). Vertical amplitude clusters/VACS (Foschi, 2014) are present in the Cenozoic succession in the south west (Figure 3.3). Despite the presence of these shallow DHIs, there are currently no significant hydrocarbon discoveries in the area to date.

The imaged PZS is of exceptional quality in this area making it an ideal location for the reconstruction of fault systems. Salt structures distort the underlying PZS imaging creating velocity artefacts (Figure 3.3).

Key reflections in the ESP and ESH area were chosen for mapping based on their high amplitude and continuity. These mapped horizons were later age calibrated from the local well successions (Figure 3.4). For reflections that could not

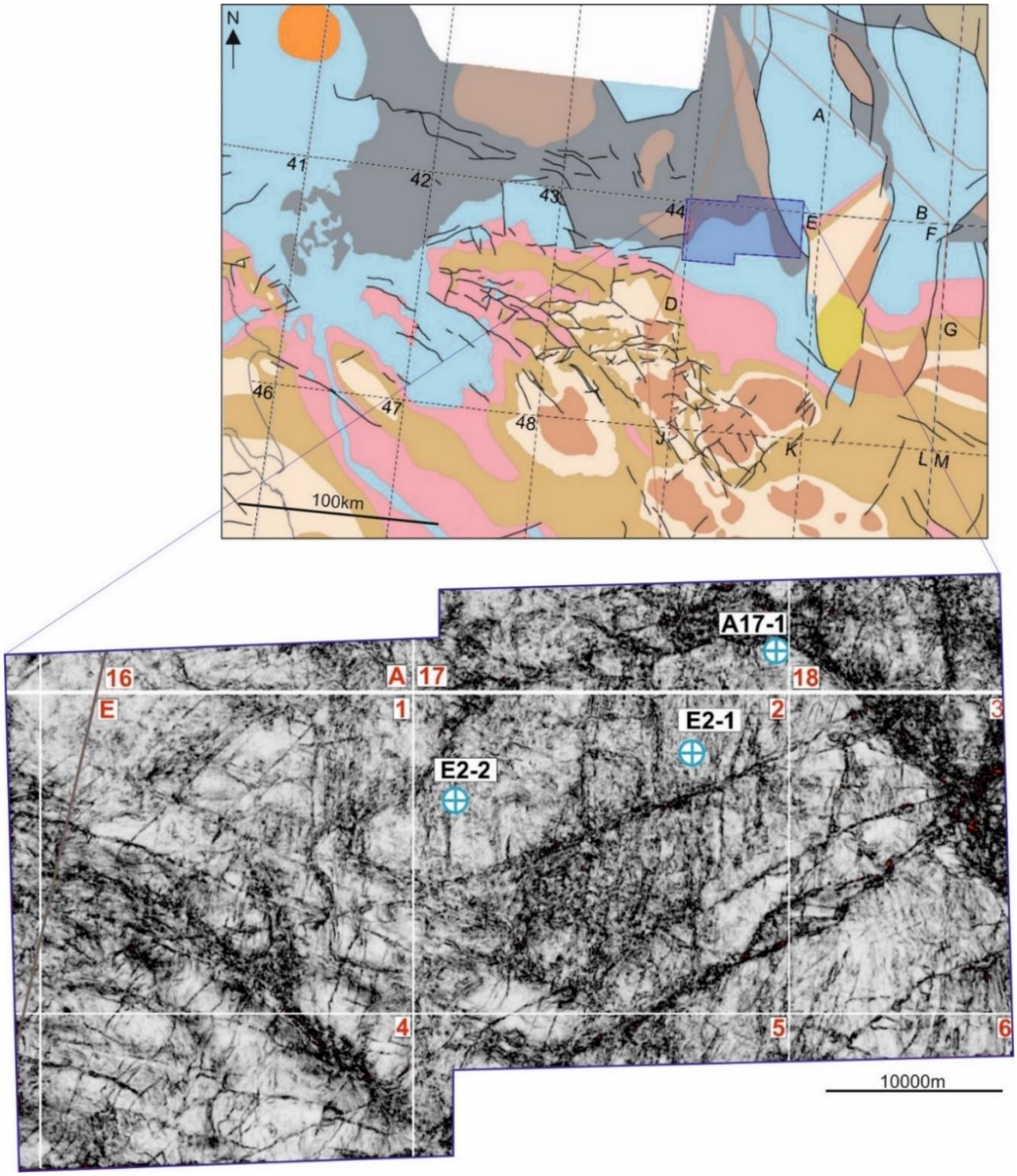


Figure 3.2 Intra-Carboniferous isoproportional slice, -50ms below the Top Rotliegend horizon on the ESP. The three wells (blue circles) have Pre-Zechstein penetrations. White lines indicate block boundaries.

be stratigraphically calibrated, such as those located in the PZS in the south west of the ESP, the seismic stratigraphy has been calibrated partially by a tie to well A-17 (see Appendix A). Since this well calibrated a relatively incomplete PZS, additional constraints on this stratigraphy were obtained from longer range correlations based on acoustic character to the equivalent section in areas of the MNSH.

3.2.2 General structural and stratigraphic context

The Mid North Sea High has recently been found to be a series of highs and lows during the Devonian, rather than a persistent high throughout the area (Ter Borgh et al., 2018). This model is similar to the onshore evolutionary history, one of granite-cored highs separated by lows (Donato et al., 1983, Fraser and Gawthorpe, 1990, Corfield et al., 1996, Besly, 1998)

The MNSH terranes were found to be partly basinal in behaviour during the Carboniferous, evidenced by the recent identification of the North Elbow Basin (Figure 3.5), north of the ESP (Ter Borgh et al., 2018). The North Elbow Basin is thought to be a continuation of the North Dogger Basin located in the adjacent UK sector (see Figure 2.17).

The ESP is the southeastern marginal high in the MNSH area (Figure 2.17). The ESH is the area of higher elevation to the NE of the area which is granite-cored (see Well A-17 in Appendix A) with a postulated underlying batholith (Donato et al., 1983, Figure 2.5). The ESH was a high during the Devonian, as indicated by the onlapping geometries of postulated Middle-Upper Devonian sediments (Figure 3.6). These Upper-Middle Devonian sediments are overlain by successive Lower Carboniferous sediments of overall uniform thickness. The overall poor calibration of the PZS in the deeper areas of the ESH necessitated the construction of a seismic

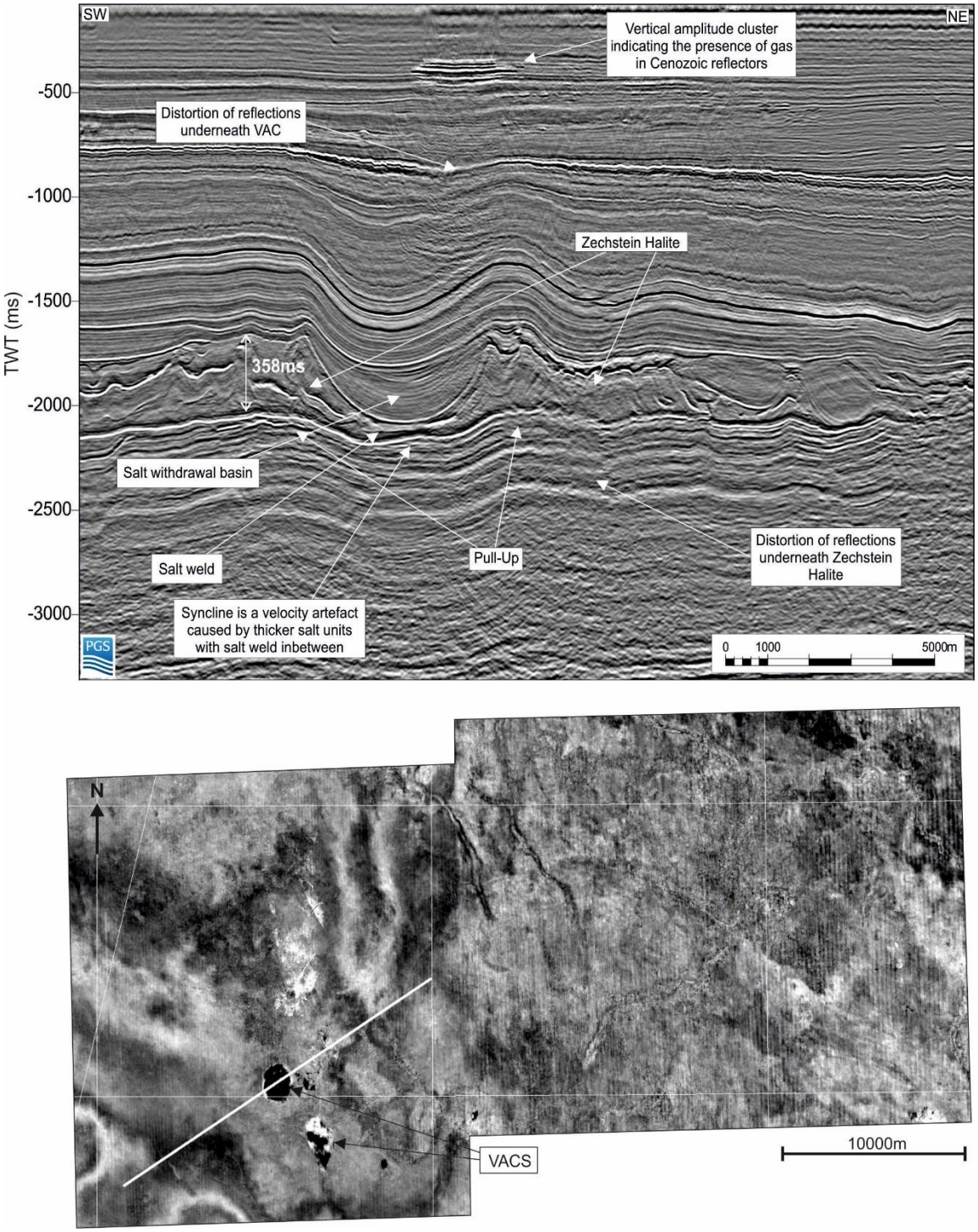


Figure 3.3 a) 3D seismic section highlighting the data quality in the ESP area. Factors that affect the imaging of the Pre-Zechstein succession are indicated b) location of section on a time slice through the Upper Cenzoic

stratigraphic framework. The Pre-Zechstein stratigraphy on the ESP has been sub-divided into seven seismic stratigraphic units, each having a distinctive seismic response (Figure 3.8).

Locally Mapped Horizon	Horizon ID	Stratigraphic Horizon	Age	Lithostratigraphic Formation	Seismic Strat Unit
Top Rotliegend	TROT	Top Rotliegend	Rotliegend	Silverpit Fm	A-E_SSU1
BPU/Unconformity 2	BPU/U2	BPU	U Westphalian - L Permian	-	
Package Z	Z	Unkown	?	Unkown	
Unconformity1	U1	U1	?	-	
Horizon A	A		Lower Namurian?	Whitehurst Grp?	A-E_SSU2
Horizon B	B				
Horizon C	C	Top Brigantian	Brigantian	Yoredale Fm	
Horizon D	D				
Horizon E	E	Top Asbian	Asbian- Holkerian	Scremerston Fm	
Horizon F	F				
Horizon G	G				
Horizon H	H				
Horizon I	I				
Horizon J	J	Top Arundian	Arundian-Courceyan	Fell Sandstone Fm	A-E_SSU3
Horizon K	K				
Horizon L	L				
Horizon M	M				
Mid Devonian 1	MDR1	Top Frasnian	Frasnian-Givetian	Condroz/Kyle Grp	A-E_SSU5
Mid Devonian 2	MDR2				

Figure 3.4 Mapped horizons in the Pre-Zechstein succession of the ESP.

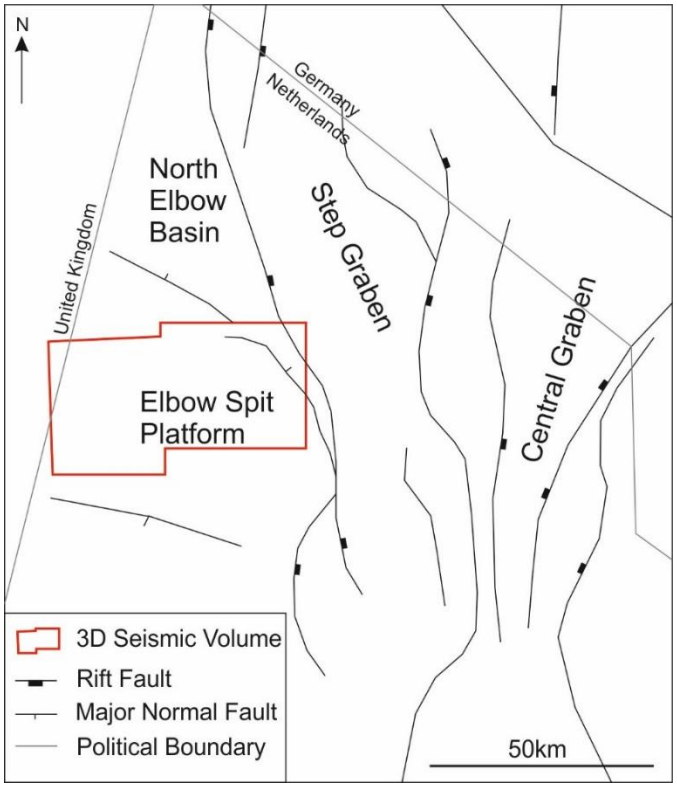


Figure 3.5 Structural elements of the northern Dutch sector from Ter Borgh et al. (2018) & Smit et al. (2016)

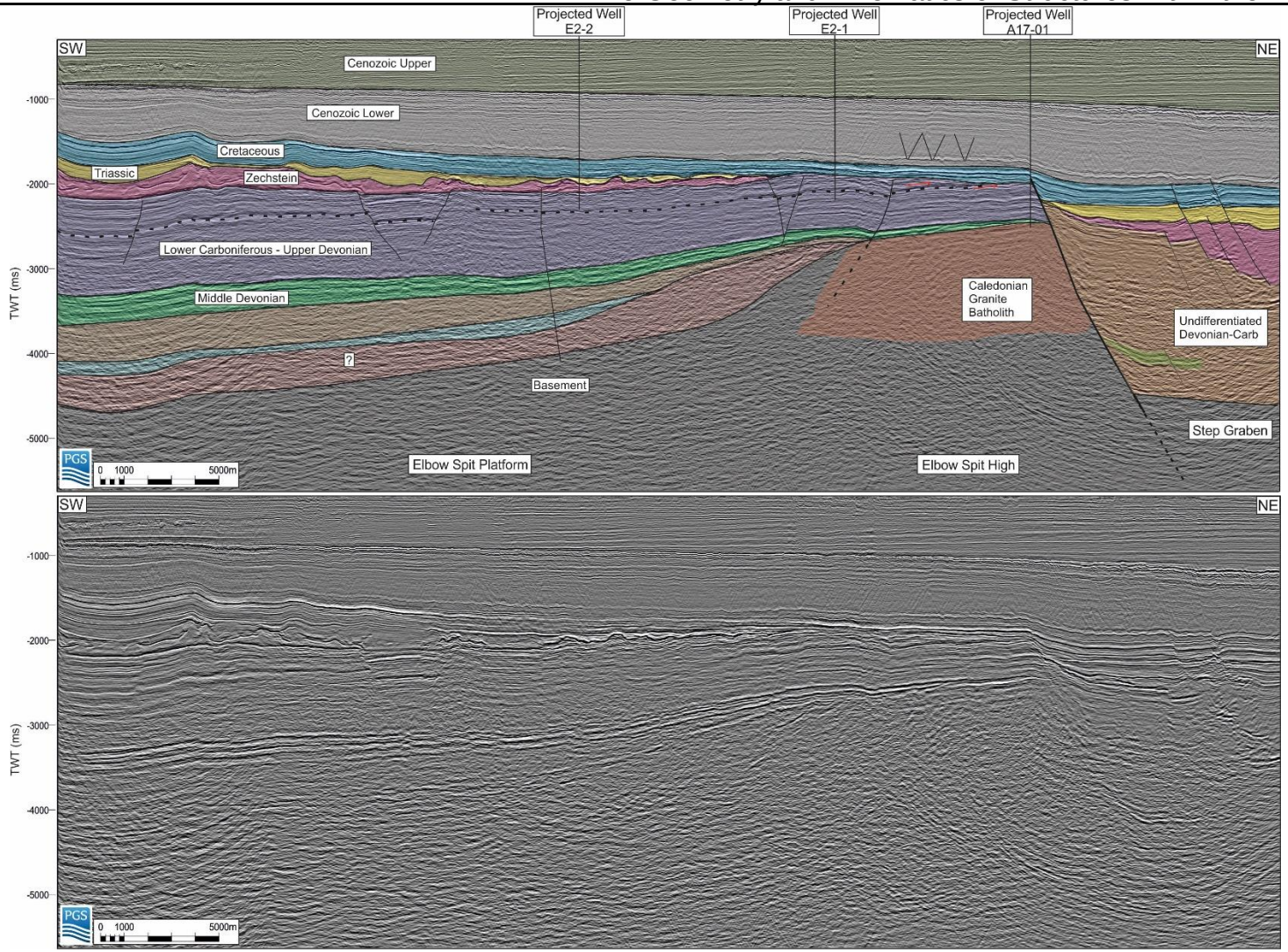


Figure 3.6 SW-NE Geoseismic section across the ESP

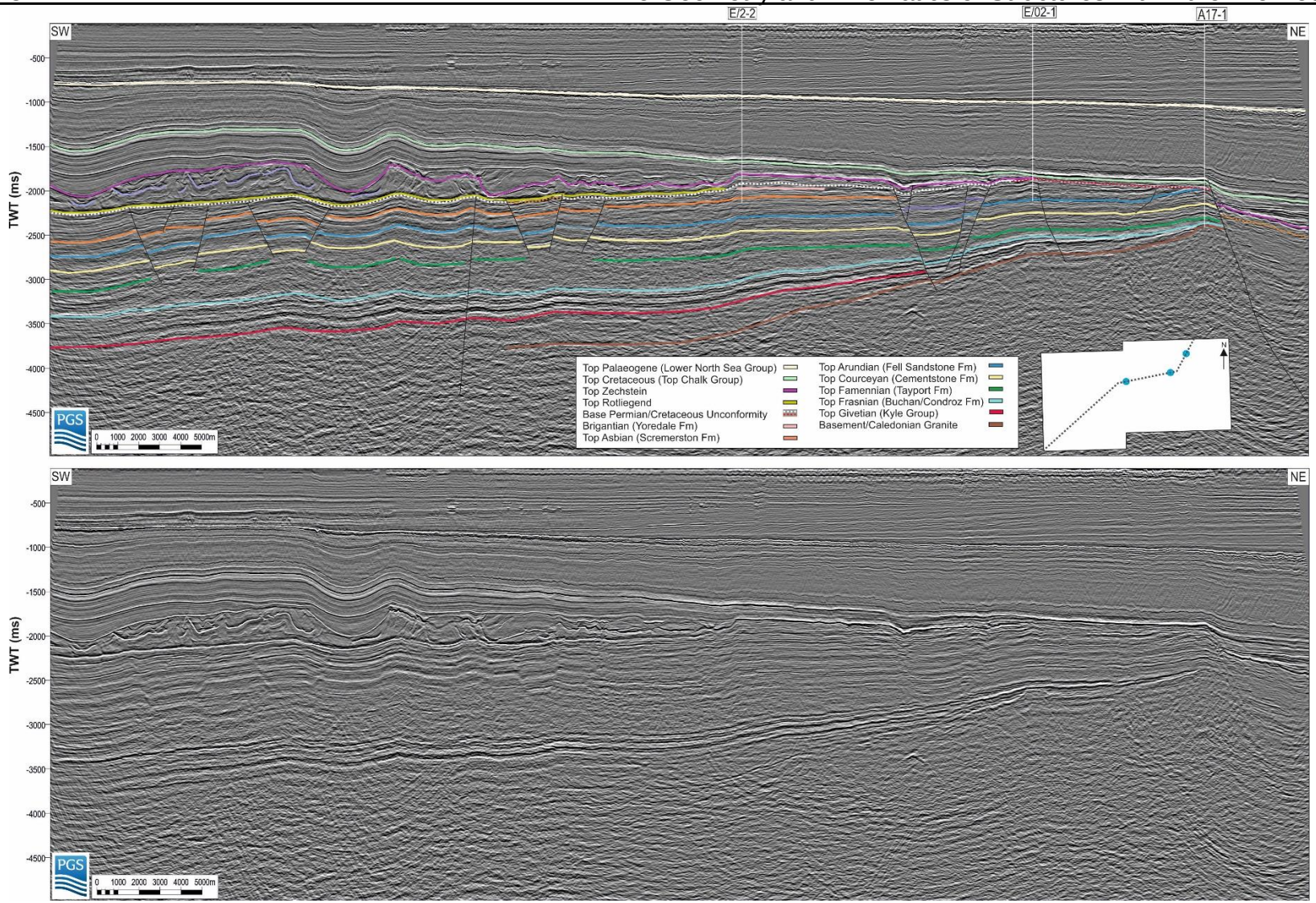


Figure 3.7 Interpreted seismic section across the ESP

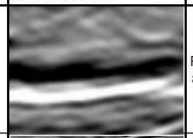
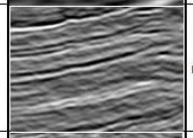
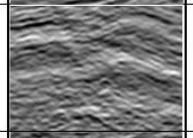
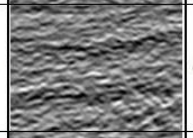
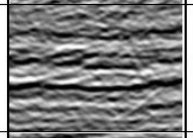
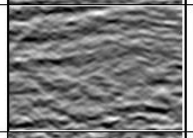
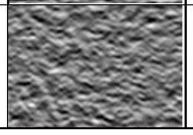
Unit Top	Unit Base	Seismic-strat Unit	Seismic Facies	Seismic Facies Description	Unit Thickness (ms)	Contact with Upper Unit	Contact with Lower Unit	Package Geometry	Chrono-stratigraphy	Litho-stratigraphy	Description	Locally Mapped Horizons	Calibrated by
Top Rotligend	BPU/Intra-Brigantian	ESP 1		Parallel postive reflection overlaying a high amplitude negative reflection	~40ms in the south west, ? In the north east	Conformable with Base Zechstein	Unconformably onlaps Intra-Brigantian/BPU	Regionally correlatable. Thins to the north east over the ESH. Deformed by faults.	Rotliegend (Permian)	Silverpit Formation	Red-brown silty claystone	TRot, BPU/U2, Z, U1	Well E2-1, E2-1, A-17
BPU/Intra Brigantian	Top Arundian	ESP 2		Coherent, high amplitude reflections with short separating intervals of lower coherence reflections. Parallel/concordant and truncated against ESP-1. Reflections become less coherent with depth.	~500ms	Truncation at the Base-Permian Unconformity	Conformable with Top Arundian/J	Regional ~4° SW dip due to regional tilting associated with footwall uplift on the ESH from movement on the NW- bounding fault. Local dip variations up to 7° due to rotation in the hanginwall of smaller scale faults.	Brigantian-Holkerian (Visean)	Whitehurst Group, Yoredale Fm, Scremerston e Fm	Yoredale Facies concisiting of marine limestones and mudstones with deltaic sandstones, siltstones and thin coal seams	A, B, Top Brigantian/C, D, Top Asbian/E, F, G, H, I,	Well E2-1, E2-1
Top Arundian	Top Famennian	ESP 3		Parallel stratified, low amplitude reflections with subordinate hummocky reflctions	~300ms	Conformable with Base Holkerian	Picked at where weak reflection coherency can no longer be recognised	Almost uniform thickness with cross-cutting faults	Arundian-Courceyan	Fell Sandstone Formation, Cementstone Formation	Massive sandstones, thin mudstones and dolomite beds. Sandstones and mudstones with thin dolomite beds	Top Arundian/J, K, L, M	Well A-17, onshore equivalent outcrop correlation (See Appendix)
Top Famennian	Top Frasnian	ESP 4		Chaotic reflections, little coherence	~300-400ms on ESP, thins on flanks of ESH	Conformable with Base Courceyan	Irregular boundary with ESP 5	Wedge geometry that is thicker in the ESP and thins of the ESH. Inferred that this packahe infills the low and onlaps the high. Fault offsets are not imaged.	Fammenian (Devonian)	Tayport Formation	Postulated overpressured mudstones	-	Well A-17, onshore equivalent outcrop correlation (See Appendix)
Top Frasnian	Top Givetian	ESP 5		High amplutude reflections with , hummocky reflections	~250ms on ESP, ~50ms on ESH	First high amplitude reflection with an irregular profile	Abrupt decrease in reflection coherence	Wedge packagae that is thickest in the ESP. Thins to the north east, onlapping the ESH. Offset by ENE- and NNE- orienatated faults.	Frasnian (Devonian)	Buchan/Kyle Group	Sandstone and dolomite beds or limestone and mudstone beds	Top Frasnian/MDR1, MDR2	Inferred from regional stratigraphy
Top Givetian	Top Basement?	ESP 6		Internal structure contains hummocky reflections with low coherency	~250ms x 5000m	More coherent reflection defines top of unit	More coherent reflection defines base of unit	Wedge shaped lense bodies that are not laterally continous	Givetian (Devonian)	Buchan/Kyle Group	Sanstone lenses/carbonate mmounds	-	Inferred from regional stratigraphy
Top Caledonian Granite	Top Basement	ESP 7		Very low coherency, low signal to noise ratio, visible diffractions, chaotic reflections	~2000ms x 15000m	Top not defined	Base not defined	Amorphous body	Caledonian Granite	-	Granodiorite	-	Well A-17

Figure 3.8 Seismic stratigraphy units in the Pre-Zechstein on the Elbow Spit Platform. Units range from Rotliegend to postulated Caledonian age.

3.2.3 Structural Sets

Variance slices through the PZS on the ESP have revealed a dense network of faults in the Rotliegend-Devonian succession (Figure 3.2). Four main sets are identified based on their distinct geometries, as inferred from their predominant strikes and relative timing relationships (Figure 3.9). A larger bounding fault is identified to the north east. Three of these sets are also identified by Ter Borgh et al. (2018) (see section 2.4.1.1).

3.2.3.1 A-E_WNW- Faults

A set of WNW-ESE (N100-N110°) orientated, normal faults have been identified in the Pre-Zechstein succession of the ESP (Figure 3.10). They are curvilinear to curved in planform view showing evidence of segmentation (Figure 3.9). They range in lateral lengths from 5-20km and have a sub-parallel alignment with a mostly regular spacing. The alignment of the array is sub-parallel to the Elbow Spit High slope contours (Figure 3.11).

A symmetrical horst and graben arrangement is observed in cross-sectional profile across most of the area, but with a change to a tilted fault block morphology upslope towards the north east (Figure 3.10). The fault planes are mostly planar with vertical extents of up to 700ms, as indicated by the observable offset of reflections within seismic stratigraphy units ESP 1-3 (Figure 3.12). Faults dip to the SW and NE at angles ranging from ~47-63° (Figure 3.13), with more SW- dipping faults overall.

The majority of the A-E_WNW- faults are truncated against the Rotliegend and their upper tips have been eroded at the BPU. The local propagation of some upper tips through the thin Rotliegend interval has occurred through a later reactivation movement. The lower tips of A-E_WNW- are not seismically resolved, the seismic data in ESP-4 does not

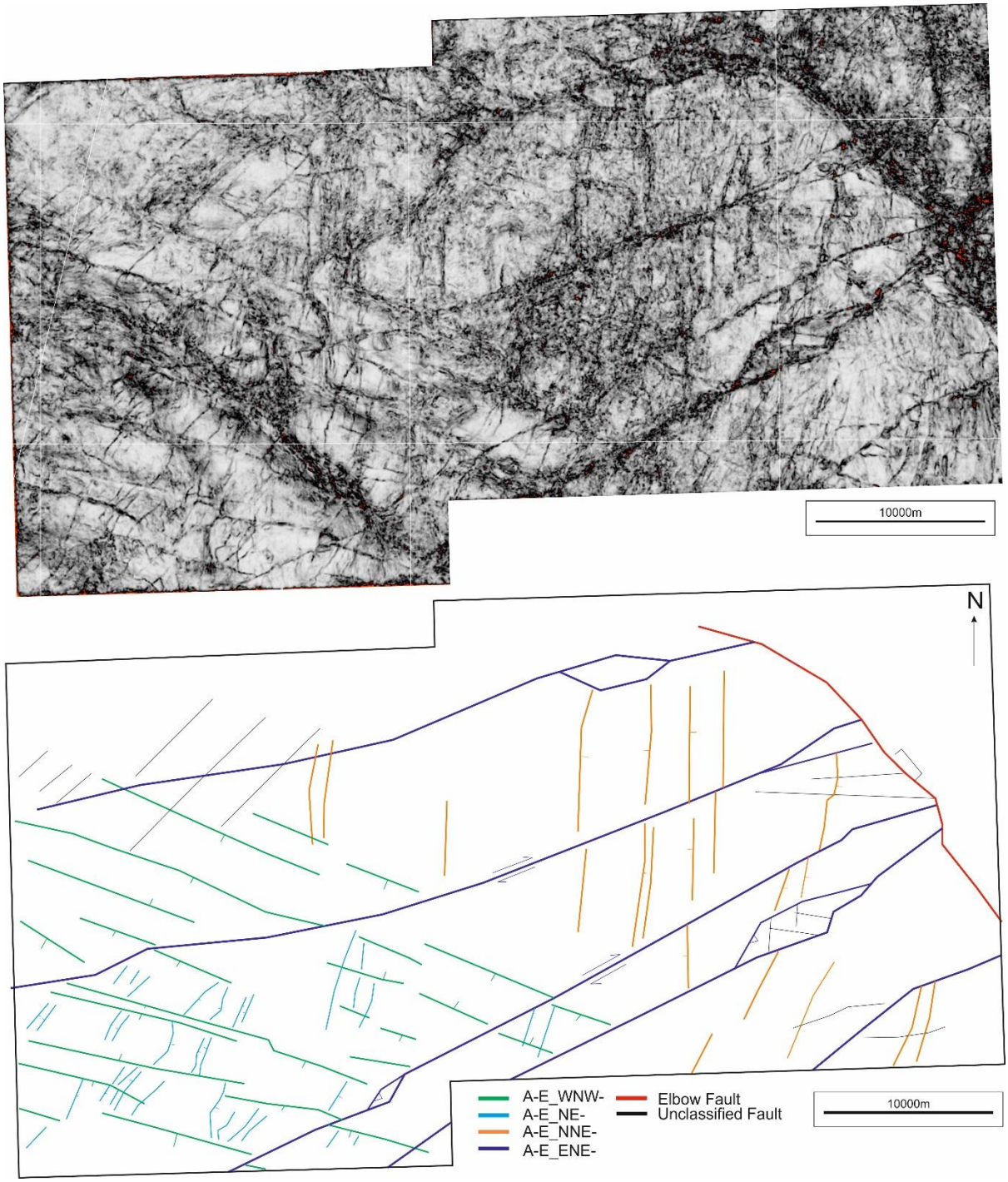


Figure 3.9 a) Intra-Carboniferous isoproportional slice -50ms below Top Rotliegend horizon/BPU b) Summary map of each fault set visible in the Brigantian and their movement sense.

contain imaged reflection offsets but ESP 5 remains undeformed by these faults (Figure 3.12), confining them to the Top Rotliegend-Top Fammenian stratigraphic interval.

Maximum throw values range from 60 to 368m(+-9m) with an average of 210m (+-9m, see section 1.5.2.3 for how error margin is determined)(Figure 3.14), recorded on various horizons within the Brigantian-Holkerian Interval (Unit ESP 2, Figure 3.8). Smaller offsets of the Top Rotliegend horizon are observed at local intervals along strike and range from 14 to 37m(+-7m). No growth packages are observed within the preserved stratigraphic intervals, something non-typical in Lower Carboniferous stratigraphy.

Fault related folds are observed on some of the faults (Figure 3.10). Some of the grabens are deformed into an anticlinal structure, in which the stratigraphy within the crest of the structure is truncated against an unconformity. This geometry is interpreted as indicating a contractional deformation occurring before the erosion and truncation during the formation of the first observed BPU in this area.

On close inspection, the presence of two Base Permian unconformities between the Lower Carboniferous and TRot is observed. U1 is compressionally deformed and represents a previous peneplanation before the grabens were folded. U2 represents the second peneplanation and erosion of stratigraphy of unknown age (Z) overlying U1. This phenomenon has not been observed previously in the ESP area and may represent the Variscan and Saalian unconformities that are elsewhere viewed as a single, composite BPU. The structural evolution between the faults and these unconformities is further investigated in Chapter 4. Soft and hard linkage structures are observed in planform and cross-section.

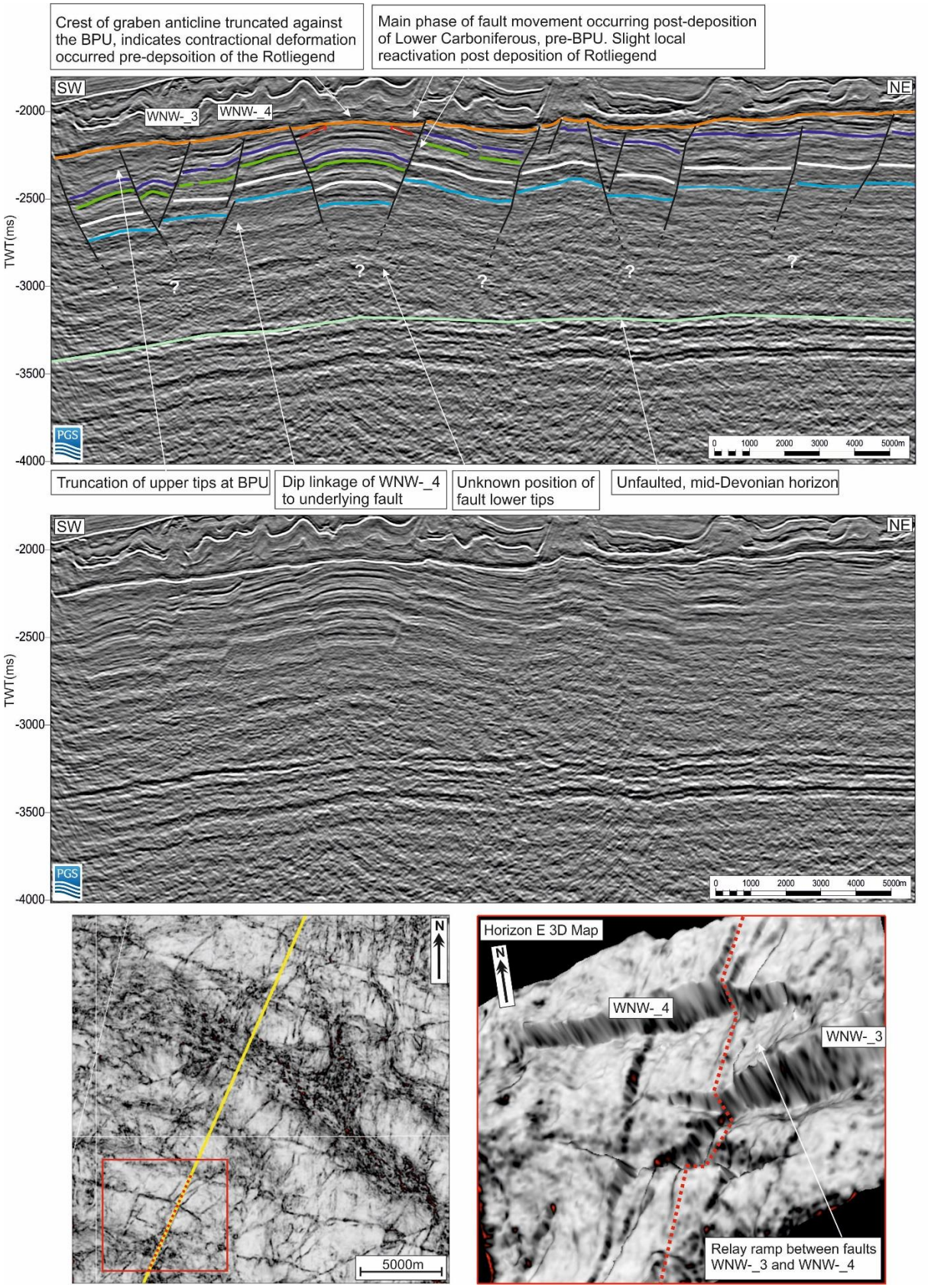


Figure 3.10 The WNW- fault set a) 2D seismic section orthogonal to WNW- trending faults (set E-A_1) b) Horizon map of Intra-Carboniferous mapped reflection, Horizon E, showing lateral linkage of WNW- faults (relay structures) c) Isoproportional slice -50ms Rotliegend showing fault trends within the Lower Carboniferous.

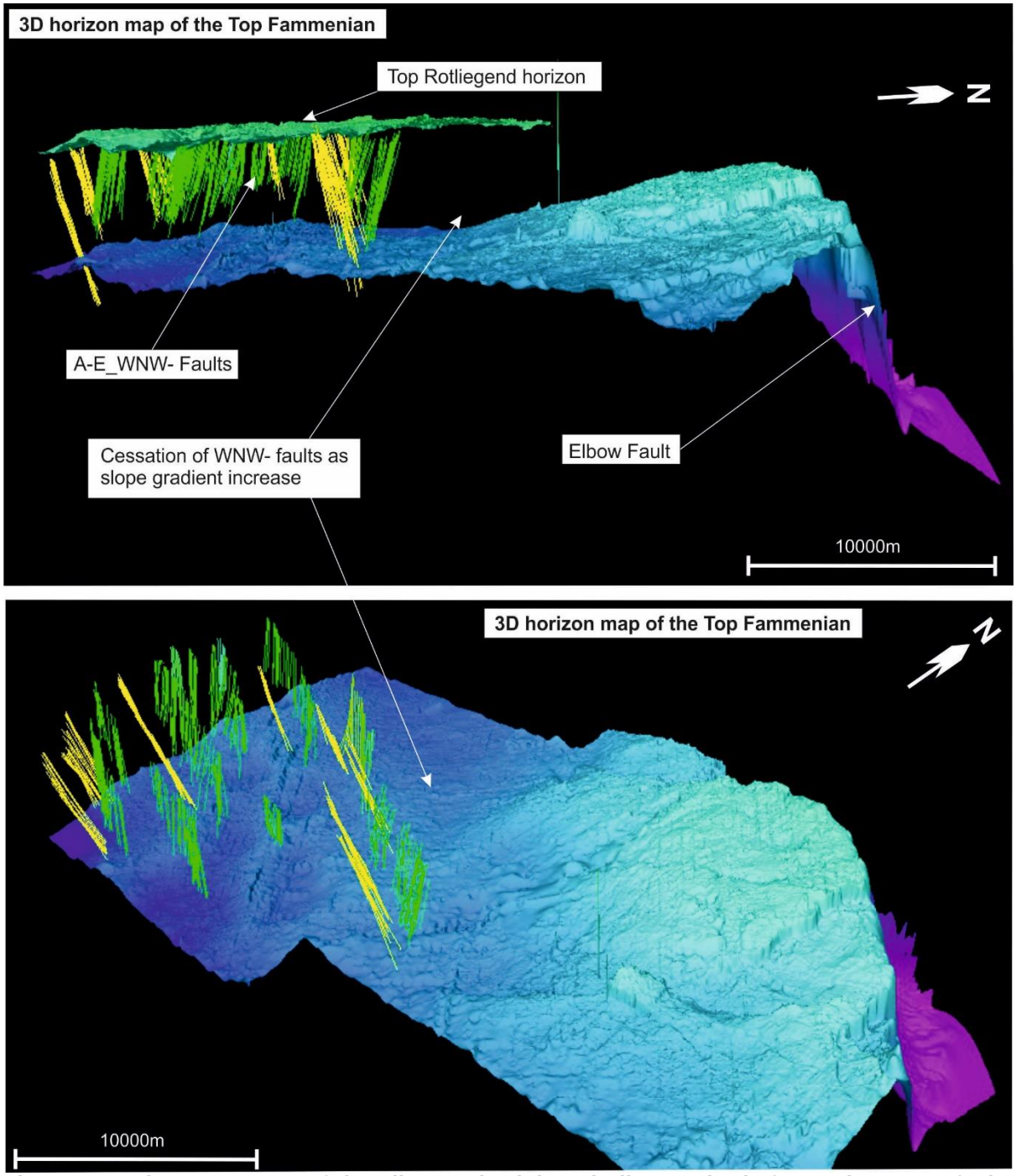


Figure 3.11 Slope geometry of the Elbow Spit High and Elbow Spit Platform. The WNW- faults are aligned sub-parallel to the slope contours.

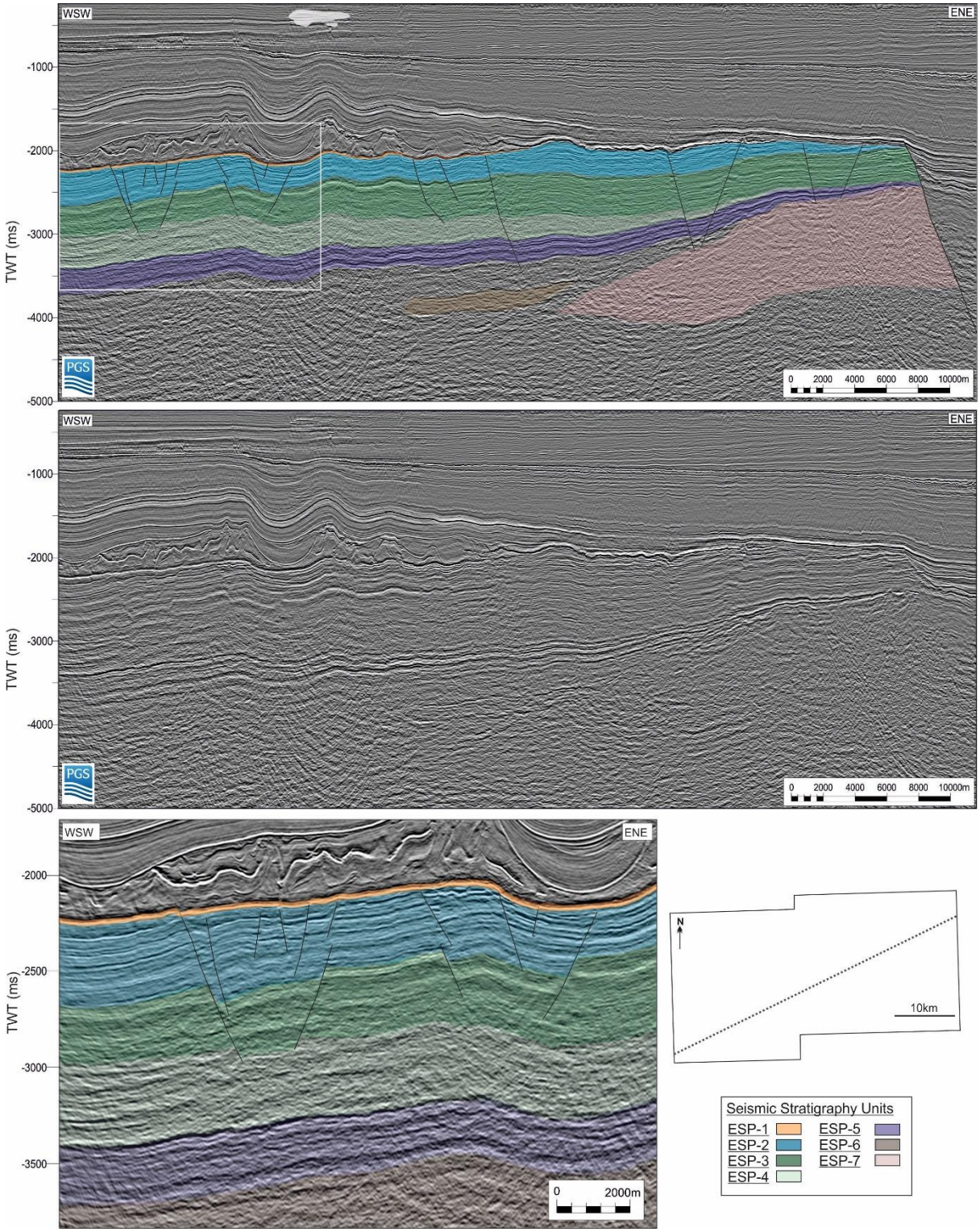


Figure 3.12 Seismic section across the ESP indicating the different Pre-Zechstein seismic stratigraphy units. The section within the white box on the first section is zoomed in on and presented by the last section.

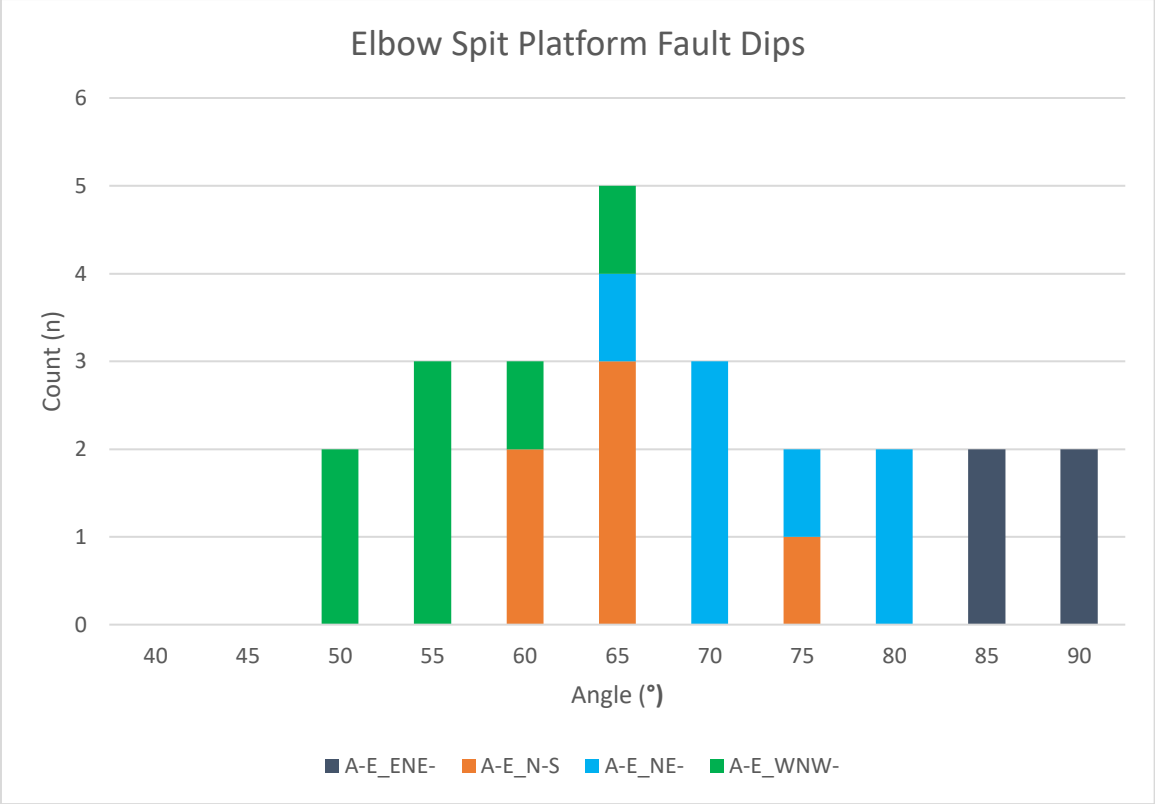


Figure 3.13 Histogram of fault dips for faults on the ESP. Different fault types are indicated by the colour key.

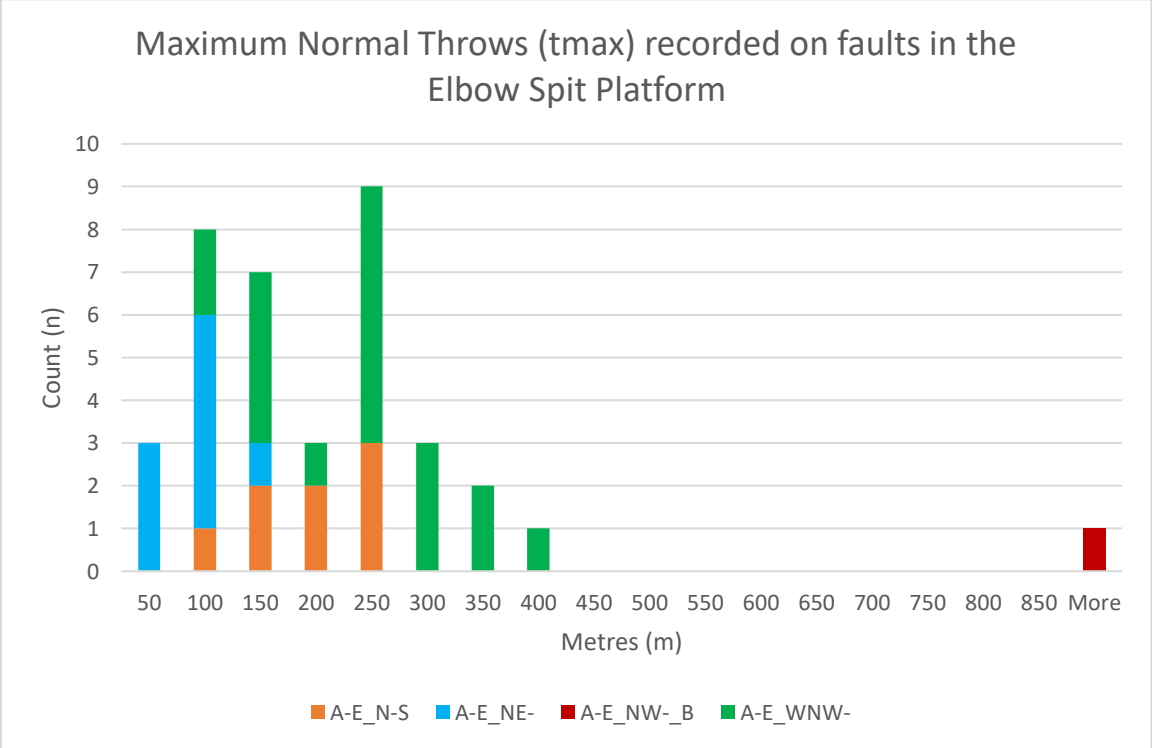


Figure 3.14 Histogram of Tmax values for faults on the ESP. Different fault types are indicated by the colour key.

Lateral linkage of faults in the form of relays and breached relays (Trudgill and Cartwright, 1994) are observed, such as those between faults WNW-_3 and WNW-_4 on the TRot horizon-variance map in (Figure 3.10).Typical segment lengths that are within the seismic data resolution range from 2-14km, but due to their curvilinear planiform geometry, these faults are likely to be further segmented.

3.2.3.2 A-E_NE- Faults

A set of NE- to NNE- (N030-N050°) orientated normal faults cross cut the WNW- faults with orthogonal intersection geometries (Figure 3.15). They have relatively short lateral lengths (1-6km) and have a linear or slightly curved planform geometry. They are best viewed in the southwest of the ESP and are spaced irregularly are clustered, but there is no obvious relationship at depth that accounts for this clustering.

Faults of this set are planar, dipping to both the WNW-ESE an ESE-WNW, with recorded dips ranging from 65-78° (avg. 70°, see Figure 3.13). There is little evidence of hangingwall folds or fault drag.

The A-E_NE- faults have a limited vertical extent in seismic section (300-600ms below the BPU) and are confined to units ESP-1 and ESP-2. The lower tips seismically terminate in unit ESP 3, in which displacement decreases to a minima (can be seen on Figure 3.15, Chapter 4, section 4.3.5.1. investigates the throw distributions).

Tmax values are relatively small, ranging from 31-104m (+-7m) (mean value 63m +-7m, Figure 3.14), recorded on horizons within the Brigantian-Asbian interval (ESP-2). The A-E_NE- faults offset Rotliegend and intra-Lower Carboniferous reflections (ESP-1 and ESP-2) by roughly similar amounts on some faults, whereas on other faults the intra-Carboniferous throws are larger than those at the TRot horizon.

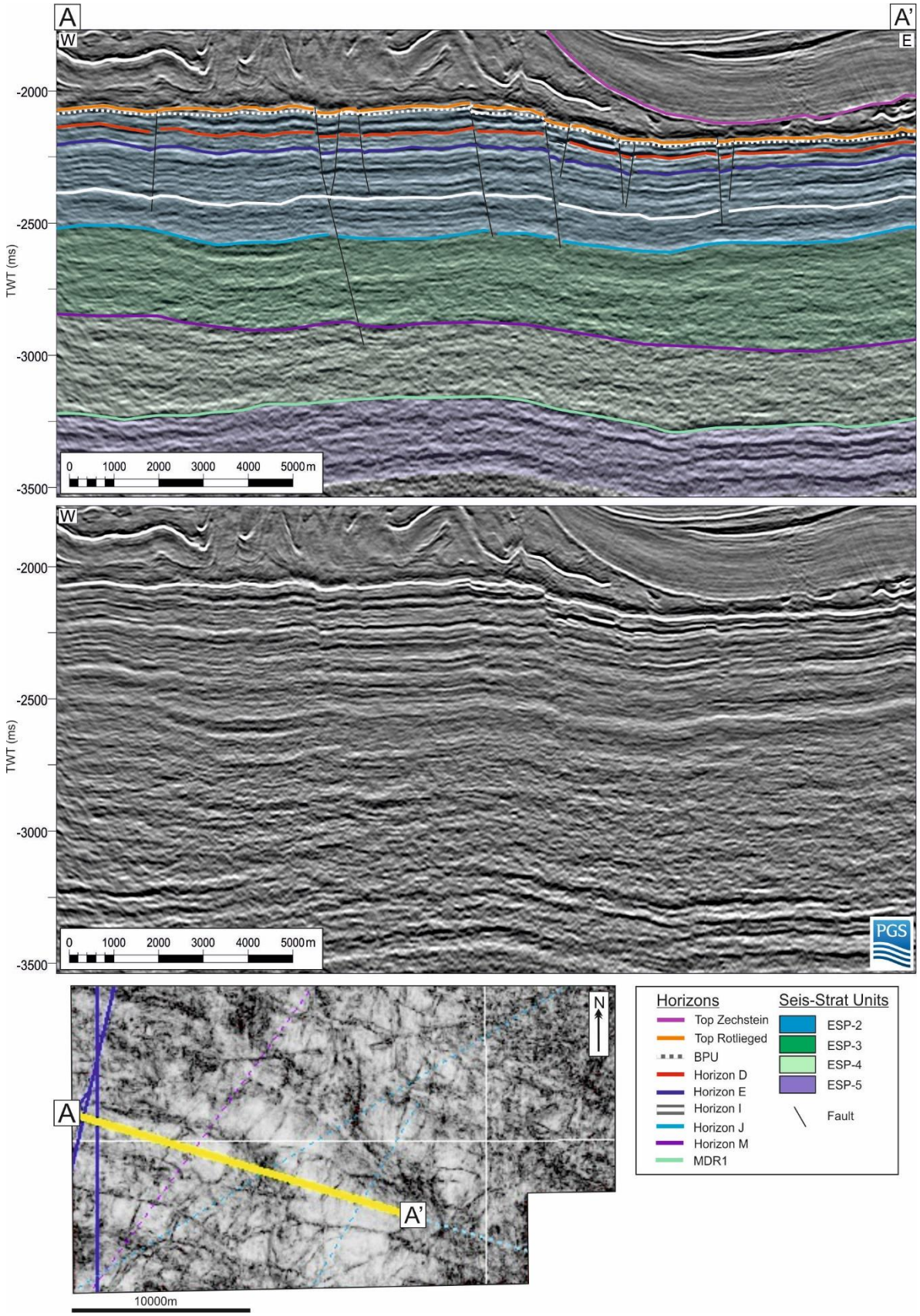


Figure 3.15 The A-E_NE- fault set a) seismic section normal to the NE- faults with mapped horizons and seismic stratigraphy units indicated b) location of seismic section on the intra-Brigantian variance slice.

3.2.3.3 A-E_NNE- Faults

A set of NNE-SSW to N-S (N005-N010°) oriented normal faults are observed in the Pre-Zechstein stratigraphy on the ESH. They have curved or linear trace geometries and lateral lengths ranging from 6000-25000. Spacings between these faults are typically irregular and non-parallel, and faults are clustered in areas.

The faults are dominantly planar, dipping to the east and west at angles ranging from 57-71° (avg. 62°, Figure 3.13). The fault planes extend vertically over 1200ms in seismic cross section (Figure 3.16).

The upper tips of these faults are truncated at the BPU/BCU, typically overlain by undeformed Cretaceous stratigraphy on the ESH. The lower tips are not imaged, with the last coherent reflection offsets of up to 140m being observed within unit ESP-5. This suggests that these faults have lower tips that terminate within the Lower Palaeozoic basement, and hence can be regarded as basement linked.

Recorded tmax values for these faults range from 78-217m (+-9m with an avg.160m, Figure 3.14), recorded on the MDR1 horizon within ESP-5. Growth packages are not observed within the stratigraphic intervals offset by the fault.

3.2.3.4 A-E_ENE- Faults

Laterally extensive, ENE-WSW (N060-N070°) oriented dextral strike-slip faults offset the PZS across the ESP and ESH (Figure 3.17). They are over 40km in lateral length and are linear and segmented. They have a slightly radial arrangement from the north east. Segment lengths range from 10-35km and are separated by structures with uplifted or downthrown PZ stratigraphy.

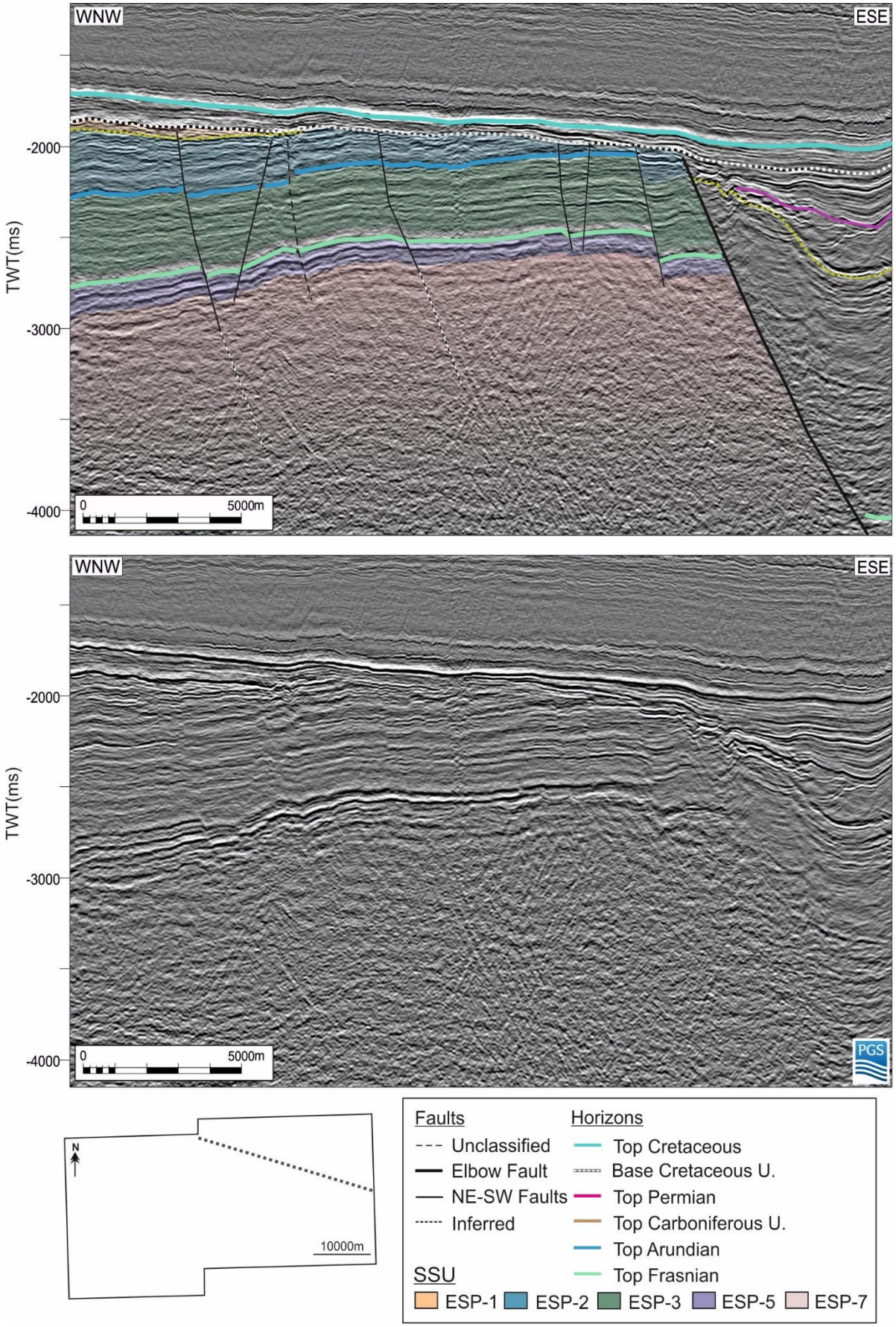


Figure 3.16 Seismic section oriented W-E normal to the A-E_N-S faults

The ENE-WSW faults are difficult to identify in seismic profile as there is only minor vertical offset of reflections. A throughgoing, narrow zone of low coherence extending up to 1500ms below the BPU, is one of the criteria used in their interpretation (Figure 3.17). They have sub-vertical fault planes with dips ranging from 84-90°. The dip angles change along the strike of the individual faults causing the dip direction to alternate from a slight northwest to slight southeasterly direction.

The vertical offset of reflections within the PZS is observed at certain points along strike that correspond to linkage (Figure 3.17). ESP-5 reflections are vertically offset, suggesting that these faults are basement-linked. The TRot horizon across the ESP is offset by these faults. No evidence of movement is expressed in the post-Rotliegend stratigraphy however, apart from a slight doming of Cretaceous stratigraphy over the crest of push-up structures (see geometry of green horizon on Figure 3.17a).

A number of different observations of the sense of slip lead to an interpretation that this fault set has an important strike-slip component. The right lateral offsets of A-E_WNW- of up to 1300m, at oblique intersections is indicative of this slip (Figure 3.17).

An uplifted area of Lower Carboniferous stratigraphy that has elliptical geometry in planform can be viewed on the TRot horizon map and is interpreted as a push-up at a restraining bend (Woodcock and Fischer, 1986). A rhombohedrally shaped structure is also observed between two ENE- faults at a point of linkage on the ESH (Figure 3.17b). It is internally faulted and upthrown to the west of the structure. The stratigraphy within the structure is truncated against the Cretaceous. The structure is interpreted as a contractional duplex at a restraining bend between two right-lateral faults (Woodcock and Fischer, 1986).

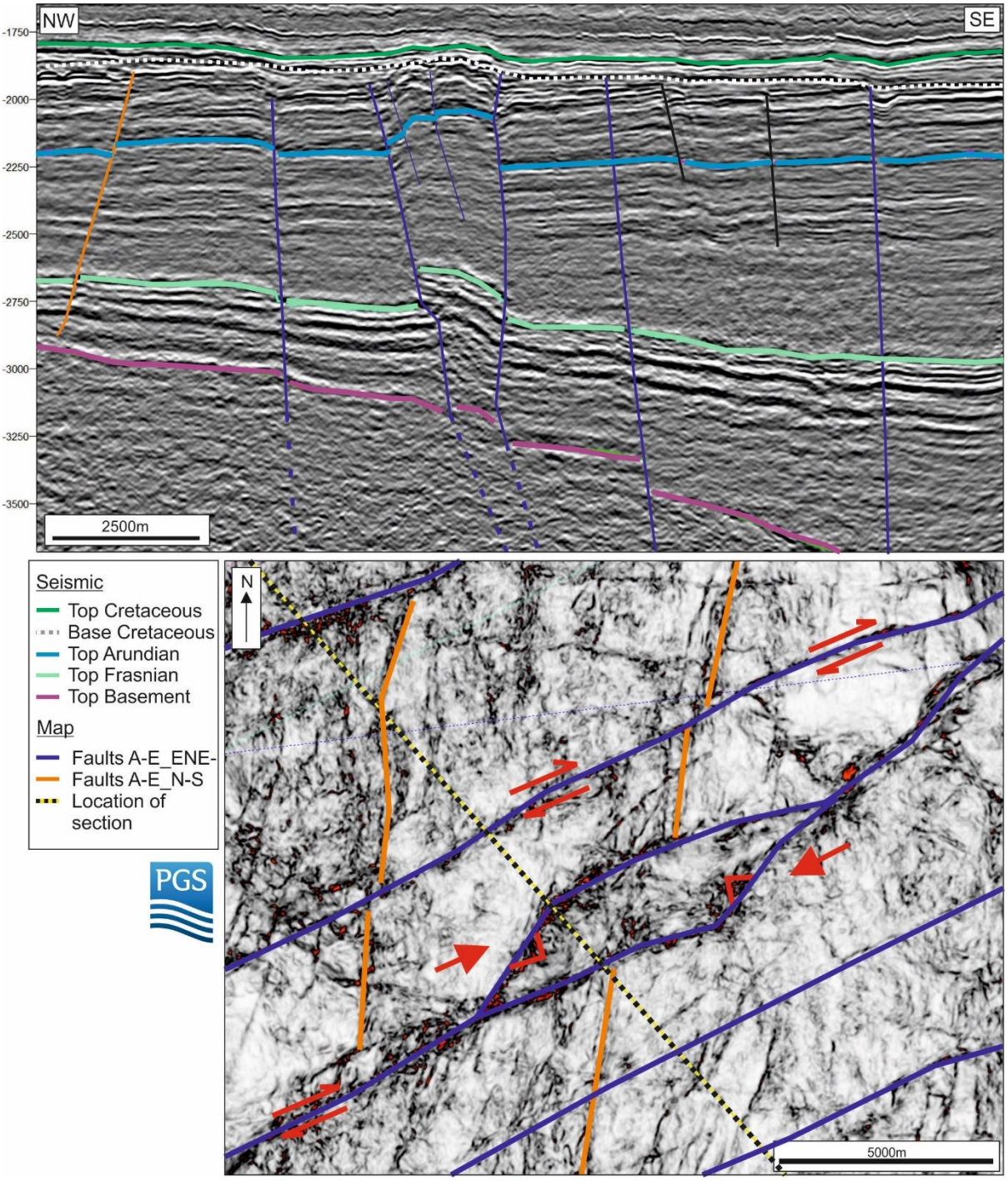


Figure 3.17 The A-E_ENE- fault set a) seismic section normal to the ENE- oriented strike slip faults b) Intra-Asbian variance slice showing the contractional duplex between the strike slip faults that may be an inverted pull apart or single phase contractional (positive flower structure). Notable right lateral offsets of the NNE- faults can be observed. The location of seismic section a. is located on the variance map by the yellow and black line.

3.2.3.5 Elbow Fault

A NW-SE (N130°) orientated normal fault with large throws of up to 2.7km (+-18m) bounds the ESH on its north east margin (Figure 3.9). The Elbow Fault is the most westerly fault connected to the Step/Central graben rift complex. The fault curves around the ESH towards the north west, with only 25km of this much larger fault covered by the 3D seismic data. Published maps (PESGB 2008; (Doornenbal and Stevenson, 2010) suggest that this fault is part of a major Mesozoic graben structure within the Central Graben, measuring over 130km in length.

The fault plane dips to the north east at an angle of ~60° and has a vertical extent of around 6.5km (Figure 3.6). The limited extent of 3D seismic data coverage of the Elbow Graben and the low coherence reflections in the deeper hangingwall stratigraphy, leads to a high degree of uncertainty when correlating reflections across the fault. The Elbow Graben offsets a succession of Base-Cretaceous to Middle-Devonian, as correlated by the Middle Devonian aged ESP 5 unit. Due to the high throw magnitude, it is suspected to offset basement reflections.

The stratigraphy in the footwall of the Elbow Fault is a succession of Lower Carboniferous-Devonian, which is then unconformably overlain by a Cretaceous interval (Figure 3.6). The stratigraphy in the hangingwall consists of a thick Devonian-Triassic succession, unconformably overlain by the Cretaceous. This erosional hiatus prevents the direct correlation of stratigraphy between the ages of Lower Carboniferous and Cretaceous across the fault.

3.3 Silverpit Basin and Murdoch Block (SB-MB)

3.3.1 Background

The Silverpit Basin (SB) and Murdoch Block (MB) are located mostly in the UK Southern North Sea, with a small portion within the Dutch Sector.

The 3D seismic data used to characterize the MB is a ~1,000km^2 volume within the PGS megamerge dataset (see Chapter 1, section 1.5.1.1) that straddles the UK/Dutch boundary within blocks 44/14, 19, 24 and D. The 3D seismic volume used to examine the SB is a ~3,000km^2 volume also from the PGS megamerge, situated in blocks 44/26-28 and 49/1-3.

Both areas contain a number of Pre-Zechstein well penetrations and hydrocarbon fields with Carboniferous reservoirs (Figure 3.18). Each area has variable data quality that is usually determined by the variable thickness of the overlying Zechstein overburden (Figure 3.19).

3.3.2 General structural and stratigraphic context

The SB and MB areas are adjacent, separated by the major NW-SE trending fault system. The Murdoch Fault Zone (Figure 2.23) is the boundary at which the dominant Pre Zechstein NW-SE trend of the Silverpit Basin changes to a more E-W dominated trend on the Murdoch Block to the northeast.

The post-Zechstein stratigraphic succession across the area is calibrated to be Permian-Triassic with an unconformity between the Triassic and Cretaceous, followed by a Late Cretaceous-Cenozoic infill (Figure 3.21). The Pre-Zechstein is calibrated to be Rotliegend-Namurian, although underlying Visean stratigraphy is inferred (Cameron et al., 1992).

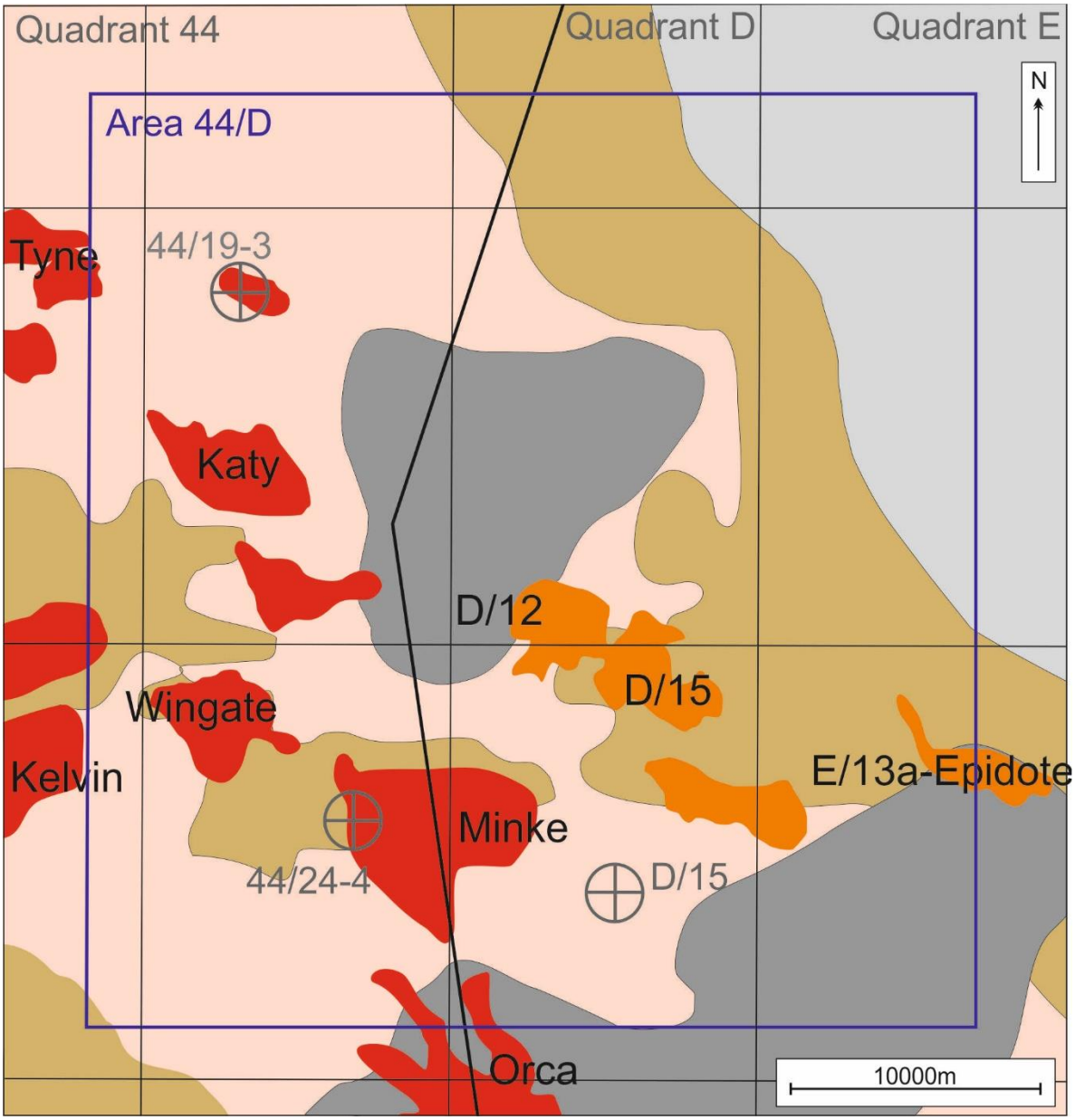


Figure 3.18 Map of the Murdoch Block indicating Base Permian Subcrop chronostratigraphy and the position of known Carboniferous Hydrocarbon fields. Light grey Westphalian A/Langsettian, Light Brown: Westphalian B/Duckmantian, Light pink: Westphalian C/Bolsovan, Dark Grey: Westphalian D/Asturian. Red areas indicate positions of UK gas fields, orange indicates the position of Dutch Gas fields. Subcrop sourced from Doornenbal & Stevenson (2010). Well and Carboniferous gas field locations sourced from PESGB 2008.

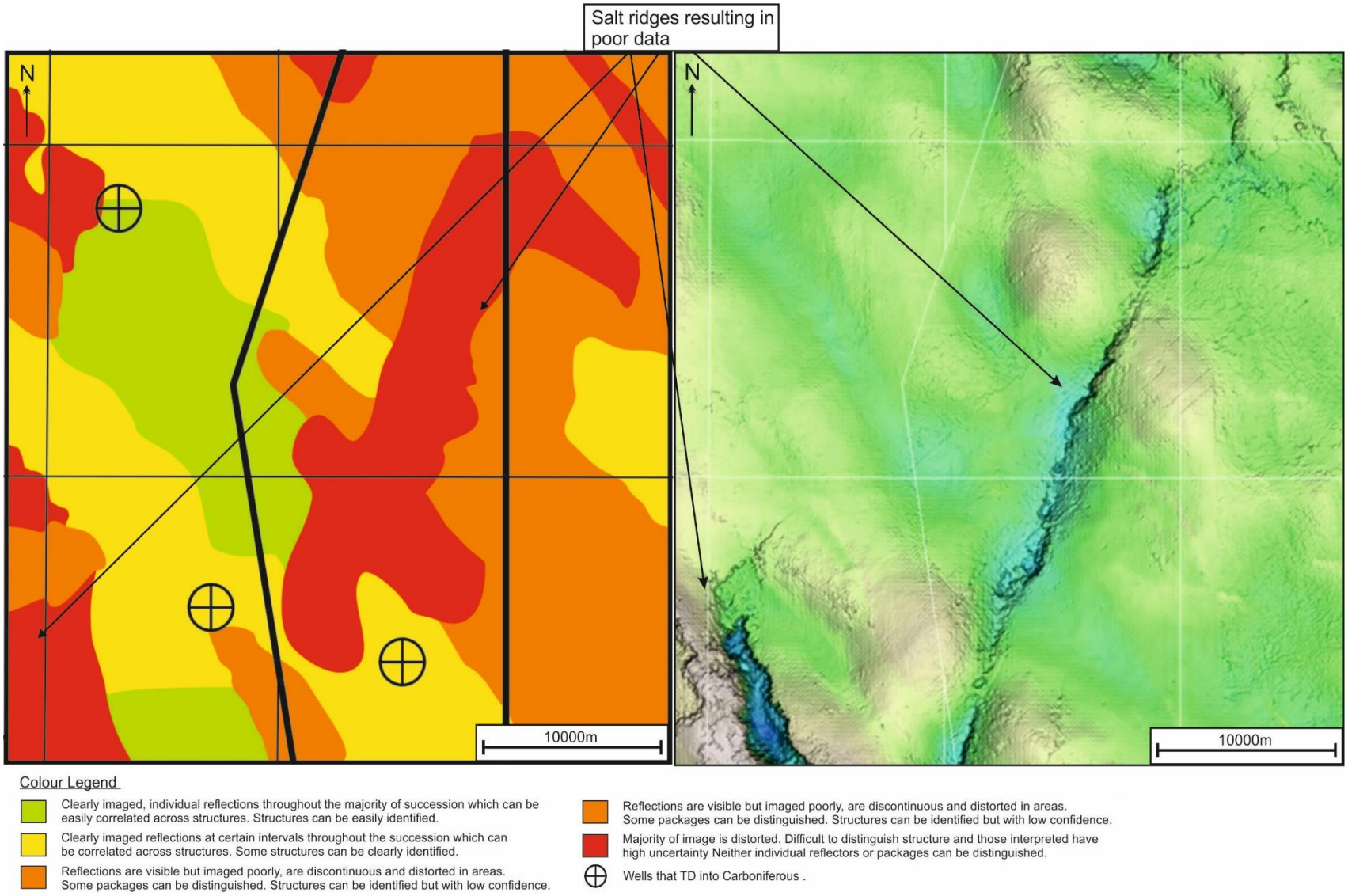


Figure 3.19 Murdoch Block a) Data quality map b) Isochore map of Zechstein thickness. Blue areas indicate thick salt structures and white/yellow where the Zechstein is thinner.

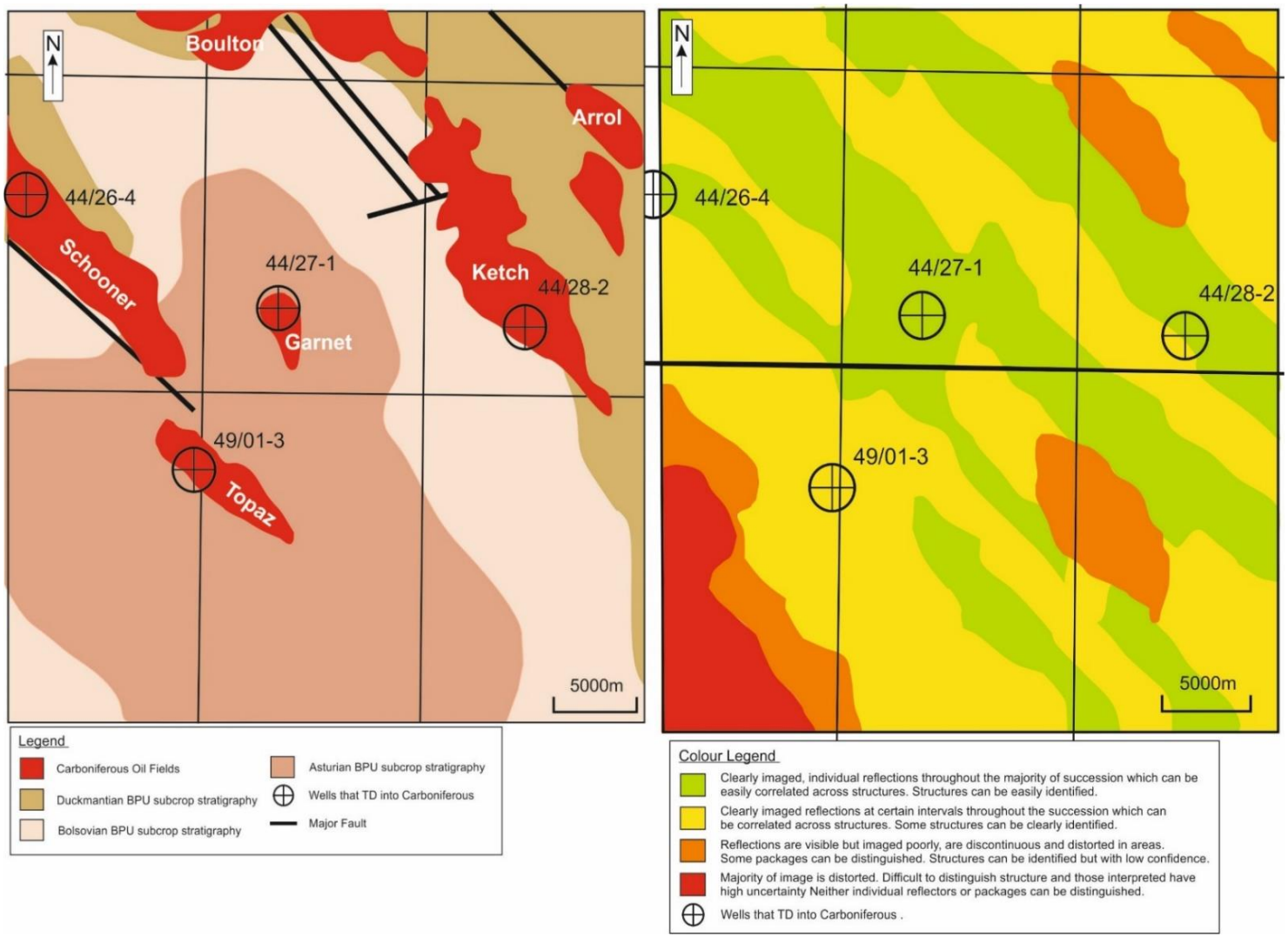


Figure 3.20 Silverpit Basin a) Base Permian Subcrop Map b) Data quality map of the Silverpit Basin case study area

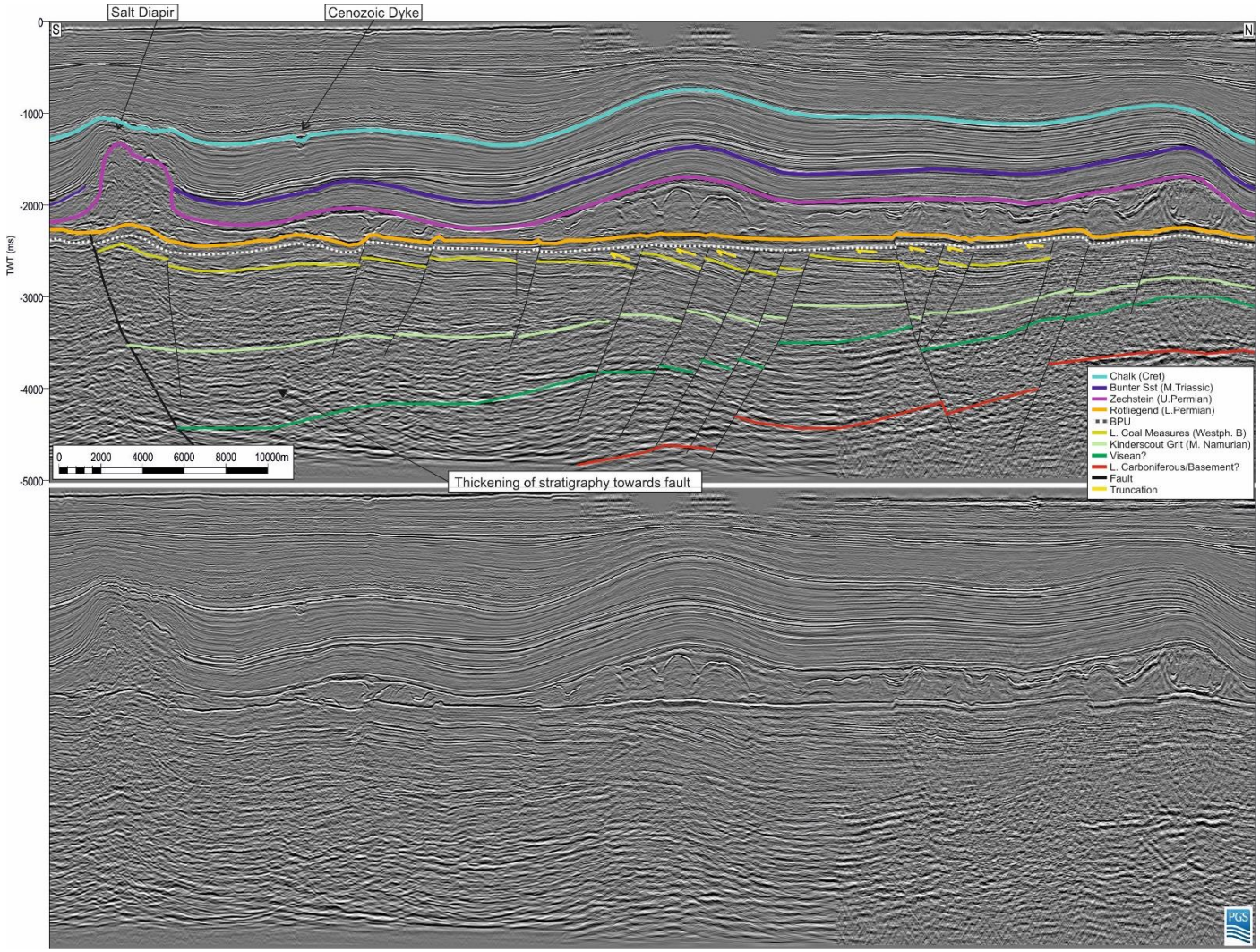


Figure 3.21 N-S Geoseismic section transecting the Murdoch Block.

The Base Permian subcrop ranges from Westphalian B-D (Figure 3.18), with the younger stratigraphy preserved in the synclines and hangingwalls. The geometry of the PZS is a wedge that thickens overall to the south, with an overall stratigraphic dip to the north (~5-8°), caused by the rotation of E-W trending faults (Figure 3.21). A network of faults and folds (described in the following sections) deforms the PZS. A seismic stratigraphic framework devised for the PZS of the central Anglo-Dutch basin has been constructed and is summarized in Figure 3.22. A more detailed account of the Silverpit Basin structure and stratigraphy can be found in section 2.5.1.

3.3.3 Murdoch Block Structural Sets

A complex network of faults is observed on the Murdoch Block. The fault patterns are strikingly different when observed on either the Top-Rotliegend horizon – variance map or intra-Westphalian isoproportional variance slices (Figure 3.23). Four main fault sets have been identified.

3.3.3.1 44-D_NNW- Faults

A set of NNW-SSE (N155-160°) normal faults are identified in the Pre-Zechstein stratigraphy in the Murdoch Block area (Figure 3.24). They are curvilinear in map view with lengths ranging from 5-13km. Their planform arrangement is parallel with regular spacing and in a slight right-stepping en echelon array.

In cross section, the faults have steep (60-74°) planar fault plane geometries that dip to the WSW and ENE (Figure 3.25). The fault planes have a vertical extent of 100ms~ below the Base Zechstein. The upper fault tips are interpreted to terminate in the basal Zechstein within the mobile evaporite units. The lower tips are interpreted to

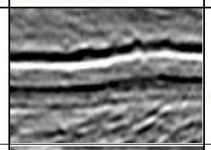
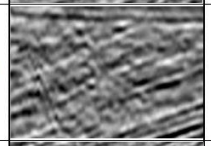
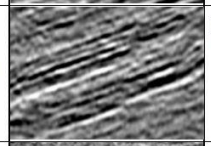
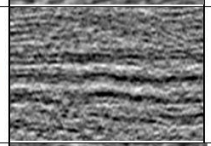
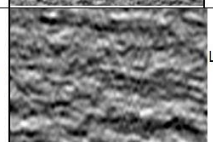
Unit Top	Unit Base	Seismic-strat Unit	Seismic Facies	Seismic Facies Description	Unit Thickness (ms)	Contact with Upper Boundary	Contact with Lower Boundary	Package Geometry	Chrono-stratigraphy	Litho-stratigraphy	Description	Locally Mapped Horizons	Calibrated by
Top Rotligend	BPU/Intra-Westphalian C-D	**ADB 1**		High amplitude, postive reflection overlaying a high amplitude negative reflection	~80-150ms, thinner in the north and thicker in the SE	Conformable with Base Zechstein - High acoustic impedance contrast between Basalanhydrite Fm and Silverpit Formation	Base of unit unconformably overlies dipping Intra-Westphalian D-C/BPU	Laterally continuous, parallel reflections, E-W channels	Rotliegend	Silverpit Formation	Red-Brown mudstones and siltstones with local halite and sandstone beds (Cameron 1993)	TRot, BPU	Wells 44/24-4 44/27-1, 44/19-3
Intra-Westphalian D-C/BPU	Intra-Westphalian C	**ADB 2**		Low amplitude, high frequency, discordant reflections,	~100-130ms	Low reflection coefficient between Silverpit Fm and Brig Fm producing non-distinct boundary	Base of unit is picked at the point where the reflections become stronger	Northward dipping. Only preserved in hangingwalls of large faults. Contains peg leg multiples that are parallel to the TRot and cross cut the dipping reflections	Westphalian D-C	Brig Formation, Ketch Member, Schooner Fm (Upper Coal Measures)	Red sandstone beds with interbedded mudstones (Cameron 1993)	-	Well 44/19-3
Intra-Westphalian C	Intra-Westphalian A	**ADB 3**		High amplitude, positive and negative reflections that are parallel and laterally continuous, seprated by intervals of discordant, low amplitude reflections	~250-400ms	Top of unit picked at the first high amplitude reflection, mapped as intra-Westphalian C	Base of unit picked where the reflections become weak and discontinuous. Mapped as intra Lower Coal Measures	Northward dipping. Offset by faults.	Westphalian C-A	Schooner Fm, Westoe Coal Fm (Middle Coal Measures)	Mudstones, channel sandstones, sandstone beds and ocasional coal seams (Cameron 1993)	intra-MCM 1, 2, intra-LCM 1, 2	Well 44-27
Intra-Westphalian A	Top Arnsbergian?	**ADB 4**		Low amplitude, hummocky reflections. Contains an interval of higher frequency negative reflections that merge due to low resolution and tuning.	~400-1070ms	Top of unit picked where the reflections become weak and discontinuous. Mapped as intra-Lower Coal Measures	Base of unit is delineated where reflection amplitude increases, signal to noise ratio decreases	Wedge shaped unit, thickens southwards. Northwards onlapping and pinch out of reflections over folds.	Westphalian A-Arnsbergian	Caister Coal Fm (Lower Coal Measures)., Millstone Grit Formation incl. Kinderscout Grit	Mudstones, seateart, coal seams and sandstone beds.	Intra-KG	Well 44-19-3
Top Arnsbergian ?	Intra-Visean	**ADB 5**		Low amplitude, low fequency, discordant, highly chaotic, low signal to noise ratio		Top of unit is delineated where reflection amplitude increases, signal to noise ratio decreases	No clear base/data extent reach	Unit geometry thickens southwards	Arnsbergian? - Visean?	Yoredale Fm? Bowland Shale Fm?-	Mudstones	-	Not calibrated, chrono and lithostratigraphy interpreted from ?

Figure 3.22 Seismic stratigraphy units in the Pre-Zechstein on the Anglo-Dutch Basin. Units range from Rotliegend to Lower Namurian.

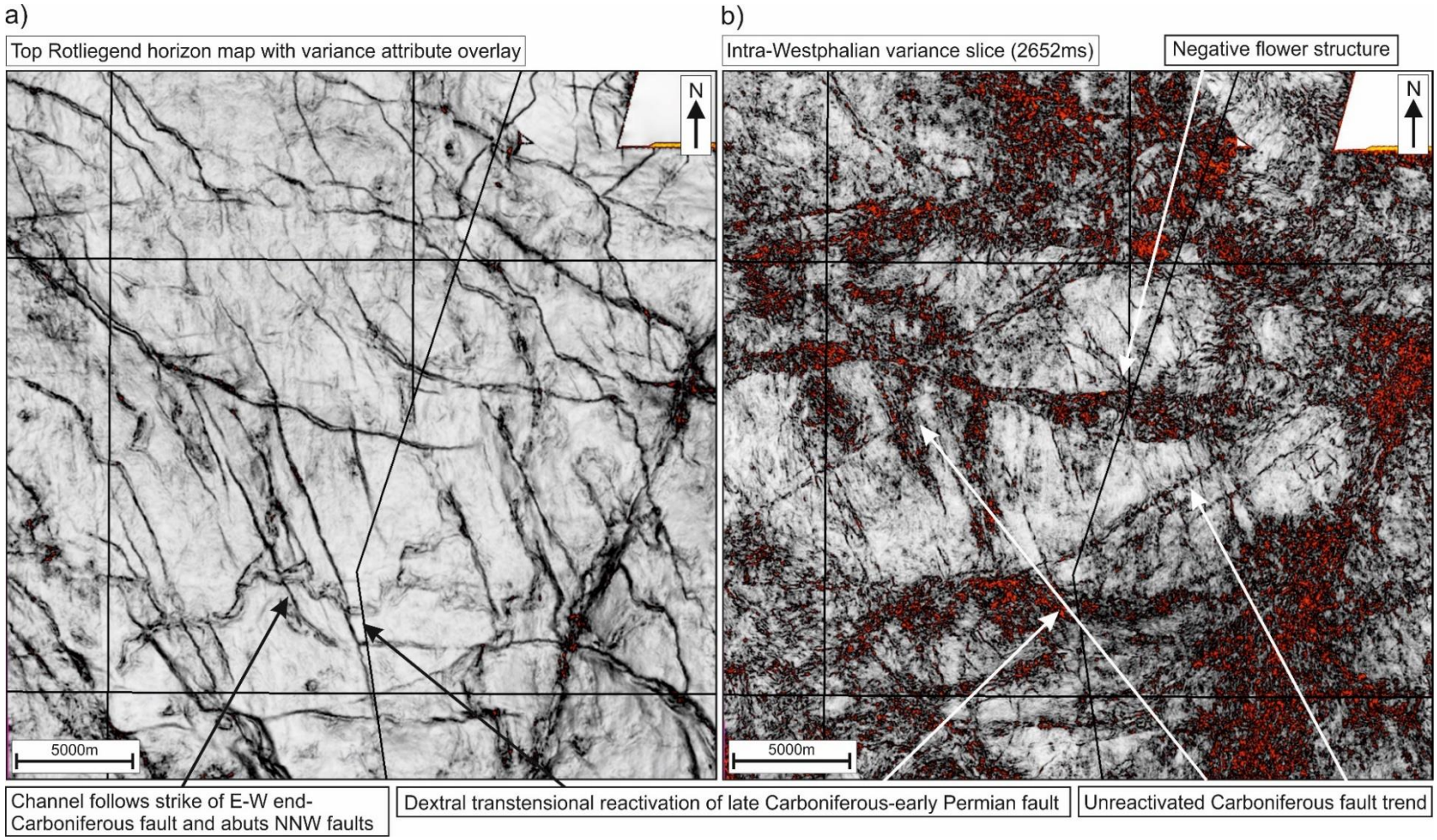


Figure 3.23 a) Top Rotliegend horizon map with variance extracted and overlaid, in the Murdoch Block. Dark areas highlight discontinues in seismic amplitude representing faults and channels. b) Isoproportional Intra-Westphalian variance slice 100ms below the base-Permian Unconformity. This slice highlights the presence of structural features that have no expression in younger stratigraphy as they have not been reactivated after the Carboniferous, notably the ENE- trend.

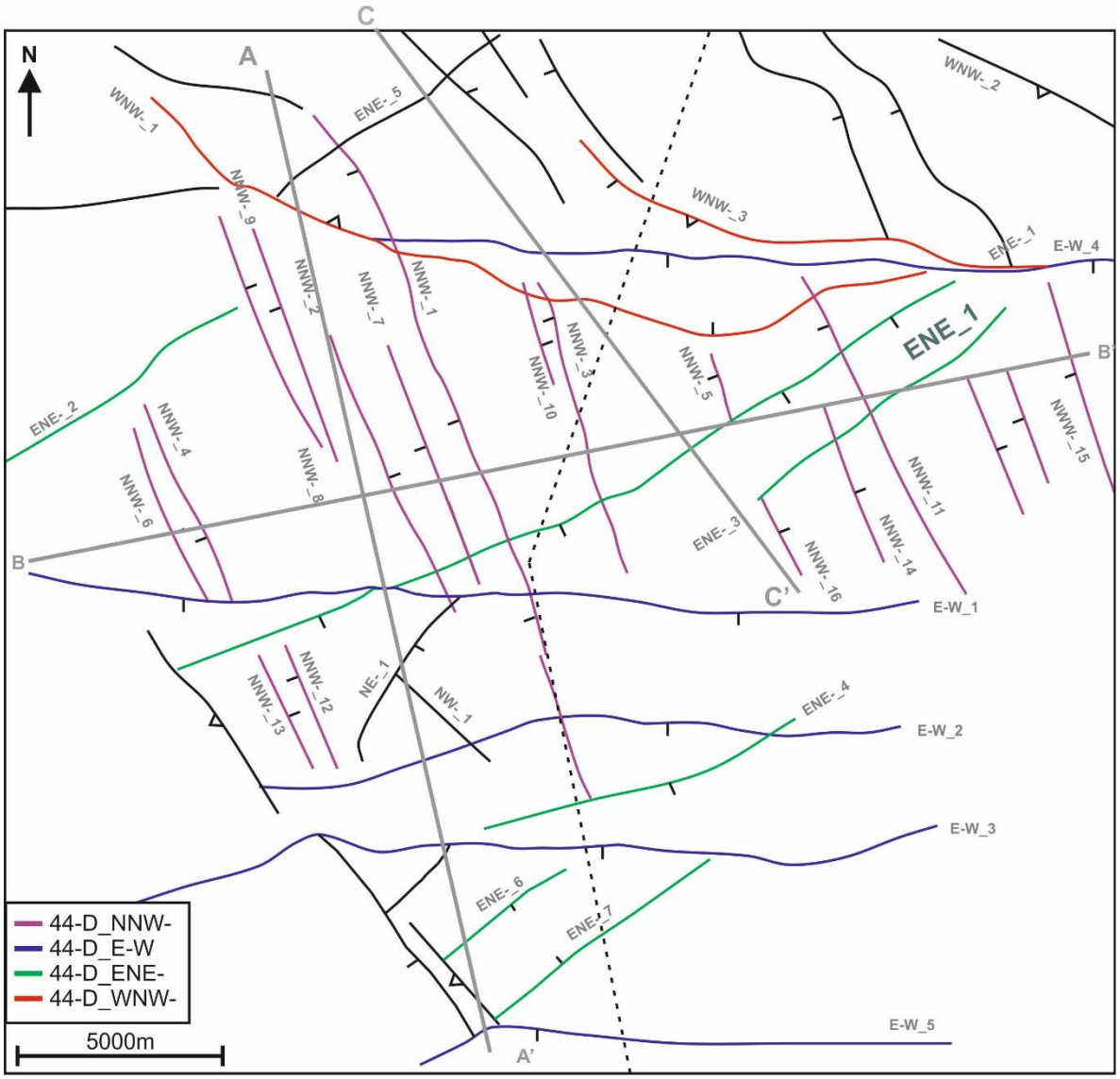


Figure 3.24 Composite fault map of all faults in the Pre-Zechstein of the Murdoch Block. Different fault sets are indicated by the colour key.

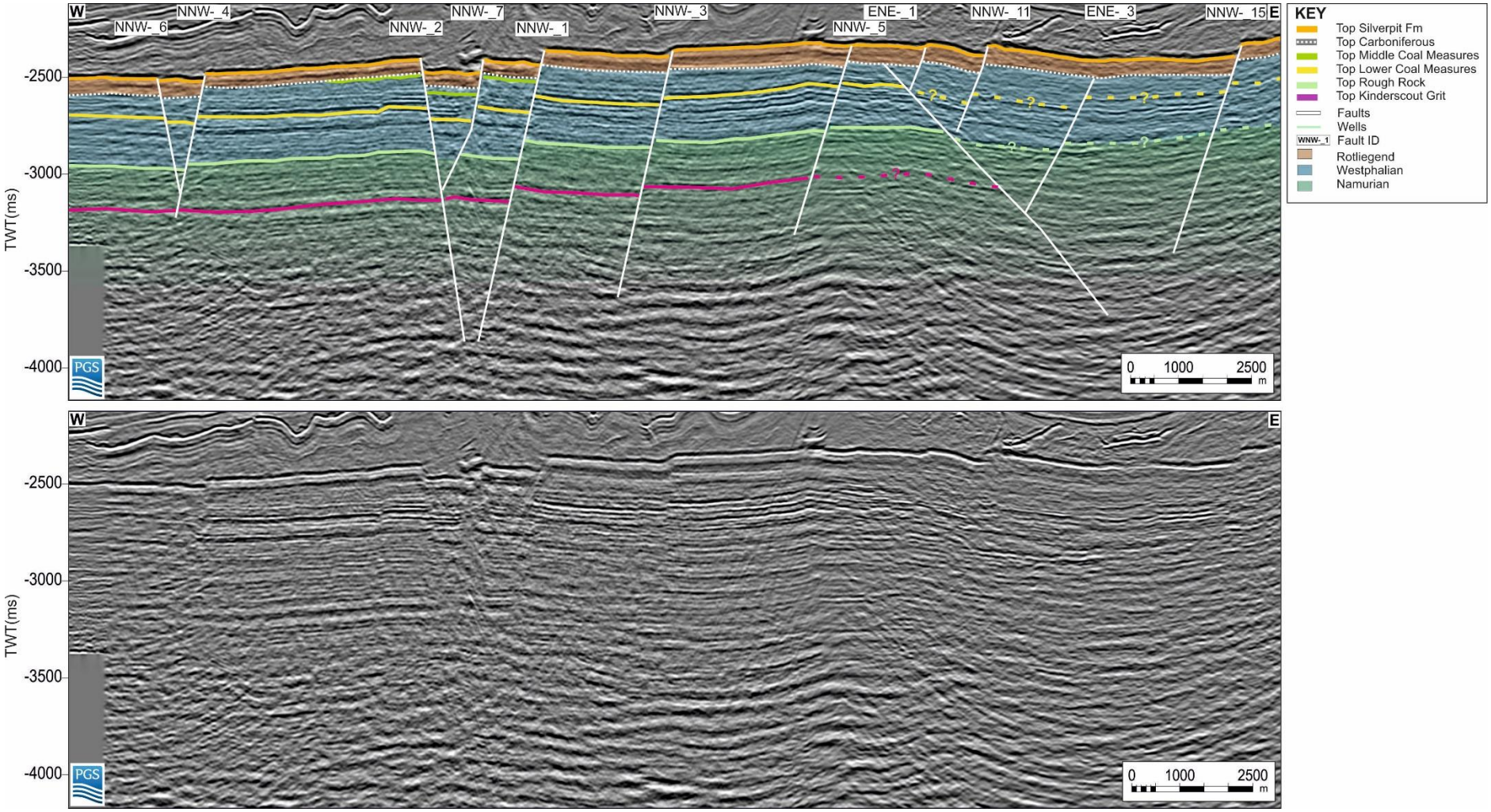


Figure 3.25 ENE-WSW seismic cross section through the PZS of the Murdoch Block, sub-normal to the NNW- faults. Location of section in Figure 3.24

terminate in the Lower Namurian, though the seismic signal becomes more distorted at and below this level, and thus the exact basal tip geometries are uncertain.

Maximum throws are recorded on both the Top Rotliegend and intra-Westphalian horizons. Tmax values and range from 47-356m (+-7m) with an average of 169m (). Some faults exhibit offset TRot and Intra-Carboniferous horizons by similar amounts, whereas on other faults the intra-Carboniferous throws are larger than those on the Rotliegend and BPU horizons.

Stratal reflections in the hangingwall show little evidence of rotation or folding. A gentle dip of <5° towards the fault plane is observed. The horizon cut-offs at the fault are sharp and clearly defined.

3.3.3.2 44-D_E-W Faults

A set of E-W (N090-N095°) net normal faults have been identified in the Murdoch Block and adjacent areas to the north (Figure 3.24). They have a curvilinear to curved planform geometry with lengths ranging from 4-22km and an irregular spacing. Fault plane geometries are planar to slightly listric, exclusively dipping to the south at angles ranging from 46-76° (avg. 55°). Stratal reflections in the hangingwall are rotated, preserving younger stratigraphy of Westphalian C-D age (Figure 3.26).

Maximum throws range from 140-801m (+- 9m) with a mean value of 418m (Figure 3.27) and are recorded on intra-Westphalian horizons such as the laterally extensive intra-Middle Coal Measures horizon (iMCM). These are the maximum retained normal throws as some faults presently show a slight reverse reactivation.

The majority of upper fault tips on E-W faults are truncated at the BPU, there is evidence of local reverse reactivation at certain points along strike however.

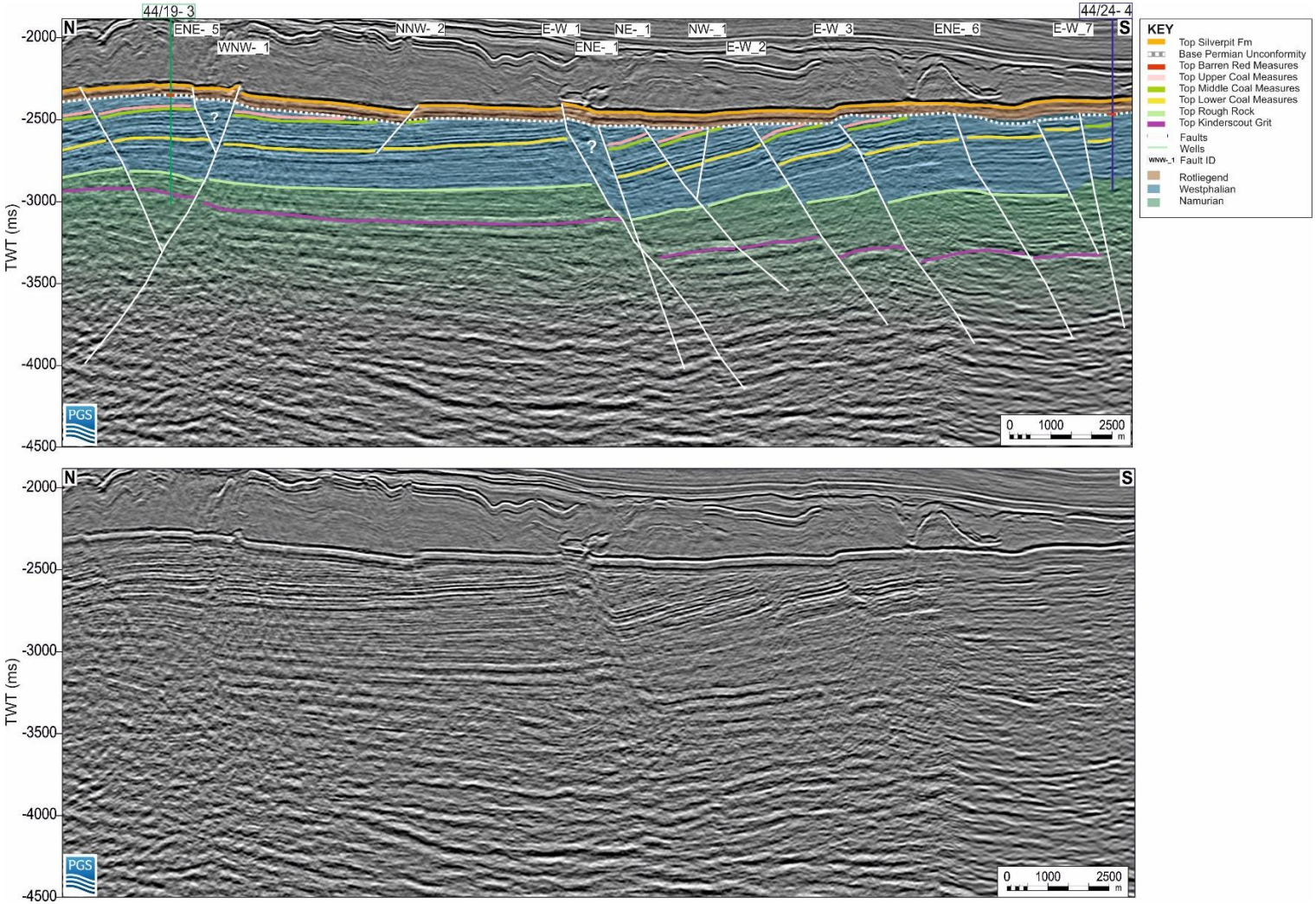


Figure 3.26 North-South seismic cross section through the the PZS of the Murdoch Block. The south dipping E-W faults offset the syn-rift stratigraphy of a alrger north dipping fault to the south of this section. Map location of section on Figure 3.24.

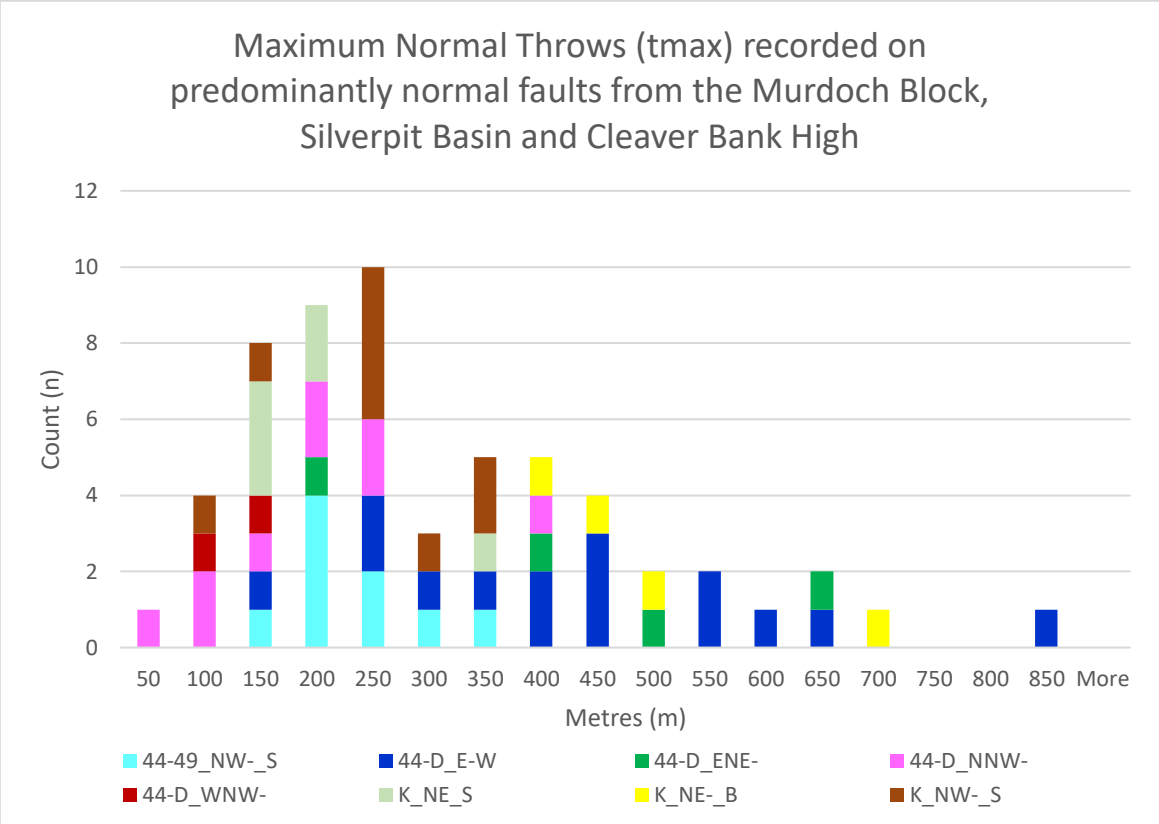


Figure 3.27 Histogram of Pre-Zechstein Tmax values on sampled faults in the Murdoch Block, Silverpit Basin and Cleaver Bank High. Different fault sets are indicated by the colour key an conform to map colour codes.

This is identified by the upwards propagation of the tips through the Rotliegend interval, into the mobile Zechstein unit. The TRot horizon is offset in a reverse sense up to ~90m at these discrete positions (see Chapter 4, section 4.3.4.1.).

The basal tips positions are uncertain due to the significant decrease in image quality with depth. The extent of the fault plane is estimated to extend up to 200ms below the Base Zechstein. The high throws indicate the large scale of these faults, which in turn suggests their basal tips are located at depth and are possibly not imaged by the seismic data. This uncertainty is explored in Chapter 4, section 4.5.1.

A right lateral offset is observed of NNW- faults at intersections with some E-W faults and push-up (Woodcock & Fischer 1986) structures are observed on some

of the E-W faults to the south. This right lateral (dextral) offset is in disagreement with the sinistral movement on these faults, proposed by Coward (1990), but due to these faults being reactivated on multiple occasions through time, a variance in offset indicators is expected.

The gross stratigraphic succession thickens to the south with an onlapping/thinning to the north. There are no growth packages observed in the hangingwall of these E-W trending faults, but a slight change in stratigraphic thickness is observed across the fault. This is interpreted to be consistent with the overall basinward thickening of stratigraphy to the south in this area (). The local nature of the reverse movement on the E-W faults may also be indicative of lateral movements. These faults were also identified by Hollywood (1993) and Schroot and De Haan (2003).

3.3.3.3 44-D_ENE- Faults

The ENE- faults are an atypical set, as though they trend ENE- (N060-N070°) and have similar planform geometries (Figure 3.24), they have contrasting cross sectional geometries (Figure 3.28). The faults are linear in map view with lengths ranging from 9-15km. They are hard to detect on seismic sections due to their high dip angles and are only imaged at certain intra-Westphalian variance intervals.

Fault plane geometries vary, with some faults exhibiting a planar geometry and others with a planar-ramp profile. Their dips range from 55-81° with the planar profiles exhibiting the steeper dips. Fault ENE-_1 dips to the SE at ~55° while ENE-_2, ENE-_3 and ENE-_5 have sub-vertical fault planes (~81°).

The upper tips of all ENE- faults are truncated at the BPU with no offset of the BPU or TRot horizon observed (Figure 3.28). The ENE- faults therefore show no evidence of reactivation that post-dates the deposition the Rotliegend. The basal

tip positions and termination nature are uncertain due to the poorer seismic image at depth. They are however estimated to extend at least 1250ms below the base Zechstein.

Maximum throws vary considerably between faults of this orientation. They are recorded on intra-Westphalian horizons and range from 157-610m (+-9m) with a mean value of 399m. Fault ENE-_1 is shallower dipping to the SSE and records a Tmax of 610m (+-9m) on the iMCM horizon. However, fault ENE-_2 has a sub-vertical fault plane with throws of ~28m on the iMCM horizon.

3.3.3.4 44-D_WNW- Faults

Faults with a WNW-ESE (N110-N120°) orientation are curved in map view with lengths ranging from 15-20km (Figure 3.24). They exhibit net normal and net reverse throw sense which changes along strike, typically at fault intersections (Figure 3.29). The WNW- orientated faults dip to the north at angles of ~54°. Detailed 3D geometries are difficult to reconstruct however due to image quality issues. The upper tips terminate into the mobile Zechstein unit, offsetting Rotliegend and Carboniferous horizons. The lower tips are interpreted to terminate below the Upper Visean, with the fault plane extending over 2000ms below the Base Zechstein.

Maximum recorded normal throws range from 72-149m (+-9m) (mean value of 110m) and are recorded on intra-Carboniferous reflections, with Rotliegend and Carboniferous horizons being offset by similar amounts. The stratal reflections in the hangingwall are folded into a rollover anticline and dip towards the fault plane.

An area of downthrown stratigraphy between faults E-W_4 and WNW-_1 is ellipsoidal in map view and contains a thicker preserved Late Carboniferous succession (Figure 3.29).

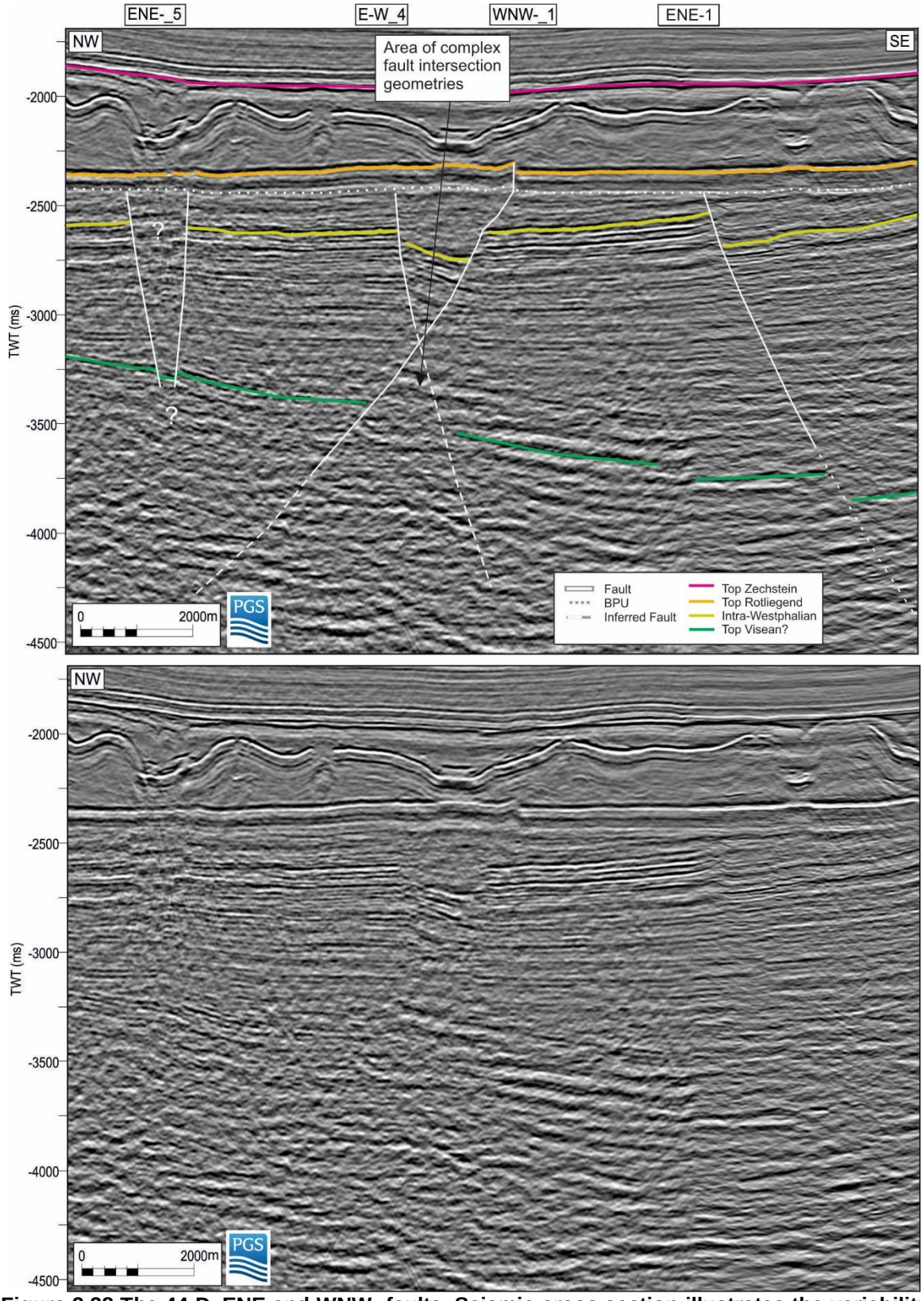


Figure 3.28 The 44-D_ENE and WNW- faults. Seismic cross section illustrates the variability between ENE- fault vertical profiles

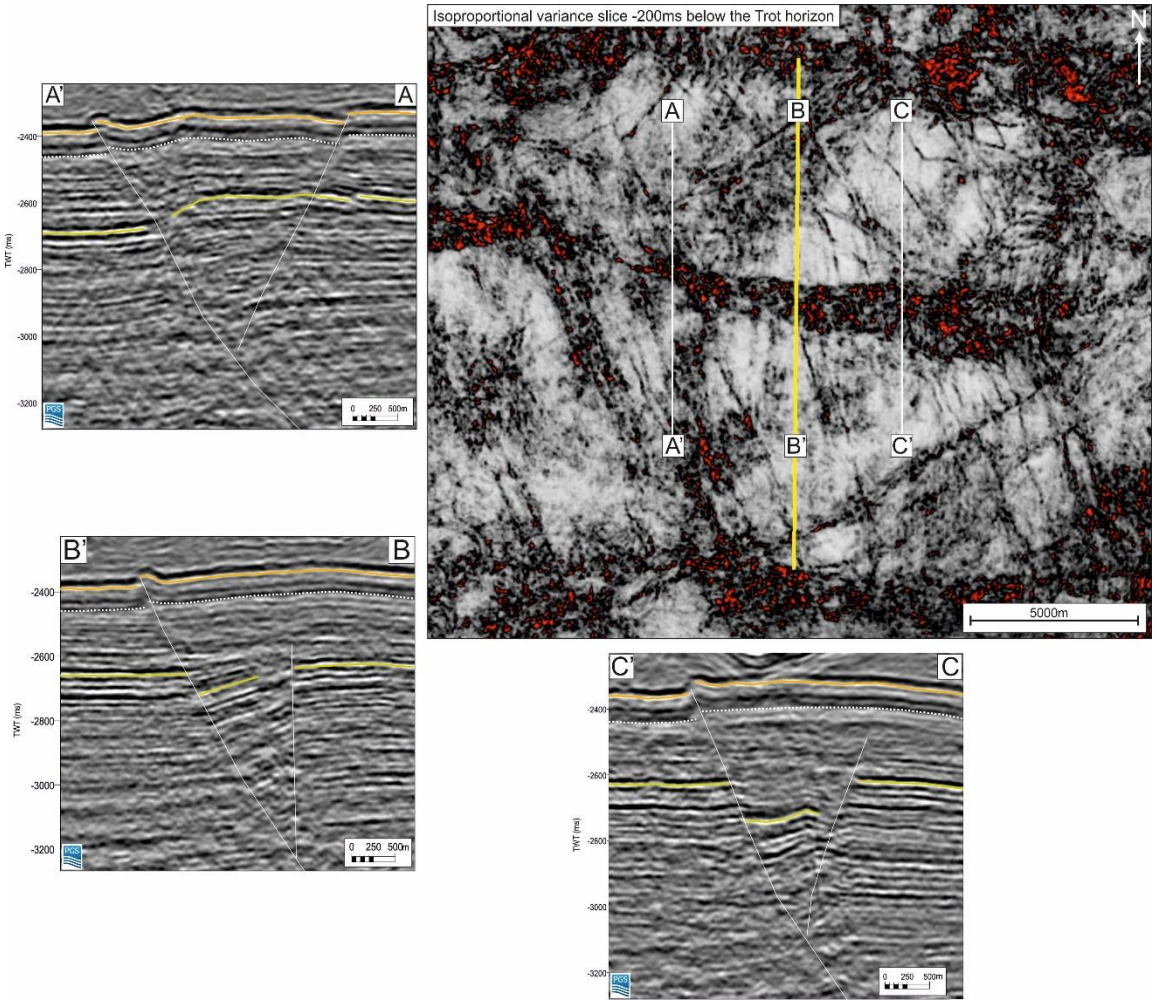


Figure 3.29 N-S seismic cross sections at three points along the push down structure inbetween WNW-_1 and E-W_4. Observed thickening of upper Carboniferous before post-Rotliegend uplift, indicating the structure formed before the deposition of the Rotliegend. This structure is interpreted as a negative flower structure.

This is interpreted to be a push-down/pull apart feature created by strike-slip movement on the E-W_4 major fault zone. The lateral slip sense of is unclear as cross cutting faults do not show obvious ofsetted relationships by this E-W fault zone.

3.3.4 Silverpit Basin Structural Sets

The southern area of the Silverpit Basin examined in this case study contrasts markedly with the other case study areas as it is dominated by NW-SE trending faults and doesn't exhibit an equally significant cross-cutting fault system. A set of folds and four sets of faults have been identified (Figure 3.30).

3.3.4.1 44-49_NW-_D Folds

The pre-Permian stratigraphy in the southern Silverpit Basin is gently folded into roughly symmetrical folds with a NW-SE (N130°) axial trend (Figure 3.31). Their lateral extent is uncertain due to image quality continuity issues at depths, but they are estimated to laterally extend over 60km. The folds have long wavelengths of ~20km and smaller amplitudes ~1.5km. Stratal reflections in the fold limbs dip ~5° when measured on seismic flattened at the BPU, giving their pre-Permian dips (Figure 3.32). The Westphalian-Visean succession is folded and there is an observable thinning of the more recent stratigraphy in the package (postulated Westphalian-Namurian, Unit ADB-4) over the fold crest.

The dipping Westphalian reflections are truncated against the BPU on each limb, and the deep fault geometry is still present when the seismic section is restored on the BPU horizon, indicating that the fold pre-dates the deposition of the Rotliegend.

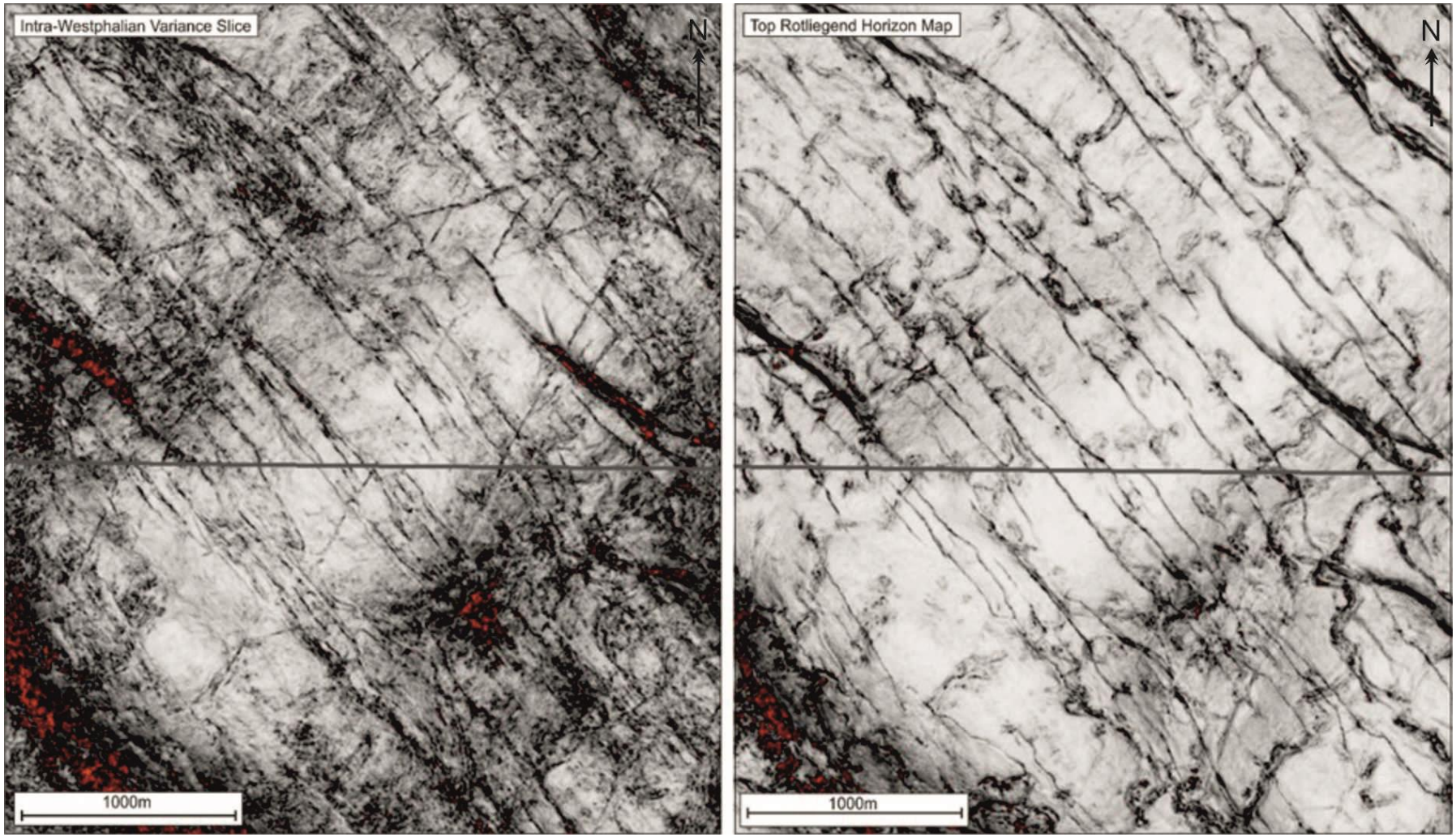


Figure 3.30 Variance slices across the Silverpit Basin case study area a) intra-Westphalian variance slice -100ms below the BPU. This slice highlights the presence of NE-SW and ENE- faults that are not visible on the Top Rotliegend horizon map. Their concealment is due to their lack of significant offset of the Top Rotliegend. b) Top Rotliegend horizon map with variance exhibiting the dominant NW-SE trend. Channels paths are unaffected by the faults indicating that the majority of faulting occurred after the deposition of the Rotliegend.

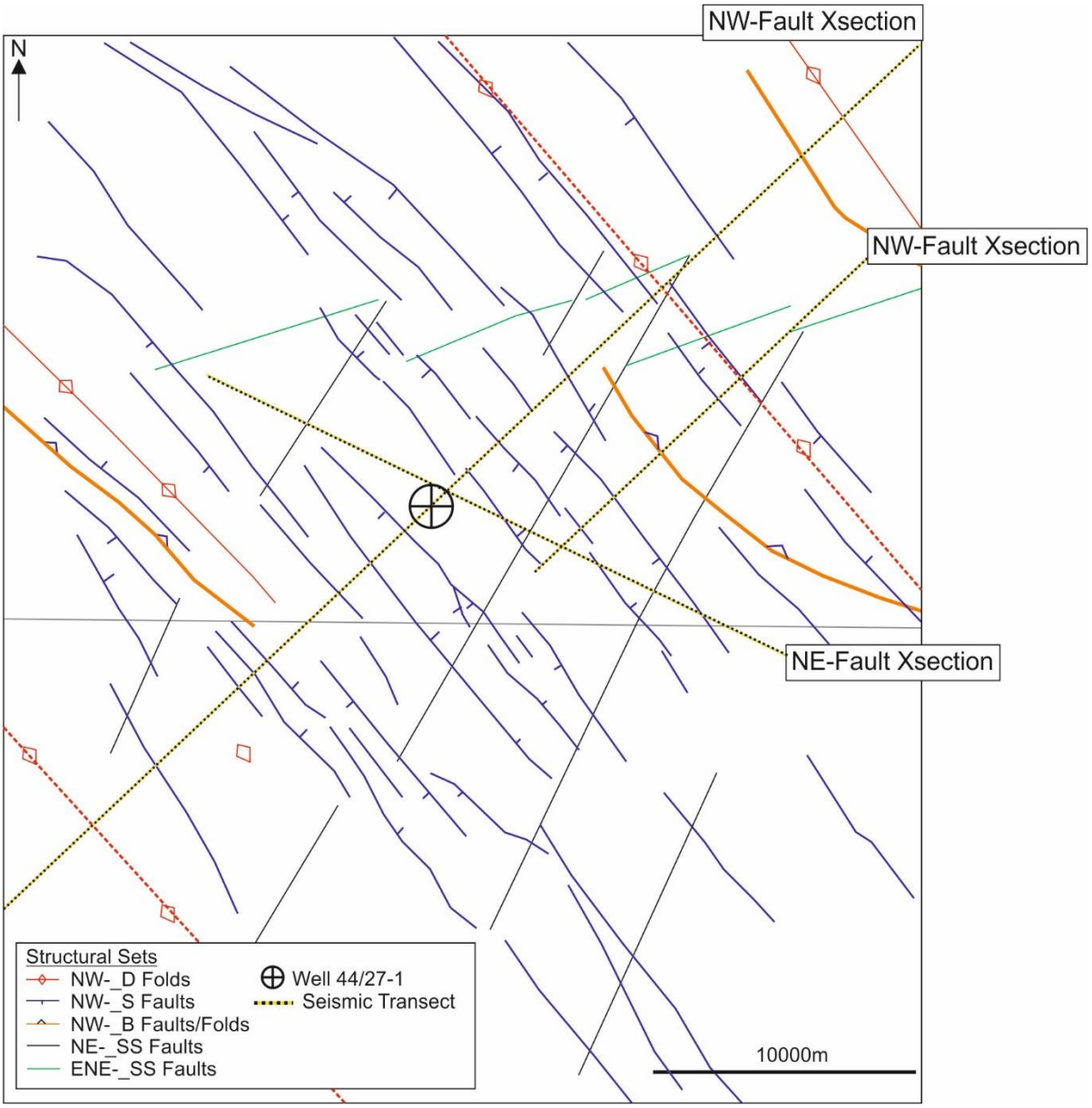


Figure 3.31 Composite structural map showing all faults and folds within the Pre-Zechstein succession in the Silverpit Basin case study area.

3.3.4.2 44-49_NW-_P Faults

A set of NW-SE (N140-N145°) oriented normal faults that are linear and curvilinear in map view and highly segmented (Figure 3.31). Lateral lengths range from 15-25km with segment lengths ranging from 2.5-10km. They are arranged in a parallel array with a mostly even spacing of 1.5km.

The faults have a horst and graben arrangement in cross section with outer bounding rotated half grabens (Figure 3.32). The fault planes have planar geometries that steepen with depth, average dips to the NE and SW in roughly equal proportions, ranging from 65-74° (mean value of 69°, Figure 3.33).

The upper tips terminate in the overlying mobile Zechstein unit, with the fault planes extending to around 1500ms below the Base Zechstein. The lower tips generally occur within seismic stratigraphy unit ADB-4 (Figure 3.32). Depending on throw magnitudes, some faults terminate mid-way through this unit while others tip out near the base. Some folding of stratal reflections underlying some NW-_P fault planes is observed within Unit ADB-5 which may indicate the termination of some lower tips into this unit.

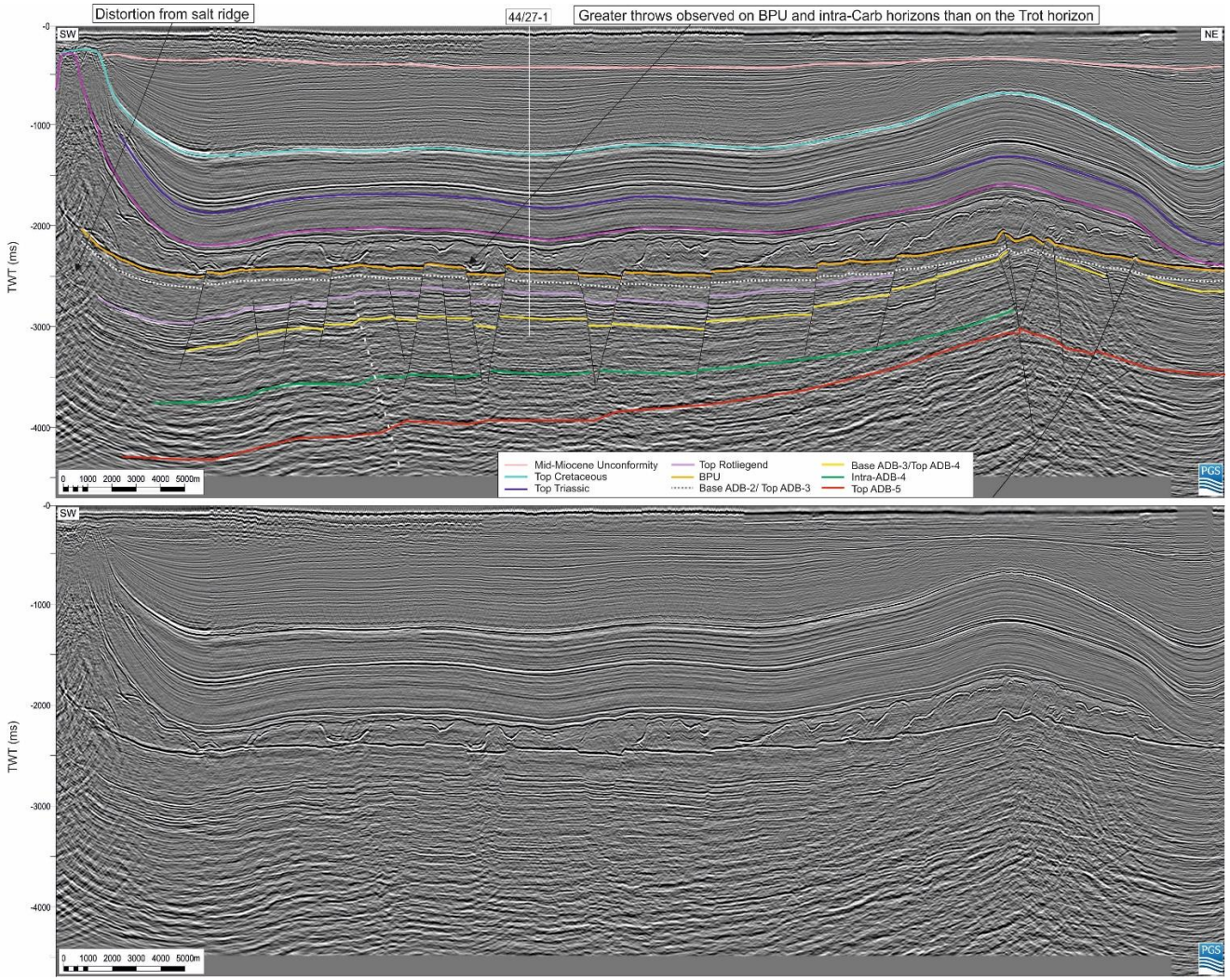


Figure 3.32 Seismic cross section normal to the NW- trending structures in the Silverpit Basin. Location of section on figure 3.30

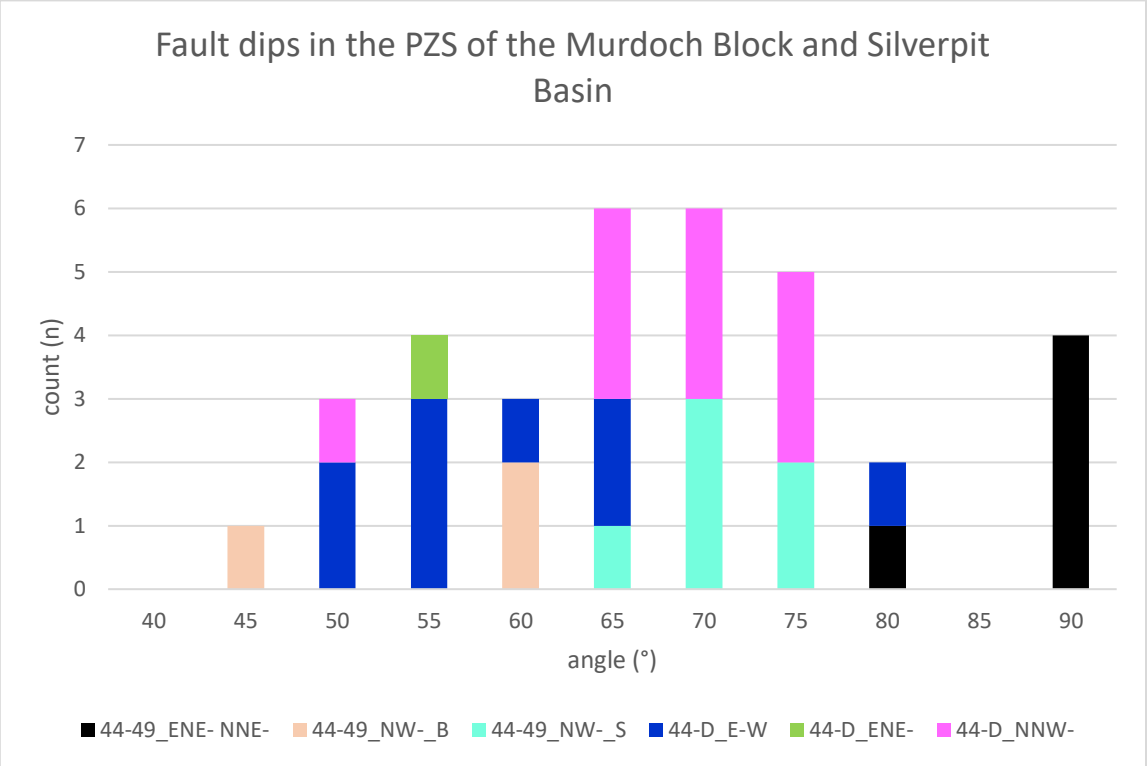


Figure 3.33 Histogram of Pre-Zechstein fault dips sampled from faults in the Murdoch Block and the Silverpit Basin. The different fault sets are colour coded and conform to map colour codes. Superficial faults with planar fault planes (i.e. NW-S and NNW-) dipped mostly from 65-70°, these angles being typical of planar normal faults. Strike slip faults (i.e. ENE- and NNE-) had the highest dip angles ranging from 80-90°. Throughgoing faults with a less planar fault plane (i.e. E-W and NW-_B sets) have dips ranging from 50-65°

Maximum throws on these faults range from 135-329m (+-7m) with a mean value of 210m, () and are measured on horizons within unit ADB-3 (Westphalian C-A). Rotliegend and Carboniferous horizons are offset with similar amounts on some of these faults, and on others the intra-Carboniferous throws are considerably higher than those on the Rotliegend.

The S/SB area exhibits one of the few examples of where free lateral fault tips can be clearly viewed within the PZS (Figure 3.34). The lateral tips of these faults overlap neighbouring parallel faults to form relays. Dip linkage (sensu Childs et al. 1995, Mansfield & Cartwright 1996), though not as clear as lateral relays, is also observed in which there is observable overlap and share of vertical displacement with isolated deeper faults in the Namurian-Visean (see Figure 4.16).

3.3.4.3 44-49_NW-_T Fault and Folds

A set of NW-SE (N130°) orientated reverse fault and associated fold structures are observed in the PZS of the southern Silverpit Basin (Figure 3.31). They are curved in map view and have lateral lengths of approximately 15-25km. They are characterised in cross section by an asymmetric southwest verging fold that deforms Carboniferous and Rotliegend stratigraphy (Figure 3.35). Seismic units ADB-1 to ADB-5 are folded in similar proportions. This is a smaller structure with a kinked geometry within a much larger uplifted 25km wide structure. Although not clearly resolved on the seismic data, brittle failure has likely occurred on these kink zones with the resulting formation of a reverse fault. Similar structures have been inferred on folds of similar geometry in thrust fold belts (Suppe, 1983). The interpreted fault plane dips range from 44-59°. The crest of the fold is deformed by smaller scale extensional faults.

The crest of the fold terminates into the overlying mobile Zechstein unit and there is no subsequent deformation expressed in the Triassic. The entire imaged PZS is deformed by the folding (~2000ms below the Base Zechstein), suggesting that these structures have a close relationship with the basement. These faults and associated folds are also identified by Leeder and Hardman (1990) and Hollywood & Whorlow (1993) who attribute their formation to buckling (see Chapter 2, section 2.5.1.2.).

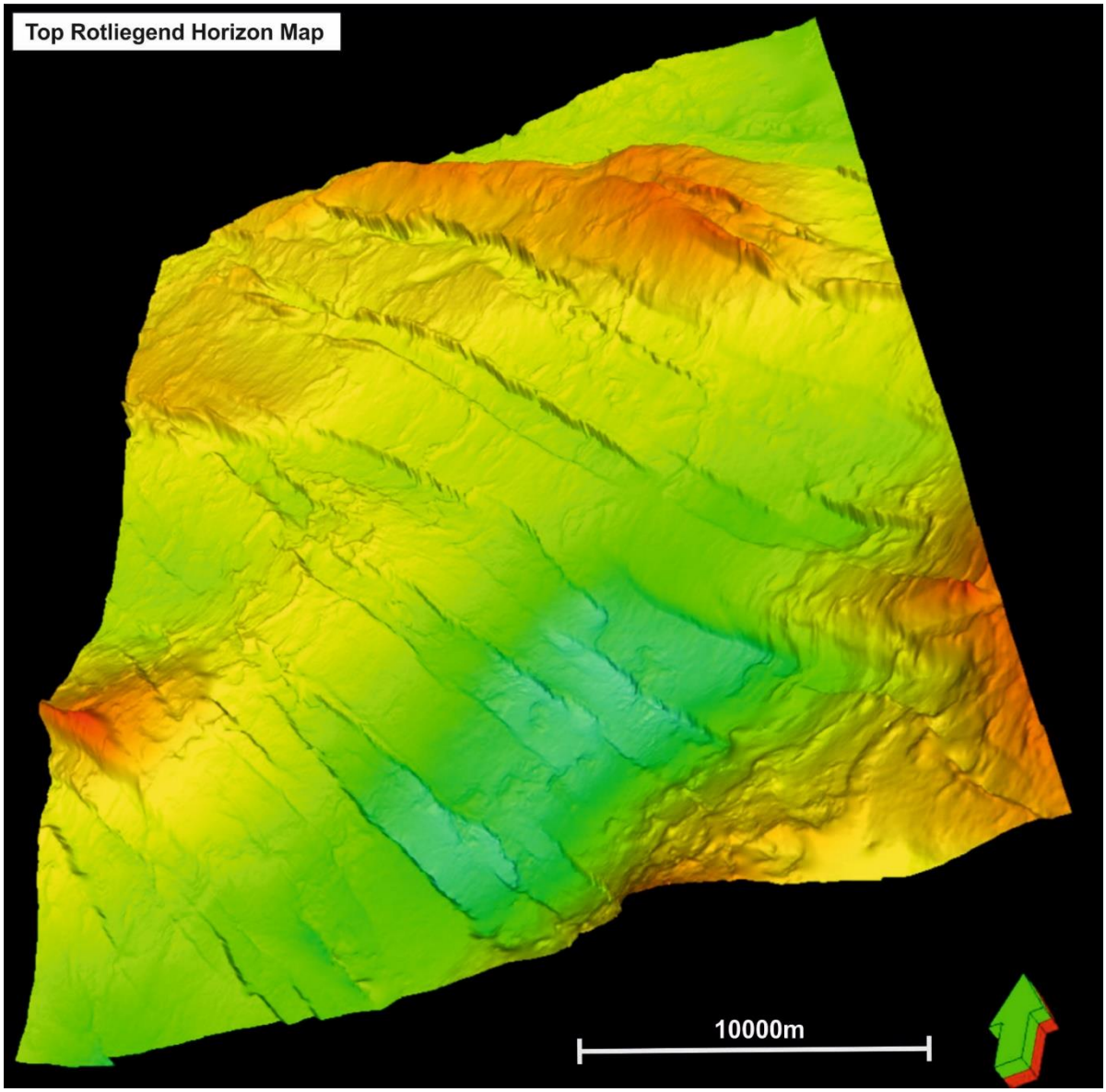


Figure 3.34 3D map of the Top Rotliegend horizon in the Silverpit Basin Case Study area. Clear dominance of NW-SE structures. The NW-_T reverse structures can be indentified by the areas of high relief (red). The areas of low relief (blue) are a seismic velocity artefact due to salt withdrawal. The prescence of salt welds in these areas produces a syncline.

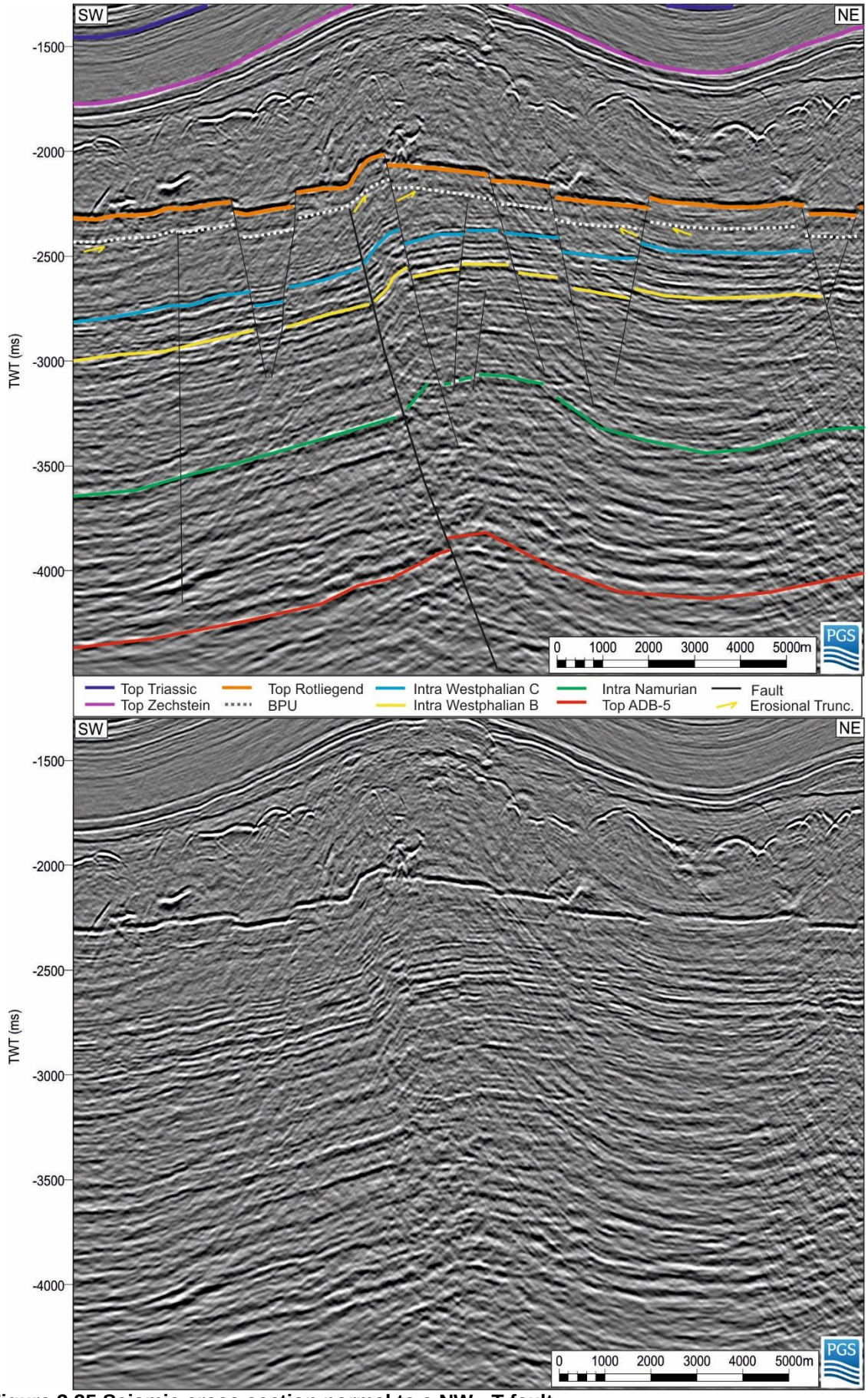


Figure 3.35 Seismic cross section normal to a NW-_T fault

3.3.4.4 44-49_NNE-_SS Faults

A group of linear, NNE-SSW (N025-N035°) orientated faults transect the S/SB. They are only recognised in map view on Intra-Westphalian variance slices and do not offset the Top Rotliegend horizon (Figure 3.30). Their lateral lengths are over 40km and they have an infrequent spacing in the S/SB. They intersect the NW-_P faults sub-orthogonally (Figure 3.31).

The faults appear on seismic cross sections as sub-vertical (dips range from 88°-90°) zones of distorted and disturbed reflections, sometimes accompanied by slight vertical offsets ranging from 62-123m(+-7m) (see Figure 3.36). The downthrown side often changes along strike, as does the throw value. This vertical zone of disturbance typically extends throughout the full imaged PZS (2000ms below the BPU). The Rotliegend and younger intervals are not deformed by these faults (Figure 3.30). Slight lateral movements are observed in the form of the offset (~150m) or slight bending of the NW-SE faults in a right and left-lateral sense. Based on these observations, these faults are interpreted to be strike-slip faults.

3.3.4.5 44-49_ENE-_SS Faults

A set of ENE- (N075°) trending strike-slip faults that are previously undiscovered in the S/SB and transect the Pre-Zechstein succession. They are linear to slightly curved in map view and like the NNE- faults, they are only visible on an intra-Carboniferous variance slice (Figure 3.30). They have abutting intersections between the NNE- faults at oblique angles, creating a zig-zag pattern (Figure 3.31). These faults have a similar cross-sectional geometry to the previously described NNE- faults. They are also expressed as a sub-vertical area of distorted reflections (dips range from 78-90°) and extend throughout the full PZS.

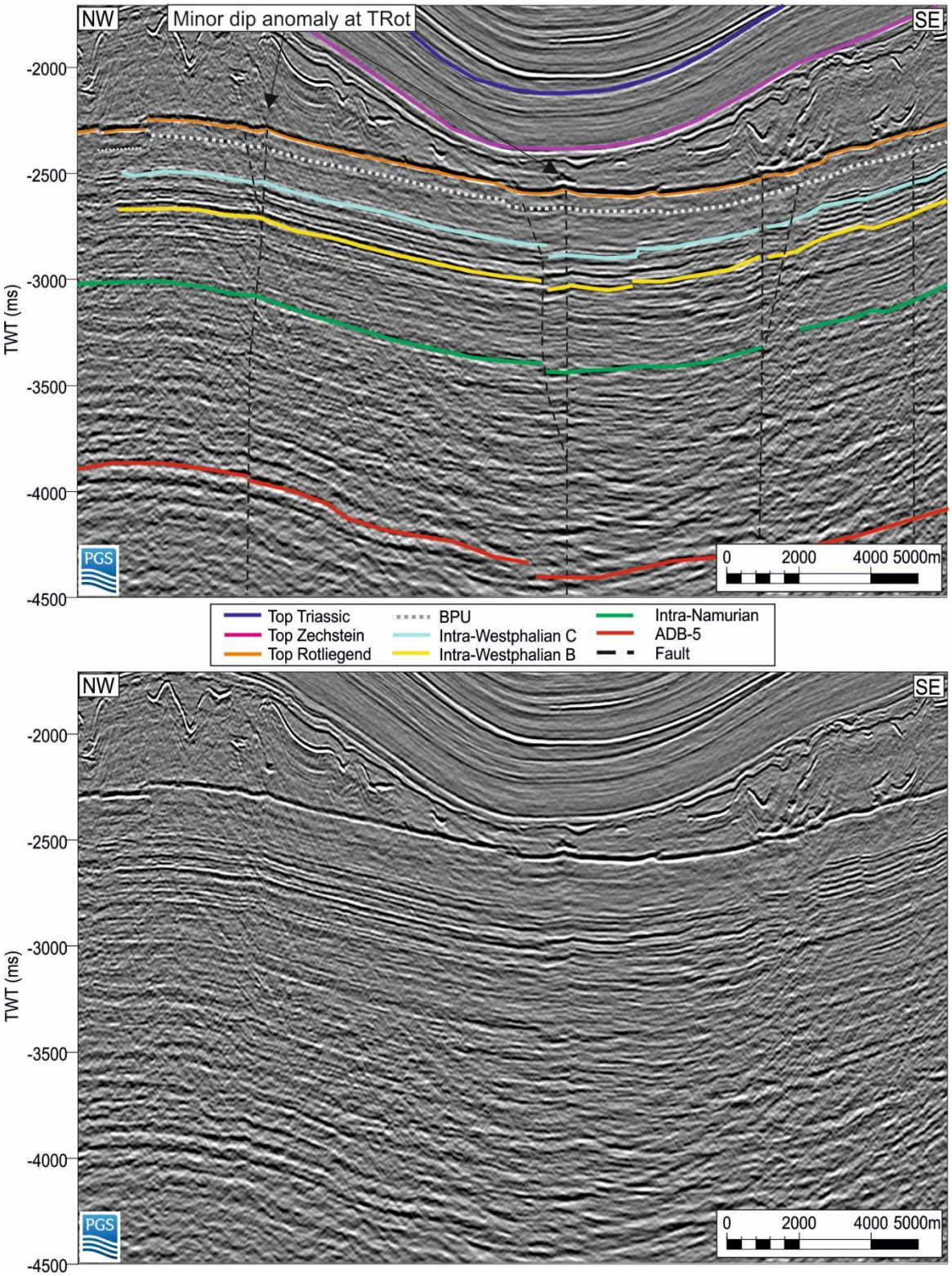


Figure 3.36 WNW-ESE interpreted seismic transect through the NE- strike slip faults. Only the strike-slip faults are interpreted in the section. Location of seismic cross section on Figure 3.30

The vertical offset of Carboniferous reflections is slightly lower than the NNE-faults, but like the NNE- faults, the downthrown side changes along strike and there is no vertical offset of the Trot horizon.

3.4 Southern Cleaver Bank High (S/CBH)

3.4.1 Background

The Cleaver Bank High is located in the Dutch Sector of the Southern North Sea. The area used to examine the CBH is a ~3000km^2 3D seismic volume within the PGS megamerge (see Chapter 1, section 1.5.1.1) located in its southern portion and is situated within Block K/1-6 (Figure 3.37). The area contains a number of key Pre-Zechstein well penetrations and Carboniferous hydrocarbon fields. The pre-Zechstein image quality is variable across the area and is likely controlled by factors such as Zechstein overburden thickness and the depth to the interval (Figure 3.37b).

3.4.2 General structural and stratigraphic context

The Pre-Zechstein structure in the S.CBH is characterised by the convergence of two regionally pervasive fault trends, NW-SE and NE-SW. A high density of faults from these trends cross-cut to form highly complex intersecting relationships (Figure 3.38). The CBH is bordered to the east by the Central Graben border fault complex in which a dominant N-S fault trend emerges.

In comparison, faults in the Post-Zechstein succession are less pervasive and the Post-ZS is dominated by folding related to salt diapirism and polygonal faults (Figure 3.39). The post-Zechstein succession consists of a large hiatus between the Zechstein and the Late Cretaceous, with local preservation of Triassic sediments in synclines between thick salt structures (Figure 3.39, Figure 3.40).

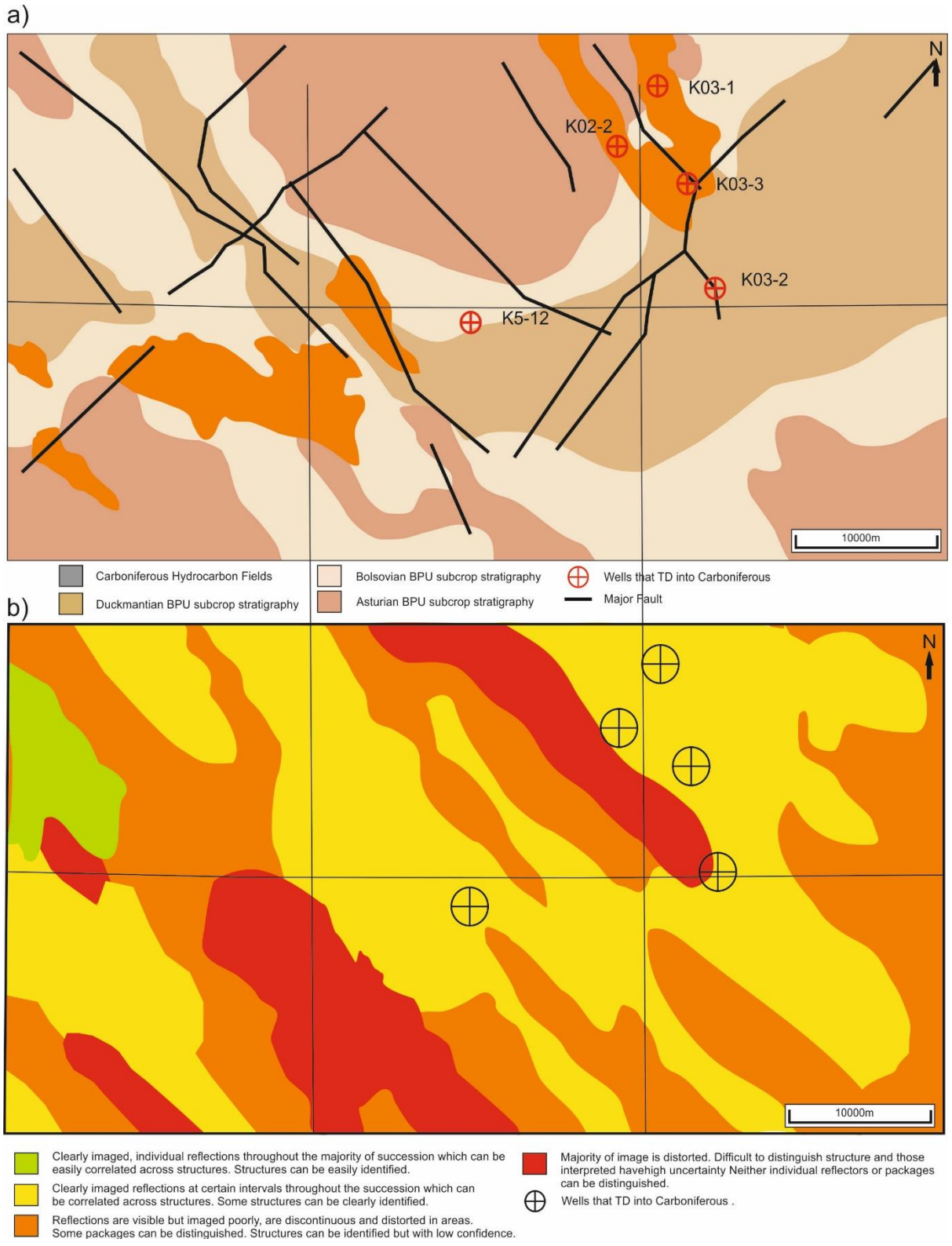


Figure 3.37 a) Structural elements and subcrop map of the Cleaver Bank High. Wells with Pre-Zechstein penetrations are indicated by the green circles. Dutch Carboniferous hydrocarbon fields are indicated by the orange polygons. Data quality map for the Pre-Zechstein succession on the Cleaver Bank High.

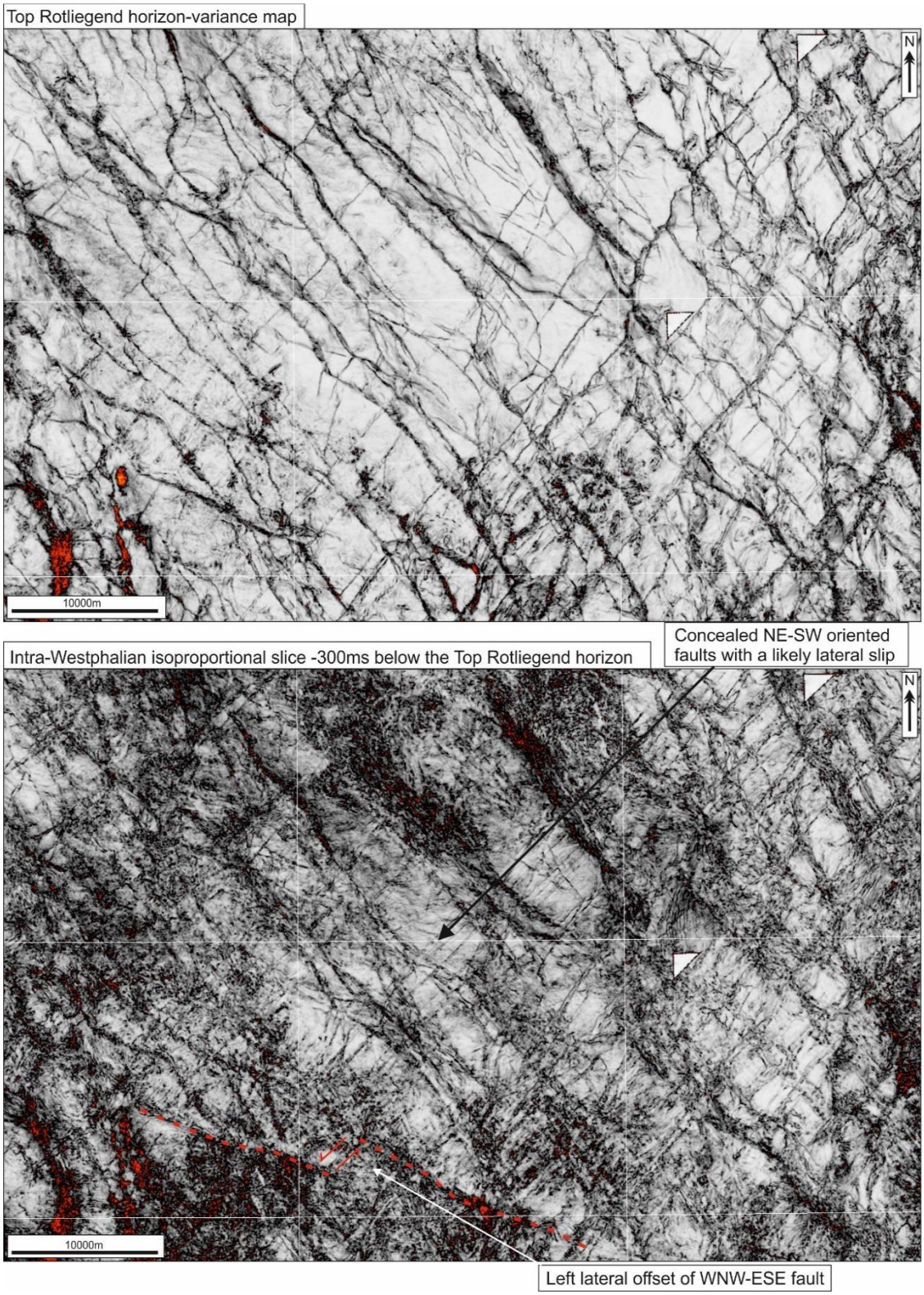


Figure 3.38 Variance maps at different intervals on the Cleaver Bank High a) Top Rotliegend horizon-variance map b) Intra-Westphalian variance slice. Orthogonal cross cutting fault trends are observed at both intervals, the Westphalian is less well imaged in this area which is reflected in the poorer resolving of faults (below). The concealed NE-SW strike slip faults laterally offset older faults (WNW-ESE) in higher magnitudes than newer faults (NW-SE).

The Pre-Zechstein succession is gently folded with Rotliegend-Lower Westphalian stratigraphy calibrated, although underlying Namurian and Visean sediments are only inferred due to lack of calibration (Cameron, 1993). The Base Permian subcrop ranges from Westphalian B-D with younger sediments preserved in the synclines (Figure 3.37).

3.4.3 Structural Sets

The Pre-Zechstein structure in the S/CBH is characterised by the convergence of two regionally pervasive fault trends that cross cut with highly complex intersecting relationships (Figure 3.38). Fold trends in the deeper succession are also recognised that show relationships with the fault sets. Two fold sets and six fault sets are described in detail in this section.

3.4.3.1 K_NW-_D Folds

The PZS in the S/CBH is folded into NW-SE (N130°) oriented folds (Figure 3.41). They are difficult to interpret in map view due to lateral data quality inconsistencies in the PZS. The folds have wavelengths of ~10km and amplitudes of ~500-700m and they deform all stratigraphic units ADB 1-5 (Figure 3.40). Similarly to the 44-49_NW-_D folds, a thinning of unit ADB-4 is observed over the deeper folded ADB-5 units. This indicates the formation of the fold prior to the deposition of the ADB-4 sequence (Lower Namurian-Lower Westphalian)(Figure 3.40).

Dipping stratal reflections at an angle of 3° are recognised on the fold limb when the seismic section is flattened on the BPU. This indicates the fold pre-dates the erosion at the BPU.

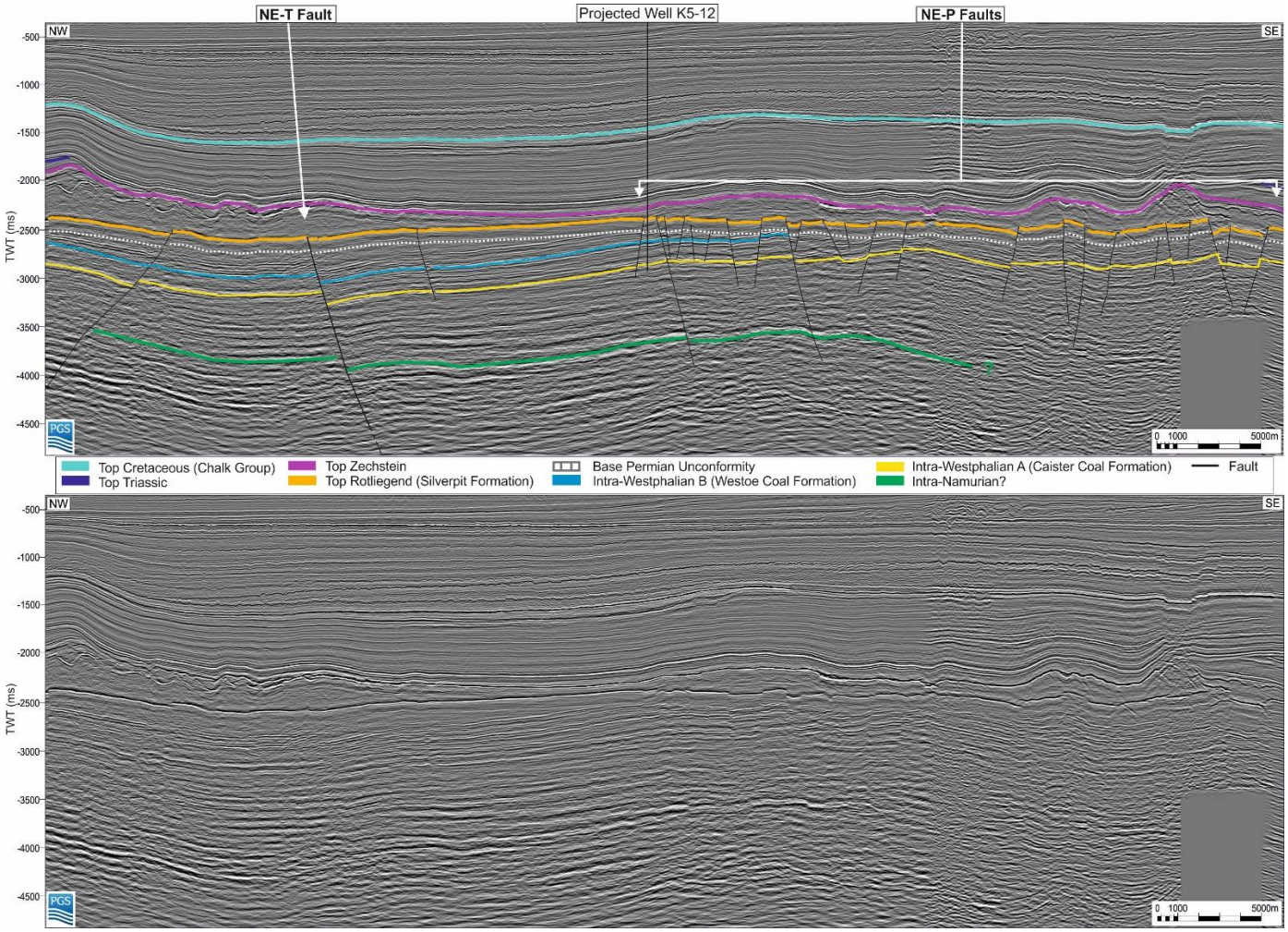


Figure 3.39 NW-SE oriented seismic cross section across the Cleaver Bank High, transecting the NE-SW structures. A NE-SW Throughgoing fault with a two stage movement history (left) contrasts the single stage, Superficial faults offsetting the crest of the long wavelength NE-SW anticlinal fold (centre). Location of transect in figure 3.37.

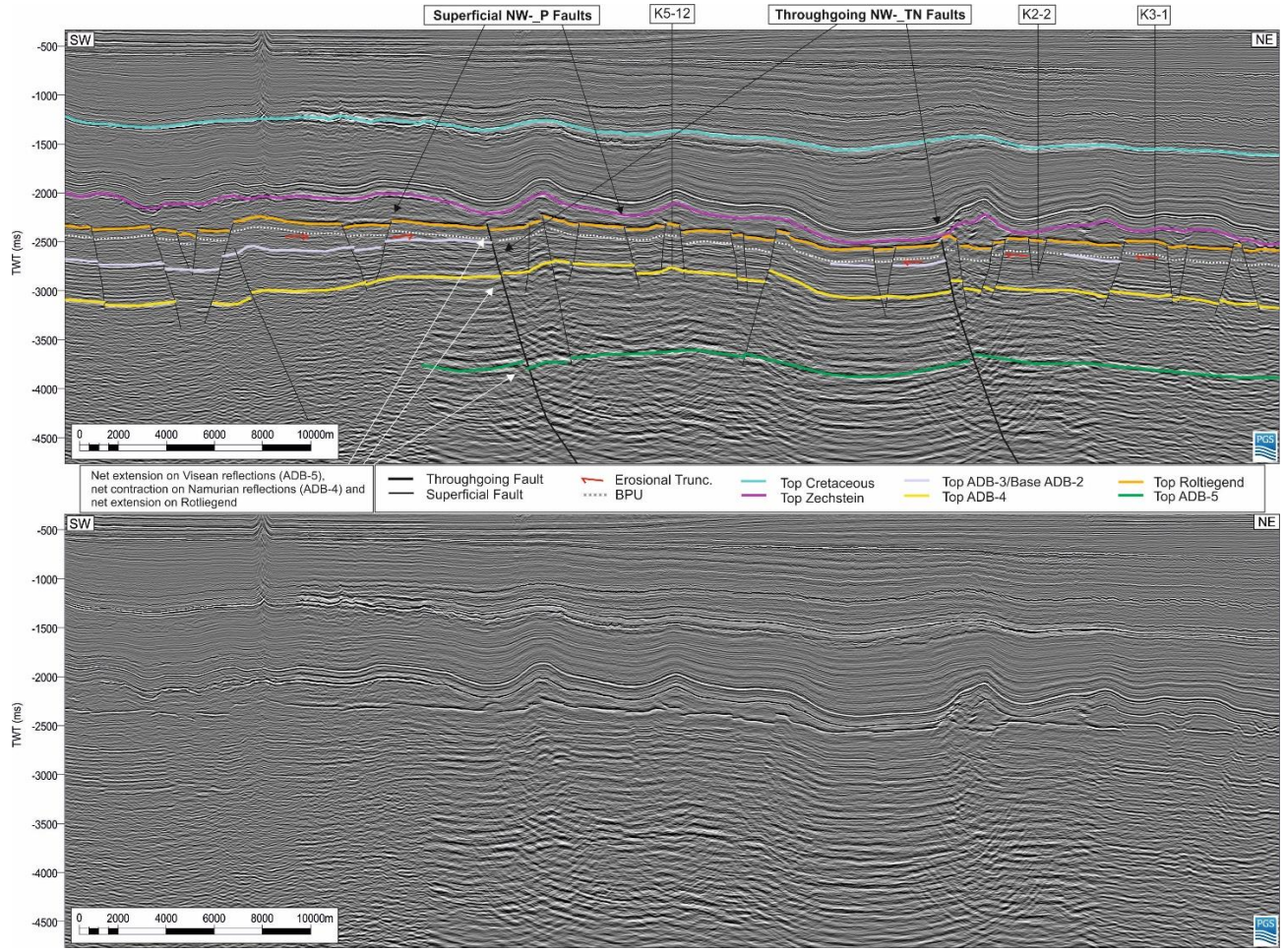


Figure 3.40 SW-NE oriented seismic cross section across the Cleaver Bank High, transecting the NW-SE structures. A clear distinction can be seen between the Throughgoing NW-_TN faults that have a large vertical extent, and the Superficial NW-_P faults. Younger Carboniferous stratigraphy appears to be preserved in the footwalls of the NW-_TN faults, indicating a pre-Rotliegend movement. Location of transect in figure 3.37. Stratigraphic correlations are highly uncertain in the PZS of this area due to poor reflection continuity. Interpretation is made based on seismic stratigraphy units.

3.4.3.2 K_NW-_BR Faults

Three distinct NW-SE (N145°) orientated fault sets are identified in the S/CBH, one of which is a set of reverse faults and associated folds. They are curved or curvilinear in map view with lengths of ~15km (Figure 3.41).

The faults have a planar fault plane geometry that predominantly dip to the NE at angles ranging from 52-71° (Figure 3.42). The upper tips propagate into the mobile Zechstein unit and the lower tips are not imaged but estimated to be located >3000ms below the Base Zechstein. The hangingwall is folded into a south-west verging monocline (Figure 3.42). It is uncertain if there are growth packages in the hangingwall as data quality is poor with increasing depth in this area.

The K_NW-_BR faults generally exhibit a reversed offset of Rotliegend and intra-Carboniferous stratigraphy by similar amounts, with maximum reverse throws ranging from 141m and 186m (+-8m) respectively. A decrease in throw towards the upper tip is observed. The fault locally downthrows Carboniferous stratigraphy towards the south west due to a faulted fold crest.

The overlying Zechstein is markedly thicker in the hangingwall and thins to the north east (Figure 3.42). Though the lateral movement of the Zechstein is complicated to reconstruct, this may indicate that there was an initially larger accumulation in the hangingwall, for which the fault would have needed to be in active extension at this time. The Cretaceous stratigraphy is thicker in the footwall above the underlying salt weld and thins over the adjacent salt walls and hangingwall stratigraphy.

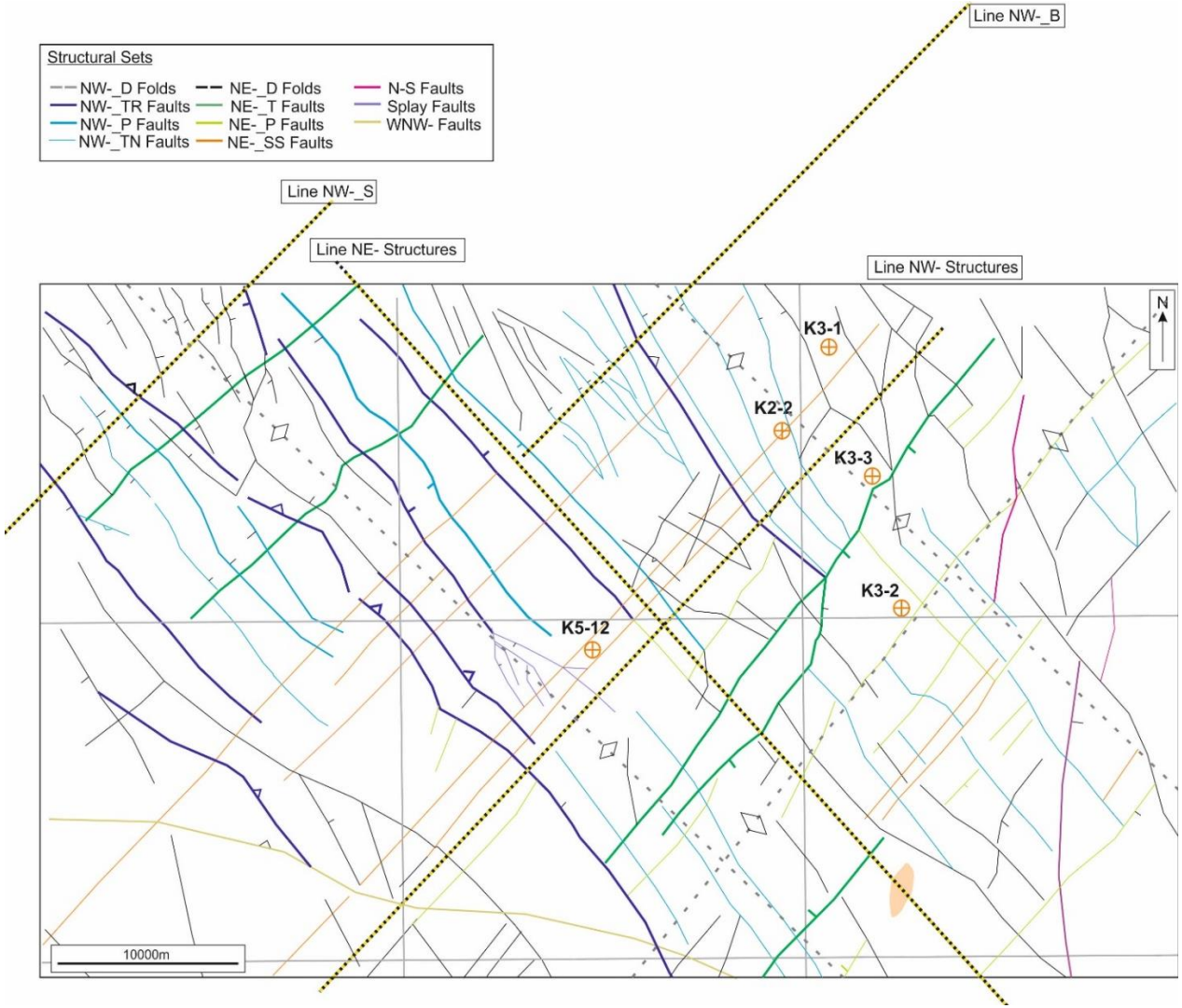


Figure 3.41 Composite structural map for all faults imaged in the PZS in the Cleaver Bank High study area. Different fault sets are colour coded.

3.4.3.3 K_NW-_BN

A set of NW-SE (N140-N145°) orientated normal faults also transect the S/CBH. They are curvilinear in map view and 15-60km and are markedly more curved close to X-type intersections with NE-SW orientated faults (NE-_SS). Some of the main fault planes exhibit bifurcation at their southern lateral tips as splays (Figure 3.41). These faults have dips similar to the NW-_BR faults with a large vertical extent (Figure 3.40). The lower tips are interpreted to be deeper than the imaged succession due to their fault plane extent. These faults are suggested to be genetically related to the NW-_BR structures but have not undergone a reverse movement.

3.4.3.4 K_NW-_P Faults

A third set of NW-SE (N140-145°) normal faults are recognised. They have a similar appearance in map view as the NW-_BN set but have a generally narrower zone of variance representing their trace (Figure 3.41).

The main differences between the NW-_P faults and the NW-_BN faults can be seen in cross section (Figure 3.40). The NW-_P faults exhibit relatively higher dips (68-80°) to the SW and NE in equal proportions. Like the others, their upper tips are located in the mobile Zechstein unit while the lower tips appear to terminate from 1-1.2s beneath the BPU, which is shallower than the other NW-SE fault planes.

The NW-_P faults generally exhibit relatively lower maximum throw values ranging from 87-328m (+-8m) (Figure 3.27), measured on intra-Carboniferous horizons. They generally exhibit slightly higher throws on intra-Carboniferous horizons than on the BPU and TRot horizons.

3.4.3.5 K_NE-_D Folds

A second set of folds are recognised in the Pre-Zechstein succession of the S/CBH which are orientated NE-SW (N040°) (Figure 3.41). They have longer wavelengths that the NW-SE folds with a higher wavelength to amplitudes (~20km and ~800m respectively) ratio than the orthogonal NW- trend (Figure 3.39).

The folded PZS has a parallel and concordant reflection configuration. Dipping Westphalian reflections are truncated against the BPU even when the seismic is flattened on the BPU horizon. This indicates the folds post-date the deposition of seismic units ADB5-2 but pre-date the deposition of unit ADB1. The fold crests are offset by a set of NE-SW orientated faults (Figure 3.39). These faults have relatively small offsets and are described fully in section K_NE-_S.

3.4.3.6 K_NE-_T Faults

A set of NE-SE (N050°) trending normal faults with lateral lengths up to 50km transect the S/CBH (Figure 3.41). They are linear or curvilinear in map view and typically spaced 7-10km apart.

Fault plane dips range from 55-58° and extend ~2000ms below the base Zechstein and possibly deeper (Figure 3.39). Their upper tips extend into the mobile Zechstein unit, with the TRot horizon recording the most recent reflection offsets. Their lower tips are interpreted to be within the deeper succession that is not imaged by the seismic due to the long vertical extent.

Maximum throw (Tmax) values range from 380-674m (+-10m) (mean value of 484m +-10m) with maximum throws recorded on intra-Carboniferous reflections. A higher normal throw is observed on intra-Carboniferous than Rotliegend reflections. Fault K_3_NE-_1 (Figure 3.39) exhibits intra-Carboniferous Tmax of ~460m (+-10m), to which throws on the TRot horizon are ~152m (+-7m).

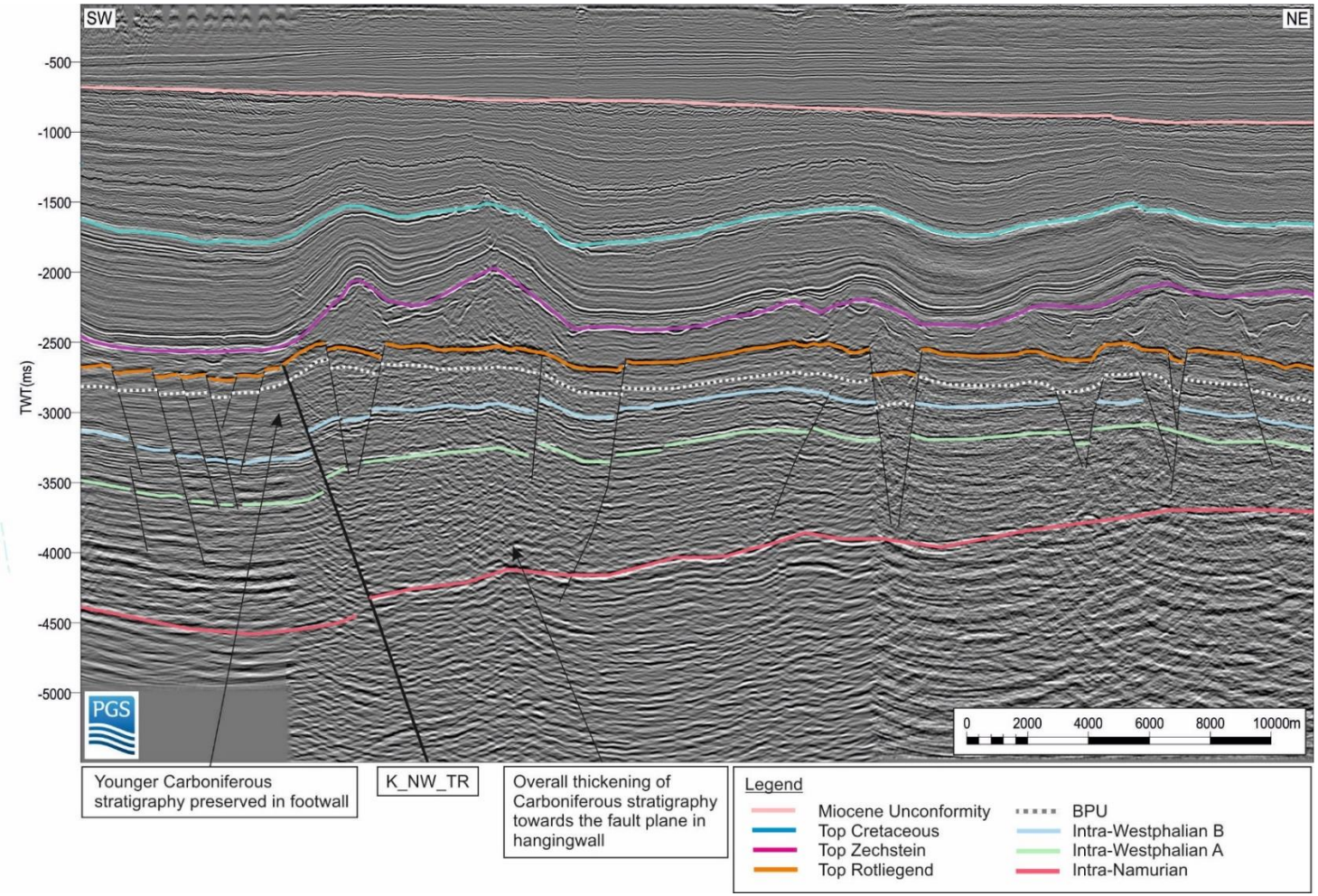


Figure 3.42 Reverse fault from type NW-_TR. The fault has younger Westphalian stratigraphy preserved in the footwall indicating that the fault has been active in a reverse sense prior to the deposition of the Rotliegend and later reactivated. It may have been active in a normal sense before the contarctional event indicated by the thickening of stratigraphy towards the fault plane in the hangingwall, however no major thickness changes are observed between the hangingwall and footwall stratigraphy. Location of transect in Figure 3.37.

The overlying Zechstein layer is relatively thin and undeformed, thickest closest to the fault plane in the hangingwall. The Upper Cretaceous unconformably overlies the Zechstein in this area and is gently folded over the upper fault tip. The Zechstein and Upper Cretaceous successions are both thicker in the hangingwall of the fault (Figure 3.39).

3.4.3.7 K_NE-_P Faults

NE-_P faults are a set of relatively shorter normal faults (N040°) that are curvilinear in map view (Figure 3.41). They exhibit complicated cross-cutting and abutting relationships with the NW- faults and therefore lateral lengths are uncertain (Figure 3.38). A higher frequency of NE-_P faults are located east of the major NE-SW trending fault and are more closely spaced in this area (~1km).

The fault planes dip steeply (65-72°), steepen with depth, and extend ~800-1000ms below the BPU (Figure 3.39). The upper tips are within the mobile Zechstein succession with the uppermost discrete offsets being observed on the TRot horizon. The lower tips of these faults appear to be located within the Namurian succession (the stratigraphy extrapolated from wells from Quadrant 44 due to limited penetrations in Quadrant K, these wells are approximately 40km but reflections can be correlated this distance with some confidence). Maximum throws on the NE-_P faults are considerably smaller than those on the NE-_B faults, and range from 110-331m (+-9m), as recorded on intra-Carboniferous horizons. Intra-Carboniferous and Rotliegend horizons display approximately equal throw values. The faults are typically located on the NE- oriented fold crests, offsetting the folded Westphalian-Rotliegend succession. A high amplitude seismic stratigraphy package underlies these faults, interpreted as ADB-5 (Figure 3.39). Although this package

has a high signal to noise ratio and low frequency, throws of up to 110m (+-9m) can still be distinguished.

3.4.3.8 K_NE-_SS Faults

A set of NE-SW orientated (N045°) linear faults appear as a faint, narrow zone of higher variance on the Top Rotliegend horizon map (Figure 3.38a). They are better viewed on an intra-Carboniferous variance slice (Figure 3.38b). They are over 5km in length and can be distinguished from other NE-SW trending faults as they sometimes appear as two closely spaced, parallel linear features (Figure 3.41). There is no expression of these faults on the overlying Top Zechstein, Cretaceous or Cenozoic horizons.

The seismic expression of these faults is poorly defined as they exhibit negligible vertical offsets of intra-Carboniferous reflections (Figure 3.41). Where they are interpreted, they have sub-vertical area of slight reflection distortion representing the fault plane, similar to the 44-49_NE- faults. Fault plane dips range from 78-90° (mean value of 86°, see Figure 3.43) and transect the PZS (within the imaging resolution). At X type intersections with NW-SE faults, the NW-SE traces are curved or have a slight offset (Figure 3.38b). Based on these observations, they are interpreted to be strike-slip faults.

3.4.3.9 K_N-S Faults

N-S (N005°) normal faults are poorly imaged and defined but are observed to the east of the S/CBH. They are poorly imaged on seismic section and best viewed on the 3D map of the Trot horizon (Figure 3.44). They are curved in planform view and reach lateral lengths over 50km. They connect closely spaced and parallel NE-_T faults, often splaying off them and joining close by NE-T faults (Figure 3.41).

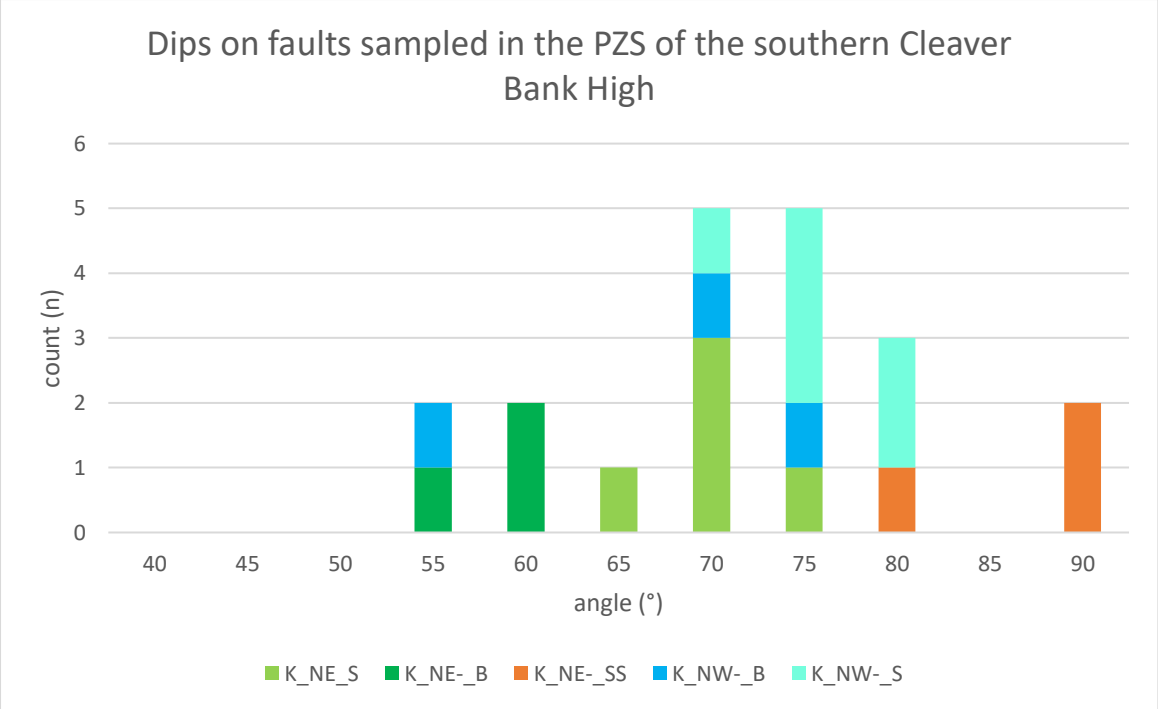


Figure 3.43 Histogram of Pre-Zechstein fault dips recorded on faults in the Cleaver Bank High. Different fault types are indicated by the colour key. Similar to the Silverpit Basin and Murdoch Block, the strike slip faults (NE-_SS) exhibit the highest dip angles. The superficial faults (NW-_S/P and NE-_S/P) exhibit the mid-range dips typical of normal planar faults. Each set of throughgoing faults have differing dips with the NE-_B faults have shallower more lystric profiles and the NW-_B faults being more variable. This is interpreted to be due to the NE-_B faults being reactivated normal lystric type faults and the NW-B faults having both normal reactivated and purely contractional origins.

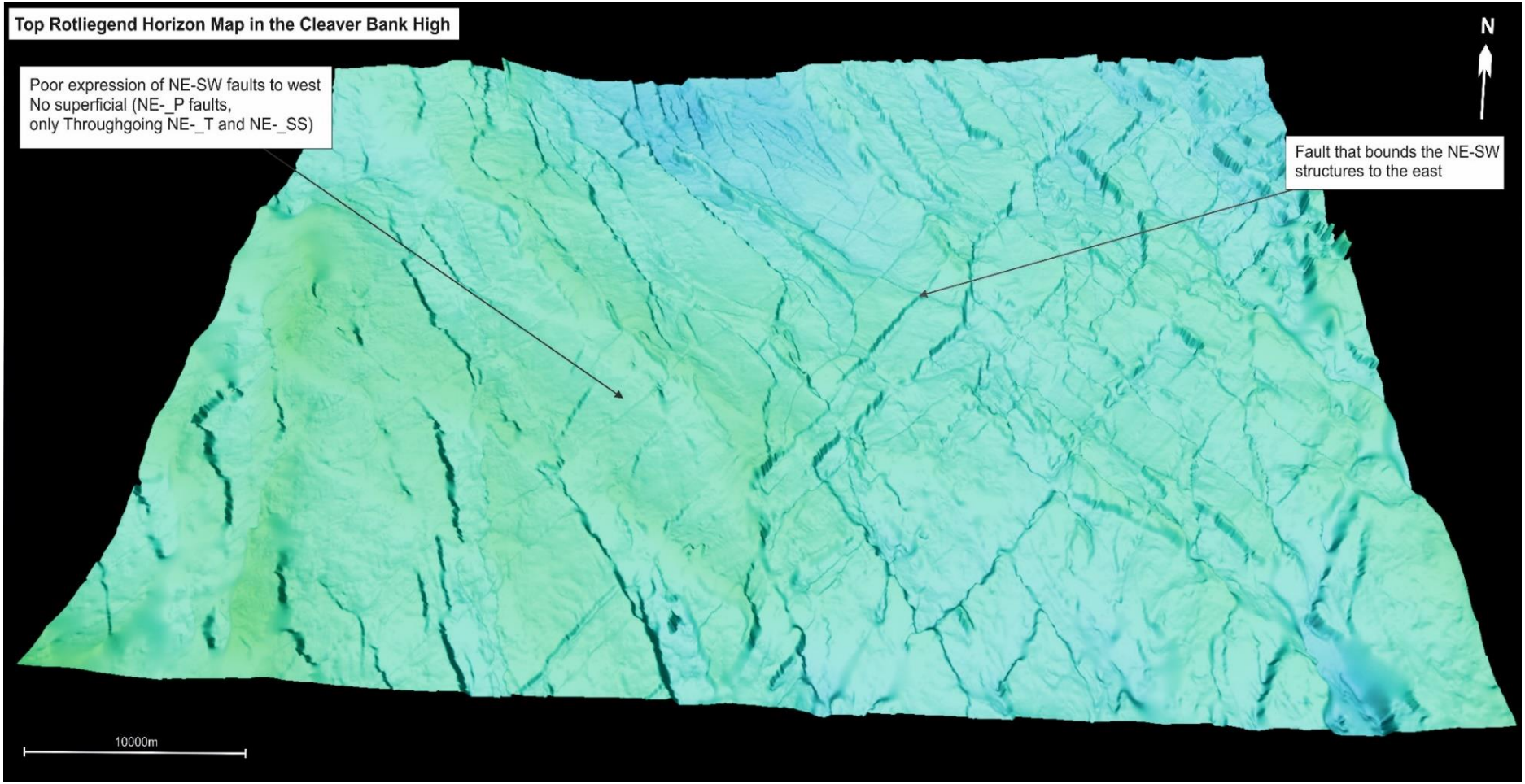


Figure 3.44 3D map of the Top Rotliegend horizon illustrating the overprinting of various fault trends creating the complex intersection geometries observed. The NE-SW faults become less frequent towards the northwest and reactivation of this trend appears to die out from the major central fault (NE-SW_T1). North-South normal faults are located to the east only. Compressional NW-SE faults can be distinguished by areas of green that represents the higher relief.

3.5 Stainmore Trough – Cleveland Basin (ST-CB)

3.5.1 Background

The Stainmore Trough – Cleveland Basin is an area in the northwest of England. The area has been examined by the observation of regional transects, constructed by the amalgamation of roughly N-S and E-W orientated public domain 2D seismic lines of varying quality and acquisition parameters (Figure 3.45).

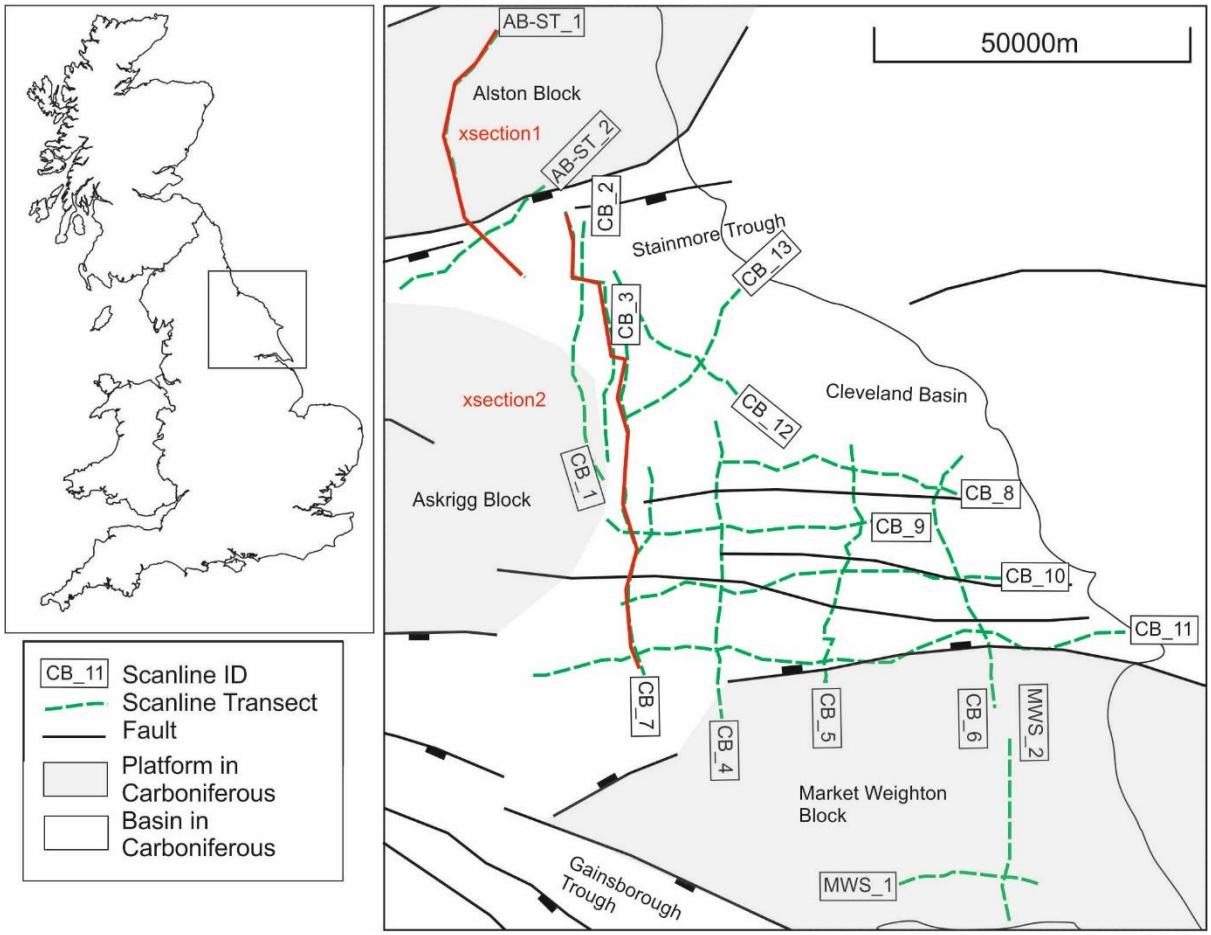


Figure 3.45 Major structural elements of the Cleveland Basin, Stainmore Trough and surrounding areas. Key transect locations are indicated.

3.5.2 General structural and stratigraphic context

The Stainmore Tough is an east-west trending half graben. The Alston Block borders it to the north and the south dipping, Lunedale, Wigglesworth and Butterknowle Faults define this boundary (see Figure 2.28). These E-W orientated faults have an en-echelon arrangement (Fraser and Gawthorpe, 2003a) and have a combined length of ~50km. Active rifting on these faults took place from the Late-Devonian – Early Courceyan evidenced from clinoforms in the Courceyan-Arundian sequence (Fraser & Gawthorpe 2003). The southwestern margin is supposedly fault bound by the Stockdale Fault (Collier, 1991) which separates it from the Askrigg Block, another granite-cored block (Bott and Smithson, 1967). To the southeast, the Stainmore Trough merges with the Cleveland Basin. The thickness of the Lower Carboniferous in the hangingwall of the Butterknowle Fault is estimated to be up to 6km (Fraser & Gawthorpe, 2003). The easterly tilt of the basin results in a progressively younger base-Permian subcrop east (Collier, 1991).

The Cleveland Basin is an east-west trending basin. The basin geometry consists of two half grabens with a series of smaller half grabens within, and a large scale transfer system at the centre (see Figure 2.28). Deposition of up to 4km of Tournaisian-Visean syn-rift stratigraphy is postulated by Fraser & Gawthorpe (2003) indicated by wedge shaped geometries on seismic. Intra-Carboniferous angular unconformities are observed in the deeper parts of the stratigraphy (see Figure 2.29). These are thought to represent the EC1/EC2, EC2/EC3 and Visean-Namurian sequence boundaries (Fraser & Gawthorpe, 2003). The pre-Zechstein stratigraphy for this area summarized in Figure 2.19. The Base-Permian subcrop consists of overall younger Carboniferous stratigraphy to the east due to the easterly structural tilt of the entire area east of the Pennines. The seismic stratigraphy for

the Cleveland Basin and Stainmore Trough was characterized by Fraser & Gawthorpe (1990) and is summarized in Figure 2.30.

3.5.3 Structural Sets

Faults observed across the Stainmore Trough and Cleveland Basin have been classified by their offset geometries. Five main sets have been recognized with further subsets. Throws discussed in the following section are intersected throws rather than maximum throws and reflect the overall throw magnitudes of the fault type rather than maximum throw of any particular fault.

3.5.3.1 Type 1 Faults

Type 1 faults exhibit at least a portion of normal throw on intra-Carboniferous horizons with no offset of the BPU horizon (Figure 3.46). Type 1 faults that exhibit throws with no syn-sedimentary packages are referred to as *Type 1a* Faults. They have relatively small throws ranging from 100-200m (+-9m) with vertical extents 1.5-2km below the BPU. They are observed in the Cleveland basin and Stainmore trough typically offsetting previously folded stratigraphy (Figure 3.47). They are interpreted to have formed after Variscan compression but before the erosion at the BPU.

Faults that show normal offsets of intra-Carboniferous reflections and syn-sedimentary packages within the Lower Carboniferous succession in the hangingwall are referred to as *Type 1b* faults (Figure 3.46). The faults are generally large scale with throws of at least 2km on basement reflections and are located at the basin margins (Figure 3.47). An example of a Type 1b fault is the Stainmore Trough bounding Butterknowle Fault (Figure 3.48). These faults are also observed in the western area in the Cleveland Basin (Figure 3.47). These faults are generally

E-W trending which is in agreement with the orientation of regional extension at the time of Late Devonian-Lower Carboniferous rifting (see section 2.3.2.1).

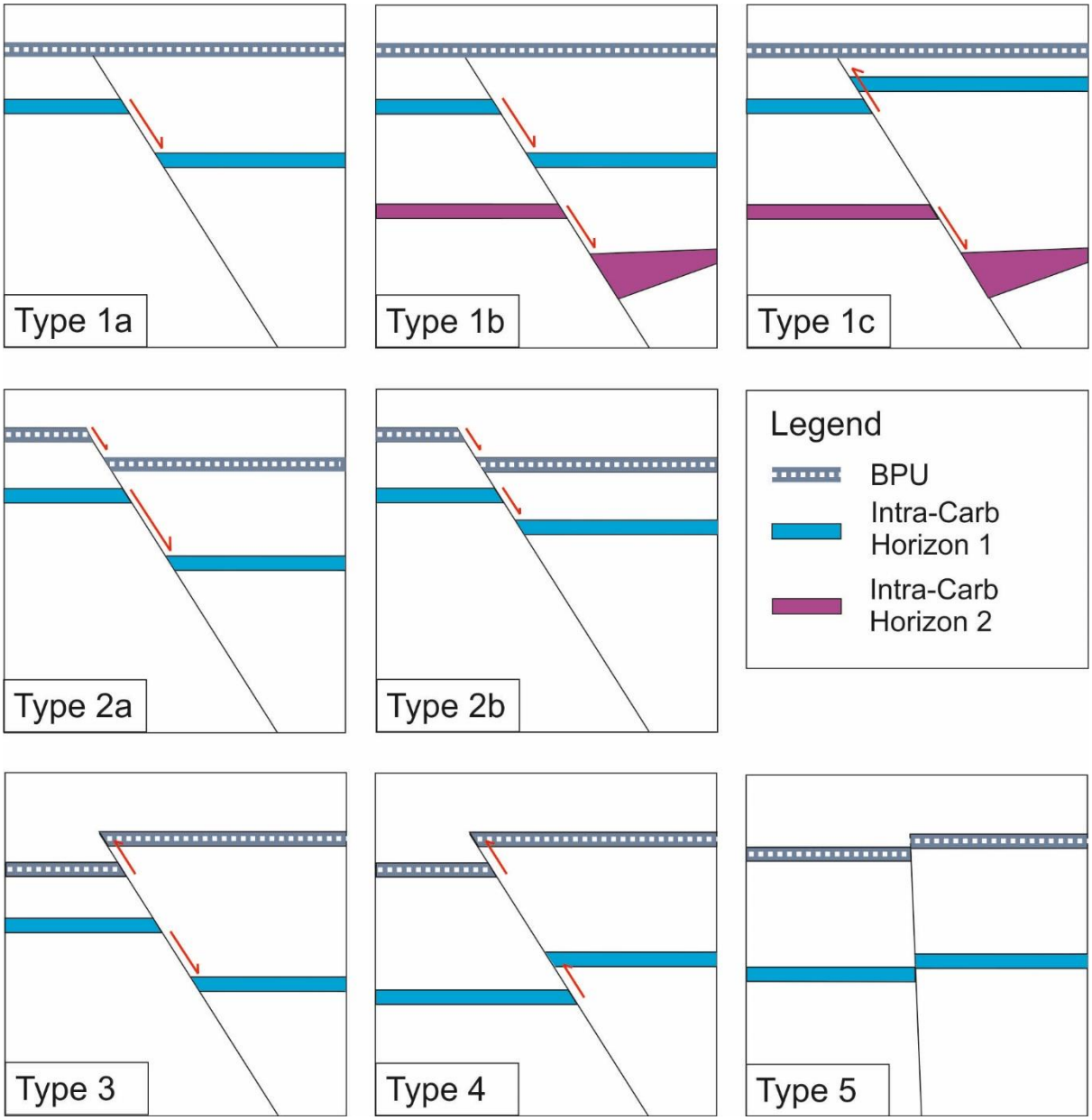


Figure 3.46 Schematic of fault types observed on seismic data from the Stainmore Trough and Cleveland Basin. These fault types are categorised based on their throw profile.

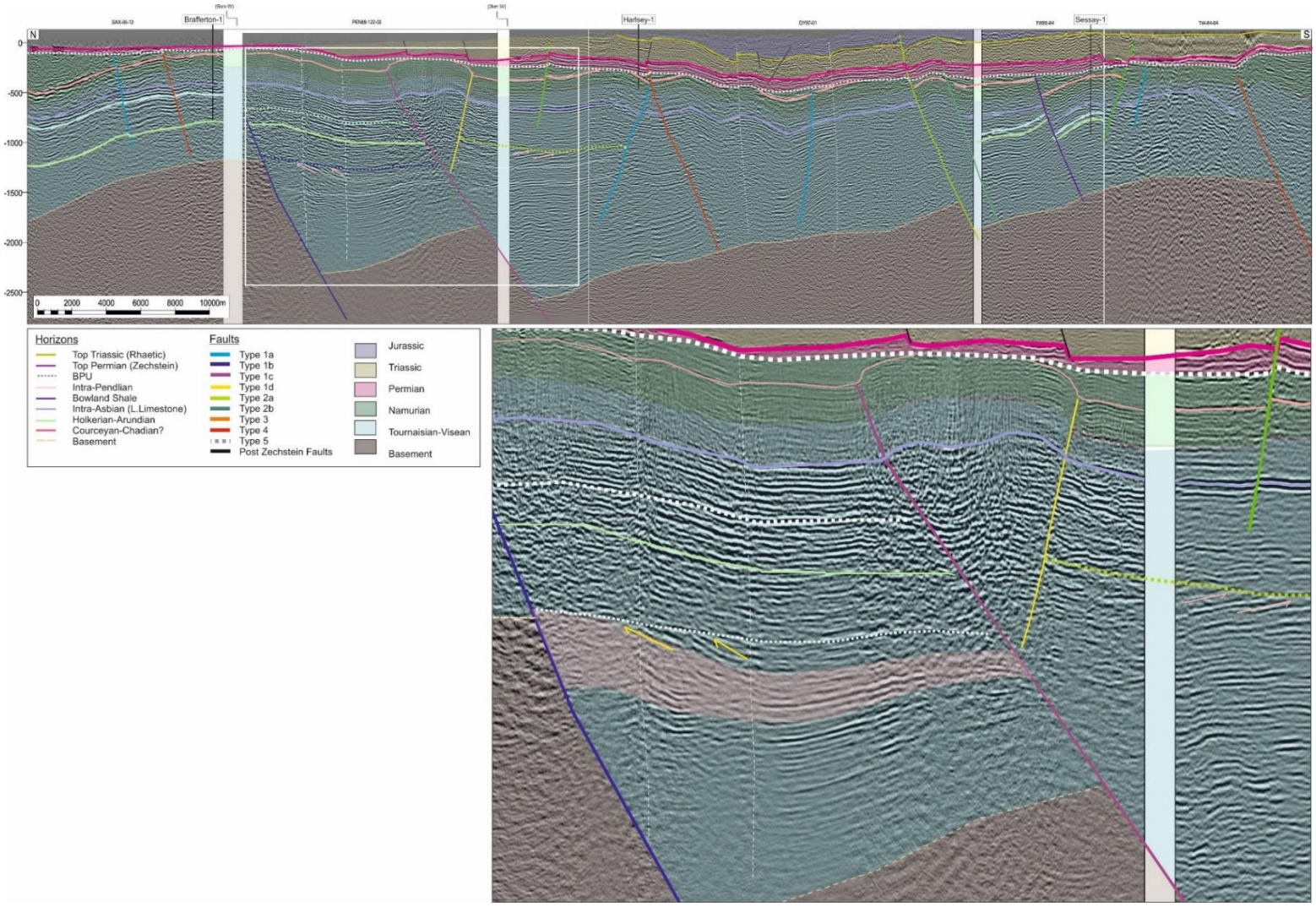


Figure 3.47 N-S composite seismic cross section that transects the western Cleveland Basin. Location of transect on Figure 3.45

Type 1c faults exhibit normal throws on Visean (Lower Carboniferous) reflections and reverse offsets of Namurian (Mid Carboniferous) reflections (Figure 3.46). They have a vertical extent of more than 5.5km with intra-Carboniferous throws of more than 2km recorded on basement reflections. They are typically half grabens with syn-sedimentary infill in the Lower Carboniferous and reverse offsets recorded on Namurian reflections.

There is an unconformity in the hangingwall of one of these faults ~800m below the mapped Asbian reflection (Figure 3.47a). This is interpreted to represent one of the angular unconformities documented by Fraser & Gawthorpe (1990). From observation of its position relative to the stratigraphic succession, it is suggested to be the Chadian-Arundian boundary.

These faults are interpreted as reverse-reactivated, normal faults which accrued normal syn-sedimentary slip in the Lower Carboniferous. Activity then ceased during the Namurian and were then reverse-reactivated at the End Carboniferous before the erosional event and subsequent Permian deposition.

Type 1d faults exhibit reverse offset of Carboniferous reflections with no offset of the BPU (Figure 3.46). They have relatively small intersected reversed throws ~150-300m (+-9m) and are observed in the Stainmore Trough and Cleveland Basin (Figure 3.49, Figure 3.47). These faults are associated with folding in hangingwalls but are also observed close to isolated folds. The folds are truncated at the BPU with no folding of the overlying Mesozoic succession. The faults are interpreted to be a brittle accompanying deformation in the buckling of the Carboniferous succession during Variscan shortening (Hollywood, 1993).

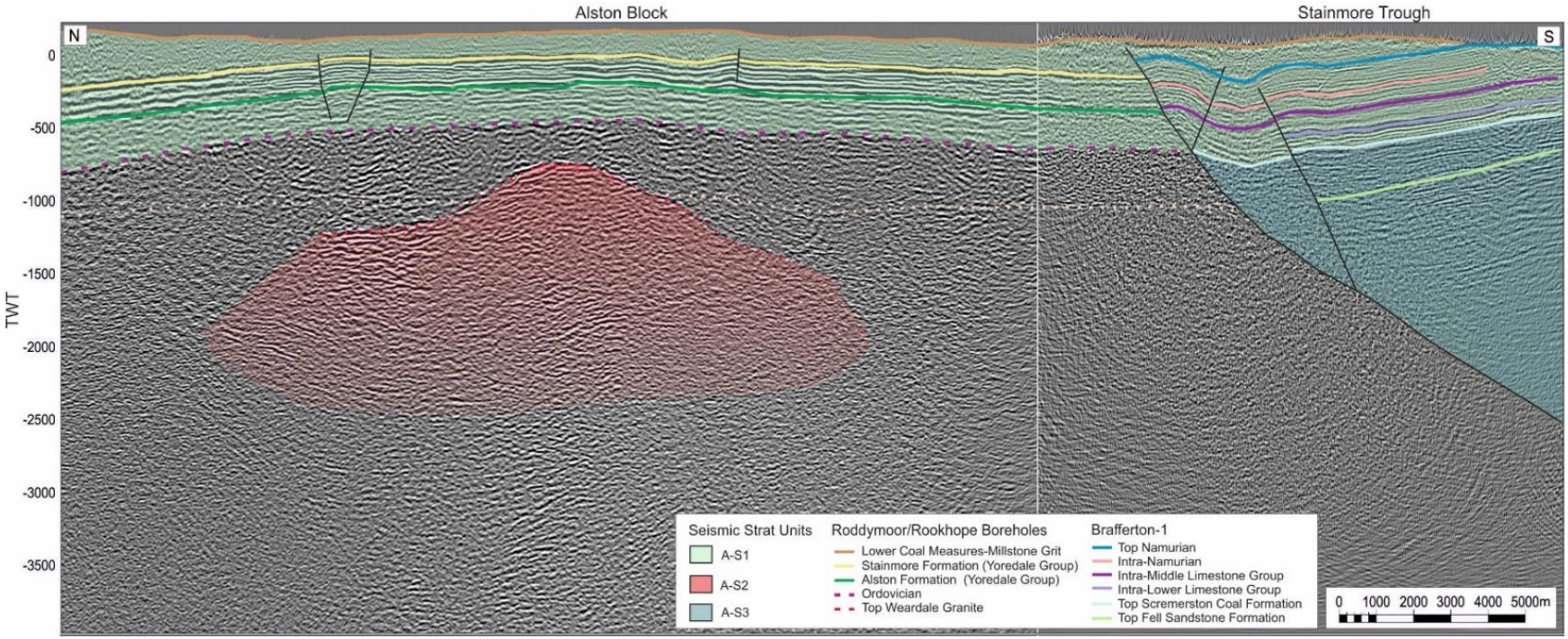


Figure 3.48 N-S seismic section transecting the Alston Block and Stainmore Trough. The large south dipping basin bounding fault (Lundale-Butterknowle Fault is a Type 1b fault with Lower Carboniferous syn-sediemntary packages in the hangingwall. Location of transect on Figure 3.44.

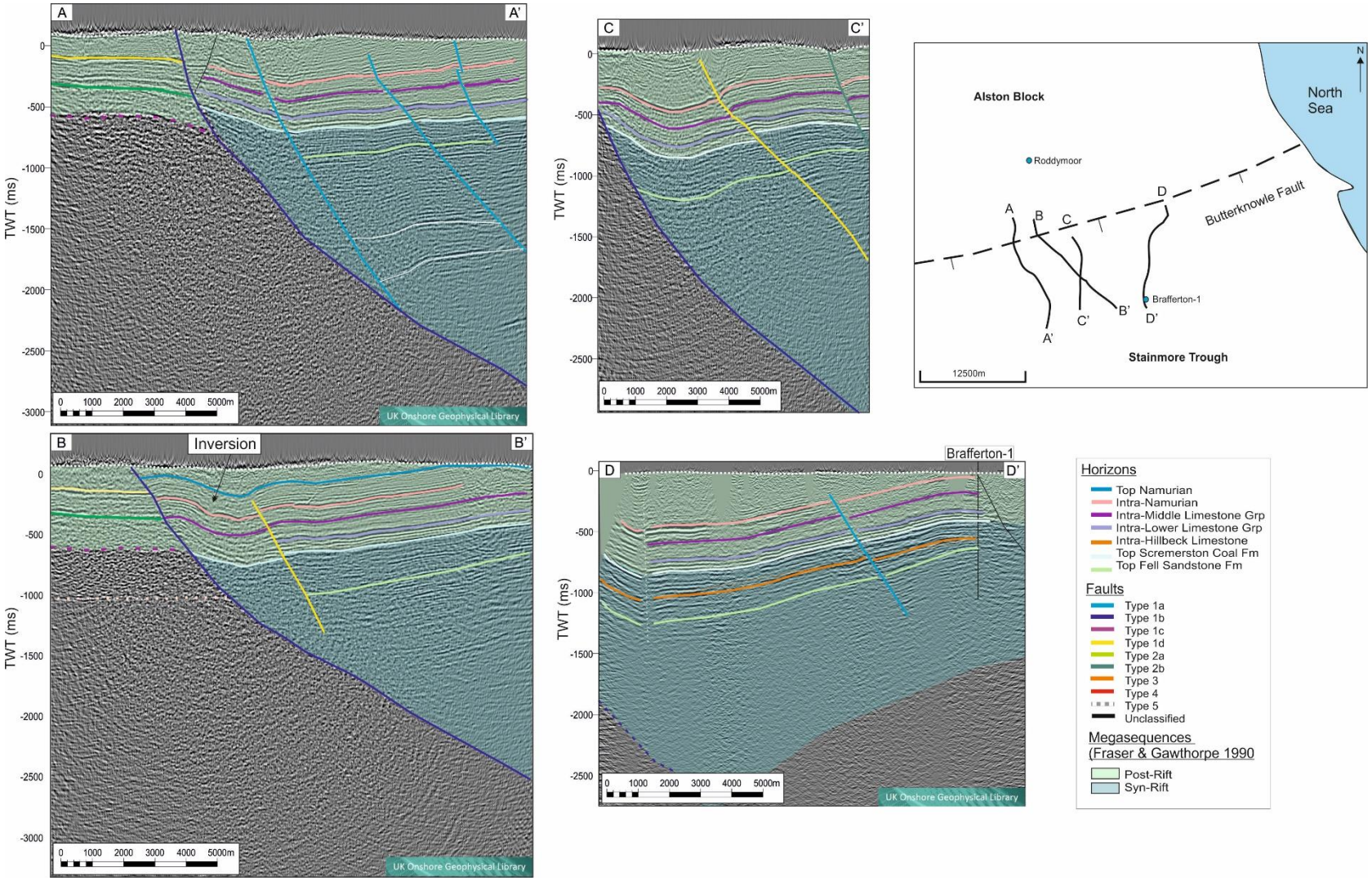


Figure 3.49 N-S interpreted seismic sections transecting the northern Stainmore Trough. Types-1a, 1b and 1d are recognised.

3.5.3.2 Type 2 Faults

Type 2 faults exhibit normal throw on intra-Carboniferous horizons and normal throw on the BPU horizon (Figure 3.46). *Type 2a* faults exhibit a higher proportion of throw on intra-Carboniferous horizons than the BPU. They are found in the Cleveland Basin where the BPU is more clearly defined and offsets of the Mesozoic are observed (Figure 3.47), though they may also be present in the Stainmore Trough area. Intra-Carboniferous throw values are uncertain due to data quality but are thought to be at least a 1km from observation of basement reflection offsets. Throws on BPU horizons are ~100m and they have a vertical extent around 4.5km.

These faults are interpreted to be Lower Carboniferous syn-sedimentary faults that have been extensionally reactivated at some point after the deposition of the Permian. The southward dipping Type 2a fault in Figure 3.49 has incurred an extensional reactivation at a time later than at least the Triassic.

Type 2b faults exhibit similar throw values ranging from ~50-160m (+-9) on intra-Carboniferous and BPU horizons (Figure 3.46). They are widely observed across the Stainmore Trough and Cleveland Basins (Figure 3.49, Figure 3.47). Upper tips are within the Mesozoic succession and in some cases have propagated near the surface. Vertical extents range from 1.8-2.8km with the lower tips typically terminating in the Lower Carboniferous and no syn-depositional packages observed. Type 2b faults are interpreted to have formed during the Mesozoic.

3.5.3.3 Type 3 Faults

Type 3 faults exhibit normal throw on intra-Carboniferous horizons and reverse throw of the BPU horizon (Figure 3.46). An example of a Type 3 fault is Fault 9 (Figure 3.47), Fault 9 has a vertical extent of ~4km and reverse throws of up

to 200m. Correlations of intra-Carb reflections cannot be made with certainty due to poor imaging, however truncation of dipping intra-Carboniferous reflections are observed in the hangingwall suggesting a normal pre-BPU movement prior to the reverse reactivation.

Type 3 faults may have had an early Carboniferous extensional movement due to their large fault plane extent, and then compressionally reactivated during one of the Late Cretaceous-Cenozoic inversion events.

3.5.3.4 Type 4 Faults

Type 4 faults exhibit reverse throw on both intra-Carboniferous and the BPU horizon (Figure 3.46). They are observed in the Cleveland Basin where the BPU is well defined, however may exist also in the Stainmore Trough (Figure 3.47). They typically have vertical extents of around ~1km and relatively small reverse throws ranging from 40-80m (+-9). They are associated with the buckling of the Carboniferous succession. Due to their roughly similar throws on Mesozoic and Carboniferous reflections, Type 4 faults may be associated with compression in the Late Cretaceous-Cenozoic.

3.5.3.5 Type 5 Faults

Type 5 faults exhibit no or minimal vertical offsets and are characterised by a vertical zone of low coherence of reflections (Figure 3.46). They are difficult to distinguish in seismic section from the widely documented dykes in the area (Hibsch et al., 1995), which also appear as the above description. These dykes however are found in the Stainmore Trough while the observed structures are present in the northern part of the Cleveland Basin. They are interpreted to be strike-slip faults through the entire succession but due to their poor seismic definition, an exact timing is unknown.

3.5.4 Coupling of the Pre- and Post-Zechstein

The Zechstein halite is a much thinner and undeformed interval onshore than offshore. Certain faults within the PZS have propagated through the Zechstein interval and clear reflection offsets can be observed in seismic (Figure 3.50). This is not observed offshore where there is a complete structural decoupling from the pre- and post-Zechstein. Figure 3.50 illustrates Pre-Zechstein faults that propagate has propagated through the Zechstein and into the overlying Mesozoic.

3.6 Dating Periods of Fault Activity

The timings of structures from the structural sets identified across the ADB and EPB are discussed based on the relative offsets of stratigraphically constrained reflections. The slip histories have been grouped on broad timings relative to the BPU offsets. The number that is bracketed at the end of each section title corresponds to the summary schematic in Figure 3.51.

3.6.1 Early Carboniferous Extensional Slip – Not Reactivated after the Early Permian

Lower Carboniferous extensional slip is constrained offshore in the ADB as the Lower Carboniferous is at depths too deep to image seismically. This has led to debate as to whether Early Carboniferous extension was accommodated in the same way as onshore. Early Carboniferous extension is evidenced onshore on the basin bounding faults of the East Pennine Basins (see section 2.3.2.1, Figure 2.6).

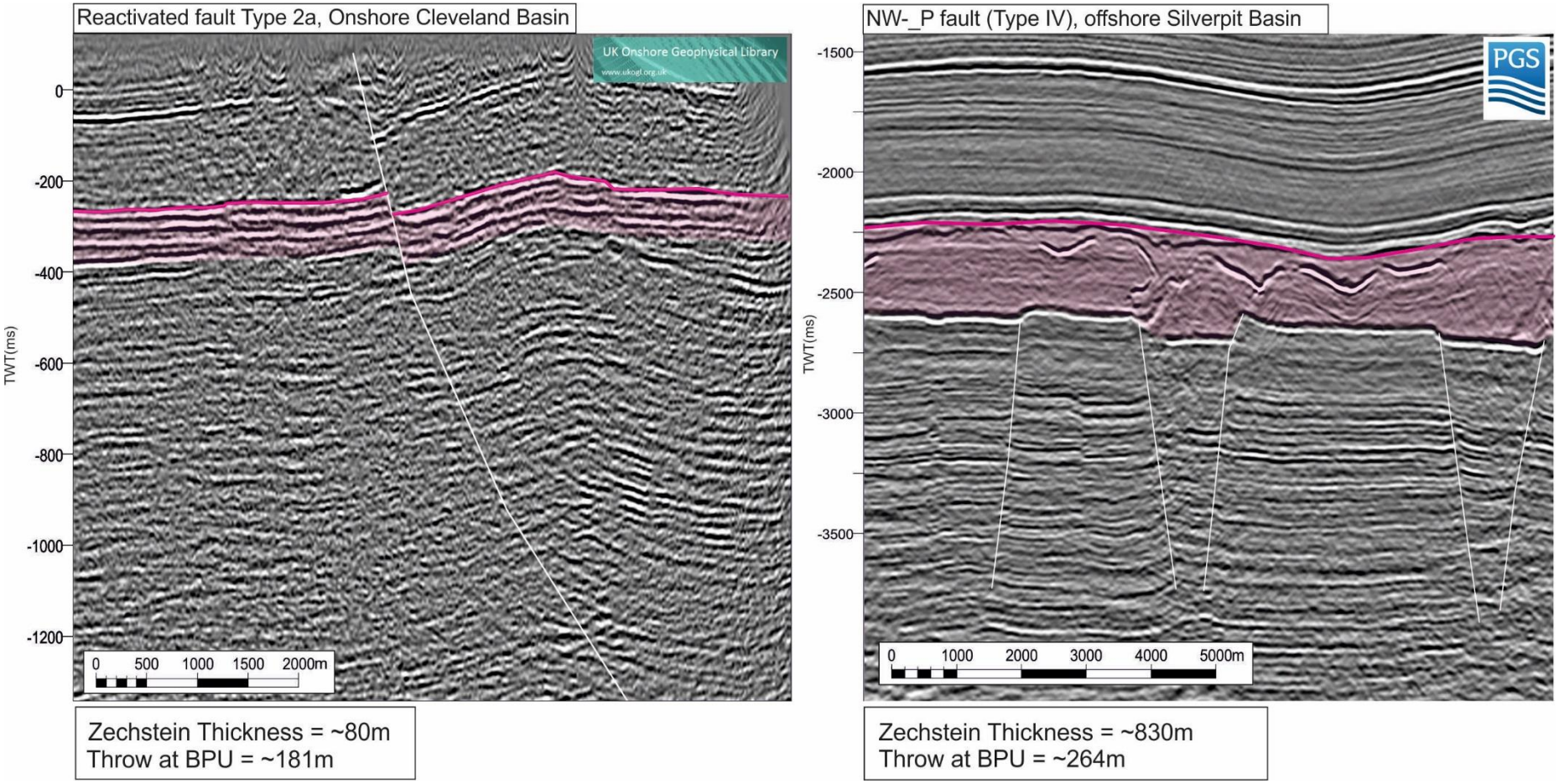


Figure 3.50 Comparison of the Zechstein succession onshore and offshore and the resulting structural coupling or decoupling. A) Onshore thin, less deformed Zechstein results in coupling of the pre and post Zechstein b) offshore thicker Zechstein succession that has undergone multiple phases of deformation and results in a decoupling of the Pre- and Post- Zechstein offshore.

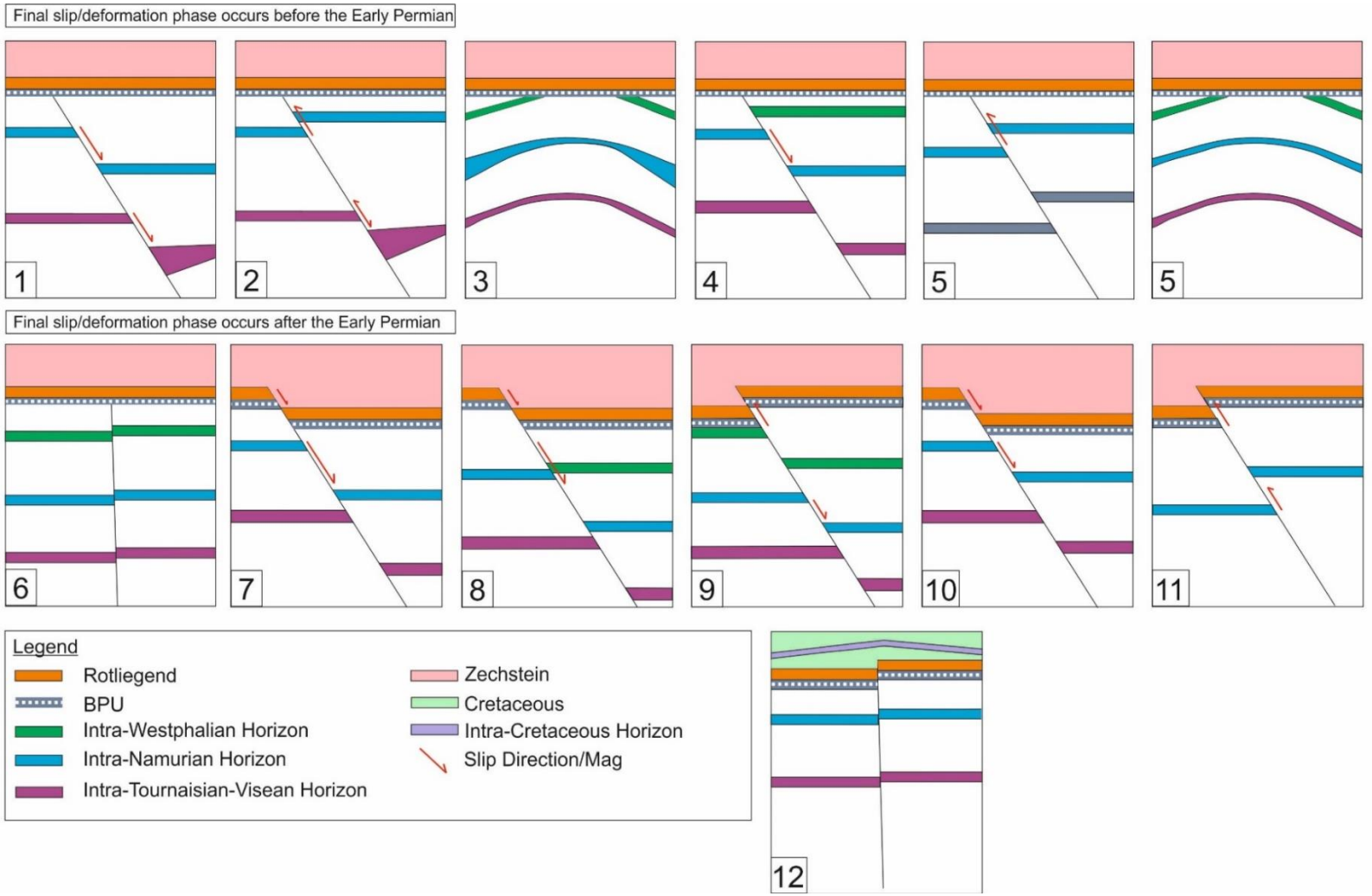


Figure 3.51 Schematic of observed fault throw profiles in 2D observed in the Pre-Zechstein succession across the Anglo Dutch and East Pennine Basin study areas. The relative fault evolution/slip history is explained in the body of text to the corresponding number along with fault examples that demonstrate this evolution.

Faults with Lower-Carboniferous, syn-sedimentary infill (ST-CB_1b and ST-CB_2b) have two main movement histories. The thinner and less deformed Zechstein interval onshore and the subsequent higher degree of coupling this that creates between the Palaeozoic and Mesozoic (Figure 3.50), and the fact that offsets are imaged by continuous, high amplitude reflections, affirms that faults truncated at the BPU that have not propagated through the Zechstein, were not reactivated after the Permian. Figure 3.51.

3.6.1.1 Late Carboniferous Extensional Reactivation (Pre-BPU) (1)

Since the ST-CB_1b faults exhibit syn-sedimentary packages of early Carboniferous age but also extensionally offset mid-Carboniferous stratigraphy for which syn-deposition is not observed (Figure 3.47), and with truncation at the BPU, their movement can be constrained to an Early-Late Carboniferous slip with cessation before the deposition of the Permian.

3.6.1.2 Late Carboniferous Compressional Reactivation (Pre-BPU) (2)

Given that the ST-CB_1c faults exhibit a reverse offset of early Namurian (Figure 3.49) reflections as well as the syndeposition activity in the Early Carboniferous, their movement can be assigned to an Early Carboniferous extensional slip with a reverse slip occurring after the deposition of the Early Namurian but ceasing before the deposition of the Permian. This reverse reactivation may be attributed to Variscan compression (section 2.3.3.1).

3.6.2 Early Carboniferous Contractional Deformation (3)

The Visean (Early Carboniferous) is a time period typically associated with regionally extensional tectonics and resulting extensional structures (see section 2.3.2.1), with compressional strain arising in Westphalian times. However, certain

structures across the ADB show evidence on seismic for undergoing a contractional phase during the Visean.

3.6.2.1 Early Carboniferous contractional deformation with a Late Carboniferous reactivation

The recognition of thinning of Namurian stratigraphy (ADB-4) over the crests of the NW-SE axial trending folded Visean (ADB-5) in the Silverpit Basin (44-49_NW-_D Folds, Figure 3.32) and S/CBH (K_NW-_D Folds, Figure 3.40) suggests that the Lower Carboniferous in the central Anglo Dutch Basin underwent a regional compressional phase during the Visean.

There is uncertainty regarding the exact timing of movement due to correlation of deep stratigraphy, however given that the folded ADB-5 Unit is thought to be Early Visean and the ADB-4 Unit Namurian, the movement is constrained to be either Visean or Namurian with cessation before the deposition of the Westphalian. The truncation of the Westphalian against the BPU suggests a Late Carboniferous compressional reactivation of these folds during the Variscan orogeny.

3.6.3 Late Carboniferous-Early Permian Extensional Slip – Not Reactivated post BPU (4)

The Late Carboniferous-Early Permian is a time period associated with regional compressive stresses and resulting compressional structures, particularly onshore UK (see section 2.3.3.1). Extensional faults that accrued slip during this time are observed in the EPB after the deposition of the Lower Namurian onshore (ST-CB_1a) and after the deposition of Westphalian D in the SB and CBH offshore.

Considering that the ST-CB_1a faults offset previously folded Lower-Mid Carboniferous (Figure 3.49), folds that are associated with Variscan N-S shortening

(Hollywood & Whorlow 1993) and that this folded stratigraphy is also truncated against the BPU, this assigns the age of the ST-CB_1a faults to after the Variscan compression but before the deposition of the Permian.

Given that the 44-D_E-W faults in the north of the ADB exhibit normal throws on Namurian-Westphalian horizons with no observable syn-sedimentary packages (Figure 3.26), it can be inferred that their movement occurred after this time but before the deposition of the Rotliegend. The 44-D_ENE- faults with normal movement can also be attributed to this timing however they are constrained to later in the Westphalian due age relationships with the pre-existing E-W faults (see Chapter 4, section 4.4).

3.6.4 Late Carboniferous Reverse Slip/Contractional Deformation – Not Reactivated post BPU (5)

The observably equal thickness of the Lower-middle Carboniferous stratigraphy across the ST-CB_1d faults and the truncation of their entrained reflections assigns their slip to the time period between the mid Carboniferous and Early Permian. Given the geological evolution (section 2.3.3.1) of the area during the Late Carboniferous, these faults are likely a result of brittle failure of buckling of the succession due to the regional N-S shortening occurring at this time (Hollywood & Whorlow, 1993).

A similar timing is proposed for the *K_NE-_D* Folds (Figure 3.39), considering that the Visean?-Westphalian stratigraphy within the fold is of equal thickness and is truncated against the BPU. The timing of folding is constrained to post-dating the deposition of the Late Westphalian but prior to the deposition of the Rotliegend.

3.6.5 Late Carboniferous Strike-Slip – Not Reactivated post BPU (6)

Considering that each of the interpreted NNE-, NE- and ENE- strike-slip faults across the SB and CBH exhibit a slight vertical offset of Carboniferous reflections (see Figure 3.36 for 44-49_NNE-_SS example) while exhibiting no vertical offset or distortion of the TRot horizon, a Late Carboniferous-Early Permian time frame is assigned to this strike slip movement. This is in agreement with the widely documented strike-slip faulting occurring at this time throughout the ADB (Coward, 1993).

Another interpretation resulting with this geometry is that the vertical offsets of Intra-Carboniferous horizons are due to the variably dipping stratigraphy in the Carboniferous succession that has been laterally juxtaposed. This would not be expressed in the TRot horizon as juxtaposing the TRot against the same TRot succession would not produce a significant enough variance in amplitudes to be reflected on the variance attribute map. This would mean the possibility of a strike-slip movement occurring after the BPU or Rotliegend. This interpretation is less likely as the strike-slip movement would have had to be a strike-slip movement that had absolutely no vertical component. Given the minimal evidence of lateral offsets of the NW-SE faults at intersections (Figure 3.31, Figure 3.41), this also suggests a Late Carboniferous movement.

3.6.6 Early-mid Carboniferous extensional slip – reactivation after the deposition of the Rotliegend

In view of the fact of their higher values of normal throw on intra-Carboniferous horizons than BPU and younger horizons (Figure 3.46), the *Type 2a* faults are interpreted to be Lower Carboniferous syn-sedimentary faults that have been extensionally reactivated at some point after the deposition of the Permian.

3.6.7 Mid-Late Carboniferous extensional slip – extensional reactivation after the deposition of the Rotliegend (7)

Ter Borgh et al. (2018) attribute the formation of the A-E_WNW- faults to Late-Devonian-Early Carboniferous regional extension. However, given that no syn-depositional Late Devonian or Lower Carboniferous packages have been observed in the hangingwalls across these faults, the fact that the upper tips are truncated against the BPU (Figure 3.10), and the observation that they appear to detach on a seismically dim layer with no observable offset of underlying reflections, an extensional slip during the mid-Late Carboniferous–Early Permian time period is instead proposed. The smaller, more localised offsets of the TRot horizon implies a slight extensional reactivation after the deposition of the Rotliegend. The detailed movement history of these faults is illustrated by Figure 4.34 and explored in more detail in Chapter 4 section 4.6.1.1..

3.6.8 Late Carboniferous Extensional Slip – Reactivated post BPU

Though these faults have formed and accrued slip prior to the Late Carboniferous and subsequently reactivated then, as the Lower Carboniferous is not clearly imaged this cannot be determined, therefore the Late Carboniferous is the most recent period of movement expressed on the seismic data.

3.6.8.1 Extensional Reactivation Post BPU (8)

In view of the fact that the normal throw values on intra-Carboniferous reflections are more than twice the values on the TRot horizon and BPU on K_NE-_T and K_NW-_TN faults (Figure 3.39, Figure 3.40), the initial timing of movement on these faults is delimited to the Late Carboniferous, with a reactivation after the deposition of the Rotliegend. Despite the Zechstein layer having a relatively thin thickness that is relatively undeformed in this area, no accurate kinematic indicators

can be derived from the Zechstein or the overlying Mesozoic. The hiatus between the Zechstein and Cretaceous on the CBH means a reactivation could have occurred during the Triassic and Jurassic, with slight normal movements also during the mid-Cretaceous indicated by the thickening of stratigraphy in the hangingwall of the NW-_TR fault (Figure 3.42).

3.6.8.2 Contractional Reactivation Post BPU (9)

Given the localised reverse offsets of the TRot horizon on the 44-D_E-W faults in the Murdoch Block area (Figure 3.26), a reverse reactivation is inferred on these previously extensional faults at some time after the deposition of the Rotliegend. Hollywood (1993) attribute this slight reverse reactivation to the Late Cretaceous compression/inversion, which had a north-south direction of regional compression.

The recognition of normal throw on intra-Carboniferous horizons and reverse throw of the BPU horizon on ST-CB_3 faults (Figure 3.46) is suggestive of a late Carboniferous extensional movement before the BPU with a reverse reactivation occurring at some time after. Their large fault plane extent is suggestive of an initial Early Carboniferous movement. Their compressional reactivation may be attributed to one of the Late Cretaceous-Cenozoic inversion events.

3.6.9 Extensional Post-BPU Structures (10)

In view of the fact that both Carboniferous and Rotliegend aged horizons record relatively similar throw values on K_NE-_P faults (Figure 3.39), and no syn-sedimentary packages are observed in the PZS, the movement on the NE-_S faults can be constrained to after the deposition of the Rotliegend. The offset of folded reflections that are postulated Late Westphalian - Early Carboniferous in age (small NE- faults on Figure 3.39) indicates that these faults formed after the Rotliegend.

Due to the small offsets on these faults, their movement history cannot be elucidated for certain due to the decoupling effect of the thick, deformed Zechstein salt layer above. Given their orientation, the most likely regional extension phases responsible for their formation could be the Early Cimmerian in the Late Triassic in which NW-SE regional extension occurred (Ziegler, 1990). However, given the fact that they are located mostly on the crests of the long wavelength folds in the PZS (Figure 3.39), these folds may have caused stress perturbations that had an effect on the clustering and preferential orientation of these faults (Rawnsley et al., 1992), meaning that E-W rifting in the Late Jurassic – Early Cretaceous may have also formed these faults, with oblique slip occurring.

The shorter K_N-S faults are interpreted to link the K_NE-_T faults, joining them and reactivating them in order to accommodate the E-W extension in the Jurassic Late Cimmerian (Cameron et al., 1992). The longer faults, such as the one in the SE corner of the area (Figure 3.41), are likely to do this but on a larger scale.

Given that the ST-CB_2b exhibit similar throw on intra-Carboniferous and BPU horizons (Figure 3.46) and no syn-depositional packages observed, these faults are interpreted to have formed during the Mesozoic.

3.6.10 Contractional Post-BPU Structures (11)

The timing of formation of the 44-49 NW-_T and K_NW-_TR faults is difficult to constrain to a specific time period. Given that the Carboniferous and Rotliegend successions have a laterally consistent thickness across the fault (Figure 3.40), the monoclines therefore formed after the deposition of the Rotliegend. The presence of the thick Zechstein halite succession and the decoupling effects this causes with the overlying Mesozoic, an upper age limit of movement is not easily constrained. The possibilities for the timing of formation of this structure are:

1. Compressional forces reactivated an area of already folded lower-mid Carboniferous stratigraphy sometime after the deposition of the Rotliegend to form the monocline (or sub-seismic reverse fault). The next regional compressional event occurred in the Cretaceous with a N-S/NE-SW direction of maximum shortening (Sub-Hercynian). Given that the structure appears to coupled with basement stresses, it is likely that it was formed during a regional tectonic phase. By referring to the regional palaeostress orientations from the Permian to Recent (Figure 2.17), the most likely timing for these faults/folds would be during the NE-SW shortening caused by the Sub-Hercynian inversion event in the Late Cretaceous (see section 2.3.6.1), that is normal to the strike on the structure. The later inversion phases throughout the Cenozoic, all related to the Alpine collision, could have also been responsible (see section 2.3.6.). This deformation is not expressed in the overlying Triassic and Cretaceous stratigraphy due to the decoupling effect of the Zechstein halite and therefore it cannot be confirmed.
2. Due to there being no expression of this fault in the Mesozoic overburden, it is possible that these structures could have formed at the end of the Permian before the deposition of the Triassic. This is unlikely however, as these structures appear to be coupled with basement stresses and the Zechstein was a time of relative tectonic quiescence (section 2.3.3.3.).

This overall thinner Cretaceous succession in the hangingwall (that thins over the salt pillows) signifies the possible combined reverse movement on the fault throughout the Cretaceous as well as coeval halotectonics occurring as shown by the growth fold in the lower part of the succession (Figure 3.42). The present day folded Palaeogene and the growth fold in the later part of this succession could be

due to halotectonics of the salt pillows or a reactivation of the NW-SW fault (or a combination of both). Quirk (1997) attribute the formation of these reverse faults to being reactivated normal Caledonian faults, which seems likely that these structures would use a pre-existing basement grain. However, the stratigraphy can be traced around the fault lateral tip and shows no evidence of prior normal movement.

Given that the ST-CB_4 faults exhibit reverse throws on both intra-Carboniferous and the BPU horizons in similar proportions (Figure 3.46), they are interpreted to have a similar movement history as the NW-_R faults and are reactivated by compression in the Late Cretaceous-Cenozoic.

3.6.11 Strike Slip Post-BPU structures (12)

Given the large stratigraphic hiatus represented by the BPU/BCU unconformities on the ESP, which has been a persistent high through the stratigraphic record, constraining the timing of movement on the set A-E_ENE-faults is difficult. The decoupling effects of the Zechstein salt layer on the flanks of the ESH also obscure the timing analysis. The observed truncation of the Lower Carboniferous succession within the push up structure (P1) at the Base Cretaceous (Figure 3.17), and the absence of growth packages in P1, this contractional duplex was created by movement that occurred before the deposition of the Late Cretaceous but occurred after the deposition of the Brigantian-Asbian succession.

The slight doming and thinning of the earliest Cenozoic stratigraphy over the crest of P1 (Figure 3.17) suggests a compressional/transtensional reactivation of this fault zone in the Early Cenozoic. The movement is therefore constrained to an initial post-Brigantian to pre-Early Cretaceous movement with a slight transpressional reactivation occurring in the Late Cretaceous. It is not possible to constrain the movement history of these faults in more detail. However, these faults

are interpreted to be in closely coupled with basement stresses and dextral strike-slip movements are observed across the ADB during the Triassic and Jurassic with the Early and Late Cimmerian events (Figure 2.17). Ter Borgh et al. (2018) assign these faults an initial later Cretaceous movement based on observation of seismic to the north east of the ESP. In view of the no or minimal vertical offsets observed on reflections surrounding faults belonging to the ST-CB_5 type, they are interpreted to be strike-slip faults with a movement analogous to the ENE- faults on the ESP, due to their extent through the entire succession. However, due to their poor seismic definition, an exact timing is uncertain.

3.6.12 Timing further investigated

Certain faults have movement histories that could not be defined by the analysis of age calibrated reflection offsets and require further investigation that will be addressed in Chapter 4, they include A-E_NE-, 44-D_NNW- and 44-49_NW-_P. This is due to contradicting kinematic indicators or very slight differences in throws on Rotliegend and intra-Carboniferous horizons.

3.7 Classification of Fault Families

Fault sets within the Pre-Zechstein succession across the ADB and EPB are classified into fault families. Fault classification (Figure 3.52) is formed by scale (throw magnitude), structural style, geometry, and orientation. A classification of faults in well imaged areas enables the correlation of structures and their movement histories in areas of poorer imaging.

3.7.1 Scale

Fault sets have first be classified by their observed maximum throws. This could have also been performed by vertical extent or lateral lengths but due to the

vertical and lateral constraints of the seismic data, throw magnitude was used instead as a proxy. Three classes are formed based throws with a difference of an order of magnitude of 10. Only one set of faults is described and identified with recorded mean throws in 10s of metres.

The majority of faults have recorded mean displacements of 100s metres. This group could be further subdivided but was not for classification simplicity. Large scale extensional faults such as the NNW-SSE trending Elbow Fault and the E-W/ ENE-WSW trending onshore grabens fall into this largest category in which recorded mean throws are 1000s of metres.

3.7.2 Structural Style

At least three structural styles have been observed across the fault sets; Throughgoing, Superficial and Layer Bound (Figure 3.53). These classifications are based on geometries alone, and the further chapters build upon these definitions introducing possible mechanisms (see Chapter 4, section 4.7).

3.7.2.1 Throughgoing Faults

Throughgoing faults have observable offsets throughout the entire imaged Pre-Zechstein Succession. Due to their large vertical extent, their basal tips are not observed on 3D seismic. Throughgoing faults range over two orders of magnitude, having maximum observed throws within the 1000s of metres range (crustal scale) and within the 100s metres range (meso-scale).

3.7.2.2 Superficial/peripheral Faults

Superficial faults have observable offsets in the upper to middle parts of the PZS. Their displacements are relatively small (10m-150m) and decrease to an area of no displacement at the lower tip which can usually be distinguished on seismic.

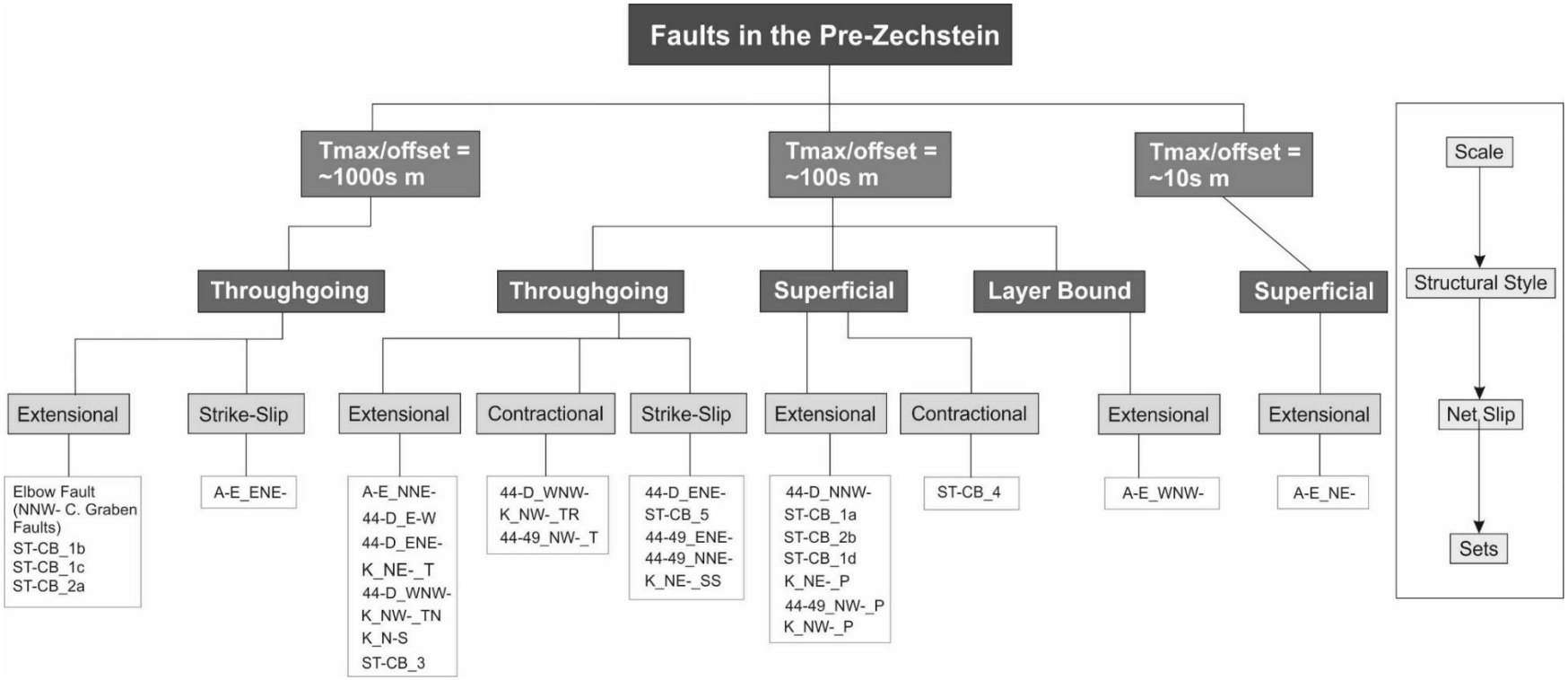


Figure 3.52 Fault classification diagram for all the fault sets identified across the study areas. The fault sets are first subdivided by mean throw magnitude, structural style, then net slip. This diagram is further built upon in the discussion when the patterns of reactivation are addressed.

3.7.2.3 Layer bound Faults

The layer bound faults offset a portion of the Pre-Zechstein succession and are observably decoupled from underlying stratigraphy by the observation of undeformed, underlying stratigraphic horizons, without the gradual decrease in throw towards this horizon (like the Superficial faults).

3.7.3 Net Slip

Net slip is considered for a classification based on geometry only. Many of the faults across the study area have been reactivated a number of times through the geological history and therefore their net slip is the simplest classification as it is performed without unravelling the complicated slip history.

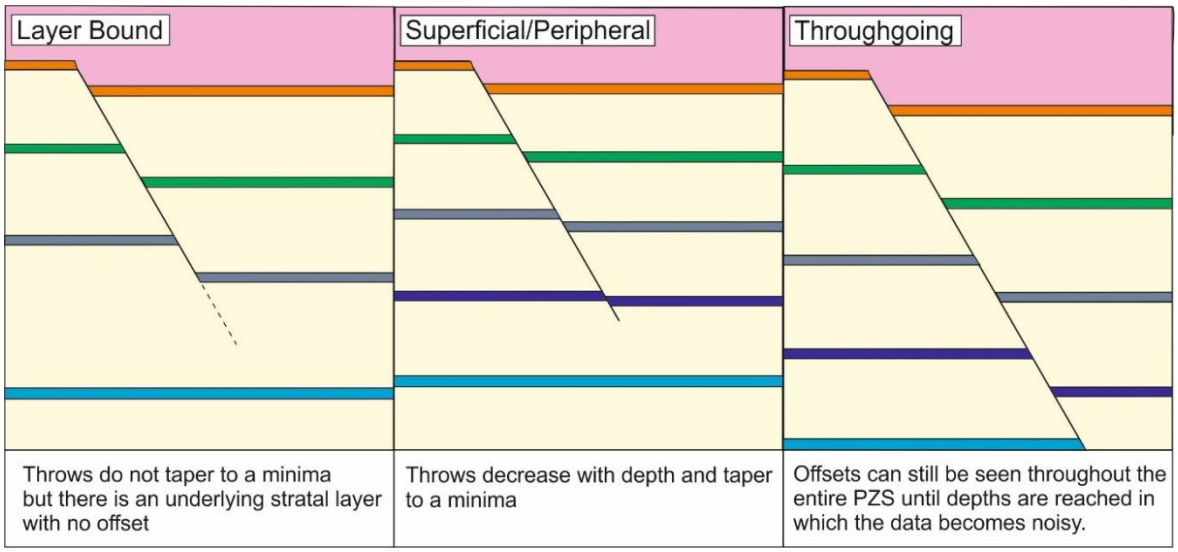


Figure 3.53 Structural style categories of faults within the Pre-Zechstein succession based on their vertical extent and basal tip geometries and relationships with underlying stratigraphy

3.8 Conclusions

1. The fault patterns across the Anglo-Dutch Basin are strikingly different at the Top Rotliegend interval compared to an intra-Westphalian horizon (100ms interval). This is due to the selective reactivation of certain faults.

2. Over 25 different faults sets with distinctive geometries have been characterized across the study areas. Their timing of movement has been assessed and grouped into 12 overall kinematic histories, these are relative timings due to the Zechstein salt decoupling effects complicating the analysis. Some genetically similar faults indicate a differential reactivation history (see above point).

3. The high length to throw ratios observed on NW-SE orientated faults in the PZ of the ADB were previously attributed to periodic reactivations. The interpretation of 3D seismic attributes and data has revealed they are highly segmented. The small throws ae therefore attributed to the fact that they are composed of many en-echelon smaller faults rather than one large master fault.

4. Faults are observed on both the 2D and 3D seismic data with throws ranging over three orders of magnitude.

5. Three structural style types emerge from the observations; Throughgoing, Superficial and Layer Bound

Chapter 4

THE KINEMATICS, STRUCTURAL STYLES AND MECHANISMS OF PRE-ZECHSTEIN FAULTS

4 The Kinematics, structural styles and mechanisms of Pre-Zechstein Faults

4.1 Introduction

This chapter presents the results from the throw distribution analysis for representative faults from six different sets from 3D seismic case study areas on the Elbow Spit Platform, Murdoch Block and Silverpit Basin (Figure 4.1). This analysis investigates the throw distributions in order to finalise structural styles, movement histories and fault formation and reactivation mechanisms.

The complexity of the structural framework of the Anglo-Dutch Basin (introduced in Chapter 3) can be attributed to the overprinting of the deformation related to numerous stress regimes through time. This is particularly evident within the Pre-Zechstein succession (PZS), in which complex cross-cutting fault networks are observed on map, variance attribute z slices and 2D and 3D seismic sections. Within these fault networks, the age and intersecting relationships are not immediately obvious from initial observation.

Interpretation of the vertical throw distributions on faults can help to constrain the timing of their formation and reactivation, as well as the mechanisms for fault formation and reactivation (Baudon and Cartwright, 2008b, Baudon and Cartwright, 2008a, Baudon and Cartwright, 2008c, Nicol et al., 1996, Watterson, 1986, Muraoka and Kamata, 1983, Barnett et al., 1987).

Observation of along strike throw distributions can provide insights into the intersecting relationships between faults within a network (Nixon et al., 2014 (Dickinson, 1954).

In a mature basin that has undergone many regional stress reorganisations, the patterns, styles and magnitude of reactivation of existing structures are often found to be highly complex. This is exemplified well by the inversion history of the onshore basins of northern England i.e. Bowland, Widmerpool, Gainsborough (Fraser et al. 1990, Fraser & Gawthorpe 1990, Corfield et al. 1996) and south west England i.e. the Bristol Channel Basin (Van Hoorn 1987, Dart et al. 1995, Kelly et al. 1999).

It is widely accepted that fault reactivation is controlled by (i) optimal orientation of the stress field for frictional slip (ii) the size of the fault (iii) overpressure and (iv) frictional resistance (Sibson, 1995, Kelly et al., 1999, Wiprut and Zoback, 2000). The specific causes of reactivation in any given basin have important implications for fluid migration and reservoir connectivity or compartmentalisation (Bailey et al., 2002, Sibson, 1995, Cartwright et al., 2007). Compartmentalization is an important issue for consideration in field development (Van Hulten, 2010), so any potential exploration programme in an inverted area in particular, should factor in an appreciation of the impact of the slip history on the security of fault baffles or seals (Manzocchi et al., 2010).

4.1.1 Project Rationale

Seismic interpretation of the relative offsets of mapped horizons on seismic sections performed for the characterised Pre-Zechstein fault sets (see Chapter 3, Section 3.6.1.4), left their timing of formation and reactivation inconclusive or uncertain, as well as their relationship to the basement/crustal scale structure. Throw mapping and analysis and interpretation of throw-depth (t-z) and throw-distance (t-x) distributions can reveal subtleties about the slip history and structural relationships that are not apparent from seismic interpretation alone.

Throw mapping has not previously been conducted on Pre-Zechstein faults across the Anglo-Dutch Basin, due to the uncertainties regarding the mapping of sub-salt reflections. Good quality 3D data and the selection of the best quality case study areas with closely spaced, good quality, intra-Carboniferous horizon correlations has enabled the vertical throw distributions on Pre-Zechstein faults to be mapped. The variable data quality meant that not all case study areas were suitable for this type of fault analysis.

4.1.2 Aims and Research Questions

This chapter has two overall aims:

1. Characterise the vertical throw distributions on faults in the Pre Zechstein succession of the Anglo Dutch Basin.
2. Investigate intersecting relationships between Pre-Zechstein faults in order to clarify their relative timing.

In detail the chapter aims to:

1. Further investigate the slip and reactivation histories and structural styles of faults across the Anglo Dutch Basin that were not fully addressed in Chapter 3 (see Chapter 3, section 3.7.11).
3. Characterise lower and upper tip fault geometries.
4. Characterise the spatial and temporal patterns of fault reactivation.
5. Discuss possible formation mechanisms that produce the distinct structural styles observed.

4.2 Data and Methods

The faults sampled for the throw-depth analysis were selected from the 3D seismic dataset only (see Chapter 1, section 1.5.1.1). The selections were based on: (1) quality of imaging of the fault planes; (2) the quality and distribution of correlative horizons to provide throw measurements at regular intervals within the interval of interest, and (3) faults being representative of a fault set, consistent with more regional seismic observations (see Chapter 3). This meant that only faults mapped in the offshore regions are contained in this study, because in the onshore region only 2D data is available, and the sampling grid is too sparse to conduct a meaningful fault analysis. All faults with throw distribution analysis presented in this chapter are located in Figure 4.1.

4.2.1 Throw-Depth Analysis

Footwall and hangingwall cut-offs of mapped horizons of known stratigraphic ages, were measured in TWT (Figure 4.2b). These measurements were performed at sampled locations along the strike of the fault plane (Figure 4.2a) and plotted against the z axis value (depth or TWT) to create a profile (Barnett et al., 1987, Mansfield and Cartwright, 1996, Baudon and Cartwright, 2008b). The hangingwall and footwall cut-off TWT or depth values were used to calculate throw values which were then plotted against footwall TWT or depth as a reference position to form the t-z plot (Figure 4.2e).

Representative faults from different fault sets were analysed in detail in order to establish timings of main phases of activity and periods of reactivation, and also to assist in the identification of specific structural styles (Detached vs basement linked).

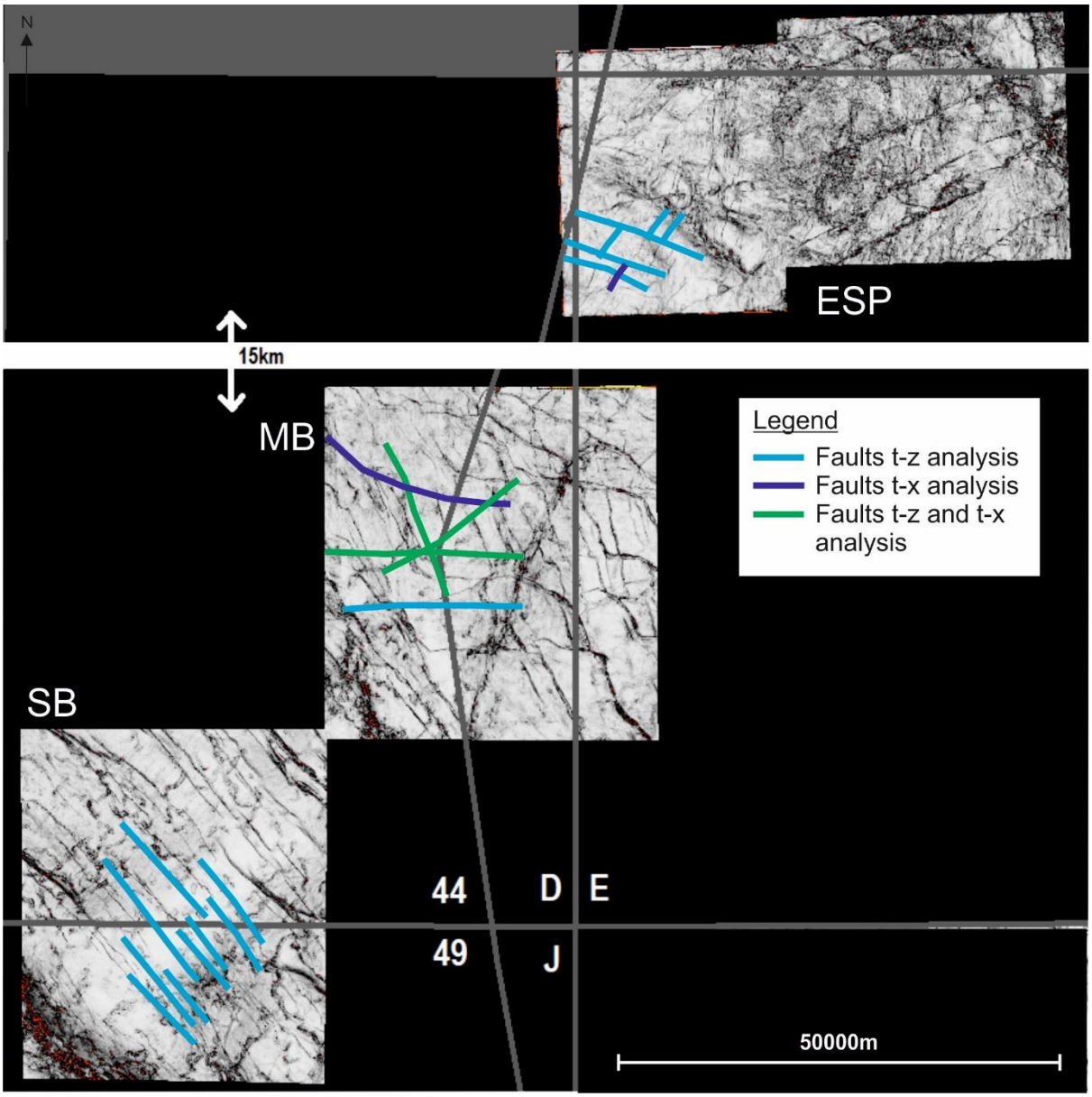


Figure 4.1 The location of each fault sampled for throw distribution analysis presented in this chapter. The coloured lines indicate the fault position, and the type of analysis performed is indicated by the key. T-Z sampling positions (MPS) are indicated by zoomed maps in succeeding figures.

The sampling strategy for throw measurement comprised two alternate methods depending on the detail and quantity of sampling required:

1. By measuring at regular intervals along strike, with sufficient sampling density as to best avoid sampling bias (see discussion in Trudgill and Cartwright (1994). Areas of poor data and regions close to fault intersections with other faults were avoided.
2. By measuring throw profiles along a transect constructed perpendicular to fault strike in areas with genetically similar parallel faults, as for example in the Silverpit Basin.

The quality of the horizon correlations across faults and the vertical distribution of correlative horizons were considered essential prerequisites in the choice of faults and measurement positions. Additional measurements were made of reflection correlations between these marker horizons as to order to reduce sampling bias, creating a more representative plot. Horizons with no observable offset were also plotted in cases where their depth provided a reference point to aid the interpretation of the fault movement history. Such horizons included the MDR1 horizon (Top Frasnian) and TRot (Top Rotliegend). Recording throw in milliseconds on time migrated seismic data was a viable proxy for throw in metres as P-wave velocity is approximately constant in this interval (Figure 4.3). A depth conversion was later performed as needed as outlined in Section 1.5.2.4 . Measurements were recorded to an error margin quantified by the processes outlined in Figure 1.12.

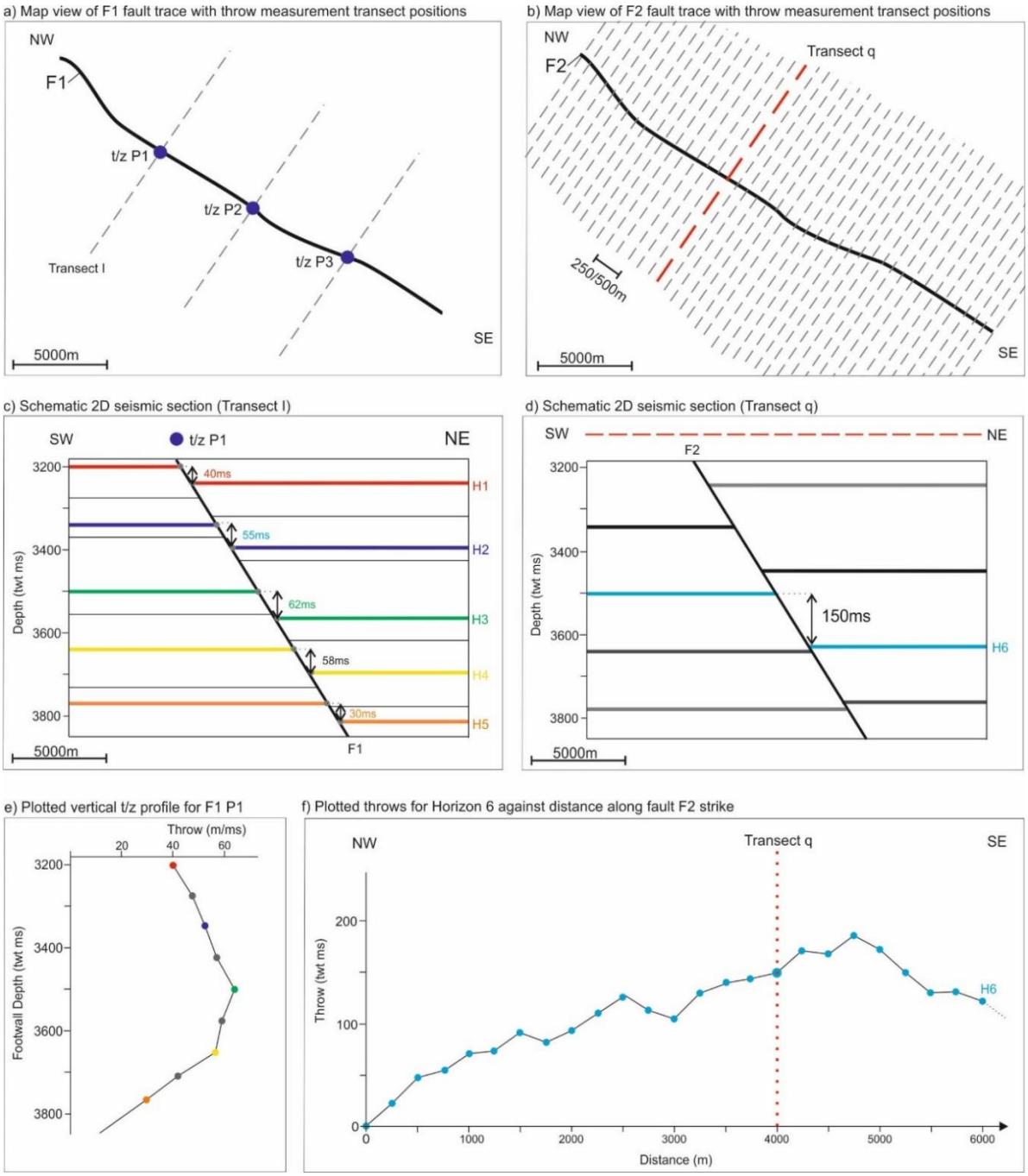


Figure 4.2 Summary of the sampling, measurement and plotting methods used in the throw distribution analysis. Schematic map view of the sampling positions and frequency for a) t-z and b) t-x measurements. c) and d) cross section of the horizon cut off measurements e) and f) resulting plotted t-z and t-x measurements

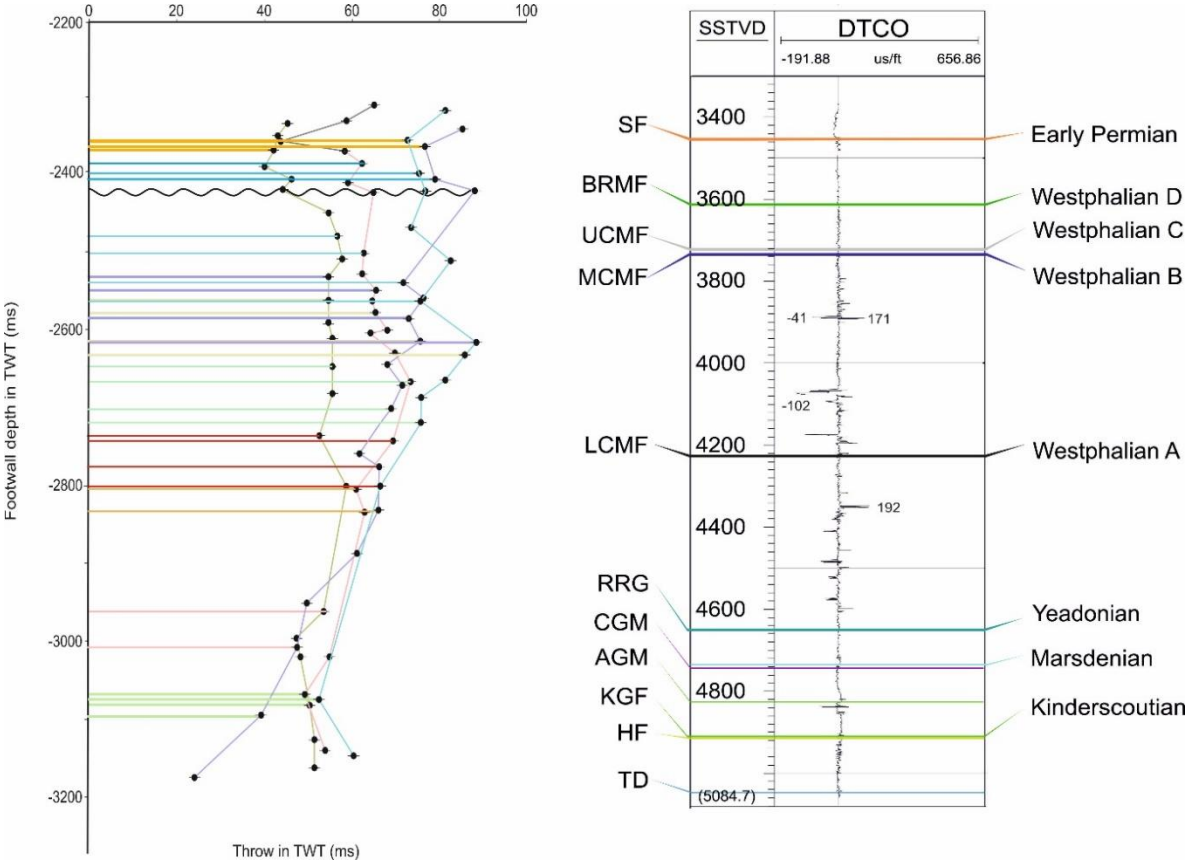


Figure 4.3 Combined plotted throws for NNW-_1 MP1-4 aligned with the sonic log for nearby well 44-19, demonstrating that changes in throw in ms are unrelated to the velocity, which stays almost constant with depth in this interval. Colours are labelled on the velocity log and conform with those on the t-z plot.

4.2.2 Throw-Distance Analysis

To examine lateral fault growth and age relationships between intersecting faults within the pre-Zechstein succession, detailed throw variations were investigated along the fault strike. In the same method conducted for measuring throw for t-z plots (section 4.2.1.), faults were chosen based on being representative of sets and having the most coherent reflection correlations across the fault cut-offs. It was a pre-requisite that these representative faults had clearly imaged cross cutting relationships.

Initial seismic interpretation was conducted using time migrated data. This was because a more accurate structural interpretation could be performed on this data type. Mapped key horizons mapped were then re-mapped on depth migrated data.

The throw was measured using the same method as previously described, but instead of measuring frequent reflections with depth, throw was measured consistently for key horizons only. The measurement position (MP) was also repeated at closer increments along strike, and the distance between such positions was determined by the length of the fault (Figure 4.2b). A compromise was made to minimise measuring time while sampling enough points to best characterise the fault.

For intersecting faults on the Murdoch Block, a throw measurement was performed for the TRot, intra-LCM_1, and intra-KG at every 250m near areas of intersection where a detailed throw profile was required, and every 500m or 750m along isolated areas of the fault trace.

4.2.3 Throw Distribution Analysis Limitations

The standard technique of measuring horizon offsets on 3D seismic data involves the following limitations and uncertainties:

- The method assumes faults are purely dip slip. In reality, most faults have some element of oblique slip (Fossen, 2016). This is likely for faults within the pre-Zechstein succession due to superposition of many deformation events and resulting multiple reactivations.
- Throw measurements reflect brittle strain, therefore elements of ductile strain such as hangingwall drag folds may invalidate measurements if not consistently included or discounted in the measurements (Walsh and Watterson, 1988a, Mansfield and Cartwright, 1996). This study recorded consistent measurements by measuring the peak amplitude of the wavelet roughly 25m from the fault plane in both the hangingwall and footwall cut-off point regardless of whether such structures were present (Figure 4.4).
- Throw measurements were made to an accuracy defined by the seismic sampling interval which is typically 2ms (Mansfield and Cartwright, 1996) but due to lower resolution in the Carboniferous interval, error bars ranged from 4-10ms. The error increases with depth due to resolution decreasing; error bars at all depths reflect the maximum error for the deepest data point.
- Poor seismic imaging of some stratigraphic layers makes it difficult to conduct a detailed throw analysis. If the reflections are discontinuous or distorted they cannot be mapped to a high accuracy around fault tips or by seismic character correlation.
- Measuring throws using this manual method is highly time consuming, especially for larger faults.

- Many of the faults did not have isolated lateral tips due to intersecting relationships, or the tip was not shown by the data extent or imaging quality. This meant that the correlation of horizons across fault cut offs was be based on seismic character, rather than the continuous mapping of a particular horizon around the fault tip (Figure 4.5).
- Defining a position for the upper and lower tips is not possible for many faults within the PZS. This is due to the fact that many if not all of these faults are truncated at the BPU and the original upper tip has therefore been eroded. Many of the lower Pre-Zechstein fault tips cannot be recognised due to the decrease in data resolution with depth. Seismically opaque successions result in the lower or upper tips being undetectable, causing many t-z plots to have final measurement points unrepresentative of the upper or lower fault tips.
- The structural analysis function in the Petrel interpretation package that automatically calculates the offset of a mapped horizon at fault cut-offs could not be implemented for this dataset. This was due to the lack of laterally consistent reflections within the Carboniferous interval.
- Many of the faults have undergone reverse reactivation, therefore the sampled normal throws are likely not representative of the greatest normal throws to occur on the fault through time (Muraoka & Kamata 1983; Walsh and Watterson (1987), (1988a); (Cowie and Scholz, 1992).

4.2.4 Seismic Attributes

The variance attribute and RMS amplitude seismic attribute were most useful to display features such as faults and channels. For the most coherent horizons, the variance attribute was extracted and overlain. This was particularly useful for the interpretation of stratigraphic features in fault blocks, such as channels.

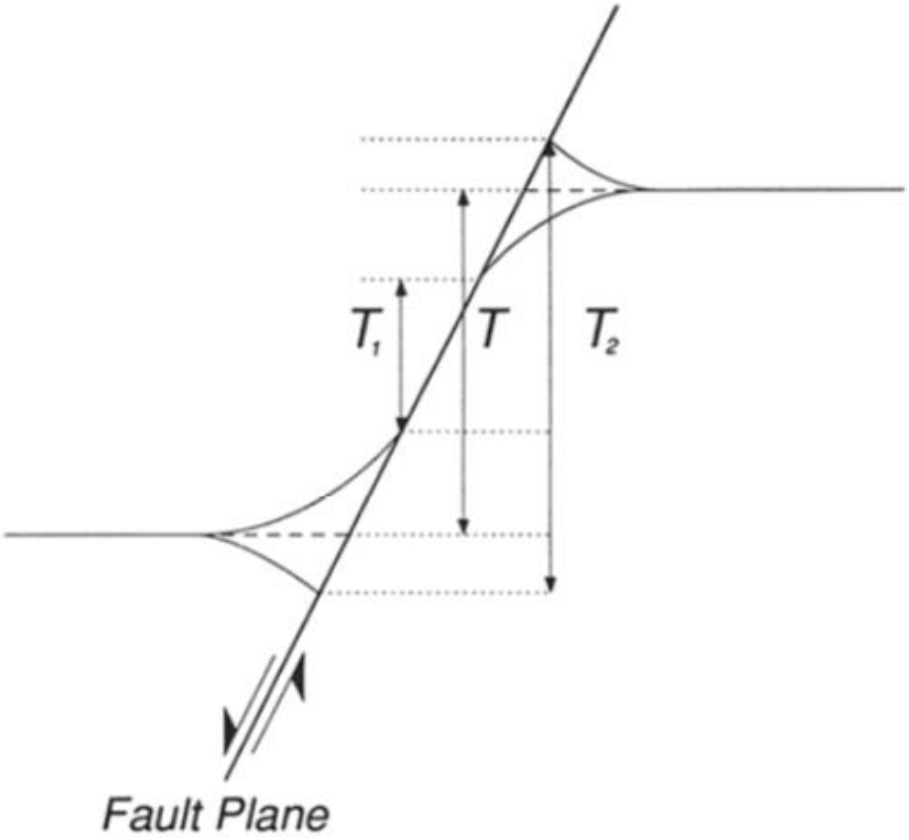


Figure 4.4 Schematic showing the corrections that were made to throw measurements for stratal folding adjacent to the fault plane From Mansfield & Cartwright (1996). In this study, T was recorded by adding or subtracting the proportion of throw accrued by the deflection.

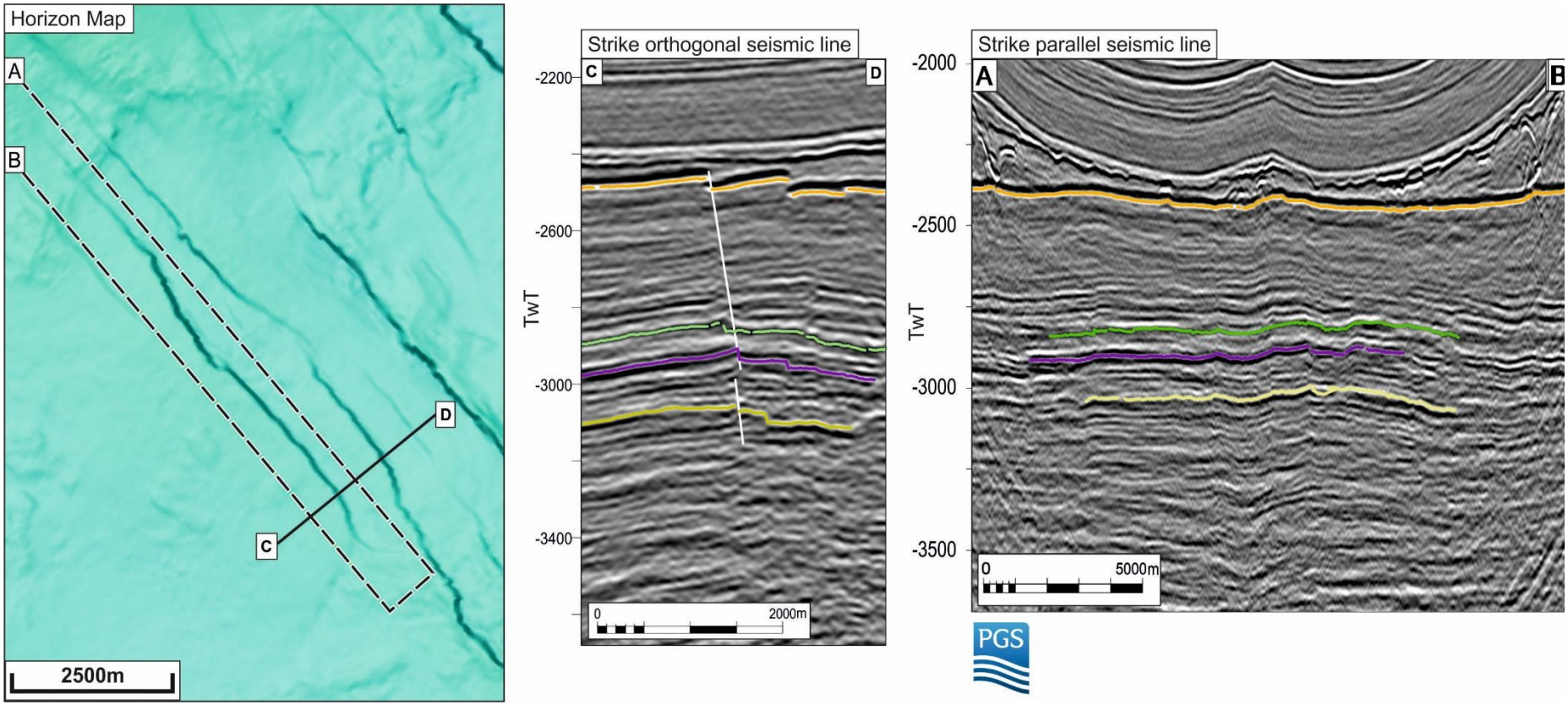


Figure 4.5 Method of correlating a horizon across a fault cut off. An arbitrary line is drawn parallel to the fault in the hangingwall and footwall that wraps around the lateral tip.

4.3 Throw-Depth Analysis

End-member profile types have been recognised and are defined below. Representative faults exhibiting one or more of these types are presented.

4.3.1 T-z Profile End-Members

The throw-depth distributions of Pre-Zechstein faults sampled across the study areas are found to exhibit a number of distinctive profile geometries (Figure 4.6). These end-member types are described below.

4.3.1.1 Type I - Beheaded, not reactivated

Type I t-z profiles (Figure 4.6ai) comprise throw measurements only from offsets of Carboniferous horizons. The first or most shallow throw measurement has an anomalously high value relative to the standard more tapered profile towards tips, giving it a 'beheaded' appearance. This is interpreted to be representative of the erosional truncation of the fault upper tip at the BPU (Figure 4.6aii). Similar t-z profiles have been attributed to later erosion of a more classical tapered geometry by Baudon and Cartwright (2008c). Profiles of this type typically display a constant shallownegative gradient from a maximum throw value (Tmax) close to the erosional unconformity downwards towards the lower tip, which is not normally imaged.

4.3.1.2 Type II – Beheaded, slight normal reactivation

Type II t-z profiles (Figure 4.6bi) have a stepped profile geometry in which the lower portion is similarly 'beheaded' as with Type I profiles, with a Tmax located at or close to the erosional surface.

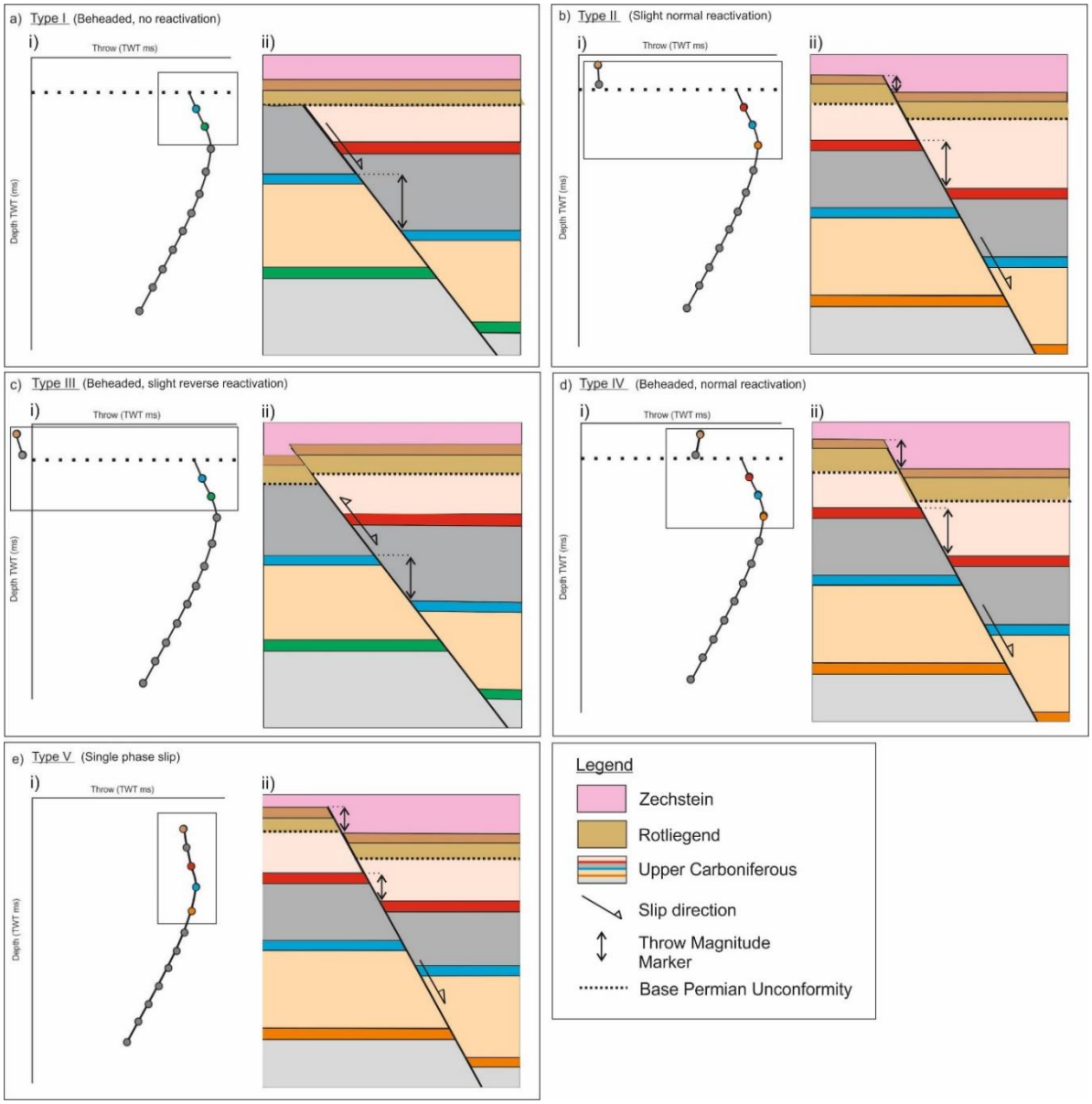


Figure 4.6 i) t-z profile end-member types observed on the faults sampled across the ADB ii) Schematic idealised cross sections expected for each profile.

They have gentle throw gradients that stay constant with depth or decrease slightly towards the lower tip which is not normally imaged. The contrast with Type I profiles is that Type II profiles exhibit a limited interval of significantly lower throw values recorded above the BPU that represent a slight reactivation of the fault (Figure 4.6bii).

4.3.1.3 Type III – Beheaded, reverse reactivation

Type III t-z profiles (Figure 4.6ci) are also 'beheaded' with a Carboniferous throw profile similar to Type I. Type III profiles however exhibit negative throw values above the unconformity. These negative throw values represent a reverse reactivation of the fault on which they are measured (Figure 4.6cii).

4.3.1.4 Type IV – Beheaded moderate normal reactivation

Type IV profiles (Figure 4.6di) are beheaded with a normal reactivation like Type II, but show a considerably higher throw magnitude on their reactivated portion. This stepped profile geometry is less obvious than Type II profiles, but is still significant enough to exceed the throw measurement error margin.

4.3.1.5 Type V – Open Top

Type V t-z profiles (Figure 4.6ei) have a mostly continuous gradient that lacks significant steps. This profile type has an 'open top' and generally exhibits maximum throws close to the first/most shallow (upper tip) throw measurement, with an overall decrease in throw towards the lower tip. The lack of a stepped profile means that Type-V profiles are the only end-member types recognised in the Pre-Zechstein that have a single phase of movement.

4.3.2 Fault examples with mostly Type I Profiles

Faults that display Type I t-z plots generally trend ENE-, WNW- or E-W and are found in the centre and northern margin of the Anglo-Dutch Basin such as the Murdoch Block, and the southern Mid North Sea High area such as the Elbow Spit Platform (*Figure 4.1*). Example faults exhibiting this t-z type and their throw profile geometries are presented as follows.

4.3.2.1 Fault ENE-_1 (Set 44-D_ENE-)

Fault ENE-_1 is located in the Murdoch block and records a net normal movement (see Chapter 3, section 3.3.3.3 for fault set description and location). Four t-z plots are presented for points along the strike of Fault ENE-_1 (Figure 4.7).

All four t-z plots have a 'beheaded' profile, due to the erosional truncation of the fault upper tips at the BPU. The plots overall show very small changes in throw gradient. Each plot has a slightly different profile geometry, in which Tmax values ranging from 116-164ms (+-5ms)/ 253-357m (+-12) are recorded on different horizons in the Lower Westphalian – Upper Namurian. Due to the significant decrease in reflection continuity between the Top Namurian and Intra-KG horizon, there are minimal data points in this interval and the gradient has been extrapolated for MP2, 3 and 4.

Detailed seismic interpretation revealed that the BPU and TRot horizons are not offset at any point along the strike of fault ENE-_1, indicating this fault has a purely Carboniferous slip history. The initial throw values recorded for the first coherent Carboniferous horizon at each position range from 116-164ms (+-5ms).

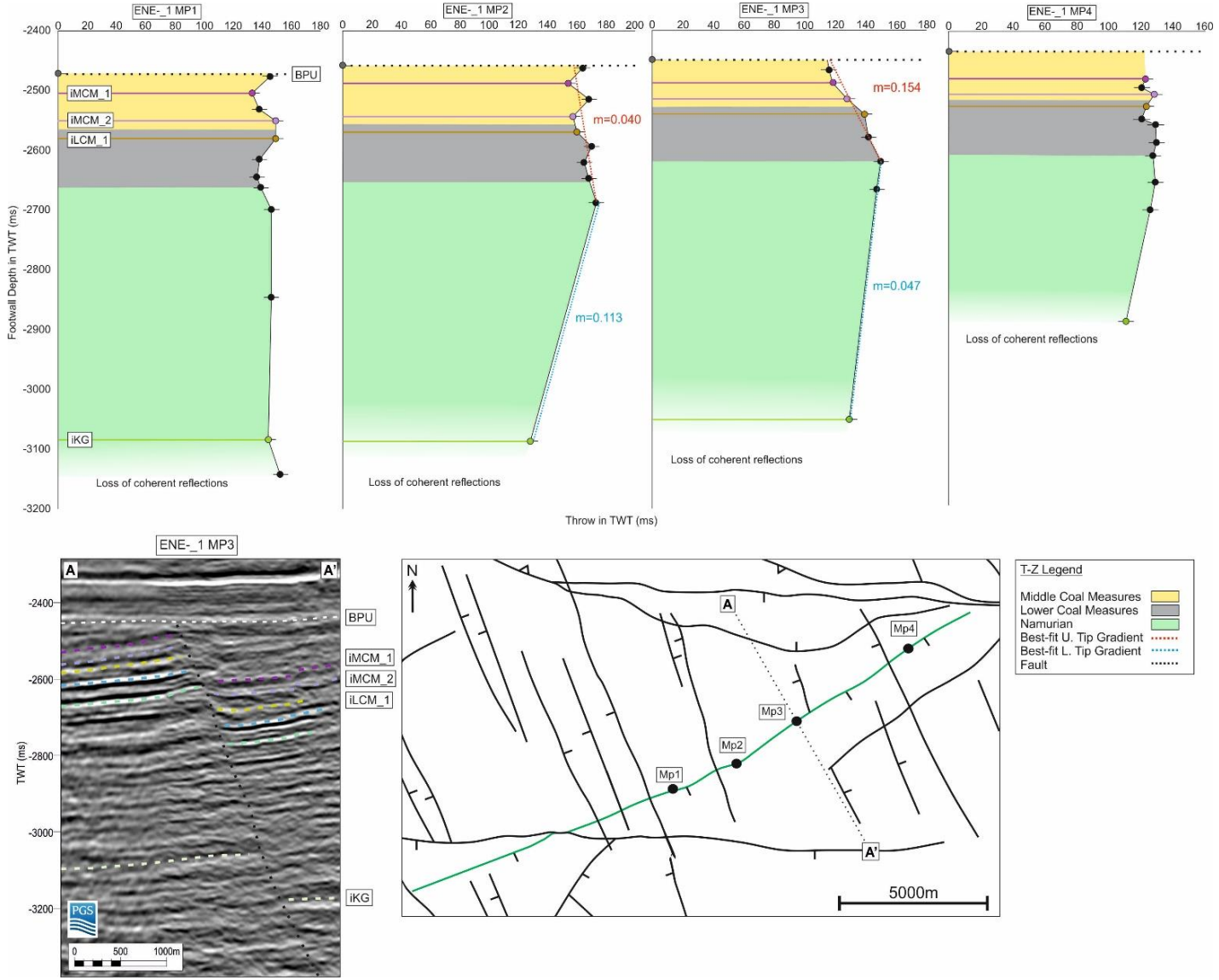


Figure 4.7 t-z plots from four selected measurement points along strike on Fault ENE-_1, located on the Murdoch Block. Location of the fault relative to the MB see Figure 4.21. Regional location of the Murdoch Block see Figure 2.20.

MP1 and MP4 show an overall constant throw value with deviations from this trend being mostly within the error margin (Figure 4.7). This profile gradient could be interpreted as representing the imaged and uneroded portion of an M-Type profile.

MP2 and MP3 have profile geometries that show a steady increase in throw (avg. gradient = 0.040 and 0.154 respectively) toward a central Tmax value in which displacement then also decreases towards the last measurement point (avg. gradient = 0.113 and 0.047).

The high throw values 128-144ms (+-5ms)/ 278-313m (+-12m) observed on the last correlative reflection (the Intra-KG horizon), and the constant throw or steady decrease in throw towards these points, suggests that the lower tips are not imaged and the fault is likely to extend beyond the last measurement point. The high throw values truncated against the unconformity, similarly indicates that the fault upper tips were originally in younger stratigraphic intervals that were subsequently eroded.

4.3.2.2 Fault WNW-_4 (Set A-E_WNW-)

Fault WNW-_4 is a normal fault in the Lower Carboniferous succession on the Elbow Spit Platform (see Chapter 3, Section 3.4.1.1 for fault set description) and is another example of a fault exhibiting Type I t-z profiles. The t-z distribution on fault WNW-_4 is presented by the four plots in Figure 4.8. Tmax values range from 65-114ms (+-4ms)/142-250m (+-9m) and are recorded in the Brigantian-Holkerian interval on different horizons. Each profile is ‘beheaded’ with no offset of the BPU or Top Rotliegend horizon. A minor fold of the TRot horizon is observed above the fault (Figure 4.8), but

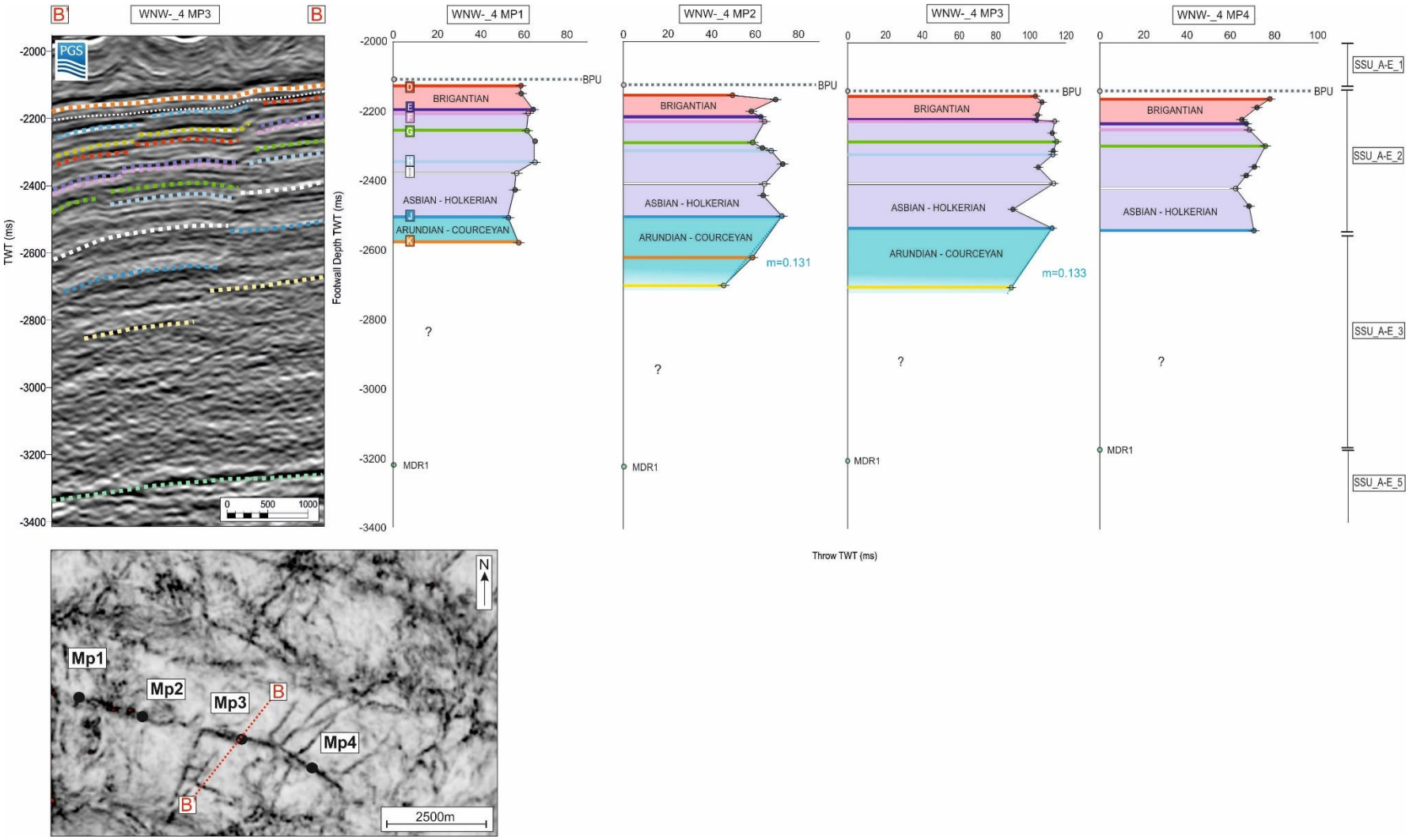


Figure 4.8 t-z plots for measurements performed at four positions along fault WNW-_4. The area represented by a question mark is where reflections can no longer be correlated. Though no offset is recorded, the MDR1 horizon depth is plotted for reference.

the folding is thought to be a product of the deposition of the Rotliegend over the incomplete planation of the hangingwall scarp at the unconformity and therefore not considered significant for offset to be measured.

The profile geometries are incomplete due to the beheading of the upper tips and the loss of reflection continuity with depth so that the lower tips are unresolved. The imaged portion of the fault however exhibits throw values that remain constant overall with depth (Brigantian-Base Holkerian), until horizon J at which throw sharply decreases (MP2 and MP3) or slightly increases (MP1).

The trend of the t-z plot between horizons D to J in Figure 4.8 exhibits minor changes in throw. The high negative throw gradient on MP2 and MP3 in the lower tip region (MP2 gradient between horizon points J-L avg. m = 0.131, MP3 gradient between horizon points J-L = 0.133). This geometry is similar to the middle and lower portion of an M shaped profile (Muraoka and Kamata, 1983).

4.3.3 Fault examples with mostly Type II Profiles

Faults that exhibit Type II T-Z profiles are found mostly on the Elbow Spit Platform and include set A-E_WNW. Two representative faults from the set have been sampled and are described below.

4.3.3.1 Fault WNW-_1 (Set A-E_WNW-)

Fault WNW-_1 is a normal fault located on the Elbow Spit Platform from set A-E_WNW- (see section 3.2.3.1. for general description of fault set). All t-z plots have a distribution typical of a Type II profile (Figure 4.6b). The strike projected t-z plots (Figure 4.9) each display a stepped profile in which a significant change in throw is observed

between the BPU and the first Carboniferous horizon (D). This difference in throw at the step ranges from 76-119ms (+-3ms)/ 176-261m (+-7m) at each measurement point and represents the slight reactivation on this fault occurring after the erosion event. The erosion event is evident from the truncation of dipping Carboniferous reflections against the Rotliegend succession (see seismic cross section in Figure 4.9).

Tmax values for the plots range from 92-133ms (+-4ms) or 202-292m (+-9m), with the positions of these throw maxima occurring within the Brigantian-Holkerian (D-H horizon interval) but on different horizons within this interval. It should be noted that these faults are beheaded and these are therefore the maximum preserved throw values. Tmax values will have been previously higher on the eroded portions.

Two distinct trends are recognised for the throw distribution on measured Carboniferous horizons for fault WNW-_1. The first is a trend that decreases in throw from a Tmax position located close to the BPU (average gradient range of 0.052 to 0.076 from points D-J) towards the lower tip (see Figure 4.9). This profile shape is observed on plots MP1 and MP3. The other profile geometry recognised shows an increase in throw in the Brigantian interval (gradients range from 0.09 to 0.305 from horizons D to E) with Tmax positions located in the Asbian-Holkerian interval on Horizons G and H. There is then a slight decrease in throw towards the last measurement point.

The measured throw values for the BPU and Rotliegend horizons range from 1-16ms (+-3ms)/ 2-32m (+-7m, converted using the average velocity of 4119m/s for the Rotliegend-Carboniferous succession from well E2-2). The measured throw values are less than the effective throw detection limit and therefore appear as folds on seismic

section. Larger values are recorded closer to the WNW lateral tip. This disparity in throw is not proportional to the Carboniferous throw values and suggests that a non-uniform reactivation of fault WNW-_1 has occurred. The observation that the highest throws overall occur at MP3, while the highest throws on Rotliegend horizons occur at MP2, supports this interpretation of a two stage movement history.

The profiles do not exhibit any of the classical M or C type profiles (sensu Muraoka & Kamata 1983) commonly seen on many faults throw distributions (Figure 4.11). This is likely due to the fact that the upper part of the Carboniferous portion of the fault has been eroded and the lower part is not imaged by the seismic. The additional throw data points on MP3 below horizon J are due to the availability of correlative horizons at that point, but not at the other measurement points.

4.3.3.2 Fault WNW-_2 (Set A-E_WNW-)

The throw distribution with depth of another normal WNW- oriented fault on the ESP is presented. The six t-z plots exhibit mostly Type II t-z profiles (Figure 4.6b). Six t-z plots are presented for fault WNW-_2, spaced approximately 1.5km along the strike of the 11km fault trace (Figure 4.10). Profiles MP3-6 have a significant step separating the pre and post BPU throw values and exhibit type II profiles, while MP1 and MP2 have only pre-BPU throw values and exhibit a Type I profile.

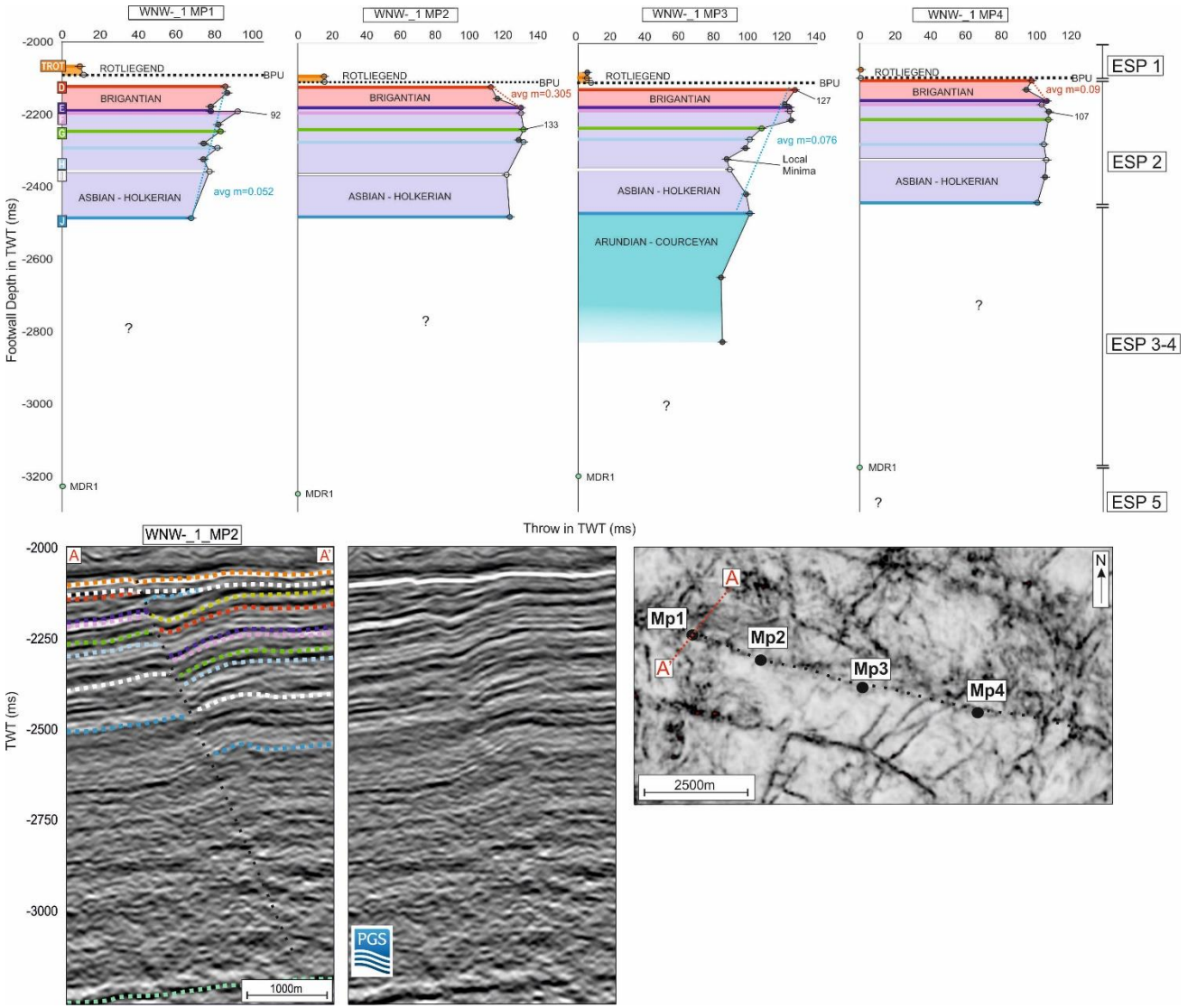


Figure 4.9 t-z plots displaying measurements performed at four positions along fault WNW-_1 on the Elbow Spit Platform. The area represented by a question mark is where reflections can no longer be correlated. Though no offset is recorded, the MDR1 horizon depth is plotted for reference.

At intersections MP1 and MP2, the Lower Carboniferous throw values show an overall slight decrease in throw from the Brigantian to Base Holkerian (horizons E-J, with gradients from 0.039-0.045) with deviations of this trend that slightly exceed the error (3ms). Maximum throws are recorded on horizons F and G and are 163ms and 145ms (+-4ms) respectively (359m and 319m +-9m, using the average velocity of 4260m/s^{-1} derived from wells E2-2 and E2-3). Intersections MP3, MP4, MP5 and MP6 have a contrasting profile geometry in which the Lower Carboniferous exhibits highest throws in the upper portion of the fault close to the BPU on horizons E to G (Brigantian-Base Asbian). The throw then decreases overall towards the lower tip exhibiting gradients ranging from 0.125-0.240 from horizons E-J. These lower tip gradients are higher than those observed at intersections MP1 and MP2, which are 0.03 and 0.045 respectively (Figure 4.10). The sharp increase in throw measured on horizon J at MP6 can possibly be explained by the fact that the measurement position on the t-z plot is located near to a relay structure.

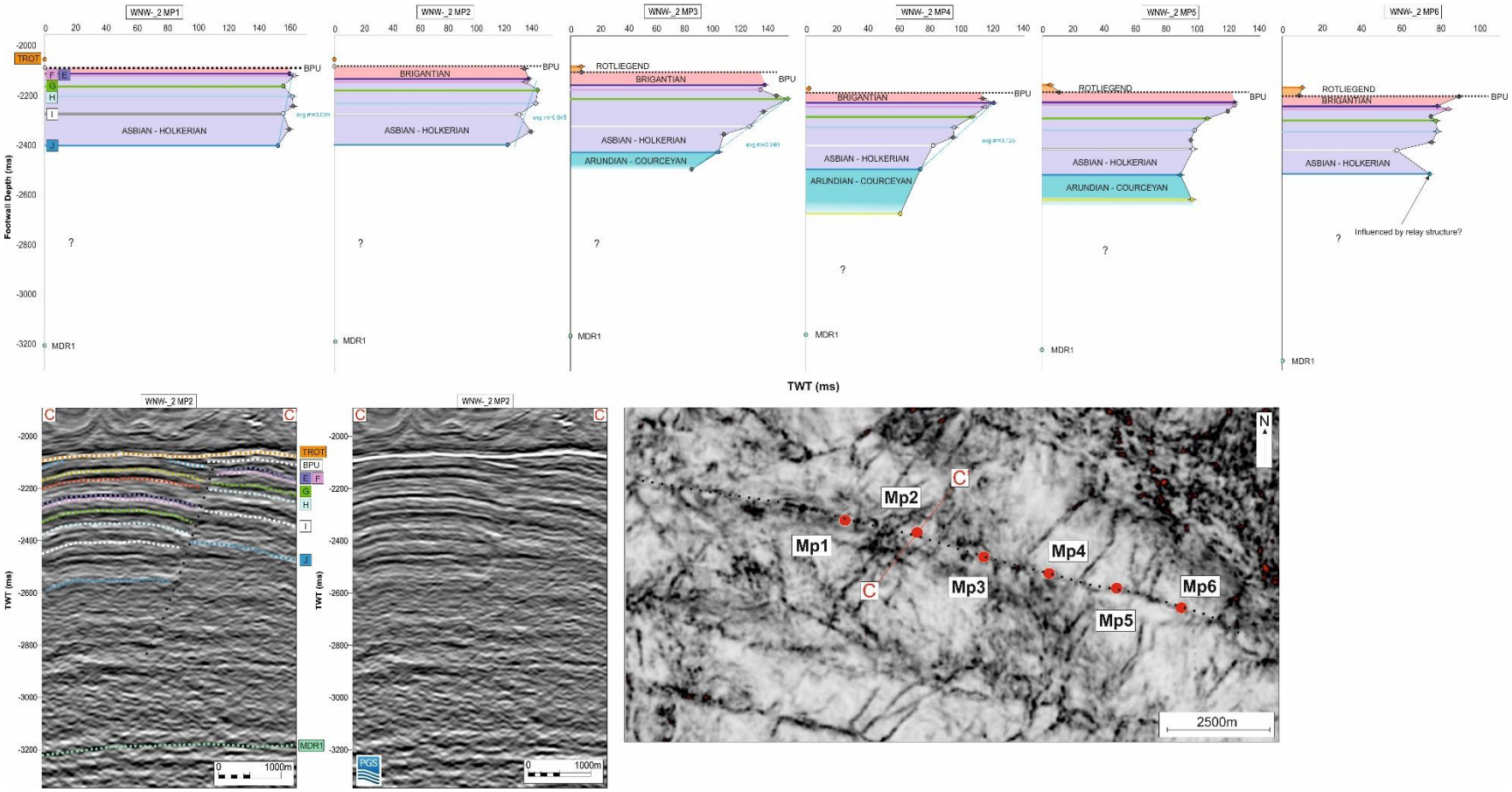


Figure 4.10 t-z plots for measurements performed at six positions along strike of fault WNW-_2 on the Elbow Spit Platform. The area represented by ? is where reflections can no longer be correlated. Though no offset is recorded, the MDR1 horizon depth is plotted for reference.

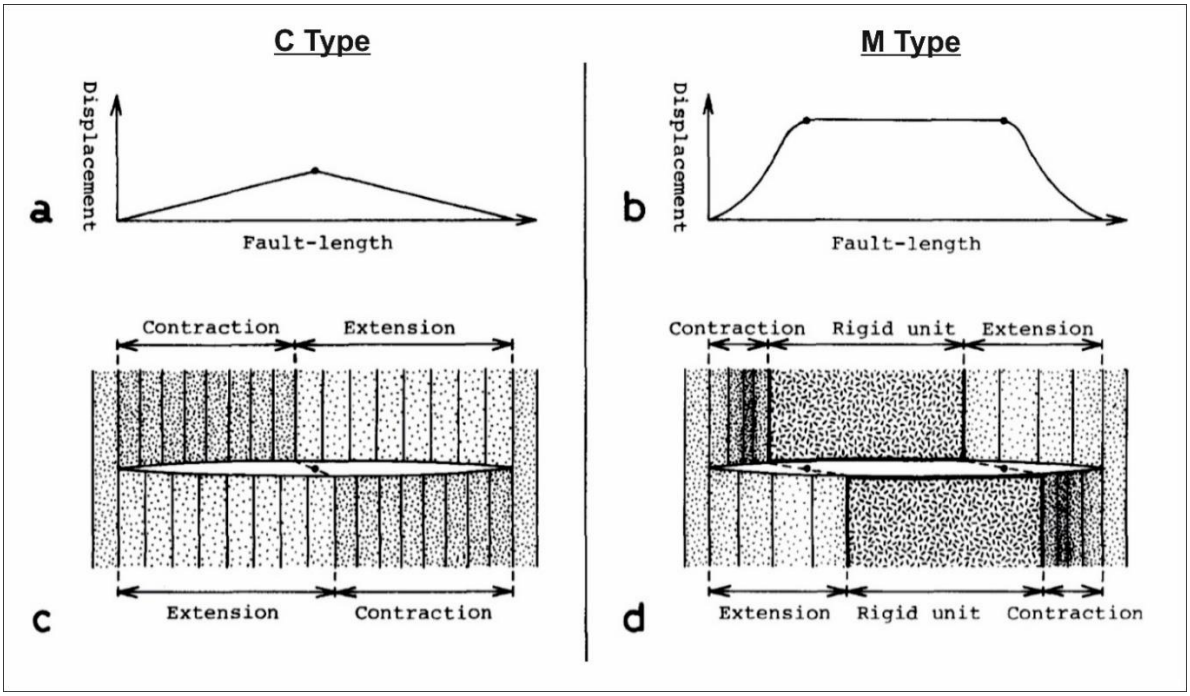


Figure 4.11 a) idealised C-type fault displacement-length profile b) idealised M-type fault displacement-length profile c) idealised strain distribution on a C-type fault d) idealised strain distribution on a M-type fault. From Muraoka & Kamata 1983.

4.3.4 Fault examples with mostly Type III Profiles

Faults with Type III profile geometries (Figure 4.6c) are found in the centre of the Anglo Dutch Basin and include some E-W trending faults belonging to set 44-D_E-W in the Murdoch Block.

4.3.4.1 Fault E-W_1 (Set 44-D_E-W)

Fault E-W-1 is a net normal fault that exhibits a reverse reactivation and evidence of oblique slip (see Chapter 3, Section 3.4.2.2. for fault set description). The throw distribution for fault E-W_1 is presented by four plots (Figure 4.12) along strike spaced approximately between 1-3km apart (different spacing due to data quality and intersections). All profiles exhibit two main portions, representing pre and post BPU offsets. The pre-BPU portion displays the Carboniferous throw values beneath the unconformity with an initial increase in throw towards a Tmax on horizon MCM_2, with gradients ranging from 0.365-0.459 between the MCM_1 and MCM_2 horizons. Tmax values on Intra-MCM_2 horizon ranging from 122-256ms (+-5ms)/ 288-605m (+-12m) based on an average velocity of 4722m/s^{-1} for the PZS taken from the wells 44/19-3, 44/24-4 and A/17-1. From this central Tmax position, there is an overall decrease in throw with depth (gradients range from 0.106-0.173), with a higher gradient observed between the Tmax and deepest measurement point on MP1 and MP2. Maximum throws notably occur in the mid Westphalian interval at each measurement point, specifically on the Intra-MCM_2 horizon.

The post-BPU portion of the plots show variability in throw values between the measurement positions indicating the non-uniform nature of reactivation along strike. Both positive and negative throws are recorded for the Top Rotliegend horizon ranging

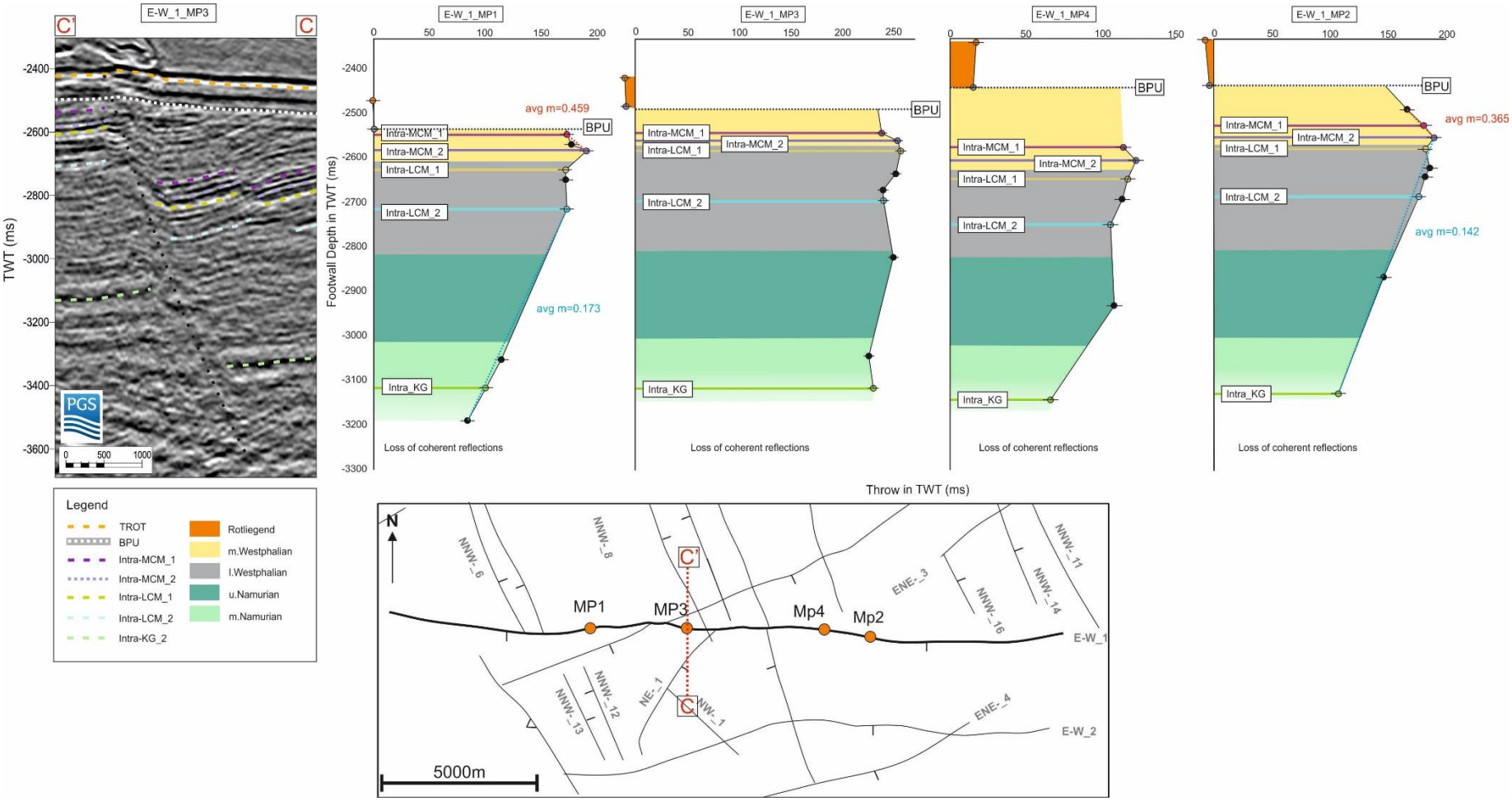


Figure 4.12 t-z plots for measurements performed at four positions along strike of fault E-W_1 on the Murdoch Block. The plots exhibit mostly type-III plots

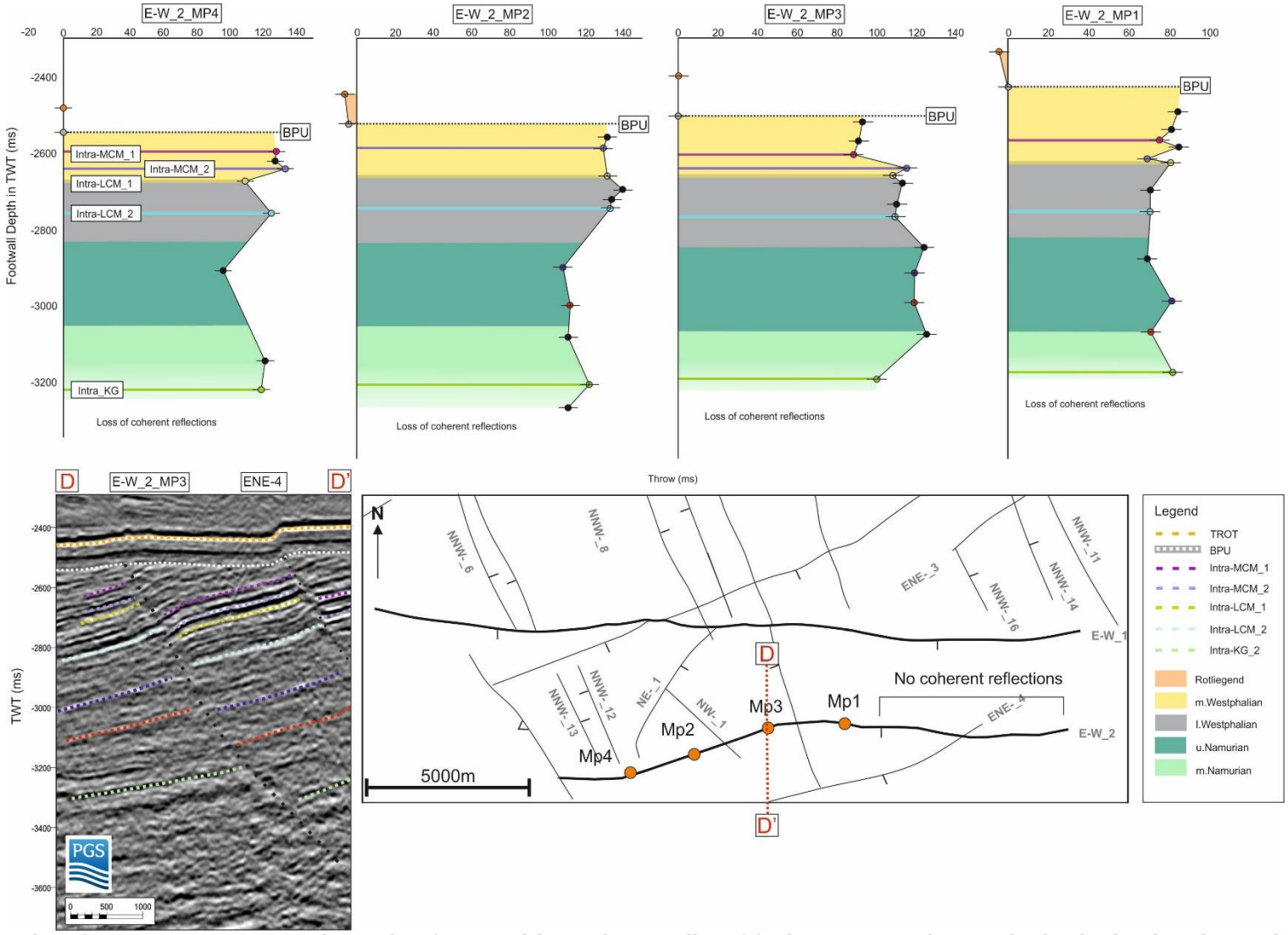


Figure 4.13 t-z plots for measurements performed at four positions along strike of fault E-W_2 on the Murdoch Block. The plots exhibit type-I and type-III plots

from -11ms to 17ms (+-4ms)/ -23 to 37m (+-9m), based on an average velocity of 4689m/s^{-1} for the Rotliegend interval, derived from the well 44/19-3. MP1-3 resemble Type III profiles but MP4 resembles a Type II profile due to the normal throws recorded on BPU and TRot horizons. This range in throws from positive to negative values exceeds the error margin, indicating that is variability is not a velocity artefact and a selectively variable reactivation has occurred.

The t-z profile geometry of the Carboniferous horizons on MP1, MP4 and MP2 may be similar to that expected for a Type C profile (Figure 4.11) if a significant portion had been eroded from the upper tip to a point above Tmax.

4.3.4.2 Fault E-W_2 (Set 44-D_E-W)

Fault E-W_2 is another example from Set 44-D_E-W of a fault that exhibits Type III t-z profiles. The throw distribution is presented by four plots along strike of the western end of the fault as coherent reflection correlations could not be mapped towards the eastern portion of the fault. Measurement positions are spaced approximately 2km apart (Figure 4.13).

Maximum throws from the sampled intersections range from 85-139ms (+-5ms) and 185-303m (+-12m derived from an average velocity of 4707m/s^{-1} for the PZS in the Murdoch Block area, sourced from well 44/19-3), with the highest throws observed on the western portion of the fault recorded on horizons within the middle-lower Westphalian. The profile geometries are irregular, atypical and varied. The only systematic patterns that can be identified on each plot are the beheaded profile and the fact that Carboniferous throw values are relatively high below the BPU, ranging from 84-131ms (+-5ms) and 182-285m (+-12m). Pre-BPU throw values show either a

slight decrease towards the last measurement point (MP4 and MP3) with punctuated areas of minima and maxima, or values remain similar with punctuated areas of minima and maxima that slightly exceed the error margin.

T-z plots MP2 and MP1 exhibit Type III profiles in which negative throws of the Top Rotliegend and BPU horizons of up to -6ms (+-3ms)/13m (+-7m) are observed. These negative throw values for the TRot are less than observed for the sampled areas of fault E-W_1. Zero throws are recorded for the Rotliegend portion at intersections MP4 and MP1, these t-z plots are therefore examples of Type I profiles. Like E-W_1, the reactivation along these faults is locally variable.

4.3.5 Fault examples with mostly Type IV Profiles

Faults with Type IV profile geometries (Figure 4.6di) are found in both the Mid North Sea High and Anglo Dutch Basin and are mostly NW-SE and to a lesser extent NE-SW trending.

4.3.5.1 Fault NE-_2 (Set A-E_NE-)

Fault NE-_2 is a NE-SW oriented normal fault from set A-E_NE-/NNE- (see Chapter 3, Section 3.4.1.2. for fault set description) located on the Elbow Spit Platform. The t-z distribution on fault NE-_2 is presented by three plots spaced approximately 500-700m apart along a ~2500m long fault trace (Figure 4.14). Each plot exhibits a similar vertical throw distribution overall. All plots have a stepped profile in which there is an abrupt shift in throw magnitudes between Carboniferous and Rotliegend horizon offsets. Tmax values range from 20-26ms (+-3ms) or 41-53m (+7m, converted using an average velocity of 4260m/s^{-1} for the upper PZS in the Elbow Spit High area, sourced from wells E/2-2 and E/2-3) and are recorded on horizons within the Asbian-

Holkerian interval, specifically marker horizons F-G. A local minima is recorded on Horizon I on MP2 but does not significantly deviate from the error margin.

The t-z plot MP1 has a Tmax close to the BPU in which there is an overall decrease in throw towards a lower tip minima at zero throw, terminating in the Arundian-Courceyan. Detailed observation at MP1 reveals an unusual variation of throw with depth in which there are a number of local minima and maxima. These are real perturbations whose amplitude exceeds the error margin (Figure 4.14). A decrease in throw from the Tmax on horizon F is exhibited with a local minima on horizon G, to which throw then increases to a maxima before Horizon I. Beneath this the throw tapers downwards to the basal tip. Notably, the Carboniferous portion of the plot consists of a central portion of fairly uniform throw values from horizons E-J. This central portion is in contrast to the basal tip taper gradient (c. 0.05) from horizons J-LP towards the lower tip. This profile is thus similar to the lower portion of an M-Type profile (Figure 4.11d, Muraoka & Kamata 1983).

The T-z profile at MP3 shares this central region of alternations of local minima and maxima as seen on MP1. If a smoothed profile is constructed through the individual throw values, MP3 resembles a C-Type profile, because the step between Carboniferous and Rotliegend measurements is less pronounced on MP3 than on MP1 and MP2 and MP3 and the change in throw less abrupt between these horizons. MP3 can therefore be interpreted as a Type V profile, which implies a single phase of movement on fault NE-_2 rather than two (Figure 4.34). The best constrained profile to judge the lower tip geometry is MP1. The sharp decrease in throw towards the lower tip at MP1 (Figure 4.14) creates a high displacement gradient (m=0.0812).

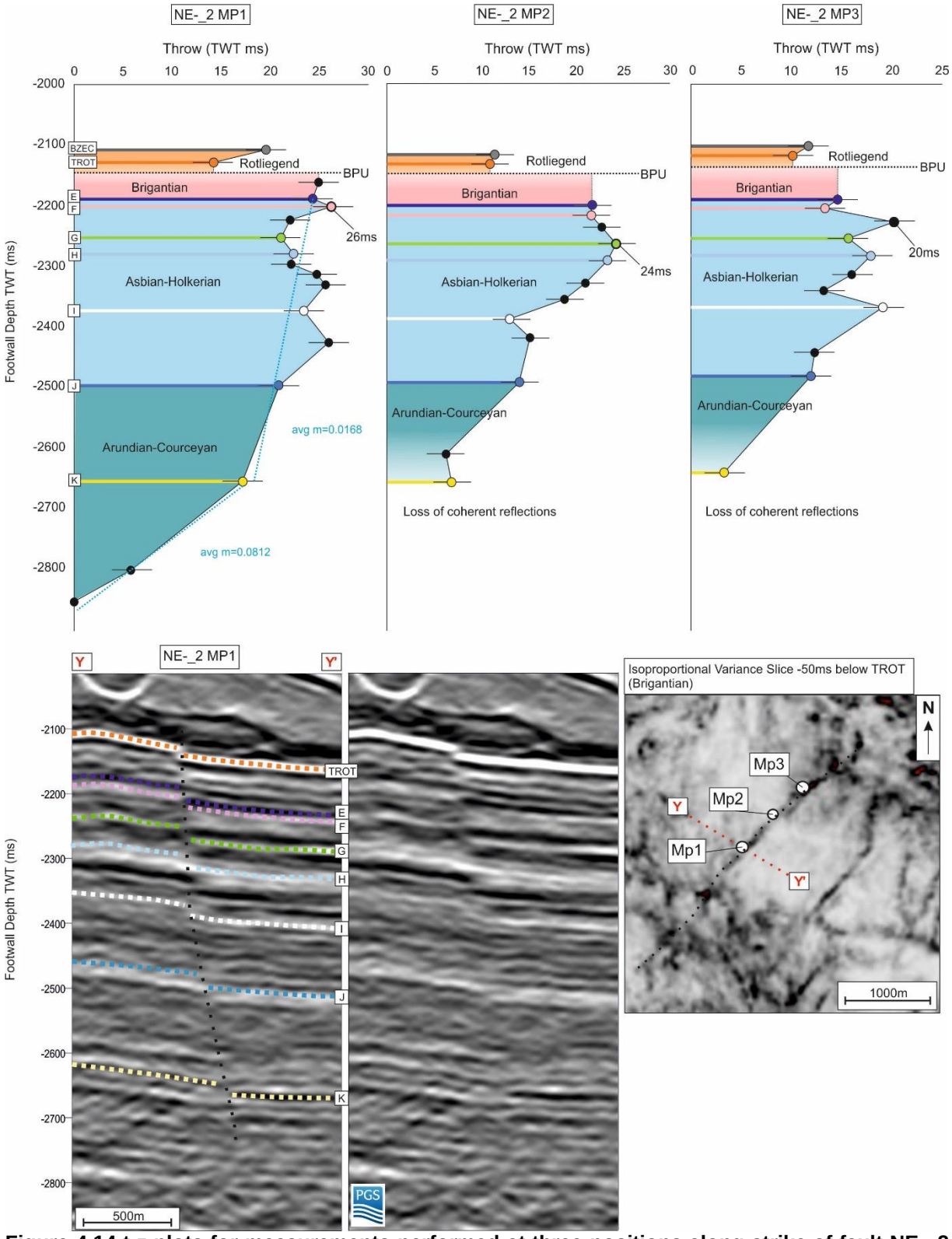


Figure 4.14 t-z plots for measurements performed at three positions along strike of fault NE-_2 on the Elbow Spit Platform. The plots exhibit type-I and type-III plots.

Although not unusually high, this basal tip gradient certainly points to the presence of a mechanical boundary beyond horizon K that has either restricted propagation or resulted in a detachment (Nicol et al., 1996).

Interpretation of the seismic section on Figure 4.14 shows the Base Zechstein reflections (above the TRot) have a slight offset and is the last coherent reflection before the mobile salt succession. The area above this is mostly acoustically opaque (halite) with a single high amplitude reflection (Z series stringer), which is not offset or deformed in a way that would suggest a relationship with the underlying fault. There is clear evidence of lateral salt flow in the area above the fault which would have erased any offset indicators related to normal throw on fault NE-_2.

4.3.5.2 NW-_P Faults (Set 44-49_NW-_P)

The t-z distribution for 44-49_NW-_P faults (see Chapter 3, Section 3.4.3.3 for general description) is sampled by a 15km transect crossing seven of these faults, normal to their strike (Figure 4.15). The sampled NW-_P faults exhibit 3/5 t-z plot types. Most of the lower tips are not imaged and therefore the deepest measurement point on the t-z plots is the last coherent reflection. Tmax values along the transect range from 30-127ms (+- 3ms)/ 71-301m (+- 7m, converted using an average velocity of 4825m/s^{-1} for the upper PZS in the Silverpit Basin study area, sourced from well 44/27-1) and maximum throws occur on horizons within the Westphalian C-D interval mostly.

NW-_1 and NW-_2 exhibit a Type V profile with ‘open tops’ but have different profile geometries. T-z plot NW-_1 has concave upper and lower tip regions and a short central area with two maximas of 53 and 48ms (+- 3ms) or 125 and 114m (+- 7m). It is uncertain whether the abrupt change in throw of 17ms (+-3ms) /40m (+-7m) is a ‘step’

as it is greater than the error margin and therefore the plot could be interpreted as a Type IV profile. Conversely, if the same steep gradient as the lower tip gradient is extrapolated into the upper tip portion where there is a lack of data points in-between the Rotliegend and the shallowest Carboniferous horizon (due to no coherent reflections in this interval), it could be interpreted as a Type V profile. The latter interpretation is thought to be more reasonable. The steep slopes and broad central region resembles an M-type profile. NW-_2 contrastingly exhibits the highest throws close to the 'upper tip' in which throw overall decreases with depth, disregarding a maxima on the intra-Westphalian B horizon (73ms/173m). There are no abrupt changes in throw value close to the unconformity and therefore it is also classed as a Type V profile, also resembling a syn-sedimentary fault geometry as seen on analogous faults in the Levant basin (Baudon and Cartwright, 2008a).

The key difference between the two type V profiles is that Rotliegend throws increase with depth on NW-_1 and decrease with depth on NW-_2. This may be an indication of how far each fault propagates into the Zechstein (see section 4.5.2.2.).

NW-_3, NW-_5, NW-_6 and NW-_7 exhibit steps in their t-z profile, with differences in throw that significantly exceed the error margin of +-3ms/7m (23-43ms/54-102m) and are therefore interpreted as Type IV profiles. The t-z plot of Fault NW-_3 (Figure 4.15) exhibits a trend in the Carboniferous portion of the profile that shows highest throw values in the Westphalian C-D interval with a Tmax of 127ms (301m) recorded on a point between the Intra-Westphalian B and B2 horizons.

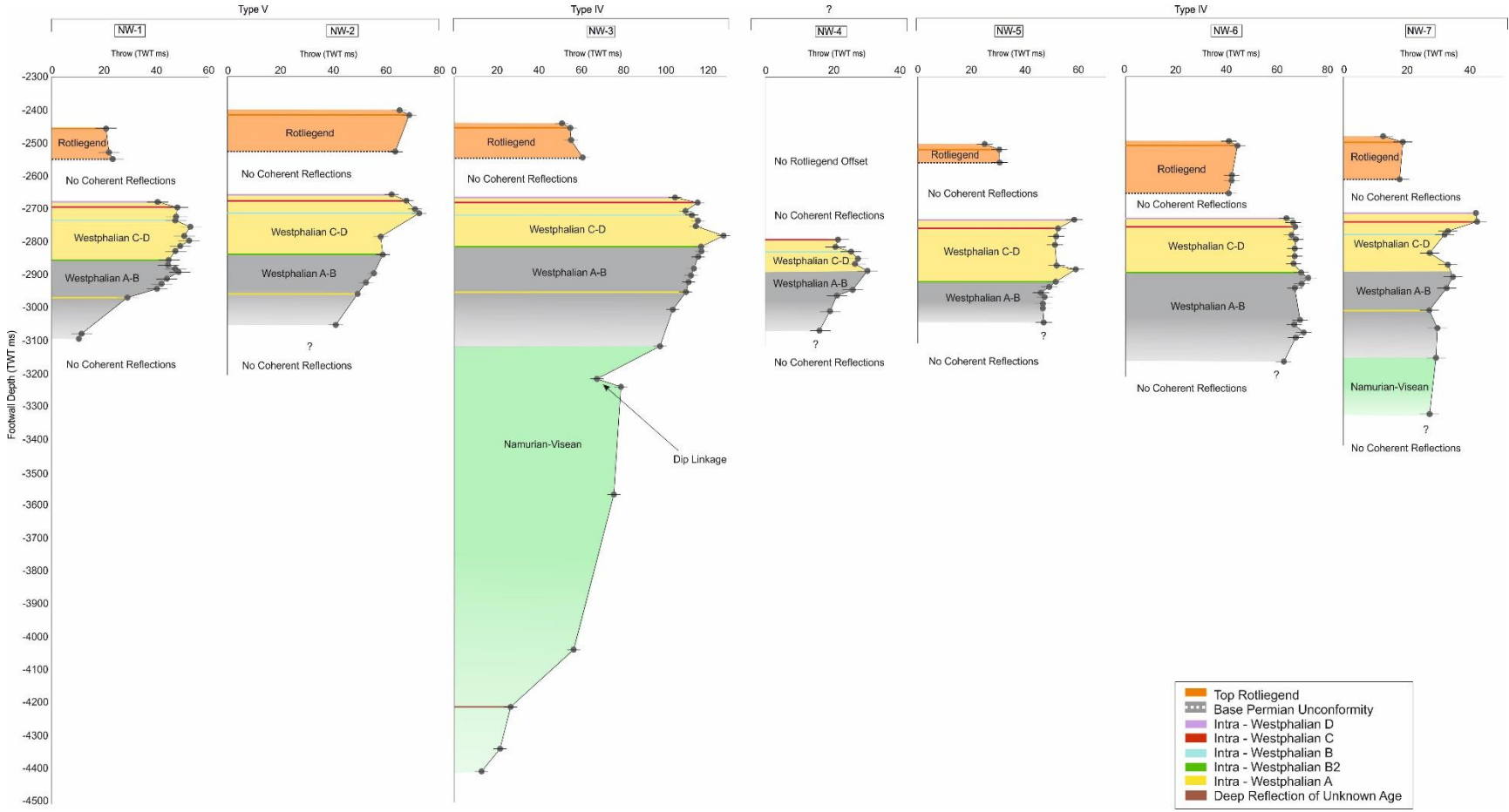


Figure 4.15 t-z plots for measurements performed at intersections with 7 parallel faults from set NW-_P in the Silverpit Basin. The plots exhibit type-I, type-IV and type-V plots. Location of transect and seismic section in Figure 4.16.

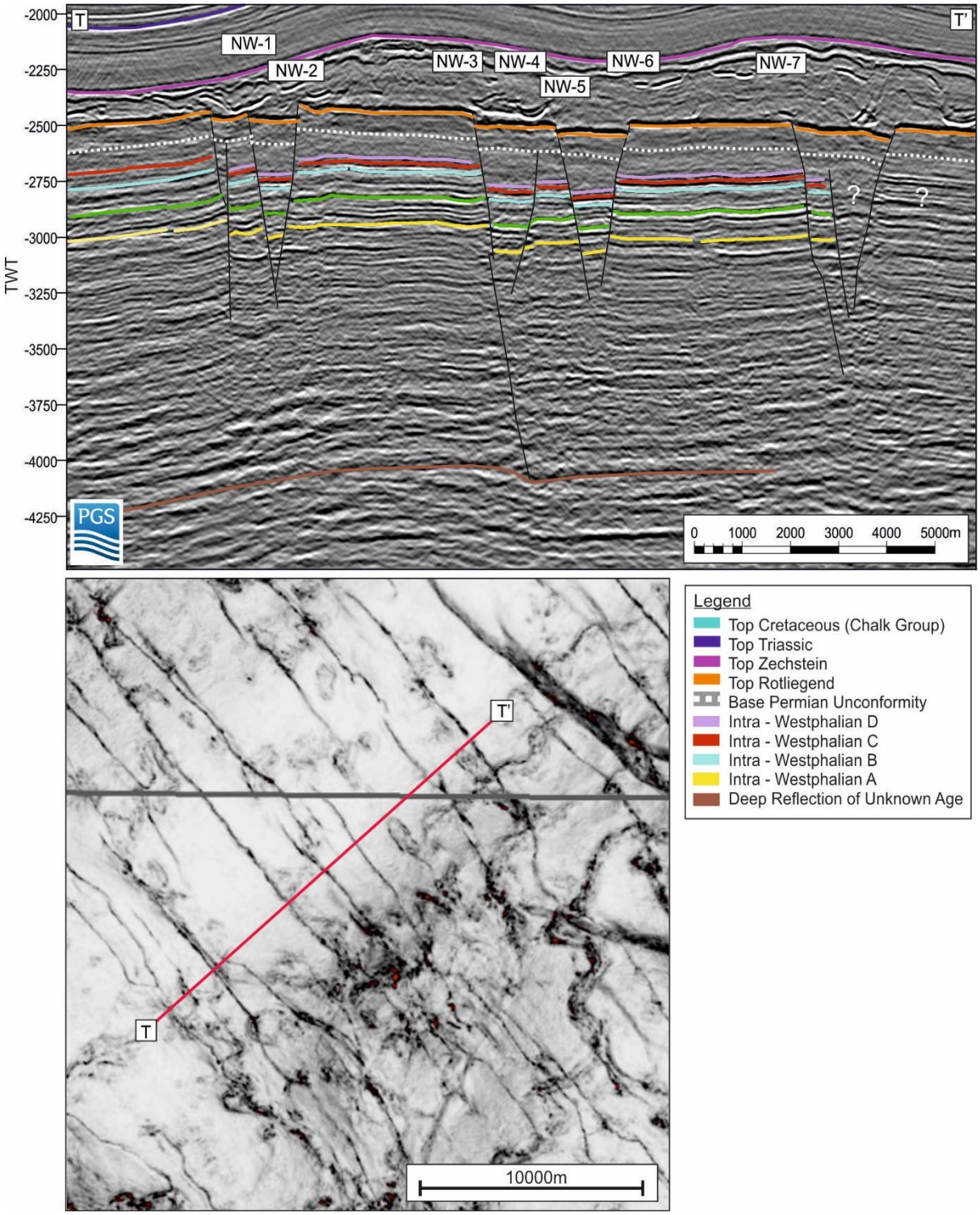


Figure 4.16 Sampling transect of faults across the NW-_P faults in the Silverpit Basin a) Seismic cross section of sampled fault intersections and measured horizon offsets. Fault names are labelled above. b) Map location of sampling transect.

Fault NW-3 is one of two on the transect for which reflection offsets can be measured close to the basal tip. This plot also exhibits a trend in which highest throws are close to the unconformity. Throw values then show an overall decrease towards the lower tip with a slight throw minima observed on a point in the Namurian-Visean succession. NW-_5, NW-_6 and NW-_7 have a similar shape to NW-_3 on their imaged portions, and are interpreted to have a throw distribution similar to NW-_3 in the Namurian-Visean succession. This is reflected on the seismic section as an area that appears as a horizontally inclined relay structure between two fault planes (Figure 4.16). These observations suggest that NW-_3 formed as two faults that linked in the slip direction i.e. by dip linkage (Childs et al., 1995, Mansfield and Cartwright, 1996, Rotevatn and Jackson, 2014).

NW-_4 exhibits a Type I profile with a beheaded upper tip at the BPU and a central Tmax of 30ms (71m) on the Westphalian B-C boundary in which throw decreases towards the upper and lower tips. These characteristics make it appear similar to a C- shaped profile that has been beheaded.

4.3.5.3 Fault NE-_1 (Set A-E_NE-)

Fault NE-_1 is a NW-SE trending fault from set A-E_NE- located on the Elbow Spit Platform. Figure 4.18 presents three t-z plots showing the vertical throw distribution for fault NE-_1. Each plot exhibits a difference in profile shape but shares the ‘open-top’ characteristic, in which the upper tip throw values on the Rotliegend horizon range from 12-15ms (+-3ms)/ 26-33m (+-7m, converted using an average velocity of 4260m/s^{-1} for the upper PZS in the Elbow Spit High study area, sourced from wells E/2-2 and E/2-3). Unlike the previously described t-z profile types with stepped profiles, the t-z plots for fault NE-_1 exhibit a continuous throw gradient with no abrupt changes (steps).

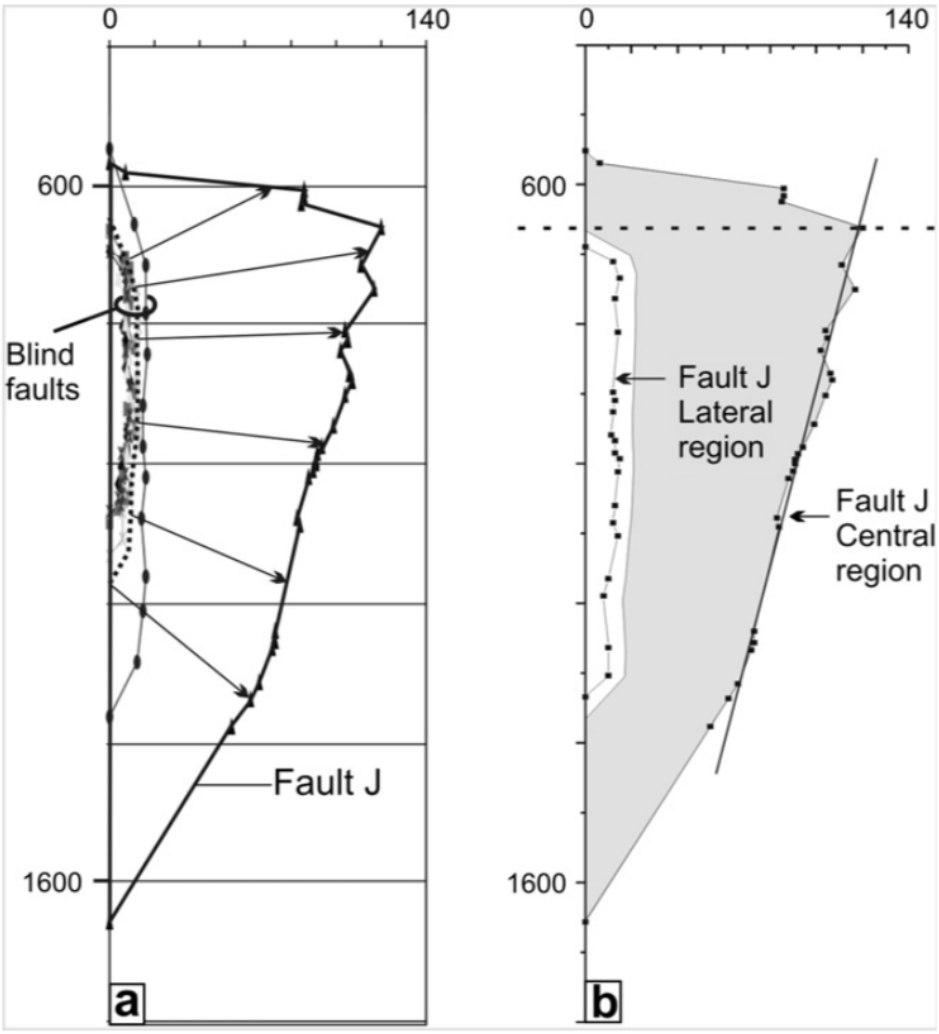


Figure 4.17 Syn-sedimentary fault t-z profile, example from Baudon & Cartwright 2008.

Maximum throws range from 15-23ms (+-3ms)/ 33-51m (+-7m) and occur on different horizons on each plot. The lower tip areas of the plots exhibit an overall sudden decrease in throw towards horizon J with a gradient of 0.064.

4.3.6 Fault examples with mostly Type V Profiles

Faults with Type V profile geometries (Figure 4.6ei) are found in both the Mid North Sea High and Anglo Dutch Basin and are mostly NE-SW and NNW-orientated.

A broad central region in which throw in this region remains more or less the same value as the upper tip, is exhibited by t-z plot MP1. Punctuated local throw minima and maxima are observed along this region. This portion of the fault is similar to that described as an M-Type profile by Muraoka and Kamata (1983). Tmax on a horizon within the Brigantian interval but this difference between this Tmax and the upper tip and lower central region is low.

A wedge shaped package seen in the hanging wall of the fault at the MP1 intersection (see blue polygon on seismic section in Figure 4.18) may be interpreted as a growth package. However, seismic interpretation and horizon flattening techniques lead to the interpretation that this feature is a lensoid body that can be traced across the fault having the same thickness in the footwall.

A contrasting atypical profile is exhibited by t-z plot MP2 which has with a single pronounced peak with a Tmax measurement in the centre of the plot in which throw decreases in a crudely linear trend towards the upper and lower tip. This is a characteristic of a C-type profile (Muraoka & Kamata, 1983), but where the average throw gradients towards the upper (0.055) and lower tips (0.104) on the plot of MP2 are much higher than what would normally be expected for an idealised blind fault, this is illustrated by the concave trend from the Tmax. This steep slope with an abrupt change in displacement towards the lower tip is a characteristic of an M-Shaped profile however, and suggests restriction from a mechanical boundary (Nicol et al., 1996).

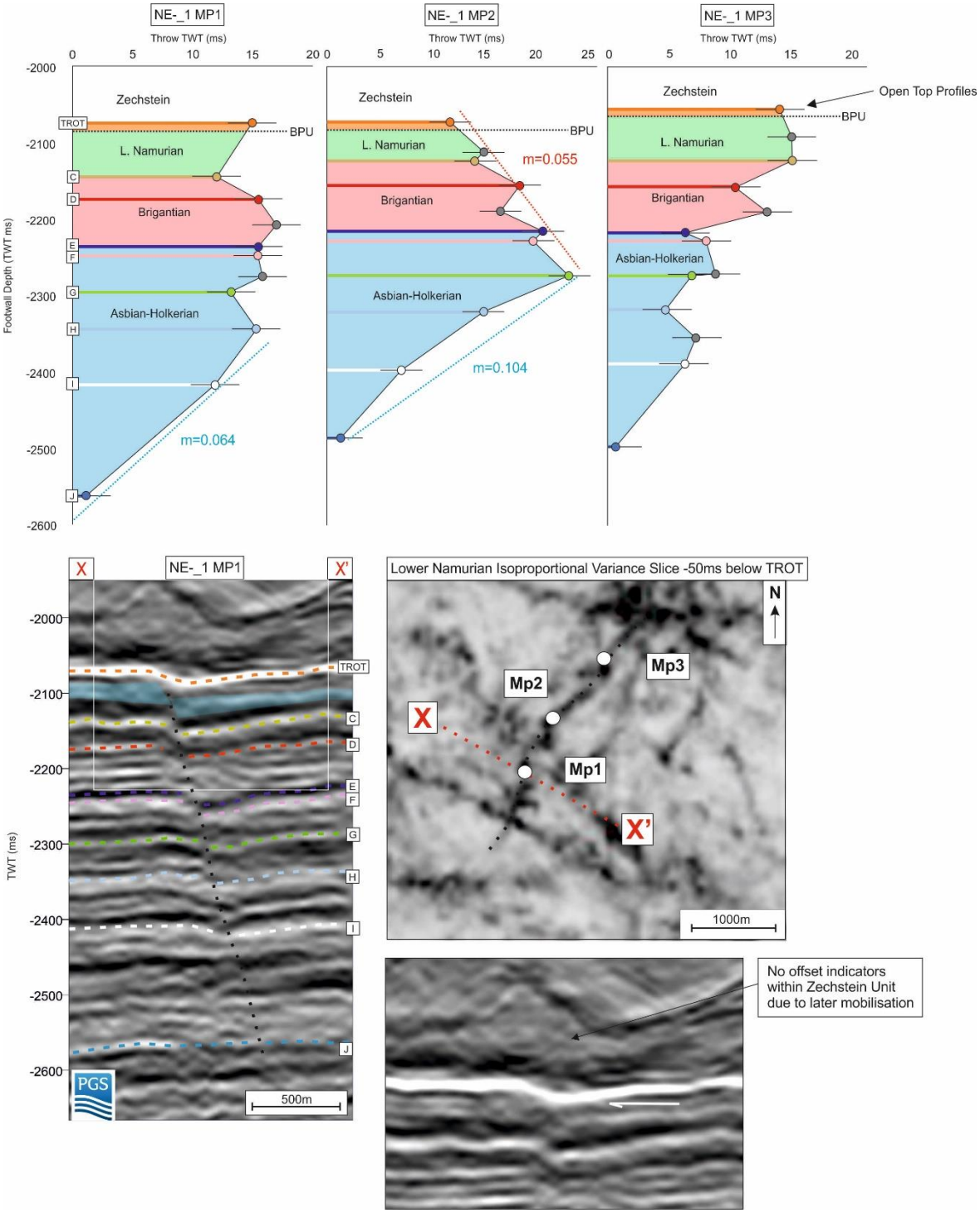


Figure 4.18 t-z plots for three measurements performed at positions along strike of fault NE-_1 located on the Elbow Spit Platform. The plots exhibit mostly type-V profiles.

Maximum throws are found in the upper tip region of plot MP3 and a Tmax is recorded on Horizon C in the Lower Namurian to Brigantian interval. There is an overall decrease from the upper tip Tmax region towards the lower tip (horizon J). This profile is similar in appearance to a syn-sedimentary fault profile such as those presented by Childs et al. (2003) and Baudon & Cartwright (2008a). However, no syn-depositional packages are observed on seismic profiles crossing this fault.

The ~850m thick Zechstein layer above the Top Rotliegend horizon is acoustically opaque above fault NE-_1 (see zoomed in seismic on Figure 4.18) and shows no syn-or post deposition deformational features related to extensional faulting, such as the deformed monoclines observed above the 'piano key faults' in the Messinian layer in the Levant Basin (Reiche et al., 2014).

4.3.6.1 Fault NNW-_1 (Set 44-D_NNW-)

Fault NNW-_1 on the Murdoch Block is another example of a fault that exhibits mostly Type V throw profiles. The vertical throw distribution along the strike of fault NNW-_1 is presented by four t-z plots (Figure 4.19). The majority of the plots exhibit a continuous non-stepped profile similar to the t-z plots for fault NE-_1. Higher throw values are recorded towards the NNW lateral tip (MP4 and MP3) with throw values decreasing towards the SSE tip (MP2 and MP1). Each plot exhibits an 'open top' with the upper tip throw measurements ranging from 44-85ms (+-3ms)/ 95-185m (+-7m). Maximum throws range from 57-88ms (+-4ms)/ 124-191m (+-9m) and are recorded on different horizons on each plot.

The t-z plots MP3 and MP4 exhibit classic Type V profiles with no significant abrupt changes in slope. MP2 has an abrupt change in throw on a point within the Rotliegend interval that is larger than the error margin (Figure 4.19). This is

measured from a point not corresponding to the unconformity position and is therefore considered to be anomalous.

Plot MP3 has a Tmax recorded close to the BPU of 88ms (192m) with throw values that show a decrease with depth towards the last measured horizon (average gradient? = 0.077) with Tmax values are at or close to the unconformity. The profile shape of MP3 resembles that of a typical of a syn-sedimentary fault (see Figure 4.17, Childs et al., 2003, Baudon & Cartwright, 2008) despite no syn-sedimentary packages observed in the hangingwall.

Above the shallowest throw measurement point, the 2.2km thick Zechstein is acoustically opaque and no evidence for the fault NNW-_1 propagating into this layer can be seen. Although the t-z plots suggest a single phase movement for fault NNW-_1 (similar to NE-_1), what appears to be footwall scarp erosion can be seen on seismic at intersections such as MP1 (see uninterpreted seismic section in Figure 4.19) complicating movement history analysis. MP1 shows a 10ms (+-3ms)/ 22m (+-7m) change in throw values between Pre- and Post BPU horizons, this change gives the appearance as a Type IV profile. Evidence from seismic for Pre-BPU offsets is an eroded footwall scarp at the BPU level in the FW.

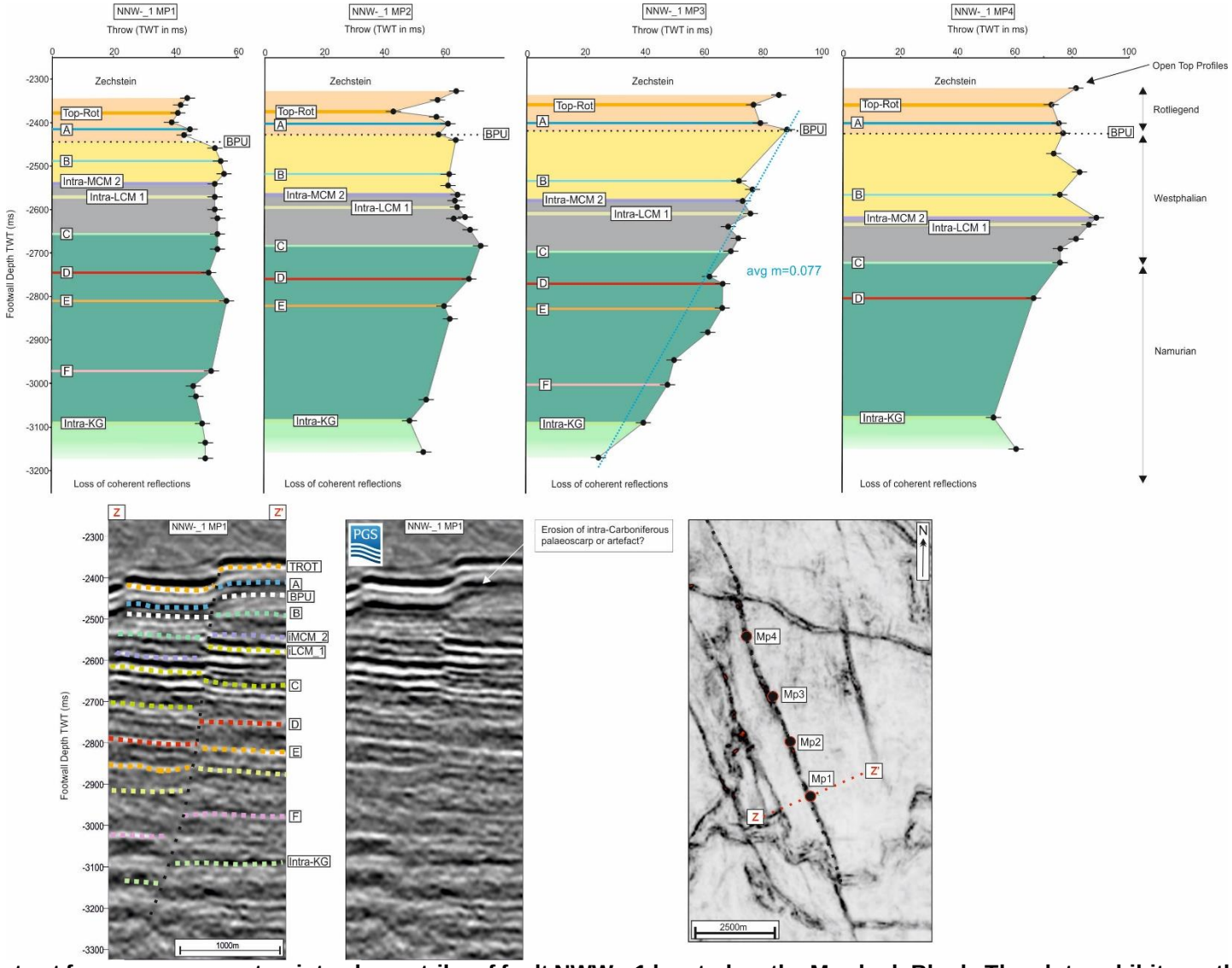


Figure 4.19 t-z plots at four measurement points along strike of fault NWW-_1 located on the Murdoch Block. The plots exhibit mostly type-V profiles.

4.4 Intersecting Relationships

The examination of relative offsets of reflections and the plotting of throw distribution with depth have aimed to estimate timing of representative faults. The faults across the study area intersect in complex cross cutting relationships (Figure 4.21). This section investigates the cross-cutting relationships in the Murdoch Block case study area using the construction of throw-distance (t-x) plots across intersecting faults in the Pre-Zechstein succession. This section aims to constrain the age relationships, with particular attention to the relationship between faults E-W and ENE- since both exhibit a pre-BPU phase of movement while one is reactivated and the other is not (see sections 3.7.3. and 3.7.7.).

4.4.1 T-x Plots

4.4.1.1 Fault NNW-_1

The throw distribution along the lateral length of fault NNW-_1 is presented by the T-X plot in Figure 4.20a. The throw on each key horizon displays an overall trend with higher throw values in the central region with a steady decrease in throw towards the lateral tips where the last recorded throws range from 15-30m (+-12m). Each of the three horizons display positive throw values that mostly overlap when plotted (Figure 4.20a). A pronounced throw minima is observed at 13km along the fault (Figure 4.20a), where each of the three key horizons record approximately zero throw. Areas of anomalous peaked maxima that deviate from this trend are present at certain points along strike, some of which align with the point of intersecting faults. The positions of these intersecting faults are labelled as solid black lines. The localised maxima labelled intra-LCMTmax exhibits a throw of 280m (+-9m) (deviating from the general trend by approximately 140m). Another localised

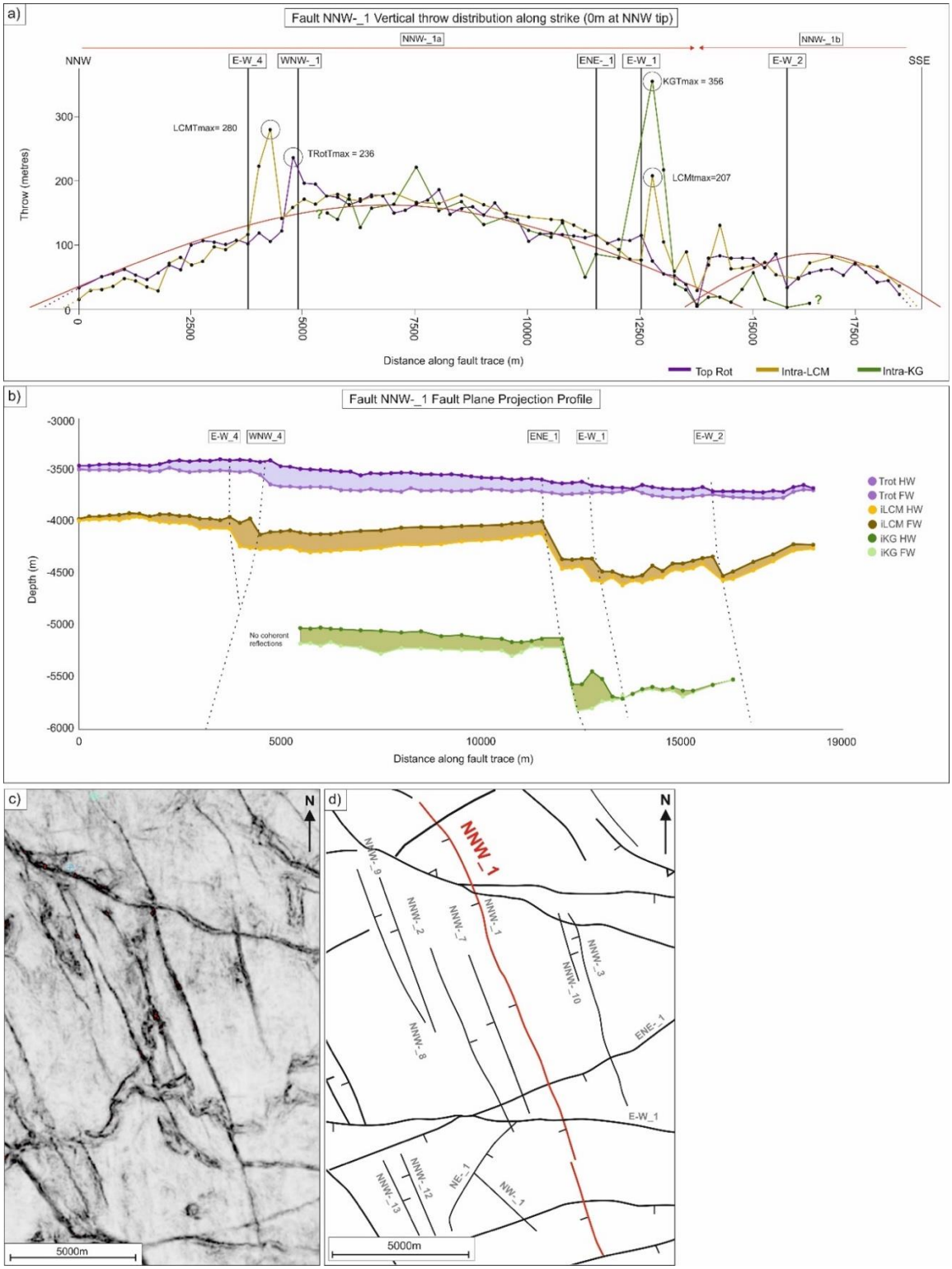


Figure 4.20 Throw distribution on fault NNW-_1 as recorded by three key horizons; Top Rotliegend, Intra-Westphalian and Intra-Namurian. a) t-x plot of the TRot, intra-MCM and intra-KG horizons b) Allan diagram of the throws on the TRot, intra-MCM and intra-KG horizons c) Top Rotliegend horizon variance map of fault NNW-_1 d) fault map of NNW-_1 and surrounding area. Throw anomalies such as the one on the IKG horizon at the intersection with ENE-1 are common at complex intersections involving 2 or more faults, they represent local reactivations involving isolated fault blocks created by the complex cross cutting geometries.

maxima (intra-KGTmax) exhibits a throw of 356m (+-12m) and a TRot maxima of 236m.

The overlapping of the three key horizons when overlain on the same t-x plot suggests a Type-V profile for NNW-_1. The fact that they overlay shows that overall the throw values are similar on Rotliegend and Carboniferous horizons being Type-IV or Type-V and suggests that fault NNW-_1 is single phase with slip occurring after the deposition of the Rotliegend (Type-V).

The throw minima at 13km may indicate that fault NNW-_1 has formed from the linkage of two fault segments (NNW-_1a and NNW-_1b). The presence of a small relay structure (Figure 4.20c-d) on the TRot horizon-variance map also is consistent with this interpretation (Cartwright et al., 1995). The recognition of this throw minima suggests that these faults grew as isolated faults and later linked, rather than growing coherently (Walsh et al., 2003).

4.4.1.2 E-W_1

The throw distribution for fault E-W_1 is presented by the t-x plot in Figure 4.22b. The t-x plot differs from the NNW-_1 profile as the each of the three key horizons display a very different geometry and do not overlay when superimposed. The lateral tips of fault E-W_1 are not imaged due to reduced image quality in these areas, though due to the decreasing throw on the western tip, it is suspected that the lateral termination is close to the last throw measurement. The throw profiles for intra-Carboniferous horizons intra-LCM and intra-KG are highly irregular and display three main ‘portions’ separated by throw minimas at 5000m, 6750m, and 7500m referred to as E-W_1a, E-W_1b and E-W_1c on the plot (Figure 4.20b). Overall, the intra-LCM and intra-KG horizons overlay with some areas that show deviations.

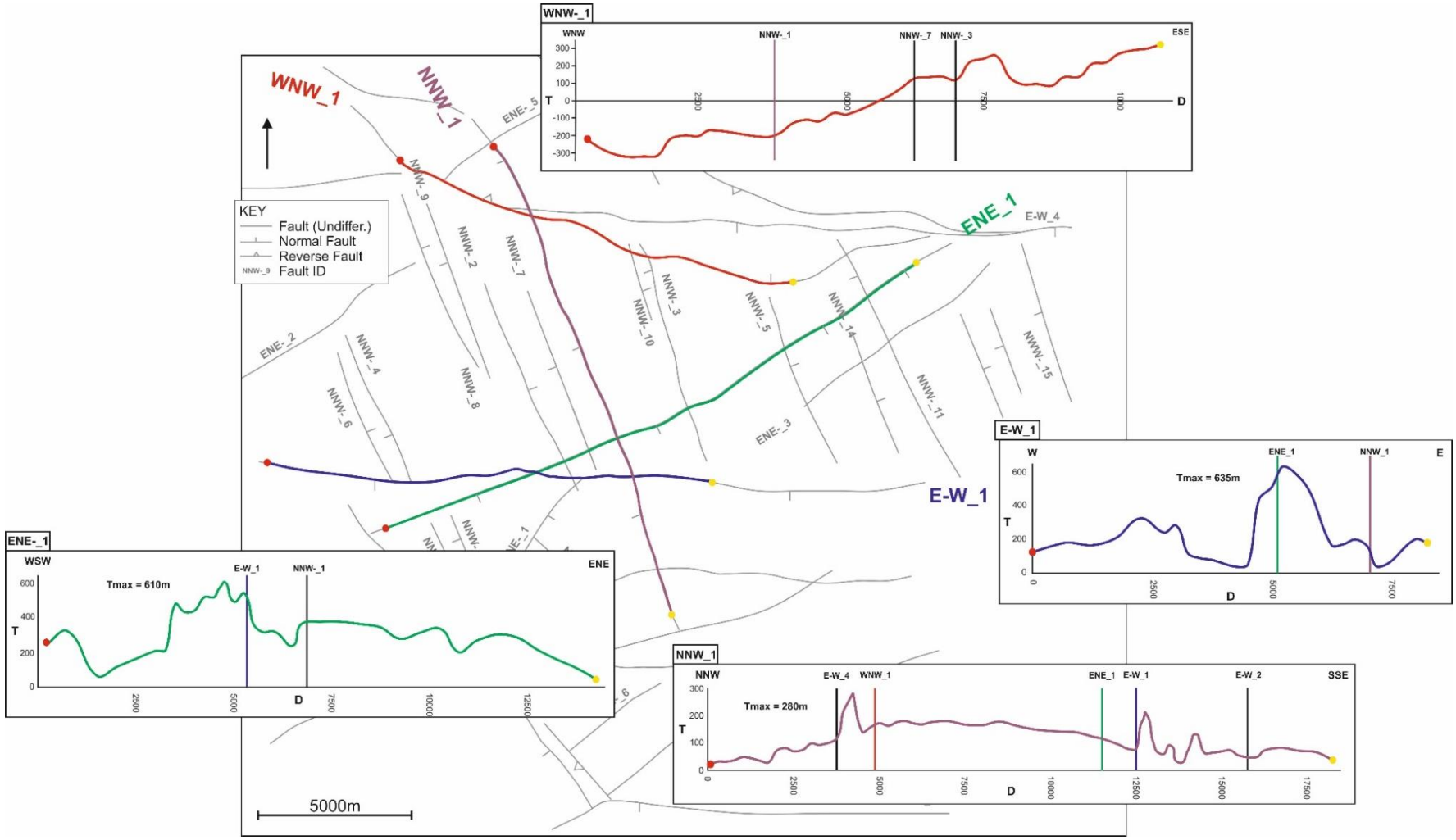


Figure 4.21 Map of four representative faults from each of the major fault sets in the Murdoch Block in which t-x analysis has been performed.

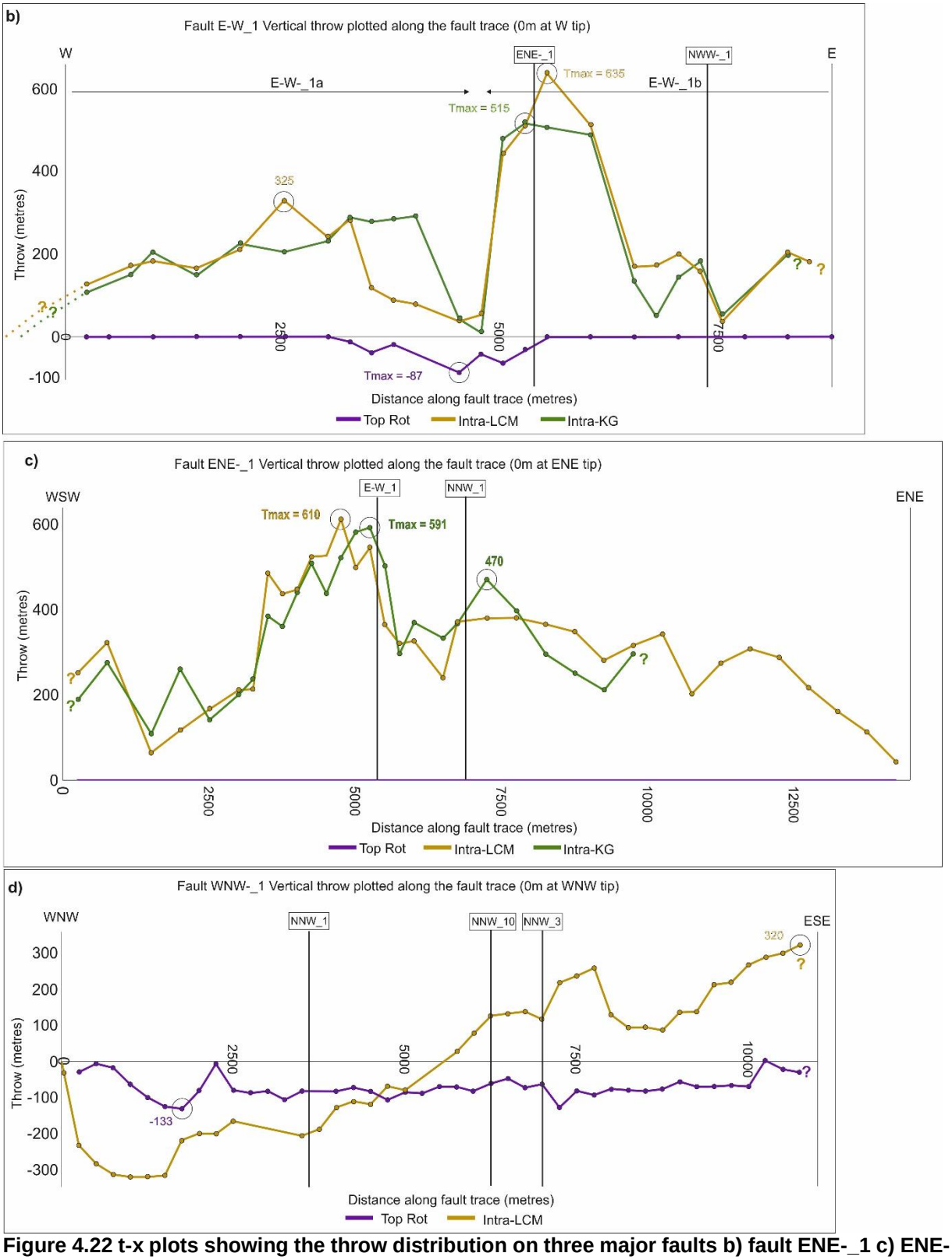


Figure 4.22 t-x plots showing the throw distribution on three major faults b) fault ENE-_1 c) ENE-_1 and d) WNW-_1.

Maximum throws of 635m and 515m (+-12) are observed on each of these horizons respectively on the E-W_1b portion close to the cross cutting intersection with Fault ENE-_1.

The TRot horizon has a throw profile that exhibits 0m across most of the fault plane but has negative throw values (reverse throw) of up to -87ms (+-9) in the area from 3000-5500m. This area also corresponds to the throw minima at 5000m. The throw minima at 7500m is close to the intersection with Fault NNW-_1. The three areas of throw minima along strike could indicate that fault E-W_1 grew as individual segments that later linked (Cartwright et al., 1995; Walsh et al., 2003).

The high difference in throws and profile geometry disparity observed between the intra-Carboniferous (intra-LCM and intra-KG) and Rotliegend (TRot) profile geometries, suggests that the main stage of movement occurred before the deposition of the Rotliegend but after Westphalian D times, with at least a two stages of movement. The atypical reverse reactivation profile observed reflects a locally upthrown portion along strike of the TRot horizon (see Figure 3.26).

The observed throw minima at 5000m is likely more pronounced than what would be expected, due to the later reverse movement at this point. This reactivation means that Horizons intra-LCM and intra-KG would have had higher throw values at the end of the Carboniferous, when restored to their pre-reactivation geometry. This highly atypical profile geometry does not resemble one of an isolated blind fault (Baudon and Cartwright, 2008c). It is likely influenced by the cross cutting intersections with faults ENE-_1 and NNW-_1 and subsequent reactivations involving this cross cutting.

4.4.1.3 Fault ENE-_1

The throw distribution for fault ENE-_1 is presented by the t-x plot in Figure 4.22c. The t-x plot is similar to that of E-W_1 in that the intra-Carboniferous horizons show a similarity in throw values. The TRot horizon however, records zero throw along the entirety of the fault strike.

The throw distributions for the intra-LCM and intra-intra-KG horizons are highly irregular and overall show a symmetry between one another when superimposed. Maximum throws on each horizon are recorded near to the point of intersection with fault E-W_1 and are 610m (+-9m) and 591m (+-12m) respectively (Figure 4.22c). Overall, the throw profiles for each intra-Carboniferous horizon crudely resembles a C-shaped profile with the exception of the high throws between ~3000m-5500m. There is a minima at around 1750m.

The throw profile is more regular towards the ENE- lateral tip where it can be seen to taper to near minimum displacement. The zero throw recorded on the TRot horizon along this fault implies that the ENE-_1 fault is beheaded and has undergone a single-phase movement with no evidence of reactivation after the deposition of the TRot horizon.

The overall profiles for the intra-LCM and intra-KG horizons crudely resemble an envelope or C-shaped profile (*sensu* Muraoka and Kamata, 1983) when a line of best fit is drawn (Figure 4.22c). The deviations from this crude geometry include the area of high throws between ~3000m and 5500m, just west of the intersection with E-W-_1.

If observed on the map, this point can be seen to be in close proximity to Fault E-W_4 (Figure 4.21). The sudden decrease in displacement gradient towards the ENE lateral tip is suggestive of the presence of a mechanical boundary restricting lateral propagation (Nicol et al., 1996), possibly a pre-existing fault. The closest structure is fault E-W_4, this is a postulated long standing major shear zone (Quirk, 1997). This restriction implies that the E-W Carboniferous faults pre-date the ENE- Carboniferous trend. The reason for ENE-_1 cross cutting E-W_1 may be due to the fact that this is a smaller fault.

4.4.1.4 Fault WNW-_1

The throw distribution along a portion of fault WNW-_1 is presented by the plot in Figure 4.22d. Only the intra-LCM and TRot horizons were able to be mapped across this fault due to loss of image quality at depth. Both horizons lose reflection coherency towards the ESE and the plot therefore does not represent the entire length of the fault. The throw distribution along this fault is complex as the along strike throws on the intra-LCM Horizon change from reverse to normal, while throws on the TRot Horizon remain solely net reversed along the mapped fault section.

The intra-LCM records highest reverse throws towards the WNW- of around 320m (+-12m) which then taper to a throw minima at around 6000m along strike. At this point, the throw values become net normal and increase east to 320m (+-12m) on the last measurement point. The TRot horizon exhibits a steady reverse throw along strike ranging from -1m to -130m (+-7m). The point at which the intra-LCM throws change from reverse to normal corresponds to a point along the strike of the fault in which the stratigraphy is downthrown between fault WNW-_1 and E-W_4.

The t-x plot displays a clear multi-stage movement history from the disparity between the intra-MCM and TRot throws. While the TRot horizon remains fairly similar along strike, the intra-MCM is reversed on fault segment A and normal on segment B (Figure 4.23). The change in Carboniferous throws along strike is less due to throw variations along WNW-_1, and more to do with the intersection with E-W_4 and the strike sip feature in-between (see figure 3.30). The most recent movement is reverse shown by net contractional displacement on the TRot horizon. This reverse movement is shown by the TRot embedded into the Zechstein (see Figure 3.26). This movement is postulated to have occurred due to regional north-south oriented compression in the Late Cretaceous Sub-Hercynian (see Chapter 2, section 2.3.6.).

4.4.2 Cross cutting fault relationships

4.4.2.1 NNW-_1 and WNW-_1

Faults NNW-_1 and WNW-_1 cross cut in the northern part of the MB at oblique angles creating an atypical X-Type intersection (Nelson, 2006) which can be viewed on the top Rotliegend horizon map (Figure 4.20). It was established from t-z and t-x analysis that the NNW-_1 faults main stage of movement was the Triassic and the reverse movement is proposed to have occurred during the Late Cretaceous (see section 2.3.6.).

A deviation from the ‘enveloped shaped’ profile of NNW-1 shows a sharp increase in throw on Horizon intra-LCM towards the intersection with WNW-_1 (see peak on segment NNW_B on Figure 4.23a). This can be explained by the extensional reactivation of WNW-_1 and NNW-_1, two faults that share fault block 3 (Figure 4.23e). This likely contributes to the anomaly close to the intersection with WNW-_1 and can

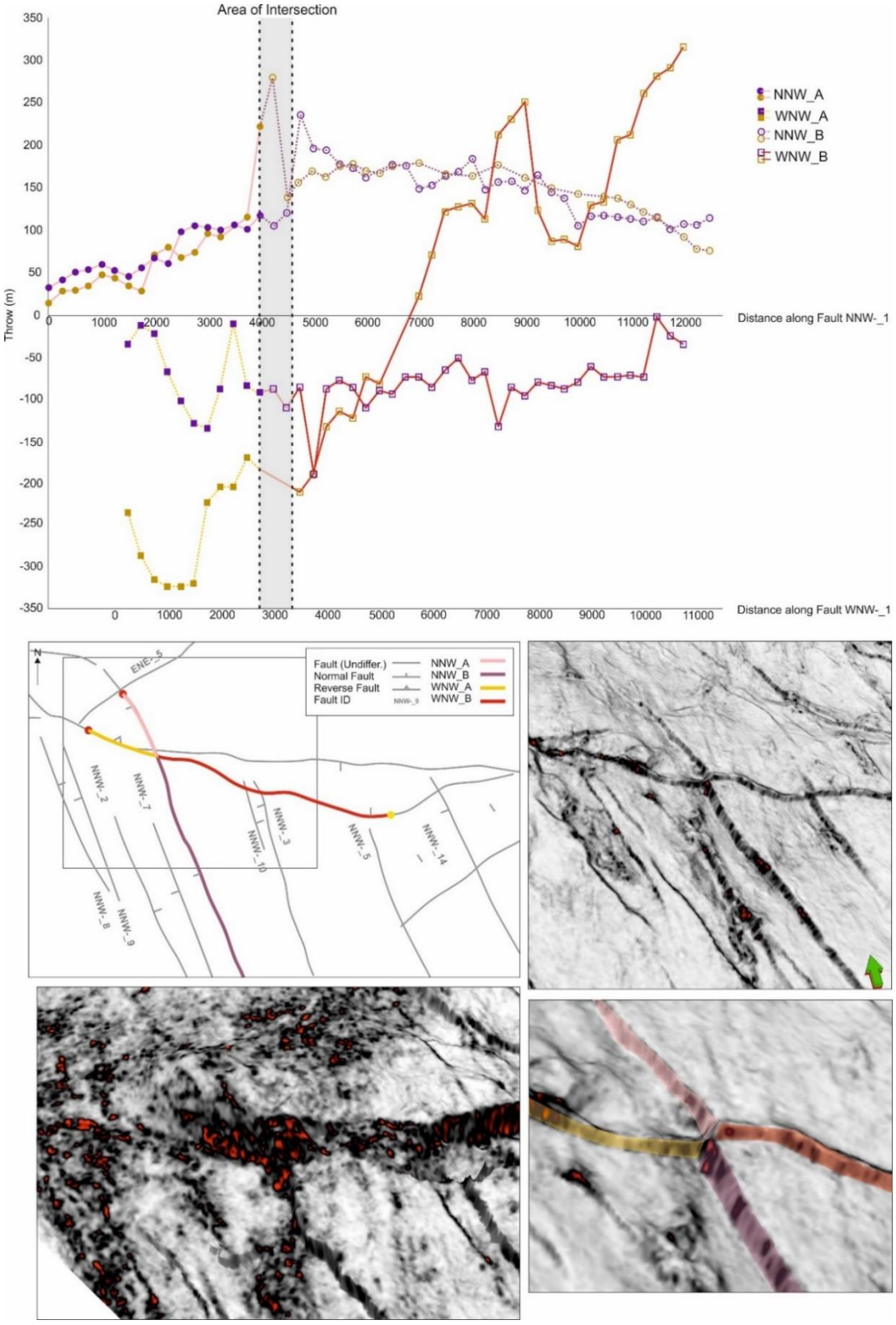


Figure 4.23 t-x plots for faults NNW-_1 and WNW-_1 overlain from the point of X-type intersection. The four fault segments created by the intersection are indicated by the colour key. Bottom left is a horizon map of the iMCM showing the subsided area between the WNW- and E-W fault that is interpreted to be a sinistral pull apart basin

be seen in 3D by the top Rotliegend horizon map as a thicker shaded area Figure 4.23e. This reactivation of Block 3 is also reflected on the WNW-_1 t-x plot by a peak negative throw on segment WNW-_B (Figure 4.23).

4.4.2.2 E-W_1 and ENE-_1

Due to their complicated intersection geometry and resolution and imaging problems, there was some uncertainty regarding which fault segments were genetically similar in this oblique X-Type intersection (*sensu* Nelson (2006). The genetically similar fault segments belonging to E-W_1 and ENE-_1 were substantiated by observation of their dip angles which were markedly different.

There is however a throw minima on fault E-W at the branch line with ENE-_1 on the intra-Carboniferous horizons (Figure 4.24a). At this point along strike, there is a throw maxima on these same horizons on ENE-_1 that corresponds to a roughly similar value as the Tmax on segment E-W_B. This may be due to reactivation before the deposition of the Rotliegend and slip occurring on fault segments EN_A and E-W_B independently (Figure 4.26).

The branch line between E-W_1 and ENE-_1 also exhibits a localised reactivation as shown by the reverse throws on the TRot horizon between 3000-5500m along strike (Figure 4.22b). This is only observed on the E-W_1 however, indicating that the reactivation was likely controlled by the preferential orientation of regional compressive stress rather than any other factors (Kelly et al., 2006). The intersection with ENE- appears to play an important role of the localisation of this reactivation, with the reverse throws being concentrated at the intersection.

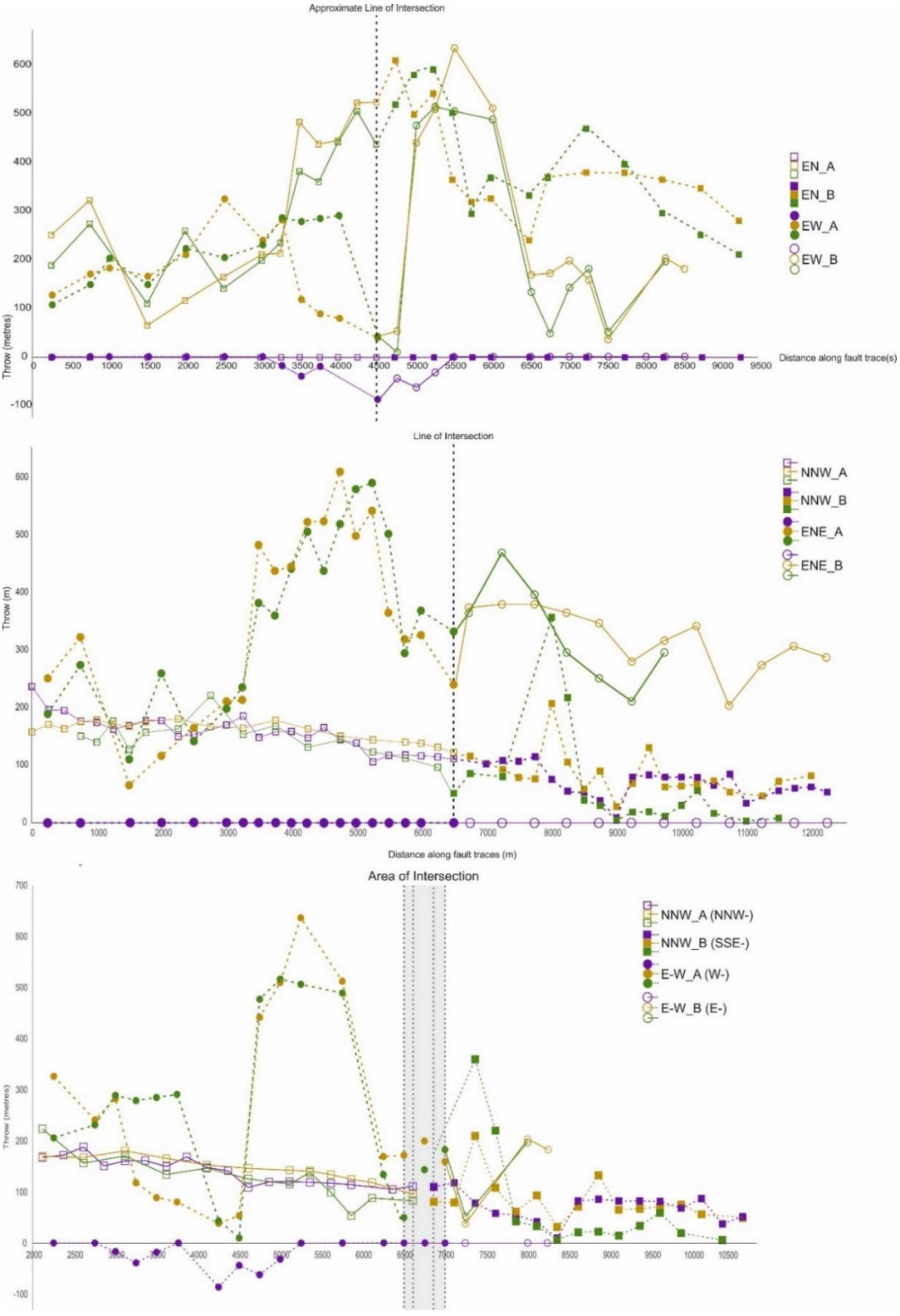


Figure 4.24 t-x plots overlain at point of intersection between faults a) ENE- and E-W b) NNW- and ENE- and c) NNW- and E-W. t-x trends at intersections for each fault are described in the text.

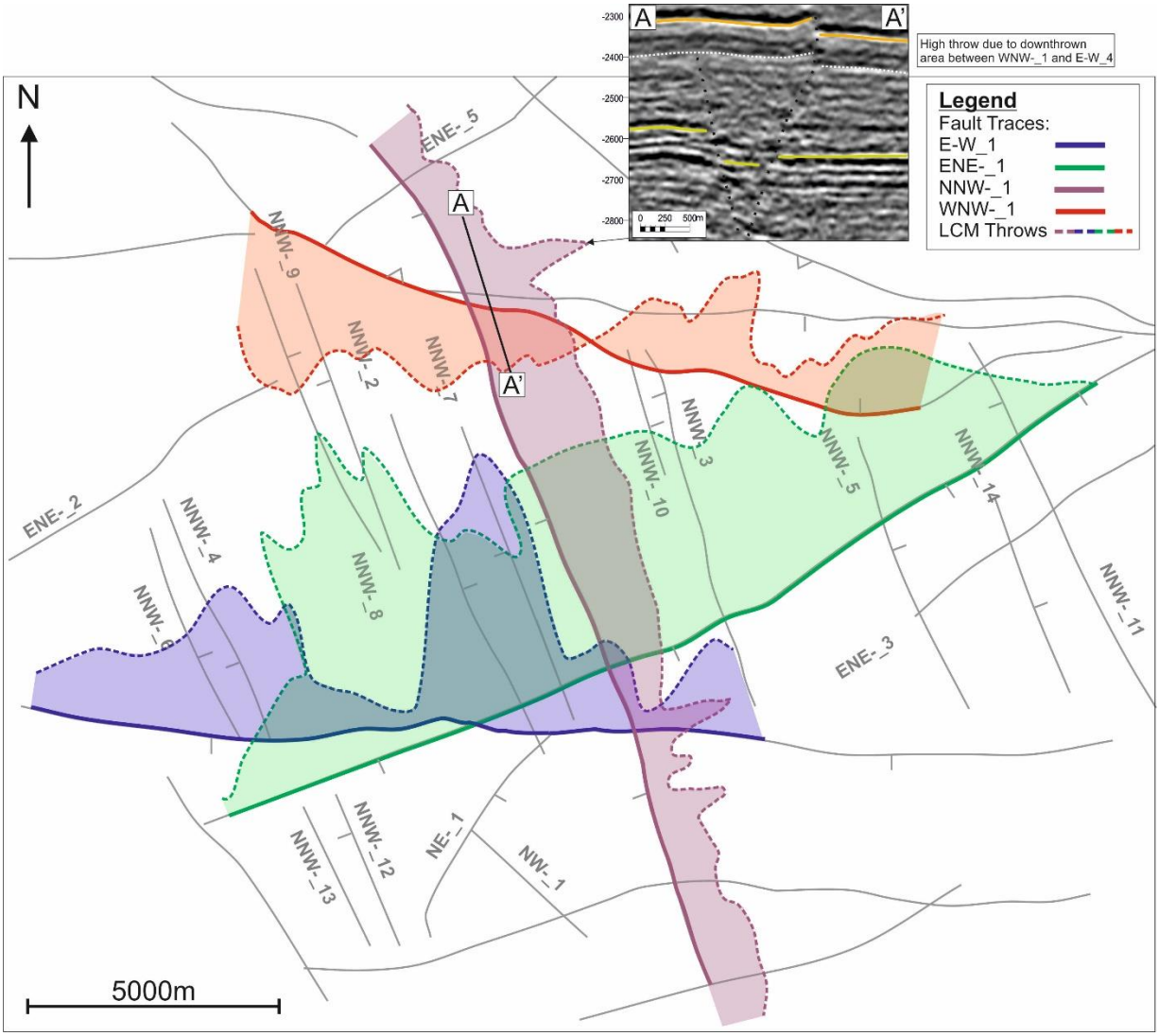


Figure 4.25 t-x distribution for the intra-MCM horizon on each of the four representative faults plotted onto the composite structural map

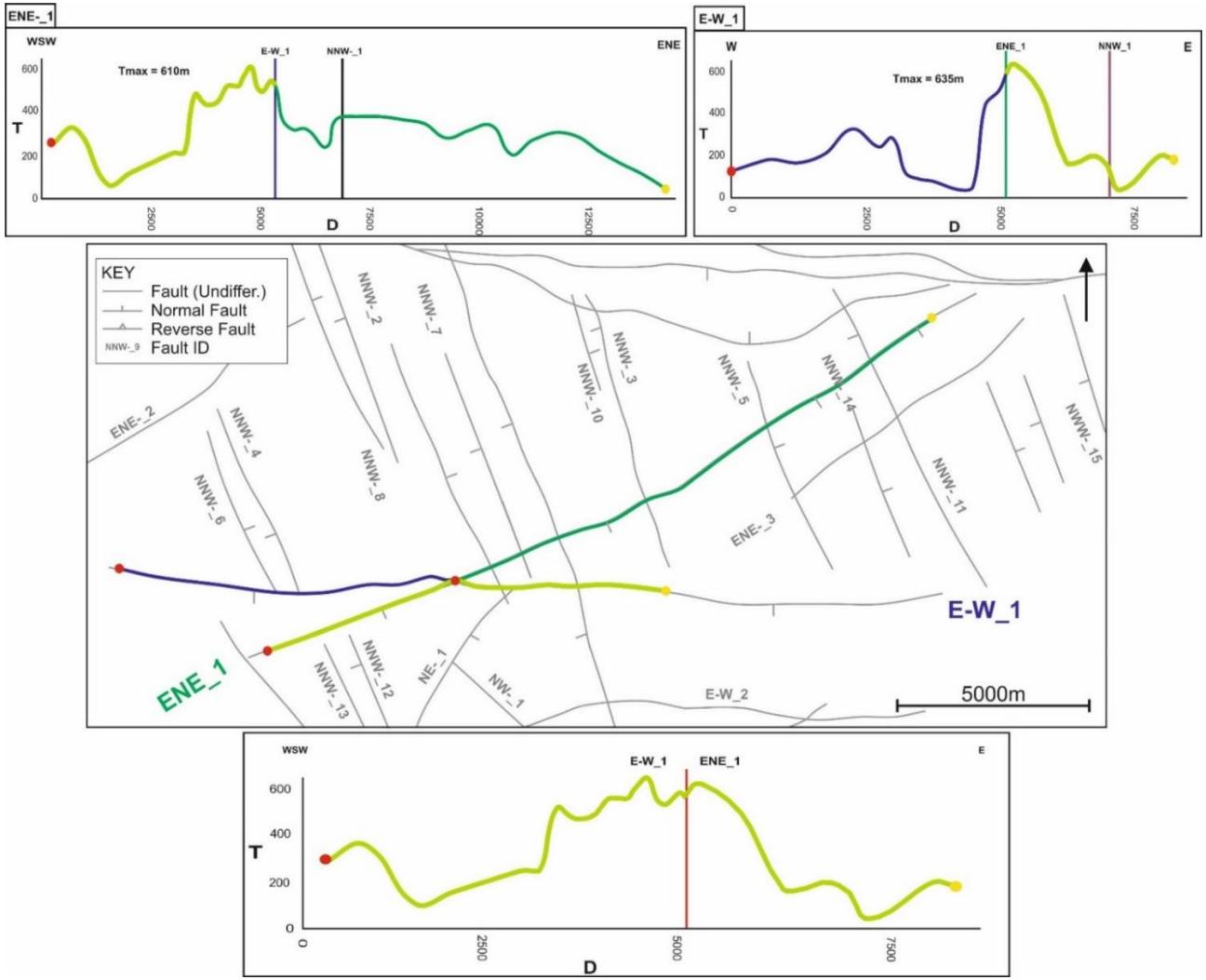


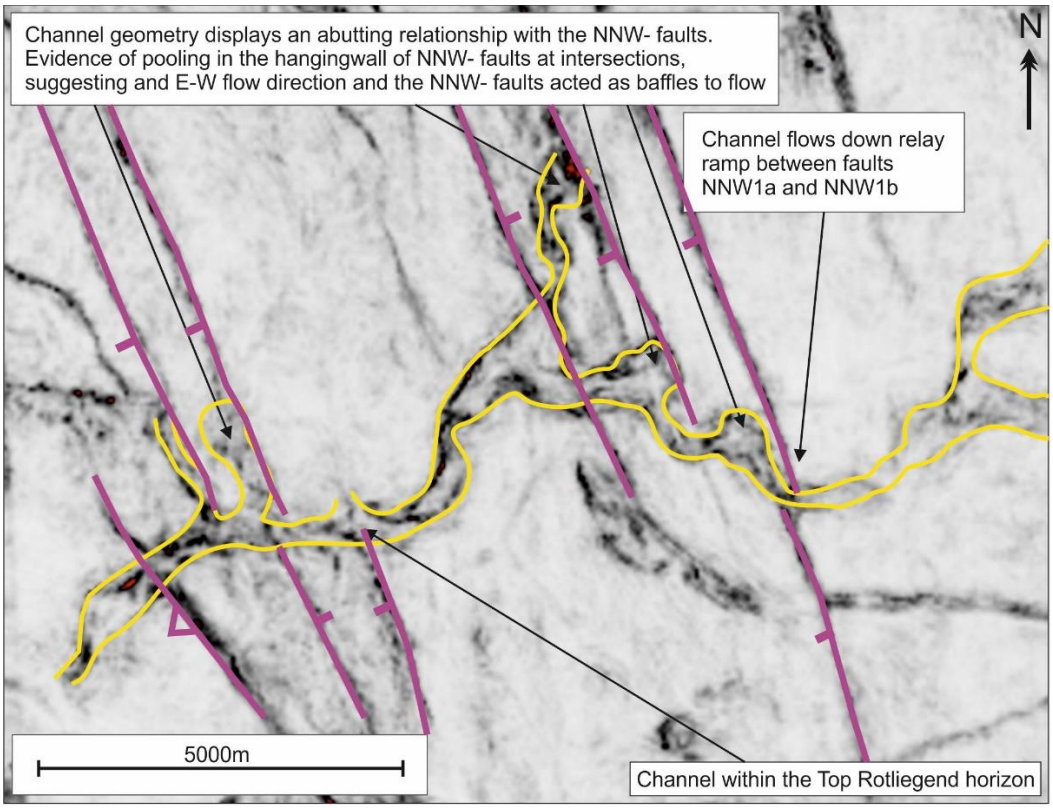
Figure 4.26 combined t-x for segments ENE_A and E-W_B on horizon intra-MCM illustrating the reactivation of these segments independently. This reactivation likely occurred before the deposition of the Rotliegend.

4.4.3 Relationships between faults and channels

An east to west flowing, sinuous channel is identifiable when the variance attribute is extracted onto the Top Rotliegend (Silverpit Formation) horizon in the Murdoch Block (Figure 4.27). The presence of a channel in this location is intriguing, as it is within the Silverpit Formation, which was deposited in a Saline Lake to Playa Lake palaeoenvironment. This dessert lake was much further north than the fluvial/aeolian systems developing to the south during the Late Rotliegend (Figure 2.15). This therefore suggests that this channel formed during the late Rotliegend at a point in time when the Silverpit Lake had evaporated. Given the ephemeral conditions of the Rotliegend, this is reasonable.

The flow of the channel follows the strike of E-W_1 (only slightly visible on the TRot horizon map) which may indicate a surface depression caused by this fault was present during the Rotliegend Figure 4.27. The flow direction of the channel changes from easterly to south-south westerly where it encounters Fault NNW-_7 to the East. The channel geometry also appears to thicken in this place as if being dammed. This would suggest the presence of a structure obstructing the easterly flow at this point in time (Late Rotliegend). Similar thickening of the channel geometry behind faults NNW-_2, NNW-_1 and NNW-_11 indicates that this abutting is not isolated to NNW-_7. Where the flow changes to a south-south westerly direction at NNW-_7, it follows the strike of NNW-_7 and changes to an easterly flow once again around its lateral tip or the point where its lateral tip appears to reach minimum displacement. The channel then appears to be blocked by NNW-_1 and follows a gap in-between NNW-_1a and NNW-1b. The channel flow path in-between NNW-_1a and NNW-_1b has been

interpreted as a relay ramp. This interpretation is supported by the throw minima observed on the NNW-_1 t-x plot separating the two fault segments NNW-_1a and NNW-_1b (Figure 4.20).



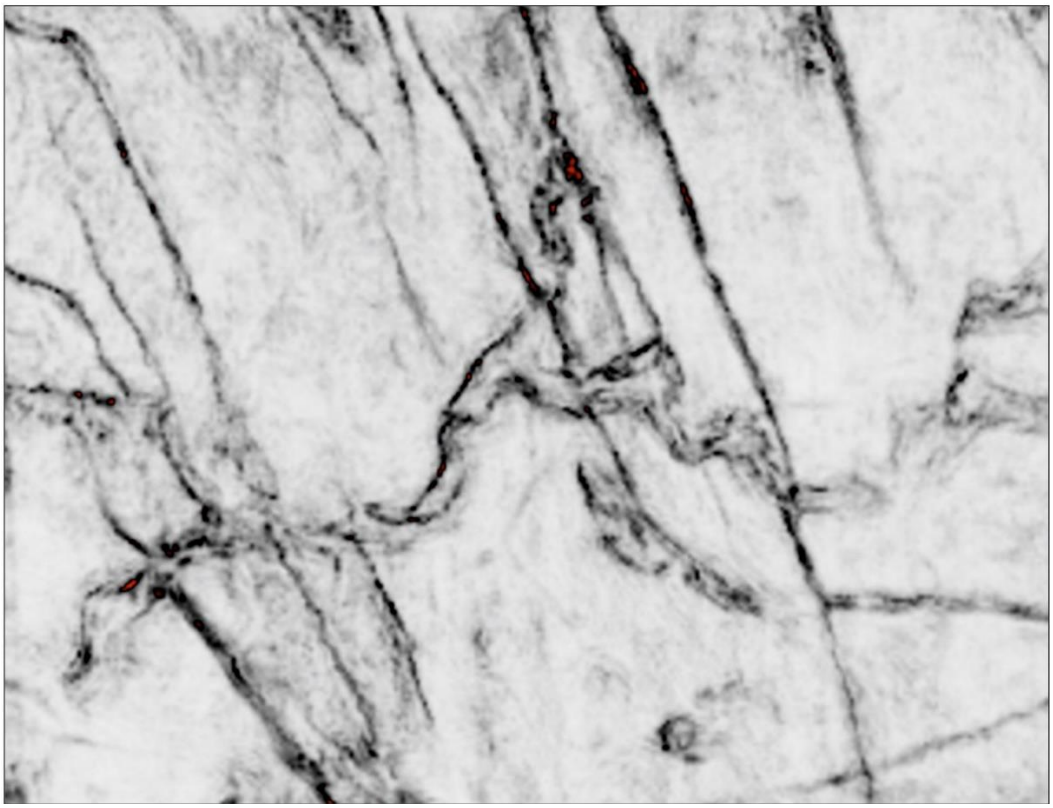


Figure 4.27 Top Rotliegend horizon map with variance overlain. An E-W trending channel (Channel A) is imaged showing flow down a relay between segments NNW-_1a and NNW-_1b, indicating these faults were present at the end of the Rotliegend.

4.5 Discussion of Fault Tip Configurations

A key uncertainty regarding the faults across the Anglo Dutch Basin are the positions of the upper and lower fault tips. This section uses the t-z analysis to estimate the geometry and nature of these unimaged or eroded fault tips.

4.5.1 Basal Tip Geometries

The lower tips of many faults presented in the results section are poorly imaged due to data limitations. In all of the surveys, with increasing depth the resolution decreases due to frequency attenuation, there is an decrease of signal to noise ratio , and the migration is more inaccurate because of greater uncertainty in the velocity model. The position of the basal tips and their relationship to the stratigraphy is discussed here from the combination of fault geometry and throw profiles.

4.5.1.1 Layer Bound Faults

It is argued here that the A-E_WNW- fault set is confined to the Lower Carboniferous to Middle Devonian (ESP-4 on seismic section) and that they are layer bound. This interpretation is based on the key observation that there is no offset of the MDR1 reflection (ESP-5, see and 3.10), correlating to the Middle Devonian aged Buchan or Kyle Group (see Figures 3.6 and 3.7). The position of the lower tips is somewhat uncertain as is the nature of their termination, because coherent reflection offsets can only be observed and mapped with confidence as far down to Horizon J (Top Arundian horizon).

The significantly high throw values recorded on the deepest coherent horizon (J) on faults WNW-_1, WNW-_2 and WNW-_4 ranging from 68-152ms, (Figure 4.8 to

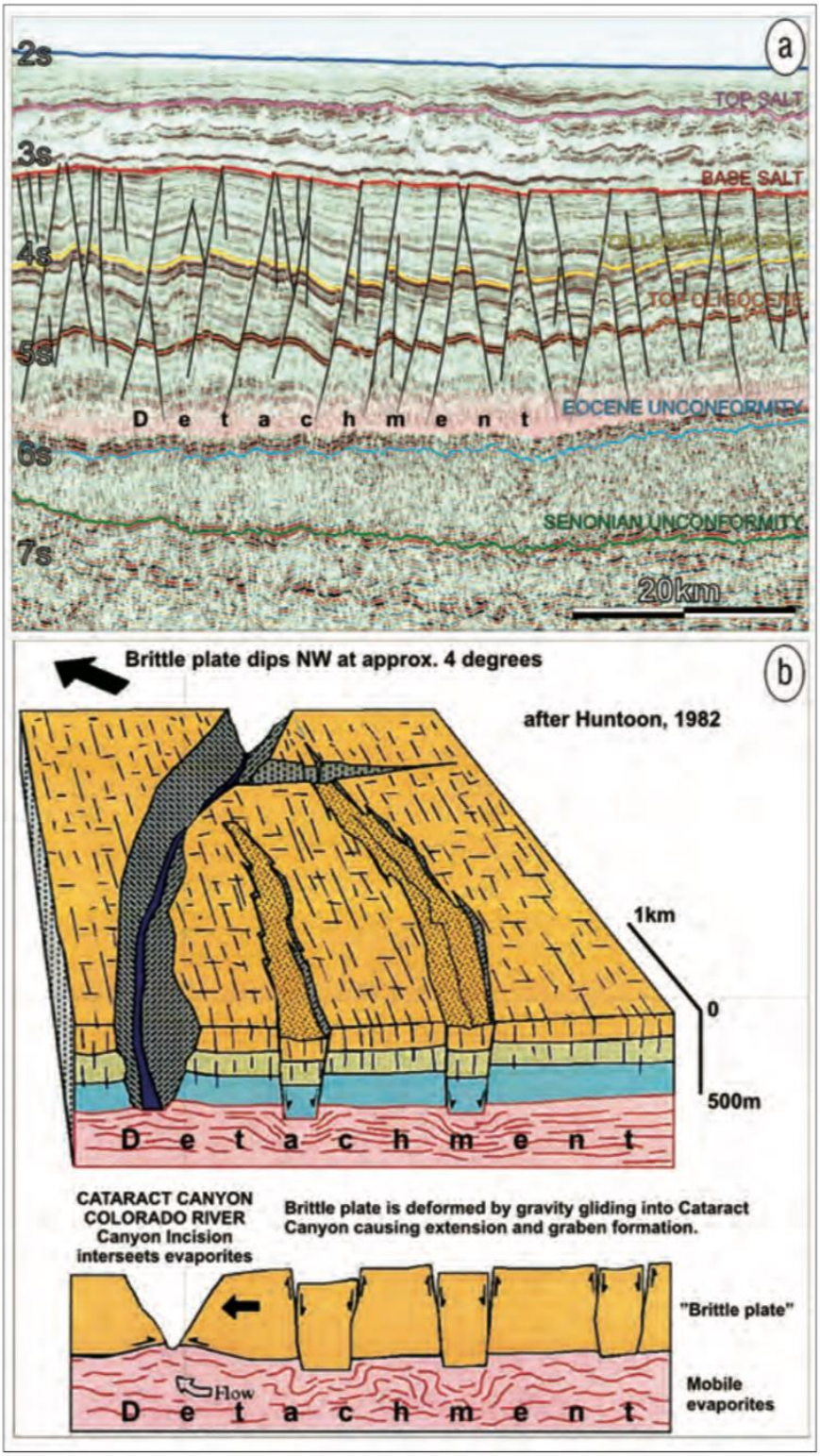


Figure 4.28 Analogous detachment faults from other areas a) the Piano Key faults in the Levant Basin, Eocene shales are the proposed detachment horizon and the faults are associated with marine slumping at the onset of the Messinian (Nader 2011). Seismic line from PGS b) Model of graben formation at a smaller scale by gravity gliding above the Paradox salt in the Canyonlands (after Huntoon 1982 and Kosi et al. 2012).

4.10) suggests that the fault tips terminate at a deeper level than the deepest imaged portion of the fault. Of the seven plots in which horizons could be correlated at deeper levels than the Arundian (Horizon J), five plots show an overall decrease in throw towards the cryptic lower tip (WNW-_1 MP3, WNW-2 MP3 and MP4, WNW-_4 MP2 and MP3 (Figure 4.9 and 4.10) compared to the two plots that show an increase in throw (WNW-_2 MP5 and WNW-_4 MP1). This is taken to suggest that the throw generally decreases in this interval. It should be noted however, that Horizons K and L are less coherent and more discontinuous and therefore more prone to interpretation and measurement error. The relatively high throw values on the Top Courceyan/Horizon L as seen on faults WNW-_2_MP4 (Figure 4.10), WNW-_4_MP2 and WNW-_4_MP3 (Figure 4.8), suggest that lower tips may be located in the Courceyan-Frasnian stratigraphic succession (ESP-4) (see Figures 3.6 and 3.7).

The t-z profile analysis therefore suggests that the A-E_WNW- faults are detached in the Lower Carboniferous-Upper Devonian (Courceyan-Frasnian). The seismic stratigraphic framework derived from seismic facies observations and stratigraphic context (Figure 3.7) suggests that this layer is predominantly mudstone. It is therefore proposed that this layer could have acted as a mechanical detachment for the A-E_WNW- faults (Tvedt et al., 2013, Morley et al., 2003, Jackson and Hudec, 2005). Similar detachment faults are observed in basins elsewhere such as the Levant Basin in the Eastern Mediterranean, in which an Eocene shale detachment horizon is postulated Figure 4.28, (Kosi et al., 2012).

4.5.1.2 Throughgoing Faults

Unlike the A-E_WNW- faults, the 44-D_E-W do not have an underlying unfaulted reference horizon (Figure 3.53) and data resolution decreases significantly permitting no coherent reflection correlations with depth. This makes it more complicated to interpret the lower tip termination positions. T-z plots end abruptly before a lower point of minimum displacement is reached and show a more or less constant throw value before this point (Figure 4.12). Faults E-W_1 and E-W_2 also have no coherent reflections that can be correlated beneath the last measurement point. Fault E-W_1 exhibits an overall decrease towards the lower tip.

Two end member possibilities can be suggested for the lower tip termination positions based on the t-z plot gradient. The first is an extrapolation with the same gradient in a typical C-shaped profile manner that is unrestricted and assumes no mechanical boundary (Figure 4.29). This unrestricted profile is indicated by the blue dotted line in Figure 4.29. The other, shown by the orange line, is where the lower tips are likely to terminate if there is a mechanical boundary causing restriction (Nicol et al., 1996). The geometry of this fault set and the long lateral lengths suggests that they have a large vertical extent and are coupled with basement stresses. The lower tips of the 44-D_E-W faults are therefore likely in the Courceyan or deeper basement levels, and mechanical restriction may have little significance due to their scale.

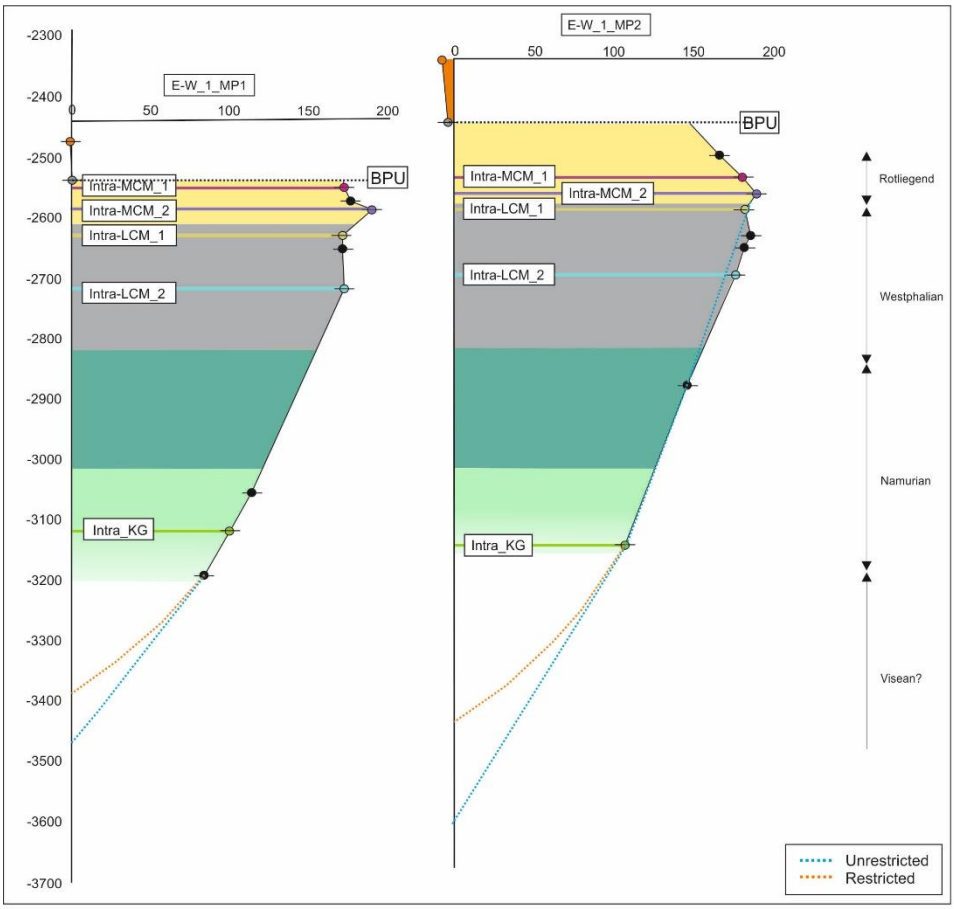


Figure 4.29 Possible extrapolation of the t-z plots for fault E-W_1 below the last coherent horizon measurement in the instance of mechanical restriction and no restriction

4.5.1.3 Superficial Faults

Superficial faults such as A-E_NE-_1 and A-E_NE-_2 (Figure 4.14, Figure 4.18) produce t-z plots with a near or fully complete lower tip region plots as their lower tips are imaged due to their small vertical extent. The t-z plots exhibit an overall decrease to a point of minimum displacement representing the lower tip.

4.5.2 Upper Tip Geometries

Most of the fault upper tips are not imaged due to erosion at the BPU or termination into the mobile Zechstein unit. Based on these truncated or beheaded throw profiles it is interesting to consider where the original upper tips might have originally been positioned.

4.5.2.1 Beheaded Upper Tip Position Before Erosion (Types I-IV)

Before reconstructing an eroded upper tip position, it is first important to assess whether or not the fault propagated in a blind fashion with its upper tip below the surface. If the tip was active at the surface (a syn-sedimentary fault propagation), then the reconstruction can be based on consideration of the regional structural evolution and the known timing of faulting within a region. The A-E_WNW- and 44-D_E-W faults are used as examples in this consideration.

It is widely accepted that the erosion at the BPU occurred during the Late Carboniferous-Early Permian (see section 2.3.3.1). Given that there are no syn-sedimentary packages observed in the preserved Courceyan-Brigantian succession, the fault activity forming the A-E_WNW- faults most probably occurred at some point during this period represented by the hiatus at the BPU. In order to crudely estimate the pre-erosional throw profile geometry and positions of the

original upper tips of the A-E_WNW- faults, we first establish whether these faults formed at the surface or blindly.

High observed throw values (up to 156ms on WNW-_2, see Figure 4.10) occur on the Brigantian horizon, which is the first pre-BPU horizon measurement. If an analogous blind fault t-z profile is used to reconstruct the tip position, then using the classical axio-symmetric distribution of displacement where the maximum throw occurs at the centre and then decreases gradually towards each tip (Barnett et al., 1987), then it may be suggested that an equal proportion of stratigraphy was in the upper portion (Figure 4.30). By the extrapolation of the same thickness of middle-Upper Carboniferous stratigraphy observed in the deeper parts of the Anglo-Dutch Basin such as the Silverpit Basin (Well 44/27-1, see Appendix A), the extrapolation of the throw plot gradient would suggest that the upper tip terminations would have been in the upper Namurian-Lower Westphalian (Figure 4.30).It is considered here however that it is more likely that these faults propagated as syn-sedimentary faults because the period of time representing the BPU hiatus at this point was one of uplift and erosion in which minimal overburden is postulated to have accumulated in the area (section 2.3.3.1). This is also consistent with depositional setting during the Namurian and Westphalian which was a large scale delta system prograding from the north (Fraser et al. 1990). Given that the Elbow Spit Platform area was a persistent Palaeozoic high through the Early Carboniferous (Ter Borgh et al. 2018), it seems even more likely that these faults formed at the surface of this delta system.

Although there is no standard method to predict the throw profile of a syn-sedimentary fault, if we use the an example of an analogous growth fault in the Levant basin presented by Baudon and Cartwright (2008), the throw distribution is skewed with a Tmax closer to the upper tip rather than centrally (Figure 4.17).

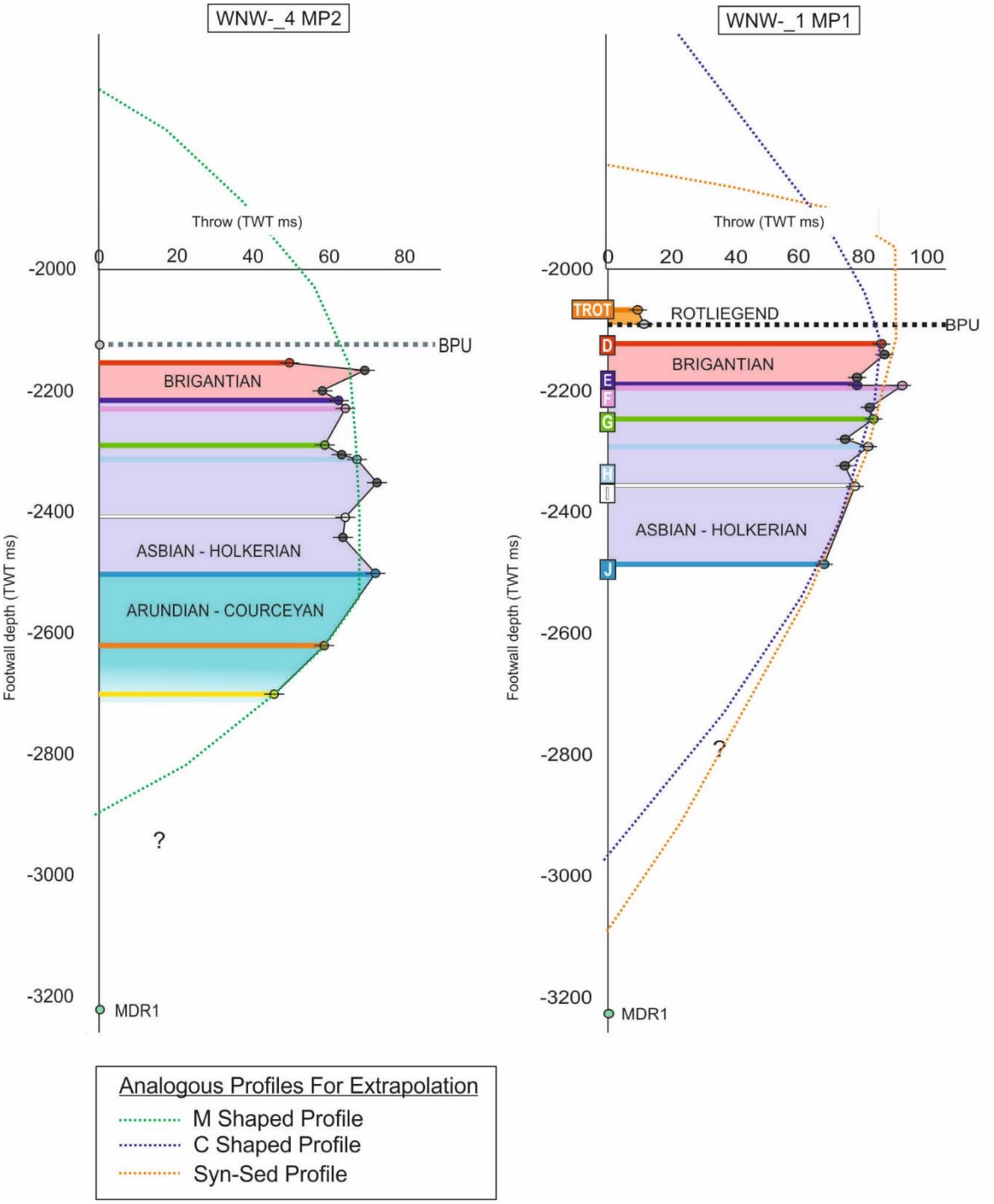


Figure 4.30 Extrapolation of t-z plots into three characteristic throw-depth distributions at two intersection points along the strike of fault WNW-_4

This would imply that the upper tips terminated in older stratigraphic intervals such as the middle-upper Namurian or later (Figure 4.30).

Differences in mechanical stratigraphy can substantially perturb a classical t-z profile (Gross, 1997, Wilkins, 2002, Nicol et al., 2003). However, this may be a major effect within the Brigantian-Westphalian interval at high resolution due to the cyclic successions of sandstones, mudstones and limestones with their different mechanical properties. At the seismic resolution, these lithologies are arranged as high frequency (m-scale) cycles (Schlager, 2004, Williams, 1993) it is therefore inferred that the bulk stratigraphic succession has similar rheological and mechanical properties.

Another uncertainty that extrapolating the t-z profile presents is whether the recorded Tmax is the greatest maximum throw at that measurement intersection point or just the greatest that has been preserved before the BPU. This problem that displacement profiles may not sample the greatest displacement (and length) of a fault is also discussed by Muraoka & Kamata (1983), Walsh and Watterson (1987), (1988a), Cowie and Scholz (1992). A method of estimating if a Tmax seems reasonable for a particular fault is by calculating the D-L ratio for the fault (bearing in mind that this fault has been reactivated in strike slip and reverse senses).

Fault E-W_1 has an estimated length (exact lateral lengths are uncertain due to decreasing reflection continuity laterally) of approximately 21km and a Tmax of 640m (+-12m) which gives a D/L ratio of 0.03. When compared to global fault D/L datasets (Cowie and Scholz, 1992, Dawers and Anders, 1995, Schlische et al., 1996, Schultz et al., 2008), the Tmax and length values of fault E-W plots inbetween the constant slop for D/L ratios of 0.1 and 0.001 (Figure 4.31). This would suggest

that the preserved Tmax value is reasonable for a fault of this length and therefore may be the greatest throw despite the erosion at the BPU.

The 44-D_E-W faults are located in the centre of the basin where the greatest amount Westphalian stratigraphy is preserved. Considering the Tmax is at a position close beneath the BPU in the preserved stratigraphy, and the fact that the BPU hiatus here is small, it is likely that these faults formed close to the surface during the deposition of the upper Westphalian to Stephanian and the syn-sedimentary packages have been eroded.

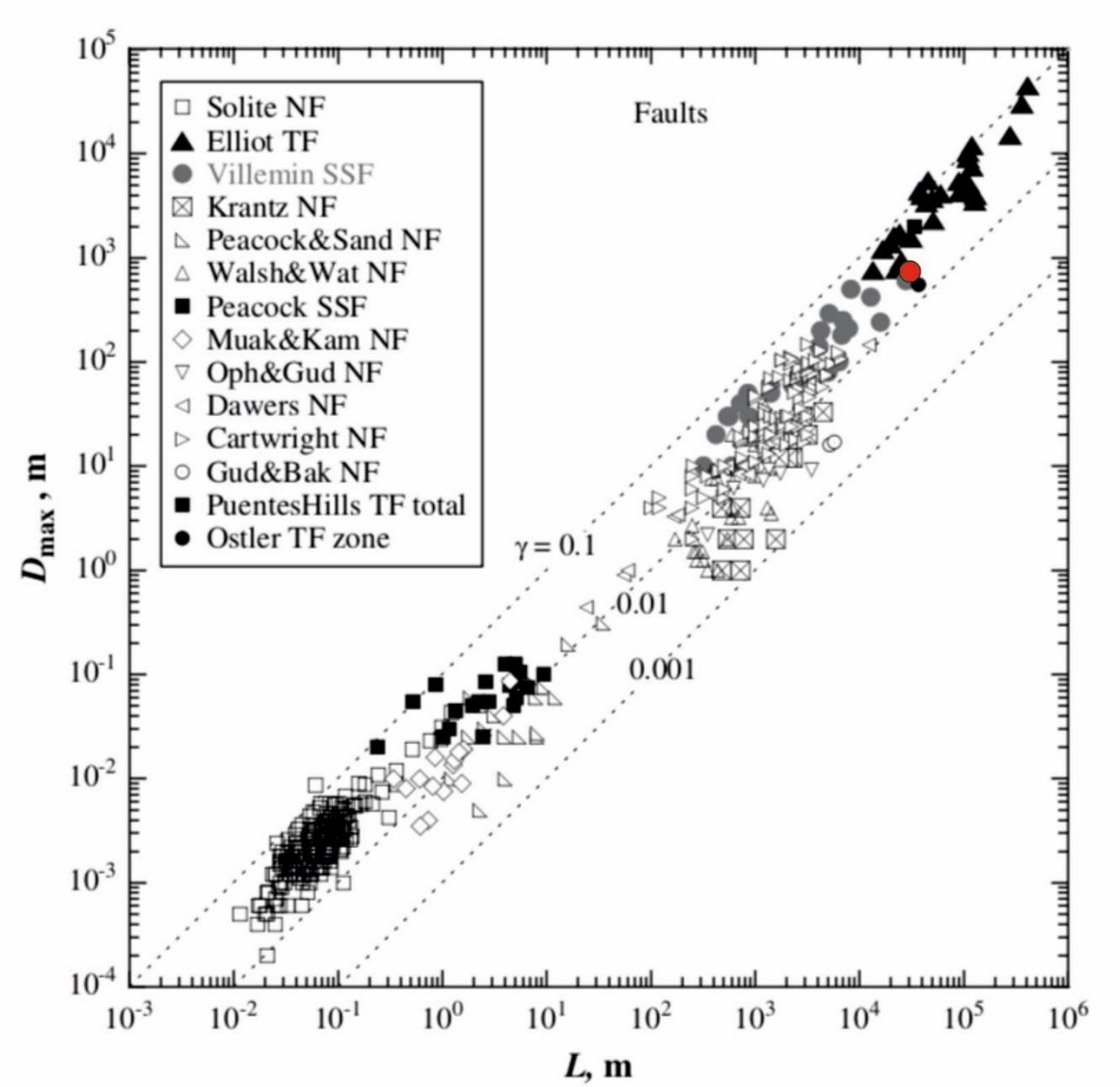


Figure 4.31 Compilation of maximum displacement and length datasets for different published fault datasets (see Cowie & Scholz 1992, Schlische et al. 1996 and Schultz et al. 2006 for data sources and discussion). Normal faults are indicated by open symbols, strike slip faults by grey symbols and thrust faults by black symblols. After (Schultz et al., 2008). The D/L measurements for fault E-W_1 plots between the constant slope for of D/L ratios of 0.01 and 0.01 among strike slip and reverse faults. This may indicate that the pre preserved Tmax on fault E-W is close to the greatest normal throw despite the erosion at the Base Permian Unconformity.

4.5.2.2 Current Upper Tip Positions (Open Top)

Considering that there is no expression of the majority of fault upper tips in the mobile Zechstein unit, due to it being largely acoustically opaque and lateral salt flow has occurred later than the fault movement, the position of the upper fault tips are therefore uncertain. The relatively low throw values at Rotliegend levels means that if the fault had propagated into the Zechstein, there would be less coupling and no expression in the overlying Triassic interval (Withjack and Calloway, 2000).

Fault t-z profiles that display open top geometries whether they are reactivated (Type II-IV) or non-reactivated (Type V profiles) show either an overall decrease in throw on the BPU and TRot horizon towards the last measured horizon offset (i.e. NW-_1 see Figure 4.15) or an increase in throw towards the last measured horizon offset (i.e NNW-_1, see Figure 4.19). The faults that show an increase in throw are postulated to have propagated further into the Zechstein unit than those that exhibit a decrease, with the Zechstein accommodating the reactivated portion of throw in a ductile manner. Since the Rotliegend is thin and in most cases only 3 horizons can be measured and correlated within the package, the geometry of the reactivated Rotliegend portion is uncertain.

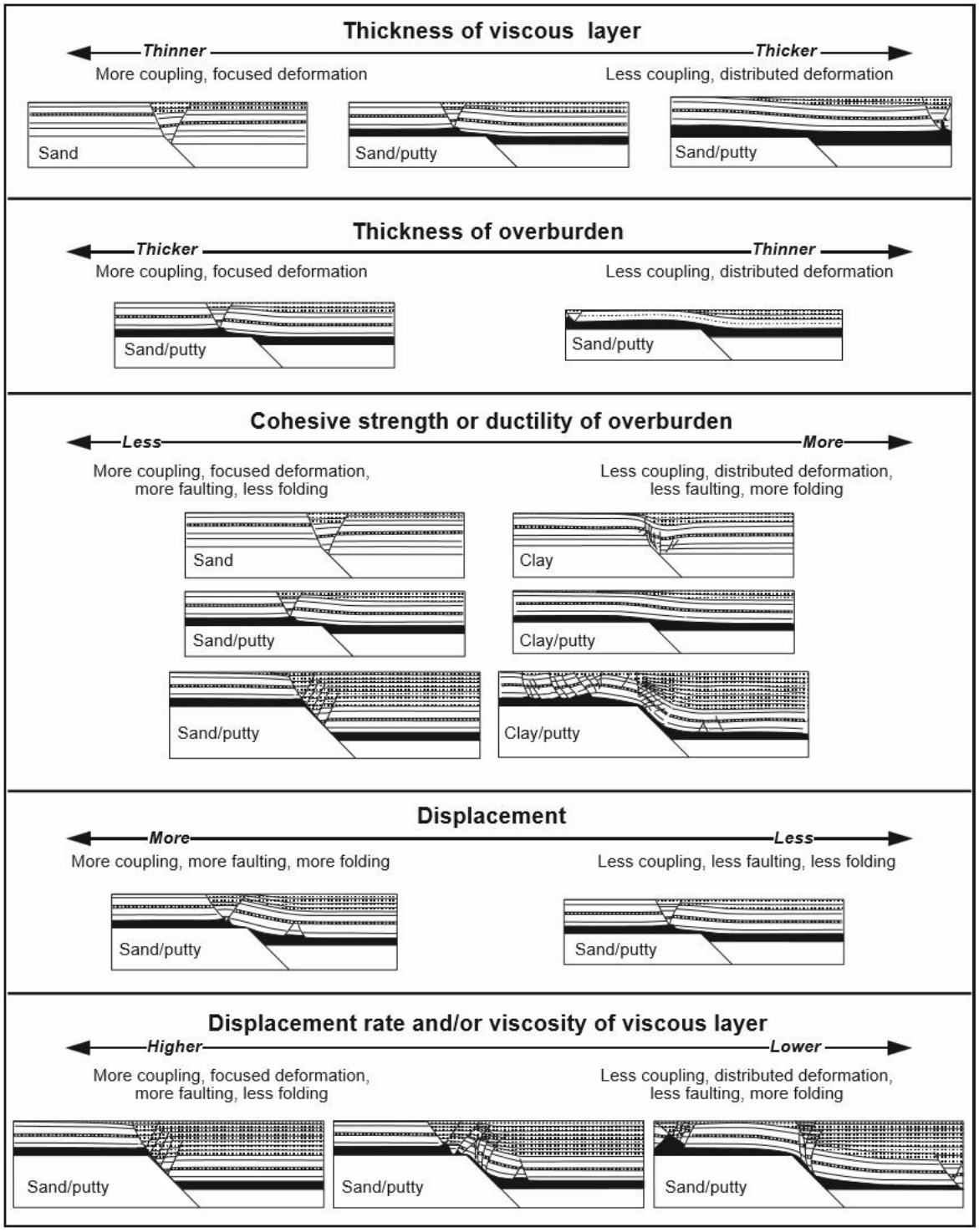


Figure 4.32 Models illustrating how the decoupling effects by a mobile evaporite layer vary due to different controlling factors (Withjack & Calloway 2000).

4.6 Discussion of Fault Slip and Reactivation Timings

The t-z and t-x profiles allow for a reconstruction of relative timing and age relationships. This section addresses the selective reactivation and local reactivation of certain faults and proposes explanations for this behaviour.

4.6.1 Fault Activity

4.6.1.1 A-E_WNW- Faults

The relatively high throw values on preserved Lower Carboniferous reflections (horizon D, intra-Brigantian, see Figure 4.8), the presence of the erosional surface (BPU), and the lack of growth packages, point towards an initial normal movement during the BPU hiatus (end of the Brigantian/early Namurian (ESP-2) and Late Carboniferous/early Permian (ESP-1). This timing of fault activity cannot be constrained any further by seismic interpretation, but observation of the throw profile and information about the geological evolution of the area can help to estimate the possible timing of formation. The formation and evolution of the A-E_WNW- faults is illustrated in Figure 4.33.

Sometime after the deposition of the Brigantian (Figure 4.34T1), prior to the deposition of the Rotliegend, normal slip occurred on the WNW- faults (Figure 4.34T2). The t-z plot analysis suggests this time may have been during the time period of the upper Namurian-Lower Westphalian (Figure 4.30). A period of erosion then occurred after the early Namurian (youngest correlatable age in the hangingwall) which eroded to the Top Asbian in the footwall creating the unconformity U1 (Figure 4.33T3). The grabens then suffered contractional strain evidenced by the folded stratal reflections in the graben into an anticline. This also folded the unconformity U1 (Figure 4.33T5) in which onlapping geometries are observed, this onlapping stratigraphy cannot be stratigraphically constrained

however, and is referred to as package Z (Figure 4.33T6). Fault activity continued on the major WNW- rotated fault blocks but ceased on faults bounding the intervening grabens at the time period represented by package Z. Erosion occurred once more creating the second observed unconformity U2 (Figure 4.33T6). Deposition of the Rotliegend occurred on U2 in which the WNW- faults were slightly reactivated at localized positions (Figure 4.33T7).

The slight observable offset of the BPU and Top Rotliegend horizon observed on certain WNW- faults on seismic (Figure 3.9) and T-Z profile (Figure 4.8, Figure 4.9, Figure 4.10) ranges from 1-15ms (+-3ms) locally on some faults at certain points. This indicates a minor local reactivation has occurred at some time after the deposition of the Rotliegend. Due to the relatively small offsets compared to the bulk stratigraphic section, and the decoupling effects from the overlying Zechstein salt layer, an upper limit for the timing of this extensional reactivation is not expressed in the overlying stratigraphic succession. The Rotliegend is thin in this area, and hence provides only a few reflections to record throw values. Therefore, the extrapolation of displacement gradients is not possible here. When observed on WNW- faults, this reactivation is non-uniform along the strike of the faults (see Figure 4.9 and Figure 4.10). This timing of extensional reactivation therefore could have occurred at any time from the Zechstein to present day (see discussion).

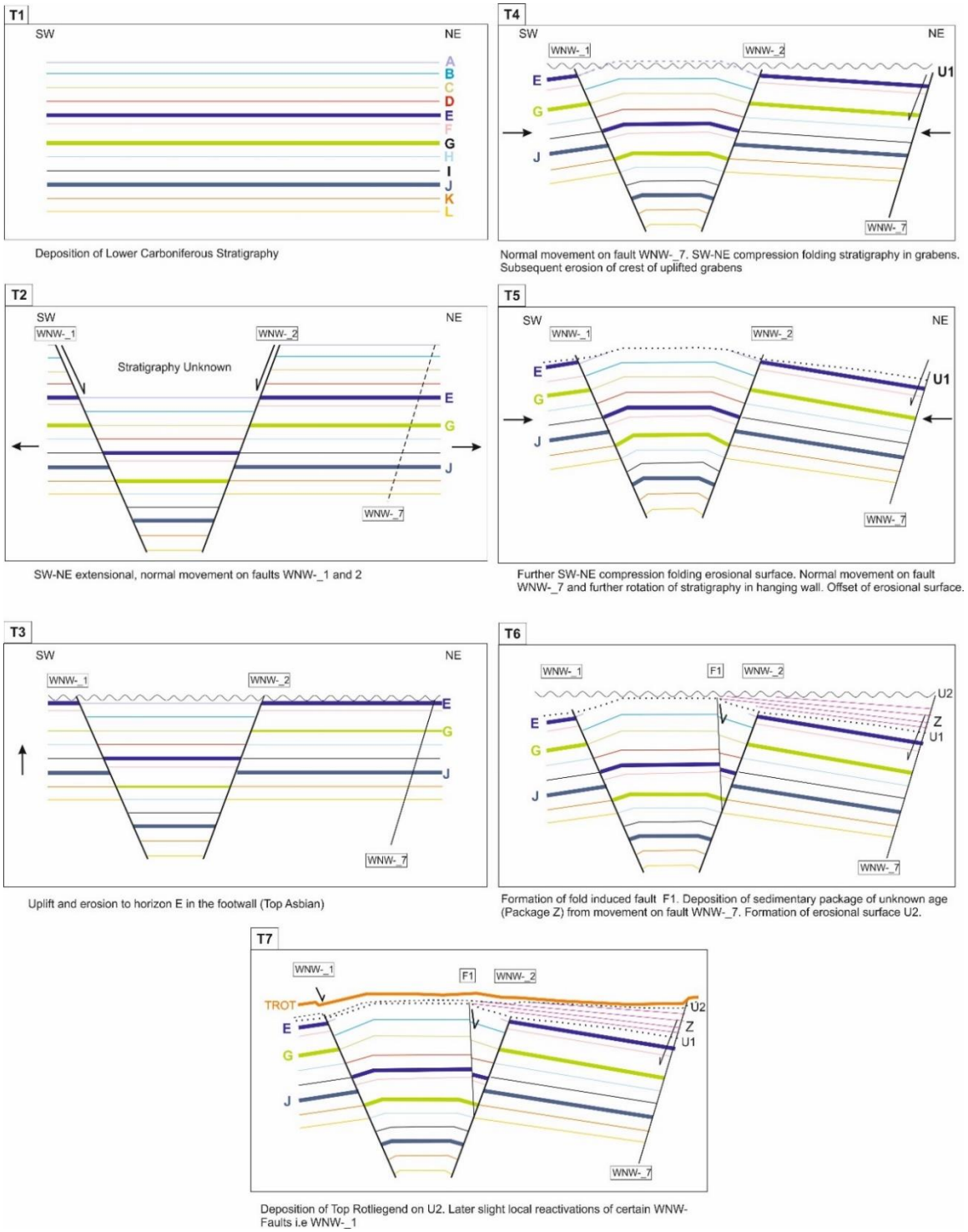


Figure 4.33 Reconstruction of the main stages of evolution for the A-E_1 fault set and BPU erosional surfaces U1 and U2. An intersection normal to the strike of faults WNW-_1, WNW-_2 and WNW-_7 is used to illustrate this. The formation of multiple unconformities are also shown. Only coherent reflections are used to illustrate the evolution. T1 represents the time when the lower Brigantian was deposited and at the surface (Before the BPU Hiatus). T2 is during the BPU hiatus when the WNW- fault initially incurred normal movement. T3 is during the BPU hiatus when the first BPU erosional surface (U1) was formed. T4 is also during the BPU hiatus when the WNW- grabens underwent contractional strain, folding the WNW-grabens. T5 shows the further folding of the grabens and folding of the unconformity in which stratigraphy of an unknown age (Z) then infills. T6 shows the formation of the second erosional surface (U2). T7 is the present day structure.

4.6.1.2 A-E_NE- Faults

The T-Z plots constructed for A-E_NE- faults (Figure 4.14 and Figure 4.18) display contrasting displacement distributions with depth, suggesting that not all NE-SW trending faults on the Elbow Spit Platform have the same movement history. Two sub-types of faults can be distinguished based on the characteristics of their t-z plots.

1. NE-/NNE- trending faults that originated before the deposition of the Rotliegend with relatively small maximum throws located in a central region of up to 25ms recorded on intra-Carboniferous horizons. These faults then underwent a minor reactivation post-deposition of the Rotliegend, with throws on Rotliegend horizons being generally 10ms less than that on intra-Carboniferous horizons. This reactivation is clearly indicated by a sharp change in throw gradient between the Top Rotliegend horizon and the shallowest Carboniferous marker horizon. Clear examples of this are illustrated by plots NE-_2_MP1, 2 and 3 and NE-_3. Due to the small throws, these faults may have been 'cutoff stretch faults' that developed to accommodate along strike variations in displacement distributions on the WNW- faults (Stewart 2001, see Figure 4.35)
2. NE-/NNE- trending faults that originated after the deposition of the Rotliegend. Typical throw plots of this type show Tmax values close to the upper tip in which throw is then constant with depth or has a steady decrease. An open top Type-V profile also observed. They key distinguishing factor is the similar throw values recorded on the Top Rotliegend horizon and the first Carboniferous marker horizon. The 'open top' on a t-z plots is usually indicative of interaction with the free surface (Childs et al., 2003; Baudon &

Cartwright, 2008a). However, with the absence of syn-sedimentary packages in this case, and the presence of the mutli-phase, deformed Zechstein halite above, it is likely that these faults formed during or after the deposition of the Zechstein, with the Zechstein layer accommodating throw.

4.6.1.3 44-D_NNW- Faults

Attempting to establish a timing of formation and slip history for fault NNW-_1 is complicated due to the t-z plots, t-x plots and fault-channel map relationships, and seismic observations individually suggesting subtly different movement histories.

The t-z plot at intersection MP1 (Figure 4.19) shows a sharp decrease in throw values by 10ms at the BPU between the Carboniferous and Rotliegend horizons. This value is greater than the error margin (6ms) which may suggest movement occurred on this fault before the BPU erosion and post-Rotliegend reactivation (Nixon et al., 2014). T-Z plots at intersections MP2, MP3 and MP4 however, do not have a stepped profile and a single phase of slip is implied. Two different timings of formation and movement are suggested by the t-z plots MP1 (1) or MP2, MP3 and MP4 (2) and are presented as follows;

Two Phase Movement (Type IV)

a. Extensional movement sometime after the deposition of the Brig Formation (U. Coal Measures Fm, Westphalian D, ~307Ma). Maximum throw of around 10ms at this time.
b. Erosion of the Late Carboniferous down to the Westphalian D
c. Fault quiescence during the deposition of the Silverpit Formation (~262Ma, Upper Rotliegend).

d. Extensional movement occurring sometime after or during the deposition of the Zechstein (~258Ma), indicated by the 'open top' profiles in which throw increases towards the upper tip. These upper tip geometries are suggested to be representative of the extensional displacement that has been accommodated by the ductile Zechstein halite layer. There is no observable offset of the Triassic stratigraphy or younger due to the presence of the Zechstein halite layer, decoupling the overlying Mesozoic stratigraphy from the upper Palaeozoic. The upper limit of fault movement is therefore unknown due to this decoupling effect.

Considering these faults show no obvious decoupling from the underlying stratigraphy, they are interpreted to be coupled with the basement (see section 3.3.3.1). The regional stresses occurring at this postulated time of formation (Late Carboniferous) is N-S/NNW-SSE compression (section 2.3.3.1). This stress regime would typically form or cause slip on NNW-SSE strike-slip/oblique slip faults, however. Although these faults are steeply dipping (mostly 65-75°, see Figure 3.28), they exhibit significant normal movement with no evidence of lateral movements. The eroded footwall scarps observed on seismic intersections normal to this fault (see uninterpreted seismic on Figure 4.19) supports this theory of two stage movement.

Single phase movement (Type-V)

a. Extensional movement sometime during or after the Late Permian, evidenced by the lack of Rotliegend syn-sedimentary packages. Given that these faults appear to be linked to the basement, this NE-SW extension probably resulted from the regional extension occurring in the Triassic Hardegsen event (Zeigler, 1990) (see Figure 2.17). This

orientation of extension is also observed on much large scale tectonic/throughgoing faults such as the N-S/NNW-SSE trending Oslo Graben (Heeremans 1996), situated to the north west of this faults set.

The T-x plot for NNW-_1 indicate a single phase movement overall. Given this postulated orientation of regional compressive stress during the late Carboniferous and the observed offset, a single phase movement is preferred.

This still means that there is complexity as to the presence of an eroded intra-Carboniferous footwall scarp (Figure 4.19), a step in t-z profile at MP1 (Figure 4.19) and the pre-existing Rotliegend NNW- feature evidenced by the blocking of the channel (Figure 4.27). A possible explanation may be the presence of a smaller scale fault that formed during the Late Carboniferous and propagated laterally after the deposition of the Rotliegend, postulated in the Early Triassic (see figure 2.17).

Since the Rotliegend channel only interacts with the southern portion of the NNW- faults (Figure 4.27), it is not possible to comment on the evolution of the northern lateral tips. Moreover, the most southern measurement point from the t-z analysis was the only plot that suggested a Pre-Rotliegend movement (Type IV profile, two phase movement, see MP1 on Figure 4.19) and was also the only intersection in which an eroded footwall scarp was observed on seismic (see seismic on Figure 4.19). From these observations, it is suggested that a smaller scale structure existed that may have later propagated into the larger scale NNW-_1 fault. This structure may have been a cutoff stretch fault (Figure 4.35) that accommodated strain variations on the large scale E-W_1 fault (Stewart, 2001). Further propagatation of the cutoff faults may have occured during Early Triassic NE-SW (Chadwick and Evans, 1995) orientated extension creating the NNW- faults currently observed.

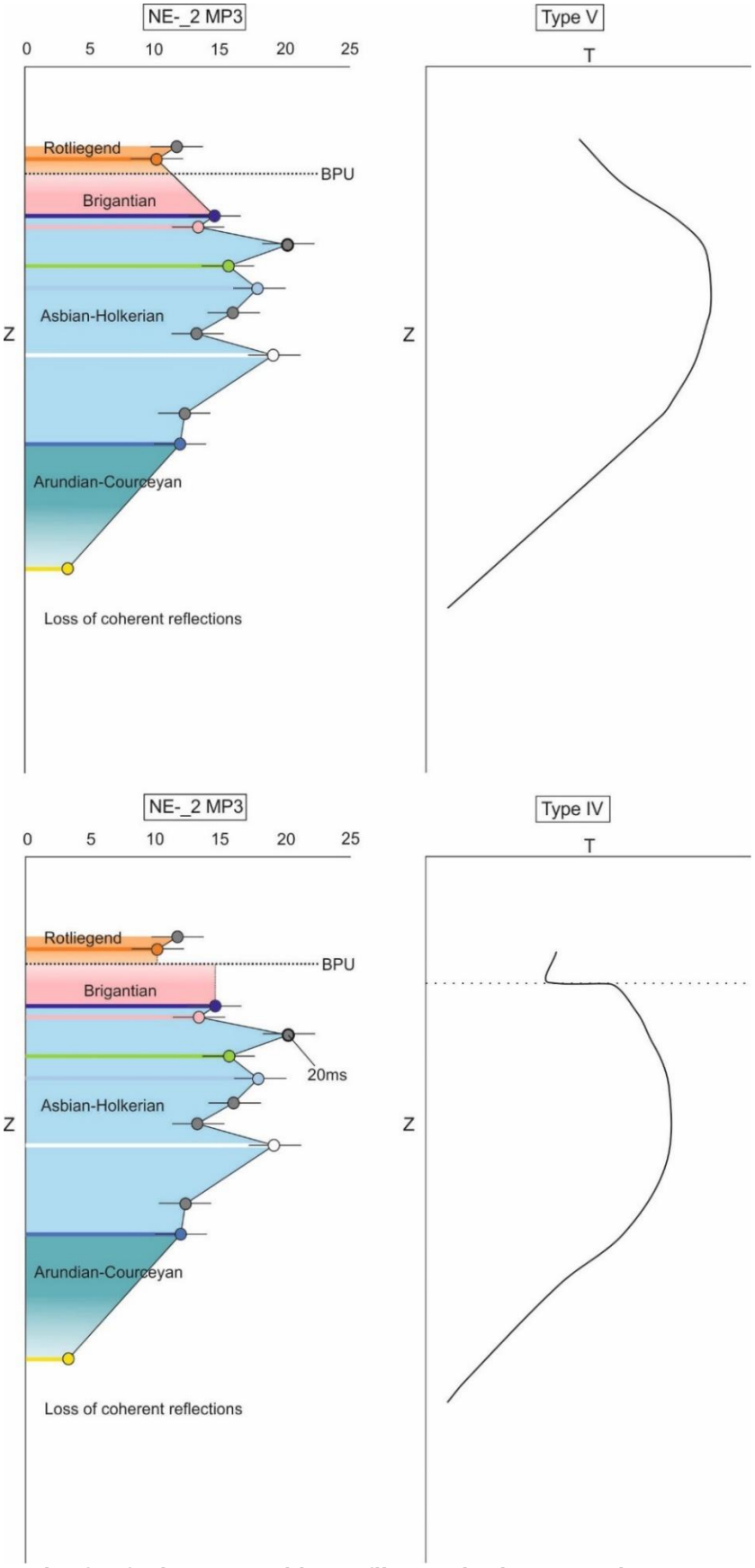


Figure 4.34 t-z plot for fault NE-_2. This profile can be interpreted as a Type-IV or Type-V profile

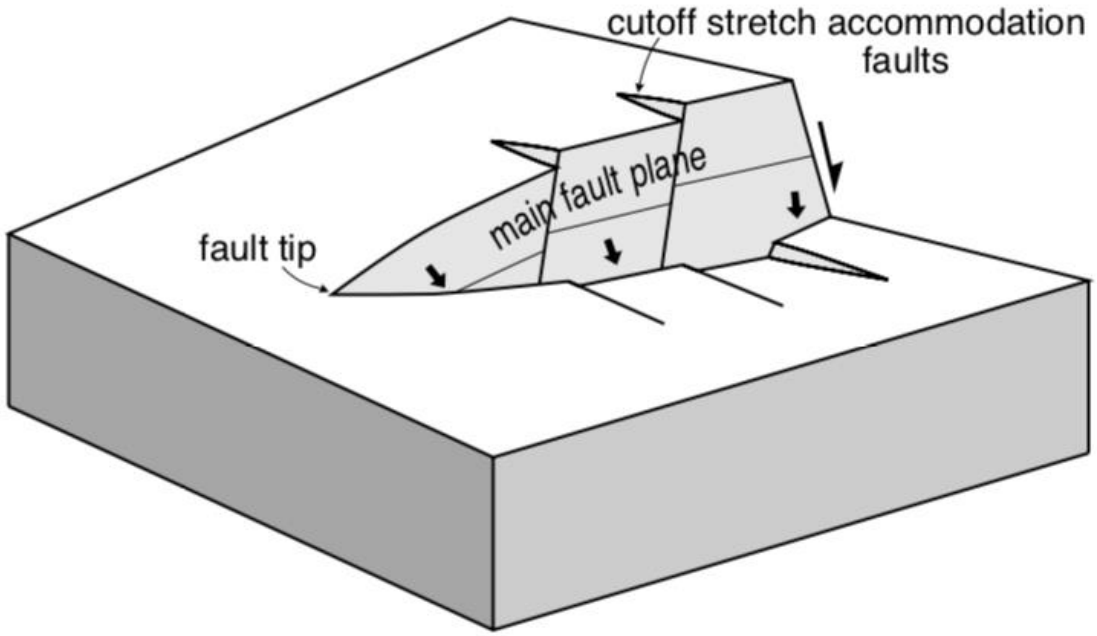


Figure 4.35 3D schematic of cutoff stretch accommodation faults that form perpendicular to a major normal fault (Stewart 2001). These cutoff faults form to accommodate the displacement variations along the major fault. This is proposed to have occurred on fault E-W_1, forming the initial NNW-SSE structures that later propagated into the observed NNW-SSE small scale faults (not to be confused with large scale NW-SE throughgoing/basement faults formed during the Caledonian orogeny).

4.6.1.4 44-49_NW-_P Faults

The 44-49_NW-_P faults exhibit three distinct movement histories as derived from the t-z plots and are subdivided into three main classes, NW-_P1 (Type-IV) and NW-_P2 (Type V) (Figure 4.15).

The history of the NW-_P1 faults began with a slight initial slip occurred during the before the Deposition of the Rotliegend as indicated by the significant step between Carboniferous and Rotliegend throws on the profiles of NW-_3, NW-_5, NW-_6 and NW-_7. A main phase of movement then occurred after the deposition of the Rotliegend. This may have been during the Early Triassic due to the extension orientation observed at this time (Chadwick & Evans, 1995). Similarly, to the case with NE-_2, it is unclear when this movement occurred as there has been clear lateral salt withdrawal in the Silverpit Basin (see seismic section on Figure 4.15) so any evidence of movement history has been erased.

For NW-_P2 faults, the continuous trend on t-z plots (see faults NW-_1 and NW-_2 (Figure 4.15) without sharp deviations in throw values close to the position of the BPU, it is inferred that slip on NW-_S2 faults occurred in a single phase. Given that the Rotliegend reflections show no evidence of syn-depositional activity, this slip phase most likely occurred after the deposition of the Rotliegend. Due to the decoupling and mobilisation of the Zechstein salt, the age limit cannot be constrained any further. Regional extension in the Triassic Hardegsen event (Zeigler 1992, see section 2.3.4.1.) occurring in an NE-SW extension direction may have been responsible for the formation of these faults, but the fact that they are not in close contact with the basement may suggest otherwise. This therefore implied the NW-_S faults have two distinct genetic origins.

4.6.2 Timing Summary for each T-Z Profile

4.6.2.1 Faults with only Type I (Beheaded)

Faults with Type-I T-Z distributions only incurred slip during the Late Carboniferous-Early Permian because no syn-sedimentary packages have been observed before the BPU erosion. Slip ceased before the BPU erosional event and these faults were not reactivated. Examples of sampled faults within this study include ENE-_1, WNW-_4, E-W faults, all located close to the basin margin.

4.6.2.2 Faults with Type I and Type II

Faults that exhibit both Type I and II T-Z profiles exhibit evidence for a main slip phase in the Late Carboniferous-Early Permian, prior to the BPU erosion. There is then an extensional reactivation phase, after the deposition of the Rotliegend. This magnitude of reactivated throw is locally variable along the fault strike with certain points along strike being unaffected (Type I). Examples of sampled faults within this study include WNW-_1, WNW-_2, and most A-E faults.

4.6.2.3 Faults with Type I and Type III

Faults showing Type I and Type III throw distributions incurred a main phase of slip during the BPU Hiatus. A slight reverse reactivation phase then occurred after the deposition of the Rotliegend, postulated to have occurred during the Late Cretaceous. The reactivated portions are locally variable along the strike of the fault resulting in both Type I and Type III profiles exhibited. Examples of sampled faults include faults E-W_1, E-W_2, (44-D_E-W faults) in the central Anglo-Dutch .

4.6.2.4 Faults with Type V

Faults that exhibit Type V profiles have a movement that has occurred after the deposition of the Rotliegend evidenced by laterally uniform stratigraphic thicknesses in footwall and hangingwall. The movement may have occurred during or after the deposition of the Zechstein and the mobility of the Zechstein obscures this timing any further. Examples from the case studies include faults NE-_1, some NW-_P faults (NW-_1 and NW-_2), NNW-_1 and NNW-_4 (most *44-D_NNW-* faults).

4.6.3 Patterns of Reactivation

Faults that are not reactivated after the deposition of the Rotliegend that only exhibit Type-1 t-z distributions include some ENE-, E-W in the northern Anglo-Dutch Basin, and some WNW- faults. These faults are from different structural style categories and orientations and therefore there must be other factors controlling their lack of reactivation history (see Chapter 6).

Faults with minor reactivations (Type II) are exclusively detached at depth from any underlying basement structure. This detachment may be a controlling factor in their lack of further reactivation, shielding them from basement stresses that would normally result in fault reactivation. Faults with beheaded profiles that have minor reactivations localised along their strike are usually controlled by proximity to cross cutting intersections (Figure 4.9 and Figure 4.24a). The possible explanation why some faults with beheaded profiles are reactivated and others are not are explored in Chapter 6.

Faults exhibiting moderate reactivation that is normal (Type IV) or Reverse (Type III) are typically Throughgoing or Superficial faults (See Chapter 6).

4.7 Discussion of Fault Forming Mechanisms

The structural styles of the faults across the ADB were initially classified in Chapter 3, section 3.8.2.1. into 'Throughgoing', 'Superficial' and 'Layer Bound'. This section discusses the possible fault forming mechanisms responsible for these structurally distinct fault types.

4.7.1 Layer Bound/Detached Faults

It has been shown that a mudstone detachment layer of Upper-Devonian-lowermost Carboniferous i.e the Tayport or Cemenstone Formations are most likely present below the A-E_WNW- faults (section 4.5.1.1.). Given that these faults are therefore not in direct mechanical continuity with underlying structure (see Figure 3.10), this strongly suggests that a mechanism other than regional tectonic extension was responsible for fault formation.

Furthermore, the orientation and sense of regional stress occurring at the suspected time of fault formation (mid-late Carboniferous) was N-S/NNW-SSE compression (see section 2.3.3.1.), and since they are not in mechanical continuity with the basement, structural inheritance from a basement fabric is also not a viable explanation. This palaeostress orientation is therefore not likely to result in the formation of WNW-ESE orientated extensional faults and strike-slip or transpressional/oblique-slip faults would be expected instead.

The A-E_WNW- faults are aligned sub-parallel to the structural contours of the Elbow Spit High (see Figure 3.13), a slope that has a present-day dip towards the SW of 0.15°. This angle is high enough to initiate sliding on a mechanically weak layer with low shear strength such as the postulated mudstone rich succession mudstone (Mauduit et al., 1997). Moreover, due to the Cenozoic regional tilting down to the NE, and the onlapping of the Middle-Upper Devonian sediments on to

the Elbow Spit High SW flank, it is likely that the slope of this high was steeper during Late Palaeozoic times. The existence of this palaeoslope during the late Palaeozoic is affirmed by the onlapping and infilling of ESP-4 (Figure 3.10).

Given that the onlap configuration strongly suggests the presence of a significant inclination for the basal detachment within the later Carboniferous, a hybrid mechanism of gravity gliding-spreading (Schultz, 2001) is considered plausible (Figure 4.36). It is therefore proposed that there was some component of gravity gliding of the competent Lower Carboniferous unit on the basal detachment, made possible by the low frictional strength of ESP-4 (Figure 4.37). This in turn, could have caused the internal extension of the translating overburden (ESP-3) in the form of the A-E_WNW- faults. This faulting is the straining of the translating and spreading sheet and includes the vertical thinning and extensional portion of the deformation (gravity spreading), in which vertical displacement is accommodated partly by the ductile mudstone succession.

For this mechanism to be a valid interpretation, the following factors must be present:

1. A slight slope present at the time of faulting (mid-Late Carboniferous). Although this is not essential if the next component is present in the system (Mauduit et al., (1997) demonstrates this process occurring on slopes of ~0° also)
2. A mechanically weak detachment horizon reducing friction.

Due to the gentle incline, it is postulated that the dominant mechanism for faulting in the imaged downslope region (A-E_WNW- fault array) is gravity spreading (by definition), with vertical shortening being accommodated by the ductile underlying mudstone layer. The effects of this can be seen on a regional

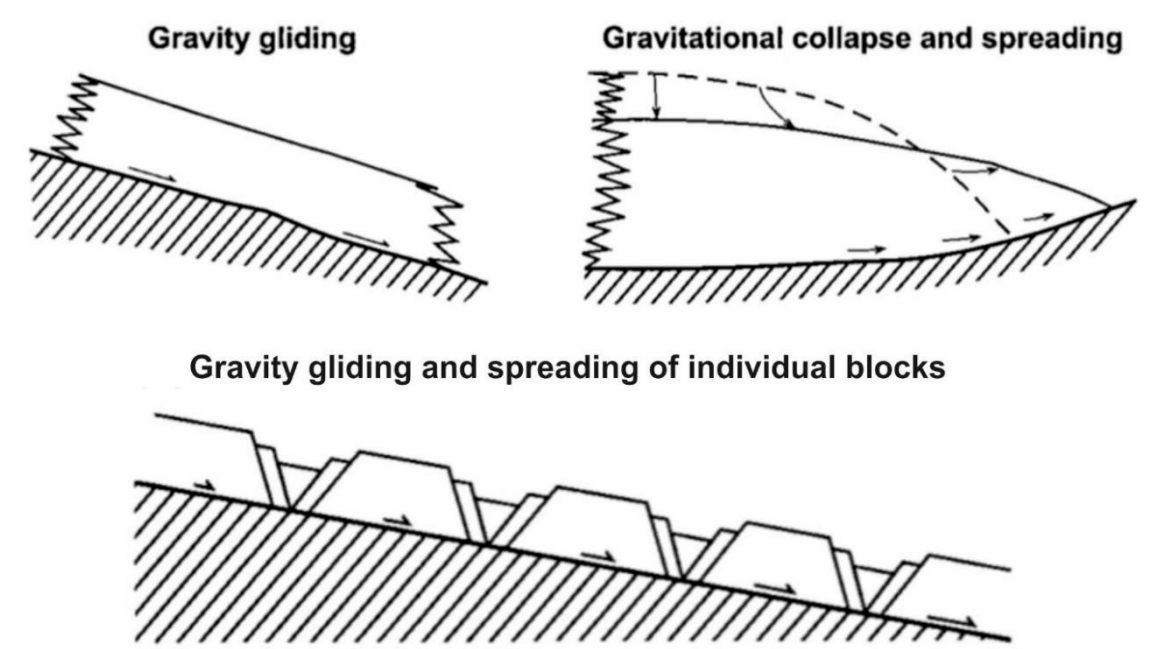


Figure 4.36 Schematic illustrating the simple systems illustrating the generally accepted concepts of a) gravity gliding and b) spreading (after Ramberg (1980) and c) Model of gravity deformation on multiple blocks in which the individual blocks are gliding but the large scale system is spreading after Schultz-Ela (2001).

section, where marker horizons appear deeper than towards the steeper portion of the slope where it is unfaulted (see Figures 3.7 and 3.10).

The gliding component of this deformation may have been initially activated by the footwall uplift resulting from the active extensional movement on the NW-SE bounding fault that has been dated to have begun in the Early Carboniferous from the correlation of reflections and offsets.

The high rate of subsidence at the beginning of the Carboniferous and the high sedimentation rates from the prograding delta system that followed in mid-Late Carboniferous times (see section 2.3.2.1) may have promoted the process by the development of overpressure in the underlying Late Devonian-Earliest Carboniferous aged mudstones that are postulated to be the detachment horizon (Osborne and Swarbrick, 1997).

The feasibility of the gravity gliding-spreading down the Elbow Spit High is further evidenced by the timing of movement on the A-E_WNW- faults. We know movement on these faults occurred during the time gap represented by the BPU hiatus (Lower Carboniferous-Rotliegend) as evidenced by the upper fault tip erosion. Therefore, the overburden would have been relatively unstable due to uplift and erosion during the Variscan tectonic phase at the end of the Carboniferous.

The minor reactivations observed on 3D seismic attributes and the offset of Rotliegend horizons in section, may have also been triggered by the NE-SW extension occurring on the NW-SE bounding fault in the Early Triassic Hardegsen event (Zeigler 1990, Ter Borgh et al., 2018) (see Figure 2.17), by footwall uplift on the Elbow fault acting to steepen the slope slightly. Conversely, the lack of significant reactivation observed on the A-E_WNW- faults may also be due to the detached nature of these faults, decoupling them from regional extensional basement stresses. Similar scale examples of arrays of extensional faults detaching in an underlying mudstone layer with an overlying salt layer are also observed on the 'Piano Key Faults' in the Levant Basin (Kosi et al., 2012). Just as the Piano Key Faults are related to mega slumps due to Messinian drawdown, the detachment faults on the Elbow Spit Platform may be related destabilisation of the Carboniferous delta top during the Namurian, due to the high influx of sediment (see LC1b on Figure 2.10). This high sediment influx from the northerly source (Fraser et al. 1990) may have also generated overpressure in the underlying fine grained succession.

The Canyonlands Grabens of SE Utah provide a classical example of dual spreading/sliding driving the extension in an overburden in which the detachment layer is represented by the Paradox Evaporite Formation (Figure 4.28)(Schultz-Ela, 2001).

In summary, it is therefore proposed that the A-E_WNW- faults formed as an indirect result of tectonic processes, due to gravity spreading and gliding mechanisms triggered by the dynamic slope of the Elbow Spit High, due to periodic movement on the Elbow Fault that bounds it to the North East (Figure 3.8b). The detachment behaviour is a consequence of weakening of shear resistance in a layer, which is a result of overpressure due to disequilibrium compaction. It can therefore be argued that if this proposed mechanism is correct, they are only an indirect consequence of regional extension.

4.7.2 Throughgoing and Superficial Faults

Given the fact that throughgoing faults produce structures that have an apparent alignment with the directions of extension with the regional stress orientations, they are interpreted to have been formed due to regional tectonic stresses. The superficial faults appear to be aligned with throughgoing structures, possibly affected by stress perturbations caused by these throughgoing structures (Figure 3.35), similar perhaps to stress perturbations leading to preferential joint directions (Rawnsley et al., 1992, Bourne and Willemse, 2001). A result from this is that they are therefore somewhat shielded or 'blocked' from further reactivation, with the reactivational strain being concentrated on the throughgoing feature due to their large vertical and lateral extent are closely coupled with basement structures, resulting in them being active more frequently through time (Walsh et al. 1991, see Chapter 6).

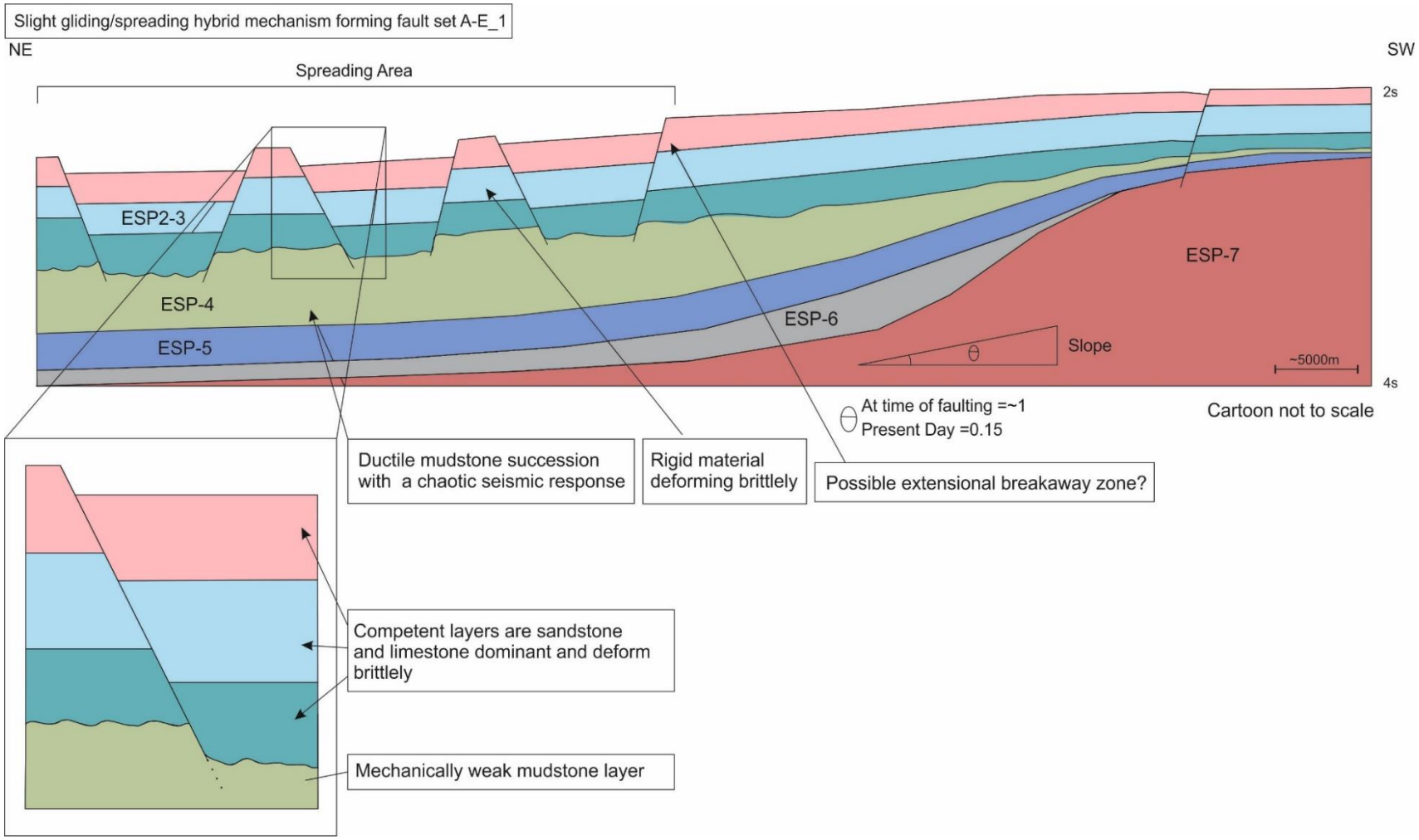


Figure 4.37 Schematic NE-SW cross section transecting the ESP illustrating the proposed gravity gliding-spreading hybrid mechanism that is forming the A-E_WNW- faults. Faults are tipping out into the mechanically weak mudstone layer that is accommodating the strain and displacement of the rigid fault blocks by ductile flow

4.8 Conclusions

1. Five main t-z profile shapes have been recognised on faults within the Pre-Zechstein succession across the study areas. Three main end member types are established in which these five sub types fit into
    a. Beheaded Single Phase – Type I
    b. Beheaded Two Phase – Type II, III, IV
    c. Post-Rotliegend Single Phase – Type V.
2. Faults may exhibit more than one type of profile due to variations in local reactivation along strike i.e. Type I and Type II. A Type V fault will only exhibit Type V profiles as they are inherently single phase.
3. Three main structural styles are recognised for the faults in the case study areas; superficial/peripheral, detached and throughgoing.
4. The timing of sub-salt structures that offset the Rotliegend section, terminating into the Zechstein, cannot be determined for certain due to the complex superimposition of at least 6 tectonic episodes in the basin.
5. The beheading of the majority of faults at the BPU and non-imaging of most fault lower tips precludes a definitive analysis of fault type and history, t-z analysis however can be used to give an estimation of these pre-erosional/non-imaged/non-preserved positions.
6. The presence of a major decoupling layer in the mobile Zechstein halite units has a profound effect on the structural evolution of fault systems in the basin. The later deformational events invariably induce some deformation of the salt with flow both laterally and vertically, and this destroys any earlier imprint of upwards fault propagation from the pre-Zechstein succession. Fault

propagation tip monoclines that are indicative of syn or post depositional movement are therefore not preserved to aid in fault dating.

7. The original thickness of the salt layer in the central Anglo Dutch Basin (before modification through later deformation), was thick enough for the salt to accommodate the strain accumulating on underlying faults during Mesozoic reactivation in a ductile manner and without there being an expression in the overburden (Withjack & Calloway 2000, Figure 4.32).
8. The Zechstein is acoustically opaque in most areas, and found above most case study faults. The faults may have propagated into the Zechstein but it is unresolved. How far they may have propagated can be crudely estimated by the gradient of the 'open top' profile.
9. The t-z and t-x analysis has highlighted subtle differences in movement history of faults previously assumed to be genetically similar (i.e. Type-IV and Type V NW-_P and NE- faults). T-x analysis has also highlighted areas along strike that have a different reactivation profile.
10. T-x analysis has shown that cross-cutting geometries of faults form complicated reactivation patterns that are determined by the intersection geometry. Local reactivations are accommodated on individual fault blocks that are preferentially aligned to the orientation of extension or compression.
11. Layer bound and peripheral class faults have exclusively normal throws with only normal (extensional) reactivation components. Their formation is usually linked to the relief produced by, and movement on, larger scale parallel or sub-parallel faults.

12. Throughgoing tectonic faults have been reverse reactivated through geological time. This is likely due to their large vertical extent enabling a prolonged close coupling with basement stresses.

13. WNW- oriented detached, normal faults in the Lower-Carboniferous – Upper Devonian on the Elbow Spit Platform that were previously attributed to forming due to regional extension, are proposed here to be formed due to gravity gliding and spreading mechanisms triggered by the dynamic footwall of the Elbow Fault. This suggests that not all faults in the Pre-Zechstein succession are formed due to regional stresses and could be instead an indirect result of extension rather than the extension itself.

Chapter 5

FAULT INTENSITY AND SPACING IN THE PRE-ZECHSTEIN SUCCESSION

5 Fault Intensity and Spacing in the Pre-Zechstein Succession

5.1 Introduction

5.1.1 Project Rationale

Characterizing the density and distribution of faults and fractures within a rock volume is of key importance to the assessment of how fluids such as hydrocarbons will flow through the unit. The presence of faults and fractures in a reservoir can either enhance or retard fluid flow and hydrocarbon production. Fracture networks such as those in low permeability sandstones and mudstones can provide conduits for gas migration and consequently enhance the permeability and productivity of the reservoir (Dewhurst et al., 1999, Caine et al., 1999, Baytok and Pranter, 2013).

Conversely, significant problems of induced seismicity can occur during fracking operations if faults are present. If hydraulic fractures intersect a pre-existing fault that is close to its critical stress state, the increase in pore fluid pressures reduce the effective normal stress, inducing slip on the fault (Clarke et al. 2019). A situation similar to this occurred in Blackpool in 2011, in which an inverted Variscan fault in the Bowland basin was reactivated in a strike-slip sense during fracking operations by Cuadrilla at Preese Hall 1 exploration well (Clarke et al 2014a). The presence of this fault was unknown, as it was not detected by 3D seismic data prior to the fluid injection (Clarke et al., 2014a, Davies et al., 2013).

It is clearly imperative for operators of shale gas plays to identify faults of all sizes prior to drilling, and one of the motivations of this thesis study has been to establish the density and distribution of faults affecting sediments of Carboniferous age on the UK continental shelf and onshore basins with a view to providing

background on the possible range of fault densities to inform future exploration activities.

Previous studies have shown fault systems follow fractal size distributions (Walsh et al., 1991, Marrett and Allmendinger, 1992, Childs et al., 1990) and therefore a quantitative characterization of the density of seismically resolvable faults can be scaled down using a power law to estimate the sub-seismic fault population density if the fault size is known (Yielding et al., 1992).

The Pre-Zechstein succession across the Anglo-Dutch and East Pennine Basins contain prospective reservoirs for tight gas (Langford et al., 2014b) and shale gas (Hughes et al., 2016, Slowakiewicz et al., 2015, Andrews, 2013) and therefore an estimation of seismic scale fault densities in this interval should be a useful constraint for input into future exploration campaigns.

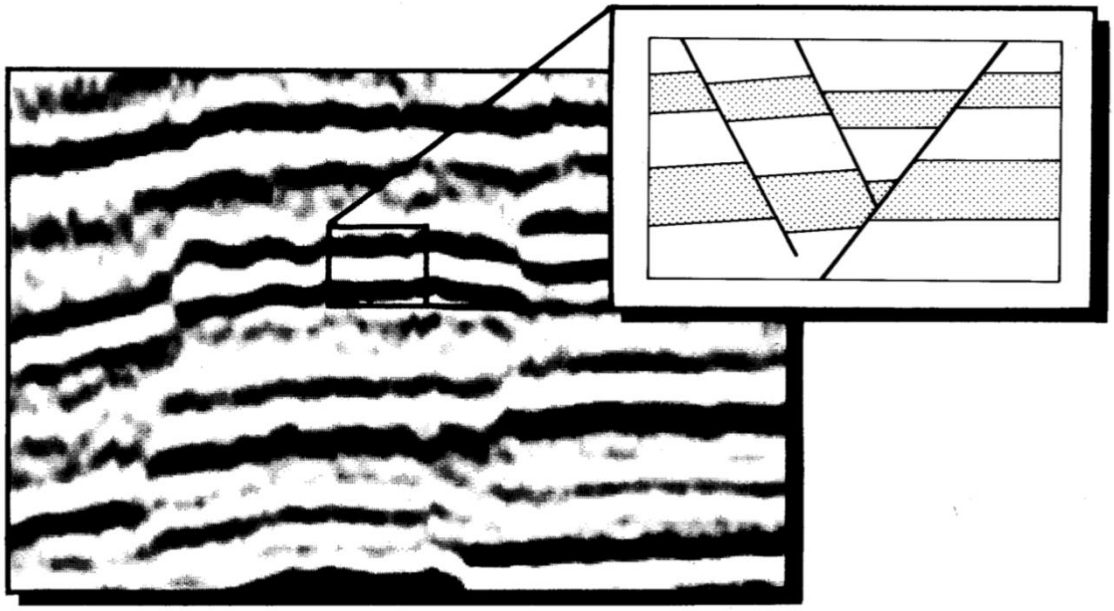


Figure 5.1 Illustration showing the possibility of faults that have offsets below seismic resolution. Medium to large offsets can be characterised by analysing seismic interpretation. (after Yielding et al., 1992)

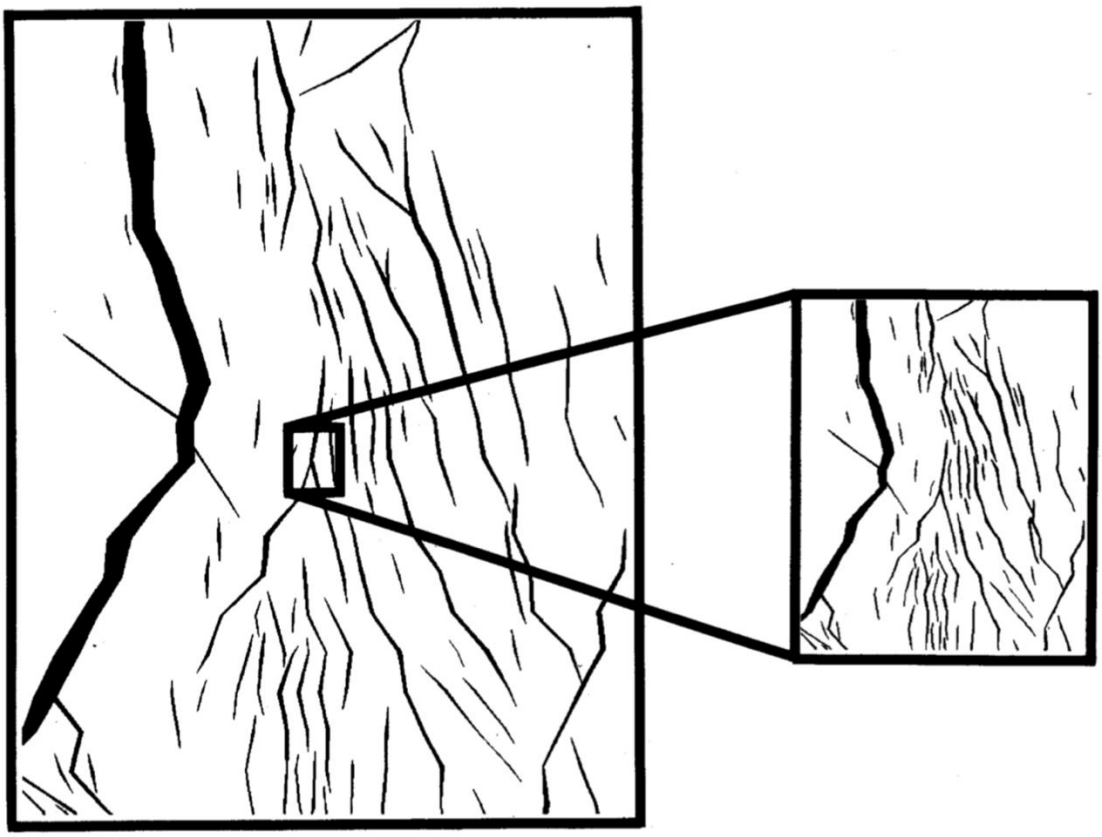


Figure 5.2 Schematic representation of a fractal/self similar fault pattern (after Yielding et al., 1992)

5.1.2 Aims and Research Questions

The aim of this study is to record and quantify the occurrence of resolved faults at seismic and map-scale the Pre-Zechstein (Devonian-Rotliegend) succession over a range of available datasets across the Pennine and Anglo-Dutch Basins. This study was conducted using a number of case study areas that have been selected based on the Pre-Zechstein imaging being of the best quality (Figure 5.3).

The key research questions this chapter will attempt to answer are:

- What is the overall density of faults within the PZS, in each case study area? How does this density of resolvable faults vary at different locations across the basin? What causes this variation?
- How does fault spacing vary between sets? Why are certain fault sets closer spaced than others?
- Is there a data type/resolution observational bias for fault distribution? Is the older onshore 2D seismic data insufficient in resolution to image faults compared to the offshore 3D?
- What implications does the spatial characterization have for the potential fluid flow and production from reservoirs?

5.1.3 Fault Intensity

Fault and fracture abundance/density in this study is defined as being the amount of faults intersected per unit distance (Walsh et al., 1991). The faults do not have to be genetically related and can be of varying attributes and orientations. Fault and fracture abundance measured by scanlines is normalized by the measure

of fault/fracture intensity. Fault/fracture intensity is the ratio of the number of faults per unit length along a sample line (Ortega et al., 2006).

5.1.4 Fault Spacing

Fault and fracture spacing is defined as the horizontal distance measured normal to genetically similar, parallel faults that form coevally (Solvia et al., 2006). In this study, fault spacing refers to the measured distance between two faults belonging to a specific characterized set.

Fault spacing is dependent on fault displacement magnitude and distribution (Crider and Pollard, 1998, Cowie and Roberts, 2001) and is a response to the stress history within the area covered by the fault population.

This study has quantified the overall fault intensity (fault abundance) and fault spacing for the pre-Zechstein succession in a number of case study areas using an established sampling method that enables the comparison of data collected from various types over a range of resolutions/scales. Alternative scanline methods were evaluated, but the selected method was preferred due to its suitability for the range of data types available to this study.

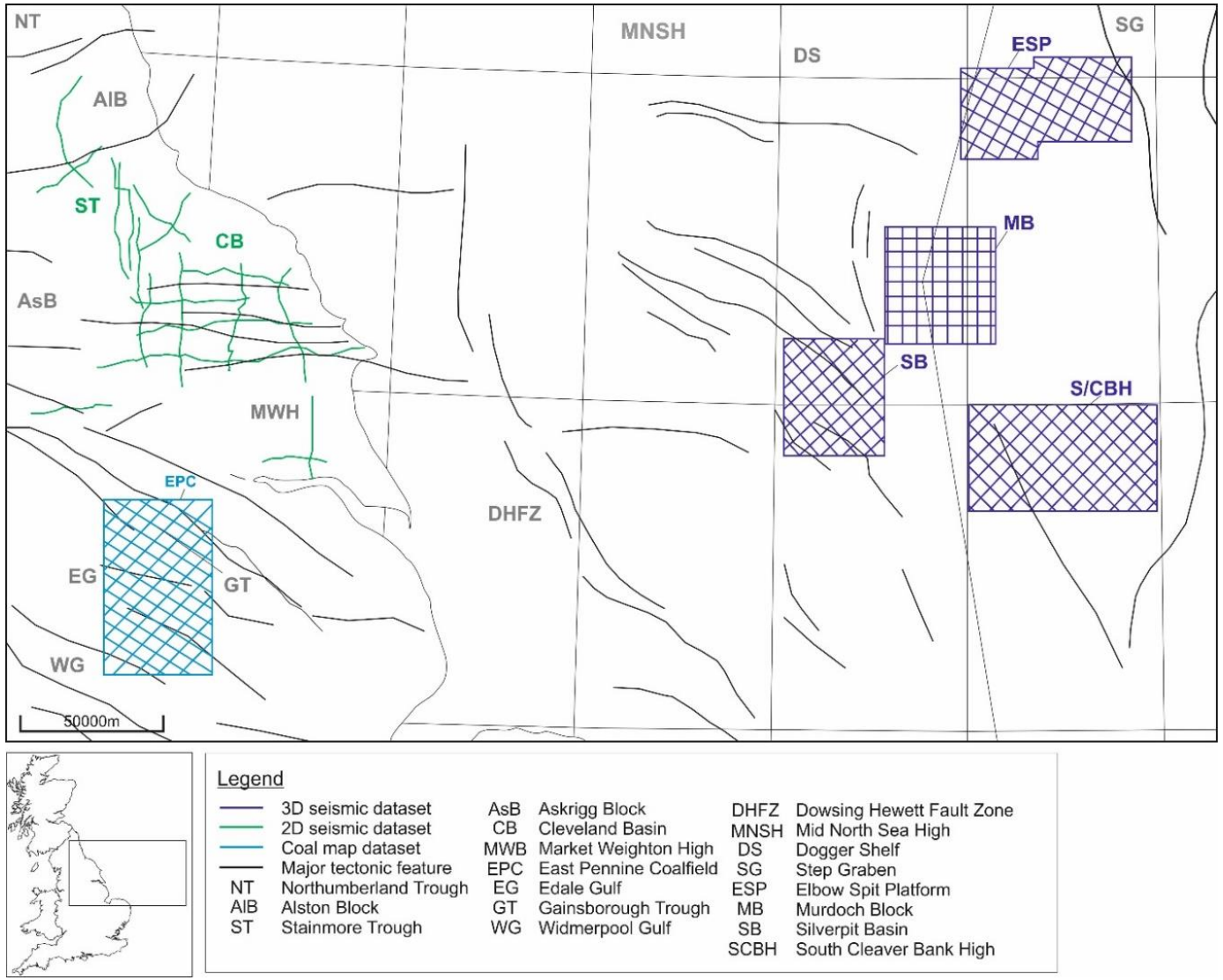


Figure 5.3 Map of the study area indicating the case study locations and their scanline survey geometry. The main structural features are incated and data types are colour coded.

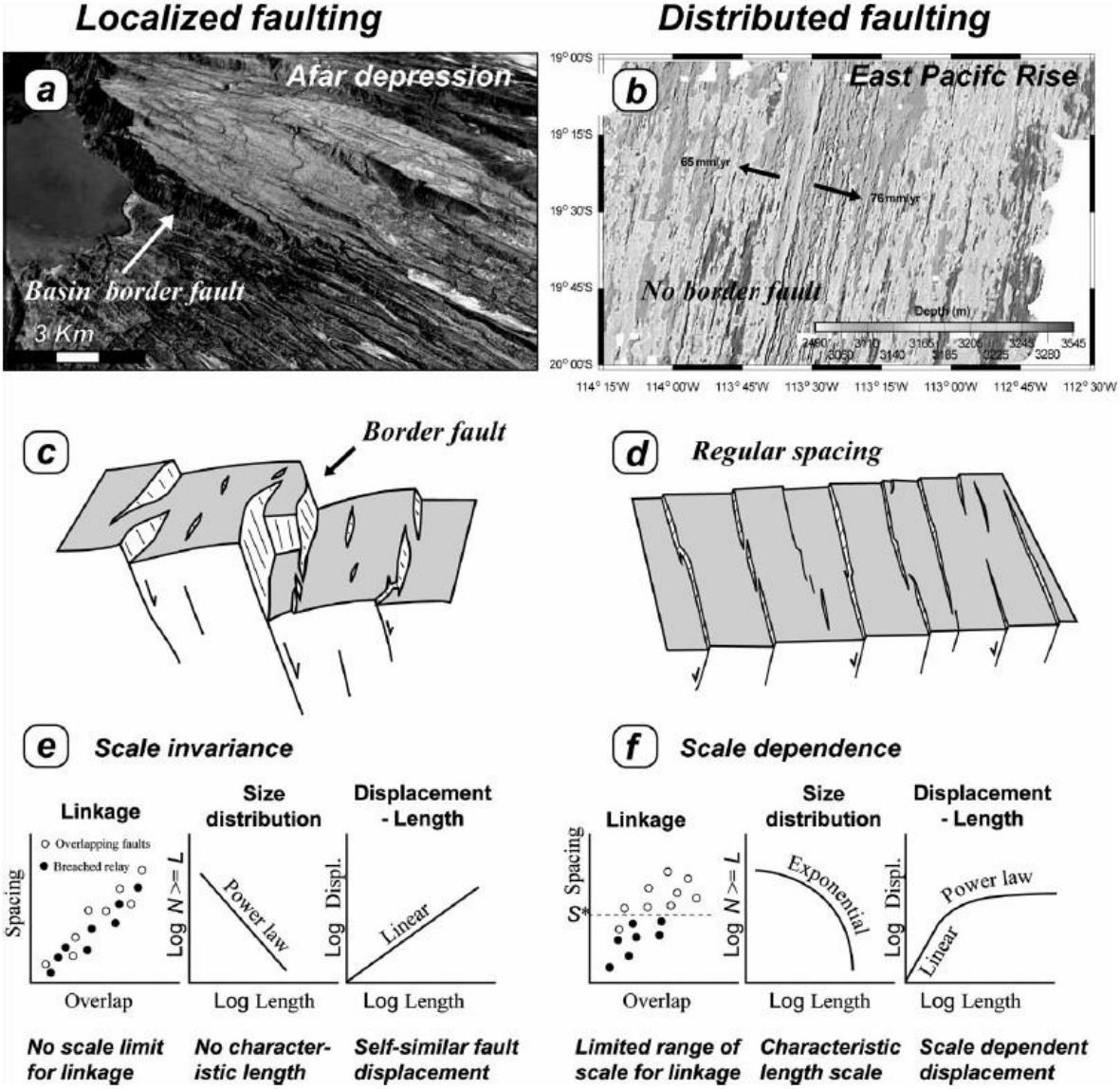


Figure 5.4 Two end-member fault population geometries with different spacing characteristics a) normal fault population with faulting localized on few large faults b) normal fault population with distributed faulting along many regularly spaced smaller faults with equal displacements c) and d) show a schematic view of the fault geometries figures e) and f) are the statistical properties characteristic to each case (Schultz et al., 2010).

5.2 Chapter Specific Datasets

The locations of each case study area within this study is illustrated by Figure 5.3. The seismic resolutions and fault detection thresholds of each dataset are presented in Figure 1.8for various areas, stratigraphy and data types.

5.2.1 3D Seismic Volumes

Selected areas from the PGS Megamerge (see section 1.5.1.1.) time-migrated 3D seismic volume were used in this study. Time-migrated data was used as fault interpretation could be performed more accurately. Throw measurements were converted from TWT to metres where necessary using the average P-wave interval velocities from local wells.

The effective throw detection threshold (ETDL) for each dataset was calculated from the dominant wavelength $\lambda = v/f$, where λ is the dominant wavelength λ, V is the P-Wave interval velocity derived from local wells, and f is the dominant frequency as computed by the Petrel function (see section 1.5.1.1.). The ETDL values were estimated to range from 42-79m in the Westphalian-Namurian succession and 51-110m in the Visean-Tournaisian (Figure 1.8).

The error for these EDL values consists of three components; 1) inaccurate or unrepresentative interval velocities from the nearest well, 2) inaccuracies in estimating the dominant frequency for the interval on the seismic data and 3) the threshold for the vertical resolution of reflection offsets may be less than $\lambda/2$ in certain areas/data types. An error of +-150ms is considered for 1) as a rounded average of the different ranges of Rotliegend-Carboniferous P-Wave velocities in the wells across the basin. The error for 2) is estimated as +-5htz due to the observational inaccuracy of the average of the dominant frequency for an interval. The combined error in the calculation of the dominant wavelength is therefore +-

15m. The error for 3) is already at the upper limit as the ETDL may be less than λ/2 in shallower PZ areas and areas of better quality imaging, giving ETDL values as λ/3 or λ/4. The value of λ/2 was therefore chosen as a consistent upper limit across all datasets.

5.2.2 2D Seismic Lines

The 2D seismic lines used in this study were selected from the UK Onshore Geophysical Library archive and have a variety of acquisition and processing parameters. Seismic lines were selected from the database and a good grid coverage was acquired. Due to the differences in acquisition dates and processing parameters, the seismic lines have varying data qualities which is clearly apparent when arbitrary transects are constructed across large areas. The minimum throw detection values for the 2D data in the ST-CB area range from 40-44m in the Westphalian-Namurian and 44-102m in the Visean-Courceyan (Figure 1.8).

5.2.3 Coal Mine Fault Map

A high quality, regional fault map for the Barnsley/Top Hard Pseudoseam was used to quantify the occurrence and distribution of faults in the Pre-Zechstein succession on a smaller scale of measurement (Figure 5.5). The 1300km^2 map is derived from extensively mined coal seams within the Westphalian. fluvial/deltaic succession of the East Pennine Coalfield and was digitized by Bailey et al. (2005). The dataset is an exceptional resource in covering a large area with a large quantity of faults mapped (n=7862). Bailey et al. (2005) used this dataset for analysis of fault population scaling properties and spatial variations of fault length and maximum throw in their study.

The Barnsley/Top Hard Pseudoseam is the most extensively worked coal seam throughout the East Pennine Coalfield and occurs stratigraphically within the upper Middle Coal Measures (Westphalian C). The map was generated from coal seam abandonment plans that were produced cumulatively during the 20th Century at a scale of 1:2500 (1cm=25m). The raw data recorded is in the form of spot heights, fault traces and throw values recorded on average every 100m along each fault trace. Most of the faults in the area are normal (Rippon, 1985), hence the throw values are a good proxy for true displacement values. The fault and seam elevation data were digitized to build the current fault map.

The quality and extent of the mine working data varies with the age of the workings. The highest quality data was derived from 1950s workings, whilst the most complete version are based on plans of the pre-1970s. The finalised map includes the highest quality data available for each mined area (Figure 5.5). The dataset includes fault traces with throws as low as ~1m (Figure 1.8).

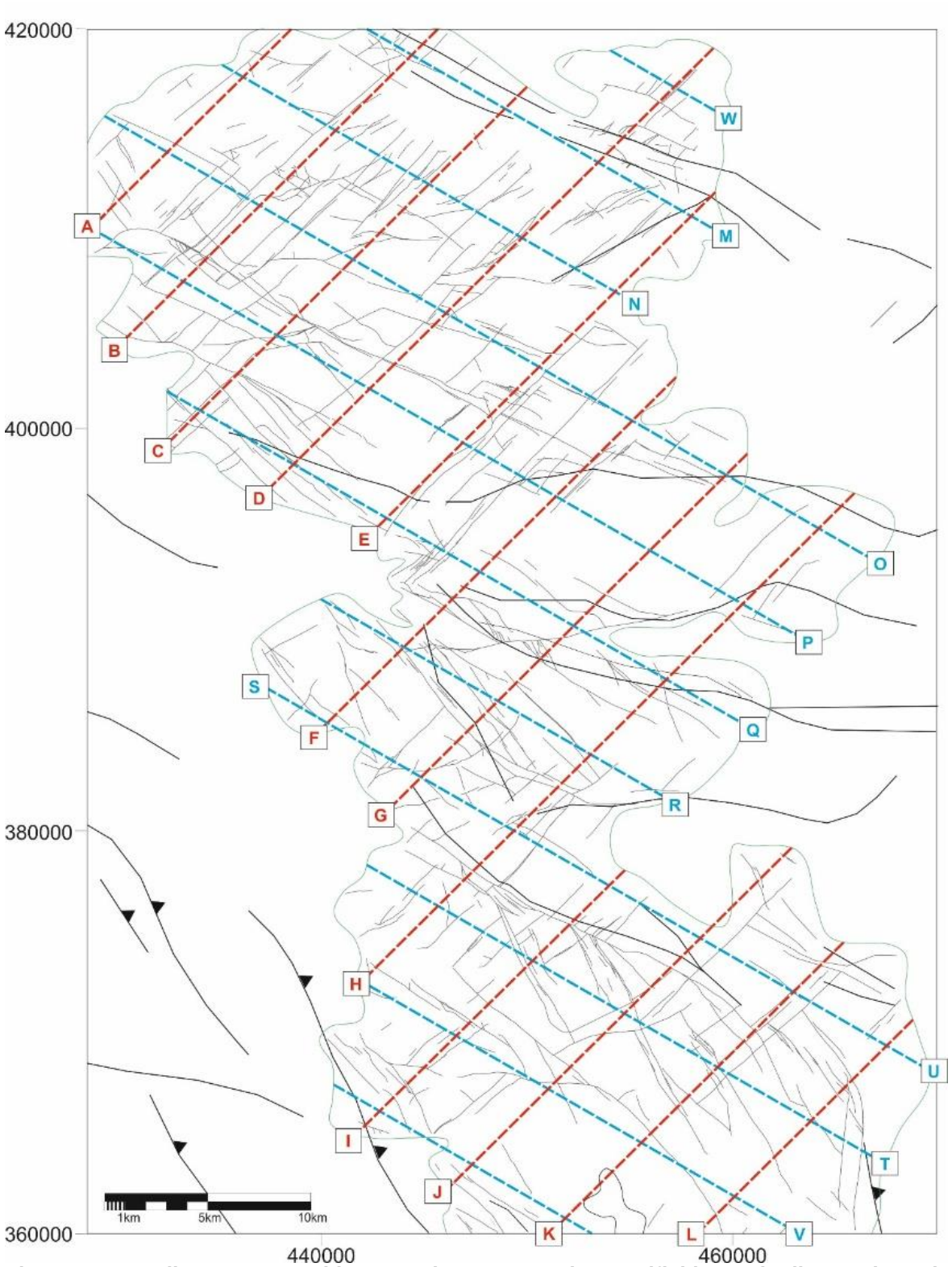


Figure 5.5 Scanline transect grid across the East Pennine Coalfield map (Bailey et al 2005). Transects have been superimposed over the Barnsley/Top Hard Pseudoseam Map. The map shows the position of all faults with a throw greater than 1m.

5.3 Methods

5.3.1 3D Seismic Dataset Methods

5.3.1.1 Sampling 3D Seismic Dataset using 1D scanlines

The approach used to quantify the presence and spatial distribution of faults was by the construction of a grid of 1D scanlines on which measurements of various fault attributes were recorded (Yielding et al., 1992, Gillespie et al., 1993, Priest and Hudson, 1981, Solvia et al., 2006). The 1D scanline approach was chosen and preferred over, for example box counting methods (e.g. Gillespie et al. 1993) in order that the distances and spacings could be measured at different scales of observation and on different data types.

5.3.1.2 Study Area Selection

The case study areas across the Anglo Dutch Basin were ideal as a basis for quantifying the fault spacing because of the clarity of fault trace expression at the Top Rotliegend horizon map. This horizon map typically reveals the nature of the complex fault patterns at this level, and when coupled with the generally sharp seismic imaging of faults in the Pre-Zechstein succession in the form of seismic discontinuities this provides a sound basis for a comparative study of fault density and spacing. The stratigraphic host intervals for the measured faults varied in each case study as the pre-Zechstein subcrop in the Elbow Spit Platform is the Rotliegend and the Lower Carboniferous, whilst the Pre-Zechstein subcrop in the Silverpit Basin and Cleaver Bank High is the Rotliegend and Westphalian.

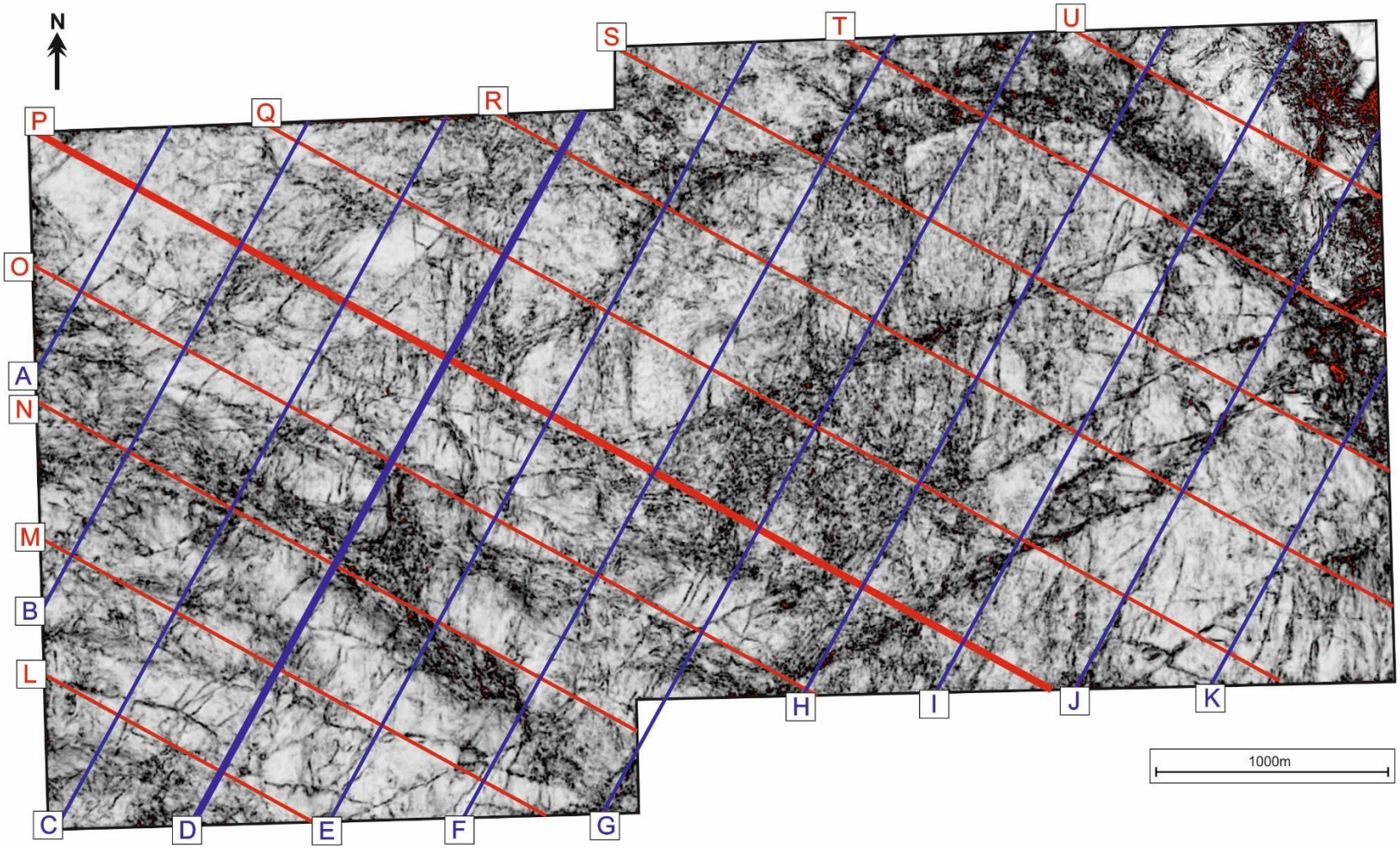


Figure 5.6 Scanline survey across the Elbow Spit Platform. Example transects in later figures are indicated by bolder coloured lines.

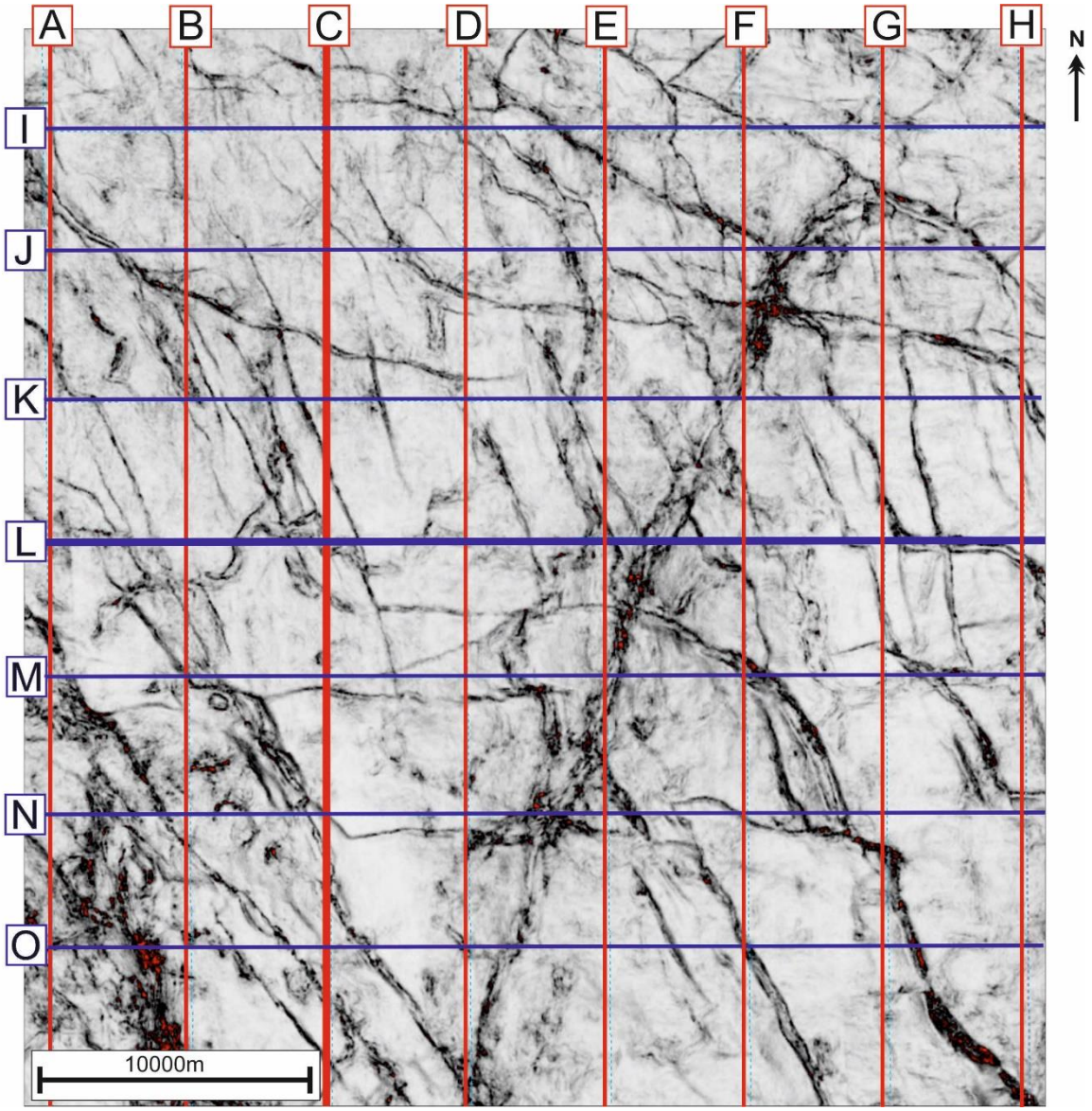


Figure 5.7 Scanline survey across the Murdoch Block. Positions of example transects in later figures are indicated by bolder coloured lines.

5.3.1.3 1D Transect Measurements

A measurement of the distance between faults intersected by the scanline were made on the Top Rotliegend horizon map (i.e. Figure 5.6). This horizon was chosen as it was the most laterally continuous and the faults offsetting this horizon often penetrated at least 1000ms downwards through the Pre-Zechstein succession, thus providing a representative measure of the fault distribution for a considerable portion of the entire Carboniferous interval. Where the faulting within the Carboniferous interval was not adequately represented by the TRot horizon map, measurements were made at some constant value of two way travel time (typically 200ms) beneath this horizon.

The distance was recorded for each fault intersected by the scanline along with other fault attributes including orientation, throw sense, dip direction, and fault type. For certain scanlines in which a laterally correlatable intra-Carboniferous reflector could be imaged, throw was recorded where the 2D seismic scanline (~BPU -100ms) was intersected. An approximate vertical fault trace length was also recorded for these examples. At least two of these ‘exact throw’ scanlines were constructed for each area in which this data was collected (Figure 5.12). Data quality was found to play a significant role in the accurate interpretation of the smaller faults in particular, and this proved to be a significant limitation on the application of a statistical approach. An example of the impact of data quality on fault interpretation is shown in Figure 5.11.

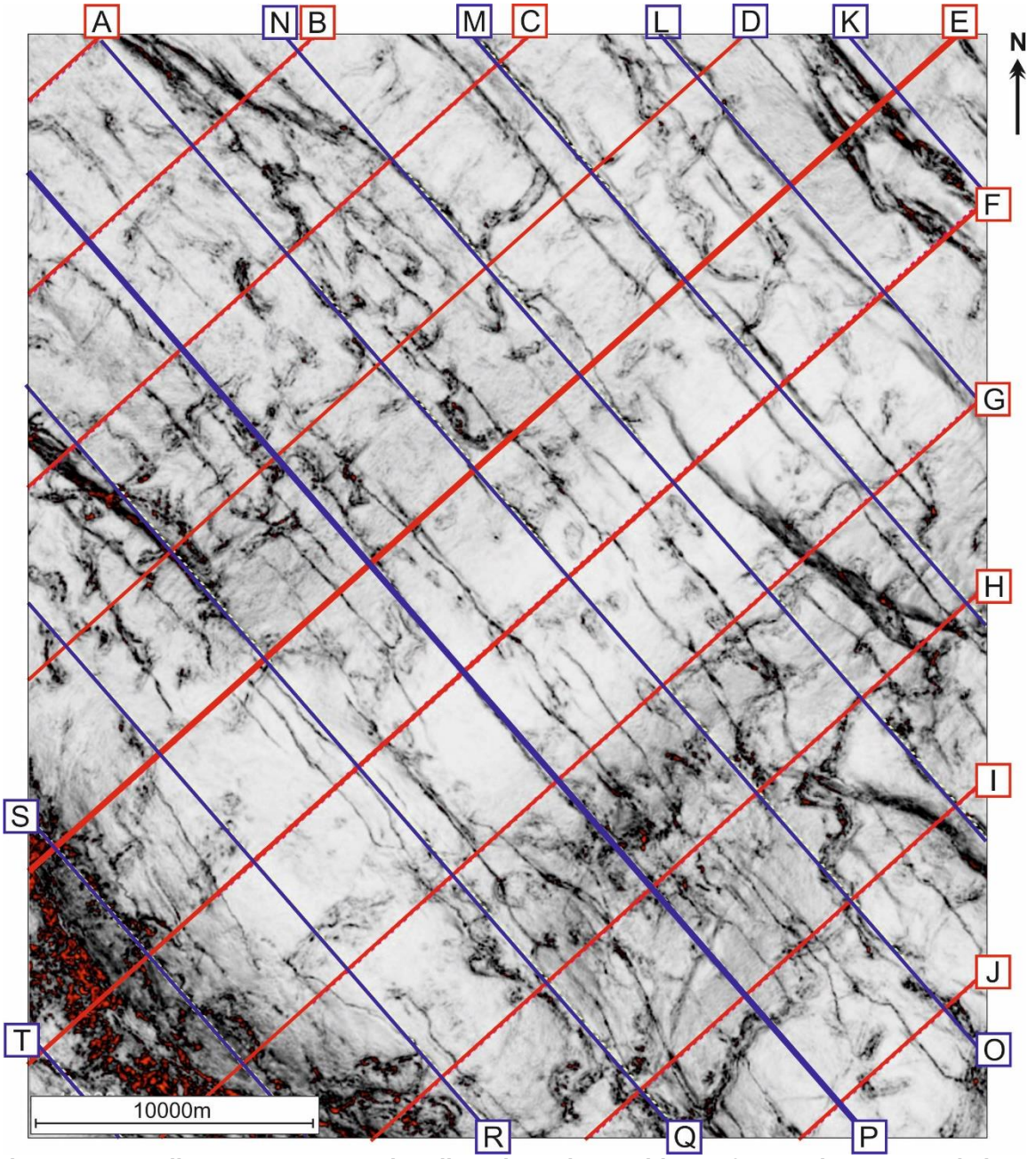


Figure 5.8 Scanline survey across the Silverpit Basin. Positions of example transects in later figures are indicated by bolder coloured lines.

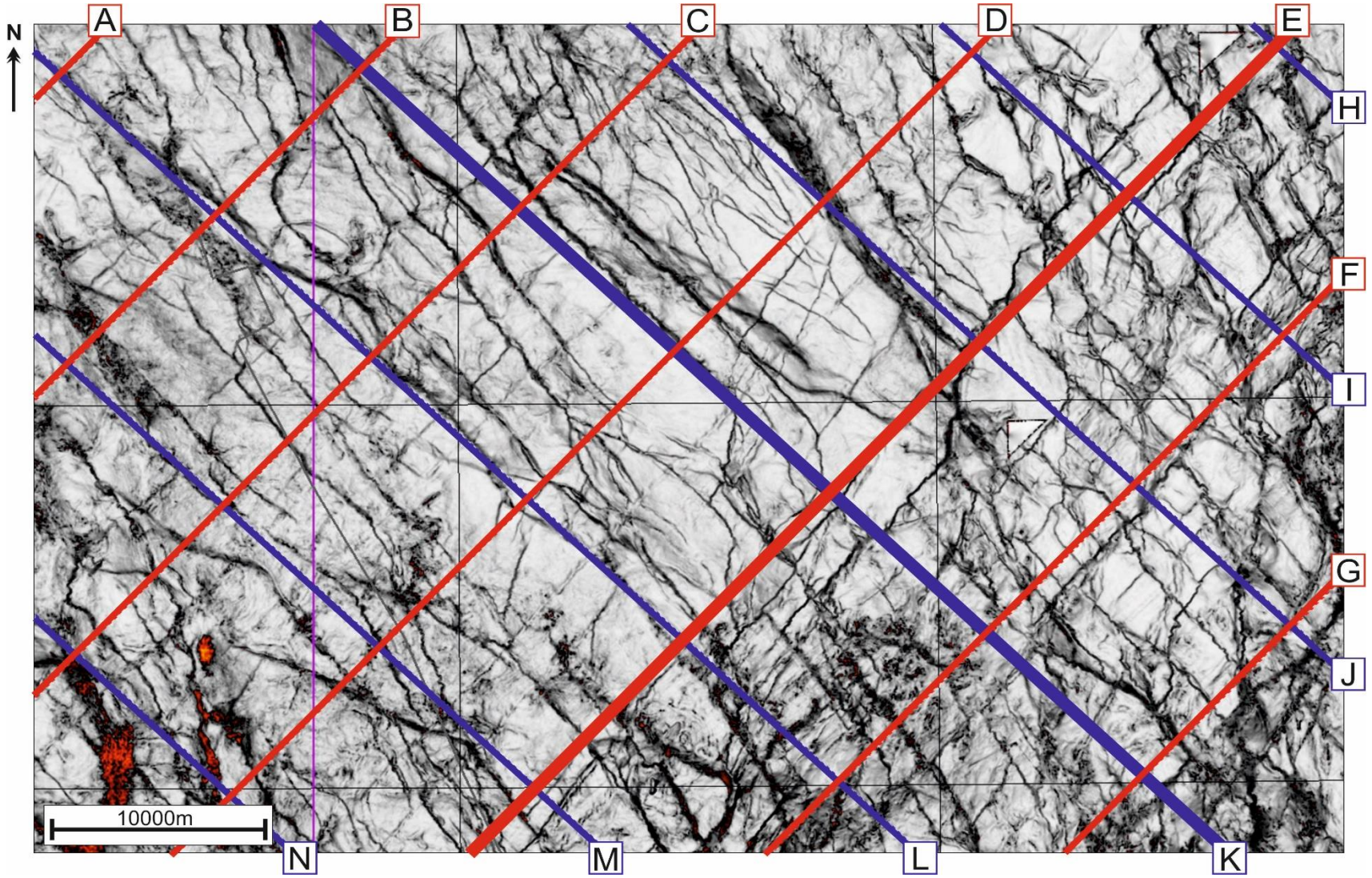


Figure 5.9 Scanline survey across the Cleaver Bank High. Example transects in later figures are indicated by bolder coloured lines.

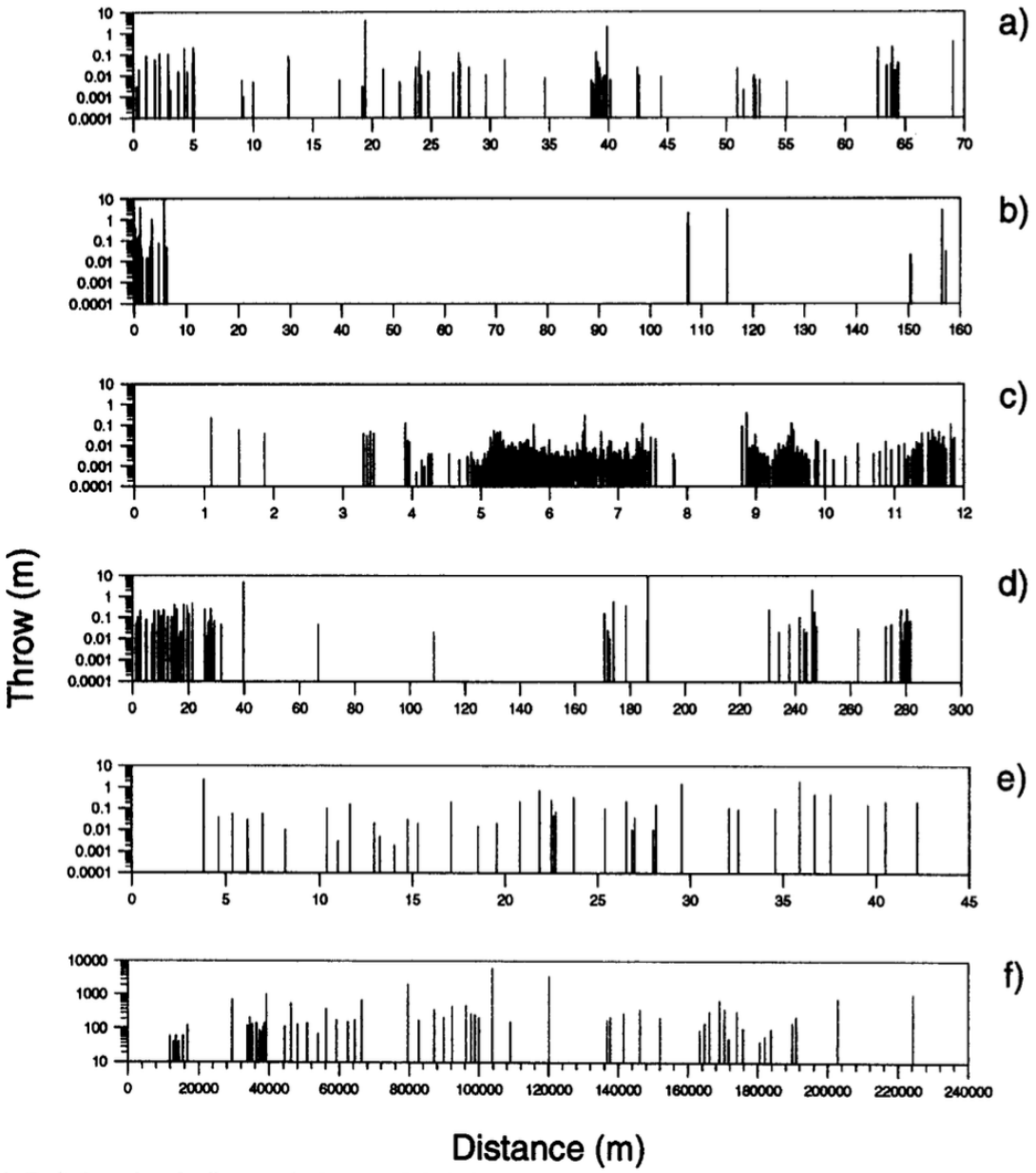


Figure 5.10 Examples of throw logs formed from 1D sampling scanlines from six other fault datasets, from various data types and localities: a) Belah Scar - Outcrop b) Round O – Quarry c) Star Crossing Quarry d) Whitworth Quarry, Lancashire e) Jamestone Quarry f) Regional seismic line from the Northern North Sea. After (Gillespie et al., 1993). The scanlines record faults at various scales of measurement and there is no obvious trend or similarities obserevd across these datasets. The spacing of faults recorded on transects a-d and f appears to be more random while transect e appears to record a more regular, systematic fault spacing.

5.3.1.4 Dataset and Scanline Production

Spacing values were plotted as distance between faults (x) versus relative size creating a scanline transect image. This presented the frequency of fault occurrence, regularity of spacing and overall density for the fault populations. For the selected scanlines in which throw was directly measured, throw was plotted as the Y-axis. Dip was also expressed by the direction of the line (Cartwright and Jackson, 2008) (see Figure 5.12 for an example).

An important caveat is that the differences in resolution and fault detection thresholds between measurements from seismic data and maps must be taken into account for a meaningful comparison between different datasets to be made. It would be expected that fault density characteristics would vary as a function of fault resolution. Two areas with similar fault populations (displacement, length, density) might appear radically different in any statistical measure, if the mapping of faults was conducted using significantly different resolution methods.

The size of faults are assigned to the fault intersection measurements using the proxy of maximum throw/lateral offset based on the scaling relationship between maximum displacement and fault length (Dawers et al., 1993, Scholz and Cowie, 1990). Fault Tmax values were previously measured for the faults within each case study area (see Chapter 3 sections 3.2.3., 3.3.3., 3.3.4., 3.5.3. and 3.6.3).

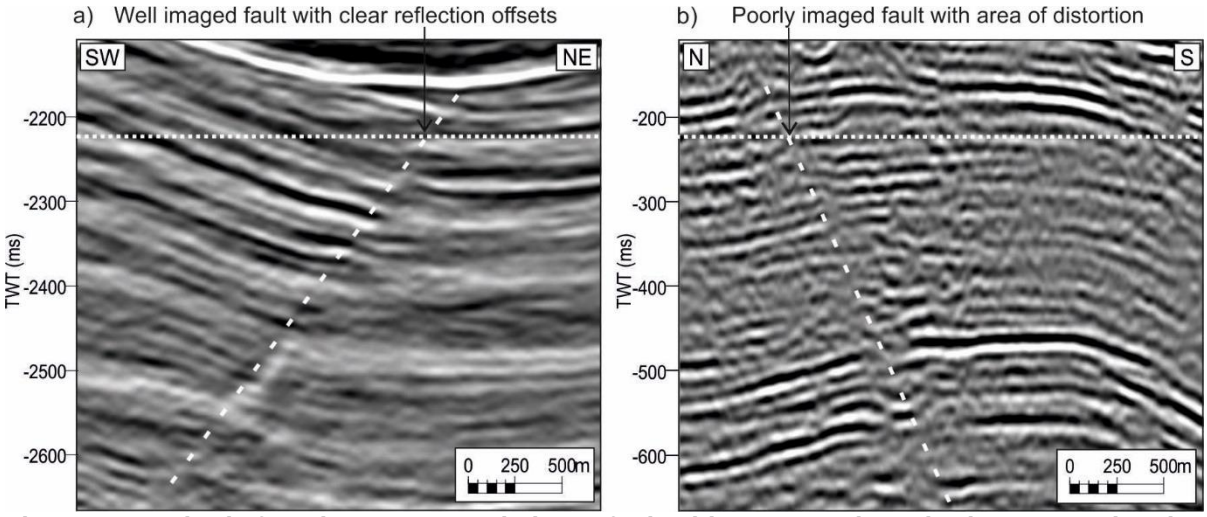


Figure 5.11 Criteria for what was recorded as a fault with an example on both very good and average seismic imaging a) Normal WNW- fault on offshore 3D data b) normal E-W fault on onshore 2D data. The white dotted line represents the scanline sampling interval; this is curved parallel to the BPU in practice.

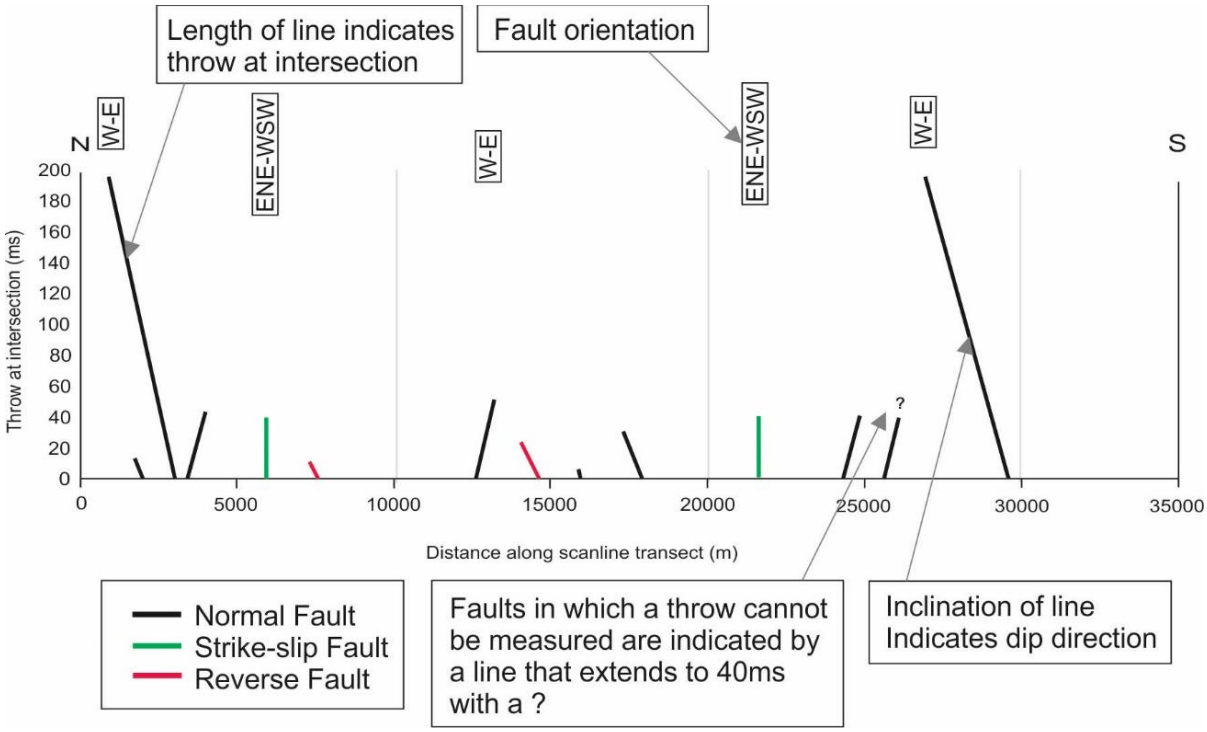


Figure 5.12 Example scanline that samples fault throw at intersection, orientation, apparent dip and slip sense

5.3.1.5 Statistical Analysis

Fault intensity (FI) and average spacing (AS) values were calculated for each scanline so that a comparison could be made between scanlines of different lengths. Fault intensity normalizes fault density for scanlines of different lengths and is the number of faults per unit length along a scanline orientated perpendicular to the fault strike (Ortega et al., 2006). Fault intensity is a measure of fault abundance and is another way of estimating the density of faults within an area. Fault intensity is most commonly determined from one-dimensional observational domains and can be calculated by the equation:

$$FI=N/L$$

Where N is the number of faults divided by L which is the total length of the scanline (Ortega et al. 2005). Average fault spacing was also calculated for each scanline. AS is the inverse of fault intensity and has the following formula:

$$AS=1/FI$$

Fault intensity and average spacing values are only meaningful when the scale of observation and fault sizes are known and considered (Ortega et al. 2005). When comparing any two datasets, normalizing fault intensities is effectively achieved by choosing a common fault detection threshold (scale of observation). Distance and spacing values were plotted as histograms to allow comparison of different case study areas and their different fault types and patterns.

5.3.2 2D Seismic Line Methods

Transects of various lengths were constructed from compiling available individual 2D seismic lines in a roughly N-S and E-W ‘grid’ (Figure 5.13). Good quality lines of various other orientations were also measured were there were data

gaps. The 2D seismic lines had been previously tied in the Z axis before any measurements were made (see section 1.4.1.2).

5.3.2.1 1D Scanline Measurements

Scanlines were constructed along the compiled seismic transects and fault spacing and throw were recorded by distance along each transect. The reference depth (in two way travel time) of these scanlines was on average 500ms below the BPU, so as to represent the fault density occurring within the central part of the thick onshore Carboniferous succession. Fault orientation was not recorded on this dataset due to the sparse 2D grid of sampling transects (Figure 5.13). For this study, faults were therefore classified based on throw type at the intersection point (see Chapter 3, section 3.6.3.).

5.3.3 East Pennine Coalfield

The East Pennine Coalfield map from Bailey et al. (2005) was chosen as an exceptional fault dataset to provide density measurements taken from an intermediate scale compared to the results from the 3D and 2D datasets. A survey consisting of two scanline orientations NW-SE and NE-SW was constructed across the digitized map spaced 5km apart (Figure 5.5). Standard measurements were made for each scanline, namely fault spacing, orientation, movement sense and gross throw magnitude. Throw measurements were not available from the 2D map, hence a simple two-fold classification of fault throw was made based on the delineation of major faults and minor faults on the original map (Bailey et al. 2005).

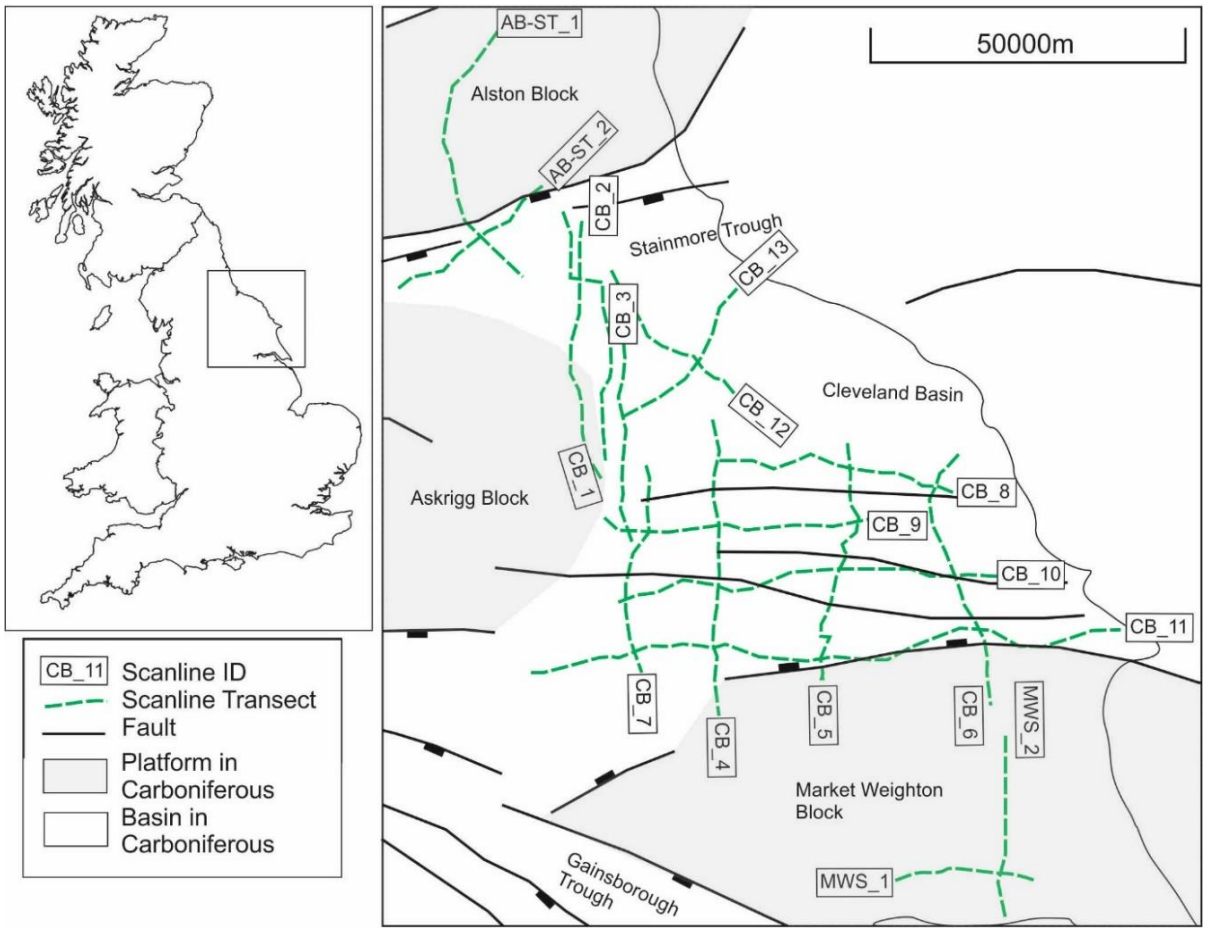


Figure 5.13 Location of the Stainmore Trough-Cleveland Basin area with 2D scanline survey superimposed. Main basin bounding structures are indicated along with Carboniferous basins and platforms.

5.3.4 Method Limitations

Notwithstanding the benefits of manual identification of faults and their characteristics using the seismic data the sampling of what are intrinsically complex topological networks in three dimensions, using a 1D scanline method has a number of limitations.

1. Non-uniformity in the source data (maps, original seismic profiles, or derivatives from seismic interpretation- horizon maps or coherence slices). The comparison of sampling results from different datasets with varying scales has been suggested to have limited value without first establishing the scales of measurement and the detection threshold (Laubach et al., 2018).

2. The use of different seismic surveys with highly contrasting acquisition and processing parameters. This variation primarily affects the statistical analysis through variation in the fault detection threshold as a function of data quality.

3. The inconsistency in the geometrical form of the scanlines. Scanlines constructed offshore from the 3D surveys provide a strong comparative basis, since scanlines could be constructed with fixed spacings on a regular orthogonal grid. This contrasts markedly with the restricted scanline geometry onshore in the Cleveland Basin, with irregular scanlines delimited by the available 2D profile geometry. The onshore seismic dataset to truncation and censoring effects, and the limited number of data points.

5.4 Fault Intensity

This section presents the results fault intensity measurements and average fault spacing (Section 5.1.3) for the case study areas.

5.4.1 Elbow Spit Platform

The density of faults in the Asbian-Brigantian (Lower Carboniferous) succession of the Elbow Spit Platform was assessed using data acquired on 20 scanlines (Figure 5.6). The seismic resolution for clearly detectable fault offsets in this interval was determined to be a minimum of 51m in this area (Figure 1.8). A total of 307 fault spacing distances were measured and recorded and presented in Figure 5.16a. The histogram shows a skewed right distribution with modal spacing values falling in the range of 0.5-1km. The histogram is similar to a negative exponential distribution such as those exhibited by joint datasets (see Figure 5.15d and e), with the first range 0-500 being the only deviation from this trend. This anomaly is interpreted to be due to the seismic resolution aliasing the smaller faults. This distribution suggests that there are a large number of closely spaced faults within the seismic resolution.

The Elbow Spit Platform has the highest abundance of faults of all the 3D seismic case study areas measured, with a fault intensity (number of fractures/scanline length) value of 0.52 (Figure 5.14), derived as an average of all scanline values of both orientations. The average spacing (AS) between faults in the area as a whole is 2.07km. This is the mean distance between faults of any type and orientation and is calculated by calculating the average spacing for each scanline (inverse of the FI value) and calculating a mean from all scanline values.

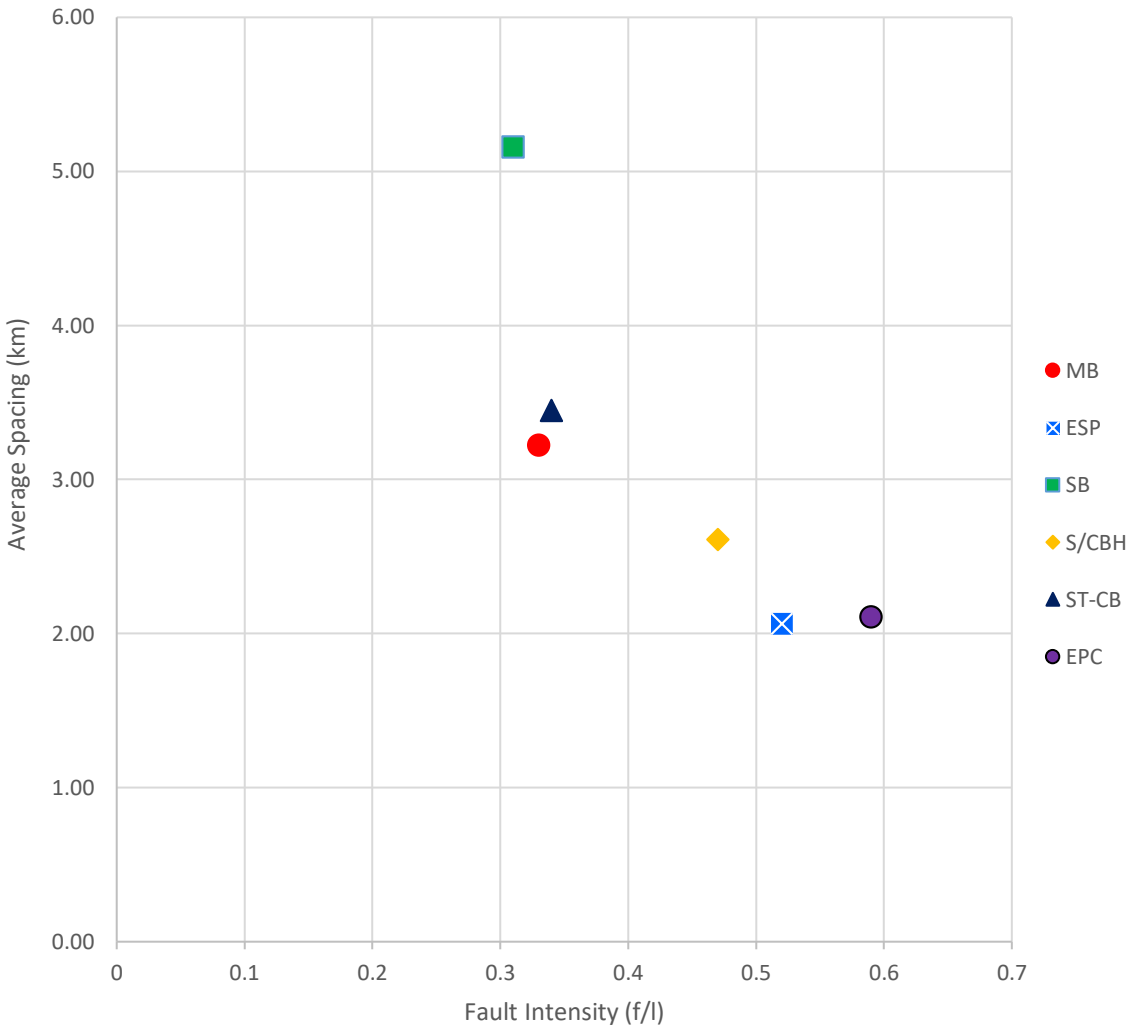


Figure 5.14 The plotted fault intensity (FI) values are calculated from the mean of all scanline FI values. FI values are expressed as a ratio of the number of faults intersected with a scanline and the scanline length. An average spacing (AS) was calculated from each scanline FI value by calculating the inverse of each scanline FI and then calculating a mean of these values to give the overall AS values for each area.

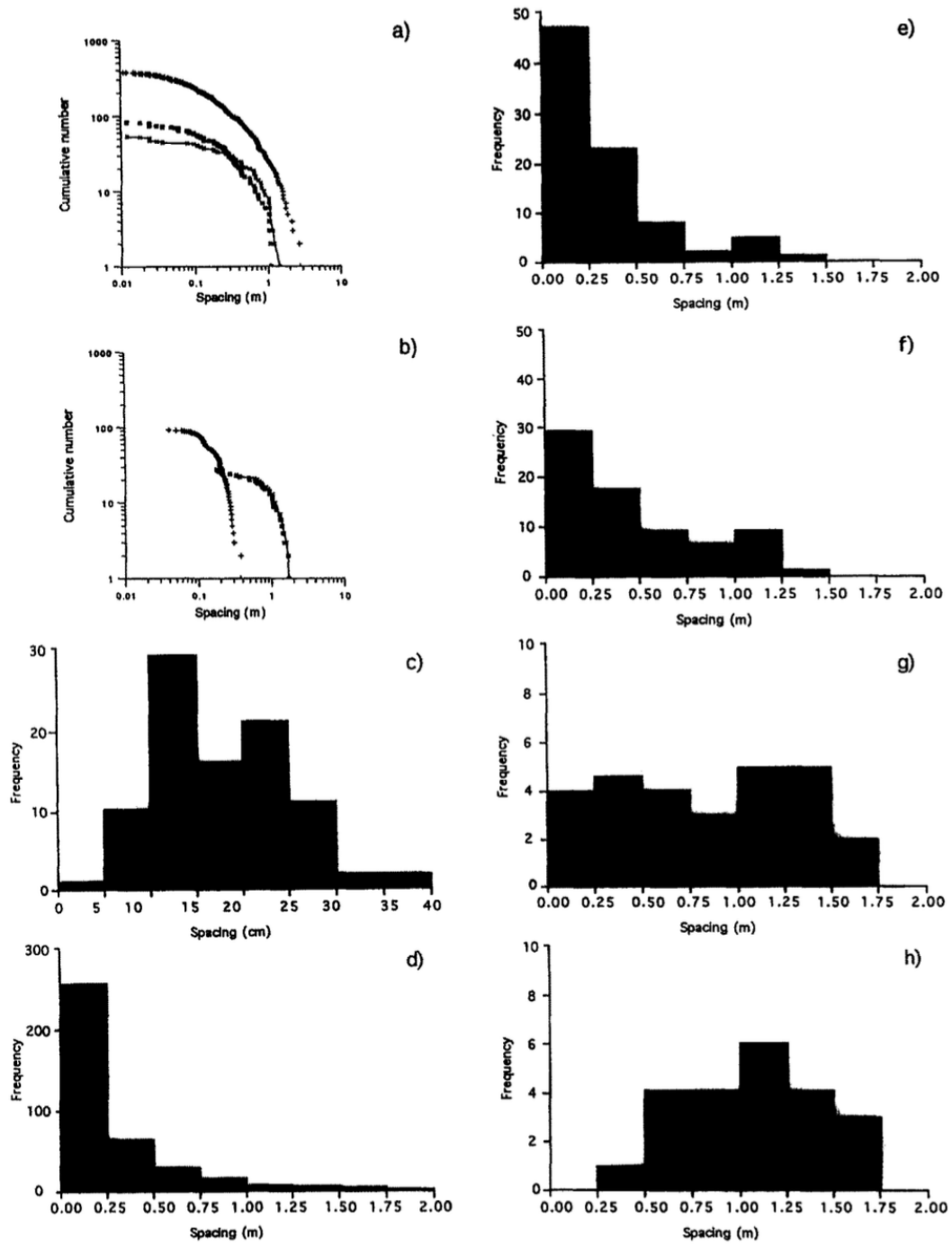


Figure 5.15 Spacing population plots for joint datasets a) and b) Cumulative frequency population curves for spacing c) – h) frequency distributions of joint spacing for six joint datasets (after Gillespie et al., 1993). Different histogram distributions are obseved for the different datasets, including: negative exponential (d and e), normal to slightly bimodal (c), skewed right (f), uniform (g) and sligtly skewed left (h).

5.4.2 Murdoch Block

The overall density of faults in the Westphalian of the Murdoch Block was recorded by 15 scanlines (Figure 5.7). The seismic resolution in this interval for the effective detection of fault offset was determined to be 73m which is the relatively highest throw detection value (see Figure 1.8). A total of 187 fault spacing distances were measured and plotted (Figure 5.16b). The distribution of the histogram is slightly skewed to higher values with two peaks. These two peaks at 1-1.5km (n=28) and 2-2.5km (n=27) are the modal spacing values encountered in this area. Spacings range exhibit a large range, from 236m-10.850km. This slightly bimodal distribution may reflect the clear anisotropy between the spacing values on N-S transects intersecting the 44-D_E-W faults that are further spaced than those on E-W transects (Figure 5.21). The anisotropy seen here is typical of spacing datasets sampled with 1-D scanlines when the fault distribution is highly skewed to a single dominant strike (See Figure 5.15c, Gillespie et al., 1993)

The overall fault intensity, calculated from the mean of each scanline fault intensity value, is 0.33 with an average spacing of 3.22km, calculated using the same method as for the Elbow Spit Platform (Figure 5.14). This is the second lowest fault intensity value for all case study areas.

5.4.3 Silverpit Basin

The dominant subcrop to the Rotliegend in this basin is the Westphalian (Chapter 2), hence the scanlines constructed here primarily record the density of faults in the uppermost preserved Carboniferous section (Figure 5.8). The effective throw detection limit for this area is 51m (Figure 1.8). The density of all faults encountered by the transects in this area is presented in the histogram in Figure 5.16c. It shows a moderately skewed distribution with a major and minor peak,

respectively at the 1-1.5km (n=29) the 3-3.5km (n=14) ranges. The spread of the histogram indicates that the distances between discontinuities in this area are mostly between 1km-3.5km with some minor outliers.

5.4.4 Southern Cleaver Bank High

This case study provided an opportunity to construct scanlines through well imaged faults primarily within the uppermost Carboniferous (upper Westphalian). The fault density was measured and recorded on 14 scanlines (Figure 5.9). The throw detection limit in this area is a throw of 42m, giving a total of 206 data points (Figure 5.16d). The histogram shows a moderately skewed distribution, weighted towards the lower end of the spacing range with three significant peaks. The majority of the counts fall in the low-moderate distance ranges. These peaks indicate the most common distances between discontinuities fall in the ranges of 500-1000m (n=34), 1000-1500m (n=40) and 1500-2000m (n=39).

The S/CBH is the second most densely populated area of seismically resolvable faults of the 3D seismic case study areas. A total fault intensity value of 0.47 is averaged from all scanlines with an average spacing of 2.61km Figure 5.14.

5.4.5 Stainmore Trough – Cleveland Basin

The distances between seismically resolvable faults in the Brigantian-Namurian? succession of the area was recorded on 17 irregular scanlines drawn along composite seismic profiles from the 2D surveys in the area. The throw detection limit for this area was 44m, not dissimilar to the values for areas offshore with well imaged faults on 3D seismic data. This is surprising given the contrast in overall data quality (Figure 5.11).

The data (N = 200) are presented in Figure 5.16e. The histogram shows a highly skewed distribution that is slightly bimodal. The dominant peaks display the

most common recorded distances displayed by the peaks representing the ranges of 500-1000m and 1000-1500m. The secondary peak is at 5000-5500m. A third (33.5%) of the measured distances are recorded between 500-1500m.

A low-medium density of faults is recorded in this area with an overall fault intensity value of 0.34 and average spacing of 3.45km (Figure 5.14). There is a higher density of faults in the interval within the basinal areas (Stainmore Trough and Cleveland Basin, (see Figure 5.30) when compared to the interval over the structural highs (e.g. Alston Block, Figure 5.30).

5.4.6 East Pennine Coalfield

The distances between faults with a throw of 1m or higher were recorded by two scanline sets in the Westphalian interval of the East Pennine Coalfield (Figure 5.5). A total of 315 distances between mapped faults were measured and plotted in Figure 5.16f. The histogram shows a negative exponential distribution with the majority of intersections being between 0-100m (n=40), to which there is an overall decrease in counts with increasing distance ranges. This is a classical distribution, seen on many fault and fracture sets from other areas in the world, particularly on joint sets (Gillespie et al 1992, see Figure 5.15e, and Priest and Hudson, 1981, see Figure 5.15a). This type of frequency distribution is typical of unrefined (all fault) datasets without lower limits of resolution (Gillespie et al., 1993).

Unsurprisingly due to the 1m offset resolution, the map of the faults in the East Pennine Coalfield records the highest density of faults with a fault intensity value of 0.59 and an average spacing of 2.11km (Figure 5.14). This raises interesting questions regarding the likely spacing of faults in areas of poor seismic control, where there is no high resolution data from coal mining or surface mapping to sample the lower throw end of the total fault population (see Discussion). Does

this distribution for the EPC give a clue to the sub-seismic distribution for the other case study areas, below the seismic resolution?

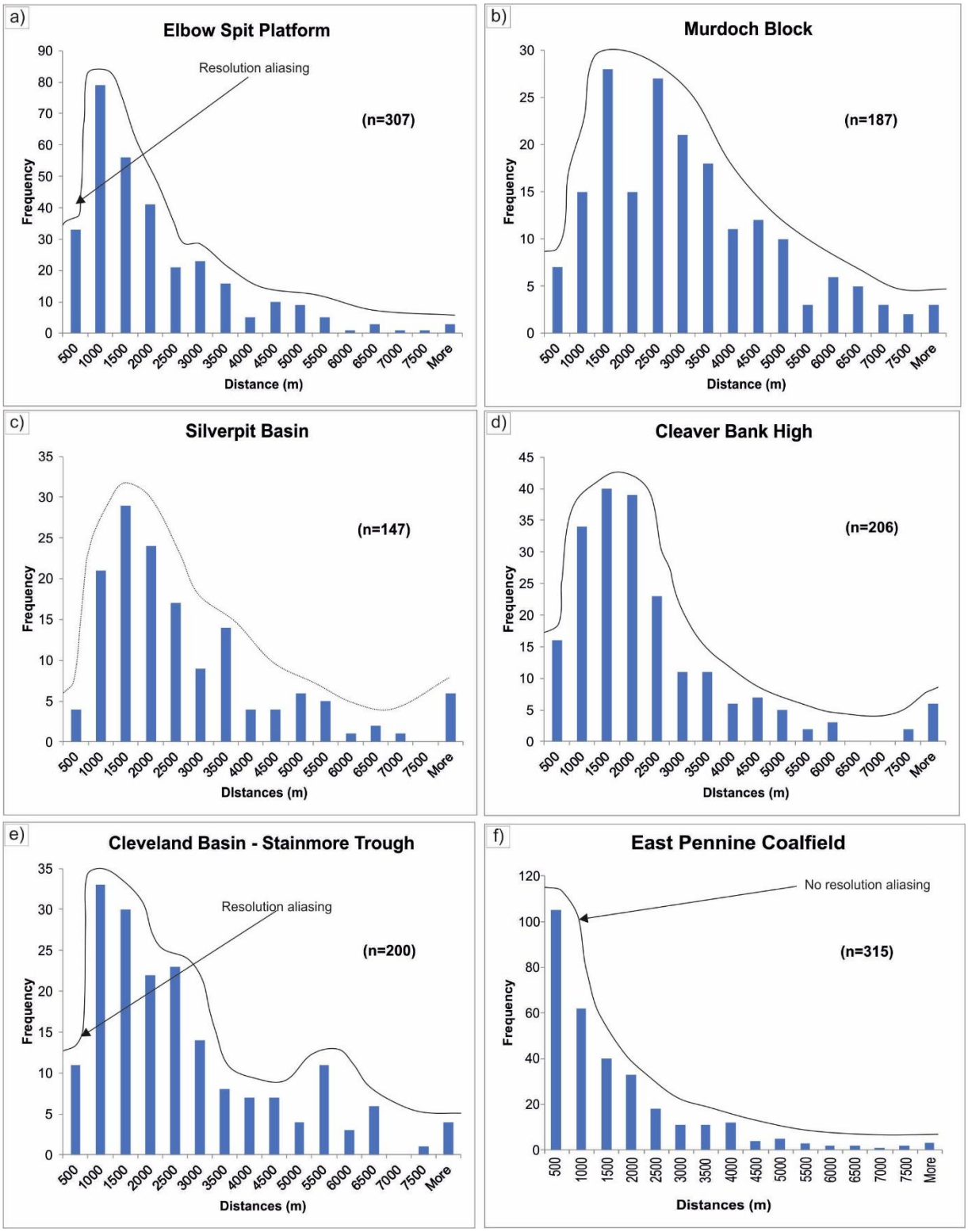


Figure 5.16 Frequency distributions for the distances between seismically resolvable faults in the Pre-Zechstein succession. A histogram is presented for each case study area. Two main end-member types of distributions are recognised: Negative exponential (a & f) and skewed right (b & c). Histograms d and e have attributes of both of these end member types. Data gaps in the 0-500 bin on plots a)-e) given by the low counts is likely due to aliasing of faults due to the seismic resolutions.

5.5 Fault Spacing Results

As previously defined in Section 5.1.4, this section presents the results quantifying the spacing between genetically similar, dominant faults in each case study area using the 1D sampling method. The aim of applying this method to the case study areas is to examine spacing and size relationships for the major fault sets, to see whether they are related, and also to see how pre-existing fault sets might influence the spacing of later, superimposed deformations (Knott et al., 1996).

5.5.1 Elbow Spit Platform

20 scanlines that transect the Elbow Spit Platform (Figure 5.6) intersecting two dominant fault types. The NE-SW transects give a good sampling of the A-E_WNW- faults. These faults have an average maximum throw value of 210m and are in the medium size class (see section 3.2.3.1.). Some A-E_NNE- (see section 3.2.3.3.) and A-E_ENE- (see section 3.2.3.4.) faults are also intersected. The fault intensity (FI) for all faults along the SW-NE orientated transects is 0.46 and the average spacing is 2.27km (Figure 5.17).

Fault orientations intersected by the NW-SE transects include NE- and NNE-extensional faults and ENE- strike slip faults (see section 3.2.3. for description and summary of fault sets). N-S trending faults are also intersected. The fault density for all faults along the WNW-ESE transects is 0.57. Average spacing of all faults along this transect set is 1.86km (Figure 5.17).

5.5.1.1 A-E_WNW-Faults

The WNW- faults are a set of normal faults in the medium throw size class (see section 3.2.3.1. for detailed description). The histogram of spacing values in Figure 5.19a shows a moderately skewed distribution with modal spacing values falling in the range of 2.5-3km. The distribution of the histogram indicates a more

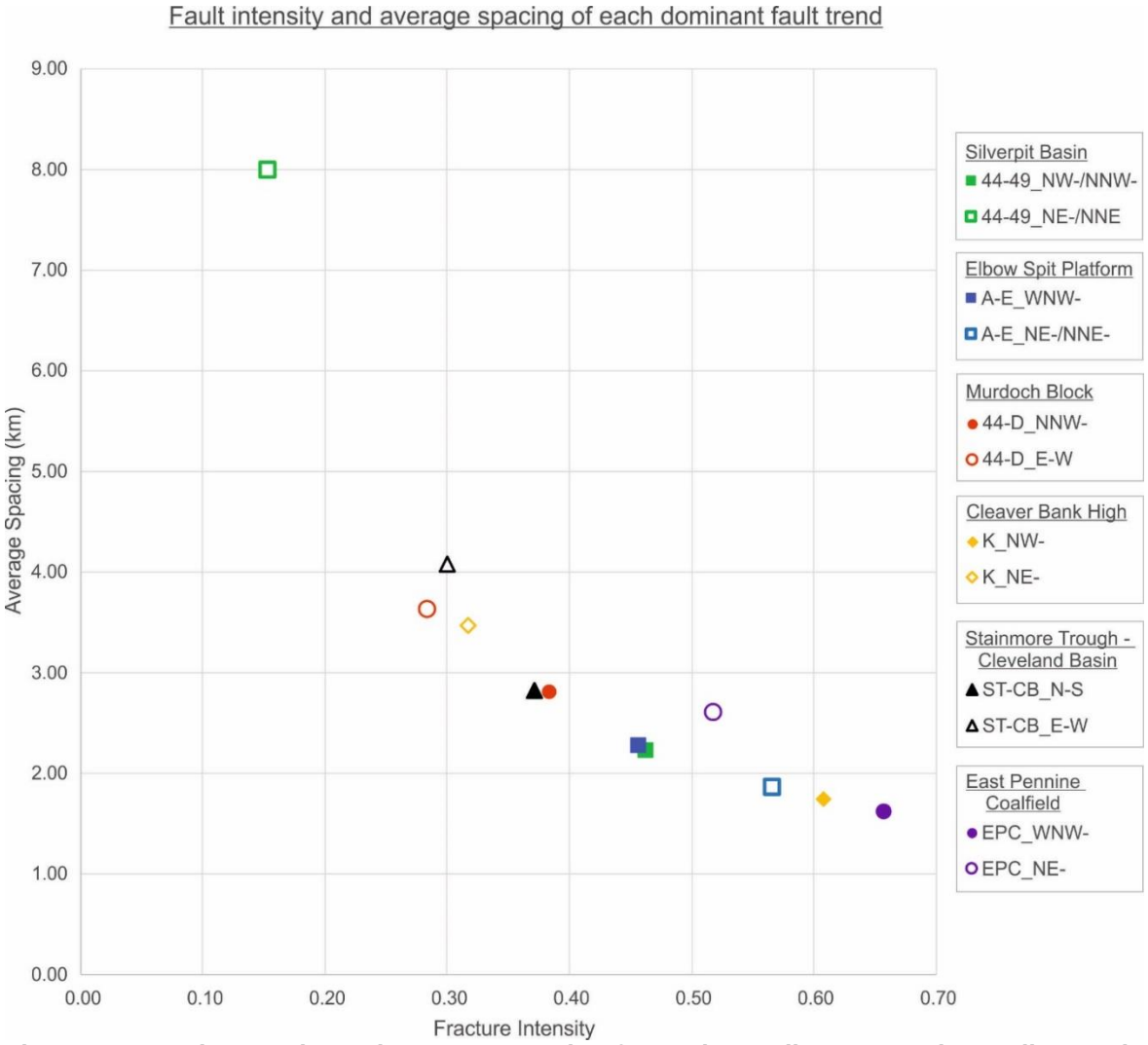


Figure 5.17 Fault Intensity and Average Spacing for each scanline set. Each scanline set is representative of a dominant orthogonal fault trend, these trends are indicated in the legend.

uneven spacing than would be expected from the Top Rotliegend horizon map (Figure 5.6). This may be due to the paucity of the WNW- faults towards the north east of the area, expressed on Transect D (Figure 5.18), in which no WNW- faults are intersected for 10.25km to the north east. Transect D intersects 7 WNW-trending extensional faults with throw values at the intersections ranging from ~25ms-140ms. The fault intensity of the WNW- faults is 0.20 and they have an average spacing of 5km. This average spacing value is likely elevated compared to the histogram modal spacing values due to this paucity WNW- faults to the NE- of the area.

5.5.1.2 A-E_NE- Faults

The NE- faults are a set of normal faults in the small throw size class (see section 3.2.3.2 for detailed description). The histogram of spacing values (Figure 5.19) shows a highly skewed right distribution with modal spacing values falling in the range of 1-1.5km. These faults are highly clustered as shown on the Top Rotliegend horizon map in Figure 5.6. The frequency distribution does not appear to reflect this clustering, and is better represented by the scanline, Transect P. Transect P (Figure 5.18) intersects 12 NE-trending net normal faults with throws at intersections ranging from ~80-20ms. The fault intensity value of the AE_NE faults is 0.24 with an average spacing of 4.12km. These values do not reflect the clustering observed on the map and highly uneven spacing recorded by the scanlines. The faults are closely spaced in clustered areas, and therefore their spacing in these clusters is closer to the modal spacing values in the frequency distribution.

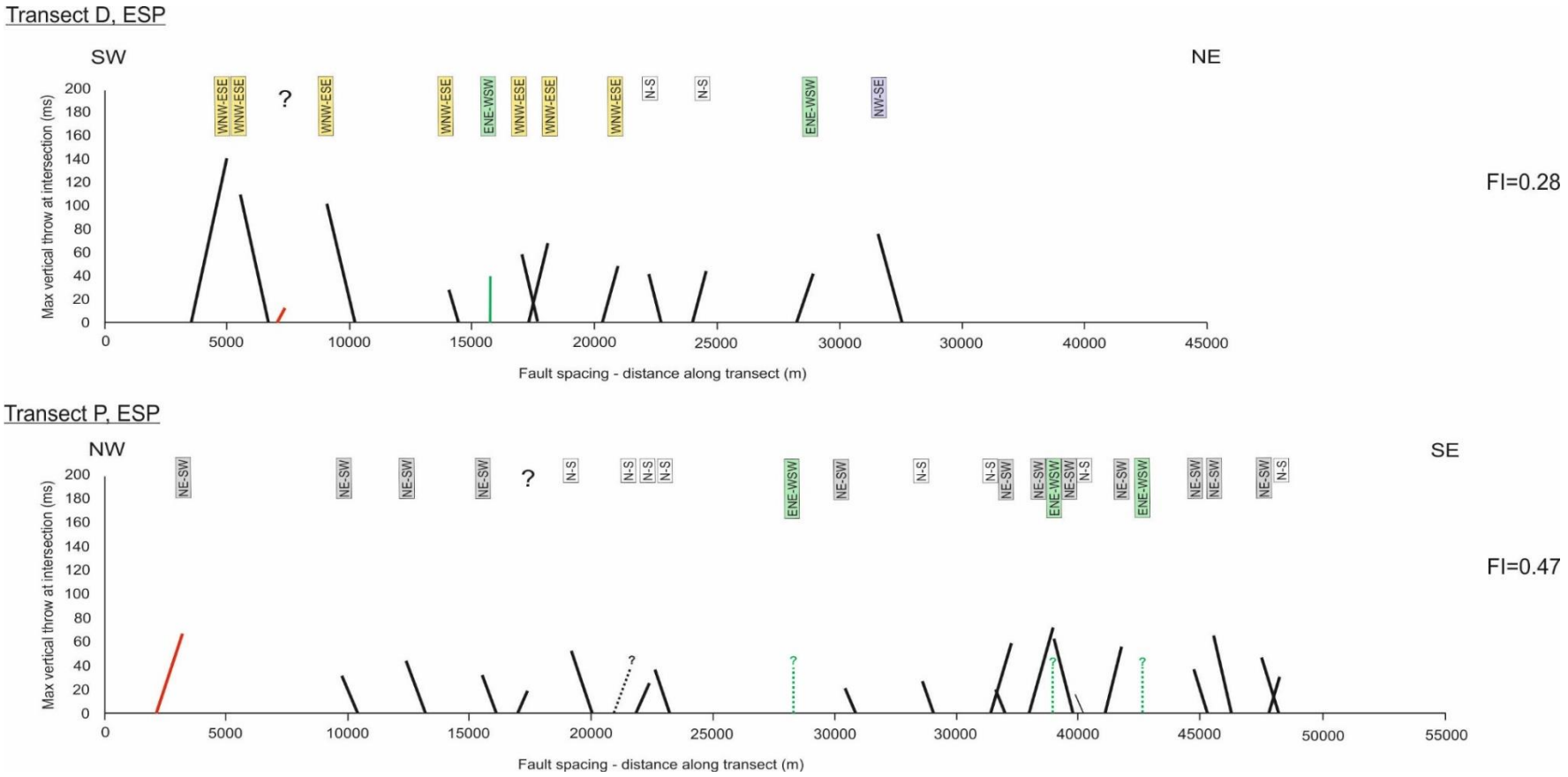


Figure 5.18 Representative scanline transects from each orientation set, sampling; fault spacing, orientation, throw sense, throw value and dip direction in the Lower Carboniferous of the Elbow Spit Platform

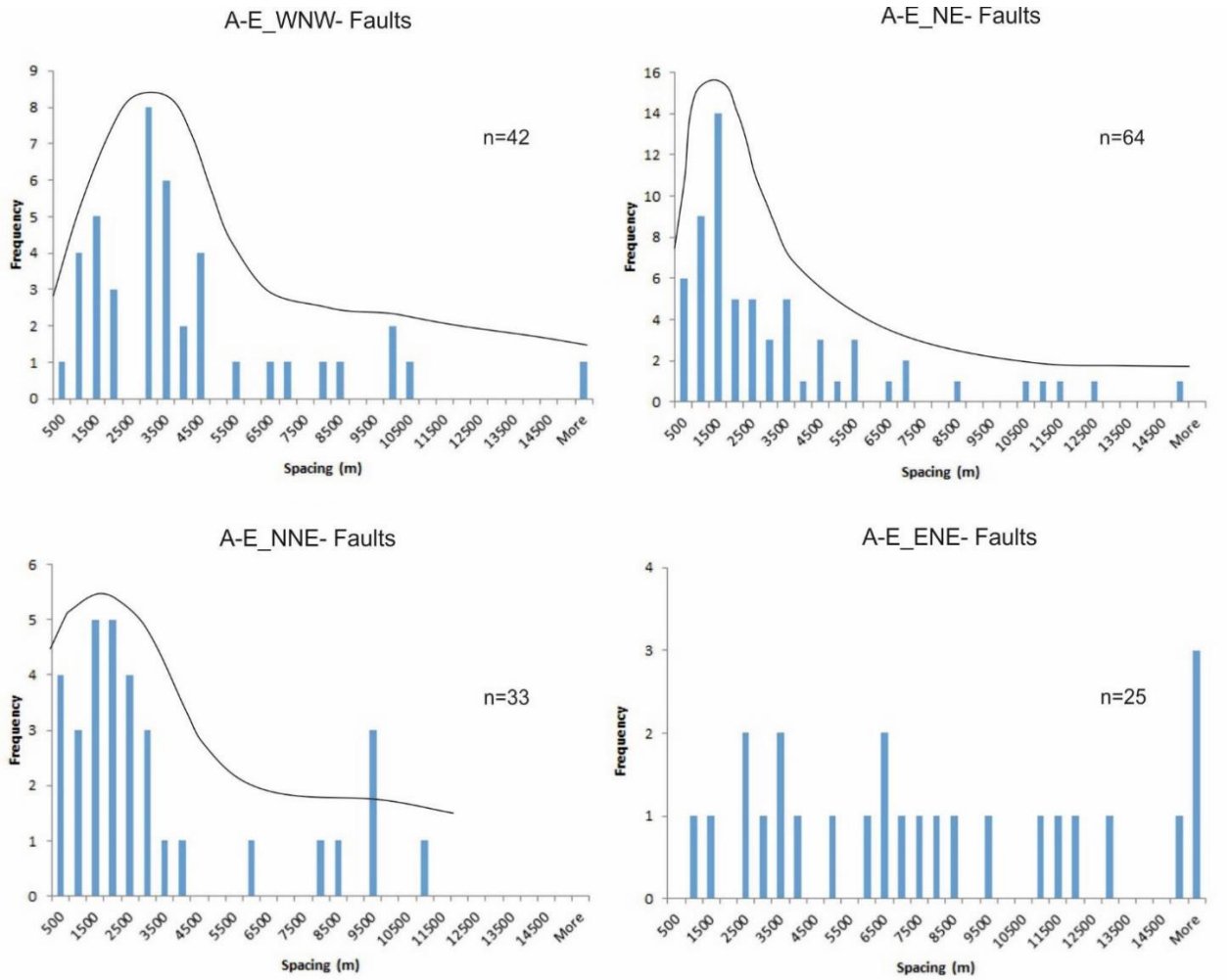


Figure 5.19 Same set fault spacings in the Elbow Spit Platform study area. Spacing distances are measured by transects normal to the dominant fault strike for the A-E_WNW- and A-E_NE- Faults. The A-E_NNE- and A-E_ENE- are sampled oblique to the transect orientations. The WNW-, NE- and NNE- faults exhibit mostly skewed right distributions suggesting overall closely, evenly spaced faults of these sets. The ENE- trending faults exhbit a random distribution, highlihting a uneven,more widely spaced fault set.

5.5.1.3 A-E_NNE-/N-S Faults

The NNE- faults have normal throws and belong to the medium throw size class (see section 3.2.3.2 for detailed description). The histogram of spacings shows a skewed distribution that is slightly bimodal. The modal ranges are 1500-2500m and 9000-9500m. This reflects the general close spacing of these faults that are clustered in the NE of the area.

Transect P (Figure 5.18) intersects 8 NNE- faults with throws at intersections ranging from 15-60ms. The fault intensity value for the NNE- faults is 0.15 with an average spacing of 6.66km. This AS value is not representative of the recorded spacing distances (Figure 5.19) as the spacings are highly irregular and clustered, similar to the A-E_NE- faults.

5.5.1.4 A-E_ENE- Faults

The ENE- strike slip faults were obliquely intersected by each transect set, and therefore their spacing values need to be evaluated with this in mind. These oblique intersections still give information of value on the spacing (see Gillespie et al., 1993 and Gomez and Laubach (2006) for discussion of this point), and have been plotted in Figure 5.19. In these cases, the spacing values are referred to as apparent spacing. The histogram shows a random distribution reflecting the uneven and sub-parallel apparent spacing of the ENE- faults (Figure 5.6, Figure 5.18).

5.5.2 Murdoch Block

The scanlines transects in the MB consisted of 8 N-S orientated scanlines (A-H) and 7 W-E trending transects (J-P). The dominant fault sets intersected by N-S orientated transects were the 44-D_E-W (see section 3.3.3 for fault descriptions). The overall fault intensity calculated for faults intersected by the N-S transects was 0.28 with an average spacing of 3.63km (Figure 5.17). The dominant fault trends

intersected by the W-E orientated scanline transects were 44-D_NNW- (see section 3.3.3. for fault descriptions). The abundance of faults intersected by W-E scanlines was higher than for the N-S transects with a value of 0.38 and an average spacing of 2.81km (Figure 5.17).

5.5.2.1 44-D_NNW- Faults

The 44-D_NNW- faults are most frequently spaced in the 1000m-2000m ranges as shown by the histogram in Figure 5.21 and show the majority of counts weighted in the range of 1000m-4500m with few outliers.

Transect L (Figure 5.20) intersects 24 faults in total and has a high FI value of 0.53 and low AS value of 1.9km. Of the NNW-SSE faults, 17 are orientated with normal throws ranging from 15-110ms, 14 of which dip to the west. One of these faults exhibits a reverse throw. The fault intensity value for the NNW- faults alone is 0.37 with an average spacing value of 2.7km. The NNW- trending faults are more frequently encountered in the Murdoch Block (0.38) and more closely spaced (2.8km) than the E-W faults (Figure 5.17).

5.5.2.2 44-D_E-W Faults

The 44-D_E-W faults have net normal throws and are in the medium throw scale range (see section 3.3.3.2 in Chapter 3). The histogram in Figure 5.21 shows that the most frequent spacing of E-W faults encountered were in the range of 2500m-3000m. This peak is only 1 count less than the other peaks at 5000m-5500m and 5500m-6000m which are thought to be representative. The data spread on the histogram shows the spacing between these faults is highly irregular, and this is also clearly seen on the TRot map (Figure 5.7).

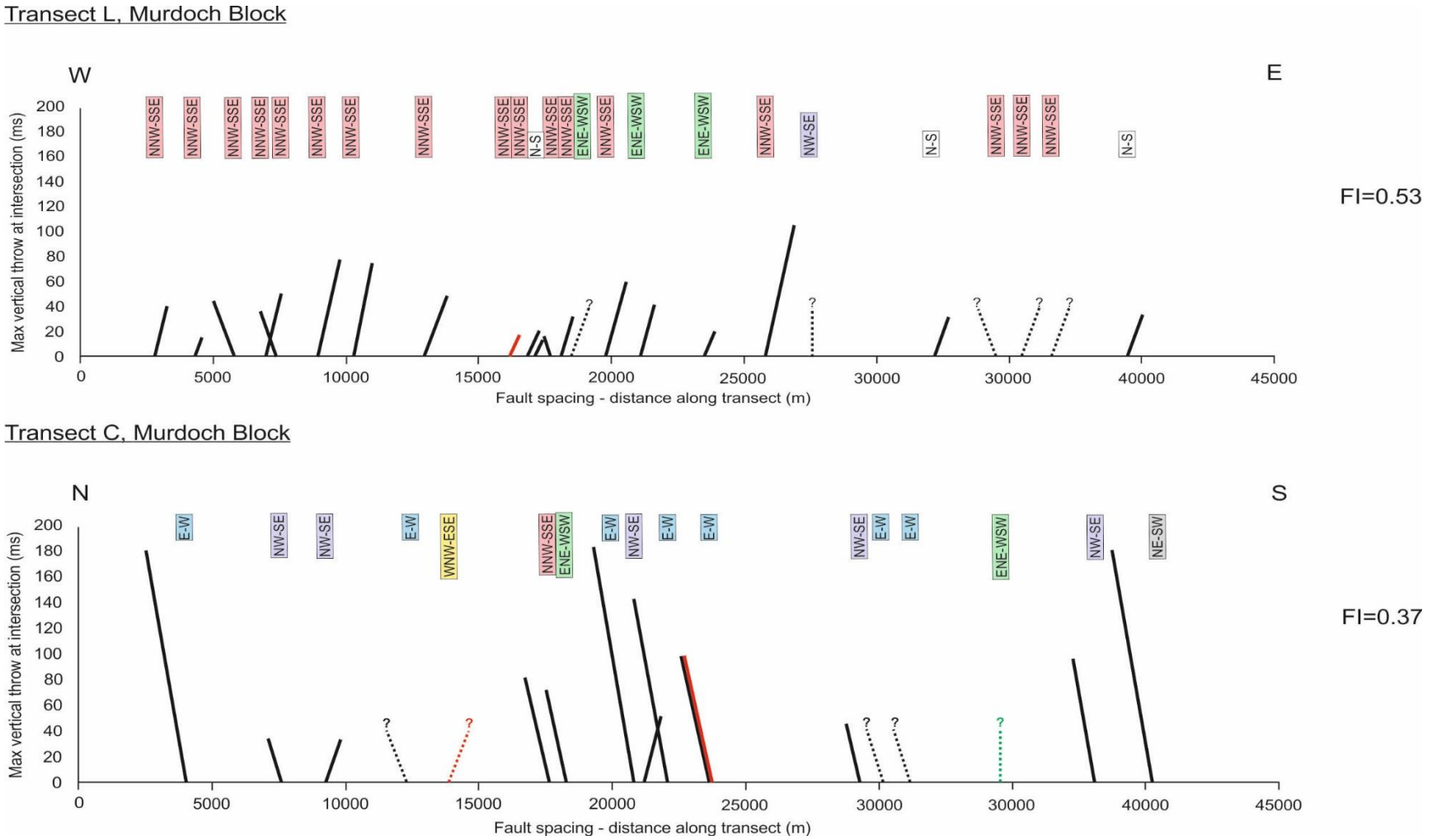


Figure 5.20 Representative scanline transects from each orientation set in the Murdoch Block. The transects sample fault spacing, orientation, throw sense, throw value and dip direction in the Westphalian interval.

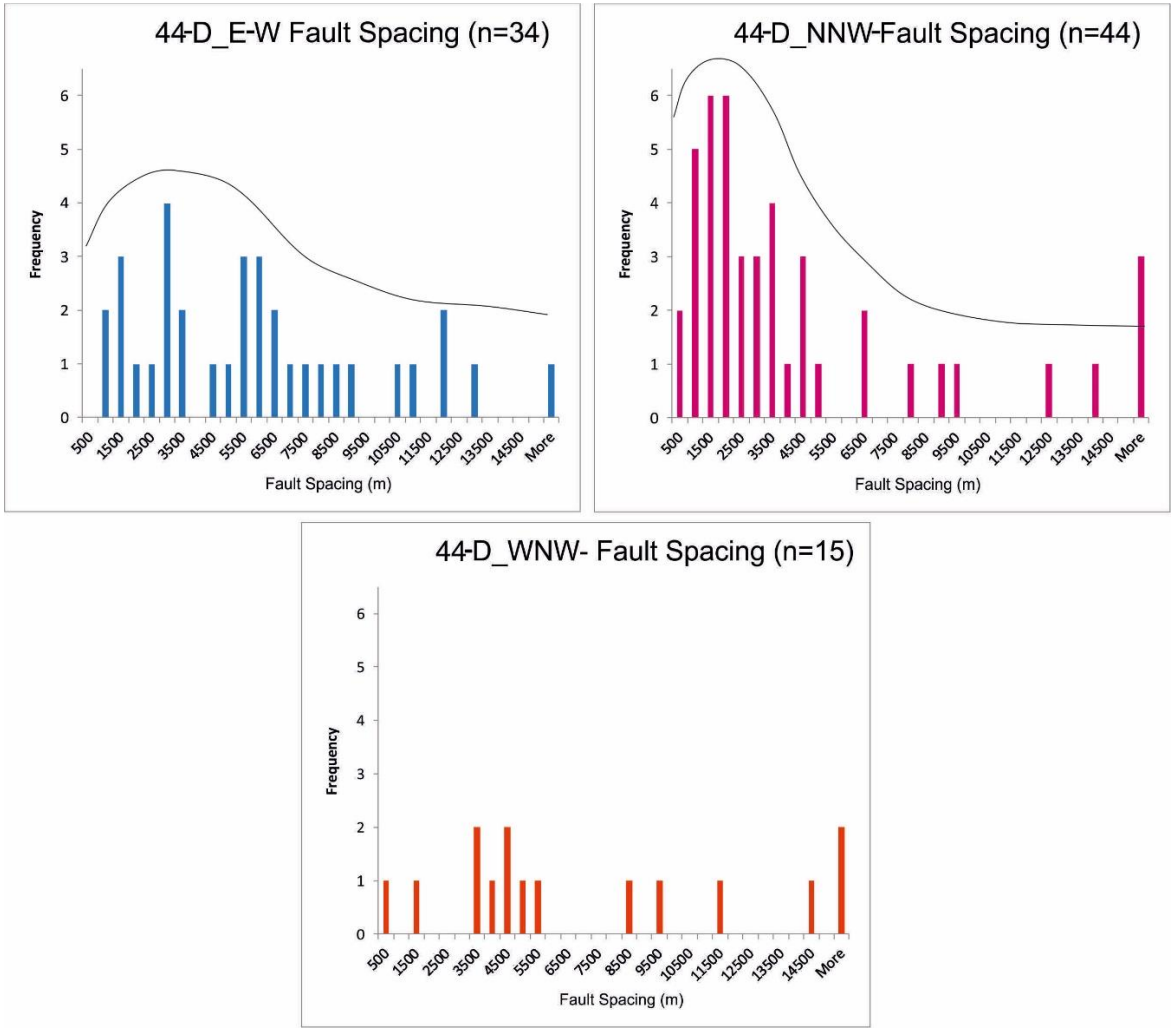


Figure 5.21 Same set fault spacings in the Murdoch Block study area. Spacing distances are measured by transects normal to the dominant fault strike for the 44-D_E-W and 44-D_NNW- Faults. The WNW- faults are sampled oblique to the transect orientations. Three main distributions are observed: Slightly skewed right to random (E-W), highly skewed right (NNW-) and random (WNW-). Three factors may be contibuting to the random distibution for the WNW- faults, 1) they are infreqently encountered in the study area and therefore there isn't enough to be represented well by a histogram distribution (n=15), 2) they are intersected obliquely by the sampling transects and 3) they have an uneven spacing.

Transect C (Figure 5.20) intersects 7 E-W faults with throws from 100ms to >200ms at these intersections and a southerly regional dip. A fault intensity of 0.16 with an average spacing of 6.25km. In summary, the E-W trending faults are more irregularly spaced than the NNW- faults, indicated by the lack of significant peaks or weighting on the E-W histogram distribution. The NNW- faults have a more even spacing indicated by the skewed right distribution (Figure 5.21b).

5.5.2.3 44-D_WNW- and 44-D_ENE- Faults

The WNW- and ENE- faults are also intersected obliquely by the scanlines. The WNW- faults are have a low frequency of intersections (n=15) and record overall uneven spacings (Figure 5.21c). Too few ENE- faults are intersected by the scanlines in the Murdoch Block area to characterize their spacing.

5.5.3 Silverpit Basin

Of the 16 scanlines that transect the SB, 9 are SW-NE orientated (B-J) and 7 are NW-SE (L-O) orientated. The dominant fault sets intersected by the SW-NE orientated transects are the 44-49_NW- normal faults (see section 3.3.4. for fault descriptions). The overall fault density for faults intersected by SW-NE transects was moderately high with a fault intensity value of 0.46 and a moderately low average spacing of 2.23km (Figure 5.17). The dominant fault sets intersected by the NW-SE Transects are NNE- and ENE- orientated strike-slip faults (see section 3.3.4. for fault descriptions). The overall fault density recorded by the NW-SE orientated transects is relatively low with and fault intensity value of 0.15 and a high average spacing value of 8km (Figure 5.17). The largest difference between the fault intensity and average spacing results is seen in this case study area. Each scanline set demonstrates the clear dominant structural fabric without a significant

orthogonal trend, an observation unique across the Anglo Dutch Basin. The underlying control of this very strong fault anisotropy is discussed in Chapter 6.

5.5.3.1 44-49_NW-_P and NW-_T Faults

The spacings of the NW-SE faults is presented by the histogram in Figure 5.22a. The modal spacing values are in the range of 1000m-1500m and the moderately skewed right distribution shows the majority of spacing values are low-medium values and therefore these faults have a mostly even spacing.

Transect E (Figure 5.23) intersects 29 faults, 24 of which are NW-SE orientated, giving the NW-SE faults an fault intensity value of 0.48 and average spacing of 2.08km. The majority of the NW-SE faults have a normal slip sense (n=21) but 3 are reverse representing the 44-49_NW-_T faults (see section 3.4.3.3). They exhibit no preferred regional dip sense, instead there are a similar number of NE and SW dipping faults, with only a few faults in sets of one direction or the other. Throw values on these NW-SE faults range from 10-140ms with an average of ~80ms. The even spacings and small throws on this fault set is similar to the distributed population geometry observed in the East Pacific Rise (Figure 5.4)

5.5.3.2 44-49_NNE- and ENE- Faults

The spacing distances are presented as a histogram in Figure 5.22b. The histogram has few counts due to low occurrence of intersections of NNE- faults. There are no significant peaks and the overall distribution suggests an irregular spacing of the NNE- faults.

Transect P (Figure 5.23) intersects 9 faults, 6 of which are the NNE- strike-slip set. The NE-SW faults have a fault intensity value of 0.12 and an average spacing of 8.33km (similar values to the transect averages). The sub-vertical dipping faults have intersected throws of between 10-35ms.

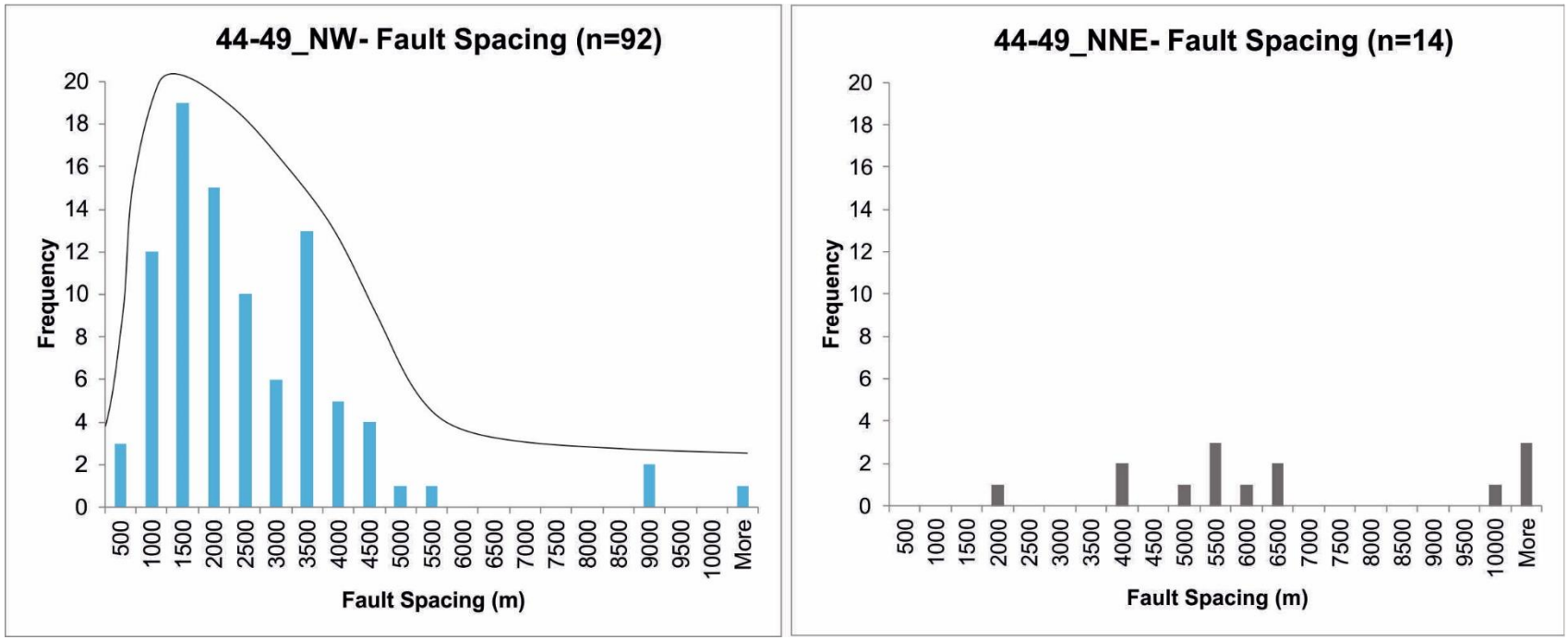


Figure 5.22 Same set fault spacings in the Silverpit Basin study area. Spacing distances are measured by transects normal to the dominant fault strike. The NW- trending faults are intersected frequently by the scanlines and exhibit a moderately skewed left distribution, suggesting a moderately uniform spacing. The NNE- faults are intersected less frequently (n=14) and the histogram reflects this, exhibiting a highly random/plateau distribution.

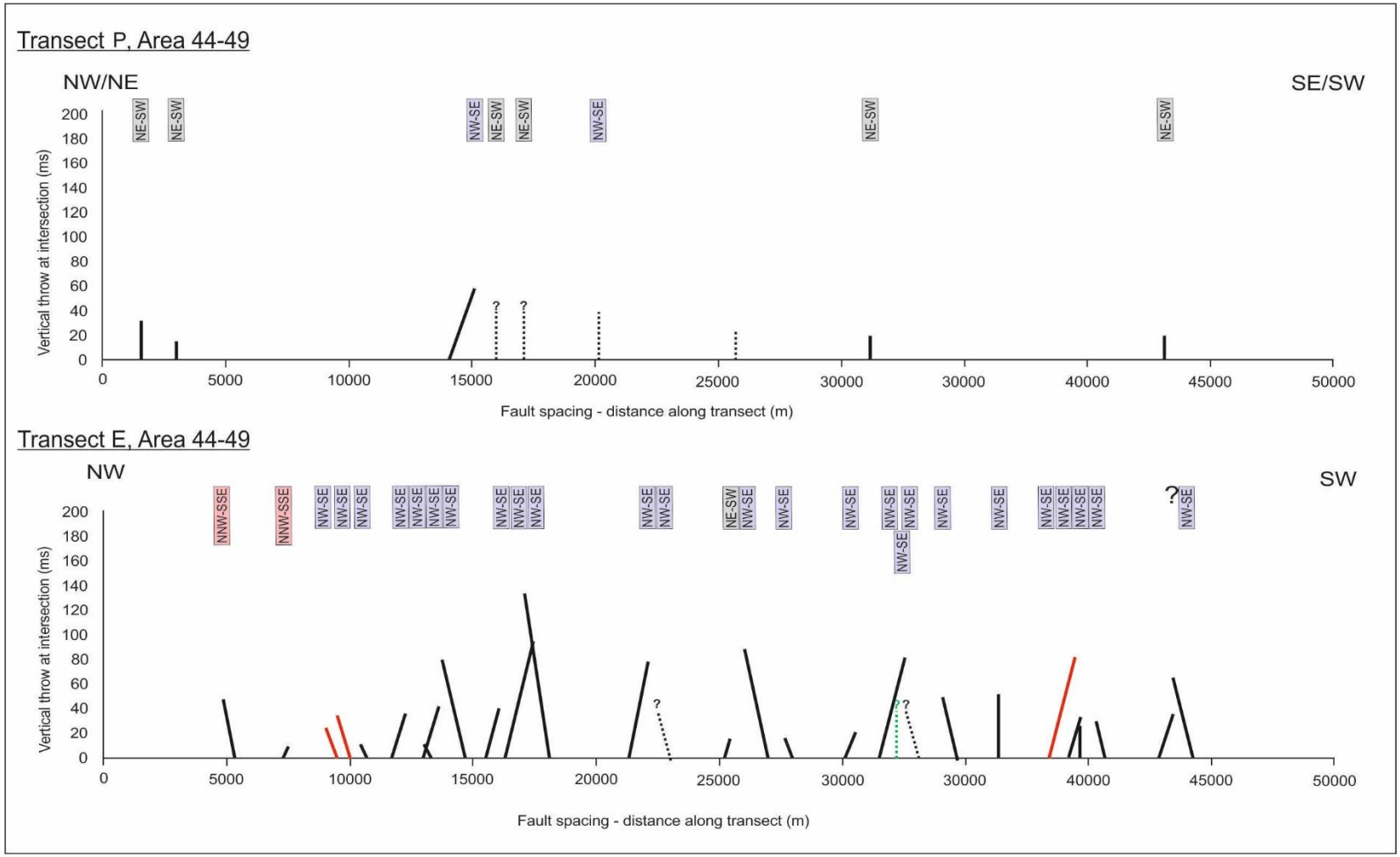


Figure 5.23 Representative scanline transects from each orientation set in the Silverpit Basin. Fault attributes sampled include fault spacing, orientation, throw sense, throw value and dip direction in the Westphalian interval.

5.5.4 Southern Cleaver Bank High

There are 14 scanlines that transect the SCBH, a set of 7 SW-NE (A-G) and 7 NW-SE (H-N). The SW-NE orientated transects mostly intersect NW- orientated faults with some NNW- and WNW- orientated faults (see section 3.5.3. for fault descriptions). The overall fault density recorded by the SW-NE orientated transects is relatively high, with a fault intensity value of 0.61 and an average spacing of 1.75km (Figure 5.17). This fault intensity value is the highest of all scanlines sets in the 3D case study areas.

The NW-SE sampling transects cross-cut the NE-, NNE- and N-S faults (see section 3.5.3 for fault descriptions). The overall density of faults recorded on this transect set is moderate-low with a fault intensity value of 0.32 and an average spacing of 3.47km (Figure 5.17).

5.5.4.1 K_NW-_TR and NW-_TN Faults

The spacing distances between NW-SE faults are presented by the histogram in Figure 5.24a. The histogram shows a highly skewed distribution with a secondary peak at the 4000-4500m range. The modal spacing distance for NW-SE faults is between 1000-1500m (n=11) with the higher values being weighted in the range of 1000-2500m (n=40). The weighting of the counts in the low-moderate range suggests a moderately uniform spacing for NW-SE faults, disregarding the peaked anomaly at 4500m. This anomaly is reflected on the TRot horizon map in the centre of the area where NW-SE faults are less closely spaced when compared to further NW or SE in the area (Figure 5.9).

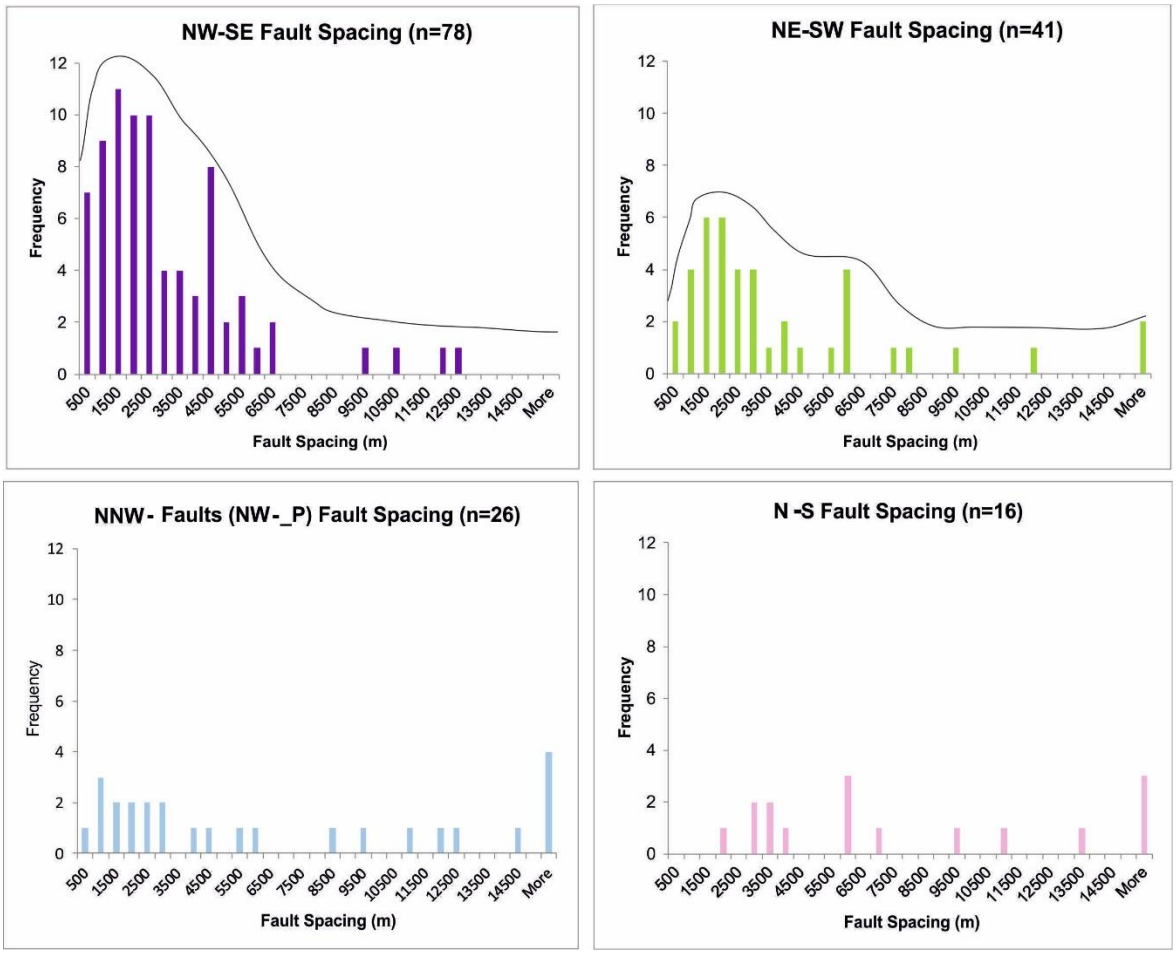


Figure 5.24 Same set fault spacings in the Cleaver Bank High study area. Spacing distances are measured by transects normal to the dominant fault strike for all sets except for N-S which are measured obliquely. The NW- and NE- trending faults exhibit moderately and slightly skewed right distributions respectively. The NNW- and N-S orientated faults exhibit highly random/plateau distributions, which may be due to them being intersected less frequently.

Transect E (Figure 5.25) intersects 28 faults and is 50km long. All faults along the scanline transect are dip-slip except for 4 faults which are in part strike-slip. There are 14 faults that are NW-SE orientated and have throw values ranging from 20ms to >200ms. No regional dip direction is observed with roughly equal proportions of NE and SW dipping faults. In summary, the NW-SE faults are closer and more evenly spacing with a higher frequency of intersections.

5.5.4.2 K_NW-_P (NNW-) Faults

The NW-_P faults have small to medium normal throws and no regional dip. The random distribution and small number of counts of NNW- faults in Figure 5.24c reflects the uneven spacing and clustering. This is also illustrated on Transect E (Figure 5.25a) that shows the clustering on the NNW- faults to the SW of the area.

5.5.4.3 K_NE-_T, NE-_P and NNE-_SS Faults

A slightly skewed right distribution is observed on the histogram in Figure 5.24b with a secondary peak at 6000-6500m. This slightly bimodal distribution reflects the irregular spacing and clustering of faults of this orientation. Fewer faults are intersected compared to the other dominant orthogonal sets in this area.

5.5.4.4 K_N-S Faults

The N-S faults are infrequent and have an irregular spacing that is shown by the random distribution and low counts presented by the histogram (Figure 5.24d). They are relatively short in map view, which also means they are not sampled as frequently.

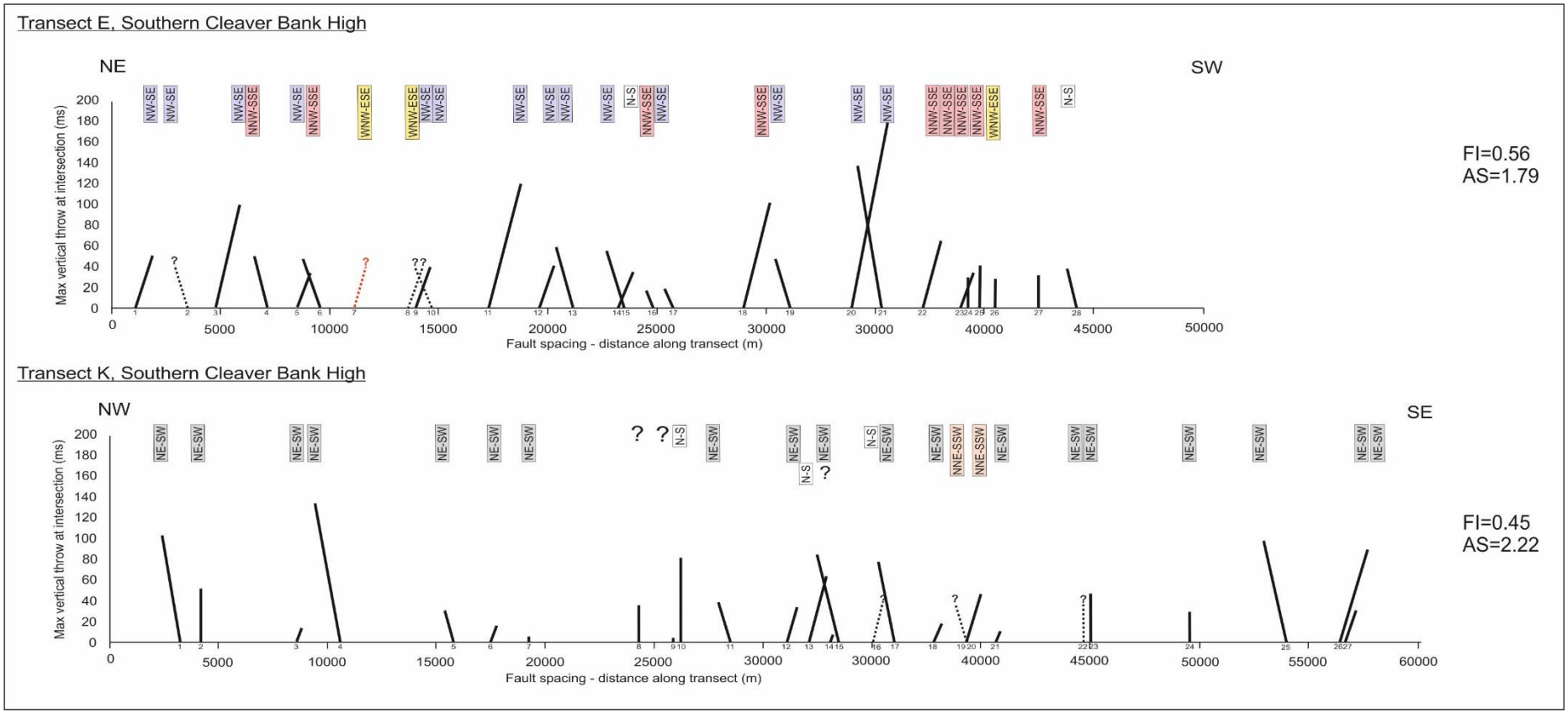


Figure 5.25 Representative scanline transects from each orientation set in the Southern Cleaver Bank High. Fault attributes sampled include fault spacing, orientation, throw sense, throw value and dip direction in the Westphalian interval.

5.5.5 Stainmore Trough – Cleveland Basin

The intersected throw values on the sample scanlines are less representative of fault size in this area due to the significant reactivations on the larger scale faults (see section 3.6.3. for fault descriptions and section 3.8. for classification).

5.5.5.1 N-S Scanlines (Mostly E-W Faults)

The N-S scanlines have an overall fault intensity value of 0.37 with an average spacing of 2.87km (Figure 5.17). The spacing between faults intersected by N-S transects are presented in Figure 5.26. The histogram shows a skewed left distribution with an anomalously low count for 0-500m spacing. The peaks range between 500-2000m accounting for 53% of the recorded distances. The distances have a total range of 6575m.

Transects CB_3 is a representative N-S scanline in the ST-CB area. An overall fault intensity of 0.34 is exhibited with and an average spacing of 2.9km (Figure 5.27a). Two out of the twelve faults intercepted are larger scale faults (ST-CB_3 and ST-CB_2a types, see section 3.6.3. in Chapter 3) with a higher proportion of smaller scale faults (ST-CB_1d, ST-CB_2b, ST-CB_4, ST-CB_1a types).

5.5.5.2 E-W Scanlines (Mostly N-S Faults)

The E-W scanlines exhibit an overall lower density of faults than the N-S scanlines with an FI of 0.30 and an average spacing of 4.08km (Figure 5.17). The histogram distribution for the E-W transects is more random than the N-S distribution and exhibits a higher range (14154m) with few significant peaks. This suggests that the faults intercepted by the E-W scanlines are further and more irregularly spaced than those intercepted by E-W transects. The E-W lines have are generally poorer imaging of the Carboniferous due to the interval being deeper, these fewer spacings may be due to resolution effects to a degree.

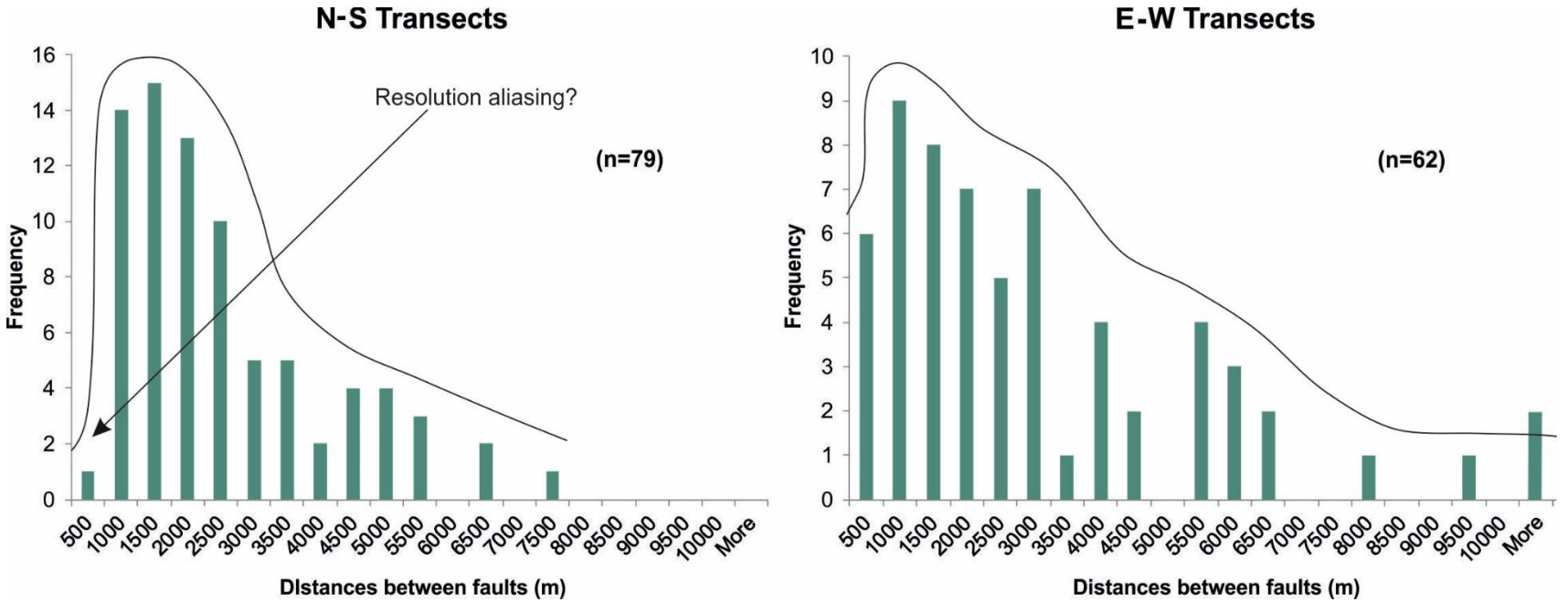


Figure 5.26 Spacings between faults on each scanline transect set the Cleveland Basin. Both distributions exhibit skewed right distributions. Would the faults intersected on the N-S transects have a negative exponential distribution if faults below the seismic resolution were also included?

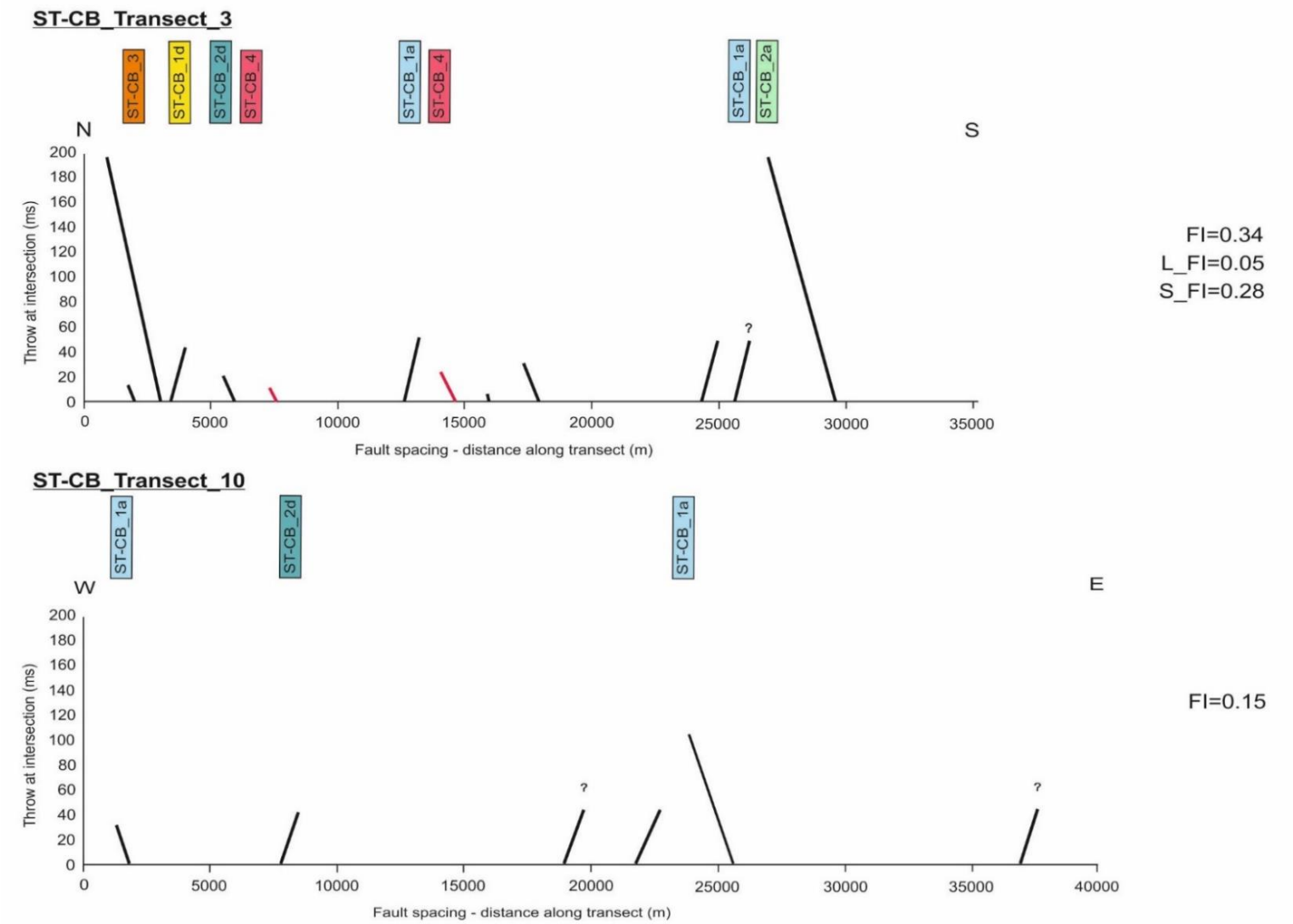


Figure 5.27 Representative scanline transects from each orientation set in the Cleveland Basin. Fault attributes sampled include fault spacing, orientation, throw sense, throw value and dip direction in the Upper Visean – Lower Namurian interval. Positions of scanlines are shown in Figure 5.13

Transect CB_10 (Figure 5.27b) reflects the less frequent and irregular spacing of the N-S faults. The faults intercepted include types ST-CB_1a and ST-CB_2b. They have generally smaller offsets than those observed on the N-S transects and the larger scale faults are not observed. A low fault intensity of 0.13 is observed with an average spacing of 7.7km.

5.5.6 South East Pennine Basin

A total of 23 scanlines transect the EPC, 12 of which are NE-SW (A-L) and 11 that are NW-SE (M-W) orientated. Faults over two orders of magnitude are intersected by each scanline orientation; larger scale Lower Carboniferous half grabens and the smaller scale faults of the East Pennine Coalfield (see Figure 2.33). The NE-SW transects intersect a higher frequency of faults with an overall fault intensity value of 0.66 (Figure 5.17). These faults intersect mostly WNW-ESE and NWW-SSE trending faults. The NW-SE transects insect less faults, as indicated by the lower overall fault intensity value of 0.52 (Figure 5.17). The dominant fault trends intersected are NE-SW.

5.5.6.1 Larger Scale Faults (Throughgoing)

The larger scale faults (indicated by the bold black lines on Figure 5.5) have orientations of dominantly E-W and WNW-ESE with lesser observed NW-SE, NNW-SSE, NE-SW, N-S. The histogram in Figure 5.28d exhibits a random distribution, with spacing values ranging from 500m to 23000m, indicating an irregular spacing of these faults across the EPC. Considerably fewer spacing measurements are recorded for these faults (n=17) which is likely due to them being an order of magnitude larger in scale. The areal extent of the data may therefore be insufficient to sample the spacing of this population.

The spacing between the E-W to NW-SE Carboniferous basin bounding faults (throws on basement reflections of >3km) across the UK is variable. Closer and more irregular spacing of these faults is exhibited towards the midlands microcraton in the South East Pennine Basin, where the troughs such as the Gainsborough and Widmerpool are thinner (15-20km wide troughs). To the north, i.e. the Northumberland Trough, Tweed basin and Stainmore Trough, they are further and more regularly spaced (~40km wide troughs). This thickness of troughs appears to increase northwards.

5.5.6.2 Smaller Scale Faults (Superficial)

The dominant fault sets intersected by all scanlines were orientated NW-SE, NE-SW and WNW-ESE with some less frequent intersections of NNE-SSW, WSW-ENE, NNW-SSE, N-S and E-W.

The spacing distances between the NE-SW faults are presented in the histogram in Figure 5.28b. The NE-SW occur the most frequently with 77 observations. The modal spacing distances between NE-SW faults are between 0-500m, with 19 observations (~25%). Over half (57%) of recorded distances fall within the range 0-1500m.

The occurrence of NW-SE orientated faults is less frequent in the East Pennine Coalfield area reflected by the fewer recorded spacings. The histogram in Figure 5.28a shows that like the NE-SW faults, the most common spacing distances for the NW-SE is in the range of 0-500m the (24.6%), however, the proportion of 0-1500m spacings is less than for the NE-SW faults (43.9%).

WNW-ESE faults were transected less frequently than the NE-SW and NW-SE faults sets in the EPC Area. The histogram in Figure 5.28c shows that the most common spacing occur in the range of 0-500m, with nearly a third (32.4%) of spacing values falling in this range. The spread of data across the rest of the histogram displays a random distribution with considerably fewer counts.

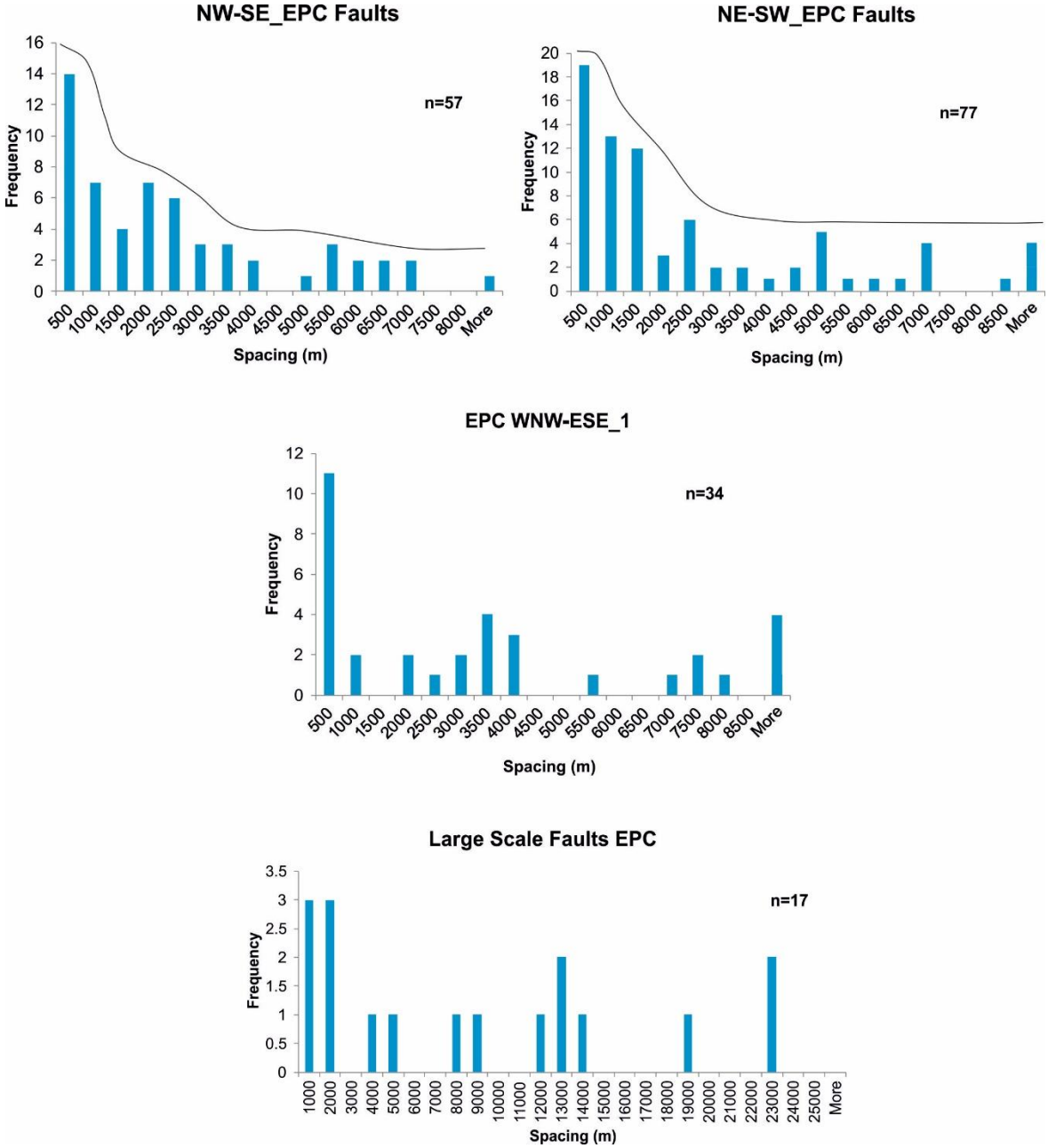


Figure 5.28 Frequency distributions for fault spacings for various fault types in the East Pennine Coalfield a) smaller scale NW-SE faults b) smaller scale NE-SW faults c) smaller scale WNW-ESE faults d) larger scale faults of varying orientations. The NW-SE and NE-SW faults exhibit slight negative exponential distributions. The WNW- faults exhibit a distribution with aspects of both negative exponential and random distributions. The Lower Carboniferous (large scale) faults exhibit a random distribution. This is likely due to them having few intersections, which in turn is due to the fact that they are an order of magnitude larger than the other faults and therefore cannot be accurately represented by such a small sampling area.

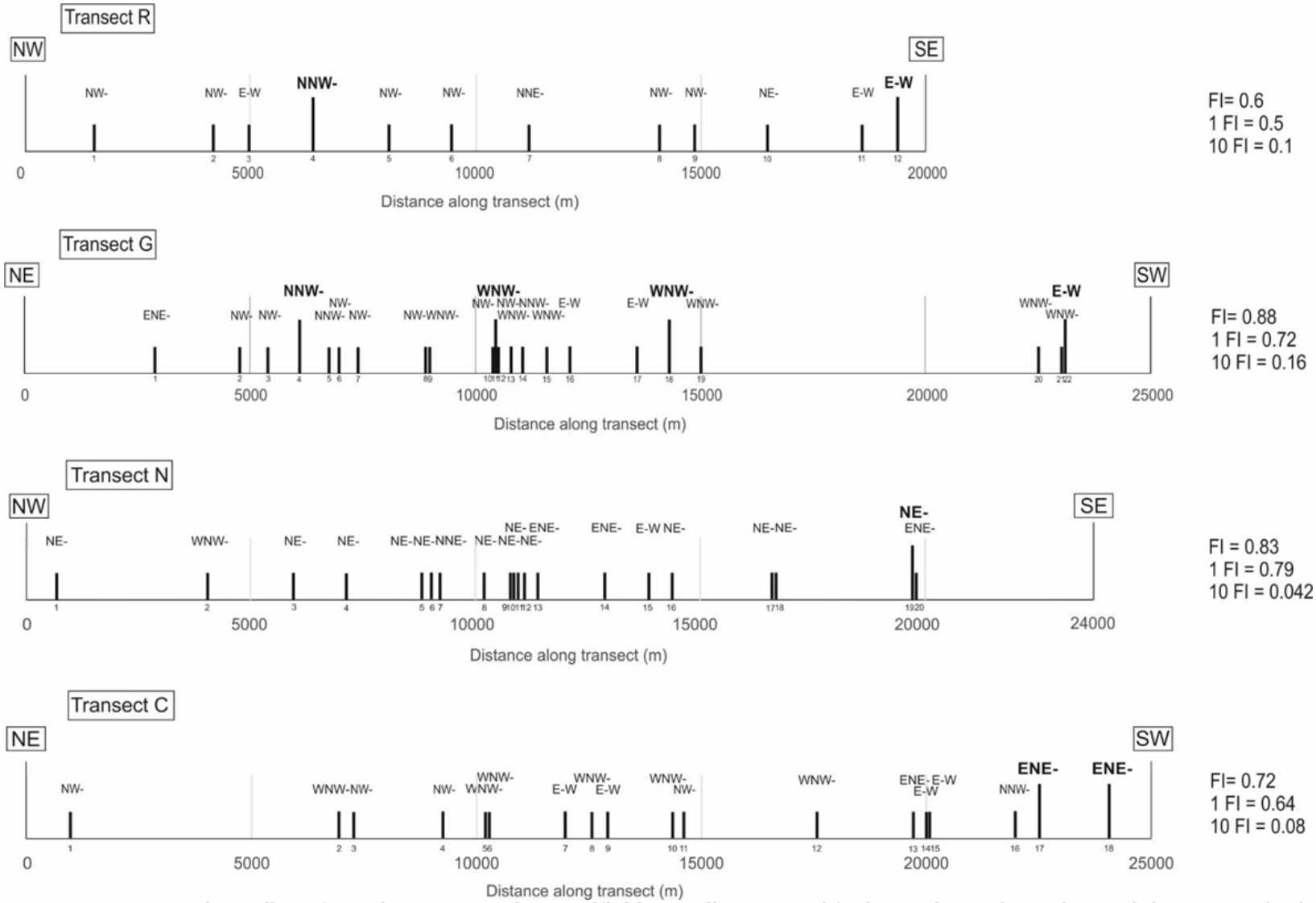


Figure 5.29 Four example scalines from the East Pennine Coalfield. Scanlines record fault spacing, orienataion and throw magnitude, as inidcated by the thickness of the fault (map proxy for fault size).

5.6 Synthesis of Key Results

The Westphalian interval of the East Pennine Coalfield records the highest fault intensity value of all case study areas (Figure 5.14). This result is reasonable because this is the only dataset records fault throws from 1-40m (Figure 1.8). Many authors have argued that fault distributions obey a simple power law distribution (Walsh et al., 1991, Marrett and Allmendinger, 1992, Childs et al., 1990; Yielding et al., 1992), whereby the frequency of smaller faults is progressively greater than larger faults. It is therefore reasonable to expect that the dataset with the lowest threshold value for detectable throw would have the highest density of faults. A separate question, however, is whether there is anything particular in the deformational history of the East Pennine Coalfield that would tend to result in an anomalously high density for faults cutting the Westphalian relative to other Carboniferous basins (see Discussion, this chapter).

The highest density of faults recorded on any of the case studies based on 3D seismic data is within the upper Visean of the Elbow Spit Platform. The Elbow Spit Platform records the highest fault intensity value of all 3D seismic datasets and has the lowest difference in fault intensity between each dominant orthogonal trend (Figure 5.17). The irregular spacing between these fault sets is represented on the scanlines by the clustering of faults (Figure 5.18). The clustering of the WNW- faults is suggested here to be due to their detached nature. The faults die out upslope where the underlying detachment horizon onlaps the slope of the Elbow Spit High (see Figure 3.6).

The lowest density of faults is recorded in the Silverpit Basin case study area. This result is not likely to be explainable by data resolution (Figure 5.31). The NE-SW

strike-slip faults in this area record the highest average spacing values of 8km (Figure 5.17) and only one spacing under 3.5km is observed in the area (Figure 5.22b). This area exhibits the highest difference in fault intensity and average spacing of each dominant fault set. This contrast in fault abundance and spacing is evident on the example scanlines in Figure 5.23. The fault pattern is strongly unimodal, with a highly skewed orientation bias towards the 'Sole Pit' trend of NW-SE. This is believed to be the result of a strong heterogeneity in the basement fabric in this area (see Figure 2.2. and Chapter 6).

The lowest threshold value of throw for fault detection is not in the onshore 2D case study area, as expected, but in the Murdoch Block area, the 2D scanlines however still appear to sample fewer faults than the 3D overall.

Areas of multiple larger scale faults (higher throws/vertical and lateral extents) such as the E-W faults in the Stainmore Trough-Cleveland Basin and Murdoch Block generally have fewer faults in between these larger faults and the minor faults that are present are small. This tendency for larger faults to dominate the strain field in extensional rift settings has been noted for the Mesozoic North Sea Rift (Walsh et al., 1990),(Walsh and Watterson, 1992), and Timor Sea of NW Australia (Meyer et al., 2002)(see Discussion).

It is also evident that throughgoing E-W trending normal faults are more widely spaced onshore than offshore and have higher throws onshore (see Figure 5.33 Transect 3 vs Transect C). It is uncertain if these two fault sets are genetically related due to the lower tip depths not being imaged offshore and thus their deep stratigraphic relationships cannot be characterized like for the E-W faults onshore for which syn-

sedimentary stratigraphy can be recognized (see section 3.6.3.). Faults whose throws fall within seismic resolution are less abundant in the footwall blocks of major bounding faults such as the Alston Block (Figure 5.30) and the Elbow Spit High (Transect D on Figure 5.18). This has also been recognized in the Forty Fathom Fault Footwall block by Knott et al., (1996), who note that faults are less common in the contractional field of normal faulted rock volumes.

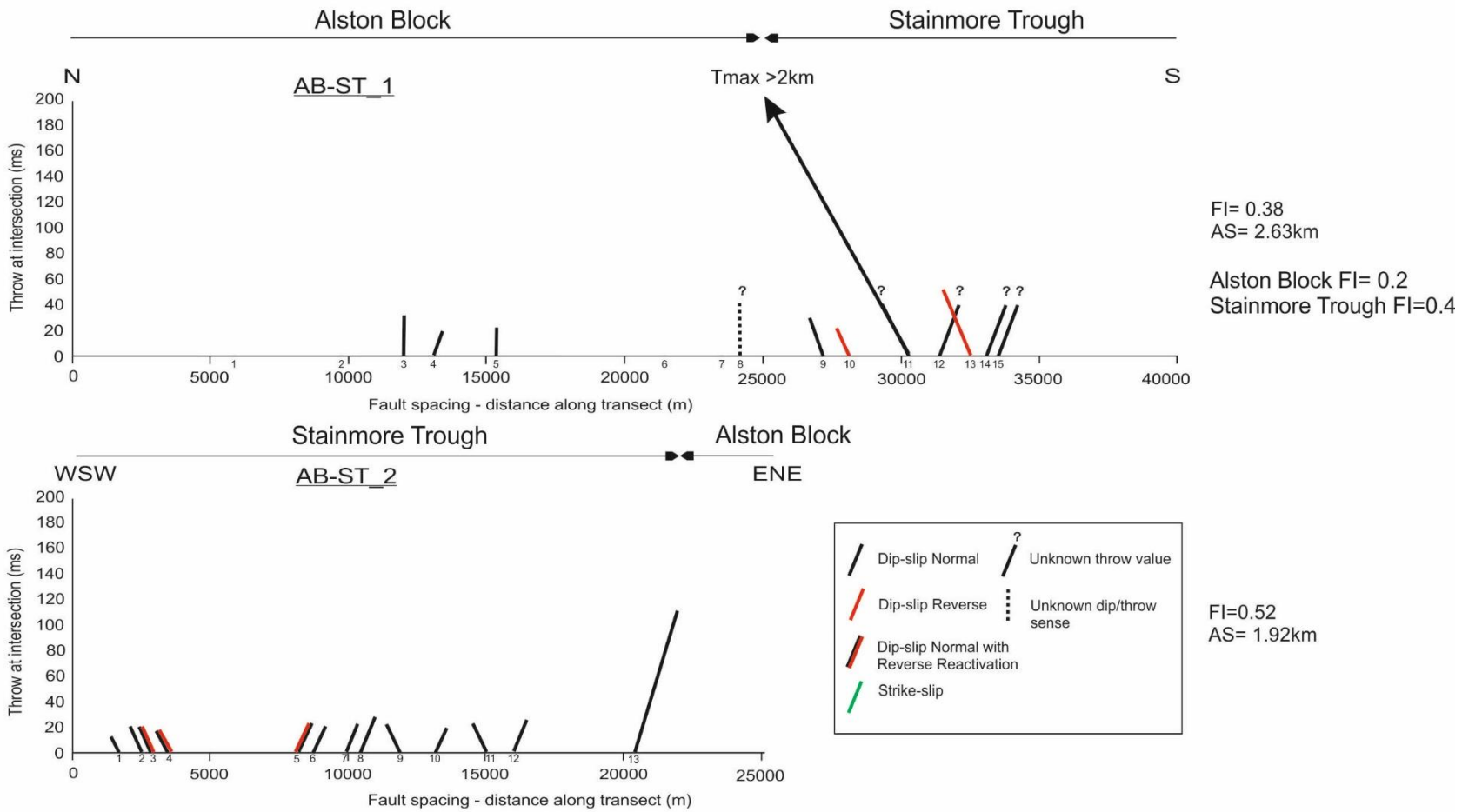


Figure 5.30 Scanline examples from the Alston Block and Stainmore Trough illustrating that there are significantly less faults observed in the footwall highs than in the hangingwalls

5.7 Discussion of Fault Abundance

The following section outlines the limitations to the fault abundance results presented in the previous sections and attempts to address the reasons behind some of the key fault intensity and frequency observations.

5.7.1 Limitations

The 1-D scanline method is widely used in fault and fracture population analysis (Priest and Hudson, 1981, Gillespie et al., 1993,). It provides a good first-order approach to the estimation of the frequency of faults populating a fixed interval of an area i.e. a horizon-based calibration. The data collection is relatively quick and simple and can be applied to multiple data types. Having a grid of two sets of orthogonal scanlines however limits the sampling to a small 1D surface and the ~5km^2 area between the scanlines cannot be extrapolated to 2D or 3D without making some key assumptions and results in uncertainty. This method is therefore good for comparing a number of areas in order to determine an area with favorable attributes that can be further investigated more detailed 2D and 3D sampling techniques.

Due to the lack of laterally coherent intra-Carboniferous horizons, the Base Permian subcrop was sampled in each area. This is a different stratigraphic interval in each area and therefore not all areas can be compared based on similar lithology and rock properties. The Stainmore Trough-Cleveland Basin and Elbow Spit Platform both have Yoredale facies of Visean (Lower Carboniferous) age, subcropping the Base Permian Unconformity (see Figure 3.7) and fault population data from these two areas can therefore be compared meaningfully, in spite of the different scan line geometries.

The East Pennine Coalfield, Murdoch Block, Silverpit Basin and Cleaver Bank High each have Coal Measure facies of Westphalian age as their Base Permian subcrop, and can also be compared accordingly. On the other hand, there are limitations regarding the comparison of the Stainmore Trough-Cleveland Basin results with the other study areas due to the ~10km, irregular arrangement between the curved scanlines.

5.7.2 Impact of data resolution on Fault Intensity results

One of the most obvious conclusions from the preceding data analysis is that generally the lower the throw detection threshold value, the higher the fault density observed (with exceptions), as exemplified by the case study of the East Pennine Coalfield (Figure 5.14). The 2D onshore seismic data is considered to be poorer in terms of fault detection of faults due to older acquisition times, imaging problems due to the lack of a third crossline dimension (Cartwright and Huuse, 2005) and aliasing and spatial resolution problems from a 2D grid. The calculated throw detection threshold derived from the sonic velocity and dominant frequency of the Base-Permian interval however gives a value that is similar to and in some cases lower than that of the 3D seismic, indicating that a viable comparison can be made between these two data types that mitigates any potential censoring effects due to resolution. This means that we can therefore reliably compare the fault density and frequency between an onshore and offshore area, these being the Stainmore Trough-Cleveland Basin and South Cleaver Bank High areas as they have roughly the same throw detection threshold value (Figure 5.31).

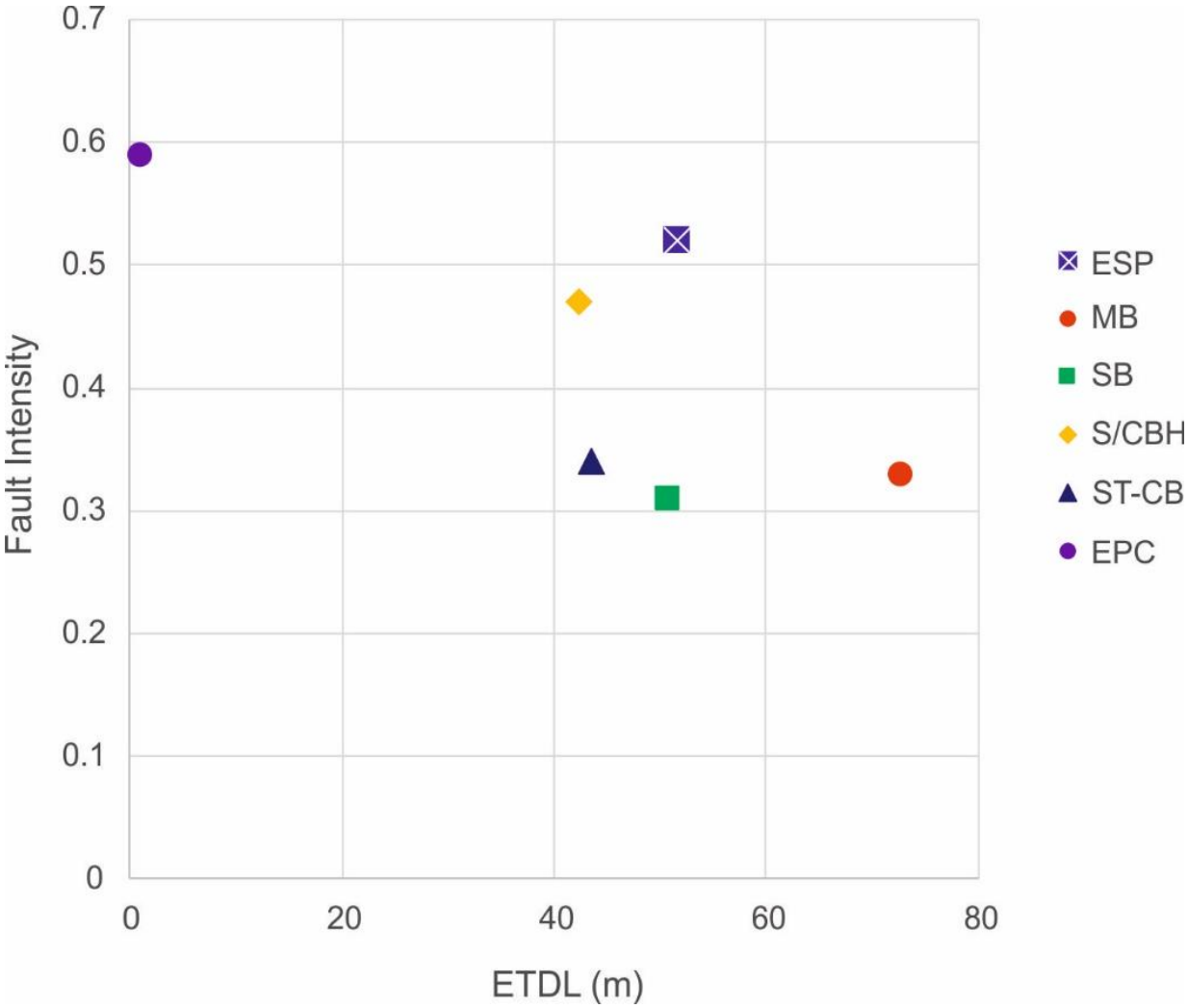


Figure 5.31 The FI and ETDL for each of the case study areas. The plot indicates which of the case study areas may have their density and spacing results affected by vertical resolution and fault detection on data. The 3D seismic data in the Murdoch Block study area has a lower vertical resolution which in turn gives a low effective throw detetction limit for faults. It is important to take this into account when comparing the fault intensity of this area to one with a higher vertical resolution /lower ETDL as the FI may be higher for the Murdoch Block if the EDTL was a lower value. This low FI value may therefore be due to either structural controls or data resolution.

Given the fact that the fault intensity for the latter area is significantly higher than the former (difference of 0.13, see Figure 5.31), the higher abundance of faults appears to be offshore appears likely to be due to purely structural controls, rather than data issues. A key difference between these two areas is the interval of measurement (see section 5.7.1.3.).

Some results however may have been affected by data resolution and having a high ETDL value, an area such as the Murdoch Block is a key example. Given that this area has a relatively low FI and a high ETDL value (Figure 5.31), this low fault intensity could due to either structural or resolution controls. The fact that the adjacent Silverpit Basin has a lower throw threshold value but has a roughly similar fault intensity, this may indicate that resolution differences in the order of 10s of metres may not have a significant effect on the frequency of faults that are resolved.

5.7.3 How does the fault intensity vary by stratigraphic interval and why?

Due to the fact that the Southern Cleaver Bank High and the Stainmore Trough-Cleveland Basin areas have similar throw detection values in the interval immediately subcropping the Base Permian (Figure 5.31), the fault density results from these two case study areas can be compared on a purely structural and stratigraphic basis as there is no resolution bias. The faults sampled in the S. Cleaver Bank High are within the Upper Westphalian stratigraphy while the faults sampled within the Stainmore Trough–Cleveland Basin area are within the Lower Namurian-Upper Visean. Given that there are significantly more faults observed within the Westphalian succession in the southern Cleaver Bank High than the Lower Namurian-Upper Visean of the Stainmore

Trough-Cleveland Basin (Figure 5.31), is there a structural or stratigraphic reason for this observation?

The once present Westphalian succession in the ST-CB area, could have also had an abundance of closely spaced faults, as observed in the southern Cleveland Basin. Scanlines taken through the Upper Visean-Lower Namurian succession of the Cleaver Bank High (Figure 5.32) show significantly lower fault abundance and higher spacing distances in this succession when compared to the Westphalian. This may be due to resolution aliasing, many of the smaller faults that are sampled on Transect K W but not Transect V have throws of 40ms or less. The seismic resolution in the Visean-Namurian interval is likely much lower, and therefore the threshold value for throw detection higher. The exact resolution at this interval cannot be calculated exactly due to lack of well penetrations calibrating the velocity. The comparison of Transect KV to Transect 3, a scanline from the Stainmore Trough – Cleveland Basin within a similar stratigraphic interval, suggests that the lack of faults recorded on KV is likely due to resolution aliasing.

A comparison can be made between areas that have sampled a similar stratigraphy but in different areas with different datatypes, such as the Visean interval sampled in areas Stainmore Trough-Cleveland Basin and Elbow Spit Platform (Transect D and P, vs 3 and 10 on Figure 5.33). Since the Elbow Spit Platform has a higher throw detection value than that for the Stainmore Trough-Cleveland Basin but also has a considerably higher fault intensity (Figure 5.31), we can therefore rule out that this difference in fault density is due to a resolution artefact. The higher fault

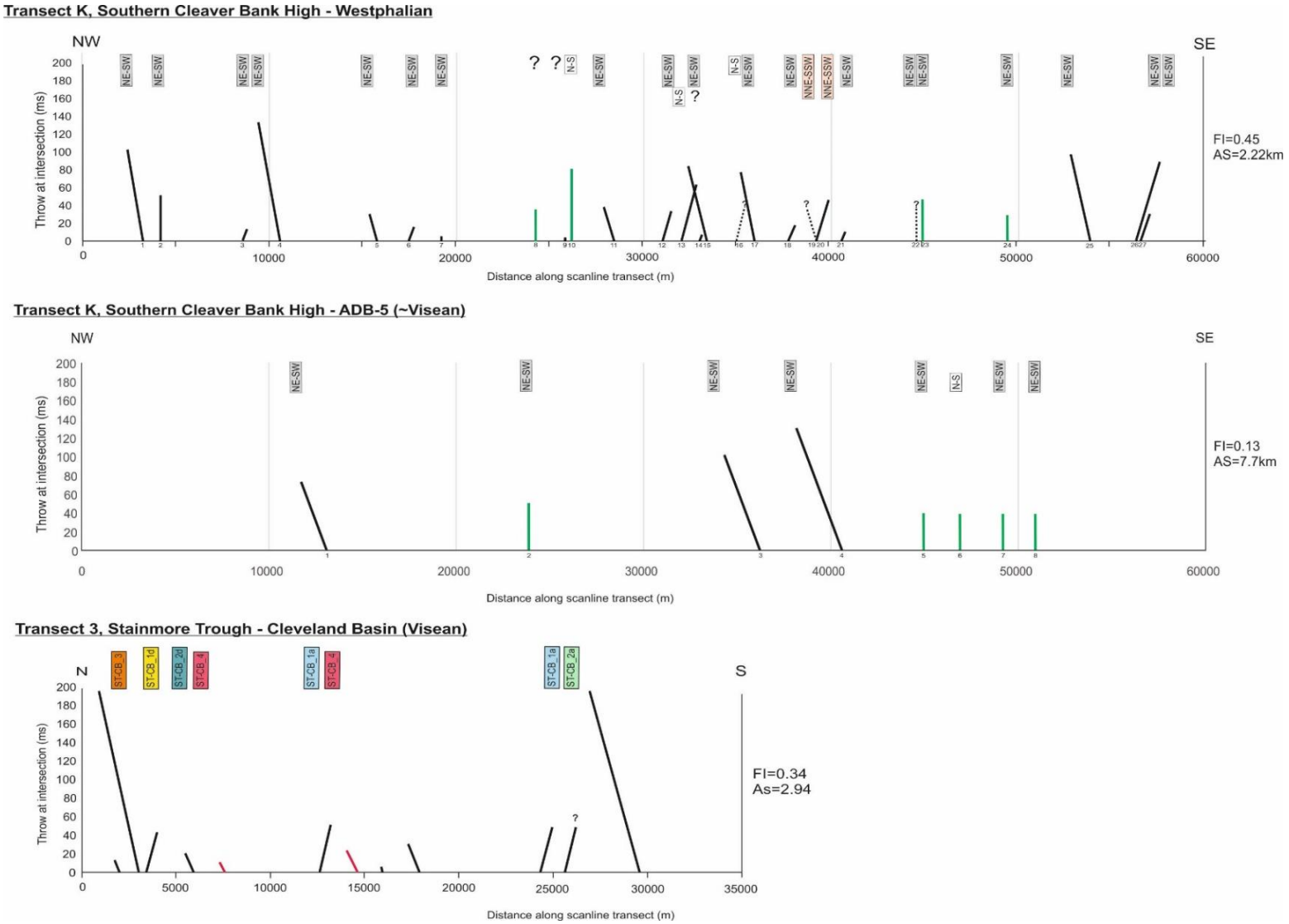


Figure 5.32 Comparison of two scanlines that sampled two different stratigraphic intervals in the Cleaver Bank high, compared with a scanline of the Westphalian interval in the Stainmore Trough-Cleveland Basin.

intensity for the Elbow Spit Platform is due to the fact that there are a higher frequency of faults with smaller and medium throws that have formed within the zone of influence of a single large scale fault. The explanation for the Stainmore Trough – Cleveland Basin is different in that there are more frequent larger dimension/throw (ST-CB_1) faults with fewer smaller faults in between (see Transect 3 on figure Figure 5.27). The mechanical reason for this may be that fewer new smaller faults have formed because the strain has been concentrated on the larger faults over time (Meyer et al., 2002) or that newer faults that have formed became inactive and did not grow to a size large enough to be represented by the seismic resolution (Walsh et al., 1991). This concentration of strain on the larger faults is evidenced by the repeated reactivations through time (see Chapter 6). Another reason for the difference in fault intensity in these two areas is that many of the faults on the Elbow Spit Platform formed due to gravity-driven processes of a non-tectonic origin (see Chapter 4 section 4.7.1) which has not been observed in the Visean onshore.

The limitations to this comparison and any comparison with the Stainmore Trough-Cleveland Basin is that there are 5 fewer scanlines, however if 15 out of the 20 fault intensity values are chosen at random from the Elbow Spit Platform the average fault intensity is crudely the same. The generally poor quality of the onshore seismic may have not imaged the smaller and medium faults, and the sparsity of the lines may have missed them in the sampling, but the calculated seismic resolution in this interval suggests otherwise (Figure 1.8).

5.7.4 Can the sub-seismic fault abundance in seismic data areas be estimated using the EPC results?

The fault spacing and abundance results for the East Pennine Coalfield may be a good indicator of the sub-seismic fault population in other sub-basinal intervals of Westphalian sampled by 3D seismic. This could be estimated by finding out the ratio of larger faults to coal map faults in the East Pennine Coalfield, and using this same scaling relationship.

For this technique to be implemented, it is necessary for throw values to be assigned to each fault on the East Pennine Coal Map dataset. When these values are assigned, a throw filter can be applied that isolates the sub-seismic (throw <40-50m) to seismic (throw >40-50m) faults for each sampling transect.

For this extrapolation to have any valid grounds, it would stand to reason that the area and interval in which this fault abundance is being estimated is 1) a similar stratigraphic interval 2) has a similar basin architecture and 3) has undergone a similar tectonic evolution to the East Pennine Coalfield. The Stainmore Trough–Cleveland Basin has a similar basin architecture to the East Pennine Basin, with roughly E-W trending large-scale faults, and is located adjacent to the EPB, however the Westphalian succession has been eroded in the Stainmore Trough-Cleveland Basin due to Variscan uplift (see section 2.6.2). Due to the generally low throw values (Bailey et al. 2005) and limited vertical extents of the EPC faults, it is unlikely that the lower tips of these faults would terminate in the upper Visean-Namurian.

An area such as the Silverpit Basin that has a roughly similar tectonic history, NW-SE basin archticture (Figure 2.23) and a preserved Westphalian interval, may be a better contender for this estimation.

5.8 Discussion of Fault Spacing Characteristics

5.8.1 Limitations

The 1-D scanline method for sampling fault spacing provides a good insight into the spacing of specific fault types when taken normal to the specific fault trend. Due to the variation in fault azimuths encountered in each area, a more rigorous approach would have involved the construction of multiple scanline orientation sets. Since it was often possible to identify two dominant fault trends in each area using horizon maps, it was decided to simply adopt a procedure of constructing an orthogonal scanline grid normal to these two dominant trends. A 2D sampling method such as box counting (Gillespie, 1993) would have removed this scanline orientation bias, however, results from 3D data (3D seismic) would not have been able comparable to results from 2D data.

5.8.2 What causes the paucity of a pervasive orthogonal trend in the Silverpit Basin

The Silverpit basin is unique among the case study areas in that it has an abnormally high difference between the fault spacing and abundance of each orthogonal fault trend (Figure 5.17). The low frequency of NE- strike slip faults is unlike that seen in any other area. The three large scale basement controlled faults in that area (set 44-49_NW-_TR, see Chapter 3 section 3.4.3.3.) that have been repeatedly

reactivated may have had a control on the spacing of the smaller scale intervening NW-_S faults and their preferential orientation. This idea that later structures are influenced by the presence of, and geometries of large scale structures that perturb the stress field is also seen by joint sets, these joint sets become aligned sub parallel when in close proximity to the large scale faults (Rawnsley et al., 1992).

This observation may however be limited by the resolution of observation, as there is a dominant E-W/WNW-ESE pattern in the East Pennine Coalfield in which superimposed smaller fault trends of NW-SE, NE-SW and WNW-ESE are observed.

Another area that exhibits this pattern is the Elbow Spit Platform, in which there is a dominant NW-SE striking normal crustal scale fault with a less pervasive orthogonal trend. Interestingly, the orthogonal trend is also a strike slip set with far and irregular spaced faults (Figure 5.6). Onshore E-W grabens also appear to have a less pervasive orthogonal trend (Figure 5.12).

In summary, areas with larger scale, Throughgoing faults appear to be less cross cut by an orthogonal trend and in two of the three cases, where present, the orthogonal trend is a set of strike-slip faults.

5.8.3 Which case study area would be most suitable for unconventional hydrocarbon production based on fault abundance and spacing?

Given that the Silverpit Basin has an overall low density of seismically resolvable faults and the widest spacing of a particular fault trend (Figure 5.14 and Figure 5.17), it may at first sight be considered an ideal area for horizontal drilling and hydraulic fracturing operations. This argument rests on the basis that there are large rock volumes where no faults would be predicted to be encountered that could potentially

be detrimental to the operation e.g. by leaking frack fluids to shallower levels, or in steering the fracks away from the target interval. Westwood et al. (2017) deem the maximum horizontal respect distance to be from 63-433m, with the values in this range depending on natural fracture intensity and failure threshold value. Wilson et al. (2018) deduced a distance of 895m between horizontal boreholes that are perpendicular to the maximum horizontal stress direction and faults optimally orientated for failure under the regional stress state. Given that the fault reactivated in Blackpool, Lancashire that caused seismicity was from 300-400m from the injection site (Clarke et al., 2014b), the figure deduced by Wilson et al., (2018) seems more likely.

This would suggest that large fault blocks such as those in the Westphalian interval of the Silverpit Basin (Figure 3.35), in which no resolvable faults are detected in areas of with dimensions of 8km x4km, are more than suitable. However, this assumes that there is no significant sub-seismic fault population. This caveat applies to any area of Carboniferous stratigraphy that represents a petroleum play where fracking may be considered necessary. There is debate as to whether fractures help or hinder production in hydraulically stimulated plays (Stephenson and Coflin, 2015). Stephenson & Coflin (2015) concluded that seismically visible features (faults or lineaments) proved to be problematic and unpredictable with success replying on the presence of a pressure-contained system. They also concluded that smalls scale natural fracture network heterogeneity made the effects variable, and that it is more helpful to consider the effects of the presence of a natural fracture network on properties of the rock body that will affect the geomechanics as a whole.

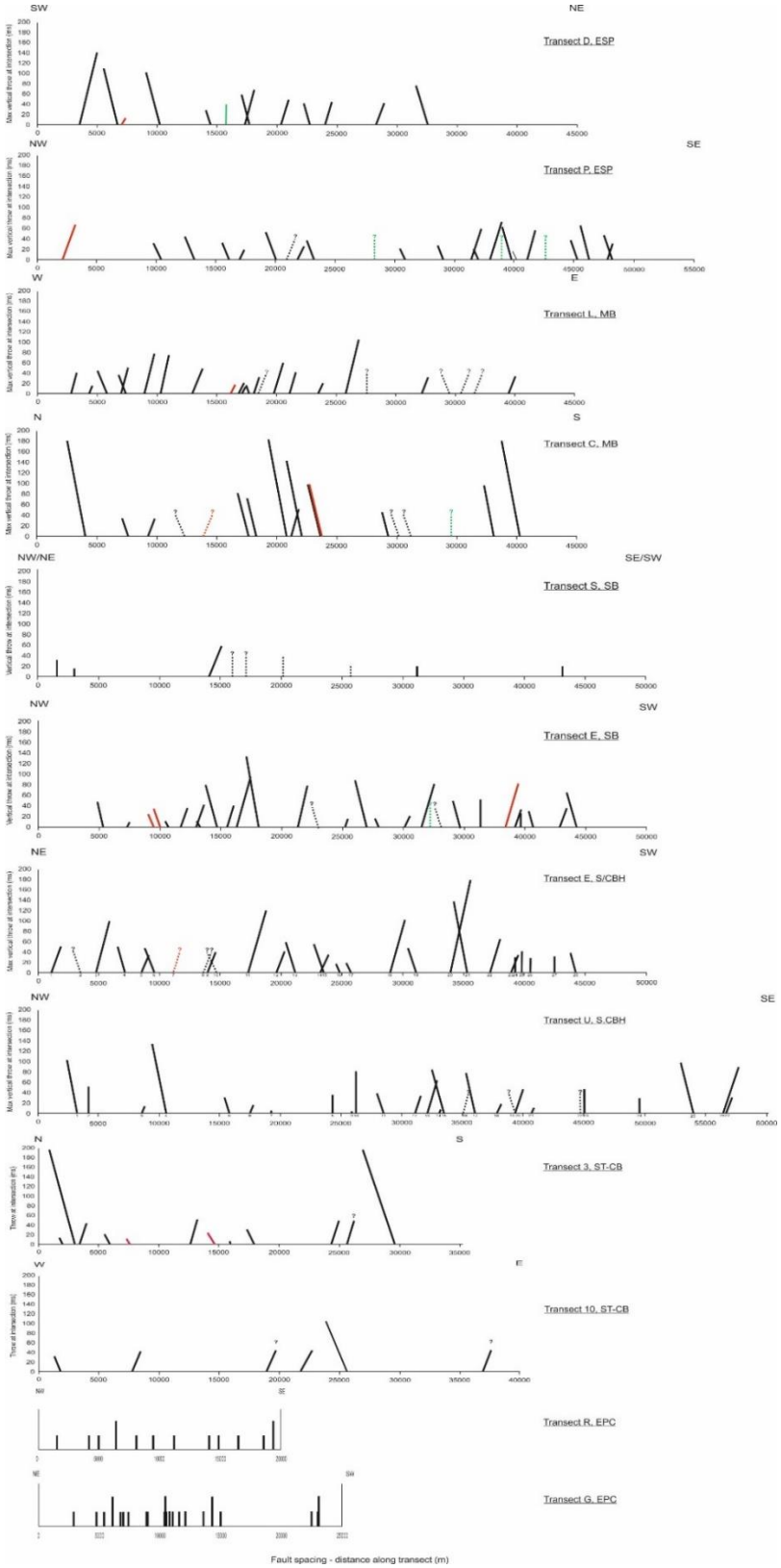


Figure 5.33 Representative scanlines from all case study areas. All scanlines can be found in Chapter 5 supplementary material.

It is therefore not possible to be definitive on what areas might have a comparably high natural fault and fracture network to that seen in the East Pennine Coalfield. It does seem likely however, that there is a significant risk that seemingly low density at seismically resolvable levels may not be true at much lower throw detection thresholds, and the East Pennine Coalfield dataset is a case in point. If we applied a throw filter at say 40m to this dataset, most of the faults would disappear. Clearly, faults with throws of say 10m could represent either a major mechanical barrier or fluid conduit during fracking operations, or could equally be stimulated to yield earthquakes above a traffic light cut-off value (Ellsworth, 2013, McGarr et al., 2015, Clarke et al 2014, Walters et al., 2015).

5.9 Further Work

Future work that would add further constraints to this dataset would be to measure the intersected throws on all scanlines rather than extrapolating the characterized throws for each fault set on every scanline. This would require a rigorous effort so would only be performed for areas on potential interest such as the Silverpit Basin.

Estimating the sub-seismic spacing by using the ratio of smaller faults using the sampling results from the EPC map could then be performed. This data can then be extrapolated to 3D seismic areas with a similar interval (i.e. CBH, SB, MB) to estimate the fault throws in these areas below ~40-60m. The additional dataset of the EPC fault throws is also required to assign to the faults on the map.

5.10 Conclusions

1 The 2D onshore seismic data appears to be as effective as offshore 3D data to capture the presence of subsurface faults. However, the poor fault definition and variability and inconsistency of image quality among different 2D seismic does not allow for the same precision in offset estimation. The inconsistency in data quality when combining multiple 2D seismic lines for a sampling transect, and the uneven sampling grid limits the comparison of these two datasets spatially, however a 1D comparison can still be made.

2. Measuring intersected throw on sampled faults on 2D scanlines is less helpful than assigning a relative size in the determination of spacing relationships. This is because the intersected throw is unrepresentative of the fault size due to variable strike positions. Reactivation histories also mean that the present throws that have been reversed may not proportional to the fault size.

3. The highest seismic scale fault abundance is recorded in the Elbow Spit High Upper Visean interval. The fault spacing distribution results from this area most resemble the negative exponential distribution curve observed on the smaller resolution fault map results from the EPC.

4. The results from the Stainmore Trough-Cleveland Basin show that the observably low fault abundance in the Lower Carboniferous section of the offshore basins in the central Anglo-Dutch Basin (areas with a Westphalian subcrop) is likely a resolution artefact.

5. The low fault abundance in the Silverpit Basin is due to anomalously high spacing due to the lack of a domain cross cutting fault trend. The few faults that are present have a low frequency and high spacing.

6. Areas with large scale throughgoing faults that are strongly coupled with the basement (i.e. Silverpit Basin, Stainmore Trough – Cleveland Basin and the Elbow Spit Platform) exhibit a significantly less dominant cross cutting fault set at the same scale of observation/seismic resolution. This is thought to be due to the stress perturbations created by the large structures that preferentially align the majority of newer structures of a similar scale parallel or sub-parallel to the throughgoing fault. This result is resolution dependent as demonstrated by the superimposition of the two cross cutting EPC fault sets (NW-SE and NE-SW) on the larger scale throughgoing/basement faults (WNW-ESE) in the Gainsborough Trough. This does not include the presence of stretch faults accommodating strain on larger faults.

7. In densely populated areas with two dominant cross cutting fault trends (i.e. Cleaver Bank High and Murdoch Block), there is a paucity of smaller scale faults with observed throws greater than ~500-800m.

8. Areas of multiple larger scale faults (higher throws/vertical and lateral extents) generally have fewer seismic scale faults in-between them. This is interpreted to be due to the decreased necessity for more new meso-scale faults to be formed through time to accommodate stress field rotations, due to the presence of the larger faults. Alternatively, faults that do form do not propagate to be seismic scale faults. The presence of one or two smaller faults around these larger faults is observed and the frequency of these faults decreases with distance from the larger fault (in agreement

with Knott et al. 1996). The presence of faults clustered around these larger faults below the seismic resolution that accommodate the displacement on likely but not quantified.

9. The quantification of fault frequency and spacing in the EPC has useful applications to the estimation of sub-seismic fault populations in stratigraphically similar intervals in areas that have undergone a similar tectonic evolution. An area such as the Silverpit Basin is an ideal candidate for this assessment.

Chapter 6

SUMMARY AND DISCUSSION

6 Summary and Discussion

6.1 Introduction

This chapter summarises and discusses the key results, conclusions and discussion points that are presented in the research chapters. The key stages of fault activity on the case study faults from Chapters 3, 4 and 5 are summarised through time and the significance of the observed fault patterns and structural styles discussed.

6.2 Phases of major fault activity in the Anglo-Dutch Basin study area

This section summarises the activity of the various fault sets through time, portrayed as a series of 'palaeotectonic' maps, inspired by Edward Tufte's 'The visual display of quantitative information.' The intention here is to present the results of the detailed structural analyses presented in Chapters 3, 4 and 5 in a simple graphical form. Only the main phases of fault activity are presented, where there is clear evidence of a fault being active in a specified time period. Times of tectonic quiescence are not discussed.

Faults that are active at the specific time periods are highlighted and their sense of displacement and magnitude indicated. The top-left inset for each main map panel indicates the interpreted direction of regional extension or contraction, or the tectonic event relevant to each specific time period (Arthaud and Matte 1977, Zeigler 1989, 1990, Van Hoorn 1987, see also Chapter 2.3).

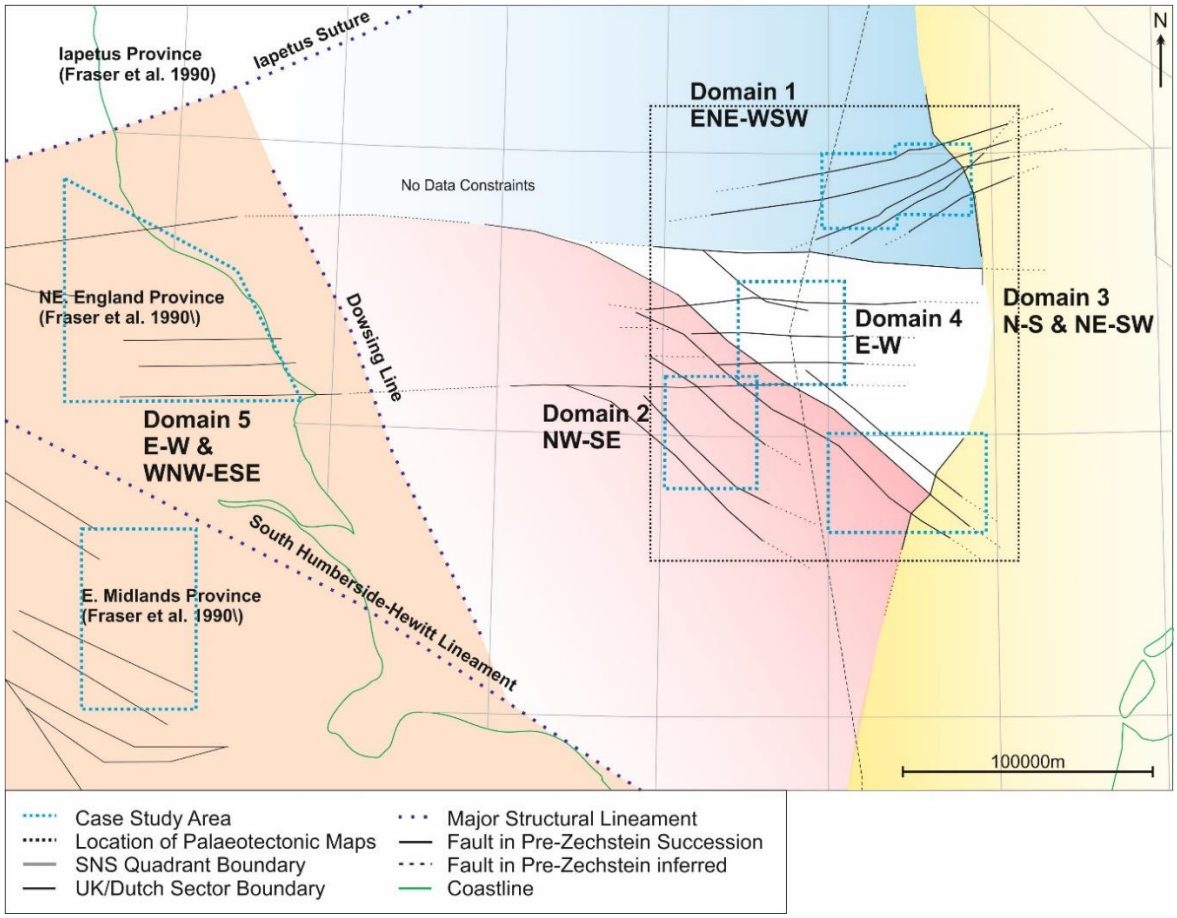


Figure 6.1 The five structural domains across the Pennine and Anglo-Dutch Basins. Domain 1) The Mid North Sea High Margin Domain is characterised by the presence of punctuated E-W normal and strike-slip faults and ENE-WSW strike-slip faults. The domain is bound to the east by a NW-SE rift fault, which marks the start of Domain 3 (The Central Graben Domain). The throughgoing faults offset the entire PZS (mostly a Visean aged base Permian subcrop to Caledonian basement) with the presence of intervening detachment and superficial faults offsetting the Upper Devonian-Lower Carboniferous. Domain 2) The Silverpit and Sole Pit domain is characterised by the dominance of NW-SE trending basement faults that have been repeatedly reactivated through time including pre- and post BPU inversions. Presence of intervening superficial faults with the same orientation. Domain 3) The Central Graben Domain is characterised by NE-SW and N-S oriented, east dipping normal faults progressing into rift faults to the east. Domain 4) The Murdoch Block-Cleaver Bank High Domain is characterised by an abundance of E-W throughgoing faults that have been reactivated frequently through geological time in all slip senses. Domain 5) The East Pennine Domain (Fraser et al. 1990) is characterised by E-W and WSW-ENE grabens and half grabens with Lower Carboniferous syn-sedimentary infill. The clear contrast in dominant fault trends and reactivation styles between the Silverpit Basin (Domain 2) and Murdoch Block (Domain 1) can be seen on 3D seismic data and published structural maps. The E-W trend intersects the NW-SE faults to the west in which this trend dies out into a dominantly NW-SE trend. This argues for the presence of a major structural boundary between these two areas, possibly marked by one of the major NW-SE trending faults i.e. the Murdoch Fault Zone.

Five structural domains are recognised in total across the Pennine and Anglo-Dutch Basins (Figure 6.1). Due to having the best 3D coverage of detailed fault geometries, I focus here on the evolution of the central Anglo-Dutch Basin.

6.2.1 Late Devonian – Early Carboniferous (Famennian-Brigantian) Rifting, (~374-329Ma)

The Late Devonian-Early Carboniferous is a time period associated with rifting and subsequently the production of syn-rift stratigraphic megasequences (Fraser et al. 1990). The 3D seismic data in the central Anglo-Dutch Basin has a vertical cut off point that typically ranges from 4-5 seconds TWT. Due to the thick Mesozoic subsidence and burial, this means that the Lower Carboniferous sediments are deeply situated and this data extent only images stratigraphic intervals and structure to depths of the Lower Namurian/Upper Visean. Fault activity during the Late Devonian and Early Carboniferous is therefore relatively uncertain in this area because most syn-sedimentary packages and lower tip regions of major faults are not imaged or are heavily affected by multiples and artefacts such as noise. This reconstruction (Figure 6.2) therefore relies heavily on postulated pre-existing, NW-SE WNW-WSE Caledonian structural fabrics (Fraser et al. 1990, Corfield et al. 1996), along with the correlation of extensional activity occurring on the WNW-ESE faults onshore and further east at this time (Fraser & Gawthorpe 1990, Corfield et al. 1996, Cartwright 1990) (Figure 6.2).

6.2.1.1 Syn-sedimentary extension on WNW-ESE oriented half grabens

The thickening of postulated Visean aged reflection packages to the south in the CADB, particularly evident in the Murdoch Block study area (see section 3.3.3.2 and Figure 3.21) is a strong indication of normal slip occurring on WNW-ESE oriented, NW dipping basement half grabens (Figure 6.2). The exact positions of

the fault planes are difficult to define in this area due the punctuated nature of coherent 3D reflections. These faults are interpreted to be reactivated Caledonian basement faults (Leeder and Hardman 1990, Fraser et al. 1990), which is why normal movement has occurred despite their strike not being optimally orientated to the N-S regional extensional stresses at this time. The reactivation that has occurred is therefore likely one of oblique-slip on pre-existing basement fabrics, which was also discussed by Oudmayer & De Jager (1993) for many fault sets in the Southern North Sea. This fault activity is also in agreement with the tectonic model for the onshore UK, in which extension was occurring on WNW-ESE and E-W half grabens (Figure 2.7 & Figure 2.8) at this time (Fraser & Gawthorpe 1990, Fraser et al. 1990, Corfield et al. 1996).

Further east, beneath the Ringkobing-Fyn High, offshore Denmark, Cartwright (1990) reported the presence of large, basement-controlled extensional faults with E-W orientations, that were active during the Late Palaeozoic, with over 3km of syn-rift fills. This perhaps gives further evidence for a more laterally extensive rift system in the central North Sea with a generally E-W trend, that developed during the Late Palaeozoic.

6.2.2 Early Carboniferous (Brigantian) Inversion (~328-326Ma)

Following Late Devonian – Early Carboniferous rifting, evidence of a contractional event is apparent in the CADB at the end of the Visean. During this time, a partition in structural styles becomes apparent, and two structural domains postulated to have been present. The deformation at this is concentrated in Domain 2.

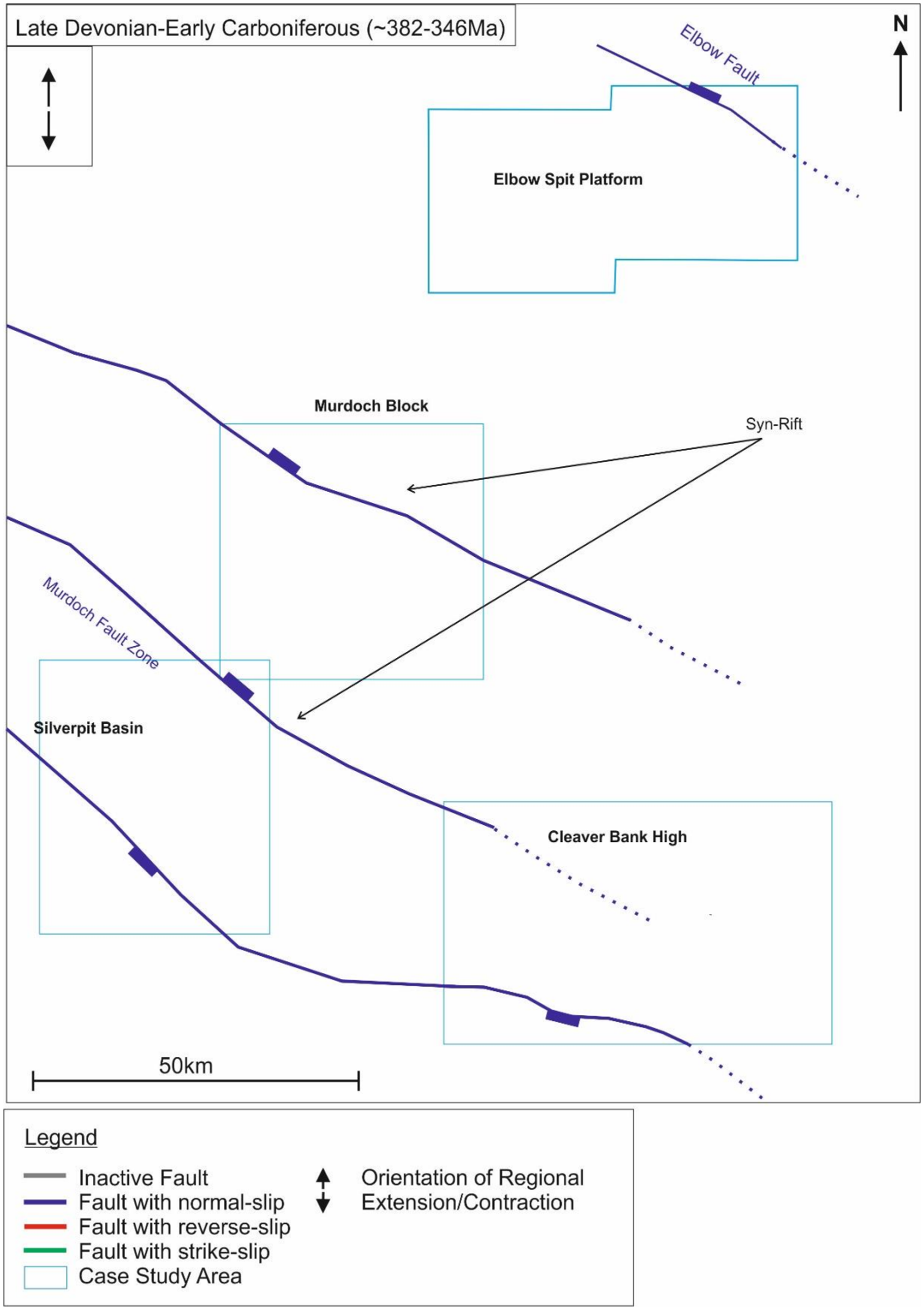


Figure 6.2 Structural map indicating the faults present during the Late-Devonian to Early Carboniferous time period in the Pre-Zechstein succession in the central ADB. Active faults and their movement sense are indicated by the colours and key. Faults outside of the Case Study areas are inferred from regional structural maps and seismic data of poorer quality. Regional N-S oriented extension induces slip on WNW-ESE Caledonian basement trends.

6.2.2.1 Domain 2

The thinning of Namurian-aged stratal reflections onto a folded Visean stratigraphic interval (that may or may not coincide with an inverted basement fault, Figure 3.32), has two possible explanations:

1) An uplift/folding/inversion has occurred during the Visean in which the Namurian sediments onlap the fold crests.
2) Active folding occurred during the Namurian, causing the thinning over Namurian stratigraphy over the fold crest (Contradicts the reported regional tectonic quiescence during the Namurian). This would indicate maximum principle compressive stresses were horizontal at some point in the mid-Carboniferous, in lieu of the reported thermal subsidence.

Model one is the most likely, despite the non-obvious fault plane/graben geometry in the onshore CADB geometry. The proposed model is an inverted half graben, with this inversion taking place at the end Visean.

Truncation of Lower Carboniferous stratigraphy is also observed in the hangingwalls of onshore E-W grabens in the Cleveland Basin (Figure 3.47), creating an angular unconformity. Fraser & Gawthorpe (1990) also discuss an inversion event at the end of the Brigantian, and this folding of Visean stratigraphy in the Silverpit Basin is proposed to reflect this inversion event and is the offshore representation.

These folds could however, be interpreted as being due to differential subsidence across the area, in which this thinning would most likely be expressed as onlap. This type of onlap may occur across a previously extended graben in which the stratigraphic sequences adjacent to the footwall flex downward.

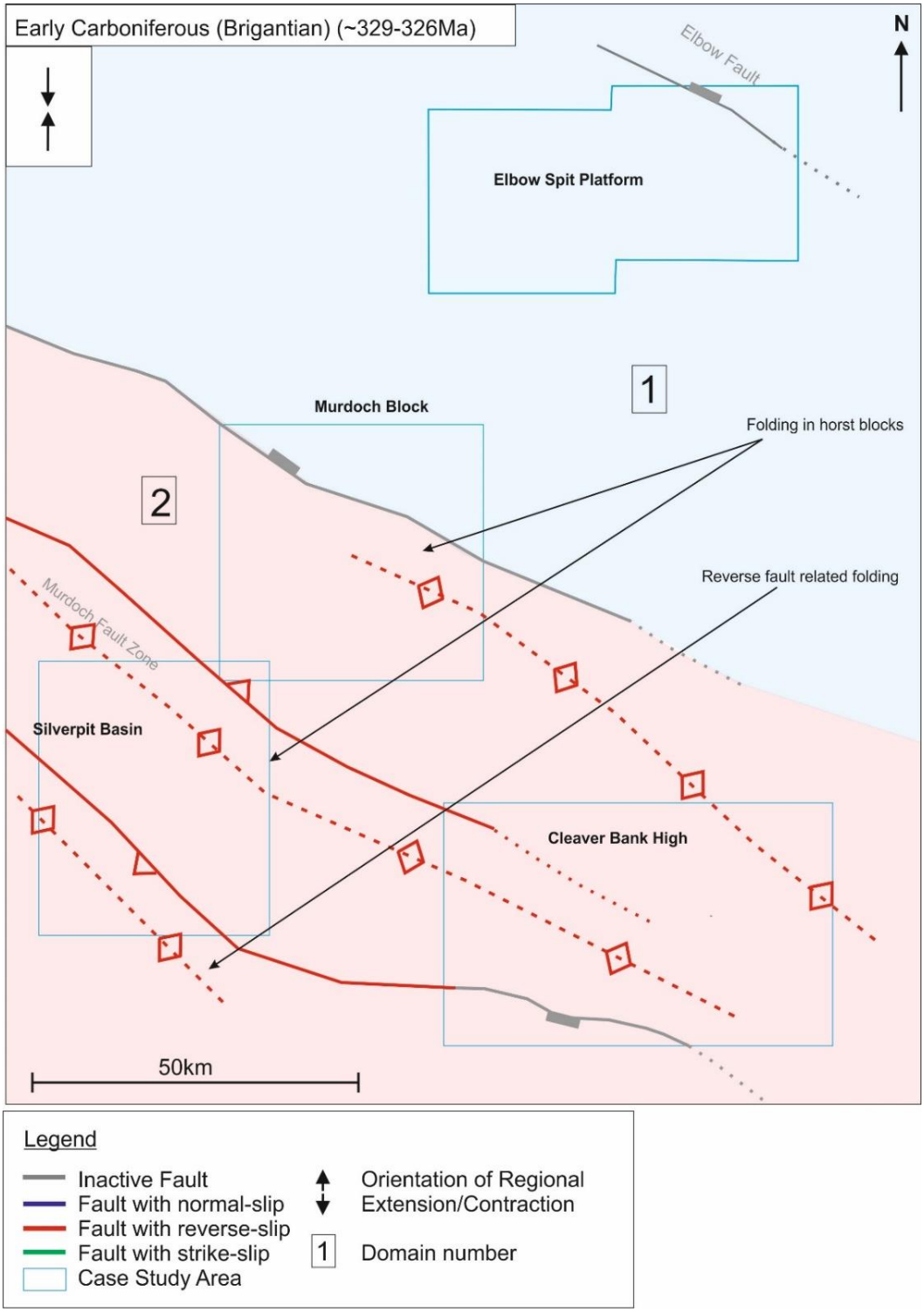


Figure 6.3 Structural map indicating the faults and folds present and active in the Pre-Zechstein succession during the Brigantian, in the central ADB. Inactive faults/folds are in grey and active faults and their movement sense are indicated by the colours and key. Faults outside of the Case Study areas are inferred from regional structural maps and seismic data of poorer quality. Folding of the Lower Carboniferous is observed on seismic data with WNW-ESE to NW-SE axial trends. This contractional activity is postulated to be related to the Brigantian inversion, also observed onshore.

6.2.3 Mid Carboniferous (Late Namurian - Early Westphalian) thermal subsidence (~321-310Ma)

The late Namurian (Arnsbergian) to early Westphalian (Westphalian A) is typically associated with post-rift thermal subsidence and overall tectonic quiescence in the central Anglo-Dutch basin (see Chapter 2.3.2.2; Schroot and De Haan, 2003). This is evidenced by the bullseye geometry of Namurian and Westphalian isopachs (Fraser et al. 1990). Non-tectonic, syn-sedimentary faulting is reported in the East Pennine Coalfield (Bailey et al 2005), East Midlands during this time, associated with delta front collapse (Fraser et al 1990).

6.2.3.1 Domain 1

Given that the BPU on the Elbow Spit Platform represents missing stratigraphy from the Brigantian–Autunian, there is the possibility of an initial normal movement occurring on the WNW-ESE detachment faults at this time (Figure 6.4). This is also in agreement with the high sedimentation rate occurring during the Namurian-Early Westphalian (Figure 2.10) causing syn-sedimentary faults gravity/ delta collapse faults (see section 4.7.1). The postulated tectonic quiescence at this time does not contradict movement on non-tectonic faults such as these. The t-z plot analysis also suggests that the A-E_WNW- faults may have incurred slip at this time (see section 4.3.3.1).

6.2.3.2 Domain 2

Seismic reflection packages displaying systematic thickening towards the south/controlling fault are observed in Domain 1 (Figure 3.21). These Namurian and Lower Westphalian syn-rift packages in the hangingwalls of WNW-ESE basin bounding half grabens in the central Anglo Dutch Basin, indicate that there was extensional fault activity during this time period (Figure 6.4), something not

observed onshore at this time (Fraser & Gawthorpe 1990) and contradicts the relative tectonic quiescence.

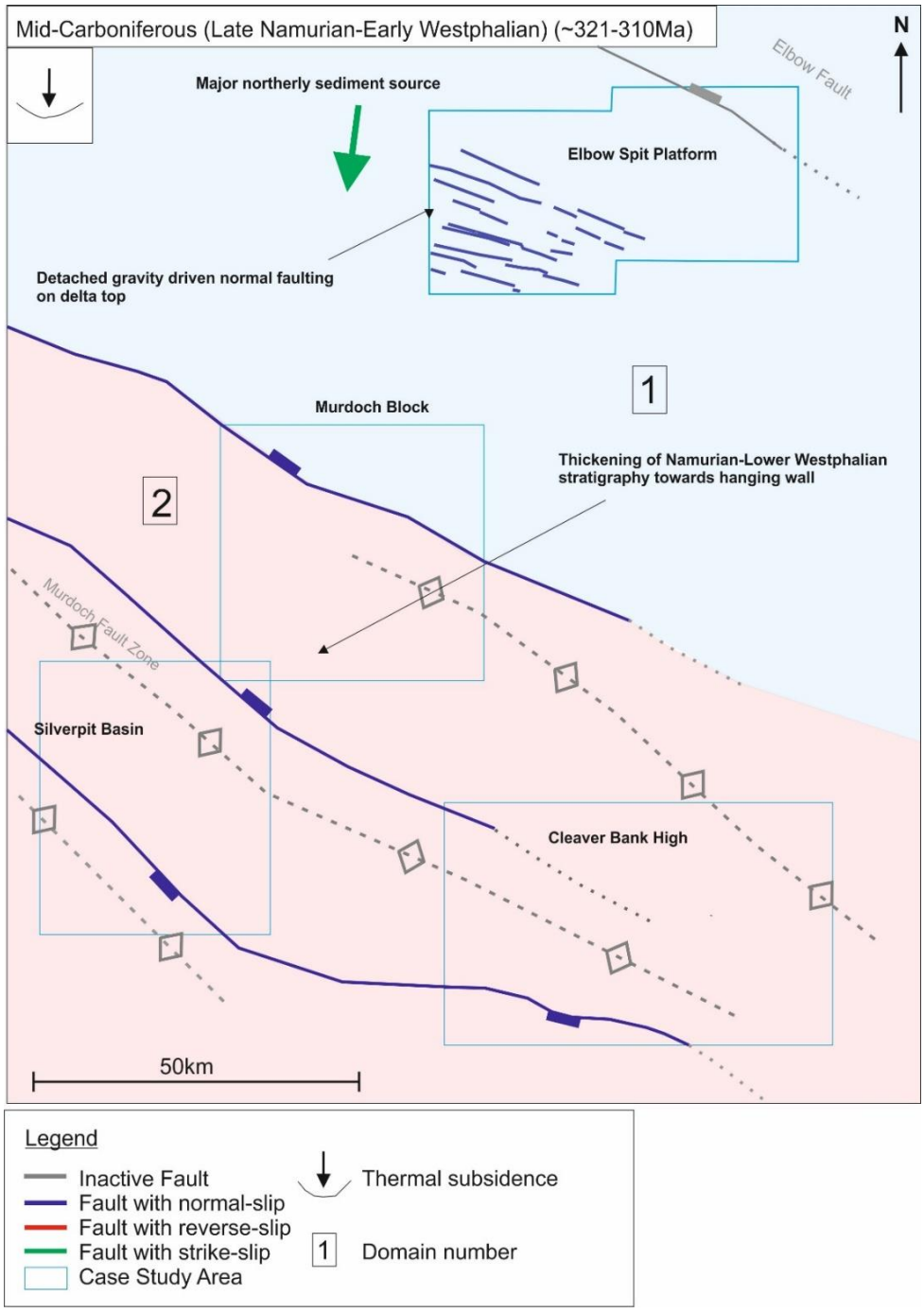


Figure 6.4 Structural map indicating the faults and folds present and active in the Pre-Zechstein succession during the late Namurian-early Westphalian in the central ADB. Inactive faults/folds are in grey and active faults and their movement sense are indicated by the colours and key. Faults outside of the Case Study areas are inferred from regional structural maps and seismic data of poorer quality. Normal slip on the WNW-ESE striking basement faults at this time is indicated by the thickening of age calibrated stratigraphy towards the south, particularly in the Murdoch Block study area. The formation of gravity driven detachment faults on the Elbow Spit Platform is postulated to have occurred at this time due to the high sediment flux possibly causing instability of the delta top/front, although the BPU erosion precludes a definitive dating.

6.2.4 Late Carboniferous – Early Permian (Stephanian-Sakmarian) Inversion (~306-290Ma)

During the time period represented by the missing stratigraphy at the BPU, almost every major fault trend displays evidence of activity in the central Anglo Dutch. This presents a major challenge for understanding the driving forces, since genuinely coeval, multi-directional extension is rare (Reches, 1983). Some minor differences in movement history have been revealed by their intersecting relationships, therefore this Variscan deformation is divided into three main phases of inversion, fracturing and strike slip.

6.2.4.1 Domain 2

Reverse movement on the basin bounding WNW_ESE trending faults in the Silverpit Basin and Cleaver Bank High (Domain 2) is evidenced at this time by the preservation of younger Westphalian stratigraphy in the footwalls of these faults (see Figure 3.21and Figure 3.40). A strike-slip reactivation of the pre-existing NW-SE faults has been proposed by previous authors (Hollywood & Whorlow 1993) in response to the NE-SW and N-S orientation of regional compression. Possibly evidence of this is the offset of E-W and ENE- features in the Murdoch Fault Zone in the Silverpit Basin. It is therefore proposed that these NW-SE basement faults in Domain 2 may have been active in a transpressional regime during the Late Carboniferous.

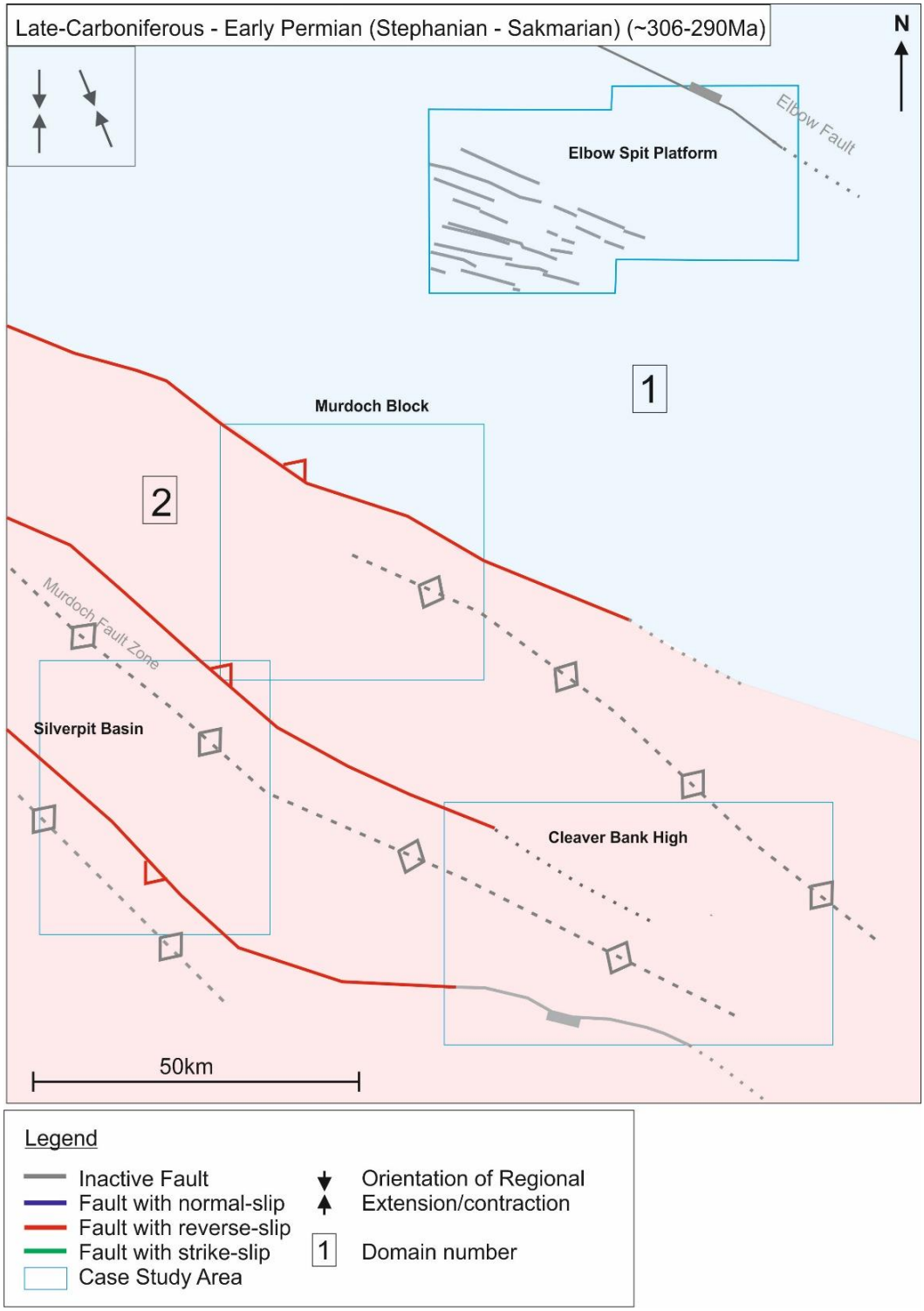


Figure 6.5 Structural map indicating the faults and folds present and active during the Late Carboniferous (Westphalian D-Stephanian) time period in the Pre-Zechstein succession in the central ADB. Inactive faults/folds are in grey and active faults and their movement sense are indicated by the colours and key. Faults outside of the case study areas are inferred from regional structural maps and seismic data of poorer quality. The inversion of the WNW-ESE basin bounding faults is evidenced on seismic data by older Westphalian stratigraphy in the hanging walls and younger stratigraphy preserved in the footwalls of these faults.

6.2.5 Late Carboniferous – Early Permian Fracturing and Strike-slip (290-285Ma)

In the later stages of the Variscan orogeny, an intense fracturing of the upper Palaeozoic is reported to have occurred (see section 2.3.3.1). The Anglo-Dutch Basin suffered extensive strike-slip faulting associated with extrusive magmatism and regional uplift, this time thermally related (Ziegler 1990, Ziegler 2004, see section 2.3.3.2). A third structural domain is recognised at this time distinguished by the presence of new E-W and ENE-WSW fault trends.

6.2.5.1 Domain 3

Given that a lateral displacement occurred on the major E-W trending faults in the southern portion of Domain 3 occurred before the deposition of the Rotliegend (see the pull apart basin with infill truncated at the BPU in Figure 3.28), it is postulated that these faults were active in a strike-slip sense during this time (Figure 6.6). Due to the lack of coherent lateral slip kinematic indicators, the actual direction of slip is uncertain, but these faults are interpreted to have been active in both left and right lateral senses at alternating, punctuated intervals through time (Schroot & de Haan, 2003). This strike-slip interpretation is reasonable at this time, considering the regional strike-slip fault regime reported by Coward (1990) (see Chapter 2.3.3.1). However, due the E-W orientation of these faults, and the N-S to NNW-SSE regional compression occurring (Corfield et al., 1996; Arthaud & Matte, 1977), a contractional reactivation would have been expected on these faults rather than the strike-slip reactivation that was in fact observed. This is suggestive of a far more complex stress regime occurring than just N-S compression.

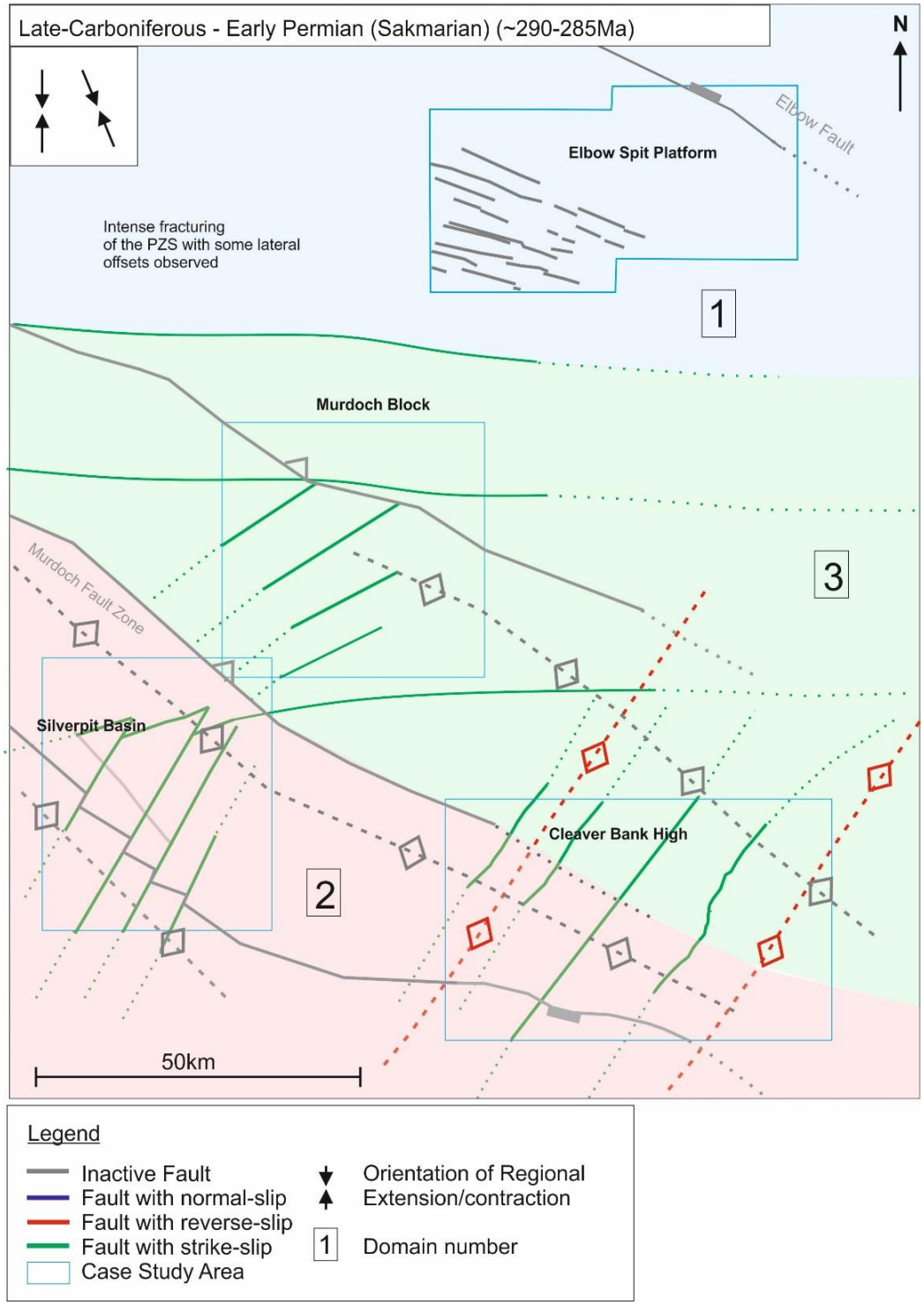


Figure 6.6 Structural map indicating the faults and folds present and active during the Late Carboniferous – Early Permian (Sakmarian) time period in the Pre-Zechstein succession in the central ADB. Inactive faults/folds are in grey and active faults and their movement sense are indicated by the colours and key. Faults outside of the case study areas are inferred from regional structural maps and seismic data of poorer quality. An intense fracturing of the crust produces E-W and NE-SW trends with postulated strike-slip activity following. The lateral slip on E-W striking zones is evidenced by pull apart basins truncated at the BPU Long wavelength folding of the PZS with axial trends of NE-SW occurs at this time.

6.2.6 Early Permian (Saalian) rifting, (~285-279Ma)

6.2.6.1 Domain 2

The extensional faulting phase on the NE-SW faults in Domain 2 is constrained to have occurred after the Late Carboniferous/Variscan aged NE-SW folding as evidenced by the offset of the NE-SW fold limb geometries (Figure 3.39). The ENE-WSW and NE-SW strike slip faults in Domain 2 were not reactivated (Figure 6.7).

6.2.6.2 Domain 3

Given the post Westphalian D pre-Rotliegend normal throws observed on many E-W orientated faults (Figure 3.26), and the fact that these faults offset the inverted syn-rift stratigraphy within the WNW-ESE grabens (Figure 3.21), it is postulated that an extensional movement occurred on these faults after the Variscan inversion but before the deposition of the Rotliegend (Figure 6.7).

Some of the ENE-WSW faults that were previously strike-slip faults in were reactivated as normal faults during this time. This reactivation appears to be somewhat enigmatic as not all the faults were reactivated. The principal factor determining the selective reactivation in this instance is interpreted to be frictional resistance related to dip, because it is observed that the faults with shallower dips were reactivated in a normal sense while those with steeper dips were not (see section 3.3.3.3 and Figure 3.33).

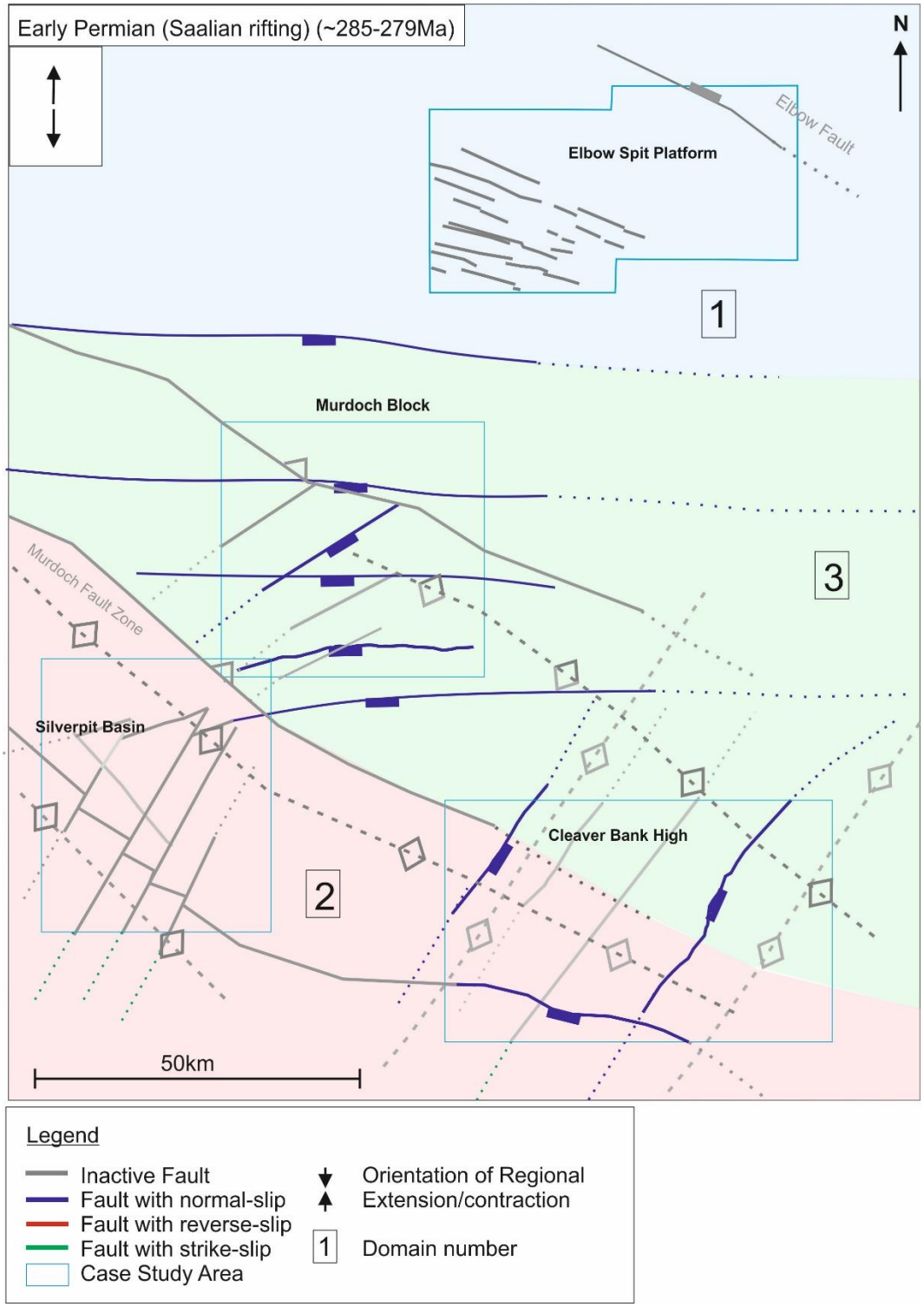


Figure 6.7 Structural map indicating the faults and folds present and active during the Early Permian (Artinskian) time period in the Pre-Zechstein succession in the central ADB. Inactive faults/folds are in grey and active faults and their movement sense are indicated by the colours and key. Faults outside of the case study areas are inferred from regional structural maps and seismic data of poorer quality. Normal movement occurred on south- dipping, E-W striking faults, and possibly on southeast dipping NE-SW faults. This extensional phase after Variscan compression is called the Saalian rifting phase.

6.2.7 Early Triassic (~255-247Ma)

On a plate tectonic scale, the Early Triassic was a time period associated with the breakup of Pangea (Figure 2.4), and on a local scale, the beginning of Atlantic rifting (see section 2.3.4.1). A fourth domain is introduced in the Anglo-Dutch Basin at this time, marked by the addition of east dipping N-S striking faults (Figure 6.8).

6.2.7.1 Domain 1

Given that the WNW-ESE faults are interpreted to be detached and gravity driven, the activity on these faults is interpreted to be controlled by movement on the bounding fault (Elbow Fault) rather than the regional extension orientation. The reactivation on the A-E_WNW- faults is therefore postulated to have occurred at this time due to the extensional activity occurring on the Elbow Fault (Figure 3.6).

6.2.7.2 Domains 2 and 3

Propagation on pre-existing NW-SE and NNW-SSE faults (Type-IV faults) and the formation of single phase (Type-V faults) occurred across Domains 2 and 4 at this time. Given that NW-SE faults are orientated optimally for extensional slip with the proposed NE-SW regional extension direction at this time (Ziegler 1990, see section 2.3.4.1), it is considered reasonable that fault slip occurred at this time. The decoupling effects of the Zechstein prevent an unequivocal age constraint.

6.2.7.3 Domain 4

An exact timing for the N-S faults cannot be constrained due to the mobile salt layer, but they interpreted to have been active after the BPU. Taking into account that they are located in close proximity, parallel alignment and eastward dipping towards to the Central Graben Rift Complex which was active at this time

(see section 2.3.4.1), and their orientation of extension is optimal for the formation of N-S faults, an extensional movement is likely to have occurred at this time.

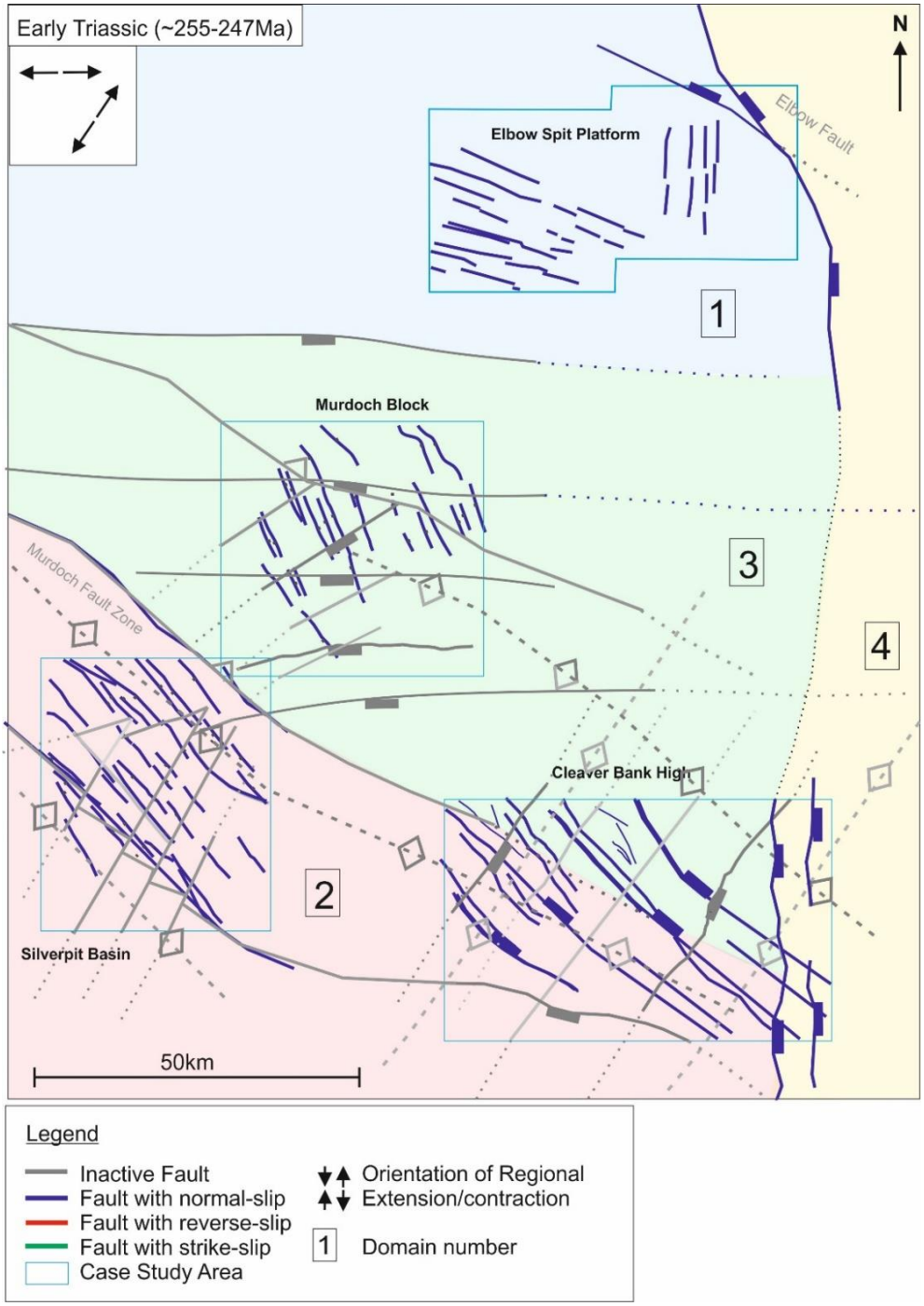


Figure 6.8 Structural map indicating the faults and folds present and active during the Early Triassic time period in the Pre-Zechstein succession in the central ADB. Inactive faults/folds are in grey and active faults and their movement sense are indicated by the colours and key. Faults outside of the Case Study areas are inferred from regional structural maps and seismic data of poorer quality. Extensional reactivation on pre-existing throughgoing NW-SE striking faults is inferred, along with the formation of new Type-V NW-SE faults due to the NE-SW and E-W regional extension occurring. Formation of new N-S faults on the ESP and CBH marks the beginning of Domain 4 influences (Central Graben Complex). Extensional movement on the Elbow Fault (top right) may have triggered the minor local reactivation exhibited on the detached WNW- faults due to footwall uplift.

6.2.8 Late Triassic- Early Jurassic Rifting (~236-224Ma)

The Late Triassic is associated with the continued early Atlantic rifting and rifting in the Central Graben (see section 2.3.5). The activity on Pre-Zechstein faults in the Anglo-Dutch Basin during the Late Triassic and Early Jurassic is concentrated in Domains 2 and 3 (Figure 6.9).

6.2.8.1 Domain 1

Due to the observed NW-SE regional extension direction, this time period is considered the most reasonable for a post-Rotliegend normal reactivation observed on Type-IV NE-SW faults and the formation of Type-V NE-SW faults.

6.2.8.2 Domains 2 and 3

Given the evidence of Post-Rotliegend normal reactivation on pre-existing throughgoing NE-SW_T (Type-IV) normal faults in the CBH and the formation of the NE-_P faults (Type-V) that offset the crests of the NE-SW folds, a Late Triassic mechanism of regional extension is attributed to the formation and reactivation of these faults.

Conversely, due to the structural relationships between the NE-_P and NE-_T faults, the formation of the NE-_P faults may be linked to the reverse movements on the major NE-_T fault that bounds Domains 2 and 3 in the Cleaver Bank High faults (see Figure 3.39). If this is the case, this normal movement on the NE-_P faults have occurred in the Late Cretaceous – Neogene.

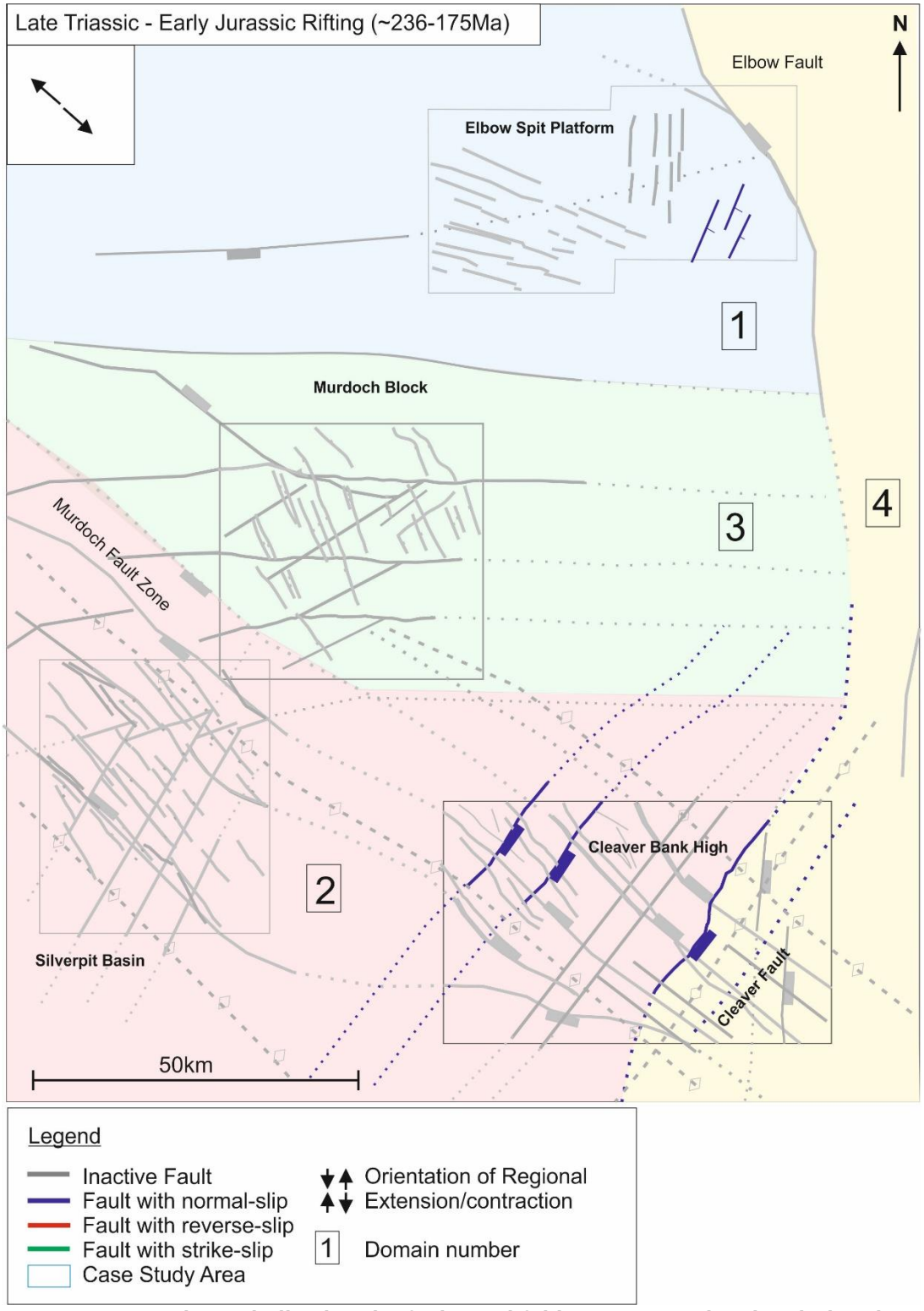


Figure 6.9 Structural map indicating the faults and folds present and active during the Late Triassic-Early Jurassic time period in the Pre-Zechstein succession in the central ADB. Inactive faults/folds are in grey and active faults and their movement sense are indicated by the colours and key. Faults outside of the Case Study areas are inferred from regional structural maps and seismic data of poorer quality. Extensional movement on NE-SW inferred from seismic evidence and is likely due to the NW-SE orientation of regional extension.

6.2.9 Late Jurassic – Early Cretaceous Rifting and Strike-slip (~151-139Ma)

Rifting in the North Sea continued with the initiation of a strike-slip faulting regime in the southern SBP, causing transtensional subsidence of N-S oriented basins (Zeigler 1990). North Atlantic rifting began in the Early Cretaceous (Pharaoh et al. 2010). Figure 6.10 illustrates the faults that are postulated to be active in the Pre-Zechstein succession during the Early Jurassic to Late Cretaceous.

6.2.9.1 Domain 1

Given the interpretation of pull apart basins associated with the ENE- faults in the Pre-Zechstein Succession on the Elbow Spit Platform (see Figure 3.17), it is likely that this regional E-W extension initiated the formation of these faults with left lateral transtensional movements. The truncation of the inverted pull apart (Figure 3.17a) against the Cretaceous succession is evidence for the later compressional reactivation of these faults in a transpressional regime.

The orientation of regional extension may have resulted in a movement on the Elbow Fault (see Figure 3.12), subsequently there is a possibility that the minor local reactivations observed on the detached WNW- striking faults may have also occurred during this time opposed to in the Early Triassic.

6.2.9.2 Domain 3

Though movement on the E-W faults at this time cannot be constrained from seismic observations due to the thick mobile salt and decoupling effects, it is possible that these E-W faults were also once again reactivated, this time in a strike slip sense. A good analogy of this is the reactivation of these faults onshore in the Cleveland Basin, on the E-W striking Flamborough Head Fault Zone (Peacock & Sanderson 1994).

6.2.9.3 Domain 4

On the premise that E-W oriented extension associated opened the North Sea rift (section 2.3.5.2, Zeigler 1990, Cameron et al., 1992) during this time period, it is likely that N-S oriented throughgoing faults in Domain 4 that were closely coupled with the basement underwent extensional slip.

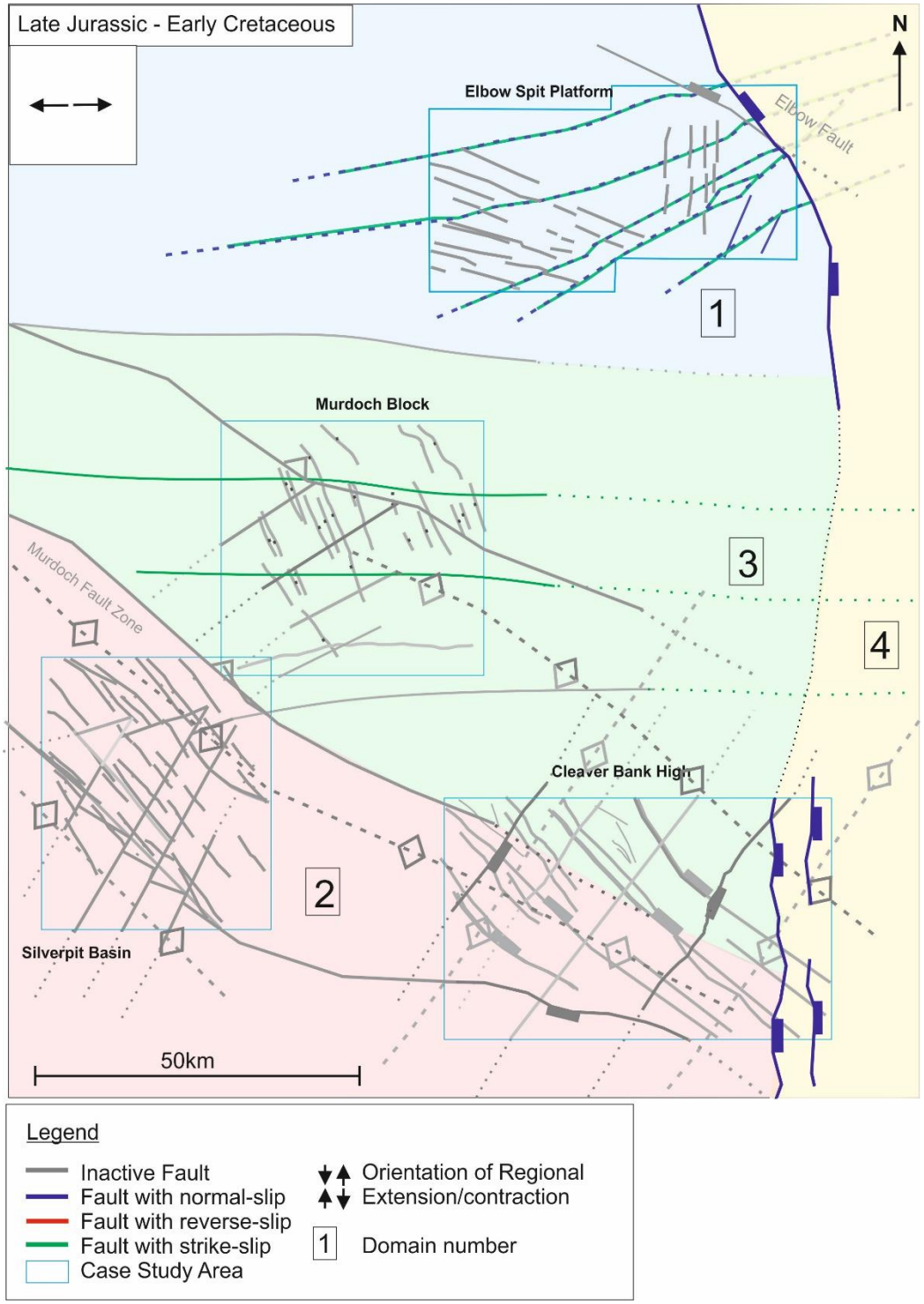


Figure 6.10 Structural map indicating the faults and folds present and active during the Late Jurassic to Early Cretaceous time period in the Pre-Zechstein succession in the central ADB. Inactive faults/folds are in grey and active faults and their movement sense are indicated by the colours and key. Faults outside of the Case Study areas are inferred from regional structural maps and seismic data of poorer quality. Normal slip on N-S bounding structures in Domain 4 is inferred due to the regional extension orientation and from seismic evidence and is likely due to the E-W orientation of regional extension. The E-W regional extension also caused the strike-slip reactivation of the major E-W faults in Domain 3 and strike-slip activity on the ENE-WSW faults in Domain 1.

6.2.10 Late Cretaceous – Cenozoic, Inversions (~89-20Ma)

Fault activity was largely governed by the far field stresses from the Alpine Orogeny in Late Cretaceous to Cenozoic times. For the Pre-Zechstein succession, this was mostly a reactivation of pre-existing structures. Active faults in the PZS in the central Anglo-Dutch Basin at this time are indicated by Figure 6.11.

6.2.10.1 Domain 1

It is unclear whether the reactivation on the A-E_ENE- faults in Domain 1, evidenced by doming of Cretaceous-Cenozoic strata, was transpressional or purely compressional (Figure 3.17). This reactivation of the A-E_ENE- faults in Domain 1 with no apparent significant reactivation of ENE- in Domains 4 and 3 is notable and may be due to the larger vertical extent of the ENE- faults in Domain 1.

6.2.10.2 Domain 2

The recognition of post-Rotliegend reverse reactivational movements on NW-SE, throughgoing faults in Domain 2, cannot be age constrained due to the decoupling effects from the mobile Zechstein unit. The reactivation of the Pre-Rotliegend NE-SW and NW-SE folds is evidenced by the folding of the Rotliegend and post-salt succession.

6.2.10.3 Domain 3

The recognition of post-Rotliegend reverse reactivations on E-W in Domain 3, cannot be age constrained due to the decoupling effects from the mobile Zechstein unit. On the premise that these fault sets are throughgoing and therefore coupled with basement stresses, it is likely that these phases of reactivation occurred during this time period, being attributed to the reported N-S to NE-SW oriented compression associated with far-field effects of the Pyrenean Orogeny (see section 2.3.6).

The magnitude of reverse reactivation on the E-W faults at this time decreases to the north. E-W faults with Type I profiles are observed in the southern part of Domain 1. Throw profiles then progressively record Type III profiles in Domain 4. Faults in the southern portion of Domain 4, appear to exhibit a higher magnitude of reverse reactivation than those in the north of Domain 4. This may be due to the increasing proximity of the Alpine Orogen to the south, and therefore these southern E-W faults are exposed to these far field basement stresses to a higher degree.

6.2.10.4 Domain 4

On the premise that these fault sets are throughgoing and therefore coupled with basement stresses, it is likely that these phases of reactivation occurred during this time period, being attributed to the reported N-S to NE-SW oriented compression associated with far-field effects of the Pyrenean Orogeny (see section 2.3.6).

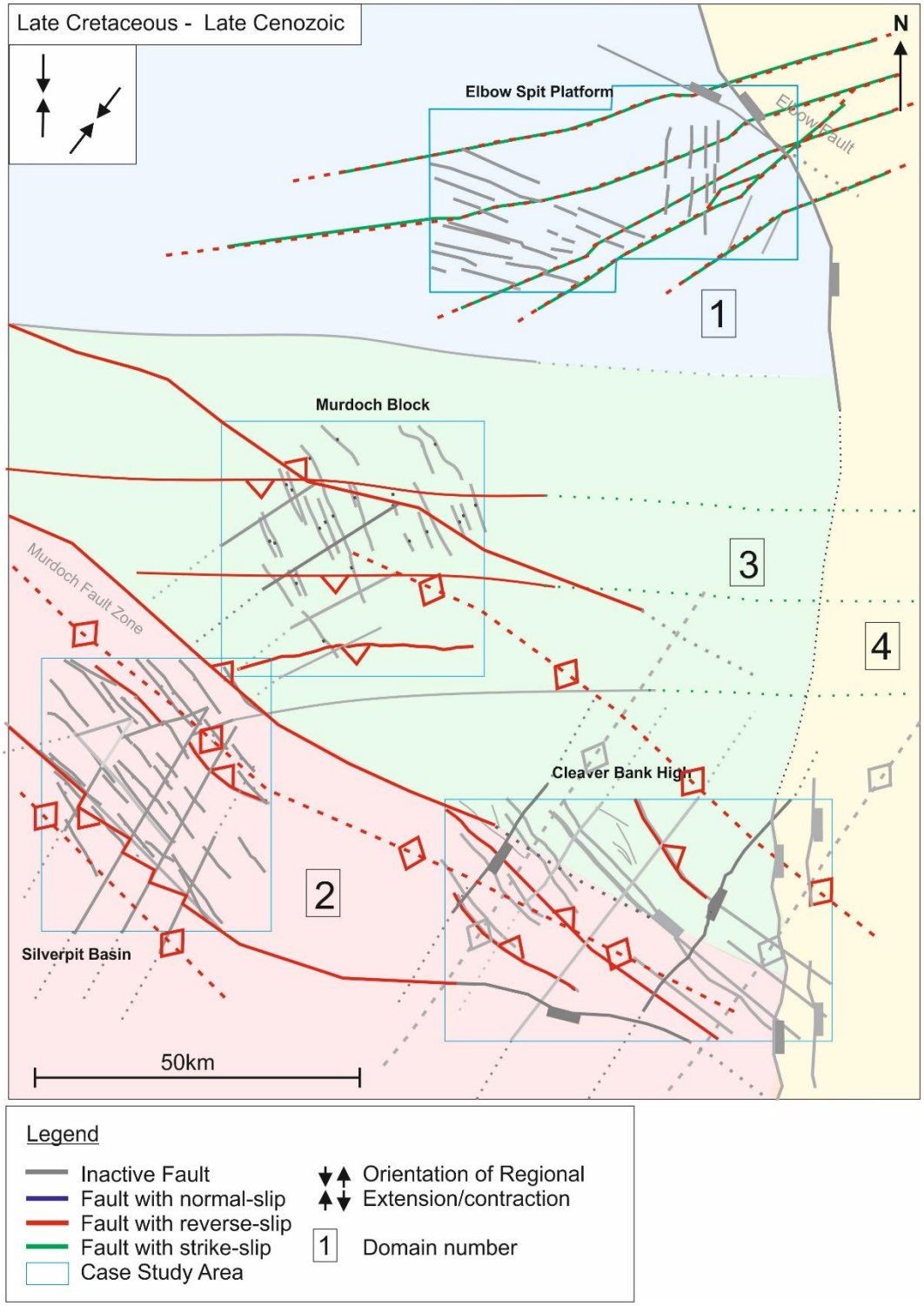


Figure 6.11 Structural map indicating the faults and folds present and active during the Late Cretaceous to Late Cenozoic (Neogene) time period in the Pre-Zechstein succession in the central ADB. Inactive faults/folds are in grey and active faults and their movement sense are indicated by the colours and key. Faults outside of the case study areas are inferred from regional structural maps and seismic data of poorer quality. A contractional reactivation of most throughgoing NW-SE and E-W structures is observed on seismic data in Domains 2 and 3 respectively. In Domain 1, a transpressional reactivation is observed on ENE- structures on the ESP.

6.3 Selective Reactivation of Pre-Zechstein Faults

From the kinematic analysis, it is uncertain what controls the selective reactivation of Pre-Zechstein faults across the Anglo Dutch Basin. A number of distinctive controlling factors that could potentially influence the degree and selectivity of fault reactivation include: (1) optimal orientation of the stress field for frictional slip, (2) frictional resistance, (3) fault dip angle, (4) fault dimensions (surface area) and (5) overpressure (Sibson, 1995, Kelly et al., 1999, Wiprut and Zoback, 2000, Bonini et al., 2012). The degree of connection with the regions of the crust where stress transmission is most acute is also a factor that perhaps should be considered, but has received relatively limited attention. Detached faults in the soft-sedimentary regime of the upper kilometre may respond to local stresses more than to regional stresses transmitted over long distances through the basement. In contrast, basement linked structures such as major graben bounding faults tend to be loci for inversion simply because they 'feel' the effects of long range crustal stress transmission (Cooper et al., 1989, Williams et al., 1989, Cartwright, 1989). The basement faults can sole out onto deeper Caledonian and Variscan thrusts (see section 2.2

The reactivation patterns and magnitudes of reactivation for the three structural style types; superficial, throughgoing and detachment (defined in section 3.7.2) are considered. Possible reasons for these selective reactivations are explored in this following section.

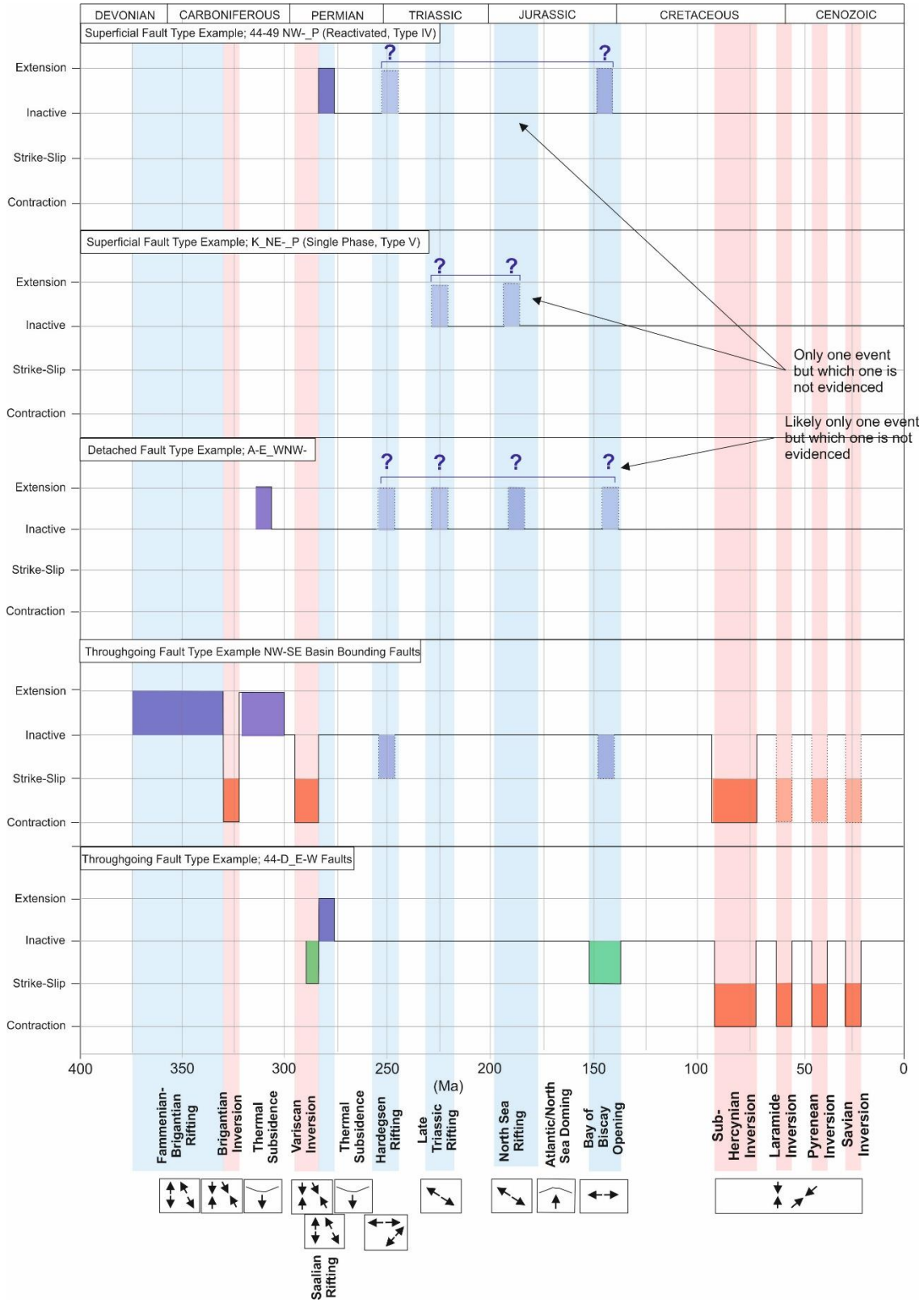


Figure 6.12 Fault activity through time for example throughgoing, superficial and detached faults. Bold lines indicate seismic evidence for fault activity during the corresponding time period while dotted line indicates the faults were possibly active. The throughgoing faults are notably reactivated more through geological time with their reactivation sense usually conforming to the regional displacement orientation. Superficial faults are active on fewer occasions with no evidence of reverse reactivation. The gravity driven detachment faults are active on fewer occasions (likely 2 max) and their movement sense does not conform to the regional displacement orientation.

6.3.1 Superficial Faults

Superficial/peripheral faults (as defined in section 3.8.2.2.) exhibit exclusively normal throws and exhibit only normal sense reactivation with small throw magnitudes. These faults are usually located in close proximity to similarly oriented throughgoing faults i.e. the NW-_P and NW_T faults in the Silverpit Basin, the throughgoing faults however may exhibit a reverse movement. Superficial faults exhibit Type-IV or Type-V throw profiles. They are also reactivated less frequently through geological time (Figure 6.12).

The small throw magnitude during reactivation may possibly be due to the stress shadow created by the local throughgoing faults (Gupta et al. 1998, Ackermann and Schlische, 1997), because the larger throughgoing faults accommodate the strain. The generally smaller vertical extents on superficial faults means that they are not in close communication with basement stresses and therefore are less likely to be reactivated (Kelly et al. 1999). This effect is then enhanced when they are in close proximity to throughgoing faults which is probably why these faults tend not to propagate into larger structures (Walsh et al., 1991, Meyer et al., 2002).

Given that reverse reactivation is not observed on superficial faults, but is observed on adjacent throughgoing faults of the same orientation, there must be a reason for this selective reactivation. An additional reason for the lack of reverse reactivation may be due to the fact that the superficial faults generally have high dip angles compared to the throughgoing faults (see superficial faults on Figures 3.12, 3.47). Local factors that increase the likelihood of fault slip such as elevated fluid pressures and increased weakness of thicker fault gouge (Kelly et al., 1999) are not

thought to be key in controls since both the throughgoing faults and Superficial faults in question are within the same succession.

6.3.2 Detachment Faults

The gravity-driven detachment faults observed only in the Upper Devonian-Lower Carboniferous of the Elbow Spit High, undergo exclusively normal throws and undergo very minor normal reactivations of very small throw magnitudes. They experience fewer phases of activity through time, as seen in the A-E_WNW- fault example in Figure 6.12. The postulated timing of reactivation does not always conform to the regional stress orientation and in some cases conforms to the timing of activity on the large-scale throughgoing faults that are in close proximity. The reactivation is locally variable and t-z profiles are Type-I or Type-II (see Chapter 4, section 4.3.3). It is suggested that the lower magnitude and less predictable reactivation profile is due to the mechanical decoupling of these faults with the underlying basement stresses, due to the situational presence of a mechanically weak detachment horizon. The faults are not reactivated as they are not in direct communication with the reactivation stresses. The minor reactivations observed may be due to the dynamics of the nearby bounding fault i.e. footwall uplift on the bounding fault increasing the slope, rather than regional extension. Their timing of reactivation is therefore unravelled by the timing of movement on surrounding crustal structures.

6.3.3 Throughgoing Faults

Throughgoing faults exhibit evidence of repeated reactivations through geological time with varied throw senses. Figure 6.12 illustrates the frequent reactivations in all movement senses of two throughgoing faults through geological time. The nature of these reactivations usually conforms to the regional stress

orientations and therefore their reactivation timing can be more easily estimated (Figures 6.1-6.12). They exhibit Type-I or Type-III throw profiles. This style of reactivation is likely due to the large vertical and lateral extent of these faults and therefore increased coupling with (distant) basement stresses.

6.4 Regional Tectonic Relationships between Structural Styles

The three different fault structural style types have been identified and discussed, however, they also have apparent relationships to one another. The most convincing examples of these observed relationships are discussed below.

6.4.1 Throughgoing (crustal/tectonic) and detachment (gravity driven)

Extensional movement on a large-scale crustal bounding fault such as the Elbow Fault is unequivocally driven by tectonic stresses. The gravity driven detachment faults located on the hanging wall block of the Elbow Fault however (A-E_WNW-) are not caused by tectonic stress, as they are decoupled from it by the detachment horizon. Their movement is an indirect consequence of the tectonic basement stresses causing uplift on the footwall block that creates topography and initiates gravity faulting. The timing of their movement is therefore constrained to the timing of footwall uplift.

6.4.2 Throughgoing (meso-scale) and superficial

Throughgoing faults across the Anglo-Dutch Basin such as the NW-_TR faults were reverse reactivated in a compressional sense during the Late Carboniferous Inversion event. The Upper Carboniferous stratigraphy in the hangingwall of the basement-linked fault has many superficial extensional faults (Figure 6.13b). Some of these faults formed before the BPU Type IV and some

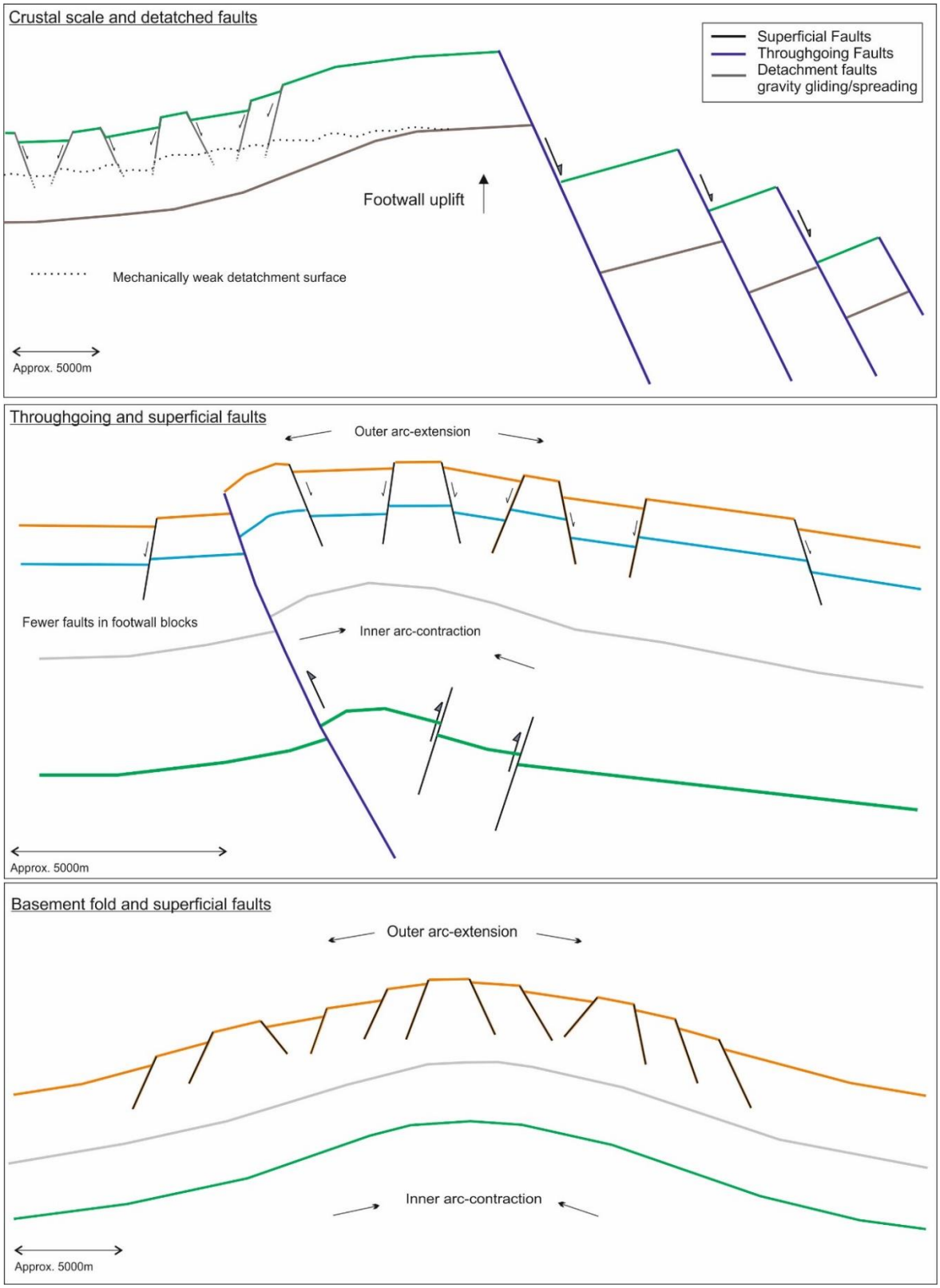


Figure 6.13 Schematic showing the structural relationships between the various structural style types

formed later (Type V). The Type IV faults are suggested to have formed as a flexural response to the compressional folding in the footwall due to late Carboniferous movements.

The Type V faults may have formed at a later compressional reactivation stage such as the Sub-Hercynian. It is suggested that these faults are formed as a response to compressional (or extensional) movement on the throughgoing fault by the flexural mechanism. This postulated mechanism is illustrated in Figure 6.13b.

6.4.3 Basement Folds and Superficial Faults

Given the fact that superficial faults have been observed in higher abundances above folds within the deep stratigraphy and these superficial faults also have an orientation that preferentially aligns with the fold axes, it is inferred that there is a link between these structures. This inferred mechanism is similar to that in 6.4.2. In which a compressional basement movement has resulted in the extensional faulting in the peripheral stratigraphy within the larger scale fold (Figure 6.13). These small-scale extensional faults are interpreted to form as a strain response to the buckle folding. In the instance that these superficial faults were detached on a horizon, the mechanism may be interpreted as gravity driven. However, these faults do not detach at a particular horizon and throw decreases systematically to an observable basal tip.

6.4.4 Fractal relationships between fault styles

As discussed in Chapter 5, fault populations have a power law or fractal relationship for size and spacing. It seems that these structural style relationships may also follow a follow a fractal pattern.

At a plate scale, using the Variscan Orogeny as an example, the throughgoing structure that controls the deformation is the plate motion (i.e. the

plate collision and resulting subduction zone). During the Variscan Orogeny, uplift was occurring as a result the imposition of horizontal compressional tectonic stresses. However, the faulting that occurs on the orogenic wedge is extensional and due to gravity driven processes.

This process is also observed in the Himalayas, in which E-W striking, gently northward dipping normal faults offset the High Himalayas and southern Tibet (Royden & Burchfiel 1987). Gravitational collapse occurs in a southward direction and also does not reflect the regional extension of the entire crust. Just as the strike of the gravity driven detachment faults on the Elbow Spit Platform align to the strike of the tectonic feature (Elbow Fault) and footwall slope contours, these E-W striking detachment faults in the Himalayas also trike parallel to the collision between India and Tibet.

The back-arc extension occurring on the overriding plate is also a consequence of this compression but is obviously extensional and therefore follows the same cause and effect process.

At a seismic scale, as previously discussed, throughgoing faults with contractional strain exhibit extensional superficial faults in the hangingwall folds. The effects from this can also be seen at a different scale of resolution, with the example of the superficial orthogonal fault trend that are observed in the Westphalian stratigraphy of the inverted half grabens in the East Pennine Basin. The footwalls of extensional crustal scale faults can exhibit detached faulting (provided the conditions are present i.e. a detachment horizon and or sufficient slope to initiate gravity driven faulting).

The faulting on the crests of the long wavelength folds observed on seismic data may have an outcrop analogue as shown in (Figure 6.14). The observation of

fractures in folded Visean limestone may be analogous to this process, in which the outer arc of the fold is heavily fractured.

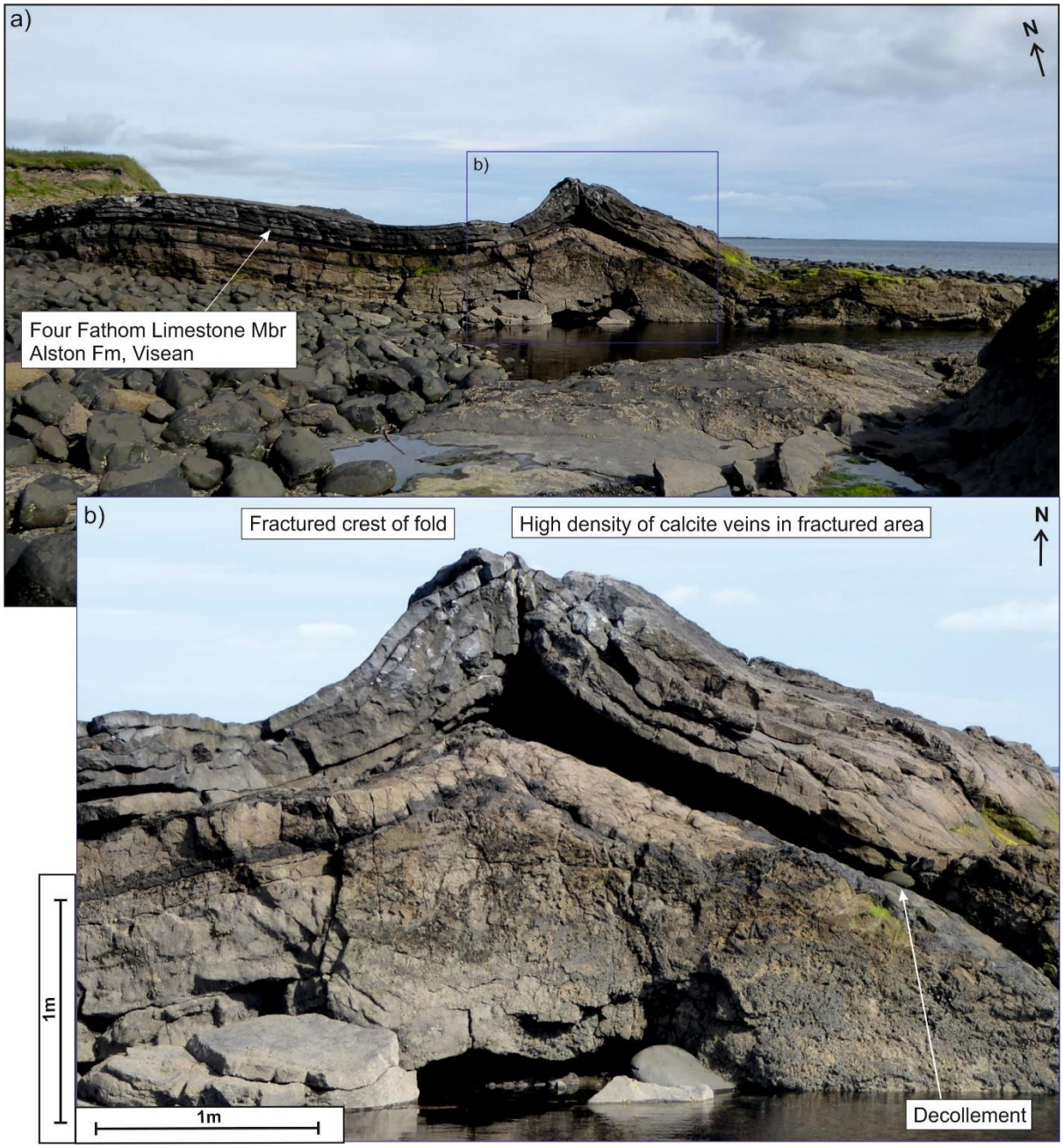


Figure 6.14 Detached fold in the Visean on the Northumberland Coast. The opening mode fractures at the fold crest along the fold axis may be a scaled down analogy to the superfical faults observed on the seismic data. Could be interpreted as a syn-rift slump fold as described in the Bowland Basin by Fraser & Gawthorpe (1990).

6.5 Open and closed faults in the Pre-Zechstein Succession

One of the key applications of this research is providing a framework that ultimately aids the assessment of fluid flow (Chapters 3 and 4) and reservoir production planning in the Pre-Zechstein (Chapter 5). Although the observation of faults on seismic data has a limited direct application in this assessment, due to being unable to image the complex fault core geometries at a necessary resolution, the characterisation of faults and fault networks in the subsurface can allow for applications of concepts and analogous comparisons to outcrop and wellbore examples.

The characterisation of fault geometries on seismic (Chapter 3) may give an insight into the fault zone/core properties, which can be used to estimate fault transmissibility. Despite there being a distinct difference in scale in this estimation, we can infer the hydraulic properties of mechanical discontinuities on seismic by applying concepts derived from surface analysis. Such analogous information includes the fault zone geometry and composition (Caine et al. 1996, Kim et al. 2004) stratigraphic juxtapositions (Knipe 1997), and amount of shale smearing that may have occurred (Engelfer 1974, Clausen et al. 2003). A crude estimation of fault transmissibility may therefore be possible.

As an example, we can consider the conventional Namurian and Westphalian sandstone reservoirs of the Millstone Grit Group and Coal Measures in the Murdoch Block of the Southern North Sea (Leeder & Hardman 1990, Fraser et al. 1990). Given that the seismic-scale fault network in the PZS of the Murdoch Block consists largely of cross cutting E-W and NNW-SSE trending Carboniferous faults, this chops up the PZS into a number of fault blocks in this area. To estimate whether these blocks are compartmentalised, we can look at the cross cutting

geometries and lithostratigraphical succession. The reflection mapping and t-z analysis revealed Tmax Namurian (intra-Kinderscout Grit horizon) throws of ~400m on the NNW- faults (see section 4.4.1.1), and ~650m on the E-W trending faults (see section 4.4.1.2). Given that we see a thick shale gouge in the fault zone of onshore south dipping E-W trending Carboniferous faults with Namurian throw magnitudes less than this (~200-300m, see Figure 6.15). This is therefore a good indication that these faults would be sealing (Knipe 1992) even without performing a complicated juxtaposition analysis (Knott 1993) between fault blocks containing this cyclic deltaic succession. The complex reactivation profiles in which individual fault blocks are reactivated at discrete times (Figure 4.20), adds to this compartmentalisation.

Another consideration in the transmissibility of seismic scale faults in the PZS of the Anglo-Dutch Basin is the fault zone/damage zone extent and composition. Given that the majority of throughgoing faults were found to have been frequently reactivated through time (Chapter 4 and Chapter 6), this knowledge of the repeated deformation may be an indication that they have a thick damage zone and the cataclasis in the fault core. Faults in the Carboniferous of the Southern North Sea have been deeply buried during the Mesozoic, contrasting to the Carboniferous fault observed on the Northumberland coast (Figure 6.15). These offshore faults in the PZS are therefore more likely to be compacted with a cataclastic core. Given that the process of cataclasis reduces grain size and pore space, porosity and permeability in the fault zone are likely reduced. Knowledge of this consistent deformation may therefore be a strong indication that these throughgoing faults offshore, act as baffles to fluid flow.

Conversely, the repeated deformation events may have enhanced permeability in certain low porosity and permeability formations. Intense sub-seismic scale fracturing (in addition to the secondary seismic scale 'superficial' faults and fracturing) may have occurred surrounding the fault plane and damage zone, particularly as a response to flexure in hangingwall anticlines. These fractures may be open (unlike deformation bands), causing an increase in permeability close to the fault plane. This therefore means that despite the impermeable properties of the fault core/plane itself due to cataclasis, a local area surrounding the fault may actually have enhanced permeability. An example of this may exist in the inverted hangingwalls of the basin bounding half grabens i.e WNW-ESE northward dipping crustal scale faults in the Silverpit Basin (see Figure 3.21) and E-W trending inverted half grabens in the Cleveland Basin (Figure 3.47 & Figure 3.49). Lower Carboniferous mudstones (i.e. the Bowland Shale Formation (Andrews et al. 2010, Hughes et al. 2016, Harvey & Gray 2012,)) are the target interval for unconvential exploration and production in northern England. Contrary to the case for conventional reservoirs, in which faults generally act as baffles to fluid flow, in low porosity lithologies. These Visean shales and heavily compacted and diagenetic Namurian sandstones that are generally poor conventional reservoirs (Leeder & Hardman 1990) may therefore contain faults that generally act as conduits for fluids (Dewhurst et al. 1999). Given the fact that Lower Carboniferous shale intervals are often found within the inversion anticlines of the basin bounding faults, this location may present an ideal site for unconvential production, as there is already enhanced permeability from fracturing. With this is mind, the chance of induced seismicity in this area may also be high, as seen in the Bowland Basin when the Variscan inverted fault was stimulated (Clarke et al. 2014). A thorough assessment of the

potential for induced seismicity on the large fault would then be essential, which may be problematic in the PZS offshore.

The estimation of the transmissibility of faults from seismic observations and timing analysis, along with the estimation of sub-seismic fault abundance (see sections 5.7.4 and 5.8.3) therefore provides a useful tool in the estimation of fluid flow in the PZS. This also provides an insight into possibly problematic areas that if hydraulically fractured may produce induced seismicity (Clarke et al 2014, Clarke et al 2019) .

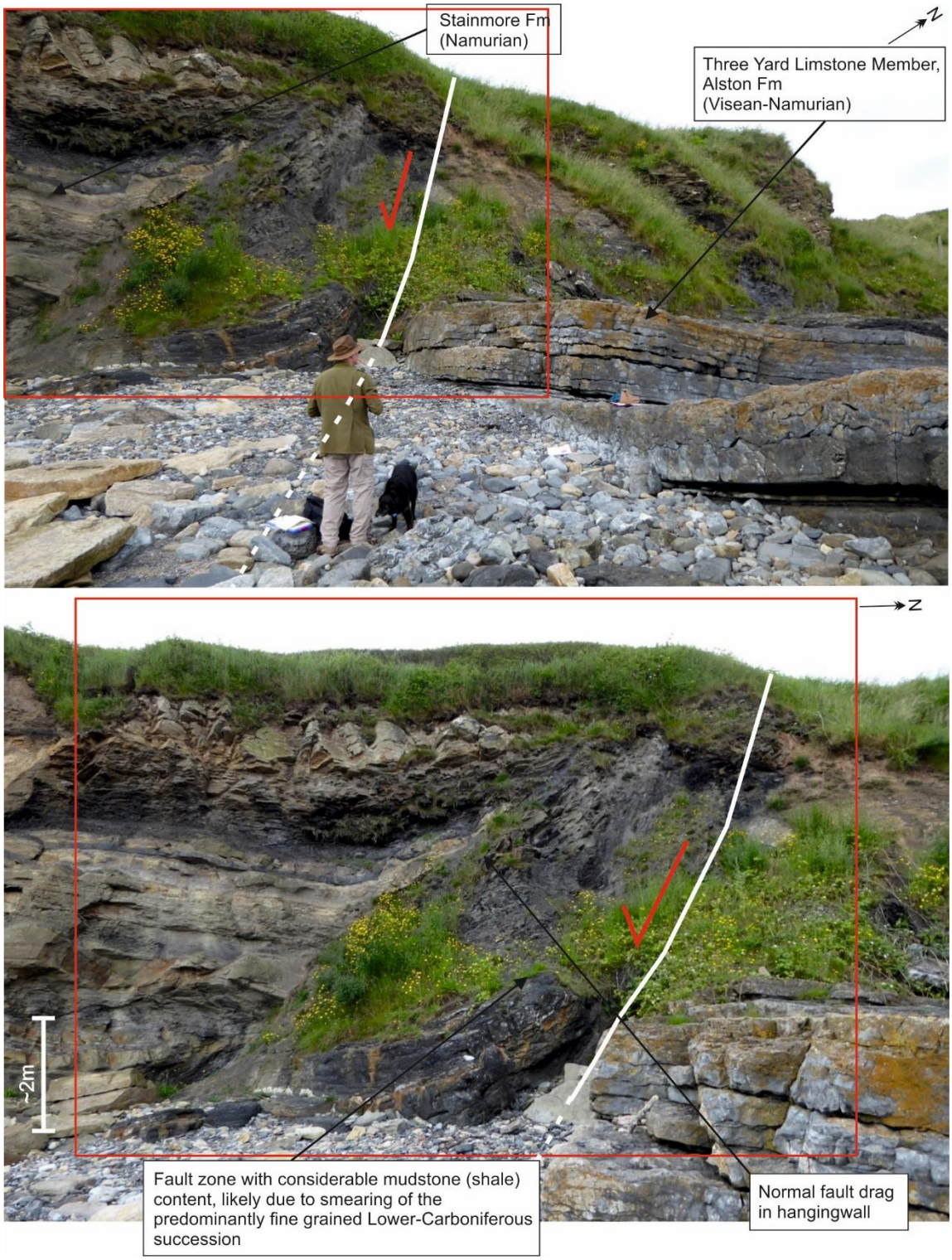


Figure 6.15 Cliff exposure of an E-W striking, southward dipping normal fault downthrowing Namurian stratigraphy against Visean, at Howick on the Northumberland coast. Displacement is unknown but is greater than the cliff face (~10m). The fault vertically extends beneath the beach and above the cliff (eroded). Due to stratigraphic thicknesses of Visean and Namurian successions in the Northumberland Trough (Calibrated by well Longhorsley 1), throw is estimated to be 200-300m. The fault zone is composed of predominantly fine grained material that has likely smeared from the high shale content of the Lower Carboniferous. This would present a baffle for fluid flow and compartmentalise the sandstones within the Stainmore formation in a reservoir situation.

6.6 Summary

- Four main structural domains are recognised in the central Anglo-Dutch Basin study area and one across in the East Pennine Basin. The clear contrast in dominant fault trends and reactivation styles between these areas suggests the presence of a major structural boundaries between these areas. These boundaries usually conform to a major crustal scale fault.
- The superficial faults are formed as a response to the hangingwall strain due to movement on basement faults. The detachment faults are a consequence of the resulting footwall elevation due to extensional movement on (crustal scale) faults, so are a consequence of a mechanically weak detachment horizon, topography and gravity. Both of these fault types are not directly connected with basement stresses, unlike the throughgoing faults, which have a kinematic history that is conformable with the regional extension or compression.
- The key controlling factors on contractional reactivation of faults are the vertical extent of the fault and the orientation of the fault. Throughgoing faults with vertical heights that extend throughout the entire Pre-Zechstein succession are the only faults in which compressional reactivation is observed. This is interpreted to be due to the direct coupling with basement stresses. The lack of fault reactivation on superficial and gravity driven detachment faults may be due to the stress shadowing of the larger faults and their decoupling from basement stresses; their formation being a response to the hangingwall strains required to accommodate movement of the basement faults (the kinematically required minor faulting). More

sporadic, non-systematic reactivation histories are therefore considered here to be the result of more specific geometrical aspects such as fault dip.

Chapter 7

CONCLUSIONS

7 Conclusions

7.1 Introduction

This chapter presents the main conclusions of the thesis. The conclusions are presented as a series of specific points. The first four conclusions are large scale regional points of relevance to the basin evolution, deformation history and fault and fractures of the onshore and offshore Carboniferous Basins of Eastern England. The remaining case study conclusions result from the more detailed semi-quantitative observations and measurements from the detailed seismic data available in the offshore part of the basin. The integrated conclusions develop a new basis for the understanding of post-Carboniferous fault and fracture formation and its relevance to secondary permeability development and the potential resource exploitation of Carboniferous stratigraphy.

7.2 Overall Conclusions

7.2.1 The onshore East Pennine Basin and offshore central Anglo-Dutch Basin together comprise five structural domains that exhibit distinctly different primary fault patterns and styles of reactivation.

The Pre-Zechstein tectonic framework onshore in the East Pennine Basin can be defined as large scale E-W to WNW-ESE striking Carboniferous half grabens, inverted in the Variscan orogeny. These basins dip eastwards off the Pennine uplift and dip gently out to sea. Good coastal exposure shows major N-S monoclines that locate the Devonian Carboniferous contact together with mesoscale E-W compressional folds and cross cutting fault sets that seem

pervasive but are sub-seismic in scale (EPC faults). These orthogonal orientations define a complex structural history onshore (Domain 5).

Offshore, the E-W to WNW-ESE basins arc slightly to the east and south east and merge with four offshore domains of the ADB. Domain 1 marks the southern margin of the Mid North Sea High and consists of a Visean base Permian subcrop in which tectonic faults can be seen to offset the Caledonian basement, and gravity driven faults detach on Upper Devonians-Lower Carboniferous shales.

The structure in Domain 2 is consistent with the NW-SE/WNW-ESE and NE-SW half graben trend onshore UK, but display a weaker Variscan inversion pattern. Domain 3 marks the area in the central ADB in which a strong E-W fabric can be observed, with possible major E-W trending shear zones that have been active at many stages through geological time. Domain 4 sees the introduction of mainly N-S structural trends that came about when rifting began in the Central Graben Complex.

It is clear from the structural examination that the intra-basinal fault and fracturing differences between the five domains is greater than the contiguity implies, and that their structural styles are domain specific, affirming that structural inheritance has been a key influence in their evolution of structural inheritance. Consequently, any assessment of fault and fracture type, orientation and density needs to be acutely aware which domain is being assessed.

7.2.2 Process of faulting and fracturing: Meso-scale faults are formed as a consequence of, or in response to, the regional tectonic stress, but not directly from these stresses.

Faults patterns across the Anglo-Dutch Basin exhibit a complex formation and reactivation history that can’t simply be explained by rotations of regional

extension and contraction. Meso-scale (superficial and gravity driven detachment faults) are formed as a response to movement on the larger scale structures, rather than to regional extension or contraction. This relationship is evidenced at many scales, where the ‘cause and effect’ is apparent. It is the regional extension and contraction on the throughgoing faults that initiates the faulting on these meso-scale structures through either a flexural response, or a consequence of increased relief (relies on the presence of a mechanically weak detachment horizon i.e. Upper Devonian mudstones). This means that the faulting regime on the superficial faults will not necessary conform to the regional tectonic stress, as it is a response to the forming large-scale structures. Deformation on these large-scale tectonic structures will cause localised stress perturbations, producing the resulting meso-Scale faults.

7.2.3 The key controlling factors for the timing and styles of fault reactivation are coupling with the basement, the relationship with crustal scale and through-going faults and the mechanical stratigraphy of the Pre-Zechstein succession.

Regionally, faults that have a large vertical and lateral extent through the Pre-Zechstein succession (throughgoing Faults) are those that have been reactivated over time, with offsets in all senses. These timings and magnitudes of reactivation usually conform to the reported regional orientation and magnitude of extension and compression at that time. Superficial and detachment faults however have smaller vertical and extents (superficial) or are decoupled from the underlying stratigraphy by a mechanically weak detachment horizon (detached). This means that their reactivation histories are limited in time and only consist of extensional reactivations, which are an indirect consequence of movement on throughgoing

structures. These smaller faults are somewhat shielded from propagating as the strain is concentrated on the larger structures that are in close proximity.

The distribution of these superfical and detachment faults is of key importance when assessing fracture and fault networks in prospective formations as this minor faulting can be the difference between compartmentalisation or connectivity of conventional reservoirs.

7.2.4 Two other profoundly different fault processes are identified that result in the detailed structural complexity of the Anglo Dutch Basin

Faults patterns across the Anglo-Dutch Basin do not easily fit a classical Anderson faulting pattern in terms of orientation or sense of displacement. This is in part due to the lack of an isotropic medium and the presence of existing faults (Caledonian structural inheritance), but also due to the effect of local strain patterns set up between large crustal scale faults, gravitational hangingwall collapse and secondary extension and compression associated with inversion related anticlines. These processes produce at least two overall types of ‘secondary’ faulting; superficial and detachment. Although both these structural style types are formed in response to the larger structures, they are different. The main difference being that the superficial faults do not detach on a particular horizon while the detachment faults are defined by dethatching at a mechanically weak horizon.

7.3 Chapter Conclusions

The following more locally based and detailed conclusions particularly highlight the outcome of the semi-quantitative work and detailed findings from some hi-resolution 3D seismic data.

7.3.1 Detailed 3D seismic interpretation and the use of seismic attributes has 1) enabled the recognition of previously undetected fault trends in the offshore Anglo-Dutch Basin and 2) highlighted the fact that large structures are highly laterally segmented.

The relatively poor imaging of the base-Permian subcrop and the presence of folding, has meant that variance slices are often not useful for observing structures at a specific stratigraphic interval. The computation of isoproportional slices at fixed intervals following the geometry of the BPU gives a more stratigraphically representative imaging of the fault patterns in the Carboniferous. This method has enabled the recognition of fault trends that were previously concealed from not being reactivated after the deposition of the Rotliegend. Such structures include the ENE-WSW faults on the Murdoch Block and Silverpit Basin.

Another advance resulting from the use of the 3D seismic data and attributes and t-x plotting identified segmentation in faults that were previously thought to be single throughgoing structures on the Top Rotliegend horizon. Fault sets such as the 44-49_NW-_P have been found to be highly segmented with relays in overlapping regions.

7.3.2 The use of 3D seismic attributes has enabled the recognition of the selective reactivation styles of faults within the Pre-Zechstein of the ADB

The Top Rotliegend horizon map is the most laterally continuous and therefore used most commonly in the regional recognition of fault trends. However, this only images faults in the Pre-Zechstein that have a component of slip after the deposition of this horizon. Many faults that are not reactivated after this have gone previously unnoticed as they are not expressed on this horizon. The comparison of

intra-Carboniferous isoproportional slices to the Top Rotliegend horizon map has highlighted the presence of faults such as the E-W and ENE- faults on the Murdoch Block, which have little expression on the Top Rotliegend but exhibit vertical throws at Carboniferous levels.

7.3.3 Only a limited comparison can be made between the resulting offshore fault network (3D seismic) to the patterns onshore (2D seismic)

Due to the largely different basin architecture onshore and offshore, each containing different structural patterns and preservation of stratigraphy, an accurate comparison between the detailed fault network is limited. An extrapolation of the Visean fault network from the Elbow Spit Platform to the Visean network onshore in the Stainmore Trough–Cleveland basin may seem reasonable, however, the effects of Variscan inversion are not as widely evidenced offshore in the MNSH region as onshore. This inversion profoundly effects the production of secondary faults and intra-Basinal structure.

7.3.4 The presence of the mobile Zechstein halite unit offshore has profound decoupling and erasing effects on the record of structural evolution of fault systems in the Anglo-Dutch Basin.

The timing of sub-salt structures that offset the Rotliegend section and terminate into the Zechstein, cannot be determined for certain due to the complex superimposition of at least 6 tectonic episodes in the basin. Lateral and vertical movements that have occurred during these episodes destroy any earlier imprint of upwards fault propagation from the pre-Zechstein succession. The original salt thickness before modification through later deformation, was thick enough for the salt to accommodate the strain accumulating on underlying faults during Mesozoic reactivation in a ductile manner and without there being an expression in the

overburden. The observation of the ‘open top’ t-z profile gradient can crudely estimate how far the fault has propagated into the Zechstein.

7.3.5 Throw distribution mapping can be performed on intra-Carboniferous horizons in areas with good reflections and enables a better estimation of fault timings, intersecting relationships and fault tip configurations

Throw distribution mapping and the characterisation of throw profile types (I-V) has highlighted subtle differences in movement history and revealed that certain faults have a pre-Rotliegend movement and have been later reactivated i.e. Type-IV faults and Type-V faults of 44-49_NW- faults.

7.3.6 Three structural style types have been recognised that have different relationships with the underlying stratigraphy

The analysis of fault geometries and the nature of their basal tip terminations has led to the characterisation of three different structural style types; throughgoing, superficial and detached. Throughgoing faults offset the entire imaged Pre-Zechstein succession (except for Type-I that do not offset the Rotliegend) and are closely coupled with basement stresses, exhibiting extensional, contractional and strike-slip movements. Superficial faults mostly offset the Upper Carboniferous and Rotliegend interval and have upper tips that terminate into the mobile Zechstein unit. Their basal tips are located within the Westphalian to Upper Namurian in which throw decreases to a minima. They exhibit exclusively normal throws despite underlying stratigraphy. Detached faults have similarly limited vertical extends and throw profiles to Superficial faults, the main difference being the presence of a clear underlying detachment, obscuring their lower tip geometries.

7.3.7 Detachment faults in the Lower Carboniferous – Upper Devonian on the southern Mid North Sea High.

A family of WNW- oriented detachment faults have been identified in the Upper Devonian – Lower Carboniferous succession of the Elbow Spit Platform. These faults were previously thought to have formed due to regional extension in the Late Devonian and Early Carboniferous, however, through detailed seismic interpretation and comparison of stratigraphically similar outcrops onshore, t-z analysis, they have been found to have formed some time between the Mid to Late Carboniferous and detach on a postulated overpressured Late Devonian mudstone succession (Tayport Formation).

Due to their decoupling from the underlying stratigraphy, the trigger for their formation is suspected to be non-tectonic. This is also in agreement with their lack of conformity with the regional orientation of extension during the Late Devonian – Early Carboniferous. This formation and minor reactivation is concluded to have occurred to periodic movements on the Elbow Fault, for which the Elbow Spit High forms the footwall. The footwall uplift occurring may have triggered the formation of these faults in a gravity gliding-spreading mechanism. The reactivation is so minor (<20ms) because they are decoupled from basement stresses. This is a key example of a family of faults that are formed as an indirect consequence of regional extension.

7.3.8 Comparing fault spacing and frequency at seismic and map scale may enable the prediction of sub-seismic fault populations in offshore areas

An orthogonal set of superficial faults in the Westphalian with throws up to a metre are superimposed over the larger scale throughgoing Carboniferous faults (Bailey et al. 2005). The Silverpit Basin has an offshore area which has a similar

basin architecture with Variscan inverted half grabens. This suggests that the fault density and spacing results from this dataset (East Pennine Coalfield map) could be extrapolated onto the offshore seismic areas by using a throw filter. This method may have useful applications to the estimation of sub-seismic fault populations in offshore seismic areas that have with similar stratigraphically similar intervals in areas that have undergone a similar tectonic evolution. An area such as the Silverpit Basin is an ideal candidate for this assessment.

7.3.9 Onshore 2D seismic data appears to be sufficient in resolution to capture the presence of faults, however, their definition of throw is poor. The 2D data however lacks the spatial extent to fully characterise the fault population that exists due to the 2D grid.

A similar frequency and spacing of faults were sampled on 1D scanlines in the Stainmore Trough-Cleveland Basin as some offshore areas. The seismic resolution in the Carboniferous interval onshore is also better than some areas offshore. This is surprising considering the age and 2D nature of the data, however may be due to the thin Zechstein overburden and the shallow depth that the Carboniferous interval is at onshore. The quality of the 2D data is still however much poorer and more prone to artefact and noise, making throw analysis uncertain. The limited spatial extent of the 2D grid also does not allow for a detailed characterisation of the detailed fault network that likely exists, as evidenced by the offshore data and coalfield maps.

REFERENCES

AIGNER, T. & BACHMANN, H. 1992. Sequence-stratigraphic framework of the German Triassic. *Sedimentary Geology,* 80**,** 115-135.

ANDREWS, I. J. 2013. The Carboniferous Bowland Shale gas study: geology and resource estimation. *British Geological Survey for the Department of Energy and Climate Change, London.* British Geological Survey.

ARTHAUD, F. & MATTE, P. 1977. Late Paleozoic strike-slip faulting in southern Europe and northern Africa: Result of right-lateral shear zone between the Appalachian and the Urals. *Geological Society of America Bulletin,* 88**,** 1305-1320.

BADLEY, M. E., PRICE, J. D. & BACKSHALL, L. C. 1989. Inversion, reactivated faults and related structures: seismic examples from the southern North Sea. *In:* COOPER, M. A. & WILLIAMS, G. D. (eds.) *Inversion Tectonics.* London: Geological Society

BAILEY, W. R., MANZOCCHI, T., WALSH, J. J., KEOGH, K., HODGETTS, D., RIPPON, J., NEIL, P. A. R., FLINT, S. & STRAND, J. A. 2002. The effect of faults on the 3D connectivity of reservoir bodies: a case study from the East Pennine Coalfield, UK. *Petroleum Geoscience,* 8**,** 263-277.

BAILEY, W. R., WALSH, J. J. & MANZOCCHI, T. 2005. Fault populations, strain distribution and basement fault reactivation in the East Pennines Coalfield, UK. *Journal of Structural Geology,* 27**,** 913-928.

BARNETT, J. A. M., MORTIMER, J., RIPPON, J. H., WALSH, J. J. & WATTERSON, J. 1987. Displacement Geometry in the Volume containing a Single Normal Fault. *The American Association of Petroleum Geologists Bulletin,* 71**,** 925-937.

BAUDON, C. & CARTWRIGHT, J. 2008a. Early stage evolution of growth faults: 3D seismic insights from the Levant Basin, Eastern Mediterranean. *Journal of Structural Geology,* 30**,** 888-898.

BAUDON, C. & CARTWRIGHT, J. 2008b. The kinematics of reactivation of normal faults using high resolution throw mapping. *Journal of Structural Geology,* 30**,** 1072-1084.

BAUDON, C. & CARTWRIGHT, J. A. 2008c. 3D seismic characterisation of an array of blind normal faults in the Levant Basin, Eastern Mediterranean. *Journal of Structural Geology,* 30**,** 746-760.

BAYTOK, S. & PRANTER, M. J. 2013. Fault and fracture distribution within a tight-gas sandstone reservoir: Mesaverde Group, Mamm Creek Field, Piceance Basin, Colorado, USA. *Petroleum Geoscience,* 19**,** 203-222.

BERTHELSEN, A. 1998. The Tornquist Zone northwest of the Carpathians: An intraplate pseudosuture. *Gff,* 120**,** 223-230.
BESLY, B. 1998. Carboniferous. *In:* GLENNIE, K. W. (ed.) *Petroleum Geology of the North Sea: Basinc Concepts and Recent Advances* Oxford: Blackwell Science.
BESLY, B. 2019. Exploration and development in the Carboniferous of the Southern North Sea: a 30-year retrospective. *Geological Society, London, Special Publications,* 471**,** 17-64.
BONINI, M., SANI, F. & ANTONIELLI, B. 2012. Basin inversion and contractional reactivation of inherited normal faults: A review based on previous and new experimental models. *Tectonophysics,* 522-523**,** 55-88.
BOTT, M. H. P. & SMITHSON, S. B. 1967. Gravity Investigations of Subsurface Shape and Mass Distributions of Granite Batholiths. *Geological Society of America Bulletin,* 78**,** 859-878.
BOURNE, S. J. & WILLEMSE, E. J. M. 2001. Elastic stress control on the pattern of tensile fracturing around a small fault network at Nash Point, UK. *Journal of Structural Geology,* 23**,** 1753-1770.
BOWKER, K. A. 2007. Barnett Shale gas production, Fort Worth Basin: Issues and discussion. *AAPG Bulletin,* 91**,** 523-533.
BROWN, A. R. 2011. *Interpretation of Three-Dimensional Seismic Data*, Society of Exploration Geophysicsts and the American Association of Petroleum Geologists.
BULAT, J. & STOKER, S. J. 1986. Uplift determination from interval velocity studies, UK southern North Sea. *In:* GRAHAM, R. H. & TROTMAN (eds.) *Proceedings of the 3rd Conference on Petroleum Geology of N.W. Europe.* London.
CAMERON, D. G., CROSBY, A., BALSON, P. S., JEFFERY, D. H. & LOTT, G. K. 1992. *The Geology of the southern North Sea,* London, British Geological Survey.
CARTWRIGHT, J. 1990. The structural evolution og the Ringkobing-Fyn High. *In:* BLUNDELL, D. J. & GIBBS, A. D. (eds.) *Tectonic Evolution of the North Sea Rifts.* Oxford University Press.
CARTWRIGHT, J. & HUUSE, M. 2005. 3D seismic technology: the geological 'Hubble'. *Basin Research,* 17**,** 1-20.
CARTWRIGHT, J., HUUSE, M. & APLIN, A. 2007. Seal Bypass systems *AAPG Bulletin,* 91**,** 1141-1166.
CARTWRIGHT, J. A. 1989. The Kinematics of inversion in the Danish Central Graben *In:* COOPER, A. H. & WILLIAMS, G. D. (eds.) *Inversion Tectonics.* London: Geological Society.
CARTWRIGHT, J. A. & JACKSON, M. P. A. 2008. Initiation of gravitational collapse of an evaporite basin margin: The Messinian

saline giant, Levant Basin, eastern Mediterranean. *Geological Society of America Bulletin,* 120**,** 399-413.
CARTWRIGHT, J. A., TRUDGILL, B. D. & MANSFIELD, C. S. 1995. Fault growth by segment linkage: an explanation for scatter in maximum displacement and trace length data from the Canyonlands Grabens of SE Utah. *Journal of Structural Geology,* 17**,** 1319-1326.
CATTO, R., TAGGART, S. & POOLE, G. 2017. Petroleum geology of the Cygnus gas field, UK North Sea: from discovery to development. *Geological Society, London, Petroleum Geology Conference series***,** PGC8.39.
CHADWICK, R. A. & EVANS, D. J. 1995. The timing and direction of Permo-Triassic extension in southern Britain. *Permian and Triassic rifting in Northwest Europe,* 91**,** 161-192.
CHADWICK, R. A. & PHARAOH, T. C. 1998. The seismic reflection Moho beneath the United Kingdom and adjacent areas. *Tectonophysics,* 299**,** 255-279.
CHILDS, C., NICOL, A., WALSH, J. J. & WATTERSON, J. 2003. The growth and propagation of synsedimentary faults. *Journal of Structural Geology,* 25**,** 633-648.
CHILDS, C., WALSH, J. J. & WATTERSON, J. 1990. A Method for Estimation of the Density of Fault Displacements below the Limits of Seismic Resolution in Reservoir Formations. *North Sea Oil and Gas Reservoirs—II.*
CHILDS, C., WATTERSON, J. & WALSH, J. 1995. Fault overlap zones within developing normal fault systems *Journal of the Geological Society,* 152**,** 535-549.
CLARKE, H., EISNER, L. & STYLES, P. 2014a. Felt seismicity associated with shale gas hydraulic fracturing: The first documented example is Europe. *Geophysical research letters,* 41**,** 8308-8314.
CLARKE, H., EISNER, L., STYLES, P. & TURNER, P. 2014b. Felt seismicity associated with shale gas hydraulic fracturing: The first documented example in Europe. *Geophysical Research Letters,* 41.
COCKS, L. R. M. & FORTEY, R. A. 1982. Faunal evidence for oceanic separations in the Palaeozoic of Britain. *Journal of the Geological Society,* 139**,** 465-478.
COLLIER, R. E. 1991. The Lower Carboniferous Stainmore Basin, N. England: extensional basin tectonics and sedimentation. *Journal of the Geological Society,* 148**,** 379-390.

COOPER, M. A., WILLIAMS, G. D., DE GRACIANSKY, P. C., MURPHY, R. W., NEEDHAM, T., DE PAOR, D., STONELEY, R., TODD, S. P., TURNER, J. P. & ZIEGLER, P. A. 1989. Inversion tectonics - a discussion. *In:* COOPER, M. A. & WILLIAMS, G. D. (eds.) *Inversion Tectonics.* London: Geological Society

COOPER, M. M., EASTON, S. D. W., LYNCH, J. J. & FOZDAR, I. M. 2005. The Caister–Murdoch System(CMS) III Carboniferous cluster development, UK Southern NorthSea. *In:* DORE, A. G. & VINNING, B. A. (eds.) *Petroleum Geology: North West Europe and Global Perspectives - Proceedings of the 6th Petroleum Geology Conference* The Geological Society.

CORFIELD, S. M., GAWTHORPE, R. L., GAGE, M., FRASER, A. J. & BESLY, B. M. 1996. Inversion tectonics of the Variscan foreland of the British Isles. *Journal of the Geological Society,* 153**,** 17-32.

COSSEY, P. J., E., A. A., A., P. M., J., W. M., A., W. M. & WRIGHT, V. P. 2004. *British Lower Carboniferous Stratigraphy,* Peterborough, Joint Nature Conservation Comitee.

COWARD, M. P. 1990. The Precambrian, Caledonian and Variscan framework to NW Europe. *In:* HARDMAN, R. F. P. & BROOKS, J. (eds.) *Tectonic Events Responsible for Britain's Oil and Gas Reserves.* London: Geological Society.

COWARD, M. P. 1993. The effect of Late Caledonian and Variscan continental escape tectonics on basement structure, Paleozoic basin kinematics and subsequent Mesozoic basin development in NW Europe. *In:* PARKER, J. R. (ed.) *Petroleum Geology of Northwest Europe: Proceedings of the 4th Conference* London: The Geological Society.

COWARD, M. P. & STEWART, S. A. 1995. Salt-influenced structures in the Mesozoic-Tertiary cover of the southern North Sea, U.K. *In:* JACKSON, M. P. A., ROBERTS, D. G. & SNELSON, S. (eds.) *Salt Tectonics: A Global Perspective.* AAPG Memoir

COWIE, P. A. & ROBERTS, G. P. 2001. Constraining slip rates and spacings for active normal faults. *Journal of Structural Geology,* 23**,** 1901-1915.

COWIE, P. A. & SCHOLZ, C. H. 1992. Physical explanation for the displacement-length relationship of faults using a post-yield fracture mechanics model. *Journal of Structural Geology,* 14**,** 1133-1148.

CRIDER, J. G. & POLLARD, D. D. 1998. Fault linkage: Three-dimensional mechanical interaction between echelon normal faults. *Journal of Geophysical Research: Solid Earth,* 103**,** 24373-24391.

DAVIES, R., FOULGER, G., BINDLEY, A. & STYLES, P. 2013. Induced seismicity and hydraulic fracturing for the recovery of hydrocarbons. *Marine and Petroleum Geology,* 45**,** 171-185.

DAWERS, N. H. & ANDERS, M. H. 1995. Displacement-length scaling and fault linkage. *Journal of Structural Geology,* 17**,** 607-614.

DAWERS, N. H., ANDERS, M. H. & SCHOLZ, C. H. 1993. Growth of normal faults: Displacement-length scaling. *Geology,* 21.

DEWEY, J. F., HELMAN, M. L., TURCO, W., D. H. & KNOTT, S. D. 1989. Kinematics of the western Mediterranean. *Alpine Tectonics,* 45**,** 265-283.

DICKINSON, G. 1954. Subsurface interpretation of intersecting faults and their effects upon stratigraphic horizons. *Bulletin of the American Association of Petroleum Geologists,* 38**,** 854-877.

DONATO, J. A., MARTINDALE, W. & TULLY, M. C. 1983. Buried granites within the Mid North Sea High. *Journal of the Geological Society,* 140**,** 825-837.

DOORNENBAL, H. & STEVENSON, A. 2010. *Petroleum Geological Atlas of the Southern Permian Basin Area.*, EAGE Publications.

ELLSWORTH 2013. Injection-Induced Earthquakes. *Science,* 341.

FOSCHI, M. 2014. Seismic Evidence for Hydrocarbon Migration. *Cardiff University,* PhD Thesis.

FOSSEN, H. 2016. Chapter 8 Faults. *In:* FOSSEN, H. (ed.) *Structural Geology* 2nd ed.: Cambridge University Press.

FRANKE, W. 2000. The mid-European segment of the Variscides: tectonostratigraphic units, terrane boundaries and plate tectonic evolution. *Orogenic Processes: Quantification and Modelling in the Variscan Belt,* 179**,** 35-61.

FRASER, A. J. & GAWTHORPE, R. L. 1990. Tectono-stratigraphic development and hydrocarbon habitat of the Carboniferous in northern England. *In:* HARDMAN, R. F. P. & BROOKS, J. (eds.) *Tectonic Events Responsible for Britain's Oil and Gas Reserves.* London: Geological Society.

FRASER, A. J. & GAWTHORPE, R. L. 2003a. *An Atlas of Carboniferous Basin Evolution in Northern England,* London, Geological Society.

FRASER, A. J. & GAWTHORPE, R. L. 2003b. Cleveland Basin. *An Atlas of Carboniferous Basin Evolution in Northern England.* The Geological Society, London: The Geological Society.

GILLESPIE, P. A., HOWARD, C. B., WALSH, J. J. & WATTERSON, J. 1993. Measurement and characterisation of spatial distribution of fractures. *Tectonophysics,* 226**,** 113-141.

GLENNIE, K. W. 1986. Development of N.W. Europe's Southern Permian Gas Basin. *Habitat of Palaeozoic Gas in N.W. Europe,* 22.

GLENNIE, K. W. 1997. History of exploration in the southern North Sea. *Petroleum Geology of the Southern North Sea: Future Potential, Geological Soc Special Publication,* 123**,** 5-16.
GLENNIE, K. W. 1998. *Petroleum Geology of the North Sea: Basic Concepts and Recent Advances*, Wiley-Blackwell.
GOLKE, M. & COBLENTZ, D. 1996. Origins of the European regional stress field. *Tectonophysics,* 266**,** 11-24.
GOMEZ, L. A. & LAUBACH, S. E. 2006. Rapid digital quantification of microfracture populations. *Journal of Structural Geology,* 28**,** 408-420.
GOOSSENS, R. F. S., E. G. 1973. The stratigraphy and structure of the Upper Coal Measures in the exposed Yorkshire Coalfield between Pontefract and South Kirkby. *Proceedings of the Yorkshire Geological Society,* 39**,** 487-514.
GOULTY, N. R. 2005. Emplacement mechanism of the Great Whin and Midland Valley dolerite sills. *Journal of the Geological Society,* 162**,** 1047-1056.
GROSS, M. R., GUTIERREZ-ALONSO, G., BAI, T., WACKER, A., COLLINSWORTH, K. B., BEHL, R. J. 1997. Influence of mechanical stratigraphy and kinematics on fault scaling relations. *Journal of Structural Geology,* 19**,** 171-183.
GUTERCH, A., WYBRANIEC, S., GRAD, M., CHADWICK, R. A., KRAWCZYK, C. M., ZIEGLER, P. A., THYBO, H. & DE VOS, W. 2010. Crustal Structure and Structural Framework. *In:* DOORNENBAL, J. C. & STEVENSON, A. G. (eds.) *Petroleum Geological Atlas of Southern Permian Basin Area.* EAGE Publications.
HIBSCH, C., JARRIGE, J. J., CUSHING, E. M. & MERCIER, J. 1995. Palaeostressanalysis, a contribution to the understanding of basin tectonics and geodynamic evolution. Example of the Permian/Cenozoic tectonics of Great Britain and geodynamic implications in western Europe. *Tectonophysics,* 252**,** 103-136.
HOLLYWOOD, J. M. W., C. V. 1993. Structural development and hydrocarbon occurrence of the Carboniferous in the UK Southern North Sea Basin. *In:* PARKER, J. R. (ed.) *Petroleum Geology of Northwest Europe: Proceedings of the 4th Conference* London: The Geological Society.
HUGHES, F., HARRISON, D., HAARHOFF, M., HOWLETT, P., PEARSON, A., WARE, D., TAYLOR, C., EMMS, G. & MORTIMER, A. 2016. The unconventional Carboniferous reservoirs of the Greater Kirby Misperton gas field and their potential: North Yorkshire's sleeping giant. *Geological Society, London, Petroleum Geology Conference series***,** PGC8.5.

JACKSON, M. P. A. & HUDEC, M. R. 2005. Stratigraphic record of translation down ramps in a passive-margin salt detachment. *Journal of Structural Geology,* 27**,** 889-911.

JARVIE, D. M., HILL, R. J. & POLLASTRO, M. 2005. *Assessment of the Gas Potential and Yields from Shales: the Barnett Shale Model,* Olkahoma Geological Survey Circular.

KEARSEY, T., ELLEN, R., MILLWARD, D. & MONAGHAN, A. A. 2015. Devonian and Carboniferous stratigraphical correlation and interpretation in the Central North Sea, Quadrants 25-44.

KELLY, P. G., PEACOCK, D. C. P., SANDERSON, D. J. & MCGURK, A. C. 1999. Selective reverse-reactivation of normal faults and deformation around reverse-reactivated faults in the Mesozoic of the Somerset coast. *Journal of Structural Geology,* 21**,** 493-509.

KIRKLAND, C. L., DALY, J. S., EIDE, E. A. & WHITEHOUSE, M. J. 2006. The structure and timing of lateral escape during the Scandian Orogeny: A combined strain and geochronological investigation in Finnmark, Arctic Norwegian Caledonides. *Tectonophysics,* 425**,** 159-189.

KLEY, J. & VOIGT, T. 2008. Late Cretaceous intraplate thrusting in central Europe: Effect of Africa-Iberia-Europe convergence, not Alpine collision. *Geology,* 36.

KNOTT, S. D., BEACH, A., BROCKBANK, P. J., BROWN, L., MCCALLUM, J. E. & WELBON, A. I. 1996. Spatial and mechanical controls on normal fault populations. *Journal of Structural Geology,* 18**,** 359-372.

KOMBRINK, H. 2008. *The Carboniferous of the Netherlands and surrounding areas; a basin analysis.* PhD, University of Utrecht.

KOSI, W., TARI, G., NADER, F. H., SKIPLE, C., TRUGILL, B. & LAZAR, D. 2012. Structural analogy between the "piano key faults" of deep-water Lebanon and the extensional faults of the Canyonlands grabens, Utah, United States. *The Leading Edge***,** 824-830.

KRAWCZYK, C. M., RABBEL, W., WILLERT, S., HESE, F., GOTZE, H. J. & GAJEWSKI, D. 2008. Crustal structures and properties in the Central European Basin System from geophyscial evidence. *In:* LITTKE, R., BAYER, U., GAJEWSKI, D. & NELSKAMP, S. (eds.) *Dynamics of complex intracontinental basins: The Central European Basin System.* Springer.

LAMARCHE, J., BERGERAT, F., LEWANDOWSKI, M., MANSY, J. L., SWIDROWSKA, J. & WIECZOREK, J. 2002. Variscan to Alpine heterogeneous palaeo-stress field above a major Palaeozoic suture in the Carpathian foreland (southeastern Poland). *Tectonophysics,* 357**,** 55-80.

LANGFORD, M. E., WESTERA, G. D., HOLLAND, B., BOCANEALA, B. & NORRIS, M. R. 2014a. Development of a Stranded Tight Gas Field in the UK Southern North Sea Using Hydraulic Fracturing Within a Subsea Horizontal Well: A Case Study. *Society of Petroleum Geologists*.

LANGFORD, M. E., WESTERA, G. D., HOLLAND, B., BOCANEALA, B. & NORRIS, M. R. 2014b. Development of a Stranded Tight Gas Field in the UK Southern North Sea Using Hydraulic Fracturing Within a Subsea Horizontal Well: A Case Study *Society of Petroleum Engineers*.

LAUBACH, S. E., LAMARCHE, J., GAUTHIER, B. D. M., DUNNE, W. M. & SANDERSON, D. J. 2018. Spatial arrangement of faults and opening-mode fractures. *Journal of Structural Geology,* 108**,** 2-15.

LEEDER, M. R. 1982. Upper Palaeozoic basins of the British Isles - Caledonide inheritance versus Hercynian plate margin processes. *Journal of the Geological Society,* 139**,** 479-91.

LEEDER, M. R. 1988. Recent developments in Carboniferous geology: a critical review with implications for the British Isles and N.W. Europe. *Proceedings of the Geologists Association,* 99.

LEEDER, M. R. & HARDMAN, M. 1990. Carboniferous geology of the Southern North Sea Basin and controls on hydrocarbon prospectivity. *In:* HARDMAN, R. F. P. & BROOKS, J. (eds.) *Tectonic Events Responsible for Britains Oil and Gas Reserves.* London: Geological Society.

LESLIE, A. G., MILLWARD, D., PHARAOH, T. C., MONAGHAN, A. A., ARSENIKOS, S. & QUINN, M. 2015. Tectonic synthesis and contextual setting for the Central North Sea and adjacent onshore areas, 21CXRM Palaeozoic Project. *British Geological Survey Research Report*.

LYNGSIE, S. B., THYBO, H. & RASMUSSEN, T. M. 2006. Regional geological and tectonic structures of the North Sea area from potential field modelling. *Tectonophysics,* 413**,** 147-170.

MANSFIELD, C. & CARTWRIGHT, J. 1996. High resolution fault displacement mapping from three-dimensional seismic data: evidence for dip linkage during fault growth. *Journal of Structural Geology,* 18**,** 249-263.

MANZOCCHI, T., CHILDS, C. & WALSH, J. J. 2010. Faults and fault properties in hydrocarbon flow models. *Geofluids*.

MARRETT, R. A. & ALLMENDINGER, R. W. 1992. Amount of extension on "small" faults: An example from the Viking graben. *Geology,* 20**,** 47-50.

MAUDUIT, T., GUERIN, G., BRUN, J. P. & LECANU, H. 1997. Raft tectonics: the effects of basal slope angle and sedimentation rate

on progressive extension. *Journal of Structural Geology,* 19**,** 1219-1230.
MAYNARD, J. R., WIGNALL, P. B. & VARKER, W. J. 1991. A 'hot' new shale facies from the Upper Carboniferous of Northern England. *Journal of the Geological Society,* 148**,** 805-808.
MCGARR, A., BEKINS, B., BURKARDT, N., DEWEY, J., EARLE, P., ELLLSWORTH, W., GE, S., HICKMAN, S., HOLLAND, A., MAJER, E., RUBINSTEIN, J. & SHEEHAN, A. 2015. Coping with earthquakes induced by fluid injection. *Science,* 347.
MCKENZIE, D. 1978. Some Remarks on the Development of Sedimentary Basins. *Earth and Planetary Science Letters,* 40**,** 25-32.
MCKERROW, W. S., MAC NIOCAILL, C., AHLBERG, P. E., CLAYTON, G., CLEAL, C. J. & EAGAR, R. M. C. 2000. The Late Palaeozoic relations between Gondwana and Laurussia. *Orogenic Processes: Quantification and Modelling in the Variscan Belt,* 179**,** 9-20.
MCPHEE, C. A., JUDT, M. R., MCRAE, D. & RAPACH, J. M. 2008. Maximising Gas Well Potential in the Breagh Field by Mitigating Formation Damage. *Society of Petroleum Geologists*.
MEYER, V., NICOL, A., CHILDS, C., WALSH, J. & WATTERSON, J. 2002. Progressive localisation of strain during the evolution of a normal fault population. *Journal of Structural Geology,* 24**,** 1215-1231.
MONAGHAN, A. A. 2014. The Carboniferous shales of the Midland Valley of Scotland: geology and resource estimation. *British Geological Survey for Department of Energy and Climate Change.*
MORLEY, C. K., BACK, S., VAN RENSBERGEN, P., CREVELLO, P. & LAMBIASE, J. J. 2003. Characteristics of repeated, Detached, Miocene–Pliocene tectonic inversion events, in a large delta province on an active margin, Brunei Darussalam, Borneo. *Journal of Structural Geology,* 25**,** 1147-1169.
MURAOKA, H. & KAMATA, H. 1983. Displacement distribution along minor fault traces. *Journal of Structural Geology,* 5**,** 483-495.
NALPAS, T., DOUARAN, S. L., BRUN, J. P., UNTERNEHR, P. & RICHERT, J. P. 1995. Inversion of the Broad Fourteens Basin (Offshore Netherlands), a small-scale model investigation. *Sedimentary Geology,* 95**,** 237-250.
NANCE, R. D., GUTIÉRREZ-ALONSO, G., KEPPIE, J. D., LINNEMANN, U., MURPHY, J. B., QUESADA, C., STRACHAN, R. A. & WOODCOCK, N. H. 2010. Evolution of the Rheic Ocean. *Gondwana Research,* 17**,** 194-222.

NANCE, R. D. & LINNEMANN, U. 2008. The Rheic Ocean: Origin, Evolution, and Significance. *GSA Today,* 18**,** 4.

NELSON, M. A. 2006. *3D Geometry and Kinematics of Non-Colinear Fault Intersections.* Ph. D, Cardiff University.

NICOL, A., WALSH, J. J., WATTERSON, J., NELL, P. A. R. & BRETAN, P. 2003. The geometry, growth and linkage of faults within a polygonal fault system from South Australia. *Geological Society, London, Special Publications,* 216**,** 245-261.

NICOL, A., WATTERSON, J., WALSH, J. J. & CHILDS, C. 1996. The shapes, major axis orientations and displacement patterns of fault surfaces. *Journal of Structural Geology,* 18**,** 235-248.

NIXON, C. W., SANDERSON, D. J., DEE, S. J., BULL, J. M., HUMPHREYS, R. J. & SWANSON, M. H. 2014. Fault interactions and reactivation within a normal-fault network at Milne Point, Alaska. *AAPG Bulletin,* 98**,** 2081-2107.

ORTEGA, O. J., MARRETT, R. A. & LAUBACH, S. E. 2006. A scale-independent approach to fracture intensity and average spacing measurement. *AAPG Bulletin,* 90**,** 193-208.

OSBORNE, M. J. & SWARBRICK, R. E. 1997. Mechanisms for Generating Overpressure in Sedimentary Basins: A Reevaluation. *AAPG Bulletin,* 81**,** 1023-1041.

OUDMAYER, B. C. & DE JAGER, J. 1993. Fault reactivation and oblique-slip in the Southern North Sea. *In:* PARKER, J. R. (ed.) *Petroleum Geology of Northwest Europe: Proceedings of the 4th Conference* London: The Geological Society.

PHARAOH, T. C. 1999. Palaeozoic terranes and their lithospheric boundaries within the Trans-European Suture Zone (TESZ): a review. *Tectonophysics,* 314**,** 17-41.

PHARAOH, T. C., DUSAR, M., GELUK, M. C., KOCKEL, F., KRAWCZYK, C. M., KRZYWIEC, P., SCHECK-WENDEROTH, M., THYBO, H., VEJBAEK, O. V. & VAN WEES, J. D. 2010. Tectonic Evolution *In:* DOORNENBAL, J. C. & STEVENSON, A. G. (eds.) *Petroleum Geological Atlas of the Southern Permian Basin Area.* EAGE Publications.

PHARAOH, T. C., WINCHESTER, J. A., VERNIERS, J., LASSEN, A. & SEGHEDI, A. 2006. The Western Accretionary Margin of the East European Craton: an overview. *Geological Society, London, Memoirs,* 32**,** 291-311.

PHARAOH, T. E., R. LEE, M 1995. The Caledonide Basement of Eastern England *Studia geoph. et geod,* 39**,** 330-346.

PRIEST, S. D. & HUDSON, J. A. 1981. Estimation of Discontinuity Spacing and Trace Length Using Scanline Surveys. *International*

Journal of Rock Mechanics and Mining Sciences & Geomechanics Abstracts, 18**,** 183-197.

QUIRK, D. G. A., J. F. 1997. The structure of the Westphalian in the northern part of the southern North Sea. *In:* ZIEGLER, K., TURNER, P. & DAINES, S. R. (ed.) *Petroleum Geology of the Southern North Sea: Future Potential.* London: Geological Society Special Publications.

RAMBERG, H. 1980. Diapirism and gravity collapse in the Scandinavian Caledonides. *Journal of the Geological Society,* 137**,** 261-270.

RAWNSLEY, T., RIVES, T. & PETIT, J. P. 1992. Joint development in perturbed stress fields near faults. *Journal of Structural Geology,* 14**,** 939-951.

RECHES, Z. 1983. Faulting of Rocks in Three-Dimesional Strain Fields II. Theoretical Analysis. *Tectonophysics,* 95**,** 133-156.

REICHE, S., HÜBSCHER, C. & BEITZ, M. 2014. Fault-controlled evaporite deformation in the Levant Basin, Eastern Mediterranean. *Marine Geology,* 354**,** 53-68.

REMMELTS, G. 1996. Salt tectonics in the southern North Sea, the Netherlands. *In:* RONDEEL, H. E., BATJES, D. A. J. & NIEUWENHUIJS, W. H. (eds.) *Geology of Gas and Oil under the Netherlands.* Springer.

RESTON, T. J. & BLUNDELL, D. J. 1987. Possible mid-crustal shears at the edge of the London Platform. *Geophysical Journal International,* 89**,** 251-258.

RIJKERS, R., DUIN, E., DUSAR, M. & LANGENAEKER, V. 2009. Crustal structure of the London–Brabant Massif, southern North Sea. *Geological Magazine,* 130**,** 569-574.

RIPPON, J. H. 1985. Contoured patterns of the throw and hade of normal faults in the coal measures (Westphalian) of north-east Derbyshire *Proceedings of the Yorkshire Geological Society,* 45**,** 147-161.

RIPPON, J. H. 1997. *Variations in tectonic style and setting in British coalfields. .* Doctoral Thesis, Keele University.

ROTEVATN, A. & JACKSON, C. A. L. 2014. 3D structure and evolution of folds during normal fault dip linkage. *Journal of the Geological Society,* 171**,** 821-829.

SCHECK-WENDEROTH, M., KRZYWIEC, P., ZUHLKE, R., MAYSTRENKO, Y. & FROITZHEIM, N. 2008. Permian to Cretaceous tectonics. *In:* MCCANN, T. (ed.) *The geology of Central Europe.* The geological society.

SCHLAGER, W. 2004. Fractal nature of stratigraphic sequences. *Geology,* 32.

SCHLISCHE, R. W., YOUNG, S. S., ACKERMANN, R. V. & GUPTA, A. 1996. Geometry and scaling relations of a population of very small rift-related normal faults. *Geology,* 24**,** 683-686.

SCHOLZ, C. H. & COWIE, P. A. 1990. Determination of total strain from faulting using slip measurements. *Nature,* 346.

SCHROOT, B. M. & DE HAAN, H. B. 2003. An improved regional structural model of the Upper Carboniferous of the Cleaver Bank High based on 3D seismic interpretation. *In:* NIEUWLAND, D. A. (ed.) *New Insights into Structural Interpretation and Modelling.* Geological Society London.

SCHULTZ, D. D. 2001. Excursus on gravity gliding and gravity spreading *Journal of Structural Geology,* 23**,** 725-731.

SCHULTZ, R. A., SOLIVA, R., FOSSEN, H., OKUBO, C. H. & REEVES, D. M. 2008. Dependence of displacement–length scaling relations for fractures and deformation bands on the volumetric changes across them. *Journal of Structural Geology,* 30**,** 1405-1411.

SCHULTZ, R. A., SOLVIA, R., OKUBO, C. H. & MEGE, D. 2010. Fault Populations. *In:* WATTERS, T. R. & SCHULTZ, R. A. (eds.) *Planetary Tectonics.* Cambridge University Press.

SIBSON, R. H. 1995. Selective fault reactivation during basin inversion: potential for fluid redistribution through fault-valve action. *Geological Society Special Publications,* 88**,** 3-19.

SLOWAKIEWICZ, M., TUCKER, M., VANE, C. H., HARDING, R., COLLINS, A. & PANCOST 2015. Shale-Gas Potential of the Mid-Carboniferous Bowland-Hodder Unit in the Cleveland Basin (Yorkshire), Central Britain. *Journal of Petroleum Geology,* 38**,** 59-76.

SMIT, J., WEES, J.-D. V. & CLOETINGH, S. 2016. The Thor suture zone: From subduction to intraplate basin setting. *Geology,* 44**,** 707-710.

SOLVIA, R., BENEDICTO, A. & MAERTEN, L. 2006. Spacing and linkage of confined normal faults: Importance of mechanical thickness. *Journal of Geophysical Research,* 111.

SOPER, N. J., WEBB, B. C. & WOODCOCK, N. H. 1987. Late Caledonian (Acadian) transpression in north-west England: timing, geometry and geotectonic significance *Proceedings of the Yorkshire Geological Society,* 46**,** 175-192.

STEPHENSON, B. & COFLIN, K. 2015. Guidelines for the Handling of Natural Fractures and Faults in Hydraulically Stimulated Resource Plays. *SPE/CSUR Unconventional Resources Conference.* Calgary, Alberta, Canada: Society of Petroleum Engineers.

STEWART, S. A. 2001. Displacement distributions on extensional faults: Implications for fault stretch, linkage and seal. *AAPG Bulletin,* 85**,** 587-599.

STEWART, S. A. & COWARD, M. P. 1995. Synthesis of Salt tectonics in the southern North Sea, UK. *Marine and Petroleum Geology,* 12.

SUPPE, J. 1983. Geometry and kinematics of fault-bend folding. *American Journal of Science,* 283**,** 684-721.

TER BORGH, M., JAARSMA, B. & ROSENDAAL, E. A. 2018. Structural development of the northern Dutch offshore: Paleozoic to present. *In:* MONAGHAN, A. A., UNDERHILL, J. R., HEWETT, A. J. & MARSHALL, J. E. A. (eds.) *Palaeozoic Plays of NW Europe.* London: Geological Society.

TOGHILL 1992. The Shelvian event, a late Ordovician tectonic episode in Southern Britain (Eastern Avalonia). *Proceedings of the Geologists Association,* 103**,** 31-35.

TRENCH, A. & TORSVIK, T. H. 1992. The closure of the Iapetus Ocean and Tornquist Sea: new palaeomagnetic constraints. *Journal of the Geological Society,* 149**,** 867-870.

TRUDGILL, B. & CARTWRIGHT, J. 1994. Relay-ramp forms and normal-fault linkages, Canyonlands National Park, Utah. *Geological Society of America Bulletin,* 106**,** 1143-1157.

TVEDT, A. B. M., ROTEVATN, A., JACKSON, C. A. L., FOSSEN, H. & GAWTHORPE, R. L. 2013. Growth of normal faults in multilayer sequences: A 3D seismic case study from the Egersund Basin, Norwegian North Sea. *Journal of Structural Geology,* 55**,** 1-20.

UNDERHILL, J. R. & PARTINGTON, A. 1993. Jurassic thermal doming and deflation in the North Sea: implications of the sequence stratigraphic evidence. *In:* PARKER, J. R. (ed.) *Petroleum Geology of Northwest Europe: Proceedings of the 4th Conference* London: Geological Society

VAN HOORN, B. Structural evolution, timing and tectonic style of the Sole Pit inversion.

VAN HULTEN, F. F. N. 2010. Geological factors effecting compartmentalization of Rotliegend gas fields in the Netherlands. *Geological Society, London, Special Publications,* 347**,** 301-315.

WALSH, J., WATTERSON, J. & YEILDING, G. 1991. The importance of small-scale faulting in regional extension. *Nature,* 351**,** 391-393.

WALSH, J. J., BAILEY, W. R., CHILDS, C., NICOL, A. & BONSON, C. G. 2003. Formation of segmented normal faults: a 3-D perspective. *Journal of Structural Geology,* 25**,** 1251-1262.

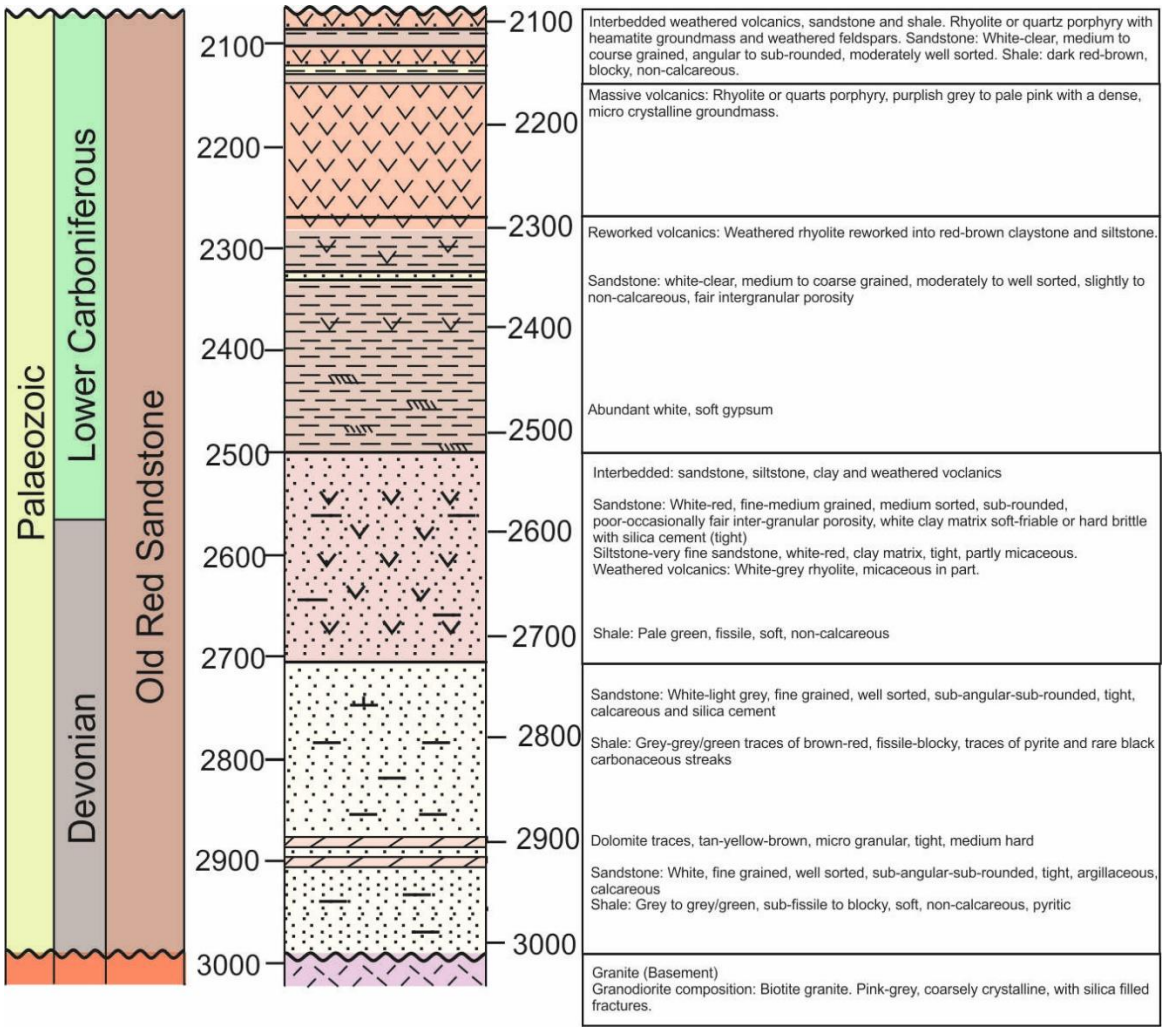
WALSH, J. J. & WATTERSON, J. 1987. Displacements of cumulative displacement and seismic slip on a single normal fault surface. *Journal of Structural Geology,* 9**,** 1039-1046.
WALSH, J. J. & WATTERSON, J. 1988a. Analysis of the relationship between displacements and dimensions of faults. *Journal of Structural Geology,* 10**,** 239-247.
WALSH, J. J. & WATTERSON, J. 1988b. Dips of normal faults in British Coal Measures and other sedimentary sequences *Journal of the Geological Society, London,* 145**,** 859-873.
WALSH, J. J. & WATTERSON, J. 1989. Displacement gradients on fault surfaces *Journal of Structural Geology,* 11**,** 307-316.
WALSH, J. J. & WATTERSON, J. 1992. Populations of faults and fault displacements and their effects on estimates of fault-related regional extension. *Journal of Structural Geology,* 14**,** 701-712.
WALTERS, R. J., ZOBACK, M. D., BAKER, J. W. & BEROZA, G. C. 2015. Characterizing and Responding to Seismic Risk Associated with Earthquakes Potentially Triggered by Fluid Disposal and Hydraulic Fracturing. *Seismological Research Letters,* 86**,** 1110-1118.
WATTERSON, J. 1986. Fault Dimensions, Displacements and Growth. *Pure and Applied Geophysics,* 124**,** 365-373.
WATTERSON, J., WALSH, J. J., GILLESPIE, P. A. & EASTON, S. 1996. Scaling systematics of fault sizes on a large-scale range fault map. *Journal of Structural Geology,* 18**,** 199-214.
WESTWOOD, R. F., TOON, S. M., STYLES, P. & CASSIDY, N. J. 2017. Horizontal respect distance for hydraulic fracturing in the vicinity of existing faults in deep geological reservoirs: a review and modelling study. *Geomechanics and Geophysics for Geo-Energy and Geo-Resources,* 3**,** 379-391.
WILKINS, S. J., GROSS, M. R. 2002. Normal fault growth in layered rocks at Split Mountain, Utah: influence of mechanical stratigraphy on dip linkage, fault restriction and fault scaling *Journal of Structural Geology,* 24**,** 1413-1429.
WILLIAMS, G. D. 1993. Tectonics and seismic sequence stratigraphy: an introduction. *Tectonics and Seismic Sequence Stratigraphy,* 71.
WILLIAMS, G. D., POWELL, C. M. & COOPER, M. A. 1989. Geometry and kinematics of inversion tectonics. *Geological Society, London, Special Publications,* 44**,** 3-15.
WILSON, M., NEUMANN, E.-R., DAVIES, G. R., TIMMERMAN, M. J., HEEREMANS, M. & LARSEN, B. T. 2004. Permo-Carboniferous magmatism and rifting in Europe: Introduction. *Permo-*

Carboniferous magmatism and rifting in Europe: Geological society of London Special Publications 223**,** 1-10.
WILSON, M. P., WORRALL, F., DAVIES, R. J. & ALMOND, S. 2018. Fracking: How far from faults? *Geomechanics and Geophysics for Geo-Energy and Geo-Resources,* 4**,** 193-199.
WINCHESTER, J. A., PHARAOH, T. C. & VERNIERS, J. 2002. Palaeozoic amalgamation of Central Europe: an introduction and synthesis of new results from recent geological and geophysical investigations. *In:* WINCHESTER, J. A., PHARAOH, T. C. & VERNIERS, J. (eds.) *Palaeozoic Amalgamation of central Europe.* London: Geological Society Special Publications.
WINCHESTER, J. A., PHARAOH, T. C., VERNIERS, J., JOANE, D. & SEGHEDI, A. 2006. Palaeozoic accretion of Gondwana-derived terranes to the East European Craton: recognition of detatched terrane fragments dispersed after collision with promontories.
WIPRUT, D. & ZOBACK, M. 2000. Fault reactivation and fluid flow along a previously dormant normal fault in the northern North Sea. *Geology,* 28**,** 595-598.
WITHJACK, M. O. & CALLOWAY, S. 2000. Active Normal Faulting Beneath a Salt Layer: An Experimental Study of Deformation Patterns in the Cover Sequence. *AAPG Bulletin,* 84.
WOODCOCK, N. H. & FISCHER, M. 1986. Strike-slip duplexes. *Journal of Structural Geology,* 8**,** 725-735.
YIELDING, G., WALSH, J. & WATTERSON, J. 1992. The prediction of small-scale faulting in reservoirs. *First Break,* 10.
ZIEGLER, P. A. 1978. North-Western Europe: Tectonics and basin development *In:* VAN LOON, A. J. (ed.) *Key-notes of the MEGS-II* Amsterdam: Geologie en Mijnbouw.
ZIEGLER, P. A. 1989. Geodynamic model for Alpine intra-plate compressional deformation in Western and Central Europe. *In:* COOPER, M. A. & WILLIAMS, G. D. (eds.) *Inversion Tectonics.* London: Geological Society.
ZIEGLER, P. A. 1990. *Geological Atlas of Western and Central Europe*.
ZIEGLER, P. A. 1992. North Sea rift system. *Tectonophysics,* 208**,** 55-75.
ZIEGLER, P. A. & DEZES, P. 2006. Crustal evolution of Western Europe. *European Lithosphere Dynamics,* 32**,** 43-56.
ZIEGLER, P. A., VAN WEES, J. D. & CLOETINGH, S. 1998. Mechanical controls on collision-related compressional intraplate deformation. *Tectonophysics,* 300**,** 103-129.

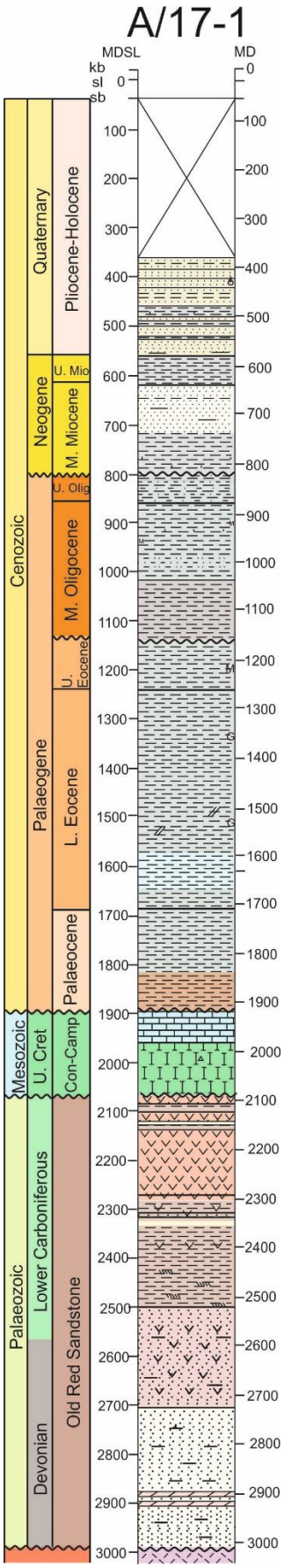
APPENDIX

Elbow Spit Platform - Well Information

Pre-Zechstein Stratigraphic succession for well A-17



Full stratigraphic succession for well A-17



Silverpit Basin Well Information

Pre-Zechstein Well Stratigraphy for wells 44/27-1, 44/26-4, 44/28-2, 49/01-3

